

**Late Pleistocene to Holocene Sedimentology,  
Palaeoceanography and Micropalaeontology of the  
Uruguayan Continental Slope**

**Cian James McGuire**

Submitted for the Degree of Doctor of Philosophy

University of Hull

Department of Geography, Geology & Environment

December 2019

Supervisors

Mike Rogerson

Dan Parsons

Liam Herringshaw



**UNIVERSITY  
OF HULL**

The copyright in this thesis is owned by the author. Any quotation from the thesis or use of any of the information contained in it must acknowledge this thesis as the source of the quotation or information

# ABSTRACT

---

## **Late Pleistocene to Holocene Sedimentology, Palaeoceanography and Micropalaeontology of the Uruguayan Continental Slope**

**Cian McGuire**<sup>1</sup>, Mike Rogerson<sup>2</sup>, Liam Herringshaw<sup>2</sup> and Dan Parsons<sup>3</sup>

<sup>1</sup> *British Antarctic Survey, High Cross Madingley Road, Cambridge, CB3 0ET*

<sup>2</sup> *Department of Geography, Geology and Environment, University of Hull, Cottingham Road, Hull, HU6 7RX*

<sup>3</sup> *Energy and Environment Institute, University of Hull, Cottingham Road, Hull, HU6 7RX*

This study utilises an extensive set of sediment cores collected from a largely unstudied contourite and turbidite depositional system located on the Uruguay continental margin to identify a method of distinguishing deposits in the deep sea that are sourced from either gravity or bottom current sedimentary processes. The cores acquired by BG Group in 2014 targeted areas of the ocean floor that encompass both Late Pleistocene to Holocene age) large sediment drifts and large downslope canyons, where turbidite and contourite deposition occurs simultaneously. Core, sediment and micropalaeontological analysis has been used to answer three basic questions 1) Do the sediments collected from different geomorphic settings owe their origin to along-slope (contourite) or gravitational (turbidite) transport? 2) Do the drift sediments contain a record of palaeoceanographic change? and 3) Can micropalaeontological analysis resolve long-standing problems with differentiating along- and down-slope processes in the geological record.



The presented study provides new data resolving these three questions for the upper, middle and lower Uruguayan slope. The new data comprises;

1. A detailed examination of the sedimentary facies of the (Late Pleistocene to Holocene) Uruguay slope, while ground-truthing interpretations from seismic and bathymetric data collected from the same area that is broadly contemporaneous
2. A reconstruction of watermass migration using stable isotope, elemental ratios and foraminiferal indices accumulated on the Uruguay slope since the Last Glacial Maximum
3. A classification of foraminiferal assemblages for that are likely to be indicative of specific sedimentary facies in turbidite and contourite deposits in order to distinguish these facies from one another in a sedimentary environment where both contourite and turbidite deposition has occurred.

This data elucidates some important new insights into the studied system and more broadly contourite and turbidite deposits globally:

1. A new model of mixed sedimentary system evolution on the Uruguay slope since the Last Glacial Maximum and how it is intrinsically linked to bottom-current/seafloor interactions
2. A new model for the flux of Antarctic sourced watermasses into the Atlantic basin across deglaciation
3. A new criterion for distinguishing contourite sand from turbidite facies by using benthic foraminiferal ecological disturbance-succession patterns

## **KEYWORDS**

Benthic Foraminifera; Palaeoecology; Contourites; Turbidites; Deepwater Processes; Mixed/Hybrid Systems; The Cold-Water Route; Ocean Circulation; Southwest Atlantic

# ACKNOWLEDGEMENTS

---

This thesis could be seen as the culmination of four years blood, sweat and tears. But I can't bring myself to think of it as such. I've learned a lot and had the privilege to work alongside some fabulously talented individuals in the lab, field, classroom, summer schools and workshops. In particular I would like to thank my supervisors Profs Mike Rogerson, Dan Parsons and Dr Liam Herringshaw who have made the last four years a wholesome and thoroughly fulfilling academic experience. I really can't thank them enough for the time and effort they have dedicated to nurturing my slow progression as a researcher.

To the technical staff and mentors that have assisted me at Hull, BOSCORF, Northumbria, BETA Analytic, Urbino, MARUM and St Andrew's. Thank you.

To my friends. Thank you for the beer, food, laughs and coming along to my weekly climbing sessions. A very special thanks go to Bas, Bobby, Chloe, Greg(s), Josh, Laura, Rita, Sergio, House Mallard, Lad Lane, and my best friend and mapping partner Dr Carl McDermott who have always been there for me.

To my family. Thank you for always being my pillars of support and continually encouraging me to do what I love. Whether it was allowing me the freedom to explore, take up (and drop) a plethora of hobbies, giving me the travel bug from an early age, or providing me with unlimited patience, inspiration, laughter and friendship. I would not be where I am today without you.

To my dearest Cécile. Words cannot thank you enough for your unfading faith and continued support through everything I've done. You closed oceans to be with me. With respect, adoration, admiration, kisses, gratitude, and love...

*Pour Cécile*

# TABLE OF CONTENTS

---

|   |             |
|---|-------------|
| <b>ABSTRACT</b> .....   | <b>I</b>    |
| <b>KEYWORDS</b> .....   | <b>III</b>  |
| <b>ACKNOWLEDGEMENTS</b> .....                                     | <b>IV</b>   |
| <b>TABLE OF FIGURES</b> .....                                     | <b>XI</b>   |
| <b>TABLE OF TABLES</b> .....                                      | <b>XXVI</b> |
| <b>TABLE OF EQUATIONS</b> .....                                   | <b>XXIX</b> |
| <b>LIST OF ABBREVIATIONS</b> .....                                | <b>XXX</b>  |
| <b>1 A GENERAL INTRODUCTION</b> .....                             | <b>1</b>    |
| 1.1 RATIONALE .....   | 1           |
| 1.2 PROJECT AIMS .....  | 4           |
| 1.3 THESIS STRUCTURE .....  | 6           |
| <b>2 LITERATURE REVIEW</b> .....                                  | <b>9</b>    |
| 2.1 CONTINENTAL SLOPE SEDIMENTOLOGY .....                         | 9           |
| 2.1.1 <i>Classifying Deepwater Deposits &amp; Processes</i> ..... | 9           |
| 2.1.2 <i>Hemipelagic &amp; Pelagic Processes</i> .....            | 10          |
| 2.1.3 <i>Gravity-Driven Mass Transport &amp; Flows</i> .....      | 10          |
| 2.1.4 <i>Turbidity Currents</i> .....                             | 11          |
| 2.1.5 <i>Bottom Current Reworked Sediments</i> .....              | 13          |
| 2.1.6 <i>Bottom Currents versus Turbidity Currents</i> .....      | 16          |
| 2.1.7 <i>Fine-Grained versus Sandy Contourites</i> .....          | 18          |
| 2.2 BENTHIC FORAMINIFERA.....                                     | 21          |

|          |  |            |
|----------|--|------------|
| 2.2.1    | <i>Introduction</i>  | 21         |
| 2.2.2    | <i>Foraminiferal Taxonomy</i>  | 22         |
| 2.2.3    | <i>The Foraminiferal Microhabitat</i>                                    | 24         |
| 2.2.4    | <i>Taphonomy of Benthic Organisms</i>                                    | 31         |
| 2.2.5    | <i>The Disturbed Microhabitat</i>  | 36         |
| 2.2.6    | <i>The Elevated Microhabitat</i>   | 40         |
| 2.3      | URUGUAY  | 51         |
| 2.3.1    | <i>Introduction</i>  | 51         |
| 2.3.2    | <i>Geological Setting</i>  | 73         |
| 2.3.3    | <i>Geomorphic Setting</i>  | 75         |
| 2.3.4    | <i>Oceanographic Setting</i>   | 78         |
| 2.3.5    | <i>Foraminiferal Setting</i>   | 84         |
| <b>3</b> | <b>MATERIALS &amp; METHODS</b>   | <b>89</b>  |
| 3.1      | INTRODUCTION AND FIELD SITE SELECTION                                    | 89         |
| 3.2      | DATA-SET   | 90         |
| 3.3      | METHODOLOGY  | 92         |
| 3.3.1    | <i>Sediment Facies</i>   | 92         |
| 3.3.2    | <i>Dating of Sediment Cores</i>  | 109        |
| 3.3.3    | <i>Stable Isotope Analysis</i>   | 113        |
| <b>4</b> | <b>SEDIMENTARY ANALYSIS</b>  | <b>115</b> |
| 4.1      | INTRODUCTION   | 115        |
| 4.2      | RESULTS  | 117        |
| 4.2.1    | <i>Selection of Core Tops and Cores for Analysis</i>                     | 117        |
| 4.2.2    | <i>Sedimentary Logging, Physical Properties &amp; Grain Size Results</i> | 122        |
| 4.2.3    | <i>ITRAX Results</i>   | 134        |

|  |            |
|--|------------|
| 4.2.4 Radiocarbon Results & Chronology .....   | 141        |
| 4.2.5 Observed Deep-Water Facies & Facies Sequences .....  | 146        |
| 4.2.6 Morphosedimentary Features.....  | 155        |
| 4.2.7 Core Correlation .....   | 163        |
| 4.4 DISCUSSION .....   | 165        |
| 4.4.1 Key Features .....   | 165        |
| 4.5 CONCLUSIONS .....  | 178        |
| <b>5 PALAEOCEANOGRAPHY.....</b>  | <b>180</b> |
| 5.1 INTRODUCTION .....   | 180        |
| 5.1.1 Background.....  | 180        |
| 5.1.2 Oceanographic Regime .....   | 181        |
| 5.2 MATERIALS & METHODS .....  | 189        |
| 5.3 RESULTS.....   | 191        |
| 5.3.1 Chronostratigraphy .....   | 191        |
| 5.3.2 Down-Core Trends .....   | 194        |
| 5.3.3 Regional Downcore Trends .....   | 204        |
| 5.4 DISCUSSION .....   | 207        |
| 5.4.1 Sediment Supply to the Ewing Terrace .....   | 207        |
| 5.4.2 Carbonate Preservation as a Proxy for Variations in Southwest<br>Atlantic Water Mass Structure ..... | 209        |
| 5.4.3 Are these signals traceable on the rest of the margin? .....   | 212        |
| 5.4.4 Glacial-Interglacial Variation of Atlantic Intermediate Waters.....                                  | 215        |
| 5.4.5 Glacial-Interglacial Bottom Water Production Around Antarctica ...                                   | 217        |
| 5.5 CONCLUSIONS .....  | 220        |
| <b>6 MICROPALAEONTOLOGY .....</b>  | <b>222</b> |

|   |            |
|---|------------|
| 6.1 INTRODUCTION .....  | 222        |
| 6.2 RESULTS.....  | 226        |
| 6.2.1 Foraminiferal Analysis .....  | 226        |
| 6.2.2 Foraminifera Observed in Sedimentary Units.....   | 228        |
| 6.2.3 Statistical Analysis.....   | 236        |
| 6.2.4 Multivariate Statistics & Foraminiferal Indices .....   | 252        |
| 6.2.5 Stratigraphy of Foraminiferal Assemblages.....  | 258        |
| 6.3 DISCUSSION .....  | 268        |
| 6.3.1 Foraminiferal Assemblages & Morphosedimentary Environments. ....  | 268        |
| 6.3.2 Benthic Foraminifera as Indicators of Strong vs. Weak Bottom<br>Currents, Stable vs. Unstable & Open Slope Environments. .... | 284        |
| 6.4 CONCLUSIONS .....   | 297        |
| <b>7 SYNTHESIS AND CONCLUSION.....</b>  | <b>300</b> |
| 7.1 INTRODUCTION .....  | 300        |
| 7.2 KEY RESEARCH OUPUTS.....  | 302        |
| 7.2.1 Verification of Morphosedimentary Environments .....  | 302        |
| 7.2.2 A Palaeoceanographic Record.....  | 303        |
| 7.2.3 A Micropalaeontological Tool to Differentiate Along- & Down-Slope<br>Transport Processes in the Geological Record .....       | 304        |
| 7.3 KEY FINDINGS AND WIDER IMPLICATIONS OF THIS RESEARCH .....  | 307        |
| 7.3.1 The Requirement for Multiscale Contourite Identification Criteria ..  | 307        |
| 7.3.2 Contourite Depositional Systems & the Currents that Create Them<br>.....  | 308        |
| 7.3.3 A Simple Unambiguous Method to Identify a Contourite Sand .....   | 309        |
| 7.4 LIMITATIONS .....   | 310        |
| 7.4.1 Facies Identification.....  | 310        |



|   |            |
|---|------------|
| 7.4.2 Carbonate Preservation – Modern versus Palaeo-Hydrography....   | 310        |
| 7.4.3 Benthic Foraminifera as Indicators of Current Velocity .....    | 311        |
| 7.5 FUTURE WORK & ADDRESSING LIMITATIONS.....                         | 313        |
| 7.5.1 Grain Size Characteristics and Foraminifera from Core Tops..... | 313        |
| 7.5.2 Precise Current Measurements from the Seafloor .....            | 313        |
| 7.5.3 Linking to Ancient Outcrop Examples.....                        | 314        |
| 7.6 CONCLUSION .....  | 316        |
| <b>REFERENCES .....</b>   | <b>325</b> |
| <b>APPENDICES.....</b>  | <b>378</b> |

# TABLE OF FIGURES

---

## Chapter 2

|  |    |
|--|----|
| Figure 2.1 The complexity of deep-marine sedimentary systems represented in a schematic diagram of environments deeper than 200 m (shelf-slope break). Reproduced from (Shanmugam, 2003). .....  | 9  |
| Figure 2.2 An idealised schematic sedimentary log through an ideal turbidite bed with the a total of nine divisions by combining the classic five divisions of the 'Bouma sequence (Bouma, 1964) and the five divisions of the 'Lowe sequence' (Lowe, 1982). A recent additional interpretation by (Shanmugam, 2016) is shown on the right, where the importance of reworking by bottom currents is shown. 12  | 12 |
| Figure 2.3 Four types of bottom currents and their depositional facies (Shanmugam, 2018) .....   | 13 |
| Figure 2.4 A summary of the traction features interpreted as indicative of deep-water bottom-current reworking by all the major types of bottom currents. From (Shanmugam, Spalding and Rofheart, 1993). B: Standard facies model of contourite sequence, linked to variation in current velocity. Modifications and variations on the standard contourite facies model, showing the range of contourite facies, sequences, and partial sequences commonly encountered (Rebesco et al., 2014)..... | 15 |
| Figure 2.5 Conceptual model showing the spatial relationship between downslope turbidity currents and along-slope contour currents. From (Shanmugam, Spalding and Rofheart, 1993). .....   | 16 |
| Figure 2.6 Summary of processes that effect the end deposit on a slope that consists of mixed depositional systems (Mutti, 1992; Mutti and Carminatti, 2012). This system results in turbidite and bottom-current deposits giving way to hybrid associations. It can be seen that the resulting sand body geometries are difficult to explain with the currently turbidite-dominated models for deep water sedimentation.....  | 18 |

Figure 2.7 Michalevich’s scheme of five classes of foraminifera where wall structure is subordinate to morphology. Main phyletic lines are Astrorhizata, Spirillinata, Nodosariata, Miliolata, Rotaliata classes (Mikhalevich, 2013). Later confirmed by the molecular studies of (Pawlowski et al., 2003). ..... 22

Figure 2.8 Molecular phylogeny of foraminifera after (Pawlowski et al., 2003) confirming Mikhalevich’s classification..... 24

Figure 2.9 Foram microhabitat cartoon by Gerhard Schmiedl showing the various foraminiferal life strategies ..... 26

Figure 2.10 There’s a close relationship between these large-scale patterns and foraminiferal microhabitats in the sediment. The TROX model proposed by Frans Jorissen reflects the influence of food inputs and oxygen on sediment microhabitats. Food increases and oxygen decreases from left to right. In oligotrophic settings foraminifera live mainly near the sediment surface because this is where food is concentrated. In eutrophic environments like OMZs, they live close to the surface because the deeper layers are anoxic. Between these extremes in mesotrophic environments species penetrate most deeply into the sediment because there’s enough food and oxygen there to sustain them..... 28

Figure 2.11 Sketch showing the various microhabitats occupied by live foraminifera (in white) in a marine benthic environment. Showing import and export from the environment. Figure reproduced by courtesy of Henko De Stigter. .... 30

Figure 2.12 Threshold friction velocity  $u^*$  measured 100 cm above the bed for foraminiferal sands of diameter  $D$  in seawater. Threshold curves are calculated from the general Shields-type curve presented in (Miller, McCave and Komar, 1977), employing two values for the effective density  $\rho_s$  of a foram test. .... 32

Figure 2.13 Threshold friction velocities for entrainment on smooth and rough surfaces for peneroplids..... 33

Figure 2.14 Summarised schematic from (Duros et al., 2017) which documents the various foraminiferal responses observed along the Capbreton canyon axis and adjacent terraces. .... 39

Figure 2.15 Epibenthic colonisation structures in high-energy environments in the Gulf of Cadiz from (Schönfeld, 2002c). With a schematic current strength section with distance from the sediment (not to scale) indicates the different hydrodynamic environments. Frequent species are marked in bold. Epibenthic foraminifera prefer elevated positions on hydroids (grey lines) or large fragments of deep-water corals (stippled)..... 41

Figure 2.16 Epibenthic colonisation structures in low-energy environments from (Schönfeld, 2002c). A schematic current strength section with distance from the sea floor (not to scale) indicates the different hydrodynamic environments and the transition layer, where suspended particles are concentrated. Frequent species are marked in bold. They concentrate on a distance of 3-28 mm above the seabed. .... 43

Figure 2.17 Geographic and oceanographic setting and study region. Salinity at 700 m depth. AAIW Antarctic Intermediate Water, r-AAIW Reversed Antarctic Intermediate Water, CDW.Circum Polar Deep Water, AABW Antarctic Bottom Water, NADW North Atlantic Deep Water. Sediment cores are indicated in yellow. .... 51

Figure 2.18 Offshore geology of Uruguay from (Soto et al., 2011)..... 74

Figure 2.19 Morphosedimentary map of the Uruguayan margin. The oceanic Segment IV and V defined by (Franke et al., 2006) and (Soto et al., 2011) are included. Abbreviations: SCS=Submarine Canyon Systems; TSZ=Transfer System Zone. From (Hernández-Molina et al., 2016).. With study area outlined by the dashed black line. .... 75

Figure 2.20 Seismically generated present-day seafloor bathymetry. A complex seafloor morphology is observed. Yellow arrows highlight the scoured and deformed pockmarks in the dune fields associated with the (southward flowing) AAIW(R-AAIW) and Upper Circumpolar Deep Water (UCDW) circulation (reproduced with permission of BG Group). Geomorphic settings include: Submarine canyons-systems (SCS); drift deposits (D1, D2 and D3); contourite terraces (T2 and T4) and mass-transport deposits (MTDs) are labelled in yellow. Adapted from (Hernández-Molina et al., 2016)..... 77

Figure 2.21 Modern morpho-sedimentary map of the Uruguay continental margin based on work by (Preu et al., 2013; Voigt et al., 2013; Hernández-Molina et al., 2016). Shows the Ewing terrace contourite system incised by multiple submarine canyon systems. The yellow coloured areas are the Ewing terrace that is located on the interface between AAIW and UCDW. Voigt et al., 2013 show that the lowermost portion of the AAIW contains a distinct nepheloid layer. Surface sediment facies are drawn after Bozzano, Violante, & Cerredo, 2011 and Hernández-Molina et al., 2016. The red circles show the location of cores investigated in this study. AAIW = Antarctic Intermediate Water; UCDW = Upper Circumpolar Deep Water; NADW = North Atlantic Deep Water; LCDW = Lower Circumpolar Deep Water; AABW = Antarctic Bottom Water; T2 = Terrace 2; D1 = Drift 1; D2 = Drift 2; T3 = Terrace 3; D3 = Drift 3; T4 = Terrace 4; MTDs = Mass Transport Deposits. Expansion zones relate to Holocene change and retreat of deeper water masses to increased NADW and AAIW..... 81

Figure 2.22 A: Section of salinity across offshore Uruguay. A trace of the bathymetry along the terrace shows the intersecting canyons. The red dots indicate locations of cores in this study. The dashed white line indicates the interface between AAIW and UCDW. B: Modern day carbonate ion concentration ( $\text{CO}_3^{2-}$ ) in the SW Atlantic, show in along and cross slope sections. The red dots show the location of cores. C: Turbidity depth profile taken to the south of the study area (Lamont-Doherty Earth Observatory) there is an increase in turbidity from ~700 – 1000 m where a nepheloid layer associated with the strong current activity within the range of AAIW. Prepared using Ocean Data View (<http://odv.awi.de>). The strength of the bottom currents in the northward flowing AABW, U/LCDW and AAIW control the development of the deep marine environment on a geological timescale. The Ewing Terrace is presently under the influence of AAIW (Hernández-Molina et al., 2009; Preu et al., 2013) where flow velocities can reach ~15-20  $\text{cm s}^{-1}$  at 1000 m water depth (Gwilliam, 1996) resulting in a distinct nepheloid layer within the central flow of the AAIW (Voigt et al., 2013). Approaching the AAIW/UCDW interface beneath the AAIW central flow, sediments deposit from the nepheloid layer and accumulate to form drift deposits..... 82

### Chapter 3

Figure 3.1 A) Schematic drawing of the Geotek Multi Sensor Core Logger (MSCL). B) Photo of whole core tube loaded onto the MSCL ready prior to a run ..... 99

Figure 3.2 A) Schematic of ITRAX micro-XRF sediment core scanner showing the main components in the set up. B) ITRAX with sample and measuring turret doors open. C) Core loaded onto the ITRAX prior to a run. .... 105

Figure 3.3 A) Radioactive decay (half-life) of <sup>14</sup>C. Decay is exponential over time. B) Photo of the accelerator mass spectrometer at the BETA Analytic facility in Miami, Florida, USA. C) The planktonic foraminifera *G. inflata* used in this study. Image sourced from Microtax.org. .... 112

Figure 3.4 A) Photo of the Thermo Delta V Advantage isotope ratio mass spectrometer which is interfaced with a GasBench II universal on-line gas preparation and introduction system, a PreCon Trace Gas Pre-Concentrator and a Flash 2000 Elemental Analyser at Northumbria University. B) SEM image example of *Cibicides wuellerstorfi* used in this study sourced from foraminifera.eu. C) SEM image example of *Uvigerina peregrina* used in this study sourced from foraminifera ..... 114

**Chapter 4**

Figure 4.1 Schematic diagram of core locations and morphosedimentary environments ..... 116

Figure 4.2 a) Sediment core locations, watermass positions and flow directions on the Petrel generated seabed offshore Uruguay. b) Core locations and interpreted morphosedimentary environments adapted from (Hernández-Molina et al., 2016). c) Modern day >63 micron sand distribution across the slope generated using newly acquired core top grain size data and contour map was compiled using a squared inverse distance weighted regression in ArcGIS. d) Modern day >150 micron coarse sand distribution across the slope..... 121

Figure 4.3 a) Interpreted bioturbation types in the piston cores collected from the Uruguay slope. Left image is an x-radiograph of core UPC125 (25-75 cm) and interpretive sketch of the ichnofacies. To the right is the interpreted section. b)

|   |     |
|---|-----|
| The eight piston cores and their accompanying core photographs and x-radiographs.....   | 123 |
| Figure 4.4 UPC001 (Drift 1) Photograph, radiograph, grain size and MSCL plots of physical properties against depth. Interpreted sedimentary facies demarcated by dashed lines and grouped into units of similar characteristics .....         | 124 |
| Figure 4.5 UPC032 (Drift 2) Photograph, radiograph, grain size and MSCL plots of physical properties against depth. Interpreted sedimentary facies demarcated by dashed lines and grouped into units of similar characteristics .....         | 126 |
| Figure 4.6 UPC065 (Submarine Canyon) Photograph, radiograph, grain size and MSCL plots of physical properties against depth. Interpreted sedimentary facies demarcated by dashed lines and grouped into units of similar characteristics      | 128 |
| Figure 4.7 UPC125 (Terrace 2) Photograph, radiograph, grain size and MSCL plots of physical properties against depth. Interpreted sedimentary facies demarcated by dashed lines and grouped into units of similar characteristics             | 129 |
| Figure 4.8 UPC133 (Drift 3) Photograph, radiograph, grain size and MSCL plots of physical properties against depth. Interpreted sedimentary facies demarcated by dashed lines and grouped into units of similar characteristics .....         | 130 |
| Figure 4.9 UPC154 (Terrace 4) Photograph, radiograph, grain size and MSCL plots of physical properties against depth. Interpreted sedimentary facies demarcated by dashed lines and grouped into units of similar characteristics             | 131 |
| Figure 4.10 UPC164 (Terrace 2) Photograph, radiograph, grain size and MSCL plots of physical properties against depth. Interpreted sedimentary facies demarcated by dashed lines and grouped into units of similar characteristics            | 132 |
| Figure 4.11 UPC170 (Drift 2) Photograph, radiograph, grain size and MSCL plots of physical properties against depth. Interpreted sedimentary facies demarcated by dashed lines and grouped into units of similar characteristics .....        | 133 |
| Figure 4.12 UPC001 (Drift 001) Photograph, radiograph, grain size and ITRAX plots against depth and age. Interpreted application of each elemental proxy are indicated on axis. Interpreted sedimentary facies and units are indicated on the |     |

|  |     |
|--|-----|
| right of the figure. Intervals of enhanced winnowing by bottom currents shaded in grey. ....   | 134 |
| Figure 4.13 UPC065 (Submarine Canyon) Photograph, radiograph, grain sie and ITRAX plots against depth and age. Interpreted application of each elemental proxy are indicated on axis. Interpreted sedimentary facies and units are indicated on the right of the figure. Intervals of enhanced winnowing by bottom currents shaded in grey. .... | 135 |
| Figure 4.14 UPC125 (Terrace 2) Photograph, radiograph, grain sie and ITRAX plots against depth and age. Interpreted application of each elemental proxy are indicated on axis. Interpreted sedimentary facies and units are indicated on the right of the figure. Intervals of enhanced winnowing by bottom currents shaded in grey. ....        | 136 |
| Figure 4.15 UPC154 (Terrace 4) Photograph, radiograph, grain sie and ITRAX plots against depth and age. Interpreted application of each elemental proxy are indicated on axis. Interpreted sedimentary facies and units are indicated on the right of the figure. Intervals of enhanced winnowing by bottom currents shaded in grey. ....        | 137 |
| Figure 4.16 UPC164 (Terrace 2) Photograph, radiograph, grain sie and ITRAX plots against depth and age. Interpreted application of each elemental proxy are indicated on axis. Interpreted sedimentary facies and units are indicated on the right of the figure. Intervals of enhanced winnowing by bottom currents shaded in grey. ....        | 138 |
| Figure 4.17 UPC170 (Drift 2) Photograph, radiograph, grain sie and ITRAX plots against depth and age. Interpreted application of each elemental proxy are indicated on axis. Interpreted sedimentary facies and units are indicated on the right of the figure. Intervals of enhanced winnowing by bottom currents shaded in grey. ....          | 139 |
| Figure 4.18 Composition plots of Si/Al and Ca/K for the six piston cores showing the sedimentary environments of mid slope drift (disturbed)(UPC001 and UPC065); mid slope terrace (UPC125 and UPC164) and lower slope drift (UPC154 and UPC170). ....   | 144 |



Figure 4.19 Contourite and turbidite facies observed on the Uruguay Continental Margin. A) Hemipelagic facies UPC154 B) Turbidite facies UPC065 C) Bioturbated muddy contourite facies UPC154 D) Mottled silty contourite facies UPC032 E) Very fine sand mottled contourite facies UPC125 F) Bioturbated fine sand contourite facies UPC125 G) Laminated fine sand contourite facies UPC164 H) Massive medium/coarse sand contourite facies UPC125..... 147

Figure 4.20 Core correlation panel from the upper/mid slope (left panel) and lower slope (right panel).  $\delta^{18}O$  graph from (Barbante et al., 2006). Dates were obtained in this study from discrete radiocarbon measurements of planktic foraminifera. The Holocene-Pleistocene boundary has been well constrained due to a combination of radiocarbon and carbonate appearance over the deglacial. All cores appear to show sandier facies into the Holocene, however this is an effect of increased abundance of large foraminifera tests..... 164

## Chapter 5

Figure 5.1 A: Modern annual salinity mean at 700 m water depth and flow of southern-sourced waters (black arrows) showing primary cold and warm water contributions to the South Atlantic. Southwestern Atlantic study area indicated in red. B: Enlargement of study area seabed generated in Petrel. Yellow dot indicates the location of core UPC164 on the Ewing terrace, on the interface between AAIW and UCDW. Flow paths of the main watermasses are indicated by arrows and table with upper and lower property limits. AAIW = Antarctic Intermediate Water; UCDW = Upper Circumpolar Deep Water; NADW = North Atlantic Deep Water; LCDW = Lower Circumpolar Deep Water; AABW = Antarctic Bottom Water. Prepared using Petrel, ArcGIS and Ocean Data View (<http://odv.awi.de>). ..... 184

Figure 5.2 Modern morpho-sedimentary map of Uruguay continental margin (after Hernández-Molina et al., 2016; Preu et al., 2013; Voigt et al., 2013). Shows Ewing terrace contourite system incised by multiple submarine canyon systems. Yellow-coloured areas define Ewing terrace, located at interface of AAIW and UCDW. Voigt et al. (2013) showed lowermost portion of AAIW contains distinct nepheloid layer. Surface sediment facies defined following Bozzano, Violante, & Cerredo, 2011 and Hernández-Molina et al., 2016. Red circle shows location of

core UPC164 investigated in this study. AAIW = Antarctic Intermediate Water; UCDW = Upper Circumpolar Deep Water; NADW = North Atlantic Deep Water; LCDW = Lower Circumpolar Deep Water; AABW = Antarctic Bottom Water; T2 = Terrace 2; D1 = Drift 1; D2 = Drift 2; T3 = Terrace 3; D3 = Drift 3; T4 = Terrace 4; MTDs = Mass Transport Deposits. Expansion zones relate to Holocene change and retreat of deeper water masses to increased NADW and AAIW. .... 186

Figure 5.3 A: Section of salinity across the study area offshore Uruguay. A trace of the bathymetry along the Ewing terrace shows the intersecting Montevideo Canyon and Piriápolis Canyon. The red dot indicates the location of core UPC164 used in this study. The dashed white line indicates the interface between AAIW and UCDW. B: Modern day carbonate ion concentration (CO<sub>3</sub><sup>2-</sup>) in the SW Atlantic, show in along and cross slope sections. The red dot shows the location of core UPC164 currently situated in the upper portion of the AAIW/UCDW. C: Turbidity depth profile taken to the south of the study area (Lamont-Doherty Earth Observatory) there is an increase in turbidity from ~700 – 1000 m where a nepheloid layer associated with the strong current activity within the range of AAIW. Prepared using Ocean Data View (<http://odv.awi.de>)..... 188

Figure 5.4 Age-depth model calculated from BChron R package for the 12 radiocarbon dates in Table 5.3 ..... 192

Figure 5.5 Summary of the sedimentary data collected for core UPC164 before conversion to age scale. Line scan images, radiographs, interpreted sedimentary facies, grain-size weight percentages downcore, L\* for lightness, MSCL-S physical properties and key ITRAX elemental ratios plotted as 5 point moving averages ..... 193

Figure 5.6 Age-adjusted key ITRAX elemental ratios for core UPC164. Time periods indicated across the top in pink for warming and blue for cooling in the Southern Hemisphere. Grey-shading indicates periods of more intense winnowing activity. Elemental ratio (A-H) use and key case studies listed in Table 5.4. .... 200

Figure 5.7 Summary of micropalaeontological data collected from core UPC164. A: Grey shading shows periods of increased bottom current activity overlain on sediment accumulation rate. B: Cibicidoides + Uvigerina equivalent δ<sup>18</sup>O

showing shifting position of AAIW through the last ~20 ka. C: Stable oxygen isotopes  $\delta^{18}\text{O}$  of ice core EDML. D: Austral spring (September–November) mean insolation at 60°S (Berger and Loutre, 1991; Renssen et al., 2005) E: Percentage sand fraction of core UPC164 F: %NPS is the percentage of left-coiling *Neogloboquadrina pachyderma* out of total *N. pachyderma*, with higher values reflecting colder surface conditions. G: Fragmentation Index of core UPC164. H: %warm is the combined contribution of warm planktonic foraminiferal species to the entire assemblage. I: Benthic Shannon Diversity Index showing higher diversity into the Holocene. Data recorded down core from the >150  $\mu\text{m}$  fraction. .... 204

Figure 5.8 Stratigraphic table showing sedimentary logs of each core with ITRAX Ca/Fe elemental ratios for the upper and lower slopes from South to North. Dashed lines are interpreted tie points associated with radiocarbon dates and specific fluctuations observed in the Ca/Fe record. Lines are tied to the EDML oxygen isotope record (Barbante et al., 2006)..... 206

Figure 5.9 Diagram representing the migration of main water masses present offshore Uruguay since the Last Glacial Maximum. Arrows indicate relative intensity and direction of flow. Hollow black arrows indicate the migration of interfaces in each period. Inset is interpreted position of the BMC. Location and bathymetry of UPC164 is overlain. .... 219

## Chapter 6

Figure 6.1 Location of the J14092 cruise core localities in this study and present day pathways of the Southern and Northern sourced watermasses based on (Hernández-Molina et al., 2016) ..... 222

Figure 6.2 Summarised schematic adapted from (Hess et al., 2005) which documents the various foraminiferal responses to the deposition of a turbidite. In addition is a hypothesised schematic of how foraminifera may respond to contourite deposition using various observations of the studies discussed in this chapter. .... 223

Figure 6.3 Sedimentary logs from South to North on the Upper Slope correlated to EDML Stable  $\delta^{18}\text{O}$  Isotope Ice Core Record (‰). Sampled intervals in red and

yellow (dated) dots. Cores UPC001, UPC125, UPC065 and UPC164 with corresponding clusters within each individual core (letters) and overall clusters (colour coded, 1 - 11) across study area. .... 224

Figure 6.4 Sedimentary logs from South to North on the Lower Slope correlated to EDML Stable  $\delta^{18}\text{O}$  Isotope Ice Core Record (‰). Sampled intervals in red and yellow (dated) dots. Cores UPC154, UPC133 and UPC170 with corresponding clusters within each individual core (letters) and overall clusters (colour coded, 1 -11) across study area ..... 225

Figure 6.5 Q-mode cluster analysis (UPGMA, Bray Curtis; correlation: 0.90) for autochthonous benthic foraminifera >150  $\mu\text{m}$  from all cores. Numerals indicate groups of samples with a similar composition of foraminifera, representing foraminiferal assemblages. Sample numbers indicated and coloured in accordance with overall regional assemblages. Autochthonous taxa occurring >5% abundance in at least one sample have been considered for this analysis. .... 237

Figure 6.6 Variations in relative abundances of major benthic foraminiferal taxa in core UPC001 from disturbed drift. Colours and numbers correspond to foraminiferal assemblages characterising the sample clustering across the different environments. Uncoloured numerals correspond to foraminiferal assemblages within the sediment core. Grey bars indicate periods of increased bottom current activity as represented by high values of  $\ln(\text{Zr}/\text{Al})$  ratios. Percentage gravimetric grain size >63  $\mu\text{m}$  in yellow..... 244

Figure 6.7 Variations in relative abundances of major benthic foraminiferal taxa from core UPC065 within a submarine canyon system. Colours and numbers correspond to foraminiferal assemblages characterising the sample clustering across the different environments. Uncoloured numerals correspond to foraminiferal assemblages within the sediment core. Grey bars indicate periods of increased bottom current activity as represented by high values of  $\ln(\text{Zr}/\text{Al})$  ratios. Percentage gravimetric grain size >63  $\mu\text{m}$  in yellow..... 245

Figure 6.8 Variations in relative abundances of major benthic foraminiferal taxa within core UPC125 from the upper slope contourite terrace. Colours and numbers correspond to foraminiferal assemblages characterising the sample

clustering across the different environments. Uncoloured numerals correspond to foraminiferal assemblages within the sediment core. Grey bars indicate periods of increased bottom current activity as represented by high values of  $\ln(\text{Zr}/\text{Al})$  ratios. Percentage gravimetric grain size  $>63 \mu\text{m}$  in yellow..... 246

Figure 6.9 Variations in relative abundances of major benthic foraminiferal taxa within core UPC133 on the separated drift. Colours and numbers correspond to foraminiferal assemblages characterising the sample clustering across the different environments. Uncoloured numerals correspond to foraminiferal assemblages within the sediment core. Percentage gravimetric grain size  $>63 \mu\text{m}$  in yellow. .... 248

Figure 6.10 Variations in relative abundances of major benthic foraminiferal taxa within core UPC154 from the lower slope terrace. Colours and numbers correspond to foraminiferal assemblages characterising the sample clustering across the different environments. Uncoloured numerals correspond to foraminiferal assemblages within the sediment core. Grey bars indicate periods of increased bottom current activity as represented by high values of  $\ln(\text{Zr}/\text{Al})$  ratios. Percentage gravimetric grain size  $>63 \mu\text{m}$  in yellow..... 249

Figure 6.11 Variations in relative abundances of major benthic foraminiferal taxa within core UPC164 from the upper slope terrace. Colours and numbers correspond to foraminiferal assemblages characterising the sample clustering across the different environments. Uncoloured numerals correspond to foraminiferal assemblages within the sediment core. Grey bars indicate periods of increased bottom current activity as represented by high values of  $\ln(\text{Zr}/\text{Al})$  ratios. Percentage gravimetric grain size  $>63 \mu\text{m}$  in yellow..... 250

Figure 6.12 Variations in relative abundances of major benthic foraminiferal taxa from core UPC170 on the plastered drift. Colours and numbers correspond to foraminiferal assemblages characterising the sample clustering across the different environments. Uncoloured numerals correspond to foraminiferal assemblages within the sediment core. Grey bars indicate periods of increased bottom current activity as represented by high values of  $\ln(\text{Zr}/\text{Al})$  ratios. Percentage gravimetric grain size  $>63 \mu\text{m}$  in dark yellow..... 251

Figure 6.13 Variations in assemblage indices for core UPC001. Dominance (D), Evenness (J), Shannon Diversity (H) and Fisher's Alpha Index. Fragmentation Index based in proportion of fragmented planktonic foraminifera down core. Benthic tests per gram. Relative abundances of epifaunal/shallow infaunal (green, %) vs. infauna intermediate/deep infauna (purple, %) from Appendix 3.2. Percentage gravimetric grain size >63µm in yellow. Ln(Zr/Al) ratio (blue, 3-point running average)..... 260

Figure 6.14 Variations in assemblage indices for UPC065. Dominance (D), Evenness (J), Shannon Diversity (H) and Fisher's Alpha Index. Fragmentation Index based in proportion of fragmented planktonic foraminifera down core. Benthic tests per gram. Relative abundances of epifaunal/shallow infaunal (green, %) vs. infauna intermediate/deep infauna (purple, %) from Appendix 3.2. Percentage gravimetric grain size >63µm in yellow. Ln(Zr/Al) ratio (blue, 3-point running average)..... 261

Figure 6.15 Variations in assemblage indices for UPC125. Dominance (D), Evenness (J), Shannon Diversity (H) and Fisher's Alpha Index. Fragmentation Index based in proportion of fragmented planktonic foraminifera down core. Benthic tests per gram. Relative abundances of epifaunal/shallow infaunal (green, %) vs. infauna intermediate/deep infauna (purple, %) from Appendix 3.2. Percentage gravimetric grain size >63µm in yellow. Ln(Zr/Al) ratio (blue, 3-point running average)..... 262

Figure 6.16 Variations in assemblage indices for UPC133. Dominance (D), Evenness (J), Shannon Diversity (H) and Fisher's Alpha Index. Fragmentation Index based in proportion of fragmented planktonic foraminifera down core. Benthic tests per gram. Relative abundances of epifaunal/shallow infaunal (green, %) vs. infauna intermediate/deep infauna (purple, %) from Appendix 3.2. Percentage gravimetric grain size >63µm in yellow. Ln(Zr/Al) ratio (blue, 3-point running average)..... 263

Figure 6.17 Variations in assemblage indices for UPC154. Dominance (D), Evenness (J), Shannon Diversity (H) and Fisher's Alpha Index. Fragmentation Index based in proportion of fragmented planktonic foraminifera down core. Benthic tests per gram. Relative abundances of epifaunal/shallow infaunal

(green, %) vs. infauna intermediate/deep infauna (purple, %) from Appendix 3.2. Percentage gravimetric grain size >63µm in yellow. Ln(Zr/Al) ratio (blue, 3-point running average)..... 265

Figure 6.18 Variations in assemblage indices for UPC164. Dominance (D), Evenness (J), Shannon Diversity (H) and Fisher’s Alpha Index. Fragmentation Index based in proportion of fragmented planktonic foraminifera down core. Benthic tests per gram. Relative abundances of epifaunal/shallow infaunal (green, %) vs. infauna intermediate/deep infauna (purple, %) from Appendix 3.2. Percentage gravimetric grain size >63µm in yellow. Ln(Zr/Al) ratio (blue, 3-point running average)..... 266

Figure 6.20 Variations in assemblage indices for UPC170. Dominance (D), Evenness (J), Shannon Diversity (H) and Fisher’s Alpha Index. Fragmentation Index based in proportion of fragmented planktonic foraminifera down core. Benthic tests per gram. Relative abundances of epifaunal/shallow infaunal (green, %) vs. infauna intermediate/deep infauna (purple, %) from Appendix 3.2. Percentage gravimetric grain size >63µm in yellow. Ln(Zr/Al) ratio (blue, 3-point running average)..... 267

Figure 6.20 Summary of foraminiferal proxies in relation to sediment grain size on the slope (bottom current velocity). Major indicator species are listed for each interpreted morphosedimentary environment..... 287

Figure 6.21 Phase diagram summarising the positions of each assemblage against levels of disturbance, competition for food and bottom current strength. Stippled line divided the fresh organic matter supplied via phytodetritus vs. degraded refractory material from turbidites. Solid black line marks the likely boundary where downslope transport can supply enough material from the shelf to be deposited or bottom currents are strong enough to prevent shelf material making it downslope. .... 290

Figure 6.22 Conceptual model for the succession of benthic foraminifera adapted from (S. Hess et al., 2005; Rogerson, Kouwenhoven, et al., 2006). Assemblages are outlined on the righthand side of the diagram. Key indicator taxa are named within the dashed horizontal lines for T. The T values are those adapted from (S. Hess et al., 2005). Branching structure shows the arrival of

specialist taxa into the prevailing environment. Assemblages of taxa shown here  
are site specific. .... 291



# TABLE OF TABLES

---

## Chapter 3

Table 3.1 Sediment cores used in the study of the Uruguay slope facies sequences..... 92

Table 3.2 Summary of elemental ratios used in this study, their importance and key case studies ..... 102

Table 3.3 Accelerator mass spectrometry (AMS) radiocarbon dates and calibrated ages. IRMS isotope values from *G. inflata* included ..... 111

## Chapter 4

Table 4.1 Summary of core numbers, geograpgical location and interpreted sedimentary environment from (Hernández-Molina et al., 2016)..... 118

Table 4.2 Accelerator mass spectrometry (AMS) radiocarbon dates and calibrated ages. IRMS isotope values from *G. inflata* included ..... 142

Table 4.3 Depositional Environment and locality of each piston core. .... 167

Table 4.4 The main methods of bioturbation identified within sediment under the persistent action of bottom currents and how they change with variation in bottom current velocity. From (Wetzel et al., 2008) ..... 172

Table 4.5 A comparison of the expected patterns of bioturbation in hemipelagic, turbiditic and contouritic sedimentary environments. From (Wetzel, et al., 2008) ..... 175

## Chapter 5

Table 5.1 Summary of key watermasses located offshore Uruguay, their properties and characteristic flow directions. .... 187

Table 5.2 Location of sediment core in this study..... 189

|  |     |
|--|-----|
| Table 5.3 Accelerator mass spectrometry (AMS) radiocarbon dates and calibrated ages. IRMS isotope values from <i>G. inflata</i> included ..... | 191 |
| Table 5.4 Summary of elemental ratios used in this chapter, their importance and key studies .....   | 197 |

## **Chapter 6**

|  |     |
|--|-----|
| Table 6.1 Summary of sedimentary environments and prevailing energy conditions sampled .....   | 226 |
| Table 6.2 Summary of one-way ANOSIM results for statistical significance of factor for Clusters 1 - 11.....  | 238 |
| Table 6.3 Pairwise ANOSIM p-values, uncorrected significance for each Cluster 1 - 11.....  | 239 |
| Table 6.4 Pairwise ANOSIM R values for each Cluster 1 - 11.....  | 240 |
| Table 6.5 Similarity percentage (SIMPER) analysis for benthic foraminiferal assemblages >150 µm (combined fractions) in all cores. Overall average dissimilarity: 76.59. Taxa occurring at least once at >5% abundance were included in the data matrix..... | 241 |
| Table 6.6 A comparison of the expected patterns of bioturbation in hemipelagic, turbiditic and contouritic sedimentary environments. Adapted from (Wetzel, et al., 2008) to include foraminiferal patterns. ....   | 293 |

## **Chapter 7**

|   |     |
|---|-----|
| Table 7.1 Research Objective 1 and how it has been addressed in this thesis ..... | 318 |
| Table 7.2 Research Objective 2 and how it has been addressed in this thesis ..... | 319 |

|   |     |
|---|-----|
| Table 7.3 Research Objective 3 and how it has been addressed in this thesis | 320 |
| Table 7.4 Research Objective 4 and how it has been addressed in this thesis | 321 |
| Table 7.5 Research Objective 5 and how it has been addressed in this thesis | 322 |
| Table 7.6 Research Objective 6 and how it has been addressed in this thesis | 323 |
| Table 7.7 Research Objective 7 and how it has been addressed in this thesis | 324 |

# TABLE OF EQUATIONS

---

## Chapter 3

|  |    |
|--|----|
| Equation 3.1 Equation for bulk density from GRA .....        | 94 |
| Equation 3.2 Relationship between $I$ and $\eta d$ .....     | 95 |
| Equation 3.3 Equation for p-wave velocity .....              | 96 |
| Equation 3.4 Corrected core velocity after calibration ..... | 97 |

# LIST OF ABBREVIATIONS

---

|        |   |
|--------|---|
| AABW   | Antarctic Bottom Water                      |
| AAIW   | Antarctic Intermediate Water                |
| AMOC   | Atlantic Meridional Overturning Circulation |
| BC     | Brazil Current                              |
| BMC    | Brazil-Malvinas Confluence                  |
| CDS    | Contourite Depositional System              |
| CDW    | Circumpolar Deep Water                      |
| ISW    | Ice Shelf Mode                              |
| LCDW   | Lower Circumpolar Deep Water                |
| MC     | Malvinas Current                            |
| NACW   | North Atlantic Central Water                |
| NADW   | North Atlantic Deep Water                   |
| NCW    | Northern Component Water                    |
| r-AAIW | Reversed-Antarctic Intermediate Water       |
| SACW   | South Atlantic Central Water                |
| SAMW   | Subantarctic Mode Water                     |
| SCS    | Submarine Canyon System                     |
| SCW    | Southern Component Water                    |
| TW     | Tropical Water                              |
| UCDW   | Upper Circumpolar Deep Water                |

# CHAPTER 1

---

## A GENERAL INTRODUCTION

### 1.1 Rationale

Deep sea sediment bodies are ubiquitous morphological features along continental margins. These sediment bodies can provide long-term, high resolution archives of palaeoceanography and palaeoclimate (Knutz, 2008; McCave, 2008; Nielsen *et al.*, 2008; Hernández-Molina *et al.*, 2018) they are prone to sediment instability (Laberg *et al.*, 2008; Sumner *et al.*, 2013; Moernaut *et al.*, 2014; Miramontes *et al.*, 2018), they provide a sink for carbon (Galy *et al.*, 2007; Rebesco *et al.*, 2014) and microplastics (Näkki *et al.*, 2017; Courtene-Jones *et al.*, 2019; Kane *et al.*, 2019), and can provide some of the largest and best hydrocarbon reservoirs on the planet (Nilsen, 2008; Viana, 2008). These deposits may accumulate on the continental slope via transport down the slope (by gravity) or along the slope (by ocean currents)(See Fig. 2.1). Particulate transport processes and fluxes control the geometry, distribution and internal architecture of deep-sea sediment accumulations. Therefore, it is a first-order issue to constrain when creating a detailed reconstruction of a depositional sequence. Depositional sequences form critical long-term archives (>100 years) for investigations into the response of the planet's interconnected Earth, Ocean and Atmospheric systems to environmental change, and the risks posed to coastal communities and seafloor infrastructure by natural hazards (Sumner *et al.*, 2013; Miramontes *et al.*, 2018). An understanding of sediments and associated pollutants are transported from source (on land) to sink (the deep-

ocean) and are subsequently dispersed are critical for improving societal resilience to planetary change and the hazards we face. One of the major challenges of reconstructing a depositional sequences is confidently attributing a resultant deposit to the processes that led to it's creation (Hodgson *et al.*, 2018). One such problem for deep-sea depositional sequences is, whether a deposit was formed by along- or down-slope transport processes. It is difficult to decipher from buried, fossilized depositional systems (Shanmugam, 2017).

New criteria for distinguishing contourite (along-slope) and turbidite (down-slope) sediments remain key to unlocking the unique potential of contourite systems to act as high-resolution archives of palaeoceanography and palaeoclimate. One major environmental difference between the sand bodies originating from turbiditic and contouritic processes is the variance of bottom velocity. In contourite systems bottom velocity at single sites remains relatively constant over millennial timescales e.g. (Toucanne *et al.*, 2007), however, in a turbidite system the passage of a single gravity flow event results in velocity changes over hours to days (Anschutz *et al.*, 2002). For a contourite system, this results in stable conditions and benthic communities that are in equilibrium with the bottom energy throughout deposition (Schönfeld, 2002c), but in a turbidite system disequilibrium will be expressed by the community due to high velocity sand emplacement events (Rogerson *et al.*, 2006). In principle, this means that contourite and turbidite materials should be distinguishable, even on macroscale. This PhD investigates an exceptional mixed down / along slope system of Holocene and Late Glacial age (Uruguay slope), unravel its sedimentology, constrain the controls on its changes and ultimately investigate whether benthic microfossils can reliably distinguish the mode of emplacement of the sands. In the process of

achieving that goal, it will evaluate whether the sedimentary materials on the Uruguayan slope are consistent with predictions from geophysical surveys of Hernández-Molina *et al.*, 2016 and reveal the palaeoceanographic history recorded in the stratigraphy of the cores.



## 1.2 Project Aims

This PhD thesis aims to develop a simple, unambiguous method to distinguish sediment that originate from thermohaline-induced (along-slope) currents from gravity driven (downslope) currents. However, development of a new methodology requires that the origin of the sandy deposits (in terms of their sedimentology and palaeoceanography) to be fully understood. The specific objectives to be completed are as follows:

- Collect, curate and select core sample set, through selecting, splitting, scanning logging and sampling cores from morphosedimentary environments likely to contain a range of grain sizes from both along- and down-slope deposits and by proxy low to high velocity sedimentary transport in both systems
- Use a combination of multi-sensor core logging, radiocarbon and oxygen isotopes to identify where changes in the subsurface sediments are. This will aid subsampling of core in order to avoid taking large numbers of samples
- Collect samples from key sections of core associated with these changes to conduct sediment gravimetric grain size analysis and benthic foraminifera censuses Develop and test the ability of core scanning techniques in determining sedimentological and palaeoceanographic controls in the core material with the aid of gravimetric grain size and traditional core logging techniques
- Use a combination of multi-sensor core logging, radiocarbon and oxygen isotopes to form a reconstruction of the depositional history of the chosen

sites and see how this compares to the current understanding of the Uruguayan slope

- Develop and test the ability of foraminiferal assemblages to discriminate between contouritic and turbiditic depositional systems in order to constrain reservoir geometry which will assist the hydrocarbon industry in frontier exploration
- Infer the processes responsible for each identified assemblage e.g. flow strength/sedimentological/oceanographic conditions using framework from earlier chapters and if a certain assemblage can confidently be associated with a sedimentary deposit
- Determine whether bottom currents can influence the sedimentation, stability and biology on the continental slope in order to better understand deep sea benthic communities in these environments and how often they are prone to catastrophic slope failure

### 1.3 Thesis Structure

This manuscript comprises 7 chapters:

- **Chapter 2** introduces the key body of previous work that has covered contourites, turbidites and the basis of interest from industrial stakeholders, and paleoclimate researchers. This chapter will give an overview of key concepts, processes and products occurring in contourite and turbidite depositional systems. It will also give an up-to-date understanding of the geology, sedimentology, micropalaeontology and palaeoceanography of the study area, located on the Uruguay continental margin.
- **Chapter 3** will outline the methods used in collecting, analysing and interpreting the data-sets. A variety of methods were used and this section covers standard core curation, logging, scanning and sampling protocols used. The methodology for grain size analysis, foraminifera species identification and assemblage analysis, stable isotope analysis and radiocarbon dating of carbonate in the core.

The following chapters detail the new data and knowledge gained from the Uruguay margin depositional system resolving the aims of this project.

- **Chapter 4:** Presents the results of the descriptive sedimentology so that the context of samples and materials used in later analysis are established. This is based on analysis of sedimentary facies and their sequences across 8 different newly collected piston cores located across the different morpho-sedimentary environments. We present a detailed, high resolution analysis of sediment grain size, physical properties and

geochemical of the Late Pleistocene to Holocene Uruguayan margin that characterises the 8 piston cores across a variety of grain sizes. Newly attained  $^{14}\text{C}$  dates are used to assess accumulation rates and aid core correlation. The different deepwater facies of the Uruguay margin that have been identified in this study will be compared to existing geophysical evaluation of the deposit, and the relationship between litho- and geophysical facies evaluated. The spatial and temporal evolution of the system this work develops acts as a framework for subsequent chapters.

- **Chapter 5:** The results of the paleoceanography work are presented in this chapter. Analysis of core materials revealed changes in the Uruguay slope system which must relate to changes in circulation, and these needed constraining and understanding before subsurface changes in micropalaeontology could be ascribed to different bottom energy / energy variability conditions. Newly acquired stable oxygen results allow for a greater understanding of the southern-sourced water flux and northern return flow along in the Southwestern Atlantic. Combined with grainsize data this reveals previously poorly understood changes in South Atlantic Meridional Overturning Circulation. Foraminifera were picked from over 500 samples and indices were derived and analysis of carbonate microfossil corrosion indices aid identification of corrosive glacial southern and non-corrosive northern sourced watermasses for the first time in this system. Paleoceanographic reconstruction of the watermasses offshore Uruguay reveals changes since the Last Glacial Maximum and the implications this has for global climate.

**Chapter 6:** Presents the results of the micropaleontological work. Here, a detailed analysis of the foraminiferal assemblages across the different sedimentary environments aims to test the ability of foraminiferal assemblages to discriminate between contouritic and turbiditic depositional systems. Characteristic trends within the foraminiferal and sedimentological data that aid delineation of contourites from other deepwater facies will be highlighted.

- **Chapter 7: Synthesis & Conclusion.** An examination of the potential of contourites as high resolution records of palaeoclimate and how benthic foraminifera may be added to the list of their key identification criteria. Finally, the key conclusions will be outlined and suggestions made for the future research on the use of microfossil indicators in sedimentary systems in the past present and future

# CHAPTER 2

## LITERATURE REVIEW

### 2.1 Continental Slope Sedimentology.

#### 2.1.1 Classifying Deepwater Deposits and Processes

The focus of this study is the deep marine environment, which encompasses everything in the zone below the continental shelf (700 – 3300 mbsl), including the shelf break, the continental slope and the abyssal plain. These are populated by geomorphic features such as submarine canyon systems, terraces, sediment drifts and channels may be found in Figure 2.1. Defining the processes that give rise to these geomorphic features in deep marine environments is key, as they are intimately linked to the geological evolution of continental margins and below we define the depositional processes in this environment and provide the framework for this study.

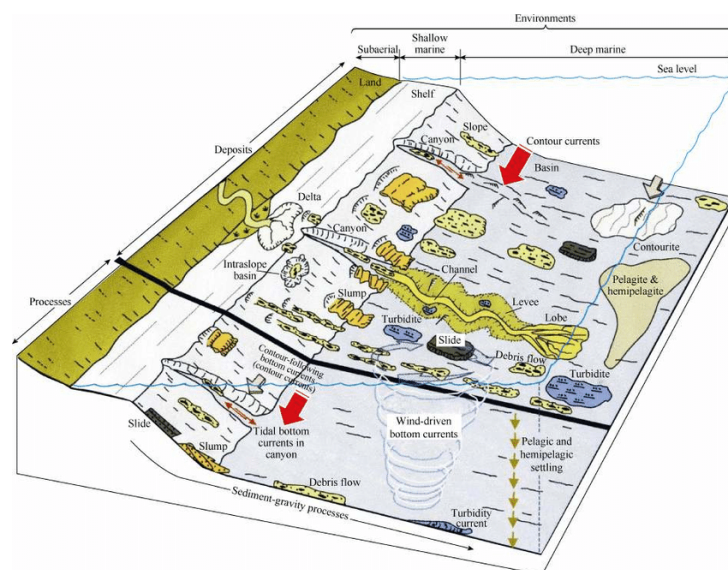


Figure 2.1 The complexity of deep-marine sedimentary systems represented in a schematic diagram of environments deeper than 200 m (shelf-slope break). Reproduced from (Shanmugam, 2003).

### 2.1.2 Hemipelagic & Pelagic Processes

Pelagites are deposits primarily composed of biogenic material that settle out from suspension in the overlying water column. *Stow et al.* (1998) gave a general definition of a hemipelagite as a fine-grained sediment that typically occurs in marginal deep-water settings (Hesse, 1975; Stow, 1985; O'Brien *et al.*, 2009). They are composed of a mixture of biogenic pelagic material (>10%) and terrigenous/volcanogenic material (>10%) where a large amount (>40%) of the terrigenous/volcanogenic fraction is silt-sized or greater (>4  $\mu\text{m}$ ). This sediment is poorly sorted due to this bi-modality of the finer clay fraction and the coarser biogenic fraction. They can be deposited by a combination of vertical settling and slow lateral advection.

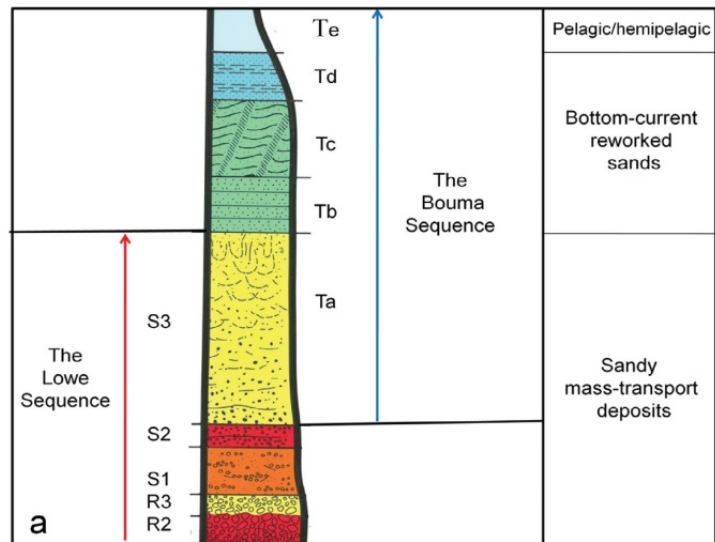
### 2.1.3 Gravity-Driven Mass Transport & Flows

Gravity driven sediment transport refers to the failure, dislodgement and gravitational movement of sediment down the continental slope (Stow, 1996)(Fig. 2.1). Once a failure occurs, the failed body of sediment moves downslope under gravitational pull when the shear stress exceeds the shear strength (Coherent). When this stress is applied, it can become a continuous, irreversible deformation of fluid and sediment that sustains the movement, becoming a flow (Incoherent) (Shanmugam, 1996; Stow, 1996) Subsequently, bottom currents may rework these sediments somewhat and produce a new type of deposit (Shanmugam, 2018). This project is not concerned with coherent flows, because although they can transport foraminiferal tests they cannot alter assemblages post-mortem (Murray, 1991).

#### 2.1.4 Turbidity Currents

A turbidity current is defined as a flow of granular materials with Newtonian rheology, i.e., no shear thinning or thickening is observed, and in a turbulent state, in which the granular materials are supported by turbulence from which deposition occurs through suspension settling (Kuenen, 1951; Sanders, 1963; Dott, 1964; Middleton & Hampton, 1976; Shanmugam, 2006, 2016). The 'classic' turbidites are the 'Bouma Sequences', deposited by low-density (i.e. low-sand concentration flow) turbidity currents (Bouma, 1962) and the 'Lowe Sequences' for coarse/sandy turbidites deposited by high density (i.e. high-sand concentration flow) turbidity currents (Lowe, 1982). These are shown in the scheme outlined in Figure 2.2.





**Total lack of empirical data for gravelly and sandy turbidity currents (i.e., high-density turbidity currents [HDTc])**

| Data Source & Information   | Importance  | Availability  |
|---|---|---------------|
| Direct measurements (Modern oceans/Lakes)   | Imperative  | Absent        |
| Sediment core (Modern seafloor)   | Imperative  | Absent        |
| Flume experiments   | Imperative  | Absent        |
| Theoretical models  | Important   | Abundant      |
| Outcrop study (All turbidite facies are based solely on the study of ancient strata using outcrops) | Unimportant (The ultimate objective is to interpret ancient strata. Therefore, facies models derived from ancient strata, without validation from modern environments promote circular reasoning) | Most abundant |

**b**

Figure 2.2 a) An idealised schematic sedimentary log through an ideal turbidite bed with the a total of nine divisions by combining the classic five divisions of the ‘Bouma sequence (Bouma, 1964) and the five divisions of the ‘Lowe sequence’ (Lowe, 1982)(S3 and Ta overlap). A recent additional interpretation by (Shanmugam, 2016) is shown on the far right, where the importance of reworking by bottom currents is shown. b) Table showing the importance of where future observations of turbidity currents should be focused in order to further our understanding of “the” turbidite sequence.

### 2.1.5 Bottom Current Reworked Sediments

Deep water masses interact with the seafloor which results in winnowing, reworking and redeposition of sediment as shown in the upper portions of Figure 2.2a. If this reworking is sustained over a period of time they become known as thermohaline-induced bottom currents (Shanmugam, 2012). However, three other types have also been recognised as outlined in Figure 2.3, with associated sedimentary structures outlined in Figure 2.4.

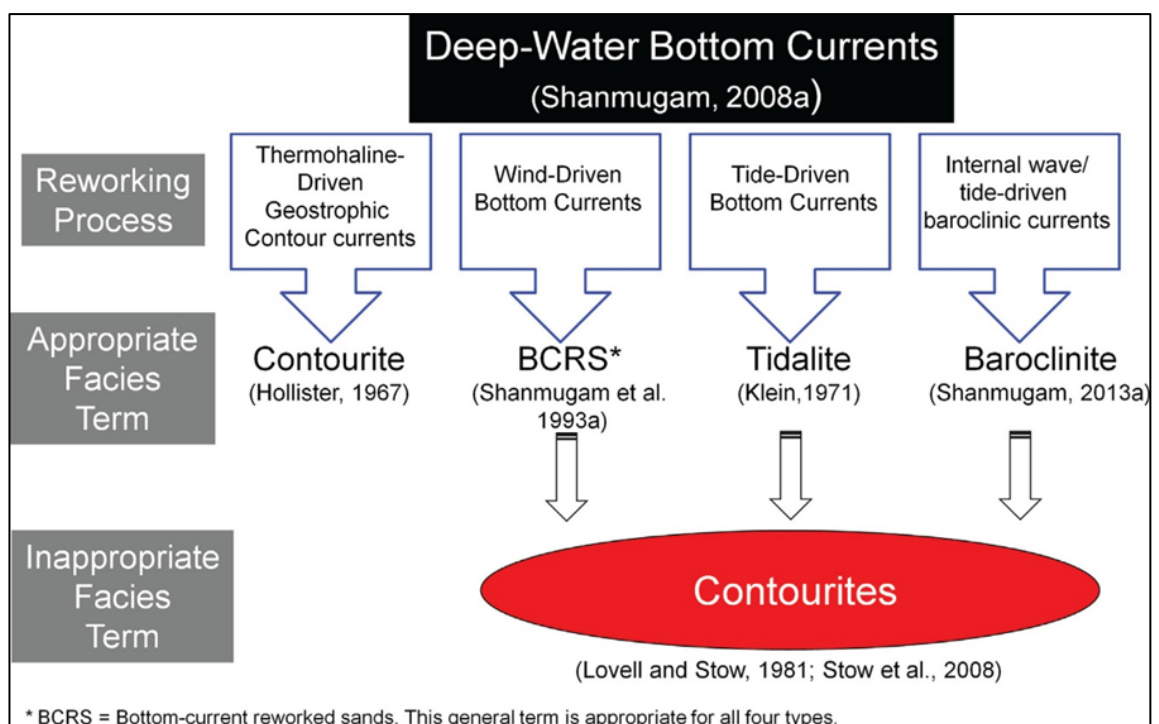


Figure 2.3 Four types of bottom currents with their interpreted reworking process and what should and should not be referred to as a true contourite (Shanmugam, 2018)

#### 2.1.5.1 Deep-Water Bottom Currents

The major types of deep-water bottom currents include thermohaline-induced contour currents, wind-driven bottom currents, deep-marine tidal currents and baroclinic tidal currents which all produce similar bedforms on the seafloor (Hsü, 1964; Hubert, 1964; Hollister, 1967; Lonsdale *et al.* 1972; Pequegnat, 1972;

Klein, 1975; Mutti, 1992; Shanmugam *et al.*, 1993; Hernández-Molina *et al.*, 2008; Shanmugam, 2008, 2013, 2016; Mutti & Carminatti, 2012; Hernández-Molina *et al.*, 2018). (See Fig. 2.3)

Contourites are sediments deposited from thermohaline induced geostrophic bottom currents (Heezen *et al.*, 1966; Faugeres *et al.*, 1984; Faugères & Stow, 1993; Hollister, 1994). Many authors are now advocating for a constraint on the nomenclature surrounding a true contourite, to “deposits from or significantly reworked by the action of stable geostrophic currents in deep water (>500 m)”(Shanmugam, 2017). Stow *et al.* (1998) proposed a general facies model for muddy and sandy contourites, based on recognised depositional patterns from the Gulf of Cadiz (Gonthier, Faugères and Stow, 1984). The model is represented as a basal inversely graded unit followed by a normally graded unit and with ubiquitous bioturbation throughout. Additional terms used for wind-driven and internal tide processes, which are described under the collective term ‘bottom current reworked sediments’ (Shanmugam, 2006, 2012; Mutti & Carminatti, 2012). Other factors that control the way a contourite can be distinguished from other deepwater facies are poorly understood and are discussed below.

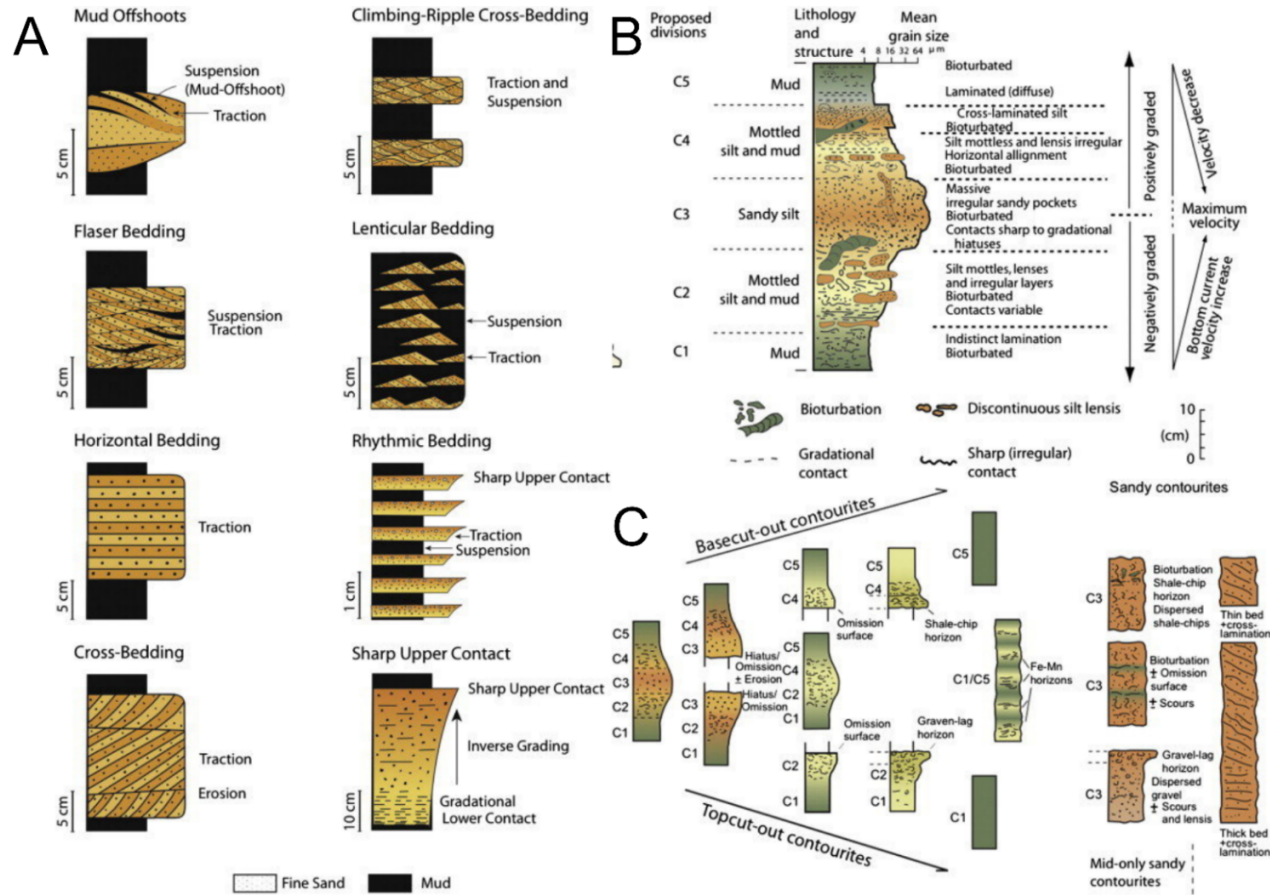


Figure 2.4 A summary of the traction features interpreted as indicative of deep-water bottom-current reworking by all the major types of bottom currents. From (Shanmugam et al., 1993) See Figure 2.2 for standard sequence. B: Standard facies model of contourite sequence, linked to variation in current velocity. C: Modifications and variations on the standard contourite facies model, showing the range of contourite facies, sequences, and partial sequences commonly encountered (Rebesco et al., 2014)

### 2.1.6 Bottom Currents versus Turbidity Currents

Distinguishing deposits of deep-water bottom currents from turbidity currents is a major challenge for deep-water sedimentology. Visually these deposits often appear identical to one another (Bouma & Hollister, 1973; Stow and Lovell, 1979; Mulder *et al.*, 2009; Shanmugam, 2017). However, there have been attempts to define some essential differential criteria between the two currents. Shanmugam (2012) (See Figure 2.5 for concept) lists 11 differences between the deposits outlined below:

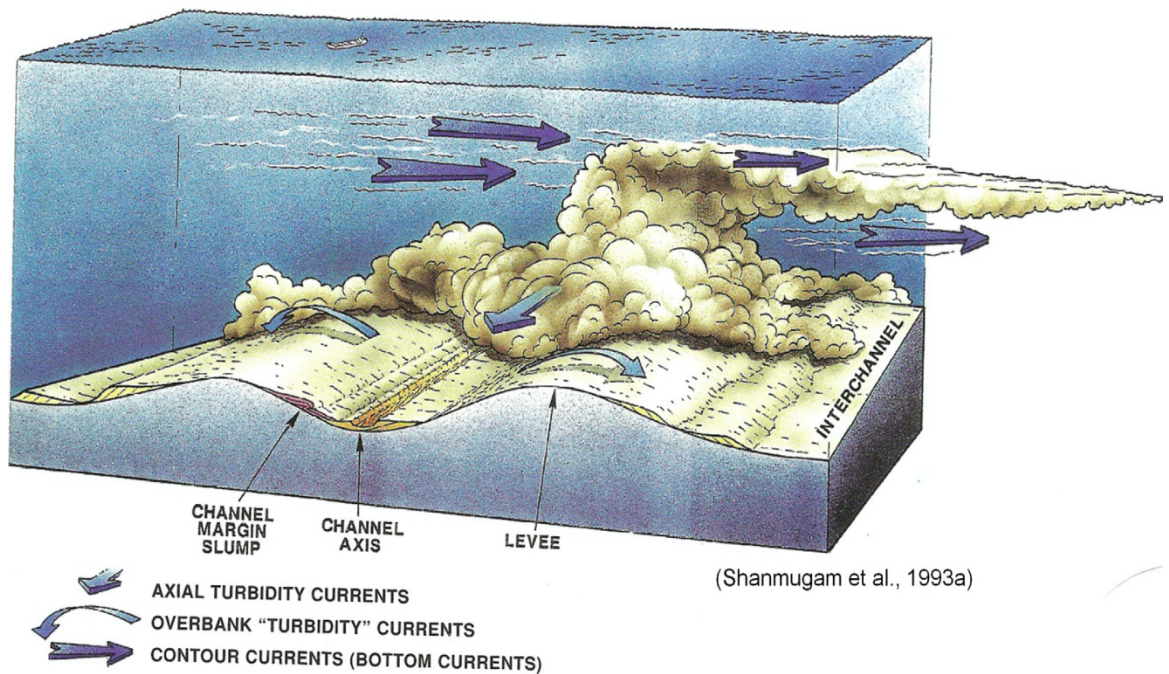


Figure 2.5 Conceptual model showing the spatial relationship between downslope turbidity currents and along-slope contour currents. From Shanmugam et al., (1993).

1. Bottom currents occur on shelf, slope, and basinal environments. However, turbidity currents are confined to the slope and basinal environments.

2. Bottom currents can be induced by thermohaline (i.e. density gradients created by surface heat and freshwater fluxes), wind or tidal forces, whereas turbidity currents are always driven by sediment gravity.
3. Bottom currents can move along-slope, in circular motions known as oceanic gyres that are unrelated to continental slopes or flow up and down submarine canyons under the influence of tidal forces. Turbidity currents that flow along-slope occur only due to constraints of seafloor topography.
4. There have been direct measurements of modern bottom current velocities, whereas direct velocity measurements from turbidity currents in the modern oceans are now only just being developed (Xu *et al.*, 2010; Xu *et al.*, 2014; Liu *et al.*, 2016; Hage *et al.*, 2018; Paull *et al.*, 2018).
5. Bottom currents vary over millennial timescales and develop equilibrium conditions. Turbidity currents are episodic or surge-type catastrophic events that do not develop equilibrium conditions (Kuenen & Migliorini, 1950; Allen, 2009).
6. Bottom currents exist without the requirement of a sediment load, whereas turbidity currents, as sediment gravity flows, cannot exist without sediment entrainment (Middleton & Hampton, 1976).
7. Bottom currents exhibit oscillating energy conditions, while turbidity currents exhibit waning energy conditions (Kuenen & Migliorini, 1950; Sanders, 1963).
8. Bottom current transport material by traction, whereas turbidity currents generally transport material in suspension.
9. Bottom current deposit are characterised by traction structures such as parallel laminae, ripple laminae and cross bedding (Hsü, 1964;



Shanmugam *et al.* 1993; Martín-Chivelet *et al.*, 2008). Turbidites are deposited by a catastrophic event of waning energy that results in a deposit of normally graded sediment (Kuenen & Migliorini, 1950).

10. Bottom current deposits are topped by a sharp upper contact (Hollister, 1967), whereas turbidites show graded upper contacts.

11. Bottom currents rework and winnow away mud resulting in well-sorted sands with good porosity and permeability (Shanmugam *et al.*, 1993), whereas turbidites are mud-rich deposits that are poorly sorted with low porosity and permeability (Sanders & Freidman, 1997).

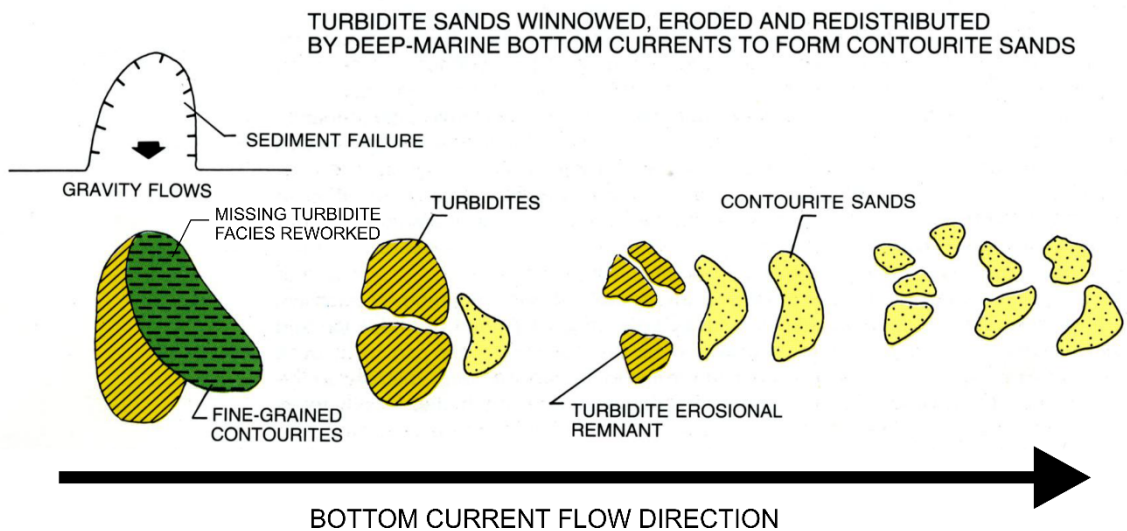


Figure 2.6 Summary of processes that effect the end deposit on a slope that consists of mixed depositional systems (Mutti, 1992; Mutti & Carminatti, 2012). This system results in turbidite and bottom-current deposits giving way to hybrid associations. It can be seen that the resulting sand body geometries are difficult to explain with the currently turbidite-dominated models for deep water sedimentation.

### 2.1.7 Fine-Grained versus Sandy Contourites

In this study, a contourite deposit is defined as being so extensively reworked by persistent geostrophic bottom currents that there are no indications of downslope processes. A contourite deposit will often contain multiple erosional/hiatal

elements, deposits should be termed contourite depositional systems adhering to sedimentological terminology defined by previous work (Hernández-Molina *et al.*, 2008). There are a variety of examples from the northeastern Atlantic (Akhmetzhanov *et al.*, 2007; Huvenne *et al.*, 2009; Masson *et al.*, 2010), to the southwestern Atlantic off the coasts of Brazil (Viana *et al.*, 1998; Moraes *et al.*, 2007a; Mutti & Carminatti, 2012) and Argentina (Preu *et al.*, 2013). The most extensively studied present-day example by far is the contourite depositional system located in the Gulf of Cadiz, NE Atlantic Ocean (Nelson *et al.*, 1993; Habgood *et al.* 2003; Hernández-Molina *et al.*, 2006, 2013, 2014). Ancient examples of contourites can also be found such as the Oligocene of Cyprus (Stow *et al.* 2002; Miguez-Salas & Rodríguez-Tovar, 2019), the Cretaceous of SE Spain (Martín-Chivelet *et al.*, 2003) and in the Miocene of Morocco (Capella *et al.*, 2018a).

Our study will be most useful identifying contourite sands in particular. There is considerably less literature surrounding contourite sands than their finer-grained counterparts. The primary body of work on sandy contourites has been assembled by Shanmugam (outlined above) with a focus on examples from the Gulf of Mexico for industry applications. The features identified in these studies have questionable origins and the criteria used to identify them as contourites cannot be directly transferred for use in identifying contourite sand examples from other oceans (Lovell and Stow, 1981; Hans Nelson *et al.*, 1993; Viana & Fauglères, 1998; Akhmetzhanov *et al.*, 2007; Moraes *et al.*, 2007a; Masson *et al.*, 2010; Hernández-Molina *et al.*, 2013). The rift in the language used to diagnose these sediments is significant and is often a source of friction between academics of either school. In bedforms, Shanmugam (2012) identified traction



surfaces and mud drapes as key criteria of bottom current reworking, whereas in examples from the Atlantic bedform features are rare and bioturbation is much more extensive, similar to those observed in muddy contourites (Stow *et al.*, 2002; McCall *et al.*, 2005; Stow & Faugères, 2008). There are two compositional varieties or facies of contourite sands depending on sediment supply and source. Both facies have a carbonate component and it is this component that is the focus of this study since these are more likely to contain significant quantities of microfossils. One type of contourite is of mixed siliciclastic-bioclastic that requires a vigorous prolonged bottom current (up to  $280 \text{ cm s}^{-1}$ ) that transports large and dense sediment grains. These deposits require an additional mechanism to enhance current velocity locally. This mechanism is usually morphological forcing where the flow becomes confined such as an oceanic gateway (e.g. Gulf of Cadiz) or erosional channels (e.g. Brazilian margin). Other contourite sands are primarily carbonate (Calcarenitic) in composition. These contourites can be entirely composed of foraminiferal sands. A number of foraminifera dominated deposits have been observed along the northern margin of Spain (Van Rooij *et al.*, 2010) and the northeast Atlantic (Huvenne *et al.*, 2009). Foraminifera require a relatively lower bottom current velocity ( $2\text{-}3 \text{ cm s}^{-1}$ ) for dispersal and deposition, which is well below the velocities described above (Kelham, 2011). The pervasiveness of foraminifera across many sandy (i.e. around  $200 \mu\text{m}$  average grain size) contourites sets the foundation for this study.

## 2.2 Benthic Foraminifera

### 2.2.1 Introduction

Foraminifera, or forams for short, are single-celled Eukaryotes of an ancient taxonomic group of amoeba. They can be traced to the Cambrian (~550 million years ago) and, since then, over 10,000 species have evolved. Of them, still nearly 9000 species can be found today, leaving the rest as extinct species confined to the rock record. Foraminifera have cytoplasm that can branch as fine strands and form dynamic nets with which they can catch food or float in the water column a test (or shell) that acts as a defense structure and buoyancy aide. Even though, most species live on the seafloor or within the first few centimetres of the surface sediment (referred as *benthic foraminifera*) and only 40 extant species inhabit the water column (called *planktic foraminifera*). However, foraminifera not only inhabit the oceans, but can also be found in brackish waters, freshwater and even terrestrial habitats (Haynes, 1981; Loeblich & Tappan, 1988; Sen Gupta, 1999b).

One distinct characteristic of foraminifera is the fact that they form shells, or *tests*. These tests are primarily composed of calcium carbonate ( $\text{CaCO}_3$ ), but some benthic foram species build their tests from sand, shell and coral fragments or even tests of other smaller foraminifera in a fascinating process of grain selection (Haynes, 1981).



Figure 2.7 Michalevich's scheme of five classes of foraminifera where wall structure is subordinate to morphology. Main phyletic lines are Astrorhizata, Spirillinata, Nodosariata, Miliolata, Rotaliata classes (Mikhalevich, 2013). Later confirmed by the molecular studies of (Pawlowski et al., 2003).

### 2.2.2 Foraminiferal Taxonomy

Benthic foraminifera can be seen with the naked eye which is relatively large considering they are unicellular organisms. Their tests are either single chambered (monothalamous) or have multiple chambers (polythalamous) and range in size from tens of  $\mu\text{m}$  to  $>10\text{ cm}$ . Most are found within the range of 100 - 500  $\mu\text{m}$  in size. Their tests have a diverse set of morphologies, these include spheres, flasks, branched or unbranched tubes (Fig. 2.7). Their test chambers can be constructed and arranged in linear, biserial (two rows), triserial (three rows), or coiled patterns (Loeblich & Tappan, 1988; Sen Gupta, 1999). There are

a large number of subgroups, but by following the scheme of Mikhalevich (2013) (see Fig. 2.7) where wall structure is subordinate to morphology, they can be ordered into five main phyletic lines:

1. Astrorhizata
2. Spirillinata
3. Nodosariata
4. Miliolata
5. Rotaliata

These morphological groups were confirmed in molecular studies by (Pawlowski *et al.*, 2003) (Figure 2.8). Morphology varies from a body that is tree-like, bush-like, spherical, or lumpish that is made up of a complex structure of fine branching tubules (see figure 2.7). Taxonomic concepts based on test morphological features from Caspers, (1980); Loeblich & Tappan, (1988); Jones, (1994); Holbourn *et al.* (2013) have been applied for this study.

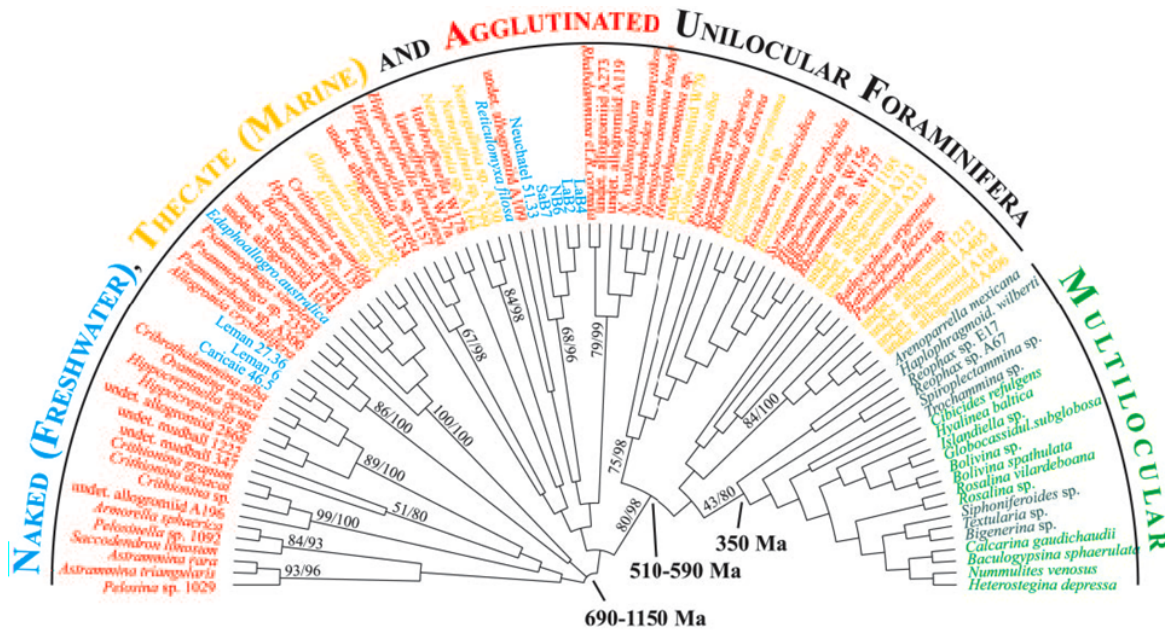


Figure 2.8 Phylogenetic relationships among early Foraminifera from rRNA gene sequences (Pawlowski et al., 2003). The types of test are highlighted with different colours. The majority are simple/early unilocular forms. Among the multilocular forms are Rotaliida in green and Textulariida in dark green. The tree was calibrated according to the fossil radiation of multilocular Foraminifera (350 Ma). Within the multilocular clade molecular data confirms Mikhalevich's classification based on morphotype to be sufficient in the identification of foraminiferal species.

### 2.2.3 The Foraminiferal Microhabitat

Benthic foraminifera have previously been used as a proxy to assess palaeoceanographic change in the north-eastern Atlantic, to reconstruct Mediterranean circulation patterns and Mediterranean-Atlantic exchange (Jorissen, de Stigter & Widmark, 1995; Jorissen *et al.*, 2007). Benthic foraminiferal species have a high taxonomic and biological trait diversity and turnover (e.g. The K-Pg boundary extinction of Cretaceous planktic species), they can therefore occupy a wide range of epifaunal and infaunal microhabitats and seafloor environments (i.e. brackish lagoons to the abyssal plain). The assemblage of benthic foraminifera species at a given site is primarily determined by the quantity and quality of the food supply and in turn the oxygen concentration

in the ambient bottom and pore waters within the sediment (See Fig. 2.9). Foraminifera utilise a huge variety of feeding mechanisms, as evidenced by the great variety of test morphologies that they exhibit. From the variety of trophic habits and test morphologies a few generalisations may be made. Branching benthic foraminifera such as *Notodendrodes antarctikos*, which resembles a microscopic tree, absorbs dissolved organic matter via a "root" system. Other sessile benthic foraminifera exhibit test morphologies dependent on the substrate on or in which they live, many are omnivorous opportunistic feeders and have been observed to consume autotrophic and heterotrophic protists (including other foraminifera), metazoans and detritus. Some suspension feeding foraminifera utilise their pseudopodia to capture food from the water column, or interstitial pore waters, *Elphidium crispum* forms a "spiders web" between the stipes of coralline algae. Infaunal forms are probably detritivores and commonly have elongate tests to facilitate movement through the substrate. Benthic and planktonic foraminifera which inhabit the photic zone often live symbiotically with photosynthesising algae such as dinoflagellates, diatoms and chlorophytes. It is thought the large benthic, discoidal and fusiform foraminifera attain their large size in part because of such associations. Foraminifera are preyed upon by many different organisms including worms, crustacea, gastropods, echinoderms, and fish. Other parameters such as water depth, water temperature and salinity are considered of minor importance, particularly in the deep sea (Murray, 2006).

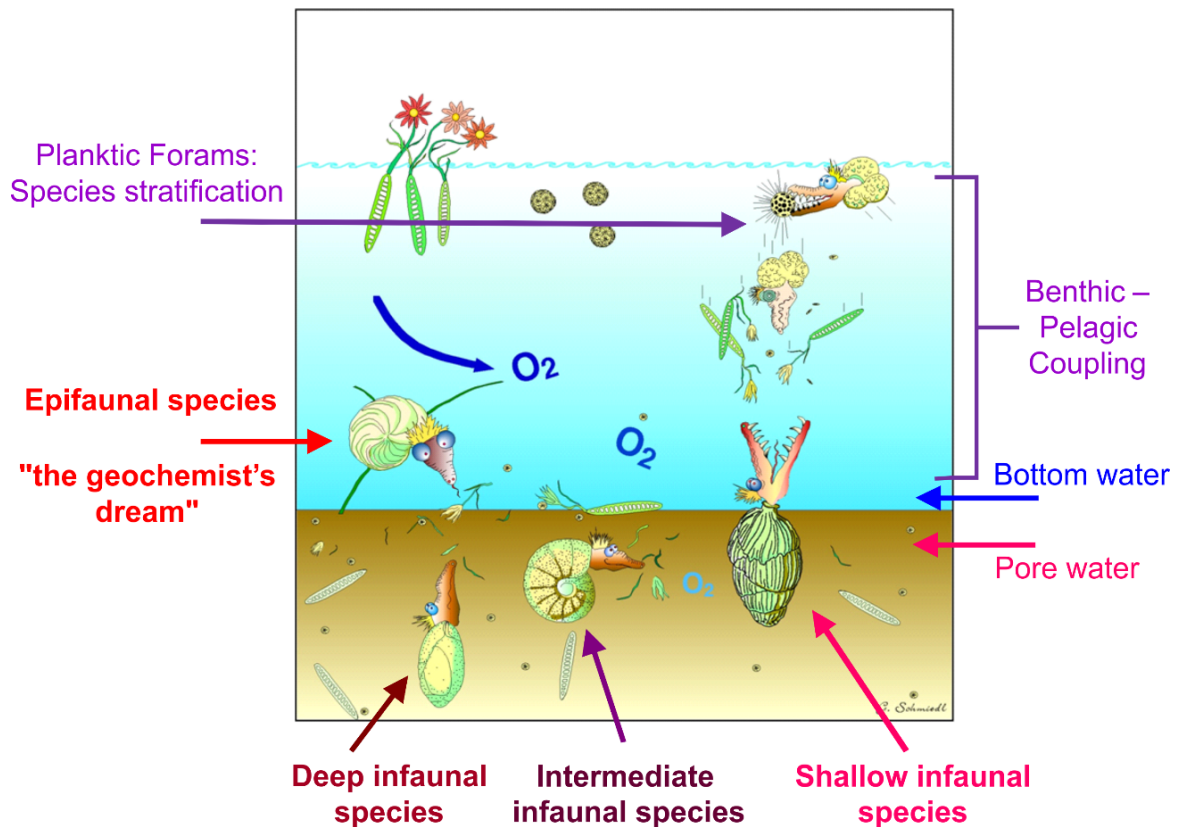


Figure 2.9 Foraminiferal life strategies cartoon by Gerhard Schmiedl showing the various foraminiferal life strategies

Several benthic foraminiferal studies have shown that certain species and overall assemblages of foraminifera show preferences for specific oxygen and/or trophic levels, whereas others are more tolerant of a wider range of oxygen availability and a more varied food source (Gooday, 2003; Murray, 2006). Benthic foraminiferal distributions are largely limited by a combination of food availability and oxygenation summarised in the Trophic Oxygen model (TROX model) of (Jorissen, de Stigter & Widmark, 1995) (See Fig. 2.10). The amount of organic matter flux to the sea floor is the main controlling factor on the distribution of species within the sediment, if oxygen of the bottom-water is not the limiting factor (Van Der Zwaan *et al.*, 1999). In this study, to aid interpretation of palaeoenvironment, palaeoproductivity and palaeoxygenation, other proxies such as number of benthic tests per gram of sediment, diversity and epifaunal/infaunal abundances are used. The number of benthics per gram of

sediment is a useful proxy to estimate past oxygen content and organic matter flux (Jorissen, de Stigter & Widmark, 1995; Van Der Zwaan *et al.*, 1999). In oxygen starved environments (hypoxic to anoxic), the number of benthics per gram generally decreases, in environments where organic matter flux to the seafloor increases, the number of benthics per gram increases (Gooday, 2003). However, increasing the flux of organic matter to the seafloor leads to a higher consumption of oxygen resulting in a decrease of benthics if a certain threshold is reached (Murray, 1998). There are some exceptions in seasonally anoxia prone basins with high primary productivity that show an increase in the number of benthics with seasonal increased oxygen (Bernhard, 2009). Therefore, benthic counts per gram is controlled by both oxygen content and organic matter flux. To understand the role of each of these factors alone, other data such as assemblages, species specific distributions and epifaunal/infaunal abundances need to be considered.



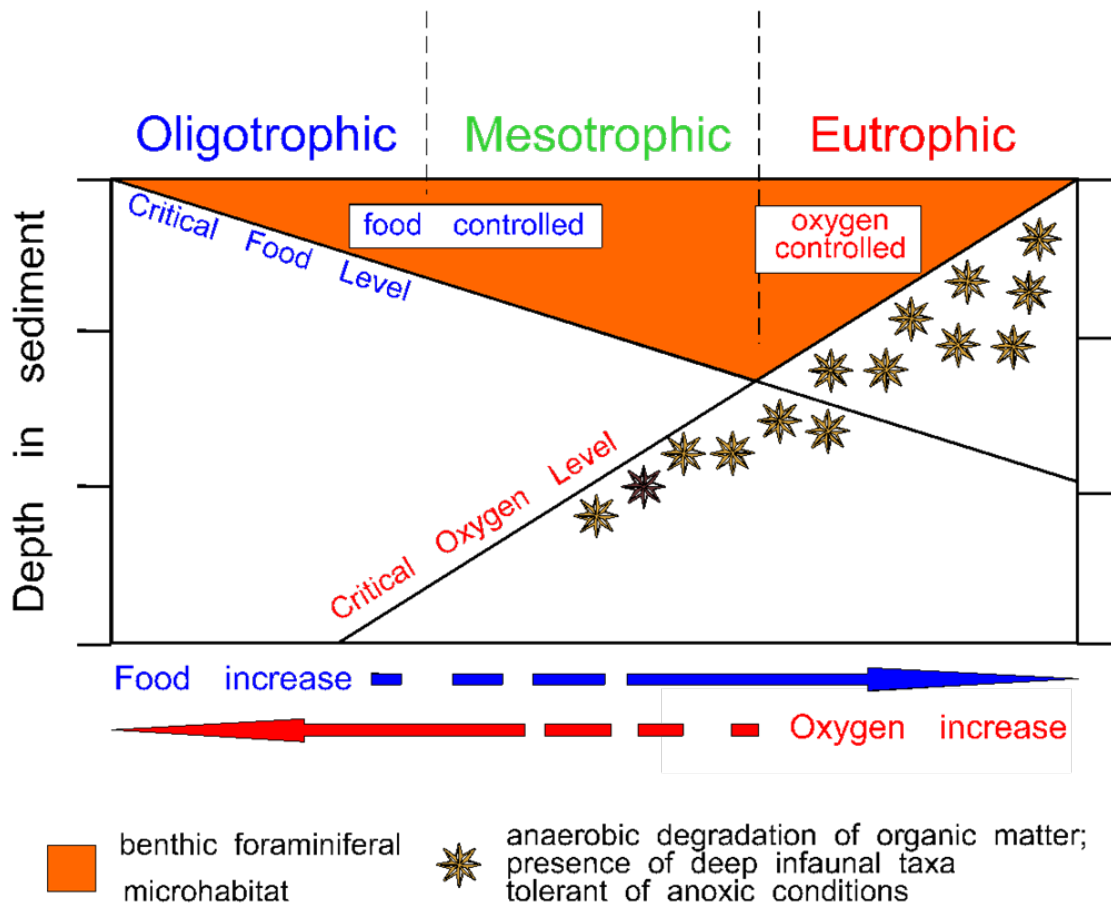


Figure 2.10 Relationship between these large-scale patterns of organic matter flux and oxygen availability and foraminiferal microhabitats in the sediment. The TROX model proposed by Frans Jorissen reflects the influence of food inputs and oxygen on sediment foraminiferal microhabitats. Food increases and oxygen decreases from left to right. In oligotrophic (high oxygen/low organic matter) settings foraminifera live mainly near the sediment surface because this is where food is concentrated settling out of suspension from the water column. In eutrophic environments like OMZs, they live close to the sediment surface because the deeper layers are anoxic. Between these extremes in mesotrophic environments species penetrate most deeply into the sediment because there's enough food and oxygen there to sustain them.

Taxonomic diversity of benthic foraminifera is another method to indirectly assess oxygen content and organic matter flux for palaeoenvironments. Generally, assemblages exposed to low oxygen and/or high organic matter flux exhibit low diversity and a dominance of a few taxa (Sen Gupta & Machain-Castillo, 1993; Van Der Zwaan *et al.*, 1999), this is also true for macroinvertebrates (Caswell *et al.*, 2018). However, low diversity assemblages also occur in oxygenated

conditions if the organic matter flux is very low (food limited) (Schmiedl *et al.*, 1998). It therefore must be used in combination with the other parameters discussed above (such as presence or absence of particular indicator species) to understand the role of diversity to estimate flux of organic matter and oxygenation of the bottom water. Fisher's alpha ( $\alpha$ ), Shannon Index (H), Evenness (J) and Dominance (D) are used here as diversity proxies (Hayek and Buzas, 2016). Diversity of species is a combined measure of both the species number and Evenness that measures how equally abundant species are in a community. The simplest diversity metric is species count per sample and it is a direct measure of species richness. The evenness measures the relative abundance of the different species that make up the benthic community of an area. The Shannon Index measures the diversity, which includes their abundances as a proportion of the total of a community. It accounts for the number of species and the evenness as a proportion of the whole assemblage in the sample. Fisher's alpha is used to describe the relationship between the number of species and the number of individuals in those species. It is independent of sample size and can be calculated knowing only species richness and the total number of individuals.

Less than 1% of surface production reaches the seafloor as organic matter (Basu and Mackey, 2018). Supply of organic matter to the seafloor through the water column is often reliant on lateral advection by intermediate to deep water currents or by slope failure and resulting turbidity currents. This is of particular importance along oceanic margins (Antia *et al.*, 1999). Importantly, laterally advected organic matter is often aged, with the more labile, easy to consume parts stripped off. The type of processes responsible for the delivery of laterally transported organic

matter to the seafloor will determine to the quantity and quality of food available for benthic organisms (See Fig. 2.11).

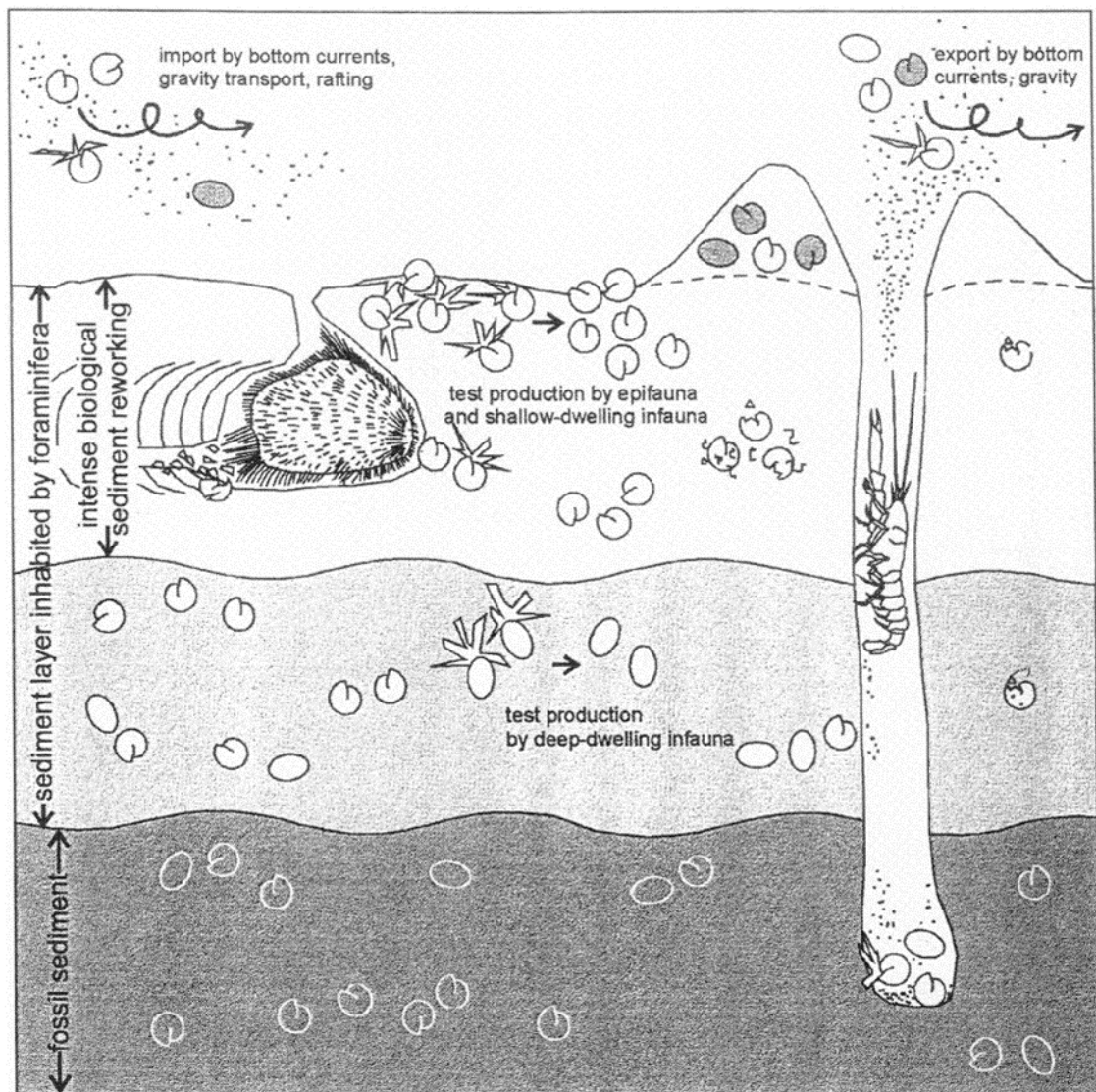


Figure 2.11 Sketch showing the various sedimentary microhabitats occupied by live foraminifera (in white) in a marine benthic environment. The deeper (often anoxic) environments (light and dark grey) are occupied by deep-dwelling benthic foraminifera and buried fossilised sediment containing dead tests. Showing import and export from the environment. Shown on the right-hand side of the figure in some cases forams live commensally with larger burrowing invertebrates, such as crustaceans and burrowing echinoderms. Figure reproduced by courtesy of Henko De Stigter.

#### 2.2.4 Taphonomy of Benthic Organisms

Taphonomy is the study of the processes that occur during an organism's death, pre-burial and post-burial. This includes decomposition, post-mortem transport, burial, compaction, and other chemical, biological or physical activity that affects the preservation of an organism. The main taphonomic processes affecting preservation of benthic organisms are post mortem transport, destruction of tests (such as fragmentation, abrasion, dissolution), and mixing of tests from different environments (Murray, 2006).

##### *2.2.4.1 Transport of Benthic Foraminifera*

The physical behaviour of foraminiferal tests in response to motion in the ocean has been documented in numerous studies. Foraminiferal tests accumulating on the seafloor are sediment and can therefore be moved and deposited by ocean currents like any sediment. Miller & Komar, (1977) examined the threshold friction velocity (or, initiation of motion) as a function of grain/test size, Figure 2.12 shows plots for two different particle densities (1.162 and 1.5 g/cm<sup>3</sup>).

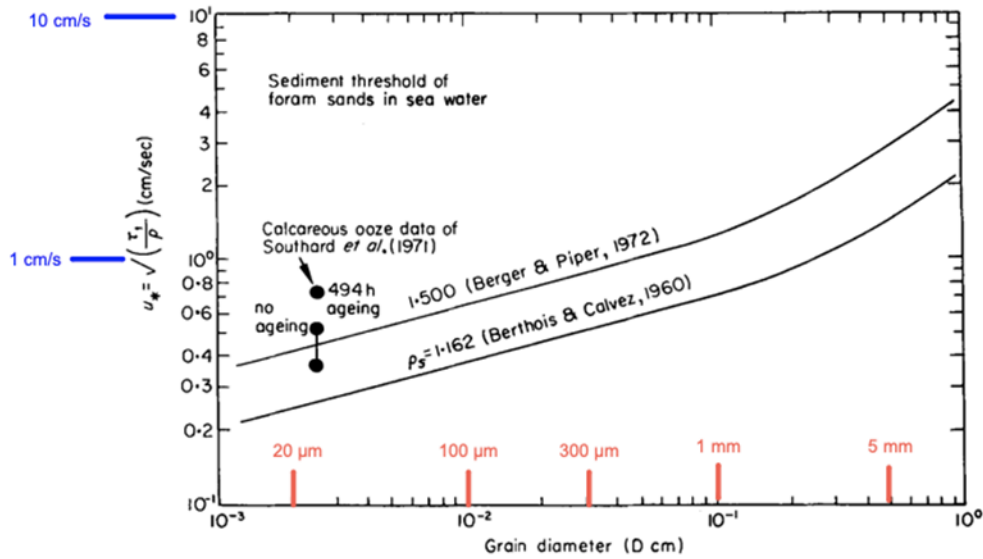


Figure 2.12 Threshold friction velocity  $u_*$  measured 100 cm above the bed for foraminiferal sands of diameter  $D$  in seawater. Threshold curves are calculated from the general Shields-type curve presented in Miller *et al.* (1977), employing two values for the effective density  $\rho_s$  of a foram test.

It takes higher velocities to initiate motion for larger test sizes, but those velocities are lower than they would be for a clast of the same size. The foram has a lower effective density due to hollow chambers in most foraminiferal species. Figure 2.12 accounts for ‘ageing’, this refers to experiments where loose foram tests were given time to de-water and compact. This implication of ageing the test is a more compacted and cohesive texture has a higher threshold velocity. Miller *et al.* (1977) advise caution for sediments where there is a mixture of terrigenous clay, which can significantly increase the cohesion effect. More recently, a study by Yordanova & Hohenegger (2007) performed similar analysis but for many different species of foraminifera. Figure 2.13 shows a selection of their plots for different species’ threshold friction velocity and an ‘entrainment’ velocity (to become suspended in the current).



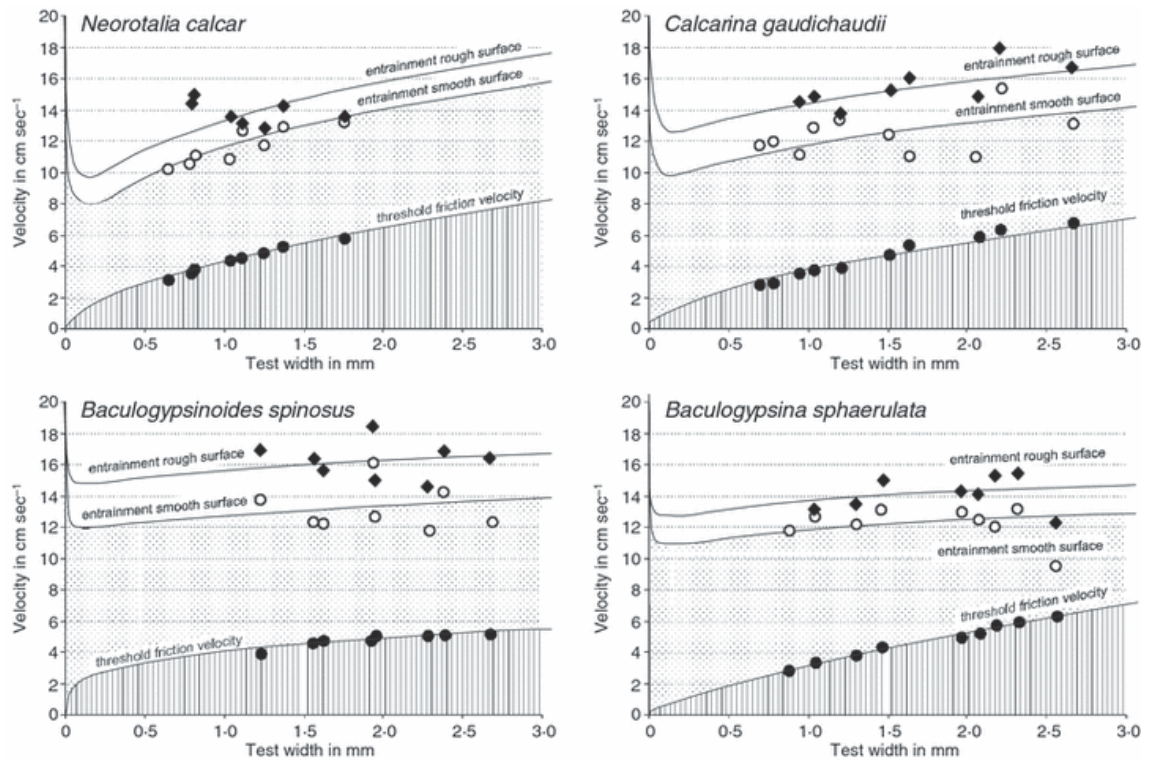


Figure 2.13 Threshold friction velocities and velocities for entrainment on smooth and rough surfaces for different growth stages of species of calcarinid foraminifera (Yordanova & Hohenegger, 2007). This group shows friction velocities similar to hyaline foraminifera. Entrainment velocities on smooth substrates increase from *B. sphaerulata* to *B. spinosus* to *C. gaudichaudii* and to *N. calcar*. Higher velocities (2 to 3 cm sec<sup>-1</sup> are necessary to entrain calcarinids from rough substrates.

These two studies suggest that well-sorted, loose accumulations of foraminiferal sediment (without any terrigenous sediment) can be moved by oceanic currents of  $\sim 10 - 20 \text{ cm s}^{-1}$  which is typical for bottom current systems in the ocean. Foraminifera can be transported by these bottom currents as well as a variety of other processes including turbidity currents, waves and by the activities of other organisms (Murray, 1991). Yordanova & Hohenegger (2007) also look at the effects of shape and morphology of different foraminiferal species and report that flatter tests have a higher threshold velocity compared to more spherical tests. Experiments involving larger benthic foraminifera show that the hydrodynamic behaviour of the test may have an important role in controlling their relative

abundance in both modern and fossilised deposits (Hohenegger & Yordanova, 2001; Yordanova & Hohenegger, 2007; Briguglio & Hohenegger, 2009; Kelham, 2011).

On the continental slope, the transport of foraminifera is primarily due to turbidity and bottom currents. Within submarine canyons this can increase the supply of shallow taxa to the deep sea (Schröder-Adams *et al.*, 2008). This results in ~3% of basinal floor, ~25% of submarine fan and 78% of submarine fan sandy assemblages being composed of tests supplied from the shelf (Jones, 2011). Within submarine fans there is a vertical variation with allochthonous assemblages confined to turbidite sequences and autochthonous assemblages associated with the deposition of hemipelagite (Bandy, 1964; Jones, 2011).

#### *2.2.4.2 Destruction of Foraminiferal Tests*

There are a variety of processes that can result in the destruction of foraminiferal tests such as, abrasion, bioerosion, chemical stress, parasites and predation (Martin & Liddell, 1991; Barbieri, 2001; Buzas-Stephens, 2005; Murray, 2006; Fontanier *et al.*, 2008). In most marine sediments, calcareous foraminifera are well preserved, however as depth in both the water and sediment columns increase there is a change from well preserved assemblages to poorly preserved assemblages (Schiebel, 2002; Schiebel *et al.*, 2007). This change is delimited by the carbonate lysocline where there is differential dissolution of delicate tests and a change to more robust foraminifera that completely alters the assemblage characteristics (Roth & Berger, 1975; Corliss, 1985).

Abrasive damage to tests would be expected to be more likely over longer transport distances. However, lab based experiments by Kotler *et al.* (1992) have

shown that this damage is rarely severe enough to destroy the foraminifera. The smaller size fractions that are easier to transport remain well preserved, even in high energy systems such as shallow channels abrasion cannot seriously damage tests as there is less chance of comminution between particles (Zhang *et al.*, 1993; Murray, 2006).

#### 2.2.4.3 Mixing

Transport, reworking of residual sediment and bioturbation blurs palaeoenvironmental boundaries by the post-mortem mixing of species and the mixing of the sediment itself (Horton, Edwards and Lloyd, 1999). Benthos can often mix the sediment so thoroughly that even short-lived radioisotopes show a fairly constant concentration within the surface mixed layer (i.e. 0 – 50 cmbsf). Some of the planktonic foraminifera on the modern sea floor can be centuries old because of bioturbation bringing fossilised tests back into the taphonomically active zone (Erlenkeuser, 1980; Keigwin and Guilderson, 2009).

For this study, an abundance of shallower water, neritic species tests together with deep water species tests in deeper marine environments is seen as an indicator of down-slope transport by turbidity currents and, potentially if tests appear in particularly high abundances, of bottom-current activity. Rogerson *et al.* (2011) found that shallow-water taxa such as *P. mediterranensis* or *Elphidium spp.* occur in both systems, but only become common or even dominant in contourite channels. This indicates a possible sorting or winnowing of transported tests by bottom currents that concentrates tests of a particular size and shape in particular areas depending on test settling velocity and bottom current velocity (Kelham, 2011).



### 2.2.5 The Disturbed Microhabitat

In addition to the post-mortem processes that effect the distribution of benthic foraminifera in the deep-sea, physical processes that disturb the benthic habitat can result in defaunation of the substrate. The subsequent recolonization of the substrate by benthic foraminifera gives rise to a succession of benthic foraminiferal assemblages. In settings prone to disturbance by intensive downslope sediment transport, such as submarine canyons, a variety of processes such as sediment gravity flows (Mulder & Alexander, 2001), slumps (Hsu *et al.*, 2008) or shelf water cascading events (Gaudin *et al.*, 2006). All of these processes supply a large quantity of laterally advected marine and terrestrial organic matter that become concentrated in canyon sediments (Rowe, Polloni & Haedrich, 1982; Soetaert & Heip, 1995; Vetter & Dayton, 1998). These processes are triggered by tectonic, climatic and meteorological events, the frequency of such is variable depending on the geographic location of the canyon. Canyons where these events are frequent are characterised by instability that constrains benthic community survival.

One such canyon is the Capbreton Canyon in the Bay of Biscay. Despite the canyon's disconnection from the Adour River, the canyon remains active today. The canyon is characterised by high organic matter input and substrate instability caused by bottom currents, environmental disturbances and re-sedimentation (Mulder & Alexander, 2001; Anschutz, *et al.*, 2002; Gaudin *et al.*, 2006). Cores collected from the canyon show a turbidite frequency of 1 per year (Brocheray *et al.*, 2014). In addition to frequent smaller scale, gravity events, there have been at least three turbidites on a larger spatial scale over the last 100 years (Mulder *et al.*, 2004). One such event occurred in December 1999 as a severe storm hit

the Atlantic coast of southern France. The storm surge resulted in the deposition of an 18 cm turbidite in the Capbreton Canyon at 467 mbsl. After the emplacement of this turbidite, there were a series of studies examining the benthic foraminiferal recovery (Anschutz, *et al.*, 2002; Hess *et al.*, 2005; Hess and Jorissen, 2009; Bolliet *et al.*, 2014). These studies documented the recolonization and subsequent recovery of the foraminiferal community on the seafloor at, 4 months (Anschutz,*et al.*, 2002; Hess *et al.*, 2005), 1.5 year (Hess *et al.*, 2005; Hess & Jorissen, 2009), 6 years (Bolliet *et al.*, 2014) and 15 years (Duros *et al.*, 2017) after the event. Four months after the event, the living component of the benthic foraminiferal assemblage was almost entirely composed of *Technitella melo*, *Cassidulina carinata*, *Fursenkoina bradyi* and *Bulimina marginata* interpreted as a pioneer colonisers after the emplacement of the turbidite (Anschutz *et al.*, 2002; Hess *et al.*, 2005). One and a half years after the event, the foraminiferal assemblages were characterised by other shallow infaunal species such as *Bolivina subaenariensis* and *Bulimina marginata* that make up the second phase of colonisers. The standing stocks of these two species were very high (>6000 benthics per 100 cm<sup>2</sup> of sediment) (Hess *et al.*, 2005; Hess and Jorissen, 2009). After six years, the benthic foraminiferal fauna still remained in the early phase of recolonization that suggest the area has been subject to smaller scale sediment instability (Bolliet *et al.*, 2014). In more distal localities that are unaffected by recent re-sedimentation processes, foraminiferal assemblages are more diverse and some specialized species occupy deeper ecological niches (Hess and Jorissen, 2009; Bolliet *et al.*, 2014). Duros *et al.*, (2017) found that sedimentary disturbance was frequent but of different magnitudes dependent on location along the canyon. This revealed that the

environment within the canyon has complex sedimentary patterns (turbidite, sediment resuspension and accumulation), and foraminifera have different responses to each of them (See Fig. 2.14). In areas more frequently disturbed, such as the middle canyon axis, lower canyon axis and lower terrace sites on the canyon were dominated by low to moderate foram standing stocks, with low diversity pioneer species *Fursenkoina bradyi*, *Reophax spp.* and *Technitella melo*, these remain in the early stage of recolonization despite frequent sedimentary events (Hess *et al.*, 2005). In locations that are unstable with a large amount of fine-grained sediment (thus a strongly food-enriched, fine sediment) such as some of the terraces down-canyon, are dominated by a low diversity/high density of secondary colonisers that are opportunistic but specialised. Upper canyon areas were less frequently disturbed after the 1999 event and therefore allowed a more diverse/lower standing stock assemblage to develop. This assemblage was again dominated by secondary colonisers *Bolivina subaenariensis* and *Bulimina marginata*. In the more quiescent sites that have not been exposed to sedimentary events a deep microhabitat develops, with a diverse/low standing stock assemblage composed of *Uvigerina spp.* and *Melonis barleeanus*. Stable conditions are more suitable for the development of a dense and diverse foraminiferal community.

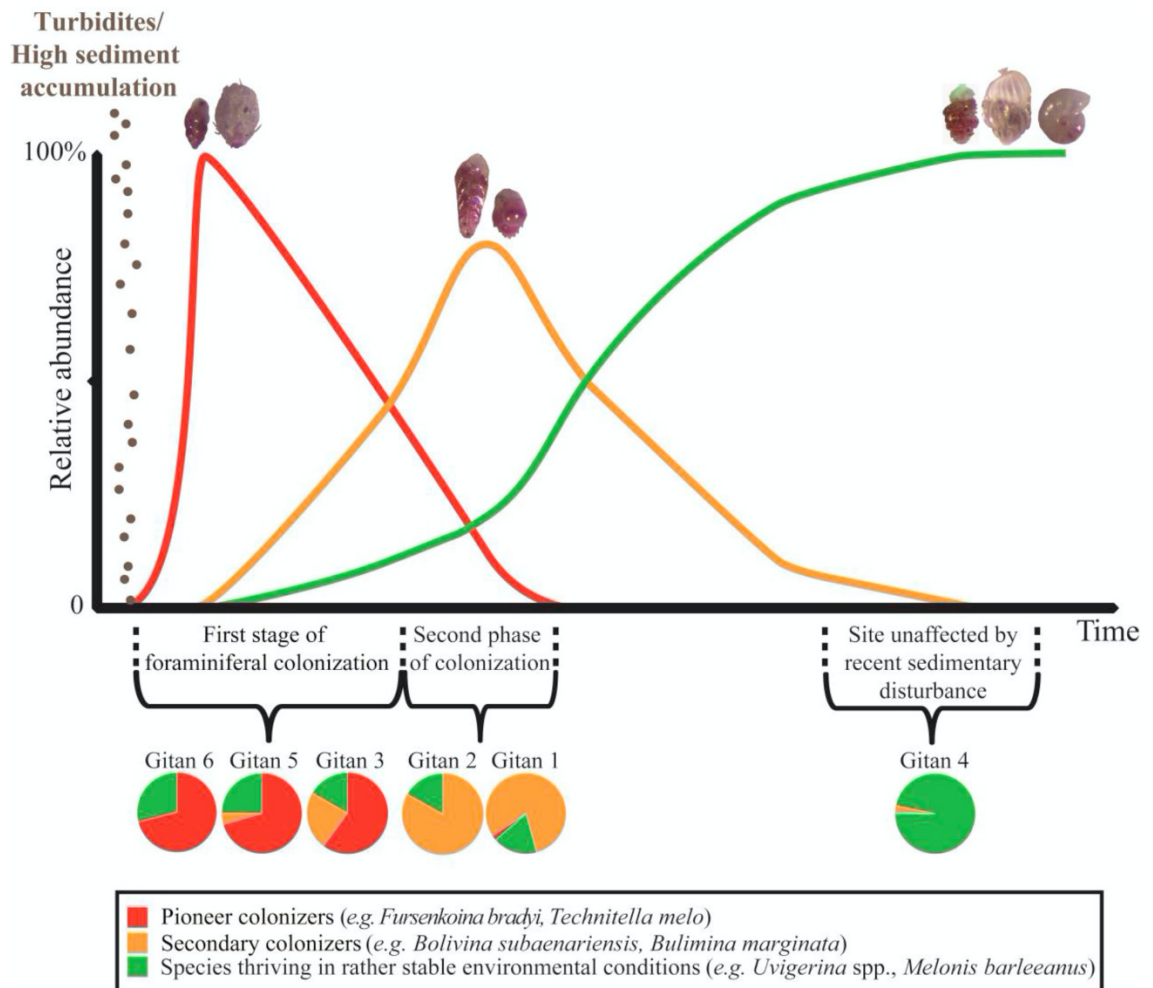


Figure 2.14 Summarised schematic from Duros et al., (2017) which documents the various foraminiferal responses observed along the Capbreton Canyon axis and adjacent terraces. With the brown stipples representing the passage of a turbidite or similar high sedimentation event.

Within the canyon assemblage, even within the most quiescent sites numerous neritic allochthonous species were identified. These dead reworked tests (*Cibicides lobatulus*, *Cassidulina carinata* and *Bulimina marginata*) were found within cores that showed no evidence for turbidite deposition. Therefore, despite sedimentary structures and living foraminifera indicating a more quiescent environment, the occurrence of large amounts of inner shelf and upper canyon fauna throughout the cores point towards the presence of processes other than turbidity currents that are responsible for downslope transport. This can be seen to be occurring even within inactive canyons such as the Cap-Ferrat canyon

where foraminifera are transported down slope in bottom nepheloid layers (Duros *et al.*, 2014). Therefore, identification of reworked shallow water foraminifera can be seen as a signal for supply from the shelf by recurrent nepheloid currents that are the result of captured and/or related down-canyon flowing of watermasses observed by Marchès *et al.* (2007) in the Gulf of Cadiz.

#### 2.2.6 The Elevated Microhabitat

Marginal basin overflow systems or areas where water masses impinge on the ocean floor downslope disturbance should have less of an influence on benthic microhabitat. Areas such as the Denmark Strait or the Gulf of Cadiz are characterised by strong bottom current regimes that favour abundances of active suspension feeders and excludes pioneering colonisers or opportunists (Schönfeld, 1997, 2002a; Rogerson *et al.*, 2011). The active suspension feeders in these setting have been classified into a group known as “elevated epifauna” as the individuals occupy elevated substrates such as cobbles, coral and kelp to feed directly from high velocity bottom currents (Schönfeld, 1997, 2002a, 2002c) (See Fig. 2.15). Therefore, it is thought that percentages of elevated epifauna are strongly correlated with the intensity of bottom currents. This relationship is observed in the present-day Mediterranean Outflow and it has therefore been suggested as a potential proxy for bottom current intensity in the past (Schönfeld & Zahn, 2000; Schönfeld, 2002a; Singh *et al.*, 2015; García-Gallardo *et al.*, 2017).

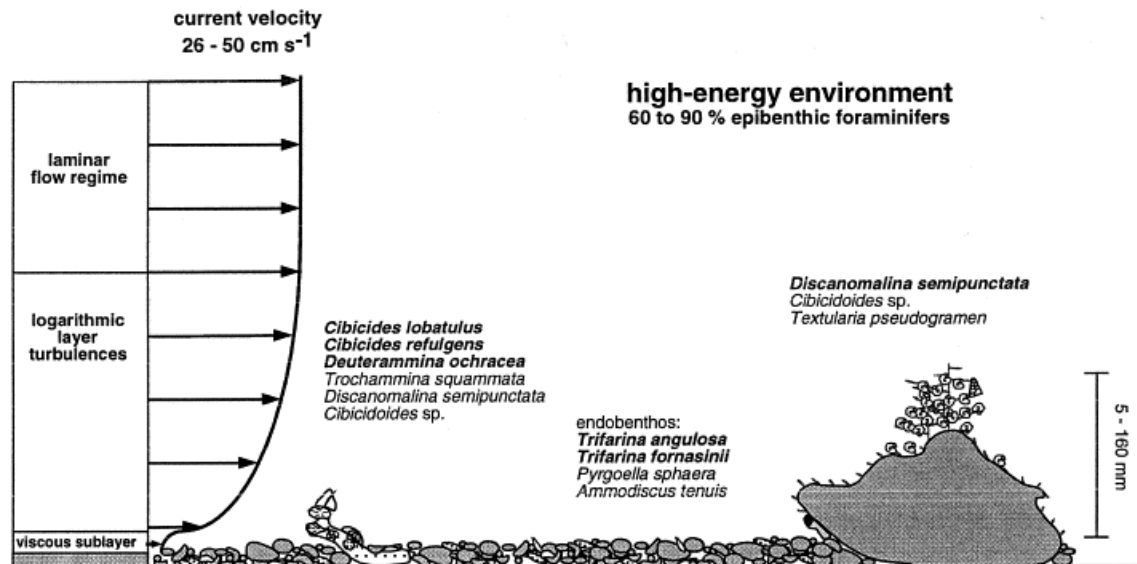


Figure 2.15 Epibenthic colonisation structures in high-energy environments in the Gulf of Cadiz from Schönfeld (2002c). With a schematic current strength section with distance from the sediment (not to scale) indicates the different hydrodynamic environments. Frequent species are marked in bold. Epibenthic foraminifera prefer elevated positions on hydroids (grey lines) or large fragments of deep-water corals (stippled).

At shallow, point-source Oceanic Gateways flow velocities can reach 80 to 300  $\text{cm s}^{-1}$  in some cases within the Mediterranean Outflow Water at the Strait of Gibraltar (Ambar & Howe, 1979; Iorga & Lozier, 1999; Candela, 2001) and then decreases with distance east to west from the gateway as it encounters slope-perpendicular ridges or canyons and spreads as it interacts with ambient North Atlantic Central Water. As the current spreads and descends from the gateway it splits and forms an upper, high-velocity limb and a lower, low-velocity limb (Thorpe, 1976; Baringer & Price, 1999). The upper limb slows down to 100  $\text{cm s}^{-1}$ , before slowing down further to 13  $\text{cm s}^{-1}$  in more distal settings off Cape San Vicente (Meincke *et al.*, 1975; Ambar & Howe, 1979; Hans Nelson *et al.*, 1993). In the lower limb, currents are slow, recorded as only 5-10  $\text{cm s}^{-1}$  (Heezen, 1969).

The Mediterranean Outflow has resulted in large geomorphic features in the western Gulf of Cadiz where it has resulted in the build-up of contourite drift bodies, that are sandy to silty in composition that have been sorted under the bottom currents (Faugeres *et al.*, 1984; Gonthier *et al.*, 1984; Stow *et al.*, 1986; Faugères *et al.*, 1999). Other deeper watermasses in the regions such as the North Atlantic Deep Water show much slower velocities (Zenck, 1980). The sediments that lie beneath these watermasses are either hemipelagic silty clays or foraminiferal oozes (Lebreiro *et al.*, 2003)

The bottom sediments that cover the depth interval also show a decrease in current strength from east to west. Schönfeld (2002b) was able to discern different biofacies under weak (Fig. 2.16) and strong (Fig. 2.15) near-bottom currents. Proximal to the Strait, hard rock outcrops and gravel lags dominate (Heezen, 1969; Nelson *et al.*, 1993). In these high velocity bottom current eastern sections, the assemblage is dominated by epibenthic species *Discanomalina semipunctata*, *Cibicides lobatulus* and *Cibicides refulgens*. These species attach themselves to objects larger than 5-7 mm at prominent points within current velocities of 26-50 cm s<sup>-1</sup>. These substrates provide a microenvironmental stability and provides a higher yield of advected organic matter at a distance from the sediment surface. Along the main current flow path the seafloor is composed of sand and sandy silt, while outside and in between the core flow paths, silt and clayey silt dominate (Nelson *et al.*, 1999). Along the western sections, these finer sediments become more frequent, which leads to an epibenthic assemblage of *Crithionina pisum*, *Trochammina squammata*, *Saccamina sphaerica* and *Rosalina anomala* attached to *Rhabdammina abyssorum* tubes and other small objects. The fauna are not as elevated as in higher velocity settings, never

reaching a height above 28 mm. The height of the fauna is related to the transition layer above the sediment with a high concentration of suspended particulate matter. The lateral flux of particulate matter decreases with height above the sediment in these lower energy environments ( $4-25 \text{ cm s}^{-1}$ )(Fig. 2.16).

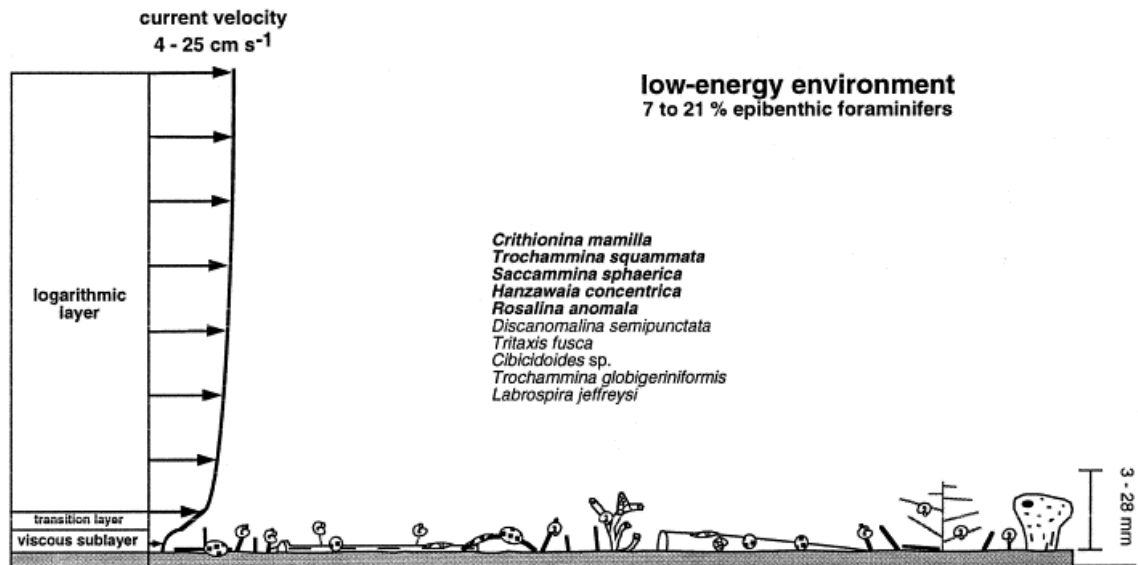


Figure 2.16 Epibenthic colonisation structures in low-energy environments from (Schönfeld, 2002c). A schematic current strength section with distance from the sea floor (not to scale) indicates the different hydrodynamic environments and the transition layer, where suspended particles are concentrated. Frequent species are marked in bold. They concentrate on a distance of 3-28 mm above the seabed.

Elevated positions do not therefore provide a better food supply. Comparing and contrasting high versus low current velocity sedimentary environments reveal that substrate stability may be a factor in benthic foraminiferal colonisation structures, standing stock and assemblage composition. Critically, Schönfeld (2002b) found that specialised shallow infaunal taxa such as *Trifarina angulosa* have adapted to survive in similar environments as other typically epibenthic species. The position of epibenthic foraminifera above the sediment surface in both high and low current velocity environments is related to the height of the greatest abundance of lateral flux of suspended food particles within reach from the ocean



floor. Therefore, co-occurrence of epibenthic foraminiferal species and certain species of shallow infaunal taxa may provide a proxy for the influence of bottom current velocity.

## 2.3 Uruguay

### 2.3.1 Introduction

The continental margin offshore from Uruguay (See Fig. 2.17) is an ideal locality for the study of deep-water sedimentary processes. The various types of sediment transport processes mentioned previously are present here including gravitational downslope and thermohaline along-slope sediment transport are all located in close vicinity to one another as shown in Figure 2.17 (Lonardi & Ewing, 1971; Klaus & Ledbetter, 1988). The modern ocean margin offshore from Uruguay is subjected to strong thermohaline along-slope currents and a high amount of fluvial sediment input via the de la Plata River. The modern suspended load is  $\sim 80 \times 10^6 \text{ t year}^{-1}$  that is made up of 75% coarse to medium silt, 15% fine silt and 10% clay (Giberto *et al.*, 2004). The combination of high sediment supply and strong oceanographic circulation results in the slope hosting an extensive mixed depositional system where turbidite and bottom-current deposits result in hybrid facies associations. Hybrid facies association is the vertical and lateral association of facies produced by genetically distinct processes (turbidity currents and bottom currents). These facies result in sand body geometries which are difficult to explain with turbidite-dominated models for deep-water sedimentation (Mutti, 1992). The setting offers the opportunity to investigate interactions between different sediment transport processes and has only recently received specific interest for the collection of core and geophysical data. However, in addition to the region being complex from a sedimentological perspective, it is also an extremely dynamic region oceanographically. Both types of influence affect the subsurface history, and so are reviewed here.

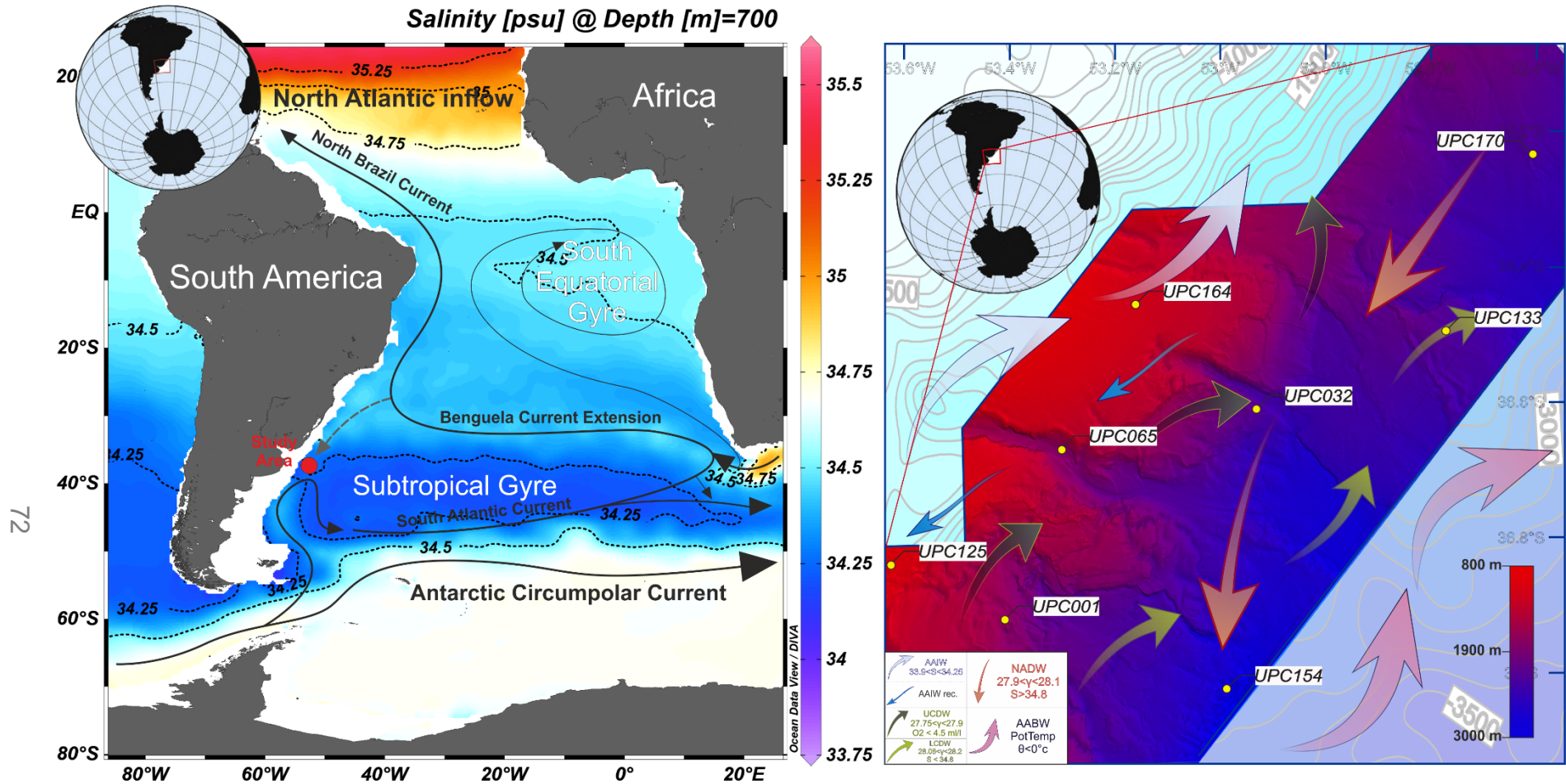


Figure 2.17 Geographic and oceanographic setting and study region. Salinity at 700 m depth represented by the dashed lines. AAIW Antarctic Intermediate Water, r-AAIW Reversed Antarctic Intermediate Water, CDW.Circum Polar Deep Water, AABW Antarctic Bottom Water, NADW North Atlantic Deep Water (summary information given in lower left of bathymetry). Sediment cores (UPC####) are indicated in yellow. Maps generated through OceanData Viewer CTD data and seismic data with Petrel.

### 2.3.2 Geological Setting

The continental margin offshore Uruguay is a segmented, rifted margin and is characterised by seaward dipping reflectors on seismic lines (SDRs) and >7 km-deep sedimentary basin with a volcanogenic-sedimentary infill. The depocenter is divided into four sequences (Soto *et al.*, 2011; Hernández-Molina *et al.*, 2016). The sequence begins with a prerift Proterozoic basement rock followed by a Paleozoic transition of continental to marine sediments. The second phase is a synrift Late Jurassic – Neocomian volcanic sequence with continental sedimentation. A transitional phase follows this in the Barremian to Aptian age sequence from continental to marine sediments, which varies across the basin. Finally, a drift phase begins in the late Cretaceous with transitional to marine sedimentation giving way to fully marine conditions in the Cenozoic. There are two main basins that formed at different time periods offshore Uruguay. They are the Punta del Este in the south (Late Jurassic - Cenozoic) and the Pelotas Basin in the north (Cenozoic in age, with scarce Cretaceous sediments compared to the Punta del Este). These basins are separated on the shallower shelf by a basement high named the Polonio High which acts as a sediment source area (Soto *et al.*, 2011). The area is divided by the Rio del la Plata Transfer System related to the southern boundary of the Polonio High. It divides the margin of Uruguay into two sectors that correspond to the aforementioned basins (Fig. 2.18) (Soto *et al.*, 2011; Hernández-Molina *et al.*, 2016).

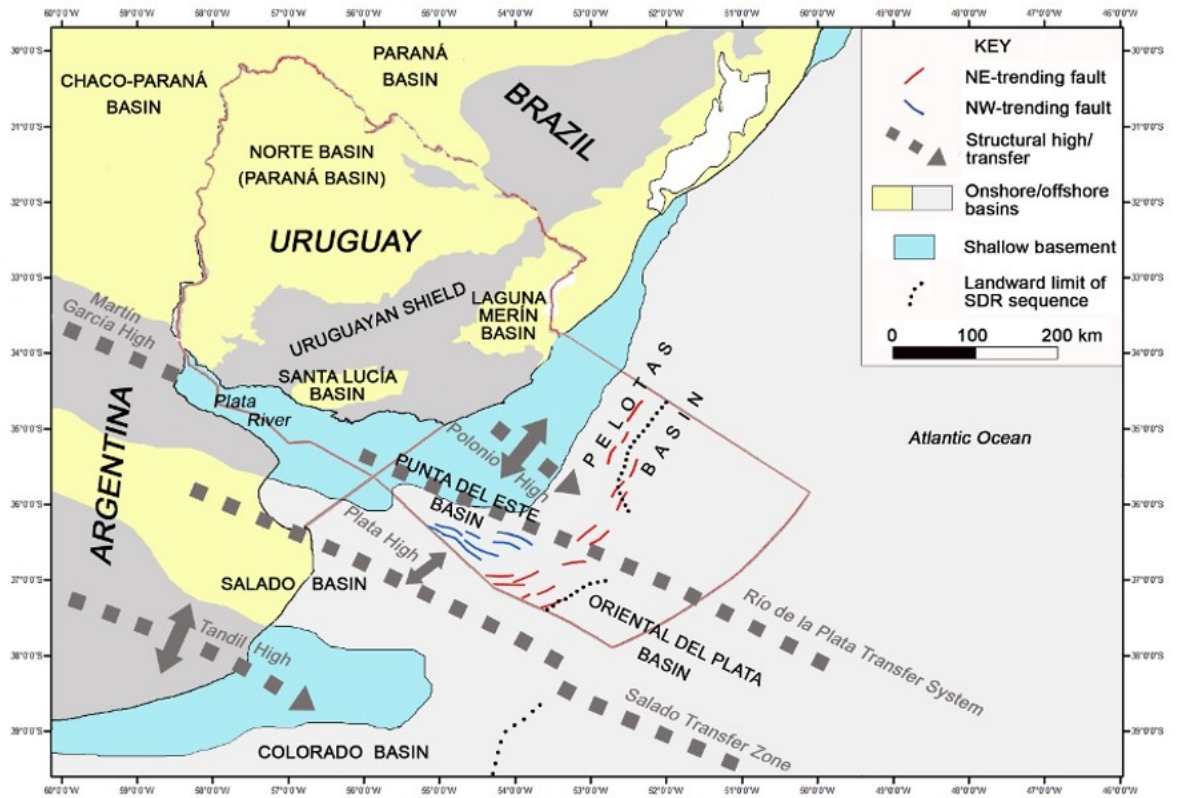


Figure 2.18 Offshore geology of Uruguay from (Soto et al., 2011)



2.3.3 Geomorphic Setting

The seafloor morphology offshore Uruguay can be divided into northern and southern zones. Both settings exhibit both large scale downslope and along-slope morphological features (See Fig. 2.19) (Hernández-Molina *et al.*, 2016).

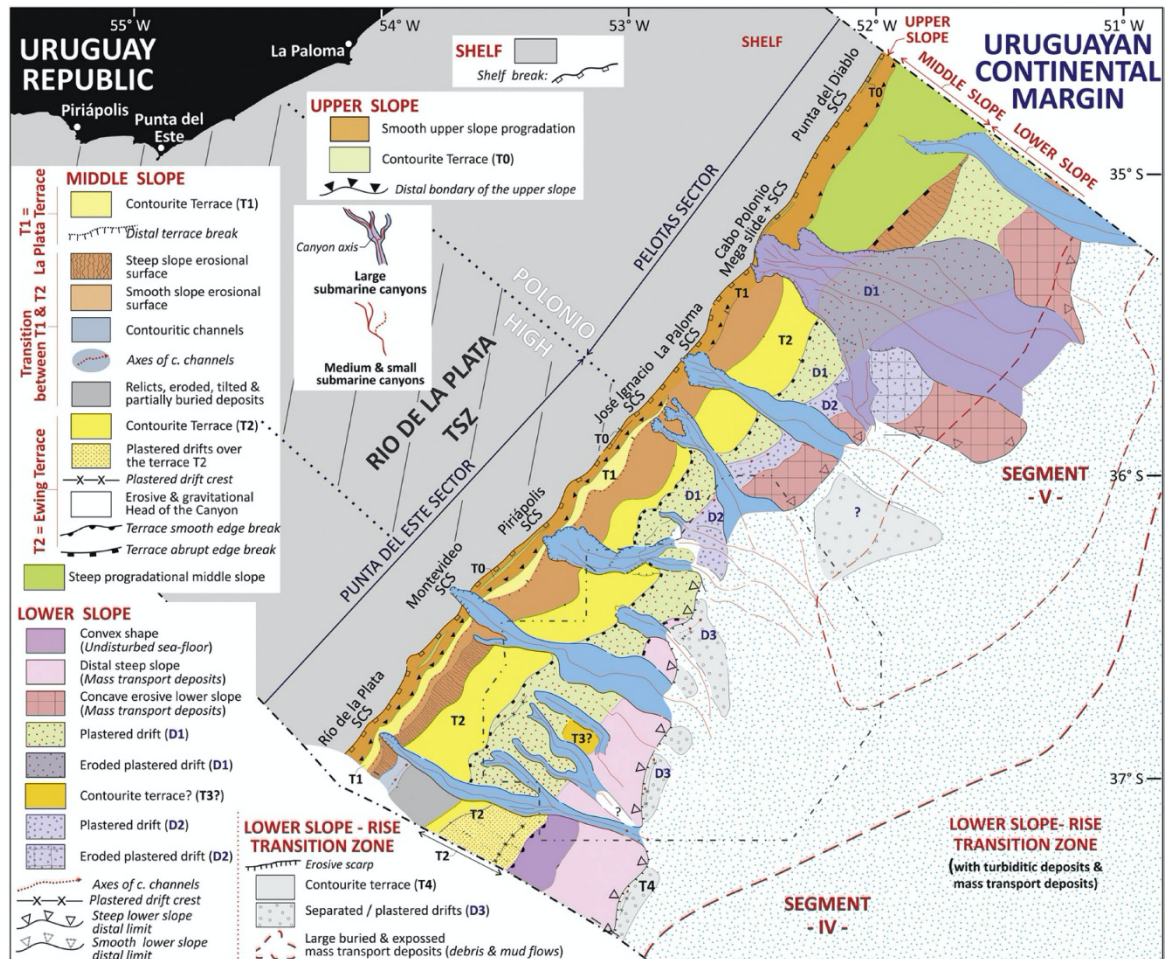


Figure 2.19 Morphosedimentary map of the Uruguayan margin. The oceanic Segment IV and V defined by (Franke *et al.*, 2006) and (Soto *et al.*, 2011) are included. Abbreviations: SCS=Submarine Canyon Systems; TSZ=Transfer System Zone. From (Hernández-Molina *et al.*, 2016).. With study area outlined by the dashed black line.

The basins are divided by the Polonio High and to the north of this downslope sediment transport processes are more abundant. (Hernández-Molina *et al.*, 2016) constructed a morphosedimentary map of the Uruguayan margin (Fig. 2.19) where they identified key morphological features of the Uruguayan margin and

their relationship to the interplay of down and along-slope processes. Downslope processes include slides, slumps and debrites, the largest being the Cabo Polonio Mega Slide that is  $>4000 \text{ km}^2$ . Debrites are seen to occupy the lower slope to rise transition where they are either exposed on the seafloor or seen buried in seismic profiles. The authors identified six large submarine canyon systems, from north to south they are: Punta del Diablo; Cabo Polonio; La Paloma; José Ignacio; Piriápolis; Montevideo and the Rio de la Plata submarine canyon systems. These canyons can be up to 6 km wide and incision depths of up to 800m. These canyons are different from the normal submarine canyons that would likely be connected to modern or ancient continental drainage channels. Instead they incise into the contourite terraces and are seen as “inactive” canyons, as they are fed sediment sourced from the terrace, and not from riverine sources. Contouritic features occur along the entire margin, even in areas dominated by downslope processes. However, a series of contourite terraces have been identified which are suitable sites of along-slope sedimentation. Numerous sand-rich deposits have been observed accumulating on the terraces that appear to be dominated by vigorous bottom current activity (Hernández-Molina *et al.*, 2018).

The contourite terraces are large sub-horizontal features that have a slight seaward tilt. Hernández-Molina *et al.*, 2016 identified 5 such terraces that are laterally continuous along the margin. These are labelled as: T0 at  $\sim 0.25 \text{ km}$  water depth, T1 at  $\sim 0.5 - 0.6 \text{ km}$  water depth, T2 (Ewing Terrace) at 1.2 to 1.5 km water depth, T3 at  $\sim 2.5 \text{ km}$  water depth and at the base of the slope is T4 at  $\sim 3.5 \text{ km}$  water depth. The locations of these terraces are shown in Figure 2.19 and 2.20 with associated drifts.

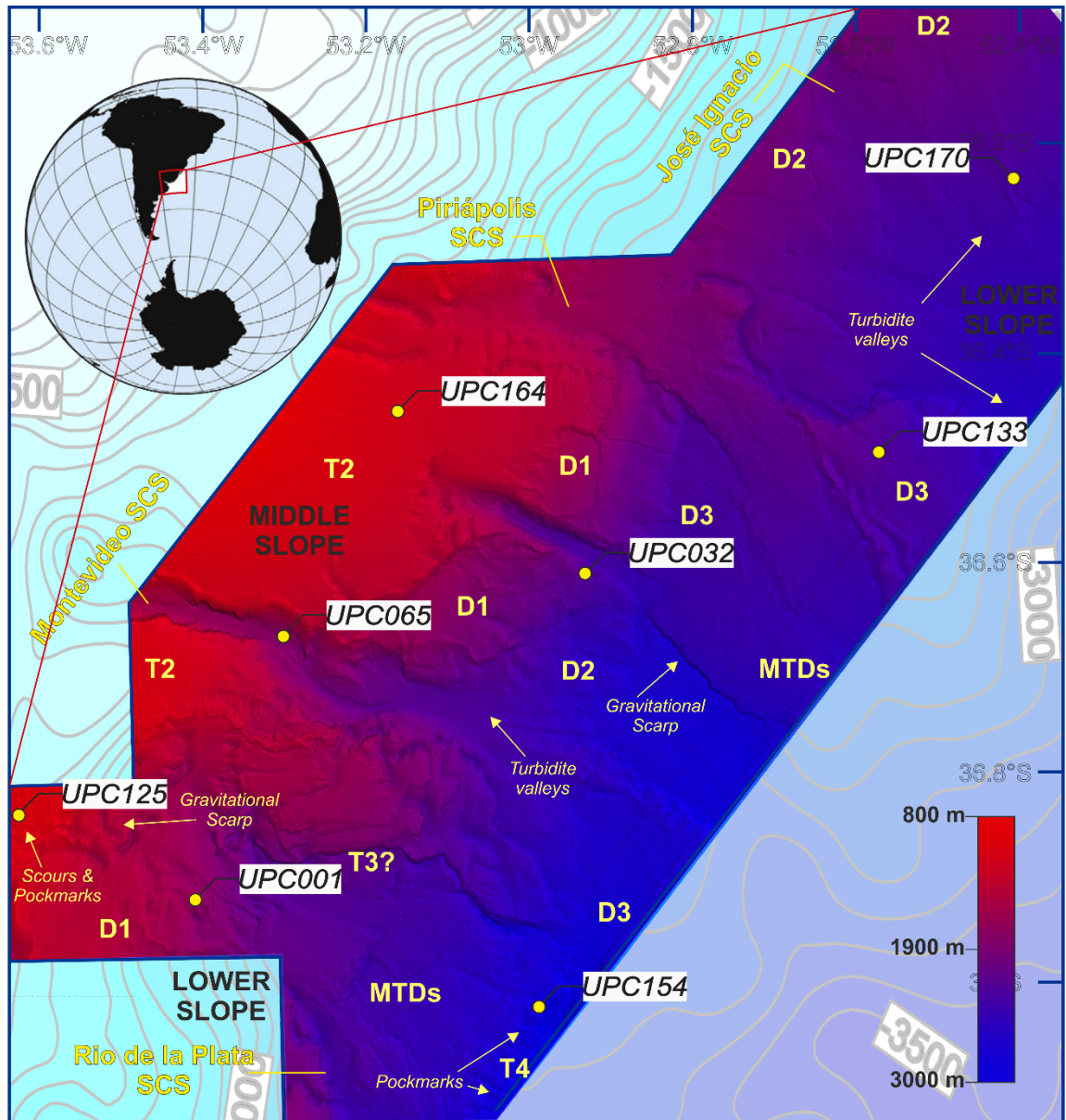


Figure 2.20 Seismically generated present-day seafloor bathymetry. A complex seafloor morphology is observed. Yellow arrows highlight the scoured and deformed pockmarks in the dune fields associated with the (southward flowing) AAIW(R-AAIW) and Upper Circumpolar Deep Water (UCDW) circulation (reproduced with permission of BG Group). Geomorphic settings include: Submarine canyons-systems (SCS); drift deposits (D1, D2 and D3); contourite terraces (T2 and T4) and mass-transport deposits (MTDs) are labelled in yellow. Adapted from (Hernández-Molina et al., 2016).



#### 2.3.4 Oceanographic Setting

The location of this study within this setting on the Uruguayan margin is vital for understanding South Atlantic oceanographic processes, as it provides evidence of a variety of critical water masses sourced from northern and southern origins that flow close to the ocean floor (See Figures 2.21 and 2.22). The upper parts of the ocean circulation offshore Uruguay contain the southward flowing Brazil Current (BC), made up of Tropical Water (TW) and South Atlantic Central Water (SACW), whereas the Malvinas Current (MC) flowing northwards is composed of Antarctic Intermediate Water (AAIW) and Upper Circumpolar Deep Water (UCDW) components. The northward-flowing Malvinas Current is topographically steered along the 1400 m isobath and is thought to be linked to the formation of the Ewing terrace (Preu *et al.*, 2013). The Brazil and Malvinas Currents converge at a point located around 38°S directly offshore Uruguay, this creates a zone known as the Brazil-Malvinas Confluence (Gordon & Greengrove, 1986; Piola & Matano, 2008; Stramma & England, 1999). This confluence is characterized by sharp gradients in temperature and salinity. Migrations of the BMC over glacial-interglacial transitions are thought to influence the stratification of the water masses below (Gordon & Greengrove, 1986; Gordon, 1989). Fluctuations on this scale are known to influence the South Atlantic subtropical gyre and therefore global ocean circulation and global climate (Stramma & England, 1999).

#### 2.3.4.1 South Atlantic Meridional Overturning Circulation

The watermasses of the southern Atlantic enter via a cold-water route through the Drake Passage or a warm-water route via the Agulhas Current (Gordon *et al.*, 1992; Poole & Tomczak, 1999). Changing contributions from the cold-water route over time have been relatively little studied compared with the warm water route. The inflow of water through the cold water route is controlled by the latitudinal position of oceanic fronts within the Drake Passage. Low-density Sub-Antarctic Mode Water (SAMW) generated in the SE Pacific is exported into the SW Atlantic north of the sub-Antarctic Front (Talley, 1999). SAMW mixes with Antarctic Waters such as CDW where it evolves to form the AAIW. Antarctic waters enter the deepest portions of the South Atlantic where Antarctic Bottom Water (AABW) (Figure 2.17) is pooled within the abyssal Argentine Basin. The entrapment of this dense, 2 km thick water mass creates a large cyclonic gyre, which begins to dominate the portions of the margin deeper than 3.5 km (Georgi, 1981; Stramma & England, 1999). The cold and low salinity ( $\theta < 0$  °C, 34.6 – 34.7 psu) AABW is one of the major components of global meridional circulation (Reid, 1996; Orsi, Johnson, & Bullister, 1999). It is formed by mixing of Ice Shelf Water (ISW) and CDW, and by coastal polynya activity around the Antarctic shelf (Stramma & England, 1999). These can be divided into ISW Mode when ice shelves are expanded over a higher sea level and Polynya Mode due to interactions between the atmosphere, sea ice and ocean on the Weddell Sea continental shelf and in polynyas. During ISW Mode, water below the ice shelves is super-cooled and flows down the slope. Whereas in Polynya Mode, surface water cools and evaporates as it comes into contact with the atmosphere and produces a dense salty water. The CDW is formed when this dense AABW enters the Antarctic

Circumpolar Current and mixes with NADW. It is thought to be entirely wind driven (Stramma & England, 1999), but perennial sea ice cover may have a moderating effect too. As CDW is advected into the South Atlantic, it is split by the southward flowing NADW into Upper and Lower CDW. (Stramma & England, 1999) (See Figure 2.22)

#### 2.3.4.2 Hydrographic Structure

Variations and changes to the meridional extent of deep to intermediate watermasses along the Uruguayan margin are poorly understood. There have been recent attempts to characterise the circulation pattern by identifying zones where different watermass strata interact with one another and where water masses are seen to interact with the ocean floor (Preu *et al.*, 2013; Hernández-Molina *et al.*, 2016). We must first assign fixed values to the physical and chemical properties of watermasses in order to understand their distribution in the deep (See Figure 2.22). By analysing these values from historical observations, Preu *et al.*, 2013 found that the boundary between north and south flowing water was not as sharp as previously suggested (Piola and Gordon, 1989) and is in stark contrast to the transition we see in the near surface layer. The SACW ( $\theta > 8\text{ }^{\circ}\text{C}$ ,  $S > 34.8$ ) is seen to detach from the margin around  $36^{\circ}\text{S}$  and the fresher, ( $S < 32.25$ ) AAIW flows northward to approximately  $30^{\circ}\text{S}$  where it deviates from the margin. The ( $S > 34.8$ ) NADW extends to  $38^{\circ}\text{S}$  (Preu *et al.*, 2013) and vertically divides  $\text{CO}_2$  saturated CDW into the fresher/warmer ( $\text{O}_2 < 4.5\text{ ml/l}$ ) Upper and salty/cold ( $S < 34.8$ ) Lower CDW (See Figure 2.22). This suggests that water masses flowing from the north and south inter-finger with one another rather than obey a defined boundary line. Therefore, any migration of the

subsurface boundaries should be defined by relative contributions of northern/southern sourced waters through time.

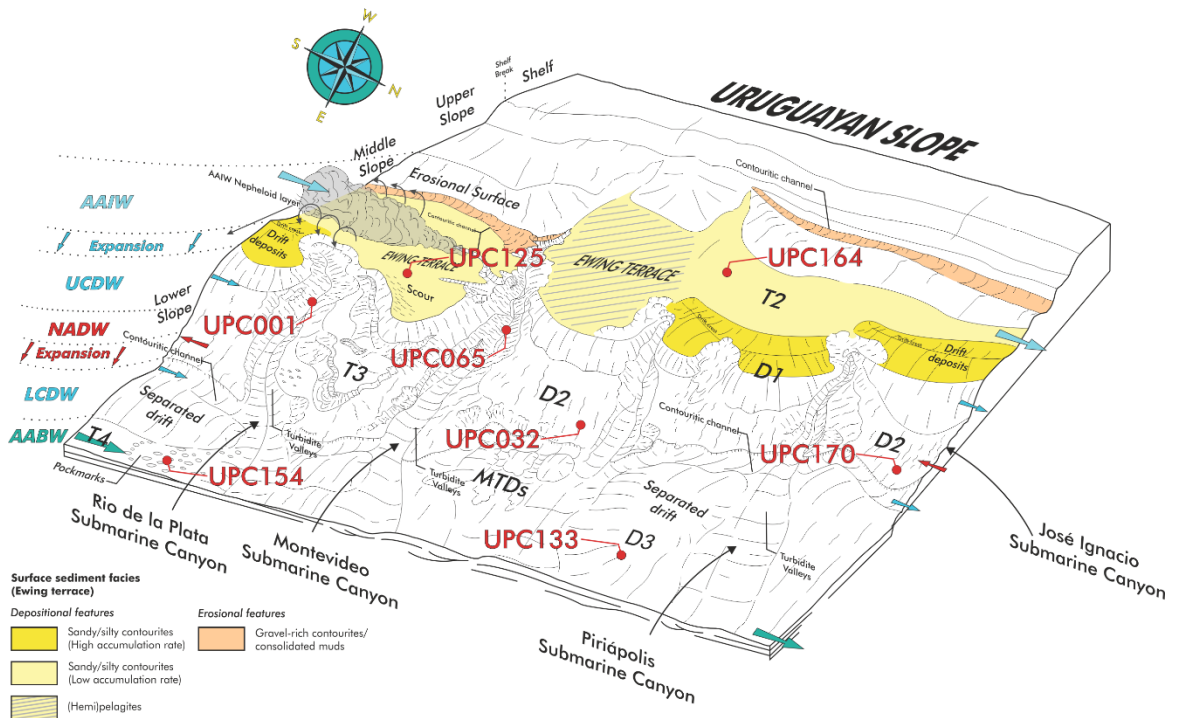


Figure 2.21 Modern morpho-sedimentary map of the Uruguay continental margin based on work by (Preu et al., 2013; Voigt et al., 2013; Hernández-Molina et al., 2016). Shows the Ewing terrace contourite system incised by multiple submarine canyon systems. The yellow coloured areas are the Ewing terrace that is located on the interface between AAIW and UCDW. Voigt et al., 2013 show that the lowermost portion of the AAIW contains a distinct nepheloid layer. Surface sediment facies are drawn after Bozzano et al., (2011) and Hernández-Molina et al., (2016). The red circles show the location of cores investigated in this study. AAIW = Antarctic Intermediate Water; UCDW = Upper Circumpolar Deep Water; NADW = North Atlantic Deep Water; LCDW = Lower Circumpolar Deep Water; AABW = Antarctic Bottom Water; T2 = Terrace 2; D1 = Drift 1; D2 = Drift 2; T3 = Terrace 3; D3 = Drift 3; T4 = Terrace 4; MTDs = Mass Transport Deposits. Expansion zones relate to Holocene change and retreat of deeper water masses to increased NADW and AAIW.

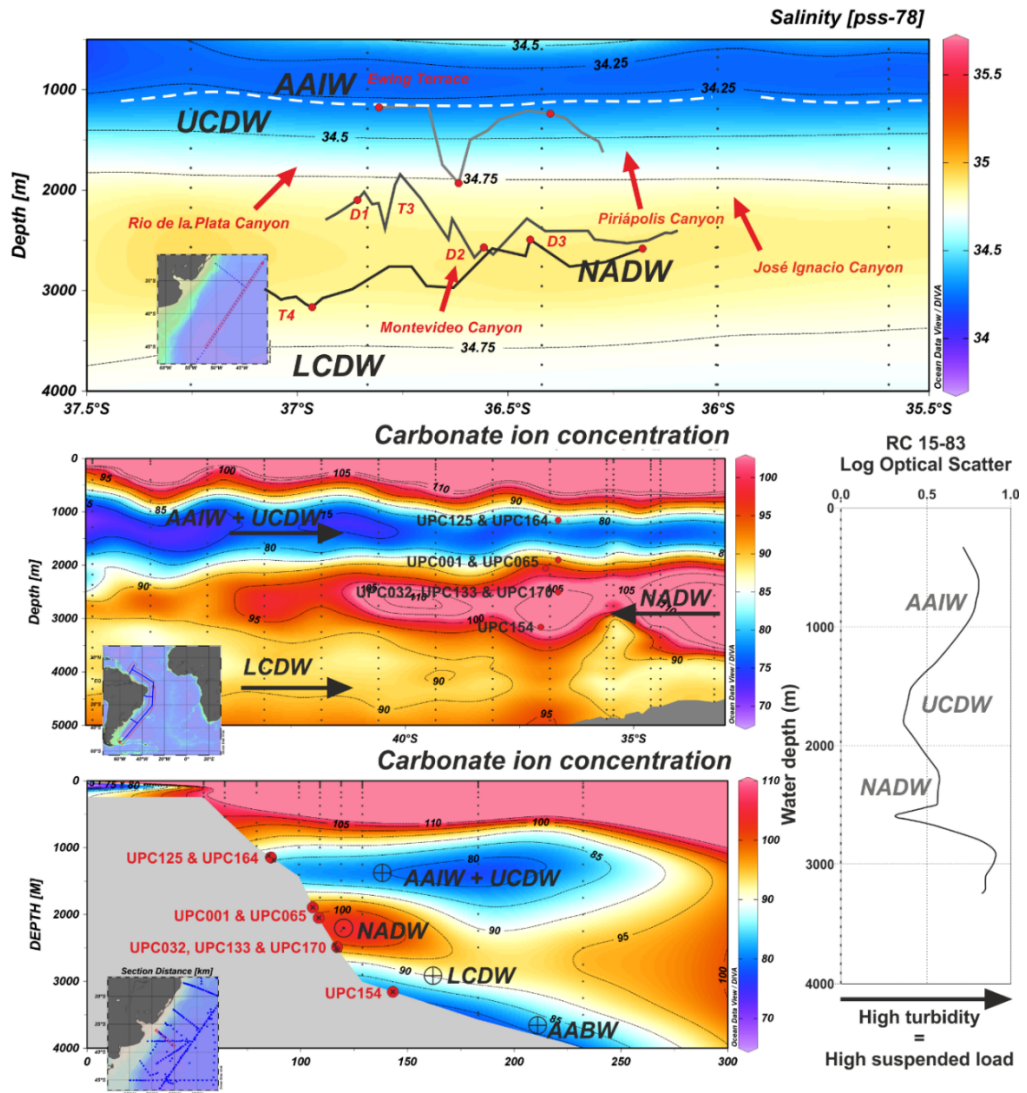


Figure 2.22 A: Section of salinity across offshore Uruguay. A trace of the bathymetry along the terrace shows the intersecting canyons. The red dots indicate locations of cores in this study. The dashed white line indicates the interface between AAIW and UCDW. B: Modern day carbonate ion concentration (CO<sub>3</sub><sup>2-</sup>) in the SW Atlantic, show in along and cross slope sections. The red dots show the location of cores. C: Turbidity depth profile taken to the south of the study area (Lamont-Doherty Earth Observatory) there is an increase in turbidity from ~700 – 1000 m where a nepheloid layer associated with the strong current activity within the range of AAIW. Prepared using Ocean Data View (<http://odv.awi.de>). The strength of the bottom currents in the northward flowing AABW, U/LCDW and AAIW control the development of the deep marine environment on a geological timescale. The Ewing Terrace is presently under the influence of AAIW (Hernández-Molina et al., 2009; Preu et al., 2013) where flow velocities can reach ~15-20 cm s<sup>-1</sup> at 1000 m water depth (Gwilliam, 1996) resulting in a distinct nepheloid layer within the central flow of the AAIW (Voigt et al., 2013). Approaching the AAIW/UCDW interface beneath the AAIW central flow, sediments deposit from the nepheloid layer and accumulate to form drift deposits.

#### 2.3.4.3 Contourite Features and their Link to Regional Watermasses

The contouritic features along the margin have a depositional, erosional and mixed origins. These form over geological timescales from the interaction of the interfaces of regional watermasses and their associated near bottom currents (Hernández-Molina *et al.*, 2009; Hernández-Molina *et al.*, 2016). The contourite features are modified locally by gravitational processes with submarine canyons and on the seaward side of drifts.

Contourite terraces on the margin form along the interfaces of watermasses, downslope of the high velocity core of the overlying watermass (See Fig. 2.21 and 2.22). The T0 terrace runs along the upper section of the SACW and is not covered by the sample set. T1 coincides with a range of depths associated with the Brazil Current and AAIW and is also not covered by the sample set. T2 matches the depth of the AAIW-UCDW interface at a depth of 1200 to 1500 metres below sea level. In the study area T3 is not very well developed but occurs in some areas around 2500 metres below sea level, this is the only terrace that does not match the depth of a modern watermass interface. To the south on the Argentine margin T3 is linked to the interface of the UCDW and LCDW (Hernández-Molina *et al.*, 2009). T4 is currently under the influence of modern LCDW but likely coincides with the depth range of the glacial LCDW-AABW interface (Preu *et al.*, 2013) This terrace was therefore likely mostly formed during glacial periods. It can be observed from our bathymetry data as having a large field of pockmarks.

### 2.3.5 Foraminiferal Setting

#### 2.3.5.1 *Are there any Uruguayan Disturbed Microhabitats?*

Within inactive canyons such as those incised into the terrace on the Uruguayan margin, foraminifera could be transported down slope in bottom nepheloid layers such as those seen in (Duros *et al.*, 2014). Therefore, identification of reworked shallow water shelf and/or terrace foraminifera can be seen as a signal for supply from shallower depths by recurrent nepheloid currents that are the result of captured and/or related down-canyon flowing of watermasses observed by Marchès *et al.*, (2007) in the Gulf of Cadiz.

Similar bottom nepheloid layer processes have been observed from the sediments sampled from the canyons that incise the continental margin offshore Uruguay and Argentina. The canyons are interpreted to be presently inactive with canyon heads disconnected from any river source. However, downslope/high rates of sedimentation are observed within canyons such as the Mar del Plata Canyon (Krastel *et al.*, 2011; Voigt *et al.*, 2013). In canyons that have a riverine connection, the surface (hyperpycnal) plumes which are generated where the river meets to ocean descend to the seabed as they are more dense due to their sediment load (Parsons *et al.*, 2001; Mulder *et al.*, 2003; Ducassou *et al.*, 2008). Hyperpycnal plumes are recognised in the sedimentary record as fine-grained turbidites. However, the Mar del Plata Canyon contains coarse-grained turbidites, which cannot be supported by this type of process. Furthermore, morphosedimentary features on the shelf such as submarine channels show that the La Plata River flowed northwards over a glacially exposed shelf (Ewing & Lonardi, 1971). Most of the La Plata River's huge sedimentary load is shown to be delivered directly to the Rio Grande Cone, located to the north of the Rio del

Plata Canyon System (Chiessi *et al.*, 2009). Any turbidite found within the canyons of the Rio del Plata system is therefore not considered to be sourced from the La Plata River.

The turbidites observed within the canyons share the same sedimentary characteristics as drift deposits on the outer edge of Terrace 2 (a grey, fine silt to sand composition) (Bozzano *et al.*, 2011). Any turbidite activity within the canyons can therefore be linked to sediment instability of drift deposits at the southern flank of the canyons. Indeed, even though northward flowing AAIW does not flow down the canyon (as it is not dense enough), vorticity conservation would argue that the flow will follow the isobaths of a slope. Therefore, the flow over a canyon will describe a cyclonic loop and will accelerate along the canyon walls (Klinck, 1996). Simulations confirm that along with this strengthening of flow along the walls, there is a general decrease in current velocity along the canyon axis. This decrease in current velocity may drastically decrease the transport capacity of the nepheloid layer and result in a considerable amount of sediment to be released into the canyon systems. Enhanced bottom current energy (as interpreted during glacial periods) would lead to enhanced accumulation of sediments. During these periods, the plastered drifts on the outer limits of Terrace 2 were growing. This makes a down-current progradation of drift deposits likely and would lead to aggradation on the southern flank and associated instability on the southern flanks of the canyon systems (Mulder *et al.*, 2006). This instability would naturally result in turbidity currents. Therefore, during periods of stronger bottom currents we would expect to see a higher degree of disturbance within the submarine canyons systems as drift progradation is promoted. This is supported by observations by Voigt *et al.*, 2013 of a coarsening of sediment within the Mar



del Plata canyon when there is a general increase in AAIW strength at the last glacial termination. Through the Holocene there is a general decrease in the current speed of Antarctic watermasses (Pahnke *et al.*, 2008). The cessation of drift construction due to more sluggish bottom current velocities through the Holocene would result in a more quiescent canyon environment. However, the drift deposits that are built upon the terrace are prone to failure by other triggers such as tectonic events. Therefore, this makes any environment downslope of a significant drift deposit prone to disturbance events such as slope failures and associated turbidity currents. The increased disturbance frequency should result in a foraminiferal microhabitat confined to the earlier stages of recolonization.

#### *2.3.5.2 Are there any Uruguayan Elevated Microhabitats?*

The Uruguayan Continental Margin is deeper and more open-slope than other well-studied contourite systems e.g. Gulf of Cadiz. This results in bottom currents that are generally weaker, with flow velocities of  $\sim 15\text{-}20\text{ cm s}^{-1}$  at 1000 m water depth according to the OCCAM Global Ocean Model (Gwilliam, 1996). These velocities are only reached within the Antarctic Intermediate Water, while other watermasses that flow along the slope are much weaker. However, we do not see a weakening of current strength away from a point-source as found at oceanic gateways. Instead, we see layers of several watermasses with cores of different physical and chemical properties with depth. Cores of the watermasses are of higher velocity and result in mainly erosive features on the slope, while the turbulent interfaces at the boundaries between the watermass cores and within the weaker watermasses are of lower velocity and form mainly depositional features. There have also been depositional and non-depositional features observed pre-, within- and post-slope perpendicular canyons. When a flow

passes over a canyon, current velocity decreases and there is potential drift sedimentation within canyons and hiatal surfaces downstream of canyons due to sediment piracy by the canyons that incise the contourite terraces along the slope. Due to the deeper more diffuse nature of bottom currents along passive margins, gravel lags and hard rock outcrops related to bottom currents are not observed on the Uruguayan Continental Margin and are more common upstream within the Drake Passage (pers. Comm. Prof. Dierk Hebbeln). Instead, within the main current flow path of the Antarctic Intermediate Water the seafloor is composed of sand to sandy silt, while in the cores of the other watermasses on the slope the seafloor is dominated by silt and clayey silt. In the slower moving watermasses and in deeper open slope environments the seafloor is occupied by hemipelagic silty clays and foraminiferal oozes (particularly within the NADW). The contourite system offshore Uruguay can therefore be seen as similar to the low energy environment observed in Schönfeld, (2002c) from the western/distal section in the Gulf of Cadiz.

Clearly, in both regions bottom currents are a major controlling factor on sedimentation and in shaping the seafloor (Stow *et al.*, 2009). They are semi-permanent features of deep ocean circulation that vary in space and velocity over a range of timescales. They result in a range of seafloor structures from small surface lineations, crag and tail structures and ripples, to the construction and maintenance of large drifts (Stow & Faugères, 2008) and the excavation of large-scale erosional features, such as terraces, abrasion surfaces, channels, moats and furrows (Hernández-Molina *et al.*, 2008). However, both regions also show evidence for episodic downslope transport, both within cores and from surface

bathymetric data. Therefore, the origin of any sediment body must be treated with caution, particularly when the context is missing.

In these deep high-energy environments, substrate properties, current strength, disturbance frequency and strategies of foraminifera result in different microhabitat colonisation structures (Schönfeld, 2002c). Therefore, the benthic foraminiferal assemblage composition should be structured by the influence of bottom currents and frequency of downslope transportation events in settings such as the Uruguayan Continental Margin.

# CHAPTER 3

---

## MATERIALS & METHODS

### 3.1 Introduction and Field Site Selection

Although the concept of developing micropalaeontological tools for deep ocean sedimentological analysis is well developed, it is generally done via a specific case study. Initial review of the literature on exposed fossil contourites and well-investigated modern sedimentary systems, three systems looked most tractable: The Oligocene of Cyprus, the modern Gulf of Cadiz and the modern Uruguay Slope. At the start of this project, an initial investigation was performed to establish which of the systems most fully satisfied the following criteria:

- Are possible to sample.
- Contain both turbidite and contourite material of the same age, verified by existing sedimentological tools.
- Contain well-preserved benthic foraminifera.

The Uruguay slope was found to be the most suitable field site for further investigation. Turbidite sourced sediments are difficult to confidently identify in the Gulf of Cadiz system and the Cypriot field sites would result in delays as we wait for appropriate sampling permissions from the Cypriot Geological Survey (Only obtained in year 3 of my PhD). However, samples collected from the type section of ancient contourites (Stow *et al.* , 2002) are promising because they contain foraminifera. There is the possibility of identifying benthic foraminifera by disaggregating these indurated sediments using acetic acid

following the methods in (Lirer, 2000), and this remains a viable counterpart to the study presented herein.

### 3.2 Data-Set

Over two hundred sediment piston cores were collected in 2014 by BG Group on cruise number J14092 from part of the region shown in Figure 2.17 mapped by Hernandez-Molina and colleagues in 2014.

Eighty-six of these were chosen on the basis of geomorphic setting (identified from the bathymetry above (Fig. 2.20), the morpho-sedimentary map (Fig. 2.19) of Hernández-Molina *et al.*, (2016) and the apparent preservation within the core tube (tested by investigating the balance of mass, as unequally filled tubes have low-density water-filled voids). Pilot samples were taken at the end of each core section (~6x down each core), eliminating the need to split all 86 cores, giving a stratigraphic sampling interval of ~1 m. This strategy is inherently useful, as a key user of our outputs will be exploration drillers in the subsurface industries. Our study mimics standard analysis of the core catcher for microfossil identification that takes place on board both research and industrial vessels. Nine cores were subsequently split, logged and scanned.

The most extensive depositional features on the margin are Drift 1 (D1) (represented by core UPC001) and Drift 3 (D3) (Cores UPC133 and UPC170). These are in the range of 10<sup>2</sup>km in size and are laterally continuous along the whole margin, only to be cut by canyons (Core UPC065), valleys and Mass Transport Deposits (MTDs). Drift 2 (D2) (Core UPC032) is poorly developed in this particular study area and where it is cored, it appears to be badly disturbed by downslope processes from failures in D1. D1 is located in the depth range

1500 to 2500 metres below sea level. These drifts on the lower Uruguayan slope have been attributed to the northward circulation of the Upper Circumpolar Deepwater (UCDW) (Hernández-Molina *et al.* 2015). However, this study and others show that some parts of D1 fall within the modern depths of weak southerly flowing North Atlantic Deepwater (NADW). D2 is located deeper than D1, between 2500 and 3000 metres below sea level, and might be linked to modern influences of both NADW and Lower Circumpolar Deepwater (LCDW). Terrace 3 (T3) located along the interface of the supposed interface between the shallower glacial UCDW and LCDW (Hernández-Molina *et al.*, 2016).

D3 (Core UPC133 and UPC170?) is a pervasive, mounded, elongated and separated drift. Towards the northern sector of our study area it is unclear if core UPC170 records D2 or D3. This area could be a locality where D3 evolves into a plastered drift. It is located >3500 metres water depth and the D3 section cored by UPC133 shows a moat on the landward side, confirming it as a separated drift. D3 is said to fall under the influence of northward circulation of Antarctic Bottom Water (AABW) (Preu *et al.*, 2013). This current widens and intensifies during glacial stages, this study confirms that AABW appears to weaken/migrate downslope through the interglacial.

### 3.3 Methodology

#### 3.3.1 Sediment Facies

##### 3.3.1.1 Visual Logging

Visual descriptions were carried out on the 8 selected piston cores from the different morpho-sedimentary environments on the Uruguay slope. The scale and resolution of the core logging was dependent on the length of the core and the overall sediment composition, with a sample collected at least every 10 centimetres. Visually some sections of these cores are difficult to log, this is where employing core-scanning techniques proved invaluable. Despite these complications, grain size variation, erosional and depositional boundaries, sedimentary features, bioturbation features, facies, sediment colour and composition were all logged with the best of care. The core logging is supported by the core scanning, discrete grain size analysis and micropaleontological analysis, methods and results are in detail below.

*Table 3.1 Sediment cores used in the study of the Uruguay slope facies sequences. Sediment cores are held at the British Ocean Sediment Core Research Facility in Southampton, UK.*

| <b>Cruise</b> | <b>Core</b> | <b>Environment</b> | <b>Core length (m)</b> | <b>Lat (°S)</b> | <b>Long (°W)</b> | <b>Water Depth (m)</b> |
|---------------|-------------|--------------------|------------------------|-----------------|------------------|------------------------|
| J14092        | UPC001      | D1                 | 5.3                    | -36.92          | -53.41           | -2053.05               |
| J14092        | UPC032      | D2                 | 5.6                    | -36.62          | -52.92           | -2513.29               |
| J14092        | UPC065      | SCS                | 5.85                   | -36.66          | -53.30           | -1896.61               |
| J14092        | UPC125      | T2                 | 4.22                   | -36.85          | -53.63           | -1121.22               |
| J14092        | UPC133      | D3                 | 3.94                   | -36.50          | -52.57           | -2451                  |
| J14092        | UPC154      | T4                 | 4.07                   | -37.03          | -52.99           | -3158.49               |
| J14092        | UPC164      | T2                 | 5.38                   | -36.46          | -53.16           | -1188.35               |
| J14092        | UPC170      | D2                 | 4.45                   | -36.23          | -52.41           | -2535                  |

### 3.3.1.2 Physical Properties MSCL – Multi-Sensor Core Loggers

Petrophysical logging was also conducted by CM at BOSCORF (<http://www.boscorf.org/instruments/mscl-s>) and provides measurements of gamma-radiation attenuation, p-wave velocity and magnetic susceptibility (See Fig. 3.1). The two former measurements are semi-quantitative guides to sediment density, and in the materials investigated here primarily reflect percentage porosity and therefore grainsize. Magnetic susceptibility is controlled by the presence of heavy minerals e.g. zirconium, titanium etc., which are transported in the silt and sand fractions. This measurement is therefore a qualitative, but highly sensitive, index of grainsize (Croudace *et al.*, 2015).



*3.3.1.2.1 Gamma ray attenuation density*

A thin gamma ray beam was produced by a  $^{137}\text{Cs}$  gamma ray source at a radiation level of 370 MBq within a lead shield with a 5 mm collimator. The gamma ray detector on the Geotek MSCL-S composed of a scintillator and an integral photomultiplier tube. Bulk rock density was computed from GRA as follows:

*Equation 3.1 Equation for bulk density from GRA*

$$\rho = 1/(\eta d) \times \ln(I_0/I), \quad (1)$$

where

- $\rho$  = sediment bulk density,
- $\eta$  = Compton attenuation coefficient,
- $d$  = sample diameter,
- $I_0$  = gamma source intensity, and
- $I$  = measured intensity of gamma rays passing through the sample.

Because  $\eta$  and  $I_0$  are treated as constants,  $\rho$  can be calculated from  $I$ . For calibration, we used a set of aligned aluminum cylinders of various diameters, surrounded by distilled water in a sealed core liner. Gamma ray counts were taken through each cylinder for a period of 4 s, and  $\ln(I)$  was plotted against  $\eta d$ . For the calibration cylinders,  $\rho$  was  $2.71 \text{ g cm}^{-3}$  and  $d$  was 1, 2, 3, 4, 5, or 6 cm. The relationship between  $I$  and  $\eta d$  can be expressed as follows:

*Equation 3.2 Relationship between  $I$  and  $\eta d$*

$$\ln(I) = A(\eta d)^2 + B(\eta d) + C, \quad (2)$$

where  $A$ ,  $B$ , and  $C$  are coefficients determined during calibration. For cores and cuttings, density measurements were conducted every 4 cm. The spatial resolution was 5 mm (collimator diameter), so each data point reflects the properties of the surrounding 5 mm interval.

### 3.3.1.2.2 *P*-wave velocity

*P*-wave (primary or pressure wave, one of the two main elastic body or seismic waves) velocity ( $V_P$ ) was measured for discrete core samples in a time-of-flight mode, by measuring sonde length and traveltime:

Equation 3.3 Equation for *p*-wave velocity

$$V_P = d/t, \quad (3)$$

where

- $d$  = distance traveled through the core, and
- $t$  = traveltime through the core.

*P*-wave velocity transducers are mounted on the MSCL system and measure  $d$  and  $t$  perpendicular to core axis at each measurement point. Total traveltime measured between the transducers includes three types of correctable delays:

- $t_{\text{delay}}$  = delay related to transducer contact faces and electronic circuitry,
- $t_{\text{pulse}}$  = delay related to the peak detection procedure, and
- $t_{\text{liner}}$  = transit time through the core liner.

The effects of delays are calibrated using a core liner filled with pure water. For routine measurements on whole-round cores in core liners, the corrected core velocity can be expressed by:

Equation 3.4 Corrected core velocity after calibration

$$V_{P_{core}} = (d'_{core} - 2d_{liner}) / (t_{total} - t_{pulse} - t_{delay} - 2t_{liner}) \times 1000, \quad (4)$$

where

- $V_{P_{core}}$  = corrected velocity through core (m/s),
- $d'_{core}$  = measured diameter of core and liner (mm),
- $d_{liner}$  = liner wall thickness (mm), and
- $t_{total}$  = measured total travel time ( $\mu$ s).

#### 3.3.1.2.3 Magnetic susceptibility

Magnetic susceptibility is the degree to which a material can be magnetized by an external magnetic field. A Barrington loop sensor (MS2C) with a 12 cm loop diameter was used for magnetic susceptibility measurements (Fig. 3.1). An oscillator circuit in the sensor produces a low-intensity ( $8.0 \times 10^{-4}$  mA m<sup>-1</sup> RMS), non-saturating, alternating magnetic field (0.565 kHz). Any material near the sensor that has a magnetic susceptibility causes a change in the oscillator frequency. This pulse frequency is then converted into a magnetic susceptibility value. The spatial resolution of the loop sensor is ~4 cm, and its accuracy is 5%. Magnetic susceptibility data were obtained at 1 cm intervals with an acquisition time of 1 s.

#### 3.3.1.2.4 Values of L, C and H

In this study, we use the lightness (L), chroma (C) and hue (H) system proposed by Giosan *et al.* (2002) to parameterise rock colour. Lightness has been used in numerous studies as an indicator of carbonate composition, as carbonate (usually white in most settings) will naturally reflect more light (Giosan *et al.*, 2002; Rogerson *et al.*, 2006). Hue and chromaticness have been shown to be sensitive to the content and redox state of iron (Giosan *et al.*, 2002). However, the response of colour to chemical and mineralogical changes is non-linear, and quantitative estimation of sediment composition is difficult (Giosan *et al.*, 2002). Here, we support colour data with chemical data from ITRAX (an instrument that records optical, radiographic and elemental variations from sediment half cores) for analysis.

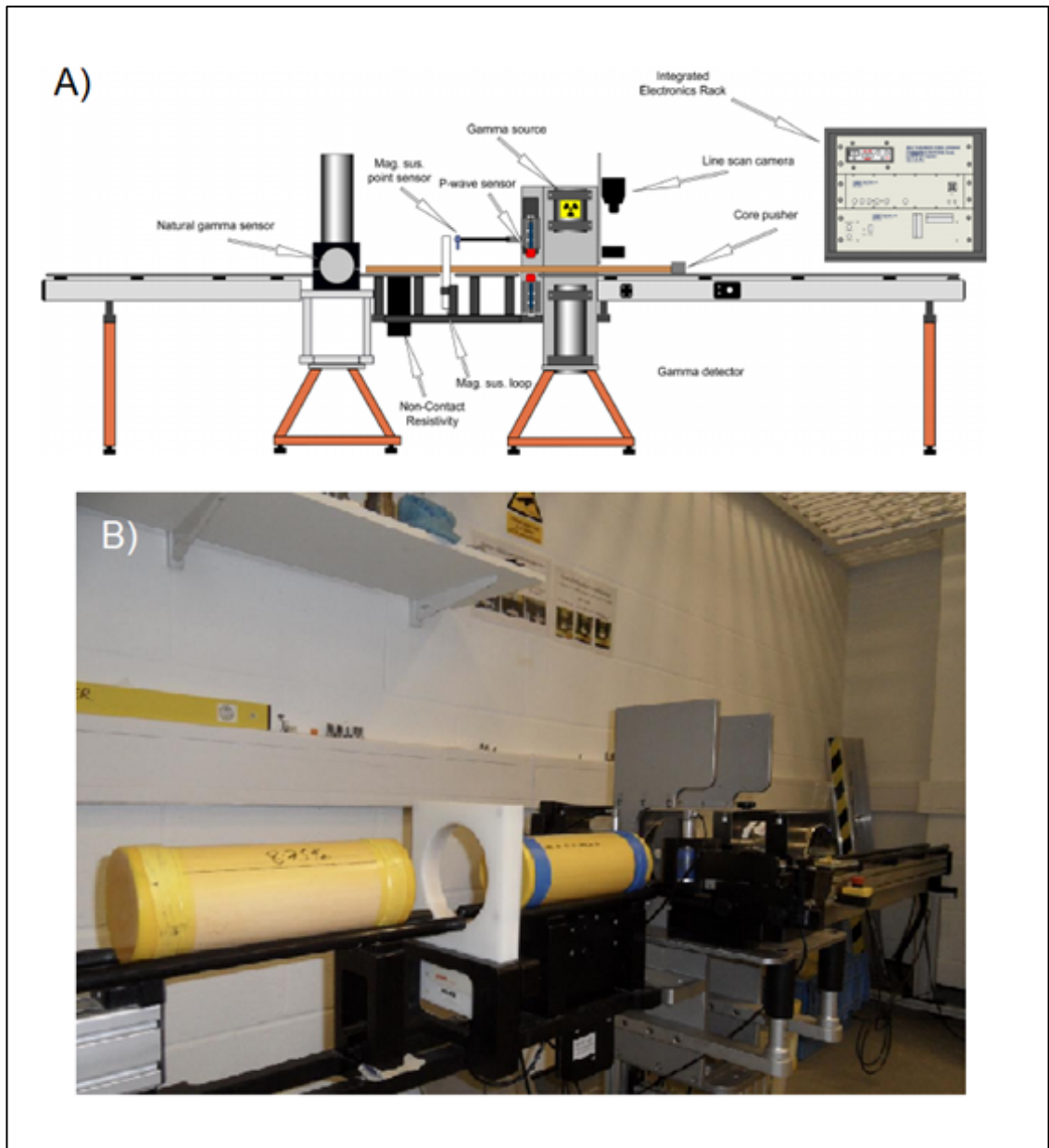


Figure 23.1 A) Schematic drawing of the Geotek Multi Sensor Core Logger (MSCL) located at BOSCORG, Southampton. B) Photo of whole core tube loaded onto the MSCL ready prior to a run

### 3.3.1.3 ITRAX – High-Resolution XRF Analysis of Sediment Cores

For sediment cores, graphic logging was supported by petrophysical and geochemical logging. XRF logging was done on the ITRAX instrument at BOSCORF (See Fig. 3.2) (<http://www.boscorf.org/instruments/itrax-high-resolution-xrf-analysis-sediment-cores>), using 60 kV and 45 maas excitement energies, with a dwell time of 800 ms, and a resolution of 200  $\mu\text{m}$ . This technique provides highly resolved, semi-quantitative measurements of the bulk chemistry of the sediment in the cores. One major advantage of the ITRAX system for facies analysis in contourite systems is its ability to produce a high-resolution optical x-ray image. This can be utilised by marine scientists to image density differences in soft sediment cores. It is a rapid and non-destructive technique for examining the internal structure of sediment cores. It reveals features that would otherwise be impossible to identify visually from the cores collected in the field site. It can be used to image bedforms, diagenetic features, bioturbation, ice-rafted debris and de-watering structures. Any feature within the sediment that exhibits a radiographic density contrast to the surrounding sediment can be imaged. This is useful when interpreting depositional environment, paleoclimate and diagenetic history of deposits (Croudace *et al.*, 2015).

ITRAX analysis is a rapid and non-destructive method of obtaining geochemical data from a core. The ITRAX instrument functions by progressively moving split core sections under a 3 kW Mo-tube X-ray source and XRF Si-drift chamber detector (Croudace *et al.*, 2006). It functions at 60 kV and 45 mA, with a dwell time of 800 ms and a resolution of 200  $\mu\text{m}$ . A sediment sample is irradiated with high energy X-rays from a controlled X-ray tube. When an atom in the sample is struck with an X-ray of sufficient energy (greater than the atom's K or L shell

binding energy), an electron from one of the atom's inner orbital shells is dislodged. The atom regains stability, filling the vacancy left in the inner orbital shell with an electron from one of the atom's higher energy orbital shells. The electron drops to the lower energy state by releasing a fluorescent X-ray. The energy of this X-ray is equal to the specific difference in energy between two quantum states of the electron. The measurement of this energy forms the basis of this analysis. Most atoms have several electron orbitals (K shell, L shell, M shell, for example). When X-ray energy causes electrons to transfer in and out of these shell levels, XRF peaks with varying intensities are created and will be present in the spectrum, a graphical representation of X-ray intensity peaks as a function of energy peaks. The peak energy identifies the element, and the peak height/intensity is generally indicative of its concentration.

On the ITRAX, the K-shell peak areas are measured automatically and converted to intensity (counts) for a designated element. The validity of the data was monitored using the distance from the sediment to the detector, element integral profiles and Compton scatter integral. No attempts have been made here to calibrate the ITRAX intensities to elemental concentrations, in their place we use element ratios. Elemental ratios reduce the effects caused by unit-sum constraint and dilution (Weltje & Tjallingii, 2008), and are a reliable indicator of semi-quantitative changes in the sediment composition. Here, selected ratios are used according to (Croudace *et al.*, 2006; Rothwell *et al.*, 2006), specifically, the element ratios listed and described in Table 3.2. Weltje & Tjallingii (2008) recommend using log-ratios to both calibrate the raw data and for comparing data as raw emission intensity is not linear with elemental concentration. They suggest



using log-ratios of intensities measured from XRF core scanners as they are related to log-ratios of concentrations by simple linear transformation.

For palaeoceanographic studies of core data, interest primarily lies in relative changes down-core and it is therefore sufficient to plot log-ratios of intensities. Weltje & Tjallingii (2008) found that records of log-ratios of intensities matched patterns of log-ratio concentrations and conclude that log-ratio intensities (used in this study) can be safely used for the purpose of qualitative interpretation or inter-core correlation without the need for calibration. Elemental ratios are used for the cross-plots in this study, log-ratios reduce scatter but show almost identical relationships. ITRAX has been used to glean information about grain size, palaeoceanographic conditions and diagenetic history of the sediment core. Ca content has been linked to glacial-interglacial cycles (Richter *et al.*, 2006). Zirconium/Aluminium (Zr/Al) peaks have been linked to Dansgaard-Oeschger events (Bahr *et al.*, 2014a) through peaks in bottom current velocity. ITRAX can also be used for heavy mineral investigations, provenance studies, organic matter content (Bahr *et al.*, 2014a) and oxygenation studies (Jansen *et al.*, 1998).

*Table 3.2 Summary of elemental ratios used in this study, their importance and key case studies that demonstrate their applications and reliability*

| <b>Elemental Ratio</b> | <b>Use</b>   | <b>Case study</b>  |
|------------------------|--|--|
| Ca/Fe                  | Carbonate stratigraphy;<br>core correlation;<br>terrigenous turbidite<br>mud discrimination. | (Rothwell and Rack,<br>2006)                                       |
| Si/Al                  | Changes in<br>aluminosilicates;<br>biogenic production                                       | (Tisserand <i>et al.</i> , 2009)<br>(Dickson <i>et al.</i> , 2010) |

|       |  |   |
|-------|--|---|
| Ti/Al | Increase in particle size, environmental energy changes  | (Spofforth, Pälike and Green, 2008)   |
| K/Al  | Provenance changes   | (Spofforth, Pälike and Green, 2008)   |
| Zr/Al | Bottom current intensity   | (van der Schee <i>et al.</i> , 2016)  |
| Mn/Al | Change in oxygenation levels   | (Spofforth, Pälike and Green, 2008)   |
| Mn/Ti | Identification of redox transitions. With loss of magnetic susceptibility records Fe reduction events                  | (Hepp <i>et al.</i> , 2009)   |
| Ca/Sr | Ice-rafted layers  | (Hodell <i>et al.</i> , 2008)   |
| Sr/Ca | Presence of high-Sr aragonite (requires shallow water source)  | (Rothwell and Rack, 2006)   |
| Fe/Rb | Mobilisation of Fe during redox related diagenesis   | (Rothwell and Rack, 2006)   |
| K/Rb  | Possibly enhanced within turbidite muds  | (Rothwell and Rack, 2006)<br>(Hunt <i>et al.</i> , 2011)  |
| Zr/Rb | Increased heavy resistate minerals   | (Rothwell and Rack, 2006)   |
| Ti/Rb | Increased heavy resistate minerals   | (Rothwell and Rack, 2006)   |
| Br/Cl | Presence of organic-rich layers, increased porosity  | (Rothwell and Rack, 2006)   |
| S/Cl  | Enrichment in organic matter   | (Thomson, Croudace and Rothwell, 2006)  |
| Mn/Fe | Identification of redox transitions, sub-oxic diagenesis   | (Marsh <i>et al.</i> , 2007)  |
| Fe/K  | Basaltic material in IRD, changes in terrigenous mineralogy, used as north/south source indicator and core correlation | (Kuijpers <i>et al.</i> , 2003)<br>(Blanchet, Thouveny and Vidal, 2009)<br>(Warratz <i>et al.</i> , 2017) |

|      |  |   |
|------|--|---|
| Ti/K | Variations in sediment source or grain size character, identification of IRD | (Brendryen, Hafliðason and Sejrup, 2010)<br>(Prins <i>et al.</i> , 2001)<br>(Siani <i>et al.</i> , 2010)<br>(Spofforth, Pälike and Green, 2008) |
|------|--|---|

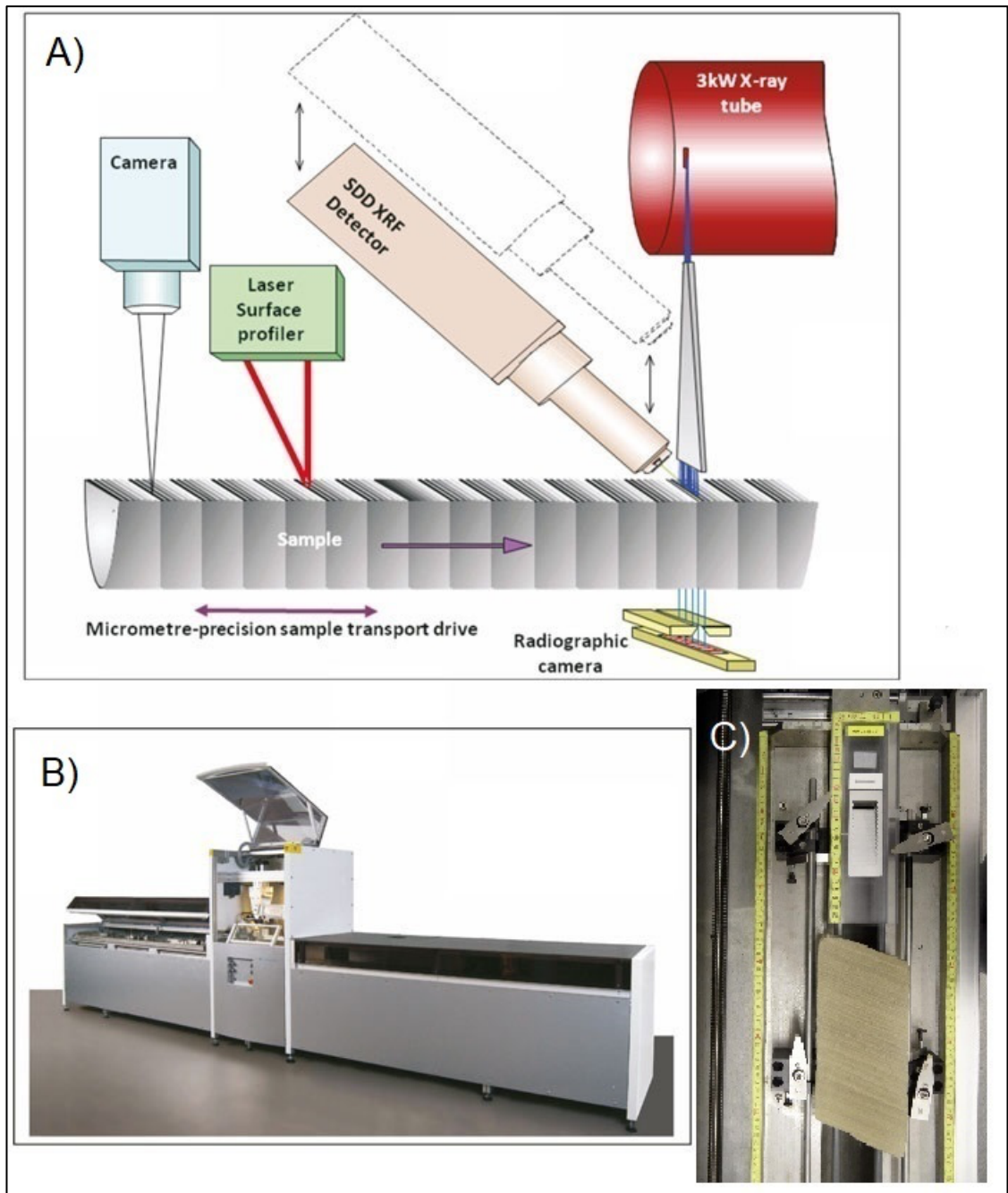


Figure 3.24 A) Schematic of ITRAX micro-XRF sediment core scanner showing the main components in the set up. B) ITRAX with sample and measuring turret doors open. C) Core loaded onto the ITRAX prior to a run.

#### 3.3.1.4 Gravimetric Grain Size Analysis

Sediment sieving was performed on discrete 10cm<sup>3</sup> sample over regular 10 cm depth intervals from the sediment core working halves. This was done to separate grain size fractions for weight percentage grain size analysis. The sample was weighed wet and then dried at 60 °C overnight and weighed again dry. This was done to estimate the water and salt content. The sample was first wet-sieved through a 63 µm mesh using ~500 ml of ultra-distilled water (15 MΩ) in a spray bottle. The water/sediment mixture was collected below the sieve in a 500 ml beaker for drying at 60 °C for ~3 days. This was done to preserve the fine fraction. The sand fraction residue collected in the sieve was transferred to a petri dish and dried overnight at 60 °C. The dried coarser residue was then dry sieved in a sieve stack consisting of mesh sizes 250 µm, 150 µm, 125 µm and 90 µm. All sediment fractions from the sample were then weighed and converted to percentages of the total weight.

#### 3.3.1.5 Micropalaeontological Investigation

To reduce the impact of post-mortem reworking Rogerson *et al.* (2006) used benthic foraminifera in the size fraction 150 µm recovered by a standard wet sieving method (Murray, 2006). Samples were dried in an oven at 60 °C overnight, split into suitably sized aliquots and picked using a damp brush into gridded micro-slides. Taxonomy was performed following (Loeblich and Tappan, 1988; Jones, 2011; Holbourn *et al.*, 2013), with additional information taken from (Murray, 2006). Following Rogerson *et al.* (2006), a total count >300 individuals were preferred for each sample but if this was not possible in these highly variable materials, whole samples were analysed.

Foraminiferal analyses (size fraction  $>150\ \mu\text{m}$ ) were conducted on 317 samples from eight cores/locality. A minimum of 300 specimens were picked from each sample, where this number of individuals could be reached. Out of the 317 samples, 45 were found to be barren of specimens and 160 contained  $<300$  forams. Large samples were split using a Green Microsplitter to facilitate counting. The number of splits was recorded and the total number of foraminifera in each sample was calculated accordingly (Schönfeld *et al.*, 2012; Appendix 3.1). Specimens of *Cibicidoides wuellerstorfi* and *Uvigerina perigrina* were extracted and used for the isotopic analyses (Section 3.3.2.) are included in the final counts. All benthic foraminifera were identified to the lowest taxonomic level and counted on a grided picking tray. Planktic foraminifera were counted for Benthic/Planktic ratios and to calculate a fragmentation index down each core as an indicator of preservational processes. Preservation of the foraminiferal tests was often poor in the lower sections of the cores with lower sedimentation rates. This complicated species identification, led to the large numbers of barren samples or samples with less than 300 individuals. A stereomicroscope LEICA STEREO EZ4 was used for the identification of individuals, which were picked, sorted and glued into grided microslides for reference and deposited in the geology collection at the University of Hull. For taxonomic references, see the appendix at the end of this thesis.

Abundances of foram taxa were classified as either epifaunal or infaunal based life position/habit. Epifaunal and infaunal taxa these were contrasted down each core to infer changes in export productivity/bottom water oxygenation throughout the studied interval in each of the interpreted environments (Jorissen *et al.*, 2007). A list of taxa with clear microhabitat (Epifaunal, shallow infaunal, intermediate

infaunal and deep infaunal) preferences was collected and considered in this analysis (Appendix 3.2) sources for this list are given in Chapter 6.

#### 3.3.1.6 Statistical Analyses

Multivariate statistical analyses were performed by using the PAST software package (version 3.0, Øyvind *et al.*, 2001) to define foraminiferal assemblages and to evaluate palaeoenvironmental changes over time. Q-mode cluster analysis (unweighted pair group method with arithmetic mean (UPGMA) algorithm, using Bray-Curtis similarity index of foram species composition) in order to group the samples according to their similarity in foraminiferal content (Chapter 6) (Øyvind *et al.*, 2001). Fifty-nine species, occurring with abundances >5% in at least one sample and representing on average 96.5% of the total sample, have been included in this analysis (Appendix 3.3). A cut-off level of 5% has been chosen to reduce noise by rare species (for this part of the analysis, not diversity calculations) and to reveal the dominant statistical patterns more clearly. This is to ensure that the clusters are distinct. Consequently, each cluster represents a group of samples with similar foraminiferal assemblages indicative of certain ecological conditions for us to distinguish between them. After all samples with the 8 cores were pooled SIMPER was used to compare Bray Curtis Similarity of each cluster (SIMPER, Bray-Curtis similarity index, all samples pooled, Chapter 6). This was done to assess which taxa are responsible for the observed differences between the groups of samples (Clarke, 1993).

### 3.3.2 Dating of Sediment Cores

Radiocarbon dating is an accurate method for dating sediments that are younger than 50,000 years (Walker, 2006). It has been widely utilised a variety of different sciences. It assesses the  $^{14}\text{C}$  isotope content of the material. In the atmosphere  $^{14}\text{C}$  combines with oxygen to form carbon dioxide and enters the carbon cycle to be used in the process of photosynthesis (Walker, 2006). The two stable isotopes of carbon are  $^{12}\text{C}$  and  $^{13}\text{C}$  and the unstable form is  $^{14}\text{C}$ . The unstable  $^{14}\text{C}$  decays towards a more stable  $^{14}\text{N}$ . The rate of this decay is called a half-life and this allows us to use the decay  $^{14}\text{C}$  for dating. The ocean is the largest carbon sink on Earth, holding 95% of the total carbon (Walker, 2006). This results in the organisms in the ocean incorporating a portion of this  $^{14}\text{C}$  into the carbonate of their tests. When the organisms die and become buried in the sediment on the seafloor they are no longer able to exchange carbon and isotope decay begins. The half-life can tell when a particular organism was buried in the sediment and therefore giving us the age of that sediment layer.

When preparing sediment samples from the cores for radiocarbon dating contamination is avoided by multiple cleaning steps of species-specific organism tests. Large samples were required of >20 cc in order to reach a sufficient amount of carbonate material, significantly less was required for the isotope analyses as only a few foram tests were needed to retrieve accurate results. To access the carbon, species-specific samples of grain sizes >150  $\mu\text{m}$  were picked in order to avoid biotic variation between species and the reworking by bottom currents (Reimer *et al.*, 2013). The forams need to be species-specific and of a similar size because isotopic fractionation differs between the species and what life stage an individual foram is in. This study used the planktonic foraminifera



species *G. inflata* as it was the only taxa abundant enough in all core samples to meet the criteria outlined above. Once the forams are washed with DI water, dried in an oven and picked into Eppendorf tubes they can be analysed for their  $^{14}\text{C}$  isotope content. The analysis was carried out by BETA Analytic in Florida using accelerator mass spectrometry (AMS) methods. The AMS measures the ratio of  $^{14}\text{C}$  to the stable  $^{12}\text{C}$  and  $^{13}\text{C}$  and uses this to calculate the progression of decay and thereby dating the sample. The carbon in the sample is first converted to graphite and bombarded by caesium ions ( $\text{Cs}^+$ ). This bombardment releases negative carbon atoms ( $\text{C}^-$ ) which are accelerated by magnets through the AMS until they are stripped of electrons and collect as  $\text{C}^{3+}$  ions of a different mass dependent on the isotopic number (Walker, 2006). The difference in mass of  $^{12}\text{C}/^{13}\text{C}$  and  $^{14}\text{C}$  can then be calculated.

The radiocarbon dates were calibrated by BETA Analytic with the high-probability density (HPD) range method using the MARINE13 calibration curve and no  $\Delta\text{R}$  (Reimer *et al.*, 2013). All ages are given in calibrated thousands of years before present (ka B.P.) (See Fig. 3.3 and Table 3.3). The errors quoted on the  $^{14}\text{C}$  age (+/- X BP) which are then used in the calibrations are strictly limited to determinate errors (the counting errors of the sample, modern  $^{14}\text{C}$  standard and background). Indeterminate errors such as sample homogeneity, relocation of samples (redeposition), and local reservoir effects in samples are not always quantifiable and should be considered in the interpretation of any calendar calibrated Conventional Radiocarbon Age. The age-depth model, sedimentation/accumulation rates and activity of the site were all calculated using the Bchron R package.

Table 3.3 Accelerator mass spectrometry (AMS) radiocarbon dates and calibrated ages. IRMS isotope values from *G. inflata* included

| Species           | Probability | Conventional age | 95.4% probability<br>Calibrated age<br>(cal ka B.P.) | Calibrated age,<br>Interpolated<br>from model |              |      |
|-------------------|-------------|------------------|--|---|--------------|------|
|                   |             |                  |  | IRM<br>S<br>d13<br>C                          | IRMS<br>d18O |      |
| <i>G. inflata</i> | 95.40%      | 1900 +/- 30 BP   | 1529 - 1358 cal BP                                   | 1470  | 1.7          | 2.59 |
| <i>G. inflata</i> | 95.40%      | 4550 +/- 30 BP   | 4835 - 4646 cal BP                                   | 4762  | 1.6          | 2.68 |
| <i>G. inflata</i> | 95.40%      | 8540 +/- 30 BP   | 9285 - 9051 cal BP                                   | 7932.5  | 1.4          | 2.73 |
| <i>G. inflata</i> | 95.40%      | 8330 +/- 30 BP   | 8996 - 8771 cal BP                                   | 8915  | 1.5          | 2.79 |
| <i>G. inflata</i> | 95.40%      | 10250 +/- 30 BP  | 11327 - 11147 cal BP                                 | 11218   | 1.3          | 3.09 |
| <i>G. inflata</i> | 95.40%      | 10470 +/- 40 BP  | 11861 - 11346 cal BP                                 | 11488   | -0.6         | 1.6  |
| <i>G. inflata</i> | 95.40%      | 10770 +/- 30 BP  | 12432 - 12046 cal BP                                 | 11698   | 1.2          | 3    |
| <i>G. inflata</i> | 95.40%      | 10580 +/- 30 BP  | 12035 - 11693 cal BP                                 | 11877   | 1.4          | 3.05 |
| <i>G. inflata</i> | 95.40%      | 10670 +/- 40 BP  | 12260 - 11825 cal BP                                 | 12022   | 1.4          | 3.13 |
| <i>G. inflata</i> | 95.40%      | 10680 +/- 40 BP  | 12294 - 11843 cal BP                                 | 12181.5                                       | 1            | 2.77 |
| <i>G. inflata</i> | 95.40%      | 10140 +/- 40 BP  | 11236 - 11040 cal BP                                 | 12726.5                                       | 1.2          | 3.2  |
| <i>G. inflata</i> | 95.40%      | 12600 +/- 40 BP  | 14218 - 13940 cal BP                                 | 13886.5                                       | 0.2          | 2.41 |

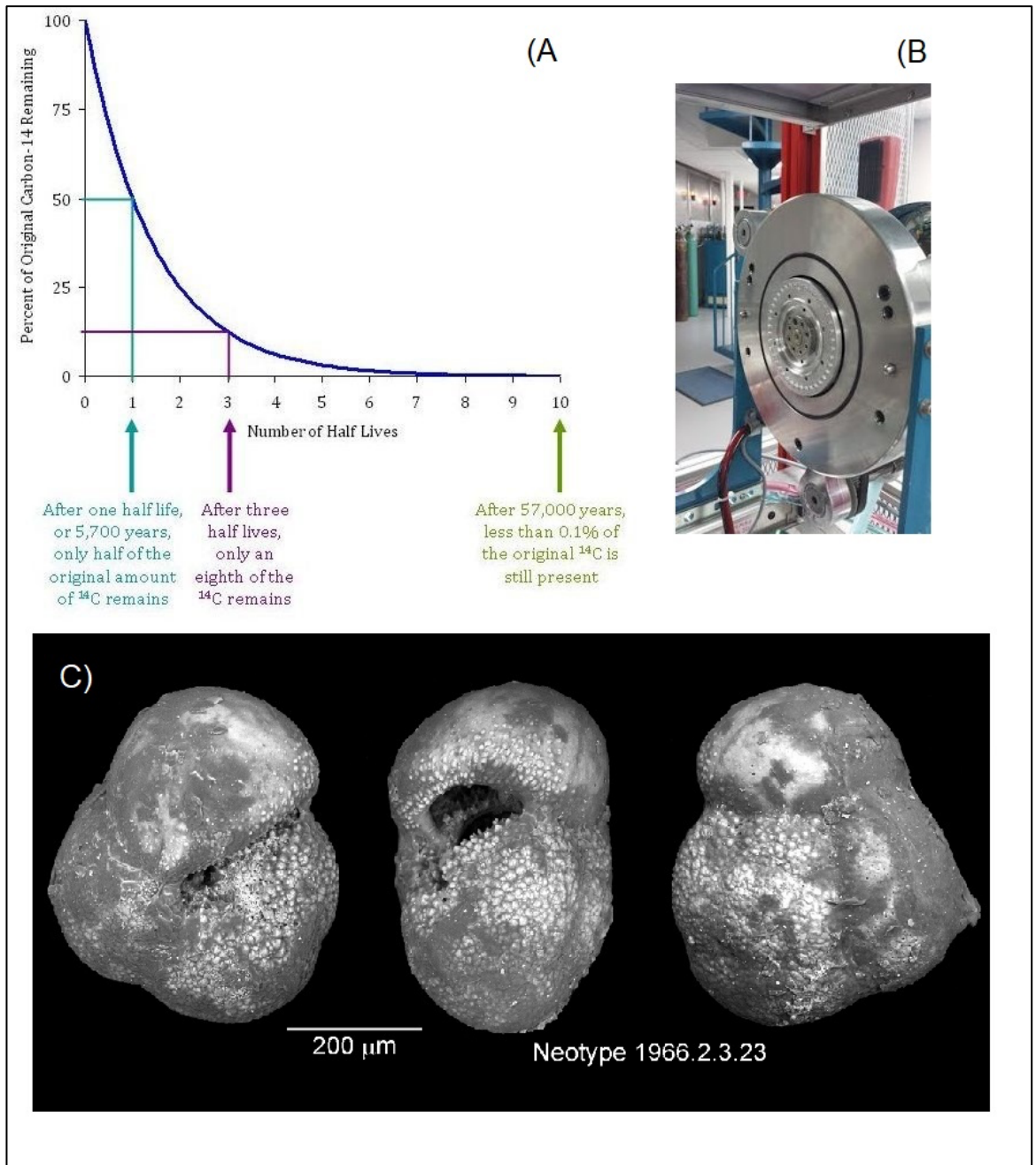


Figure 25 A) Radioactive decay (half-life) of  $^{14}\text{C}$ . Decay is exponential over time. B) Photo of the accelerator mass spectrometer at the BETA Analytic facility in Miami, Florida, USA. C) The planktonic foraminifera *G. inflata* used in this study. Image sourced from Microtax.org.

### 3.3.3 Stable Isotope Analysis

Foraminiferal  $\delta^{18}\text{O}$  and  $\delta^{13}\text{C}$  ( $\delta$  denotes the relative deviation of the molecule ratio for a measured sample from the molecule ratio of a standard) were measured on species specific samples of 3 – 10 *Cibicidoides wuellerstorfi* and *Uvigerina peregrina* tests each. Approximately 30 – 100 microgrammes of carbonate were used for isotope analysis using a Thermo Delta V Advantage isotope ratio mass spectrometer which is interfaced with a GasBench II universal on-line gas preparation and introduction system, a PreCon Trace Gas Pre-Concentrator and a Flash 2000 Elemental Analyser located at Northumbria University, Newcastle, UK (See Figure 3.4). Isotope values ( $\delta^{13}\text{C}$ ,  $\delta^{18}\text{O}$ ) are reported as per mille(‰) deviations of the isotopic ratios ( $^{13}\text{C}/^{12}\text{C}$ ,  $^{18}\text{O}/^{16}\text{O}$ ) calculated to the VPDB scale using a within- run laboratory standard calibrated against NBS standards for both C and O. Analytical reproducibility of the standard calcite is 0.1‰ for  $\delta^{13}\text{C}$  and  $\delta^{18}\text{O}$ . A single continuous stable isotope dataset from a single species cannot be generated from the entire core due to dissolution and strong ecological gradients through time. To maximise the range of the stable isotope record down-core, a composite record was generated taking into account isotope offsets between different co-existing species. It is assumed that *Cibicidoides wuellerstorfi* is calcifying in equilibrium with seawater, shows average  $\delta^{18}\text{O}$  values close to the bottom water. *Cibicidoides wuellerstorfi* disappears down-core to be replaced with a high abundance of *Uvigerina peregrina*. Therefore, *Uvigerina peregrina* was used as a replacement for *Cibicidoides wuellerstorfi* taking its shallow infaunal microhabitat effect into account as an offset ( $-0.72 \pm 0.35$ ) to true  $\delta^{18}\text{O}$  values. (Hoogakker *et al.*, 2010).

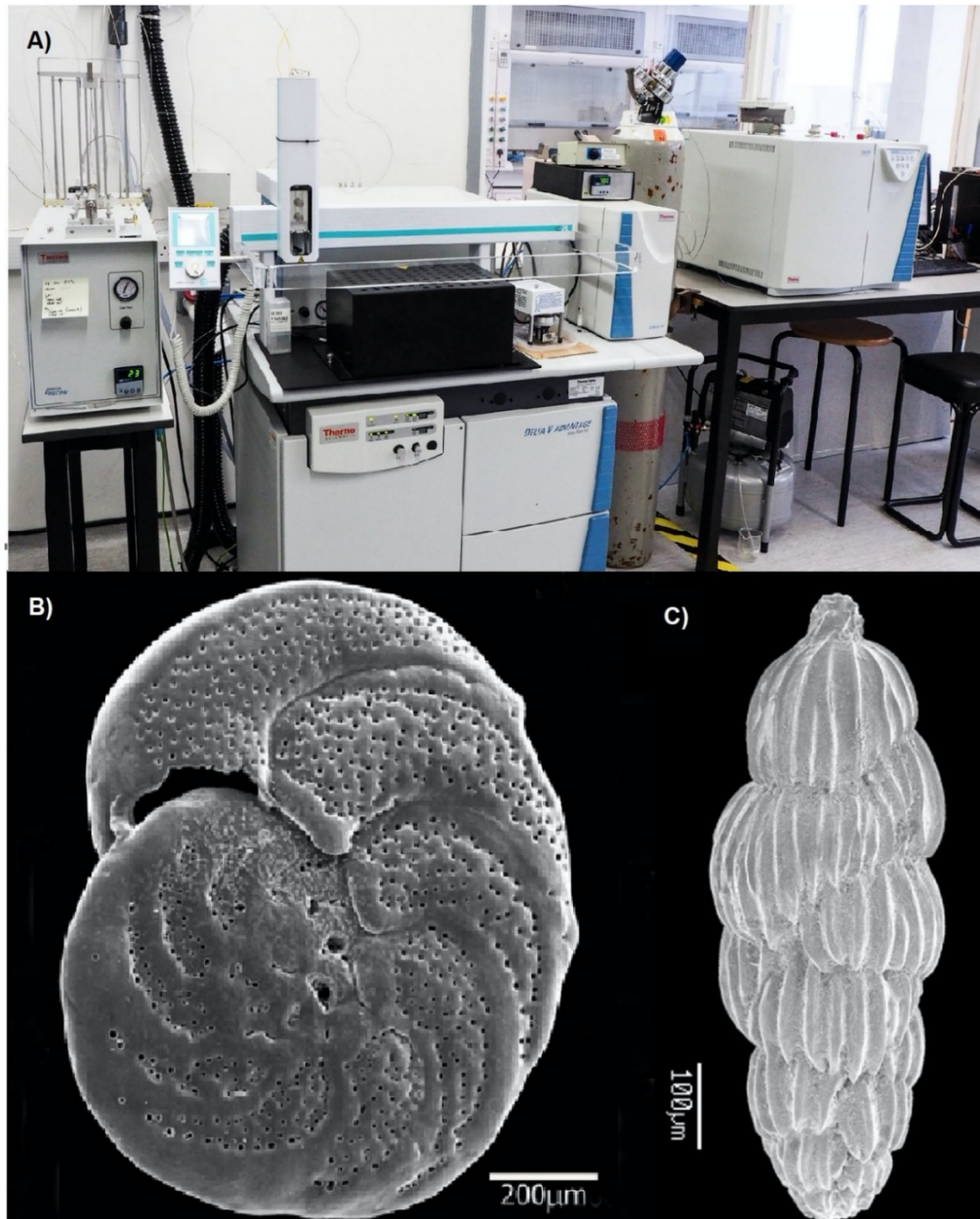


Figure 26 A) Photo of the Thermo Delta V Advantage isotope ratio mass spectrometer which is interfaced with a GasBench II universal on-line gas preparation and introduction system, a PreCon Trace Gas Pre-Concentrator and a Flash 2000 Elemental Analyser at Northumbria University. B) SEM image example of *Cibicides wuellerstorfi* used in this study sourced from [foraminifera.eu](http://foraminifera.eu). C) SEM image example of *Uvigerina peregrina* used in this study sourced from [foraminifera.eu](http://foraminifera.eu)

# CHAPTER 4

---

## SEDIMENTARY ANALYSIS

### *A Mixed Contourite Depositional System on a Passive Continental Margin*

#### 4.1 Introduction

This Chapter will report the composition, lateral and stratigraphic arrangement of sedimentary materials, and discuss how these observations fit into existing models of the Uruguay slope sedimentary system derived from geophysical analysis. A facies model for the system was developed, which will underpin palaeoceanographic (Chapter 5) and micropalaeontological (Chapter 6) objectives. This Chapter will first describe the grainsize of 77 out of the 86 core tops selected as representative of the available 212 core tops from this region. Second, it will describe the subsurface characteristics of 8 cores selected to be representative of the depositional types (Fig. 4.1) found in the core tops, six of which were chosen for further high-resolution core scanning. Third, it will compare the core top and downcore sediment types to the depositional environments identified by Hernandez-Molina *et al.* (2016) on the basis of geophysical response, to cross-validate the two approaches. Finally, it will develop a summative facies model for the region, permitting comparison of palaeo- and modern sea floor environments.

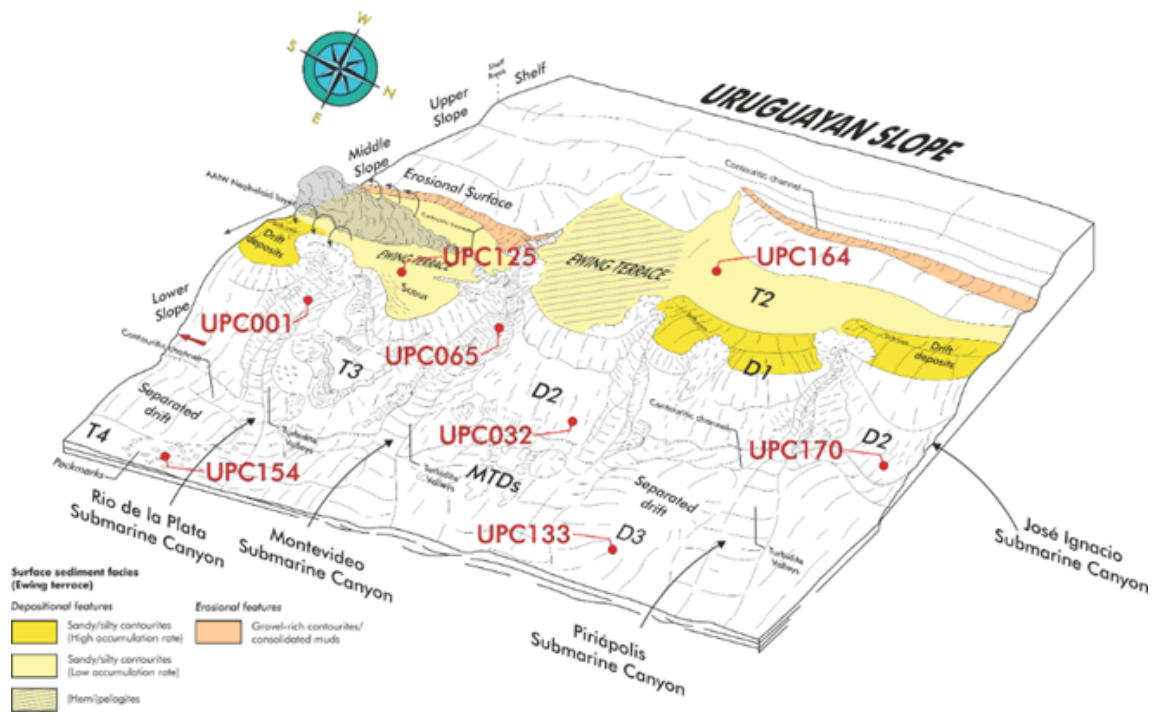


Figure 27 Schematic diagram of core locations and morphosedimentary environments off Uruguay. Study area is  $\sim 10,000 \text{ km}^2$

## 4.2 Results

### 4.2.1 Selection of Core Tops and Cores for Analysis.

A selection of 72 from the 180 core top samples were analysed by gravimetric grain size across the study area (Table 4.1). These were selected at random from the bathymetric map to obtain a representative sample set of surface sediments (0-1 cmbsf) from the slope. Gravimetric grain size results for core top samples are summarised in Figure 4.2 and the key results show that grain size across the modern Uruguayan margin (~10,000 km<sup>2</sup>) range from mud to very coarse sand. Sorting range from very poor to moderately sorted. There was a distinctive bimodal grain size distribution on the middle slope drift sediments from core top measurements, where the sediments are mud-rich (<63 µm comprises 70-80%) while also containing high percentages of medium and coarse sand (>150 micron percentages of >20%).

These sampled locations were then matched to interpreted sedimentary environments from Hernández-Molina *et al.*, (2016) and the sample set was found to cover each environment sufficiently to allow a comparison of modern surface grain size to modern interpreted sedimentary environment from bathymetric and seismic data of previous studies. Figure 4.2 showed a distinctive concentration of larger grain sizes/lack of fine fraction on the mid slope terrace (T2) suggesting stronger current activity. The bimodal and unsorted nature of the slope drift and canyon settings indicate weaker currents and hemipelagic deposition, while the mud-rich lower slope and terrace implied a quiescent environment. This evidence largely agrees with observations made by previous studies from bathymetric and seismic surveys and allowed the selection of specific full sediment cores to target each sedimentary environment.



Table 4.1 Summary of core numbers, geographical location and interpreted sedimentary environment from (Hernández-Molina et al., 2016)

| Core No. | Water Depth (mbsl) | Lat        | Long        | Environment      |
|----------|--------------------|------------|-------------|------------------|
| UPC001   | -2053.05           | -36.924475 | -53.4083588 | Drift 1          |
| UPC003   | -2205.15           | -36.868737 | -53.2626022 | Drift 1          |
| UPC006   | -2376.17           | -36.90556  | -53.2993741 | SCS              |
| UPC007   | -2030.88           | -36.853267 | -53.3836603 | Drift 1          |
| UPC015   | -1727.23           | -36.366575 | -52.9515103 | SCS              |
| UPC016   | -1735.54           | -36.389122 | -52.9189496 | SCS              |
| UPC017   | -1921.32           | -36.409082 | -52.8880374 | SCS              |
| UPC018   | -2153.75           | -36.430651 | -52.8545162 | Drift 1          |
| UPC019   | -2315.26           | -36.450076 | -52.8231931 | Drift 1          |
| UPC020   | -2357.43           | -36.471482 | -52.792952  | Drift 3          |
| UPC021   | -1926.15           | -36.494882 | -52.9157595 | Drift 1          |
| UPC022   | -2027.53           | -36.460702 | -52.8822976 | Drift 1          |
| UPC023   | -2046.34           | -36.394275 | -52.8172177 | SCS              |
| UPC025   | -2445.71           | -36.222837 | -52.5318538 | SCS              |
| UPC026   | -2403.8            | -36.196782 | -52.5069146 | Turbidite Valley |
| UPC027   | -2379              | -36.181462 | -52.4900151 | Turbidite Valley |
| UPC028   | -2353              | -36.151469 | -52.4627118 | Turbidite Valley |
| UPC029   | -2291              | -36.159146 | -52.5244349 | Turbidite Valley |
| UPC030   | -2345              | -36.17311  | -52.5040255 | Turbidite Valley |
| UPC031   | -2468              | -36.207149 | -52.4497701 | Turbidite Valley |
| UPC032   | -2513.29           | -36.618583 | -52.921055  | Drift 2          |
| UPC033   | -2582.33           | -36.596692 | -52.8996626 | SCS              |
| UPC033R  | -2588.53           | -36.595914 | -52.8986675 | SCS              |
| UPC035   | -3026.75           | -36.91654  | -52.911178  | Turbidite Valley |
| UPC047   | -2221              | -36.121844 | -52.586321  | SCS              |
| UPC048   | -2568              | -36.242137 | -52.3980638 | Turbidite Valley |
| UPC052   | -1967.23           | -36.907358 | -53.3913002 | Drift 1          |
| UPC053   | -2115.24           | -36.539009 | -53.0234345 | SCS              |

---

|        |          |            |             |                     |
|--------|----------|------------|-------------|---------------------|
| UPC058 | -2255.28 | -36.725195 | -53.2085726 | SCS                 |
| UPC059 | -1798.8  | -36.819369 | -53.3033253 | Terrace 3           |
| UPC064 | -1263    | -36.496164 | -53.1264063 | Terrace 2           |
| UPC065 | -1896.61 | -36.665504 | -53.2952865 | SCS                 |
| UPC070 | -2308.6  | -36.881965 | -53.3384067 | SCS                 |
| UPC081 | -1895.64 | -36.832516 | -53.3177981 | Terrace 3           |
| UPC083 | -2165.47 | -36.865755 | -53.322436  | Terrace 3           |
| UPC087 | -2413.31 | -36.921172 | -53.2508894 | Terrace 3           |
| UPC091 | -2644.1  | -36.878949 | -53.0243631 | Turbidite Valley    |
| UPC094 | -2945.89 | -37.033022 | -53.038993  | Pockmarks Terrace 4 |
| UPC099 | -3042.41 | -37.079049 | -53.0532845 | Pockmarks Terrace 4 |
| UPC102 | -2933.09 | -37.121702 | -53.0945621 | Pockmarks Terrace 4 |
| UPC104 | -2726.85 | -36.846571 | -52.9912956 | Turbidite Valley    |
| UPC105 | -2732.17 | -36.791325 | -52.93678   | MTD                 |
| UPC106 | -2929.9  | -36.754193 | -52.8999323 | Turbidite Valley    |
| UPC108 | -2421.81 | -36.29971  | -52.6756042 | Drift 2             |
| UPC109 | -2433.06 | -36.350173 | -52.6519866 | Turbidite Valley    |
| UPC110 | -2355.29 | -36.367102 | -52.6686941 | Turbidite Valley    |
| UPC114 | -1373    | -36.358993 | -53.1226705 | Terrace 2           |
| UPC118 | -1599.87 | -36.464536 | -52.9589768 | Terrace 2           |
| UPC119 | -1371.52 | -36.424925 | -53.0211904 | Terrace 2           |
| UPC121 | -1476    | -36.342272 | -53.0789629 | SCS                 |
| UPC122 | -1154.19 | -36.504248 | -53.2110137 | Terrace 2           |
| UPC123 | 1194.3   | -36.456356 | -53.162929  | Terrace 2           |
| UPC124 | -1710.71 | -36.63271  | -53.414625  | SCS                 |
| UPC125 | -1121.22 | -36.848313 | -53.633011  | Scour Terrace 2     |
| UPC126 | -1813.79 | -36.832586 | -53.4151823 | Scour Terrace 2     |
| UPC127 | -2359.73 | -36.295563 | -52.6833075 | Drift 2             |
| UPC128 | -2546    | -36.457355 | -52.633024  | Turbidite Valley    |
| UPC130 | -2571    | -36.447885 | -52.6254338 | Turbidite Valley    |
| UPC132 | -2559.1  | -36.576179 | -52.6444766 | Drift 3             |
| UPC133 | 2451     | -36.503157 | -52.5727512 | Drift 3             |

---

---

|         |          |            |             |                  |
|---------|----------|------------|-------------|------------------|
| UPC136  | -2499    | -36.554527 | -52.6722774 | Drift 3          |
| UPC137  | -2535.53 | -36.59547  | -52.7134335 | MTD              |
| UPC139  | -2499    | -36.529169 | -52.7061566 | Drift 3          |
| UPC142  | -2682.11 | -36.763564 | -52.9812463 | Turbidite Valley |
| UPC145  | -1595.39 | -36.494209 | -52.9821766 | Drift 1          |
| UPC148B | -2622    | -36.514112 | -52.4821983 | Drift 3          |
| UPC149  | -1437.84 | -36.912907 | -53.5673064 | Drift 1          |
| UPC158  | -1115.79 | -36.737498 | -53.4904684 | Terrace 2        |
| UPC159  | -1460.25 | -36.639907 | -53.2399401 | Terrace 2        |
| UPC160  | -1310.81 | -36.455209 | -53.0593882 | Terrace 2        |
| UPC161  | -1241.64 | -36.420002 | -53.1285043 | Terrace 2        |
| UPC162  | -1285.35 | -36.444659 | -53.0784208 | Terrace 2        |
| UPC170  | -2535    | -36.231584 | -52.4125589 | Turbidite Valley |
| UPC171  | -2260.92 | -36.139409 | -52.5581642 | SCS              |
| UPC172  | -2425    | -36.194747 | -52.4704114 | Turbidite Valley |
| UPC177  | -2377    | -36.165621 | -52.4752585 | SCS              |
| UPC182A | -1036    | -36.459587 | -53.2758593 | Terrace 2        |

---

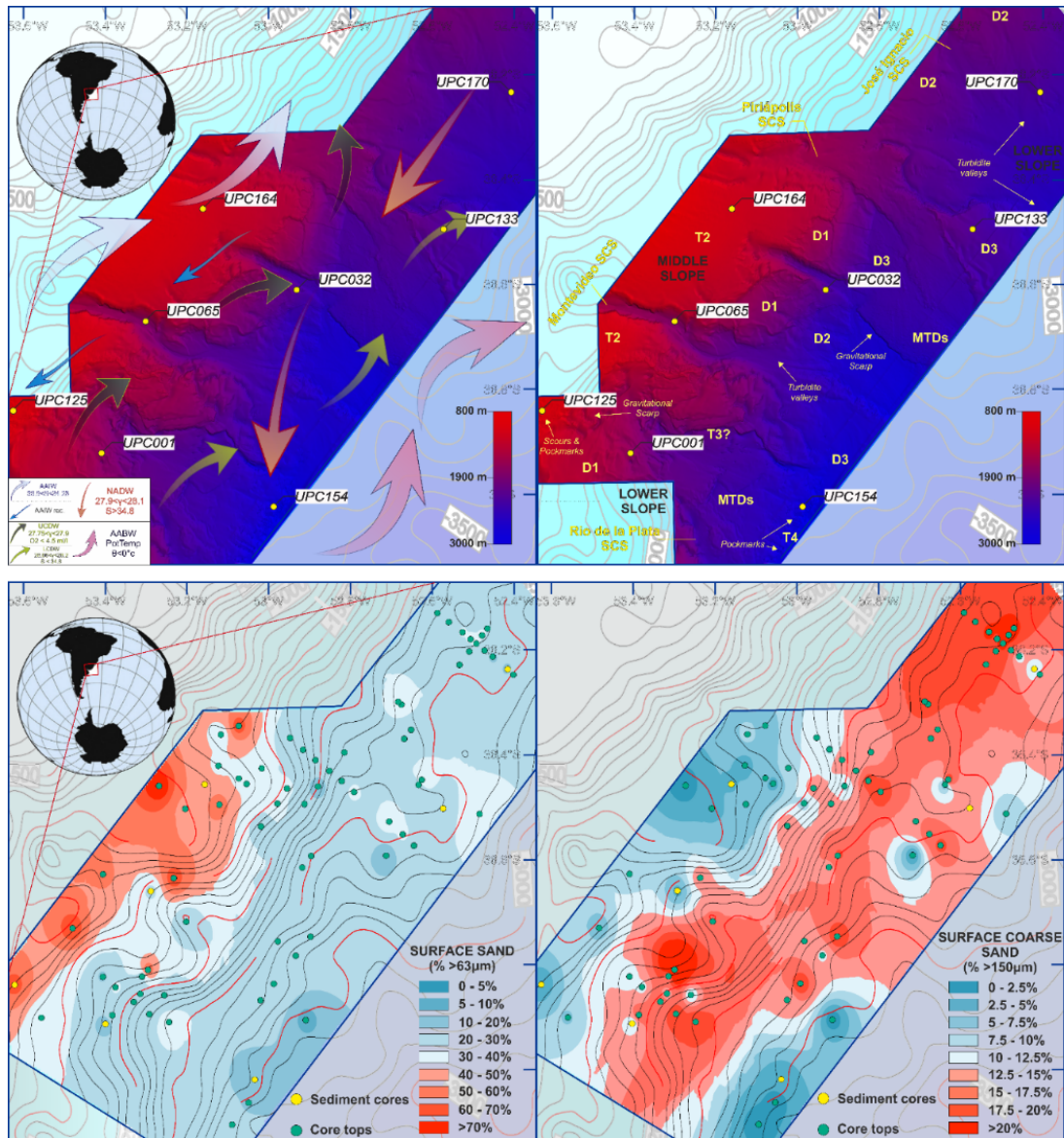


Figure 28 a) Sediment core locations (Table 4.1), watermass positions and flow directions on the seismically generated seabed offshore of Uruguay. Polygon indicates area surveyed with high resolution seismic and bathymetry b) Core locations and interpreted morphosedimentary environments adapted from (Hernández-Molina et al., 2016). c) Modern day  $>63 \mu\text{m}$  sand distribution across the slope generated using newly acquired core top grain size data and contour maps were compiled using a squared inverse distance weighted regression in ArcGIS. Yellow dots indicate full sediment cores, while green dots indicate areas where core top (0-1 cmbsf) were sampled. d) Modern day  $>150 \mu\text{m}$  coarse sand distribution across the slope.

#### 4.2.2 Sedimentary Logging, Physical Properties & Grain Size Results

Eight sediment cores were selected and have been logged in detail (Appendix 4.1). From these it was possible to identify grain size trends, abrupt depositional or hiatal surfaces and degree of bioturbation. Fining upwards grain size trends and mud caps were identified in the canyons. Distinctive green and orange muds were apparent in the deeper lower slope and terrace (T4) with a high degree of bioturbation. Figure 4.3 highlights an example of the mid slope terrace (T2) where the sediment was sandy, had developed sediment structures such as cross bedding and had extensive, large scale bioturbation structures. A more detailed bioturbation log was sketched to aid interpretation of the clearer structures seen in this core. From these observations it was possible to target sampling for gravimetric grain size sampling to further the interpretation made visually.

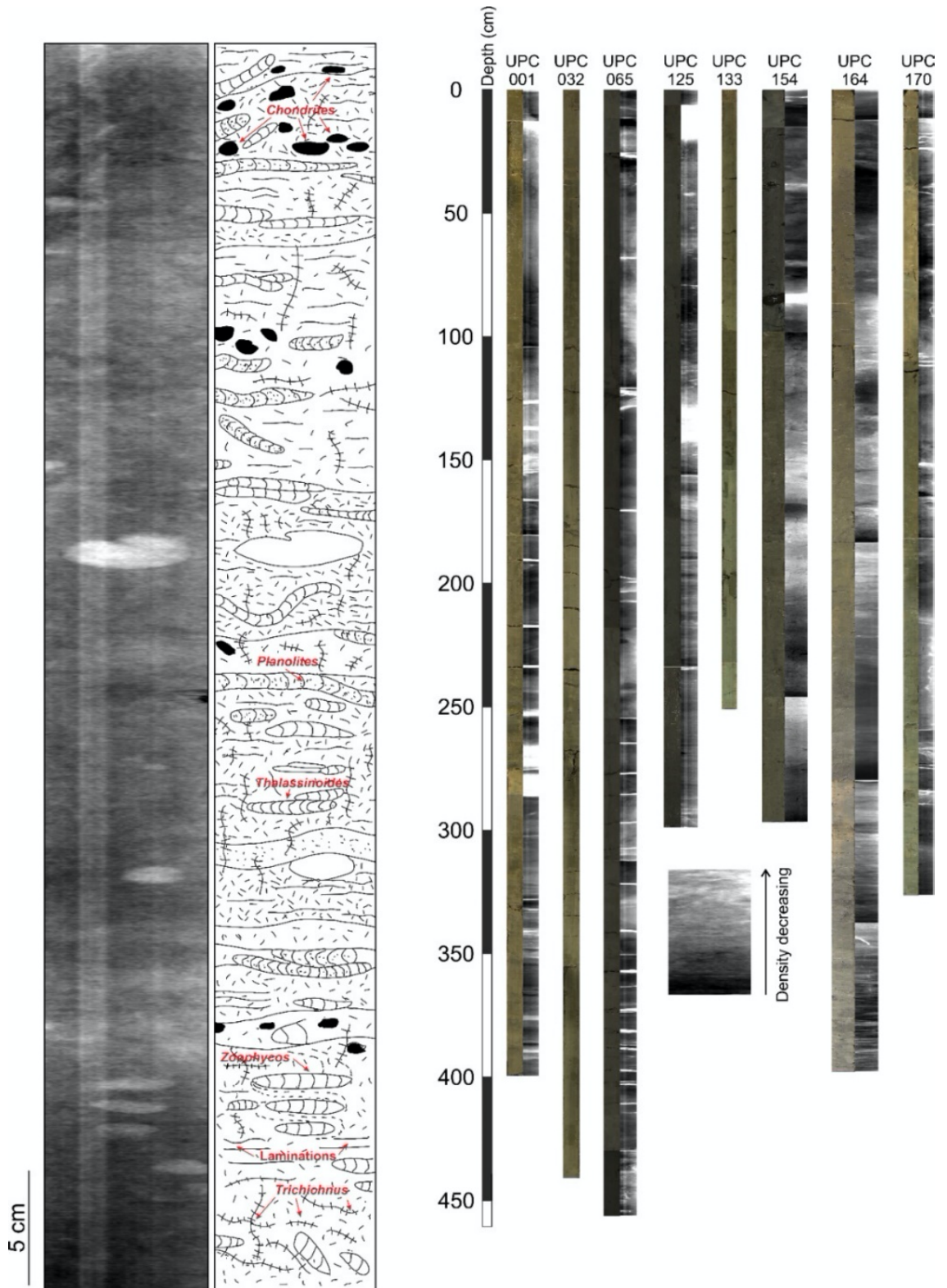


Figure 29 a) Interpreted bioturbation types in the 8 piston cores collected from the Uruguay slope. Left image is an x-radiograph of core UPC125 (25-75 cm) and interpretive sketch of the ichnofacies. Lighter areas indicate low densities while darker areas indicate higher density material. To the right is the interpreted section. b) The eight piston cores and their accompanying core photographs and x-radiographs.



Gravimetric grain size fractions of >250, 150-250, 125-150, 90-125, 63-90 and <63 microns are plotted against depth in Figures 4.4 to 4.11. Cores from the middle slope contourite terraces (UPC125, Fig. 4.7 & 164, Fig. 4.10) contain the highest proportion of larger grain sizes, while the deeper contourite terrace and canyons show the highest proportion of smaller grain sizes (UPC065, Fig 4.6 & UPC154, Fig.4.8). There are distinctive shifts in grain size from small to large sizes within the drift and deeper terrace cores (UPC133, Fig. 4.7, UPC154, Fig. 4.8 & UPC170, Fig. 4.11).

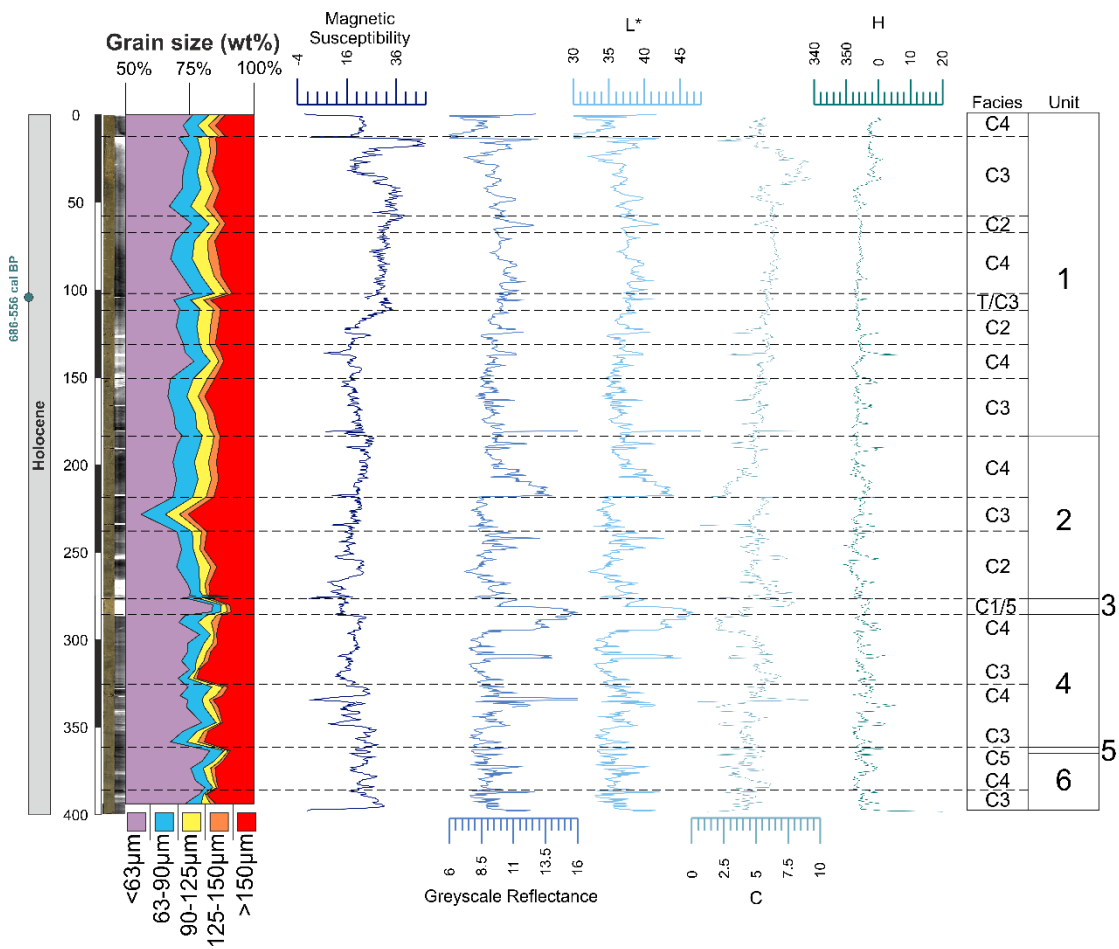


Figure 30 UPC001 (Drift 1) Photograph, radiograph, grain size and Multisensor Core Logger (MSCL) plots of sediment physical properties against depth in seafloor. Interpreted sedimentary facies demarcated by dashed lines and grouped into units of similar characteristics of grain size, bioturbation, sedimentary structures and MSCL values of colour (L\*(lightness), C(Chroma), H(Hue)) and magnetic susceptibility.

Magnetic susceptibility in the drift and higher accumulation areas of the mid slope terrace cores UPC001, UPC032 and UPC125 have more gradual changes through time than cores from the canyon (UPC065) and lower accumulation areas of the mid slope terrace (UPC164). UPC065 and UPC164 are punctuated by higher values that correspond with changes in measured grain sizes. Cores on the lower slope drifts and terraces (UPC133, UPC154 and UPC170) contain a single dominant peak twice the size of the background, that marks the transition from mud dominated sediment to more sand-rich sediment and this provides a potential marker across the slope for core correlation.



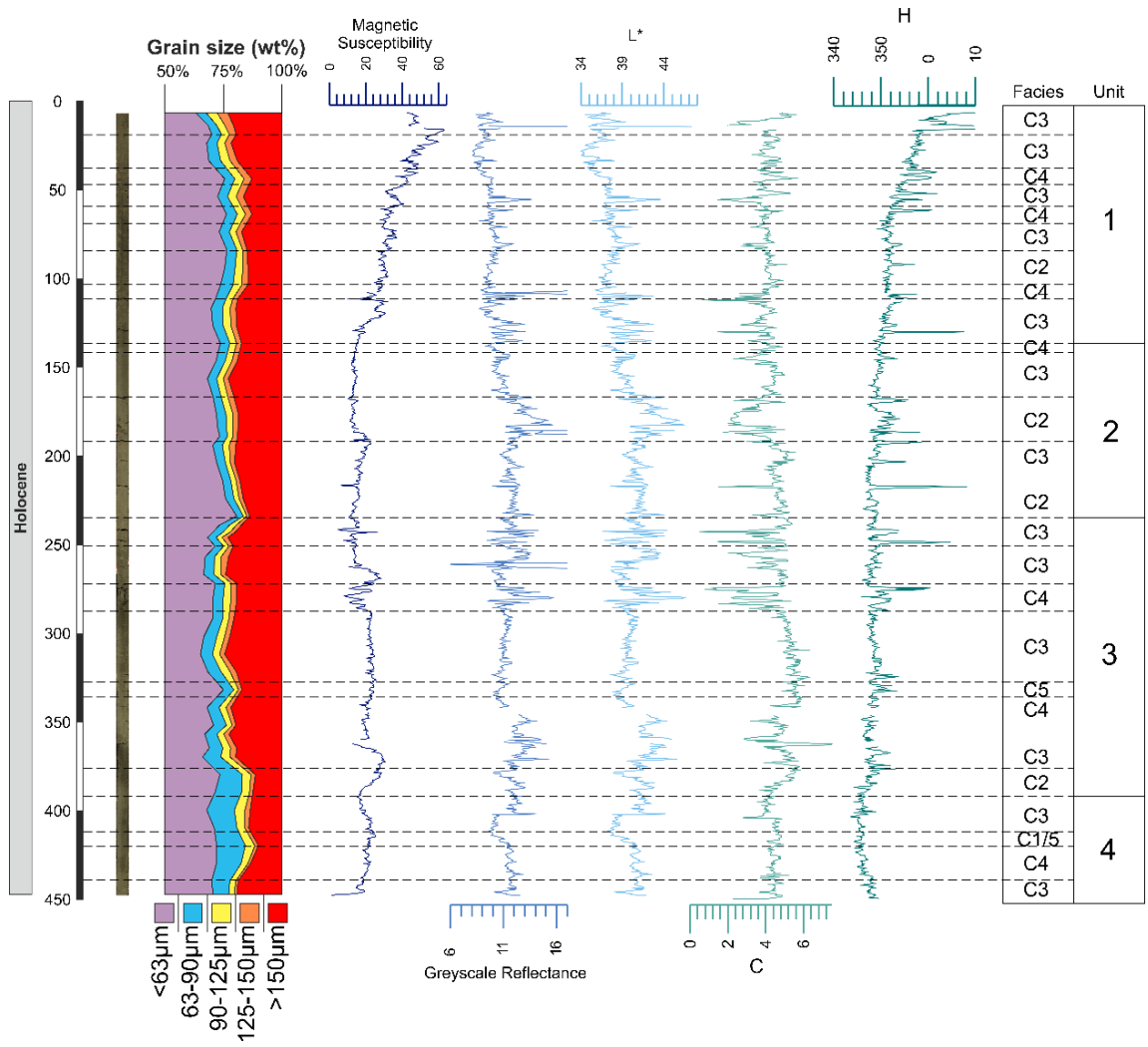


Figure 31 UPC032 (Drift 2) Photograph, radiograph, grain size and Multisensor Core Logger (MSCL) plots of sediment physical properties against depth in seafloor. Interpreted sedimentary facies demarcated by dashed lines and grouped into units of similar characteristics of grain size, bioturbation, sedimentary structures and MSCL values of colour (L\*(lightness), C(Chroma), H(Hue)) and magnetic susceptibility.

Colour values of L\* (Lightness), C (Chroma) and H (Hue) for the sediment were used to estimate carbonate content and potentially for the identification of any redox horizons. L\* is Greyscale reflectance, which reflects the presence of inorganic carbon in marine sediments (Giosan, *et al.* 2002). High proportions of carbonate are observed continuously throughout cores from the midslope drifts and areas of the mid slope terrace that have high accumulation rates (UPC001, UPC032 and UPC125) where we see a variable L\* values down core. In the lower slope cores (UPC133, UPC154 and UPC170) we only see these variations in the upper portions of the core, indicating that in these areas carbonate is absent at depth. Core UPC164 from the mid slope terrace is problematic, as the lower sections (> 130 cmbsf) of this core are actually carbonate-free (see below) but still show large variations in the L\* record. These L\* values appear to be a surface-shine artefact, and reflect the large grain size changes within this section of core. This is supported by a distinct shift in H (hue) values at this depth in UPC164, showing a major change in sediment composition where carbonate is absent. In the lower (carbonate-free) sections of the UPC164 H values swing towards the yellow-green values in the spectrum, as opposed to higher blue reflectance in the upper core that indicates more abundance of carbonate in the sediment matrix.

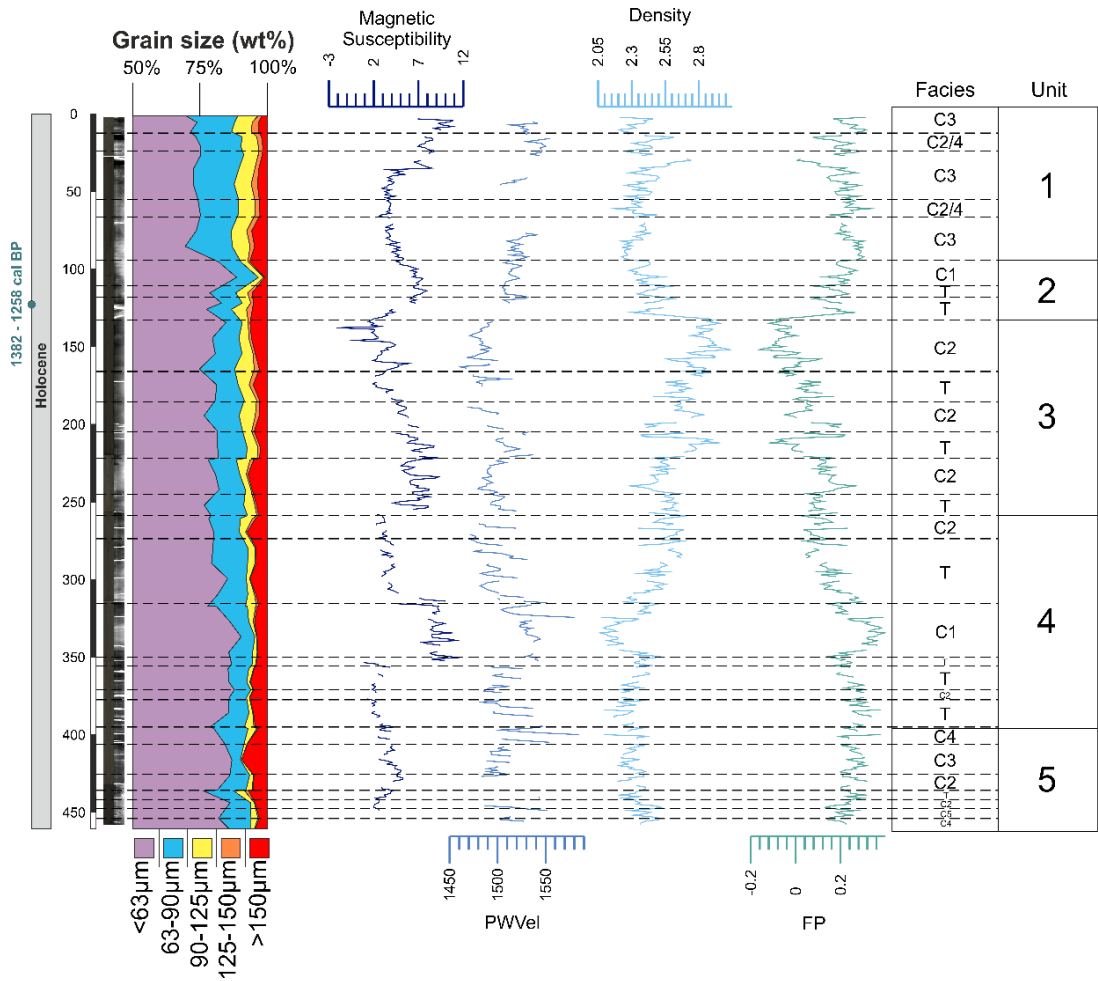


Figure 32 UPC065 (Submarine Canyon) Photograph, radiograph, grain size and Multisensor Core Logger (MSCL) plots of sediment physical properties against depth in seafloor. Interpreted sedimentary facies demarcated by dashed lines and grouped into units of similar characteristics of grain size, bioturbation, sedimentary structures and MSCL values of colour (L\*(lightness), C(Chroma), H(Hue)), magnetic susceptibility (proxy for sand), P-wave velocity (density/porosity), Gamma ray density (density useful of identifying clays) and FP (calculated Fractional Porosity)

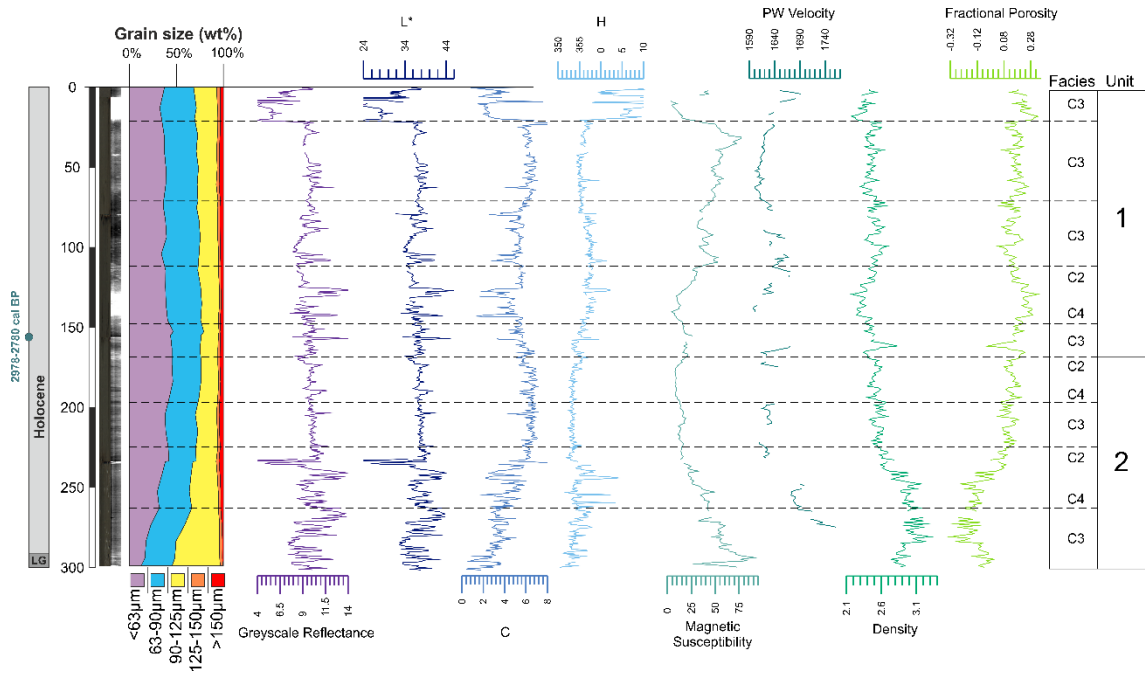


Figure 33 UPC125 (Terrace 2) Photograph, radiograph, grain size and Multisensor Core Logger (MSCL) plots of sediment physical properties against depth in seafloor. LG on timescale = Last Glacial. Interpreted sedimentary facies demarcated by dashed lines and grouped into units of similar characteristics of grain size, bioturbation, sedimentary structures and MSCL values of colour (L\*(lightness), C(Chroma), H(Hue)), magnetic susceptibility (proxy for sand), P-wave velocity (density/porosity), Gamma ray density (density useful of identifying clays) and FP (calculated Fractional Porosity)

MSCL measurements were particularly useful in cores UPC154 and UPC170 where a distinct shift in magnetic susceptibility, p-wave velocity and fractional porosity is found at 80 and 190 cm sediment depth in each core respectively, separating different phases of sedimentation. Above this peak in each core there is a noticeable increase in grain size, replacing more clay-rich sediments below the peak. A similar increase in grain density is observed in UPC164 between 200-275 cm that can possibly be explained by either an increase in grain size or a potential shift in sediment composition due to a change in provenance.

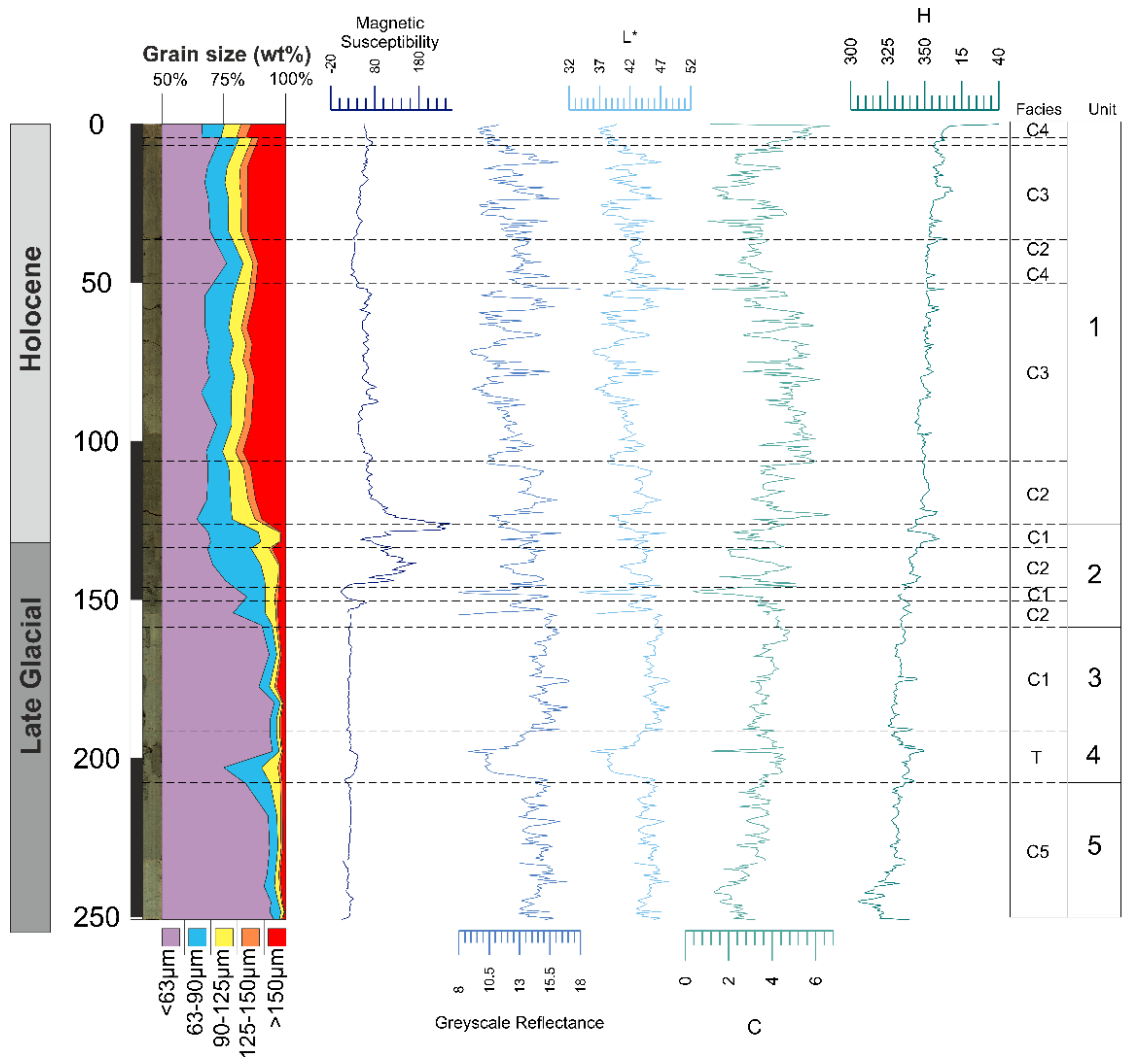


Figure 34 UPC133 (Drift 3) Photograph, radiograph, grain size and Multisensor Core Logger (MSCL) plots of sediment physical properties against depth in seafloor. Interpreted sedimentary facies demarcated by dashed lines and grouped into units of similar characteristics of grain size, bioturbation, sedimentary structures and MSLC values of colour ( $L^*$ (lightness),  $C$ (Chroma),  $H$ (Hue)) and magnetic susceptibility.

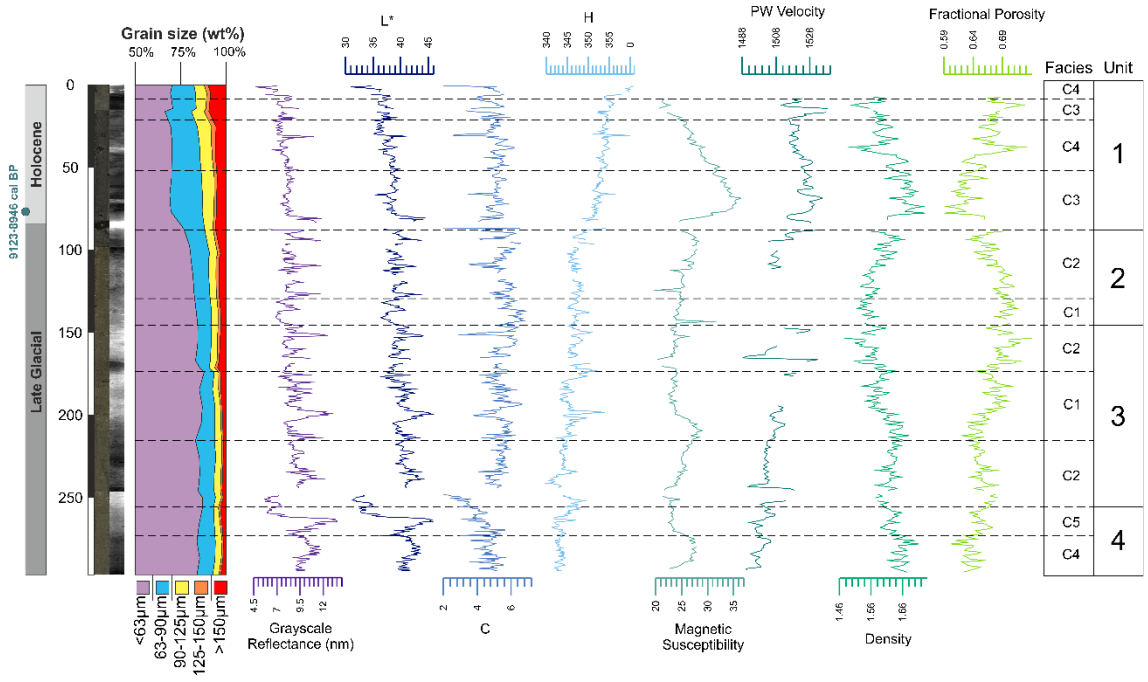


Figure 35 UPC154 (Terrace 4) Photograph, radiograph, grain size and Multisensor Core Logger (MSCL) plots of sediment physical properties against depth in seafloor. Interpreted sedimentary facies demarcated by dashed lines and grouped into units of similar characteristics of grain size, bioturbation, sedimentary structures and MSCL values of colour (L\*(lightness), C(Chroma), H(Hue)), magnetic susceptibility (proxy for sand), P-wave velocity (density/porosity), Gamma ray density (density useful of identifying clays) and FP (calculated Fractional Porosity)

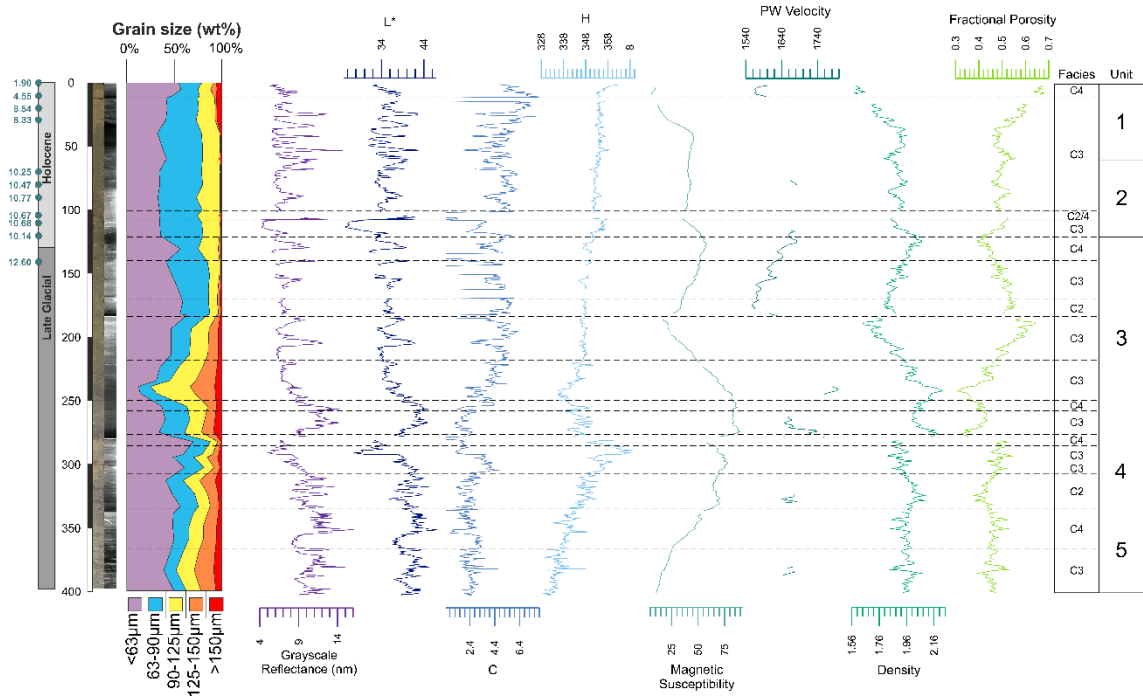


Figure 36 UPC164 (Terrace 2) Photograph, radiograph, grain size and Multisensor Core Logger (MSCL) plots of sediment physical properties against depth in seafloor. Interpreted sedimentary facies demarcated by dashed lines and grouped into units of similar characteristics of grain size, bioturbation, sedimentary structures and MSCL values of colour (L\*(lightness), C(Chroma), H(Hue)), magnetic susceptibility (proxy for sand), P-wave velocity (density/porosity), Gamma ray density (density useful of identifying clays) and FP (calculated Fractional Porosity)

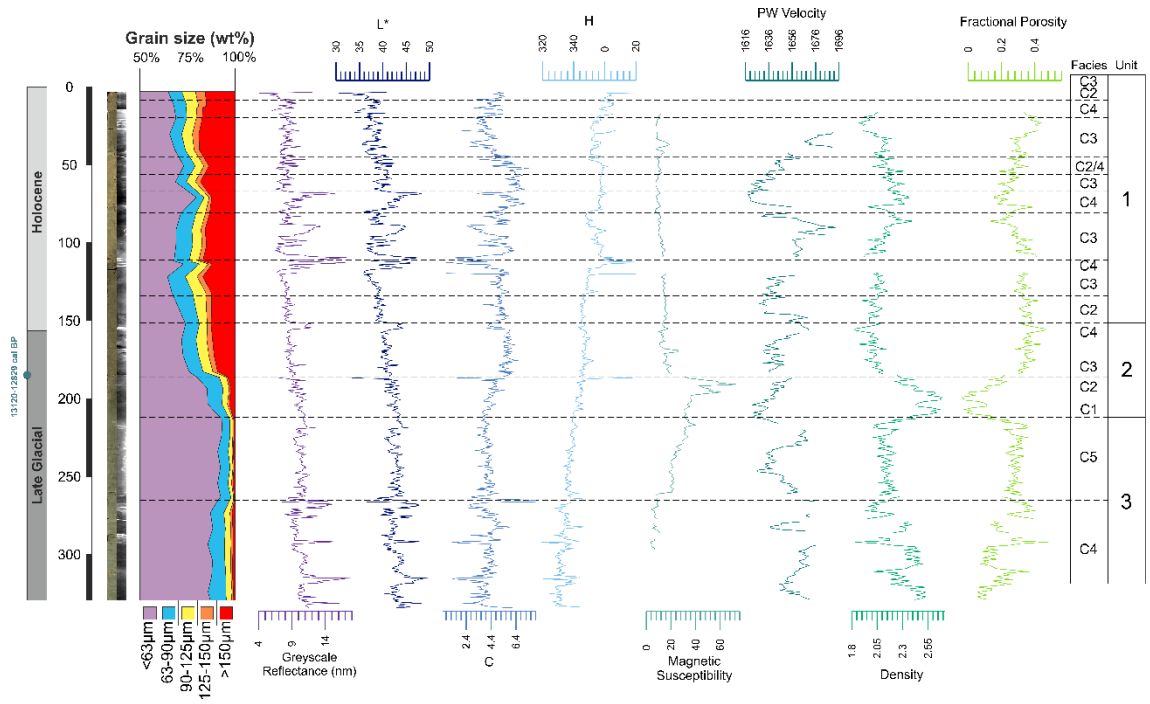


Figure 37 UPC170 (Drift 2) Photograph, radiograph, grain size and Multisensor Core Logger (MSCL) plots of sediment physical properties against depth in seafloor. Interpreted sedimentary facies demarcated by dashed lines and grouped into units of similar characteristics of grain size, bioturbation, sedimentary structures and MSCL values of colour (L\*(lightness), C(Chroma), H(Hue)), magnetic susceptibility (proxy for sand), P-wave velocity (density/porosity), Gamma ray density (density useful of identifying clays) and FP (calculated Fractional Porosity)



4.2.3 ITRAX Results

A total of 18 elemental ratios were calculated for down-core trends from raw count (kcps) data from the ITRAX measurements (Table 3.2). These have been plotted as log ratios (Weltje & Tjallingii, 2008) with a 5-point moving average against depth down-core in Figures 4.12 to 4.17. (Appendix 4.3)

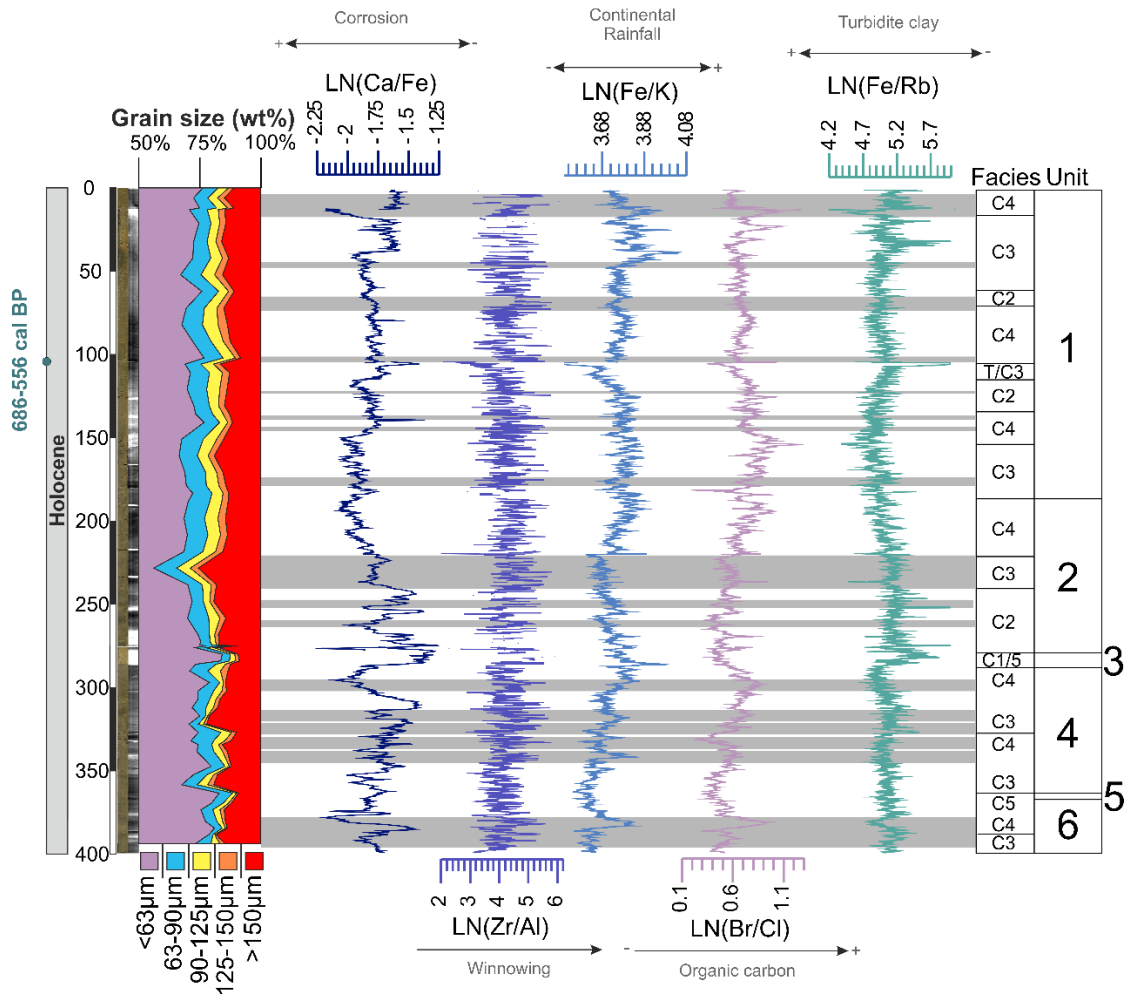


Figure 38 UPC001 (Drift 001) Photograph, radiograph, grain sie and ITRAX plots against depth and age. Interpreted application of each elemental proxy are indicated on axis. Interpreted sedimentary facies and units are indicated on the right of the figure. Intervals of enhanced winnowing by bottom currents shaded in grey.

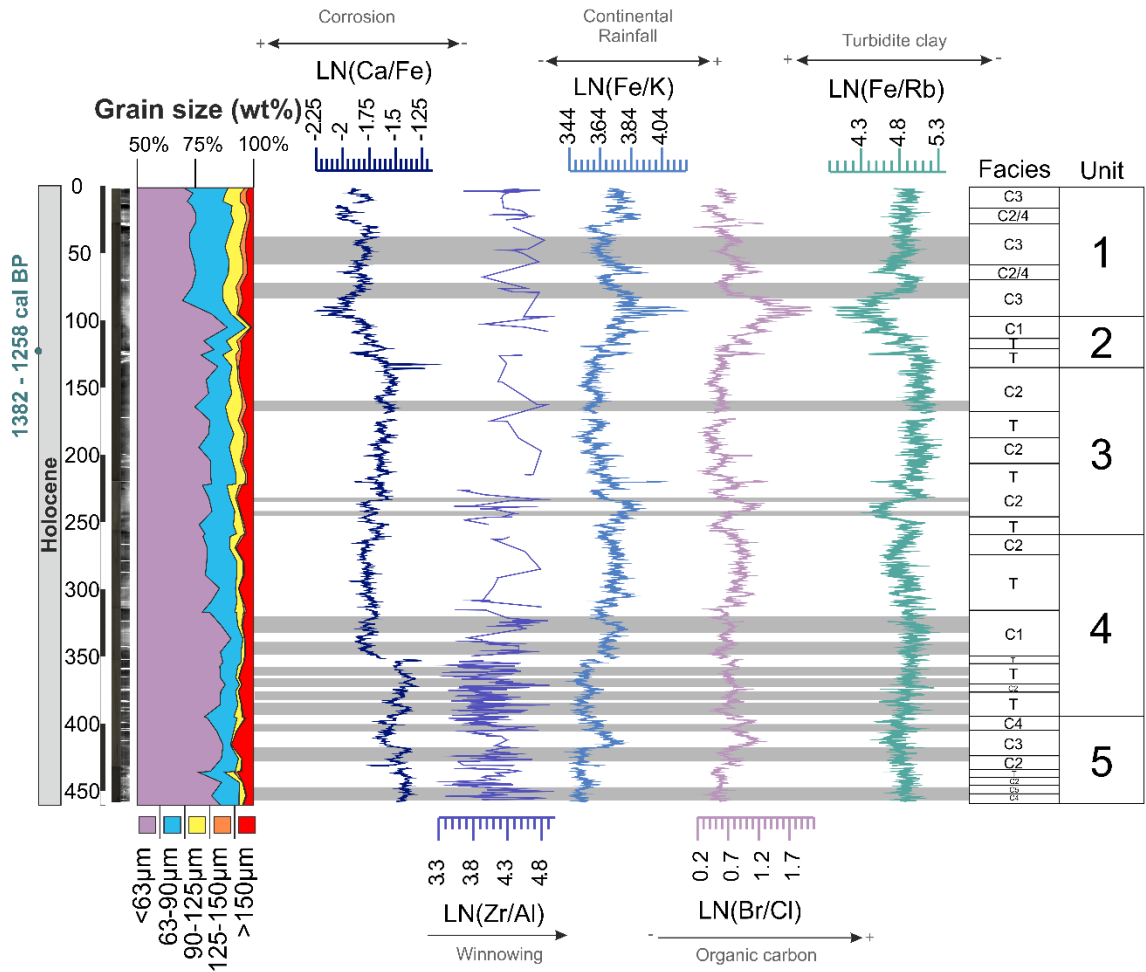


Figure 39 UPC065 (Submarine Canyon) Photograph, radiograph, grain sie and ITRAX plots against depth and age. Interpreted application of each elemental proxy are indicated on axis. Interpreted sedimentary facies and units are indicated on the right of the figure. Intervals of enhanced winnowing by bottom currents shaded in grey.

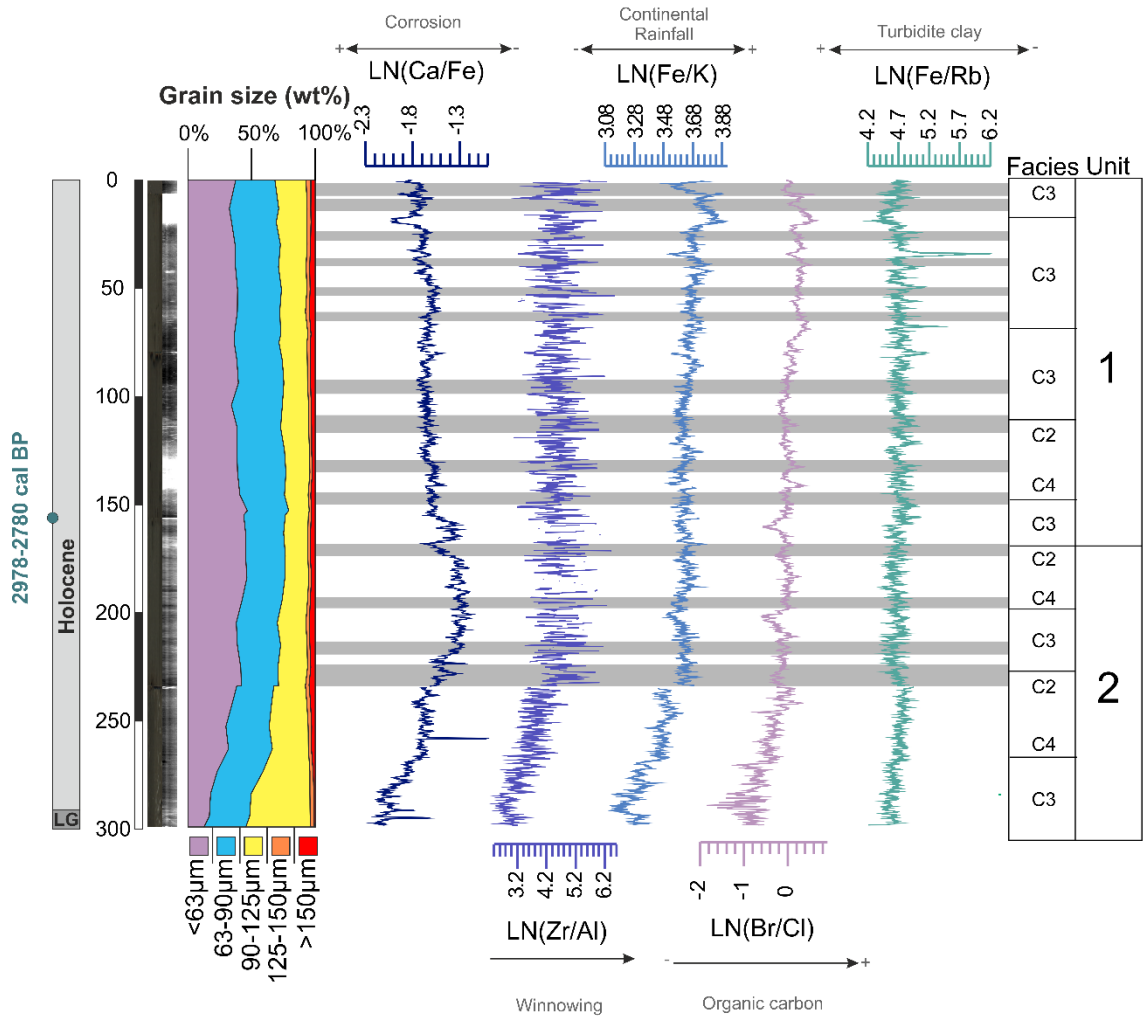


Figure 40 UPC125 (Terrace 2) Photograph, radiograph, grain size and ITRAX plots against depth and age. Interpreted application of each elemental proxy are indicated on axis. Interpreted sedimentary facies and units are indicated on the right of the figure. Intervals of enhanced winnowing by bottom currents shaded in grey.

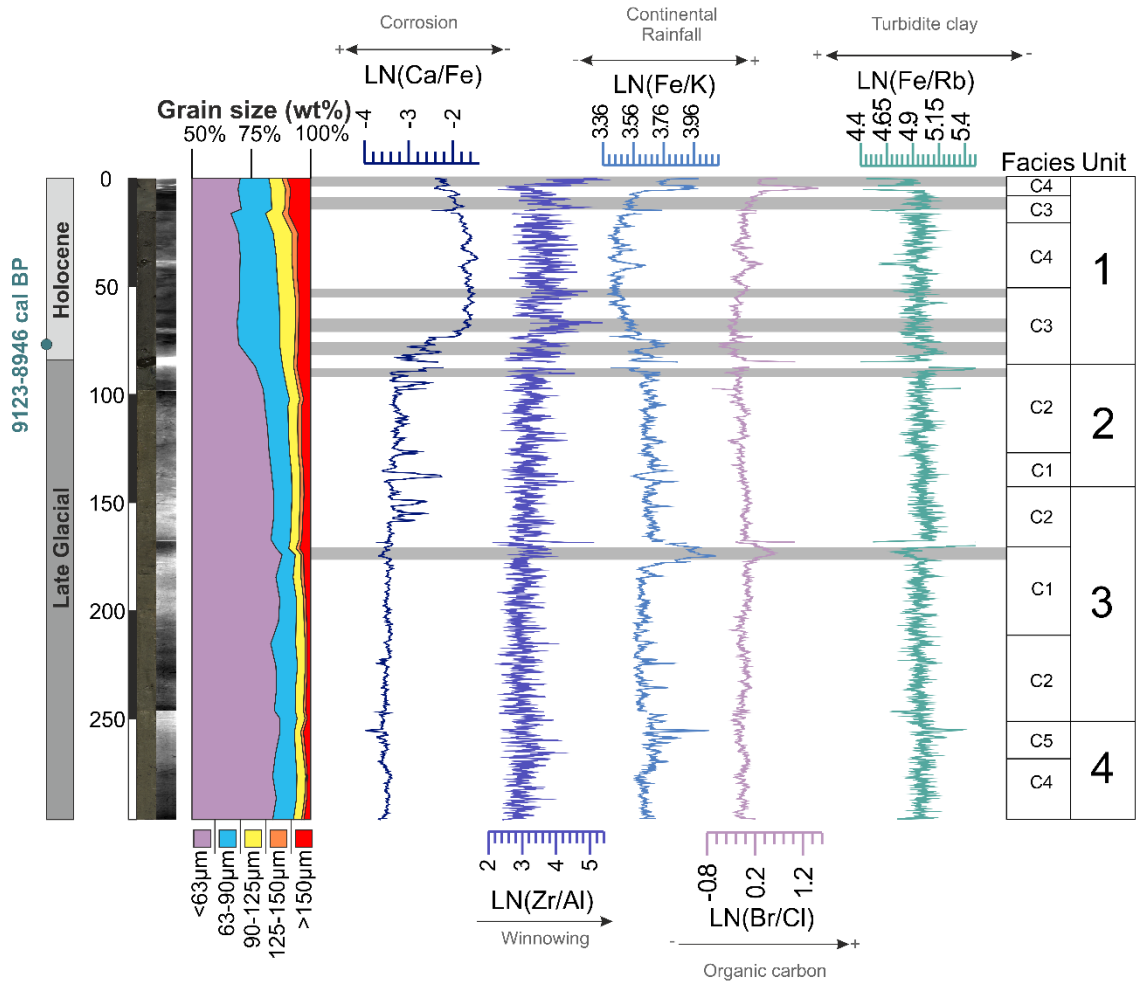


Figure 41 UPC154 (Terrace 4) Photograph, radiograph, grain sie and ITRAX plots against depth and age. Interpreted application of each elemental proxy are indicated on axis. Interpreted sedimentary facies and units are indicated on the right of the figure. Intervals of enhanced winnowing by bottom currents shaded in grey.

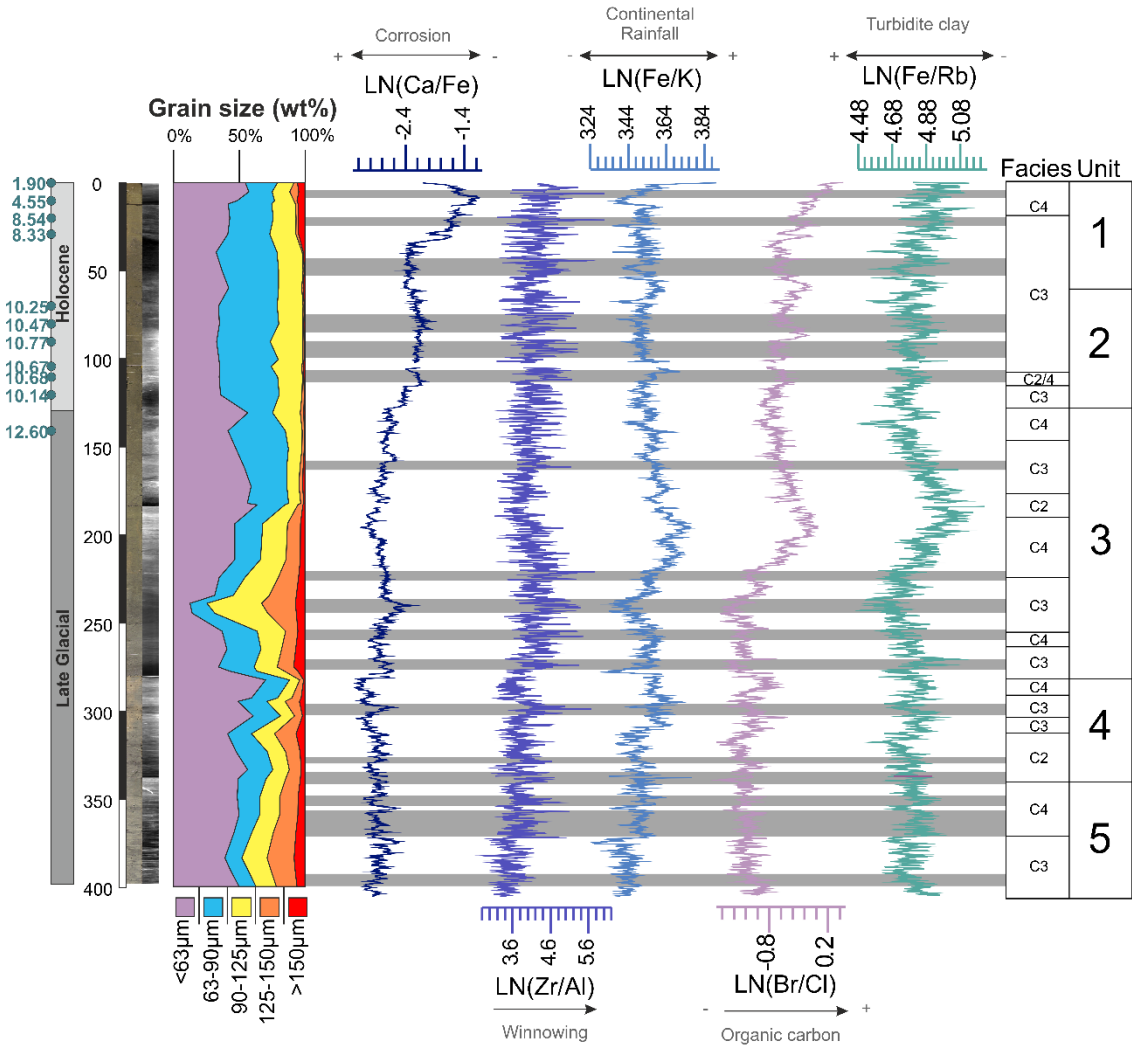


Figure 42 UPC164 (Terrace 2) Photograph, radiograph, grain sie and ITRAX plots against depth and age. Interpreted application of each elemental proxy are indicated on axis. Interpreted sedimentary facies and units are indicated on the right of the figure. Intervals of enhanced winnowing by bottom currents shaded in grey.

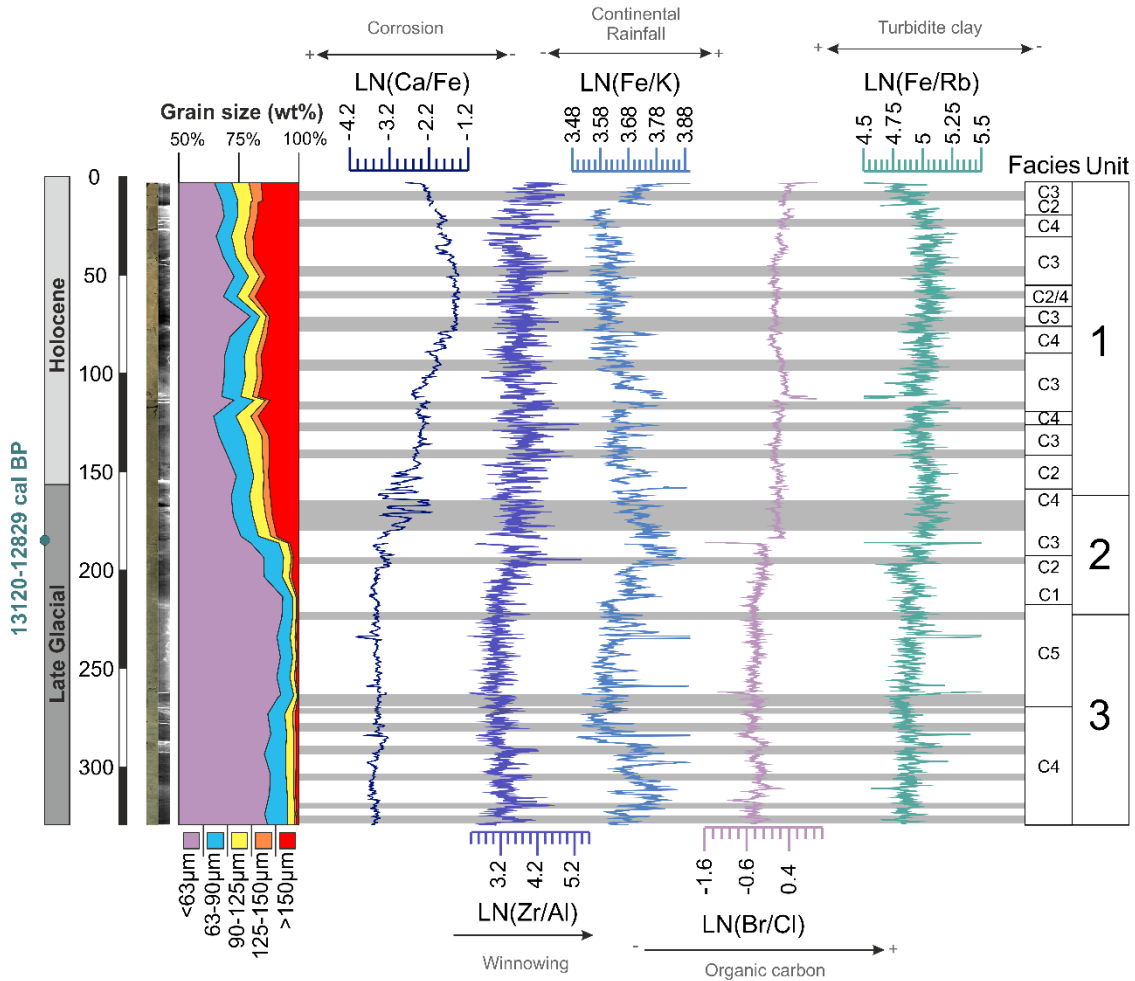


Figure 43 UPC170 (Drift 2) Photograph, radiograph, grain sie and ITRAX plots against depth and age. Interpreted application of each elemental proxy are indicated on axis. Interpreted sedimentary facies and units are indicated on the right of the figure. Intervals of enhanced winnowing by bottom currents shaded in grey.

Cores UPC001 and UPC065 contained highly variable Ca/Fe (-2 to -1.25) , with a general increasing trend downcore that suggests an increase in carbonate (from -2 to -1.25) with sediment depth (Figures 4.12 and 4.13). UPC125 showed relatively consistent values with depth (~-1.5), with a slight decrease in values (-2.2) within the lowermost, coarser grained section of the core at 240-300cm. Within UPC164 high Ca/Fe values (-1.3) were observed in the uppermost 30 cm of core that gradually decrease with depth to values around -2.5. Cores UPC154 and UPC170 have shown similar trends where high ratio values were observed

in the upper 75 and 150 cm respectively (~-1.4), before abruptly decreasing down-core (-3.0).

No trend was evident when cross correlating Zr/Al (a proxy for bottom current velocity) with grain size in UPC001 or UPC065 ( $r^2 < 0.1$  with grain size), but all other cores have shown increasing Zr/Al values towards the upper sections of the cores. Highest values of Zr/Al were observed in cores UPC125 (5.2), UPC164 (5.4) and UPC170 (5.0) ( $r^2 > 0.2$  with grain size). These  $r^2$  values would improve with discrete XRF measurements on the discrete measured sediment grain size samples.

Ratios of Fe/K were plotted as proxies for variations in sediment source and terrigenous input to the marine environment. All of the cores show increased values in the uppermost sections of core with the exception of UPC154 (the deepest core) that has significantly decreased Fe/K in the upper 80 cm of core. This long-term trend is punctuated by peak and troughs of Fe/K values, reflecting more event-like deposition from a source with different mineralogy (e.g. UPC154, 160 cm).

#### 4.2.4 Radiocarbon Results & Chronology

A total of 17 sediment samples were submitted for radiocarbon dating. Twelve of these were from UPC164 for a detailed palaeoceanography study in Chapter 5, and five of these were taken from the boundary of significant shifts in sediment composition and texture observed within cores UPC001, UPC065, UPC125, UPC154, UPC164 and UPC170. The error on dates for all the samples falls within 600 years BP (Table 4.2). This resulted in an age range for the sediment cores of Pleistocene and Holocene age and reach a maximum recorded age of 12600 +/- 40 BP and a minimum age of 1070 +/- 30 BP. It is assumed that all of the sampled sections young towards the present day as we have no means of dating all of the core tops.

There were a few anomalous age results within core UPC164 from the mid slope contourite terrace (See Table 4.2) that are likely due to the high level of sediment reworking in the system. Therefore, the single age points from the other cores should be treated with some caution. Particularly, when carbonate content is so limited at the selected levels. However, the radiocarbon results have aided core correlation and has given a better understanding of the accumulation rates in different depositional environments.



Table 4.2 Accelerator mass spectrometry (AMS) radiocarbon dates and calibrated ages. IRMS isotope values from *Globorotalia inflata* included

| Core No. | Probability | Conventional age | Calibrated age<br>95.4% probability<br>(cal ka B.P.) | Calibrated age,                             |                      |              |
|----------|-------------|------------------|--|---|----------------------|--------------|
|          |             |                  |  | Interpolated<br>from model<br>(cal ka B.P.) | IRM<br>S<br>d13<br>C | IRMS<br>d18O |
| UPC001   | 95.40%      | 1070 +/- 30 BP   | 686 - 556 cal BP                                     | N/A   | 1.90                 | 2.58         |
| UPC065   | 95.40%      | 1770 +/- 30 BP   | 1382 - 1258 cal BP                                   | N/A   | 1.60                 | 2.32         |
| UPC125   | 95.40%      | 3110 +/- 30 BP   | 2978 - 2780 cal BP                                   | N/A   | 1.90                 | 2.6          |
| UPC154   | 95.40%      | 8420 +/- 30 BP   | 9123 - 8946 cal BP                                   | N/A   | 1.40                 | 3.04         |
| UPC170   | 95.40%      | 11510 +/- 40 BP  | 13120 - 12829 cal BP                                 | N/A   | 1.30                 | 3.31         |
| UPC164   | 95.40%      | 1900 +/- 30 BP   | 1529 - 1358 cal BP                                   | 1470  | 1.70                 | 2.59         |
| UPC164   | 95.40%      | 4550 +/- 30 BP   | 4835 - 4646 cal BP                                   | 4762  | 1.60                 | 2.68         |
| UPC164   | 95.40%      | 8540 +/- 30 BP   | 9285 - 9051 cal BP                                   | 7932.5                                      | 1.40                 | 2.73         |
| UPC164   | 95.40%      | 8330 +/- 30 BP   | 8996 - 8771 cal BP                                   | 8915  | 1.50                 | 2.79         |
| UPC164   | 95.40%      | 10250 +/- 30 BP  | 11327 - 11147 cal BP                                 | 11218                                       | 1.30                 | 3.09         |
| UPC164   | 95.40%      | 10470 +/- 40 BP  | 11861 - 11346 cal BP                                 | 11488                                       | -                    | 0.60 1.60    |
| UPC164   | 95.40%      | 10770 +/- 30 BP  | 12432 - 12046 cal BP                                 | 11698                                       | 1.20                 | 3.00         |
| UPC164   | 95.40%      | 10580 +/- 30 BP  | 12035 - 11693 cal BP                                 | 11877                                       | 1.40                 | 3.05         |
| UPC164   | 95.40%      | 10670 +/- 40 BP  | 12260 - 11825 cal BP                                 | 12022                                       | 1.40                 | 3.13         |

|        |        |              |                   |         |      |      |
|--------|--------|--------------|-------------------|---------|------|------|
|        |        | 10680 +/- 40 | 12294 - 11843 cal |         |      |      |
| UPC164 | 95.40% | BP           | BP                | 12181.5 | 1.00 | 2.77 |
|        |        | 10140 +/- 40 | 11236 - 11040 cal |         |      |      |
| UPC164 | 95.40% | BP           | BP                | 12726.5 | 1.20 | 3.20 |
|        |        | 12600 +/- 40 | 14218 - 13940 cal |         |      |      |
| UPC164 | 95.40% | BP           | BP                | 13886.5 | 0.20 | 2.41 |

---

The radiocarbon results in this study include 12 species-specific samples from the planktonic foraminifera *Globorotalia inflata* in the size fraction >150  $\mu\text{m}$ . (Table 4.2). The radiocarbon dates were calibrated by BETA Analytic with the high-probability density (HPD) range method using the MARINE13 calibration curve and no  $\Delta R$  (Marine Reservoir Offset) (Reimer et al., 2013). All ages are given in calibrated thousands of years before present (ka B.P.).

#### 4.2.4.1 Rates of Sediment Accumulation

The dates show that accumulation rates of sediment are very different between core sites. The cores located on the middle slope drifts show the highest accumulation rates (UPC001 = 161 cm/ka) with the submarine canyon core (UPC065 = 110 cm/ka) following close behind. Cores from the mid slope terrace show two different accumulation rates depending on their position relative to the Montevideo Submarine Canyon. UPC125 positioned on the terrace to the south of the canyon shows a much higher rate of accumulation (52.1 cm/ka) when compared to UPC164 (9.4 cm/ka) position to the north of the canyon, both of these cores are at similar water depths. The deeper terrace and drift cores UPC154 (8.3 cm/ka) and UPC170 (13.9 cm/ka) have similar, slow accumulation rates.

#### 4.2.4.2 Elemental Ratio Cross Plots

Elemental ratio cross plots were constructed to easily visualise and identify sediment composition changes that could give evidence towards changing provenance within each identified depositional environment. Of all the cross plots possible, Si/Al and Ca/K were found to be most useful. These elemental ratios accentuate any differences in the chemical composition between cores and sedimentary units (Figure 4.18). There were clear differences in sediment composition depending on the position of the core on the slope. For instance, UPC001 and UPC065 had very similar compositions of Si/Al and the Ca/K record shows no carbonate free intervals. This is likely due to high rates of sedimentation in these areas being sourced from the mid slope terrace. While UPC164 and UPC125 were both located on the mid slope contourite terrace, so it was expected that they would be very similar compositionally. However, UPC125 appears to be enriched in Ca/K compared to UPC164. This is due to reduced carbonate content in the lower sections of core UPC164 compared to UPC125. The two cores differed greatly in terms of accumulation rates, which appeared to be much higher on the terrace to the south of the Montevideo Canyon compared to the terrace north of the canyon. UPC154 and UPC170 were both located on deeper contourite drifts. UPC154 is located in the south and showed similar compositions to other cores located in the southern portion of the study area. There was evidence for reduced carbonate accumulation/preservation in the lower portions of the core. UPC170 is located in the north and shows a very scattered distribution compared to other cores, this could be the result of a slightly different sediment source compared to the other cores. This may be due to an

increased northern-sourced sediment influence in the northern sectors of the study area (Figure 4.2)

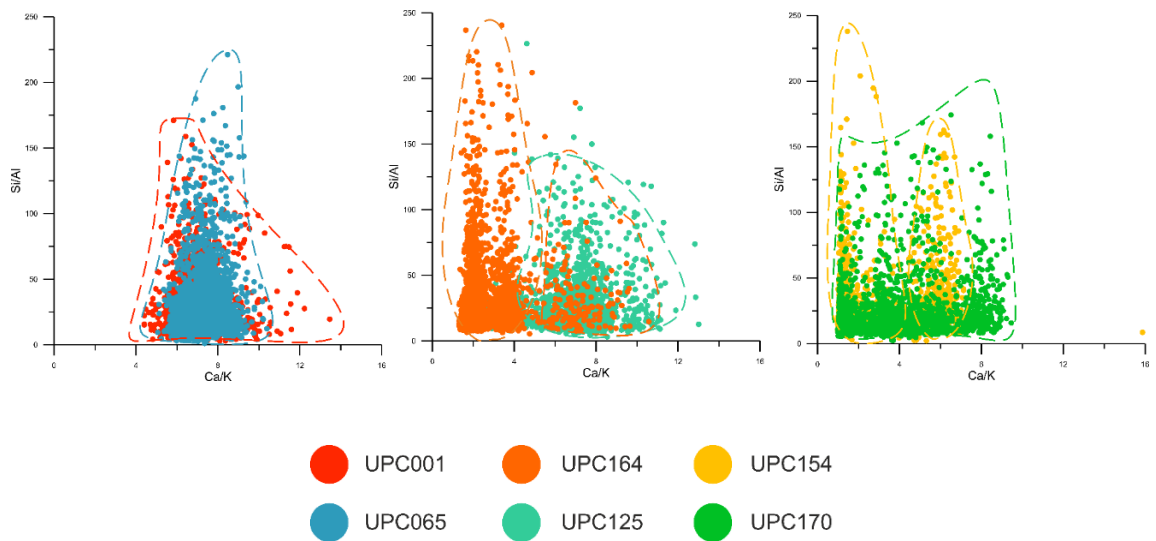


Figure 44 Composition plots of Si/Al and Ca/K for the six piston cores showing the sedimentary environments of mid slope drift (disturbed)(UPC001 and UPC065); mid slope terrace (UPC125 and UPC164) and lower slope drift (UPC154 and UPC170).

#### 4.2.5 Observed Deep-Water Facies & Facies Sequences

Eight sedimentary facies were observed within the Uruguayan slope system. A) An olive green, bimodally sorted, hemipelagic mud facies, labelled as C1 and C5 facies (UPC154). B) Turbidite facies composed of brown mud and fining upwards sand deposits with black mud caps, categorised as Ta to Te facies (UPC065). C) Bioturbated, olive green, muddy contourite facies, also grouped in with C1 and C5 (UPC154). D) Mottled, dark brown, silty contourite facies, identified as C2 and C4 (UPC032). E) Orange to light brown, very fine sand mottled/bioturbated contourite facies, also grouped into C2 and C4 (UPC125). F) Dark to light brown, bioturbated fine sand contourite facies, C2 and C4 facies (UPC125). G) Light to medium brown, laminated fine sand contourite facies, into C3 facies (UPC164). H) Dark brown, speckled, massive medium/coarse sand contourite facies, into the C3 facies (UPC125). These facies are shown in Figures 4.4 to 4.11 and 4.12 to 4.17. Figure 4.19 is a summary of how these facies appear visually in the cores, without the aid of core scanning techniques.

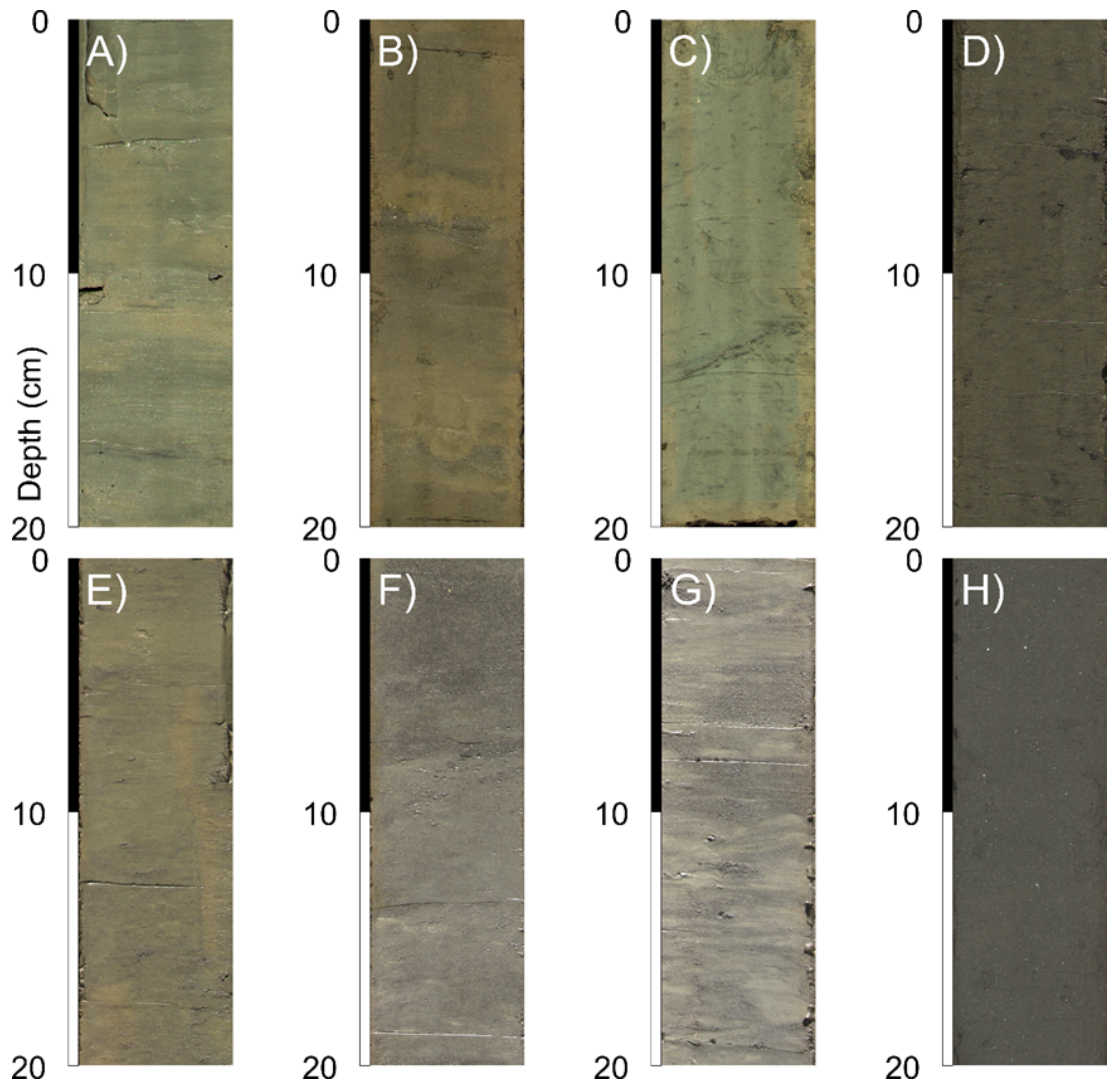


Figure 45 Contourrite and turbidite facies observed on the Uruguay Continental Margin. Photographed using an MSCL-CIS with Minolta camera attachment. A) Hemipelagic facies UPC154 B) Turbidite facies UPC065 C) Bioturbated muddy contourrite facies UPC154 D) Mottled silty contourrite facies UPC032 E) Very fine sand mottled contourrite facies UPC125 F) Bioturbated fine sand contourrite facies UPC125 G) Laminated fine sand contourrite facies UPC164 H) Massive medium/coarse sand contourrite facies UPC125.

#### 4.2.5.1 Hemipelagic, Non-Depositional/Hiatal, C1 and C5 Facies

Hemipelagic facies are defined as homogenous sediment and often showing distinct olive-green to orange-brown colouration. Biogenic material is mainly composed of the tests of planktonic foraminifera. It is fine-grained and bimodally sorted due to finer clay and coarser fraction of biogenic material (Figure 4.19 A, UPC170 210-230 cm). Hemipelagic facies have the highest reflectance (>12 nm),

lowest magnetic susceptibility ( $<17 \times 10^{-8} \text{ (m}^3/\text{kg)}$ ), moderate to low velocity ( $1555 \text{ m s}^{-1}$ ), lowest density ( $<2 \text{ g cm}^{-3}$ ), and relatively moderate porosity (35%). Ca/Fe ratios are low ( $<-2.58$ ), as are Zr/Al ratios ( $<3.8$ ). Fe/K are the same as other mud-rich facies at  $\sim 3.6$ . Mn/Fe ratios are very low ( $<4.8$ ), Fe/Rb ratios are low ( $<4.6$ ), K/Rb are low ( $<1.1$ ), Zr/Rb are low ( $<0.45$ ) and Ti/Rb are very low ( $<0.9$ ). Hemipelagites are more common in the deeper drift cores and along slope from submarine canyons and can be observed in cores UPC154 (130-300 cm), UPC133 (125-250 cm) and UPC170 (210-230 cm). Here they are labelled as C1 and C5 contourite facies as they are often found alongside each other on the transitions from/to coarser facies in contourite settings. Non-depositional surfaces are particularly common in UPC164 at 120 cm and between 250 – 310 cm, these are often found in coarser sediments.

#### 4.2.5.2 Turbidite Facies – Ta to Tc & Absence of Td/Te Bouma Divisions

Typical deep-water turbidite facies with identifiable Bouma sequences. These deposits showed repeated fining upwards sequences of fine sand/coarse silt to mud. Many turbidite beds were missing true turbidite mud caps (division Te). Within core UPC065 the maximum sand content rarely reached above 40%. The turbidites observed in this environment have relatively low magnetic susceptibility ( $\sim 20 \times 10^{-8} \text{ (m}^3/\text{kg)}$ ), with very low p-wave velocity ( $\sim 1500 \text{ m s}^{-1}$ ). These facies had a moderate to high density and low fractional porosities ( $\sim 15\%$ ). Ca/Fe ratios were the highest in these facies at  $>-1.6$ . Zr/Al ratios were high at  $>4.0$ , with moderate Fe/K ratios and some of the lowest Ti/K ratios. Mn/Fe ratios were relatively high ( $>-4.5$ ). Br/Cl ratios were the highest in these facies ( $>1.0$ ). Turbidite facies showed the lowest Fe/Rb ratios ( $<4.3$ ), but this varies with grain size. K/Rb was very high at  $>1.3$ . Zr/Rb and Ti/Rb were also high at  $>0.5$  and 1.2

respectively. The fine-grained sand/silt beds were often cross-laminated and rarely showed intense bioturbation of other facies (Figure 4.19 B, UPC001 360-380 cm). Broken shelly material was found in many of the sandier beds. Foraminiferal tests were in low abundance. Sharp contacts were common between silt-mud to coarser event beds. Sediments were much more mud-rich than other facies observed in the area. Td and Te muddy and fine silt facies were often missing and replaced with facies showing more indications that it is in fact C2 or C4 in the contourite sequence. These were mottled (from pervasive bioturbation) with lenses of coarser silt, commonly seen in sections from UPC001, 55-100 cm and UPC065, 125-240 cm.

#### *4.2.5.3 Bioturbated Muddy Contourite Facies – C1 and C5 divisions*

Similar muddy content as hemipelagic facies. However, the muddy sections here are often entirely bioturbated. There are no visible structures and the sediment appears massive. These facies had a high reflectance at ~11 nm, with moderate magnetic susceptibility and p-wave velocity at  $\sim 35 \times 10^{-8}$  ( $\text{m}^3/\text{kg}$ ) and  $\sim 1580 \text{ m s}^{-1}$  respectively. The facies have some of the lowest densities  $\sim 1.85 \text{ g cm}^{-3}$  and some of the highest fractional porosity  $\sim 40\%$ . They contained some of the lowest Ca/Fe ratios compared to other facies ( $< 2.6$ ) and Zr/Al ratios ( $\sim 3.2$ ). Fe/K ratios were high ( $> 3.6$ ) and Ti/K ratios are similar to other mud-rich facies ( $\sim 0.06$ ). Mn/Fe ratios were moderate  $\sim 4.5$  and Br/Cl were moderate and similar to other mud-rich facies  $\sim 0.5$ . Fe/Rb ratios were high  $> 4.9$ , K/Rb ratios were moderate  $\sim 1.1$ , Zr/Rb ratios were low  $< 0.45$  and Ti/Rb ratios were high at  $> 1.2$ . One of the main reasons these facies can be identified as contouritic is the identification of small scale burrows are visible with diameters of only a few millimetres which are known to be pervasive in contouritic settings. These might be identified as



*Chondrites* (4.19, C) as these are a small-scale branching tunnel system, commonly seen in these settings. There was some shell material present and the facies contain foraminifera. The presence of biogenic material results in the contourite facies being bimodally sorted. These facies are common in UPC133, UPC154 and UPC170 on the deeper sediment drifts.

#### 4.2.5.4 Mottled Silty Contourite Facies – C1, C2, C4 and C5 Divisions

These facies were commonly found in UPC032, UPC133 and UPC170. They grade into muds and fine sands within the deposit, often found as lenses within muddier facies a common feature of deposits that are contouritic in nature. Mottled silty contourite facies had very low reflectance at <8 nm, with relatively low to moderate magnetic susceptibility ( $\sim 28 \times 10^{-8} \text{ (m}^3/\text{kg)}$ ) and p-wave velocity ( $\sim 1550 \text{ m s}^{-1}$ ). The facies had a moderate density ( $\sim 2.13 \text{ g cm}^{-3}$ ) and very low fractional porosity values (10%). Ca/Fe ratios were high ( $>1.8$ ). Zr/Al were moderate to high at  $\sim 3.97$ . Fe/K ratios were low  $<3.5$  and Ti/K ratios were similar to other mud-rich facies  $\sim 0.06$ . Mn/Fe ratios were low at  $<4.6$  and Br/Cl are moderate and similar to other mud-rich facies ( $\sim 0.5$ ). Fe/Rb ratios were high at  $>4.9$ , K/Rb ratios were very high  $>1.3$ , Zr/Rb were low  $<0.45$  and Ti/Rb ratios were very high  $>1.4$ . These were intensely bioturbated silts that appear mottled on the cut surface (Figure 4.19 D). The bioturbation results in any sedimentary structures being destroyed and the facies being poorly sorted. Small-scale burrows were present with larger-scale burrows including *Planolites* and *Thalassinoides* seen in x-radiograph images.

#### 4.2.5.5 Very Fine Sand Mottled Contourite Facies - C2, C3 and C4 Divisions

Very fine and fine sand material were often seen as lenses within other facies or thicker beds. These facies were commonly highly bioturbated and had a mottled

appearance similar to the silt facies resulting in these facies being identified as contouritic in origin (Figure 4.19 E). These facies had moderate to low reflectance of  $\sim 8.5$  nm and moderate magnetic susceptibility of  $\sim 25.28 \times 10^{-8}$  ( $\text{m}^3/\text{kg}$ ). P-wave velocities were high at  $\sim 1600$   $\text{m s}^{-1}$  and so were densities at  $\sim 2.25$   $\text{g cm}^{-3}$ . Fractional porosity was relatively moderate at  $\sim 27\%$ . Ca/Fe ratios were high ( $> 1.8$ ), with high Zr/Al ratios of  $> 4.3$ . Fe/K ratios were high at  $> 3.6$  and Ti/K ratios were very high  $> 0.15$ . Mn/Fe ratios were low  $< 4.6$  and Br/Cl ratios were moderate similar to other mud-rich facies at  $\sim 0.5$ . Fe/Rb ratios were high  $> 4.9$ , K/Rb ratios were high  $> 1.2$ , Zr/Rb values were moderate at  $\sim 0.5$  and Ti/Rb ratios were moderate to low at  $< 1.1$ . Within these facies large-scale burrows were much more common up to one centimetre in diameter. Spherical and elongate burrows of 10 cm in length were observed. These were identified as *Planolites* and *Thalassinoides*.

#### 4.2.5.6 Bioturbated Fine Sand Contourite Facies – C2, C3 and C4 Divisions

Found as discrete layers within the cores and were highly bioturbated and could therefore be interpreted as contourite sands (Figure 4.19 F). These facies had moderate reflectance ( $\sim 9$ ) and magnetic susceptibility ( $\sim 30 \times 10^{-8}$  ( $\text{m}^3/\text{kg}$ )). P-wave velocities and densities were high at  $1650$   $\text{m s}^{-1}$  and  $> 2.2$   $\text{g cm}^{-3}$  respectively. These facies had a very high fractional porosity of  $> 40\%$ . The facies had moderate to high Ca/Fe ratios  $\sim 2.1$ . Zr/Al ratios were very high at  $> 4.5$ . Fe/K ratios were high ( $> 3.6$ ) and Ti/K were moderate at  $\sim 0.05$ . Mn/Fe ratios were very low  $< 4.8$ . Br/Cl ratios were low at  $\sim 0.1$ . Fe/Rb ratios were high at  $> 4.9$ , K/Rb ratios high  $> 1.2$ , Zr/Rb ratios were moderate at  $\sim 0.5$  and Ti/Rb ratios were very high  $> 1.3$ . Sharp boundaries were observed with large-scale bioturbation working

sediment down from these surfaces. These trace fossils were similar to those found in the very fine sand facies but were more difficult to identify precisely.

#### *4.2.5.7 Laminated Fine Sand Contourite Facies – C3 Division*

In these sandier facies (>70% sand) there was a marked reduction in bioturbation. They showed clear sedimentary structures of lamination and cross-lamination (Figure 4.19 G). However, they could be seen to contain coarsening upwards sequences (without sharp lower contacts) and were therefore interpreted as contourite sand beds and not sand emplaced by a downslope event. These facies had very high reflectance (>12 nm), magnetic susceptibility (>75  $\times 10^{-8}$  ( $\text{m}^3/\text{kg}$ )), p-wave velocity (>1700  $\text{m s}^{-1}$ ) and density (>2.7  $\text{g cm}^{-3}$ ) values. Fractional porosity was also relatively high at >30%. Ca/Fe ratios were moderately low at <-2.3. Zr/Al ratios were moderately high >3.9. Fe/K ratios were low at <3.19 and so were Ti/K ratios at <-0.2. Mn/Fe ratios were high at >-4.4. Br/Cl ratios were very low at <-1.0. Fe/Rb ratios were low at ~4.5. K/Rb were moderate at ~1.2. Zr/Rb ratios were low at <0.5. Ti/Rb ratios were high at >1.2. They would often show gradational boundaries with finer silty beds. Erosive contacts were common on upper and lower bed boundaries. Any bioturbation that was present will be made up of large-scale burrows centimetres in length. These sandier facies were rich in biogenic material in the form of benthic and planktic foraminifera.

#### *4.2.5.8 Massive Medium/Coarse Sand Contourite Facies – C3 Division*

Some of these facies showed faint lamination. However, medium sands were more often than not massive and showed no indications of any sedimentary structures (Figure 4.19 H). These facies had low reflectance <8.5 nm. They have very high magnetic susceptibility (50  $\times 10^{-8}$  ( $\text{m}^3/\text{kg}$ )) and p-wave velocities (>1650

m s<sup>-1</sup>). These facies had the highest densities of >2.8 g cm<sup>-3</sup>, with a low fractional porosity <20%. Ca/Fe ratios were very high >1.6. Zr/Al ratios were also very high at >4.8. Fe/K ratios were very high at >3.6 and Ti/K ratios were moderate at ~0.05. Mn/Fe ratios were very low at <0.5. Br/Cl ratios were low ~0.0. Fe/Rb ratios were very low at <4.4. K/Rb values were very low at <0.8. Zr/Rb were very high at >0.9 and Ti/Rb ratios were low at <1.0. They showed similar contacts and boundary types as the laminated sand facies and were therefore thought to be sourced from alongslope sediment transport. These facies were rich in broken shelly material and other biogenic material such as benthic and planktic foraminifera.

A summary of the key sedimentary facies is as follows:

***Hemipelagic facies*** – olive-green to orange-brown, poorly sorted, low density, Ca/Fe and Zr/Al values.

***Turbidite facies*** – fining upwards sequences, low porosity, high Ca/Fe and Br/Cl values and absence of intense bioturbation.

***Bioturbated muddy contourite facies*** – low density, Ca/Fe, Zr/Al values. Lots of small scale bioturbation with no visible sedimentary structures.

***Mottled silty contourite facies*** – lenses of silt in muddy matrix, low porosity, high Ca/Fe and Zr/Al values. Larger burrows become identifiable.

***Very fine sand mottled contourite facies*** – identifiable as lenses of sand, high velocity and porosity values and high Ca/Fe, Zr/Al and Fe/K values. Large burrows become dominant.

***Bioturbated fine sand contourite facies*** – discrete sand beds that are highly bioturbated. High velocity, density and porosity values. Ca/Fe, Zr/Al and Fe/K values are all high.

***Laminated fine sand contourite facies*** - >70% sand, reduced bioturbation, sedimentary structures become visible, very high magnetic susceptibility, velocity, density and porosity values. Lower Ca/Fe, Zr/Al and Fe/K values.

***Massive medium/coarse sand contourite facies*** – massive/structureless sands. High magnetic susceptibility, velocity and density values with reduced porosity. Very high Ca/Fe, Zr/Al and Fe/K values.

#### 4.2.6 Morphosedimentary Features

The sedimentary analysis represents each depositional environment from the morphosedimentary map constructed in the previous study from bathymetric and seismic data by Hernández-Molina *et al.*, (2016) outlined in chapter 2 section 2.3.4.3. Below each core is matched to its interpreted sedimentary environment from previous studies. The aim was to cross-validate the dominant depositional processes present at each site.

##### 4.2.6.1 UPC001 – Unstable Zone of Contourite Drift 1

Core UPC001 (Figures 4.4 & 4.12) was composed of silty to sandy units and appears to show a mixed contourite-turbidite deposition (C1 to C5 and Tc to e). The units have been defined by sharp basal contacts and muddy caps. Here it was interpreted as a plastered drift deposited by contouritic processes and periodically exposed to downslope turbidites that were either reworked or sourced directly from upslope. It was located on Drift 1 (identified by Hernández-Molina *et al.*, 2016) downslope of failure escarpments cut into the drift.

The core has been divided into 6 units. The upper 1.8 m of the core was interpreted as silty contourite drift deposition, showing cyclic grain size changes (C1 to C5). This section of the core shows less evidence of downslope processes. The cyclic variation in grain size could be due to variations in strength of the overlying NADW. Many primary structures such as laminations and cross bedding have been destroyed by intense bioturbation.

The lower units from 1.8-4 m contain repeated downslope event beds that were likely turbidites, with some showing evidence of reworking. These were the only facies of pure turbidite mud cap in the studied cores as evidenced by the high

K/Rb elemental ratio and scarcity of foraminifera tests (defined as C1 to C5 due to reworking but could also be identified as Tc to Te). Generally, this portion of the core was less abundant in foraminifera tests than the upper portion. The reduction in foraminifera counts and a more variable Ca/Fe record for carbonate within this lower section may be evidence for a dominance of downslope deposition in this period.

The facies identified in this core largely agree with the unstable drift morphosedimentary zone identified by Hernández-Molina *et al.* (2016) as most of the sediment was sourced from downslope transport processes that have been intensively reworked by alongslope bottom currents.

#### 4.2.6.2 UPC032 – Contourite Drift 2

The piston core UPC032 (Figure 4.5) was collected from the drift adjacent to the mouth of the small submarine canyon in the centre of the study area. Hernández-Molina *et al.*, 2016 defines this area of the slope as Drift 2. However, it appears to extend as a lobe to the south of the canyon as sediments exiting the canyon mouth get reworked by the southward flowing NADW current (Figure 4.2 a). . The 4.5m core was divided into 4 units, all were similar and the only deviation from the trend was the lowermost 75 cm where there appeared to be a reduction in grain size. It contained the highest percentages of >250 µm sediments in the study area. However, this fraction was entirely composed of large planktic and benthic foraminifera. Once the carbonate was excluded it was in fact a silty-muddy drift. The cyclic nature of grain size changes was continuous down core on a 1 to 3 ka wavelength.

The core was intensively bioturbated throughout and showed multiple coarsening upwards and fining upwards sequences. These facies were bounded by sharp/erosional and gradational contacts. With limited data collected on this core it can still be interpreted as showing many of the classification criteria of a silty contourite drift (Figure 4.20) (C1 to C5).

#### 4.2.6.3 UPC065 – Montevideo Submarine Canyon System

Located in the central axis of the Montevideo submarine canyon. The core was divided into five separate units with downslope deposition being the main process of sediment emplacement. Contourite reworking varies from almost total drift deposition in the uppermost 80 cm.

The sediments were interpreted from the limited data set as silty contourite drift deposition (C1 to C5) as the core was intensively bioturbated throughout and shows multiple coarsening upwards and fining upwards sequences. These facies were bounded by sharp/erosional and gradational contacts. With limited data collected on this core it could still be interpreted as showing many of the classification criteria of a silty contourite drift that is in agreement with the morphosedimentary zone of Hernández-Molina *et al.* (2016). There appears to be two full turbidite sequences with mud caps intact at 80-125 cm, 270-320 cm and 320-375 cm (Ta to Te). Other fining upwards sequences were missing muddy caps and often showed a coarsening upwards into silty drift facies, that may be interpreted as reworked turbidites.

Voigt *et al.* (2013) observed drift sedimentation within canyons on the Argentine slope to the south of our study area. High sediment deposition rates were linked to sediment being deposited into the canyon from the nepheloid layer of the



along-slope current of the AAIW. As the AAIW moves over the canyon the increase in depth from the terrace results in a velocity decrease and an associated reduction in carrying capacity for sediment load. Similar processes are thought to be acting in the Montevideo canyon from the observations made here. In the absence of an obvious continental source for these middle slope terrace canyons, they are assumed to be fed sediment entirely derived from the terrace itself.

Although the canyon is fed from a contouritic source, downslope processes are still likely to operate within the canyon itself. Evidence for this includes the multiple fining upwards sequences that appeared to be more event-like than continuous rain of fine sediment from currents in the water column above. This interpretation furthers the work of Hernández-Molina *et al.* (2016) & others. Total counts of benthic foraminifera remained low throughout the core and are dominated by deposit feeders and deep infaunal species. Bioturbation was much lower within the canyon than other settings on the slope, with only some large-scale bioturbation observed within the core. The reduction in fauna indicate an environment that is less favourable for benthic organisms than the open slope.

#### 4.2.6.4 UPC125 – Scoured Contourite Terrace 2

Recovered from the scoured and pockmarked middle slope contourite terrace identified by Hernández-Molina *et al.* (2016) (Figure 4.2). The core contained some of the coarsest sands collected in the study area (C2 to C4). The sediments in UPC125 were interpreted as a contourite sand deposit under the influence of high velocity AAIW on the midslope terrace. The core has been divided into 2 units as there appears to be some cyclicity in grain size that is linked to variations in the strength of AAIW through time. The upper unit begins at 160 cm, it coarsens

upwards and was composed of >40% sand, with large-scale (planulites) bioturbation present. The lower unit was composed of a coarse sand (>40% sands) that fines upwards into amalgamated finer sand beds that are both rich in angular terrigenous sediment grains. The entire core was rich in benthic foraminifera and siliceous microfossils such as radiolaria. Large-scale bioturbation was pervasive throughout the core but was difficult to identify due to the coarse sediment. The sedimentary facies identified in this core agree with the morphosedimentary interpretation of Hernández-Molina *et al.* (2016) as this zone of the slope being under the influence of high velocity bottom currents as evidenced by the numerous scour marks on the seafloor.

#### 4.2.6.5 UPC133 – Separated Contourite Drift 3

UPC133 was collected from the separated drift on the lower slope interpreted and labelled Drift 3 by Hernández-Molina *et al.* (2016) (Figure 4.2). The core was the first of the deep drift cores discussed here, all of which showed a similar trend of a fine-grained/carbonate free section, followed by a transition to a coarser-grained section with carbonate material. The sediments in UPC133 were interpreted here as silty contourite drift deposition (C1 to C5, with Tb to Td). Additional geomorphological information from bathymetry and seismic interpretations of Hernández-Molina *et al.* (2016) allow it to be characterised as located on a large separated mounded drift. The core has been separated into five units, however it can be divided into two modes. The upper section from 0-120 cm showed typically silty contourite drift deposition and was extensively bioturbated throughout. It was rich in calcareous and agglutinated foraminifera. The lower section 120-250 cm transitions to a carbonate-free hemipelagic

sedimentation under weak bottom current influence as seen from the multiple siltier lenses seen within this section.

#### 4.2.6.6 UPC154 – Contourite Terrace 4 Pockmarks

This core was retrieved from the pockmarked area of the lower slope Terrace 4 identified by Hernández-Molina *et al.* (2016). The core showed a similar transition to the one seen in UPC133. However, here the sediments were more mud-rich in the upper section that contains carbonate.

The sediments in UPC154 were interpreted as muddy contourite deposition on the terrace (C1 to C5). The core has been divided into four separate units, but as with UPC133 it has two main modes of deposition. The upper section from 0-80 cm was more typical of muddy-silty contourite drift deposition. It was extensively bioturbated and had a high foraminifera content. It had abundant angular to sub-angular terrigenous grains and angular grains of carbonate material (rip-up clasts?). The lower section from 80-300 cm was composed of hemipelagic sedimentation with a minor bottom current influence. It had the distinct orange-brown colour of pelagic sedimentation and was mostly carbonate-free in this lower section. However, this section still contained extensive small-scale (mm) bioturbation and silt lenses that were rich in angular terrigenous grains. These interpretations were in large agreement of those made by Preu *et al.* (2013); Hernández-Molina *et al.* (2016) & others that this area of the slope is a relict contourite erosional feature on the slope.

#### 4.2.6.7 UPC164 – Contourite Terrace 2 Sediment Waves

UPC164 was collected from the sediment-starved middle slope contourite terrace. The sediment within the core was sand-rich and was quite similar to core

UPC125 (C2 to C4). However, discontinuities were more common within this core and overall it appeared to have a slower rate of sediment accumulation. It showed the same carbonate trend as the deeper drift sediments, with the upper portion of the core being carbonate-rich and the lower sections being carbonate-free. The surface of the terrace in the locality surrounding the core appeared to be part of a sediment wave/dune field from bathymetry data (Hernández-Molina *et al.*, 2018).

The core has been divided into five separate units based on modes of deposition of the facies. The two uppermost units from 0-120 cm. The base of these units had a sharp contact with those beneath and deposition appeared to slow dramatically towards the top. Grain size was less variable here when compared to the units below and carbonate was much more abundant here than in the lower sections. From 120-280 cm there was a large unit of amalgamated contourite sands. There was a generally trend of fining upwards through this unit and its lower contact at 280 cm was sharp. Carbonate increases from the base of this unit towards the upper contact. However, it was carbonate poor throughout with an abundance of angular to subangular terrigenous grains. Large-scale bioturbation has not removed all evidence of primary sedimentary structures here, as there is faint cross-lamination in the lowermost most parts of this unit. From 280-310 cm there was a much finer unit that has a distinct orange to yellow colouration. Oxide nodules and terrigenous grains were abundant, as well as evidence for lamination. The section was free of carbonate and evidence of bioturbation. The lowermost unit from 310-400 cm was composed of another amalgamated contourite sand that was carbonate free, but had plenty of siliceous microfossils such as radiolaria. It was rich in large angular terrigenous grains and

showed evidence for large-scale bioturbation throughout. It was clear that the terrace has been exposed to a variety of different depositional processes through time. This variation in depositional processes was much clearer here than in core UPC125 as the lower accumulation rate has allowed a greater time period to be recorded. This agrees with the interpretations made by Hernández-Molina *et al.* (2016) that this was a post-canyon contourite terrace zone, that was characterised by low sediment accumulation rates.

The interpretations of core UPC164 will be expanded in Chapter 5 in a more detailed palaeoceanography study. The terrace was interpreted as having formed along the turbulent interface of the AAIW and UCDW watermasses.

#### 4.2.6.8 UPC170 – Drift 2 and Turbidite Valleys?

UPC170 was collected from the middle slope Drift 2 in proximity to where it had been incised by turbidite valleys (Figure 4.2). The core showed an identical trend of deposition as seen in the other drift cores UPC133 and UPC154 (C1 to C5). However, here the carbonate upper section of core has a greater thickness and has much more carbonate material such as foraminifera when compared to the other drift cores. The sediments in UPC170 were interpreted as silty contourite drift deposition. Additional geomorphological information from bathymetry and seismic interpretations of Hernández-Molina *et al.* (2016) allow it to be characterised as located on a large plastered drift. The core has been separated into three units, however it can be divided into two modes. The upper section from 0-210 cm was characterised by silty to sandy contourite drift deposition. It showed evidence for bi-gradational grain size changes with sequences cut out by discontinuities. The sediment was extensively bioturbated and was rich in benthic foraminifera. The coarsening upwards sections of this upper unit was rich

in a variety of angular terrigenous grain lithologies. The lower unit from 210-320 cm transitions to a carbonate-free hemipelagic sedimentation under weak bottom current influence in the lowermost portion where it seems to transition to muddy contourite drift deposition. This lower section was entirely carbonate-free and terrigenous grains were less abundant. The facies interpretations made in UPC170 agree with the morphosedimentary zone interpreted by Hernández-Molina *et al.* (2016).

#### 4.2.7 Core Correlation

Visual inspection supported by MSCL, ITRAX and  $\delta^{18}\text{O}$  data permits correlation of the lower slope drift and terrace sediments (UPC133, UPC154 and UPC170) with the upper/mid slope drift, terrace and canyon sediment records (UPC001, UPC032, UPC065, UPC125 and UPC164) (Figure 4.20). The  $\delta^{18}\text{O}$  graph from (Barbante *et al.*, 2006) was used to tie into global palaeoclimate records. Dates were obtained in this study from discrete radiocarbon measurements of planktic foraminifera. The Holocene-Pleistocene boundary has been well constrained using a combination of radiocarbon and carbonate appearance over the deglacial. All cores appeared to show sandier facies into the Holocene, however this was an effect of increased abundance of large foraminifera tests.

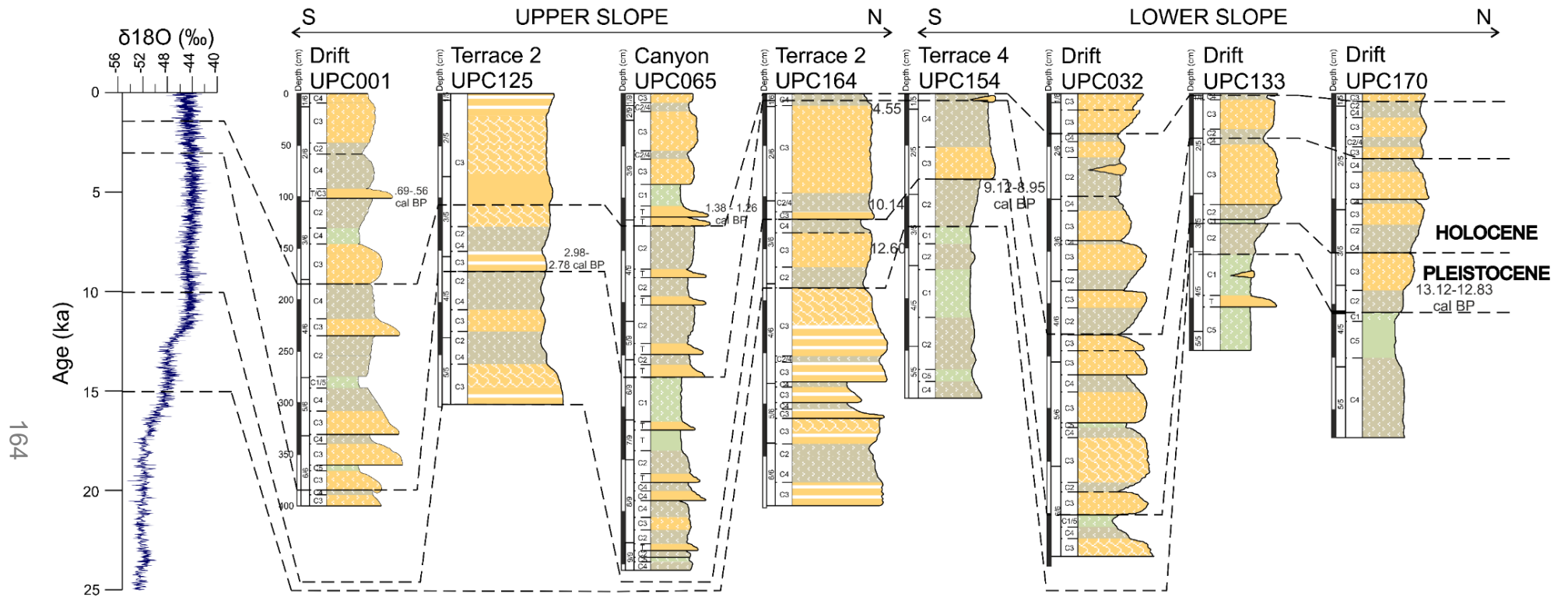


Figure 46 Core correlation panel from the upper/mid slope (left panel) and lower slope (right panel).  $\delta^{18}O$  graph from (Barbante et al., 2006). Dates were obtained in this study from discrete radiocarbon measurements of planktic foraminifera. Dashed green indicates C1 and C5; dashed brown indicates C2 and C4, dashed yellow indicated C3; striped yellow indicates C3 with lamination and block yellow indicates Ta to Td.

## 4.4 Discussion

### 4.4.1 Key Features

The finer grained contourite facies (C1, C2, C4 and C5 - muds and silts) show certain features that make them identifiable. Their characteristic high level of bioturbation that destroys/obscures any evidence of bedforms and gradational fluctuations in grain size that have been linked to changes in bottom current velocity (Stow *et al.*, 2009). This makes the finer grained facies of contourites easy to distinguish from other fine-grained deep-water deposits such as pelagic/hemipelagic and turbidites. Other deep-water facies (turbidites included), do not show bi-gradational units or anywhere near the levels of bioturbation observed in the fine contourite facies because of the event like nature, a large amount of coarse sand can be deposited instantaneously. This event does not give enough time for organisms to reworked the sediment and can often remove the entire top layer of sediment through erosion and destroy any evidence of life. Sand facies in contourites and other deep-water deposits are more difficult to distinguish from one another. Contourite sands are observed to have many different facies and associations that can appear like other deep-water sands (Shanmugam, 2018). The different features of contourite, turbidite and other deep-water facies at core and sediment scale are discussed below and are compared to large scale bathymetric and seismic morphosedimentary interpretations made in the study area.

#### *4.4.1.1 Identifying Contourite Facies in a Mixed Depositional System*

In this study, the cores examined exhibited various mixed depositional environments of varying facies. However, there is some element of bottom current influence observed in all of the cores that were split. The visual logging of



facies aided by the use of x-radiography has enabled the identification of possible processes that formed each sedimentary unit. Here, we highlight the key sedimentary features within the facies to set up the framework of how biology (microfossils) might aid us further in the recognition of contourite facies without relying on the techniques used so far.

#### 4.4.1.1.1 Discontinuities

At least seven of the eight sediment cores logged display at least some evidence for bottom current in the variety of boundaries between different facies in the sediment. There are subtle differences in the facies sequencing in bottom current sediments. Abrupt boundaries are often found to separate a sand unit (C3) from surrounding muds and silts (C1 and C5) and can be interpreted to indicate a sudden increase in bottom current velocity. Bioturbation can be seen to be particularly intense along these hiatuses as there is time for benthic organisms to burrow deep into the underlying sediment (Wetzel *et al.*, 2008). This results in many of the hiatuses in the sediment record being mixed and homogenised into the units above and below the contact. For a contact to be preserved/visible in the sedimentary record usually requires a change in sediment grain size or type to highlight the contact and the burrows reworked new sediment into old sediment and vice-versa (Miguez-Salas *et al.*, 2019). This indicates that in parts of the study area, bottom currents reached velocities that are capable of maintaining a sediment load and even becoming erosive. Erosional hiatuses are linked with the coarser sediment facies within the core set, this extends from fine sand upwards. These cores are often positioned in the proximity of the high velocity AAIW along the mid-slope Terrace 2 (Hernández-Molina *et al.*, 2016)

such as UPC125 and UPC164. However, we also observe discontinuities in some of the sandier drift cores such as UPC001, UPC032 and UPC170.

*Table 4.3 Depositional Environment and locality of each piston core.*

| Core No. | Water Depth (m) | Locality   | Depositional Environment |
|----------|-----------------|------------|--------------------------|
| UPC001   | -2053.05        | Midslope   | Drift 1                  |
| UPC032   | -2513.29        | Lowerslope | Drift 2                  |
| UPC065   | -1896.61        | Midslope   | Submarine Canyon         |
| UPC125   | -1121.22        | Midslope   | Scoured Terrace 2        |
| UPC133   | -2451           | Lowerslope | Separated Drift 3        |
| UPC154   | -3158.49        | Lowerslope | Pockmarked Terrace 4     |
| UPC164   | -1188.35        | Midslope   | Drift Terrace 2          |
| UPC170   | -2535           | Lowerslope | Drift 2/Turbidite Valley |

On the mid-slope Terrace 2, amalgamated massive sands and cross-laminated sands are common. The sand beds are divided by erosional surfaces and hiatuses which indicate an even greater increase in bottom current velocity. Within the sandier drift cores, we instead see a cyclic nature to bed transitions. The sand units in the drifts are often composed of fine bioturbated sands and their cyclicity from coarser to finer grain sizes and gradational, non-depositional

and bioturbated contacts indicates that bottom currents increase in velocity periodically, whereas in between much calmer conditions prevail. This mode of cyclicity is similar to that seen in ancient examples from Cyprus, clearly seen in outcrop (Miguez-Salas *et al.*, 2019).

The difference between erosional and discontinuous contacts found in contouritic settings compared to other deep-water sedimentary processes such as those observed in turbidites and debrites relate to subtle differences related to facies sequencing (Rebesco *et al.*, 2014). In the few full turbidite sequences we see in core UPC065, muddy facies are below erosional contacts. This indicates a very rapid change in depositional strength from slow (<10 cm/s) to vigorous (>25 cm/s) (Stow and Smillie, 2020). Events such as these where there has been a catastrophic change in energy are never seen in contourite depositional systems. In a contourite facies sequence it is more common to observe gradual increases in grain size (reverse grading) that shows a more gradual increase in energy, that can still reach a point where erosion and non-depositional bottom current velocities can be achieved. Beyond the erosional contact, a fining upwards normally graded facies is often observed that indicates a weakening bottom current. Contourites display a much more diverse set of boundary types when compared to turbidite boundaries. Contourite sequences display a broad set of gradational, non-depositional to erosional boundary types. Gradational contacts are not observed in turbidite sequences (Rebesco *et al.*, 2014). These are observed in finer-grained contourite sequences such as those observed in the Drift 1, 2 and 3 sediment cores. Gradations in grain size correspond to variations in the strength in bottom currents and in these finer grained contourite sequences they do not reach the threshold for non-depositional velocities.

#### 4.4.1.1.2 Sedimentary Structures

Preservation of primary sedimentary structures in contourites is entirely dependent on grain size. In contourite sands it is easier to preserve structures such as laminations. Finer grained contourites often have their primary sedimentary structures destroyed by the reworking of bioturbation (Wetzel *et al.*, 2008). There is a significant decrease in the intensity of bioturbation within medium to coarse-grained sands, but it is still pervasive within fine sands.

Many of the sands in this study show some evidence for primary sedimentary structures, however it is often lost in beds that are massive and structureless. Massive and structureless units may be the result of the fluidised soft sediment being disturbed during core collection and destroying any evidence of primary structures. For example, core UPC158 that was split but not used in this study due to its coarse, sandy nature it was totally fluidised within the core tube. However, cores such as UPC125 appear to have survived core collection undeformed despite being coarse grained throughout. Yet, many units in this core appear to be absent of any primary sedimentary structures. This could be linked to higher accumulation rates in UPC125 when compared to other sandy settings such as UPC164 that preserve sedimentary structures and have a lower accumulation rate. Examples of primary sedimentary structures such as laminations and cross-laminations are also quite localised within sand units and do not continue for very long intervals within the cores. Preservation of primary structures is not as extensive as those seen elsewhere in the Atlantic Ocean (Stow *et al.*, 1998) or ancient outcrop examples (Capella *et al.*, 2017).

Within the turbidite successions we see a full suite of primary sedimentary structures typical of those in the turbidite facies models described in previous

chapters (Bouma, 1964). This is due to the sudden emplacement of sediment that is not exposed to prolonged intervals of bioturbation. There is some evidence for minor bioturbation in the finer muddy turbidite caps where there has been a brief hiatus between sand emplacement events.


#### 4.4.1.1.3 Using biology to identify contourite facies

X-radiograph imaging has greatly aided the identification of bioturbation in our sediment cores and it has been used with equal success in other studies (Wetzel *et al.*, 2008). X-radiographs are quick and easy to interpret otherwise invisible changes in density of sediment whether that be between a burrow and surrounding sediment or internal primary sediment structures. Ichnology has a promising future in contourite research, defining an ichnofacies model for contourites may aid in their identification, however only a few studies have attempted to use trace fossils to define these facies (Löwemark *et al.*, 2004; Baldwin *et al.*, 2007; Wetzel *et al.*, 2008; Miguez-Salas *et al.*, 2019). In these studies, many of the authors have linked grain size to bioturbation style and extent of recolonization in an attempt to interpret sediment transportation processes where they are not immediately identifiable. Extensive bioturbation has been used as one of the key criteria in the identification of fine-grained contourites as this is a unique environmental setting in the context of the studied areas (Stow and Faugères, 2008). However, bioturbation can occur in any environment where there is a sufficient food supply to sustain a benthic community, where accumulation rates do not out-run bioturbation/recolonization rate and the substrate is suitable for habitation. Therefore, presence of extensive burrowing communities is not restricted to contourite environments and should be used only to provide further evidence for depositional regime. Figure 4.4 from

Wetzel *et al.*, (2008) summarises how benthic communities change with grain size. A change in grain size is used as a proxy for current velocity, the strength of a current determines the ability of benthic organisms to stabilise themselves onto/within a substrate and ultimately amount, mode and type of food delivered to the site.

Bioturbation tends to be absent in turbidites due to the catastrophic emplacement of the turbidite event beds. Any organisms inhabiting the seafloor sediment are removed as the turbidite passes over the area. The speed at which the sand bed is emplaced inhibits any reworking of the bed. Some bioturbation may still occur in the fine turbidite cap of the succession, but this is only possible if the time period between subsequent emplacement events is enough for benthic organisms to recolonise the substrate, leaving a gap of unbioturbated sediment. This poses an unfortunate problem that turbidite and contourite sands may show similar low bioturbation rates and cannot be distinguished from one another. While it is possible to distinguish contourites from turbidites in the finer fractions using bioturbation rates (Wetzel *et al.*, 2008), it remains difficult, if not impossible using ichnotaxa alone. In this study, we find using the same approach of the bioturbation studies (Figure 4.4) that focus on grain size and disturbance-succession patterns it may be possible to distinguish contourite and turbidite sands from one another using other benthic organisms such as foraminifera (Chapter 6).

Table 4.4 The main methods of bioturbation identified within sediment under the persistent action of bottom currents and how they change with variation in bottom current velocity. From (Wetzel et al., 2008)

| Substrate              | Mud  | Silt       | Fine Sand   | Medium Sand               | Coarse Sand   |
|------------------------|--|------------|---|---------------------------|---|
| Current velocity       | Low Energy   |            |   |                           | High Energy   |
| Sedimentary process    | Settling   | Deposition |   | Winnowing                 | Erosion   |
| Laterally advected POM | Deposited  |            |   | Suspended                 |   |
| Extent of Bioturbation |  |            |   |                           |   |
| Current effects        | Import of juveniles, larvae, POM   |            |   | Removal of POM, juveniles |   |
| Feeding Strategy       | Temporary Interface feeding - <b>Deposit feeding</b>                               |            | Filter feeding - <b>Interface/Deposit feeding</b> |                           | <b>Filter feeding/Interface feeding</b> (deposit feeding) |
| Dominant Trace Fossil  | Small Scale Bioturbation ← → Large Scale Bioturbation - - -                        |            |   |                           |   |

#### 4.4.1.2 Facies

Subjecting the cores to visual, gravimetric grain size, x-radiography and MSCL analyses has allowed the identification of a number of facies. These sequences are based on grain size trends, sedimentary structures and degree of bioturbation.

The cores collected from the mid-slope terrace (UPC125 & UPC164) show the greatest accumulations of contourite sands. Sand units here can often reach 1-1.5 m in thickness. The drifts show more of a cyclic pattern in deposition, dominated by silts and fine sand units, they appear to switch for periods of weak bottom current velocities to periods of higher velocity capable of transporting fine sand. The silt and sand beds range in thickness from 0.5-1 m in thickness. Meanwhile, the submarine canyon core is dominated by fine silt and mud deposition with intermittent influxes of thin (<20 cm) units of coarse silt/fine sand beds that fine upwards into mud caps. The sediment bed type, thickness and grain size are dependent on sediment influx, persistence of bottom current

influence versus downslope influence, and erosion and deposition of sediment. Vigorous bottom current alongside the deposition of the finer-grained facies, has formed a number of different facies sequences. Bottom currents appear to even have a role in the facies sequences observed in the shelter of the submarine canyons that incise the slope (Voigt *et al.*, 2013). These include turbidite beds with top cut out, turbidites with reworked finer units and bi-gradational sequences that can have their tops and/or their bases cut-out (Rebesco *et al.*, 2014). Here, we link changes in grain size to changes in bottom current velocity. Therefore, any changes observed in grain size can be linked to a changing transport capacity of currents and mode of deposition in any of the morphosedimentary environments.

Turbidite silt and sand facies (Ta to Td) are typical of other fine-grained turbidite facies observed elsewhere (Stow and Shanmugam, 1980). However, a significant number of the sequences are missing their finer fractions (Te). Many of the beds within the expected turbidite setting show evidence for bi-gradational grain size changes more typical of a drift deposit. We attribute these features to the reworking of sediment into the submarine canyons by strong and persistent bottom currents acting on the terrace above. As the current passes over the canyon it loses sediment carrying capacity and drops its load, thus feeding the canyon (Voigt *et al.*, 2013). Despite a bottom current source, it appears that within the canyon, there are still down-canyon processes that move the sediment towards the mouth. Evidence for gravity driven transport are in the multiple fining upwards sequences within the core. There is very little bioturbation particularly within the coarser units due to the rate of disturbance and sediment removal by the turbidity current.



Silt-very fine sand contourite facies (C1 and C5) in contrast to fine turbidites are heavily bioturbated and this action of benthic organisms has destroyed any evidence of primary sedimentary structures. Extensive bioturbation in these units leads to a mottled appearance on the split core surface. This level of bioturbation is possible due to the ongoing steady and total sediment reworking by slow moving bottom currents. These currents enhance ventilation and nutrient delivery to the sea floor sediments that encourages the growth of benthic communities. Finer grained turbidites like these are generally found in drift or flysch settings with gradational contacts between each unit (Stanley, 1993).

Fine contourite sands (C2 and C4) also contain an ichnofabric, however the burrows in this grain size are wider and longer overall by several cm. Some evidence of primary sedimentary structures may be seen due to less pervasive sediment reworking by benthic organisms due to the stronger current velocities that could both prevent organisms from establishing themselves on the seabed and/or restrict a high quality food supply from the water column. The larger grain size indicates higher velocity bottom currents, which will prevent colonisation of the seafloor by smaller organisms and juveniles of larger taxa. This results in a community of larger (> sand to gravel-sized) and deeper burrowing benthic species (Wetzel *et al.*, 2008). These units are typical of drift settings and will show gradational contacts with finer sediments and may show internal hiatuses in sedimentation.

Medium – coarse contourite sands (C3) are often massive and these are observed most commonly on the mid-slope terrace. They are broadly structureless with only some evidence of localised primary sedimentary structures. Boundaries to other finer units are often abrupt and erosional as seen

in core UPC164. In UPC125 we see a sequence of amalgamated sands with an increased thickness than those seen in UPC164.

It is observed that contourite sands mainly accumulate on top of the mid-slope terrace (Figure 4.2). The drifts and deeper localities in the study areas show a marked reduction in sand content. This shows that grain size reduces away from the high velocity AAIW bottom current core (Hernández-Molina *et al.*, 2016). It is likely that this bottom current can transport sand facies a significant distance along the terrace. Through time it may be possible to track changes in the strongest bottom current by the proportion of sand in a particular interval. This could allow the mapping of past bottom current routes and positions on the slope.

Table 4.5 A comparison of the expected patterns of bioturbation in hemipelagic, turbiditic and contouritic sedimentary environments. From (Wetzel, *et al.*, 2008)

|                              | Hemipelagic                          | Turbidite                                  |  | Contourite                                |                                       |
|------------------------------|--------------------------------------|--|--|---|---------------------------------------|
|                              |                                      | Mud  | Sand                                       | Mud                                       | Sand                                  |
| <b>Sediment Accumulation</b> | Continuous and slow                  | Instant & rapid                            | Instant & rapid                            | Semi-continuous deposition with reworking | Intermittent deposition & reworking   |
| <b>Organic Matter Influx</b> | Vertical flux                        | Vertical flux & suspension transportation  | Vertical flux & suspension transportation  | Vertical flux and lateral input           | Vertical flux & lateral input         |
| <b>Fauna Stability</b>       | Continuous                           | Death & decolonisation in turbidite events | Death & decolonisation in turbidite events | Continuous                                | Deep infauna may survive              |
| <b>Fauna Abundance</b>       | Average/Low                          | Dependent on frequency of turbidite events | Low  | Very high                                 | Fine Sand = High<br>Coarse Sand = Low |
| <b>Bioturbation Rate</b>     | Average - regulated by vertical flux | Generally low                              | Low  | Very high                                 | Fine Sand = High<br>Coarse Sand = Low |

#### 4.4.1.3 Bottom Current Reworked Turbidites

It is rare to find contourite deposition as the only depositional process in any environment. In the study area there is evidence for other depositional processes even under the strongest intermediate depth currents, there is interbedding of

different depositional process facies and reworking acting together. It is important to first distinguish a contourite as a thermohaline-driven bottom current. The features identified in this study within contourite sands and muds show gradational transitions, few bedform features and a high level of bioturbation. It is important to note, however, that bottom current sands and muds can be deposited by other oceanographic processes such as wind-driven currents, internal tides, internal waves, benthic storms and tsunamis (Shanmugam, 2018). These deposits have a wider range of features than the ones listed above for true contourites (Stow & Smillie, 2020).

The deposition of downslope (turbidite) and along-slope (contourite) processes are synchronous on the Uruguayan Continental Slope, and if there is a pervasive high velocity current, bottom current reworked sands are formed. The deposits formed from the winnowing of downslope turbidite deposits have become a particular interest to researchers (Shanmugam, 2006; Mulder *et al.*, 2008). The current will scavenge finer particles from the turbidite plume and redistribute them along the slope (See Figures 2.5 and 2.6 in Chapter 2). This has been observed along the Brazil Margin (Moraes *et al.*, 2007b) and the French Margins (Savoie, Piper and Droz, 1993). This interaction can also be observed at the facies scale as turbidites that have been modified (Stanley, 1993). The turbidite beds show normal grading as is the norm, but its cap has been reworked by contourite activity (Mulder, Faugères and Gonthier, 2008). These types of altered turbidite beds have been observed in the Columbia Channel on the Brazil margin (Faugères *et al.*, 2008). This study has observed similar beds with the cores from drifts (UPC001 & UPC032) and within the submarine canyon (UPC065).

The reworked turbidites in the drift sediments (UPC001 & UPC032) could be periodically delivered from the shelf and reworked along the terrace. The reworked turbidites from the submarine canyon (UPC065) are likely formed as a sediment laden current passes over the deeper cut in the terrace, the current loses velocity and drops its sediment load into the canyon. The extent of sediment reworking is dependent on the velocity of the current and therefore its transport capacity for sediment.

At higher velocities, bottom currents can erode and completely remove and redistribute turbidite deposits. The eroded sediment will be deposited along-slope in another location where the transport capacity of the bottom current is weakened. When the current isn't strong enough to transport the sand fraction of the downslope deposit, it will only transport the finer material. This leaves a relatively well-sorted sand body behind. These winnowed sand bodies are becoming increasingly important to understand as they have promising hydrocarbon reservoir and carbon capture potential in the deep-sea.

Mixed contourite-turbidite systems similar to the one presented in this study where there are significant quantities of reworked sand bodies have been studied in detail from the Gulf of Mexico (Shanmugam, 2014; Shanmugam, 2016). However, care should be taken to ensure that the sediment deposit is sourced from a true contouritic process and not from other bottom current processes that may be just as influential in reworking sands in the deep-sea. The study of deep-water mixed systems is a burgeoning area of research and there must be an interdisciplinary approach in understanding how to characterise the different processes interacting with deep-water particles, whether it be sediment, biogenic material, or microplastics.

#### 4.5 Conclusions

The study of the Quaternary sedimentary system on the Uruguayan Continental Margin has brought the complexity of these systems and the varied deposits they contain into focus. The sediment grain size on the margin is seen to be entirely dependent on bottom current strength and position on the slope through time. The deposition and reworking of sand fraction in particular is seen to be focused on midslope terraces throughout the Late Pleistocene and Holocene. By using a mixture of bathymetric, facies and sedimentary data it is clear that contouritic features are difficult to identify in a deep water setting. Many of the features identified can also be attributed to those seen in other deposits such as turbidites. Positive identification of a particular sediment facies as contourite is extremely challenging. Mud-rich contourites are easily misidentified as pelagic and hemipelagic sediments, whereas silty to sandy contourites can be confused with turbidites and vice-versa. However, using a combination of colour, sediment structures and bioturbation from core scanning, along side detailed physical properties and elemental ratio proxies from ITRAX, it was possible to separate facies from one another in both mud and sand-rich environments.

Despite these complications, the core data do validate the interpretations and morphosedimentary map by Hernández-Molina *et al.* (2016). Each environment interpreted on the morphosedimentary map is seen to have a higher level of complexity on glacial-interglacial timescales than alluded to in these studies, but the overall geological interpretations of each environment are correct from the sedimentary ground-truthing presented in this chapter as sedimentary processes identified in each sediment core fit the interpreted features.

At the sediment core scale, careful evidence must be collected to identify facies to confidently distinguish between deep water processes, particularly in mixed systems such as this where they can be interbedded or be deposited as hybrid beds. Facies models for turbidites such as the Bouma Sequence are very good for the identification of turbulent, event-like deposition in an area that has a characteristic normal grading trend. Contourite facies models, such as the bigradational sequence of Stow *et al.* (2008) show a more gradual transition from fine to coarse sedimentation where there is a waxing and then a waning of bottom current flow velocity. However, this doesn't account for partial sequences or the importance of bioturbation that assisted in the identifications made here.

An understanding of palaeoceanographic and tectonic regime is essential for a positive identification of a particular deposit as contourite in origin. Therefore, chapter 5 will focus on a palaeoceanographic study of core UPC164 from the contourite terrace as this core appears to be located on a critical oceanographic watermass interface and contains one of the most extended Late Pleistocene and Holocene sedimentary records in the study area. However, at the finer scale, sedimentary identification presents new problems that require new tools for positive identification at the sediment core to outcrop scale. Chapter 6 will therefore present one such tool that may aid positive identification of a deposit as contourite.

# CHAPTER 5

---

## PALAEOCEANOGRAPHY

### *Migrations of Antarctic-Sourced Water in the Southwest Atlantic Since the LGM*

#### 5.1 Introduction

##### 5.1.1 Background

A vital aspect of conducting any contourite research is understanding how global and regional palaeoceanography has impacted the deposits in the selected study area. This work is costly and time consuming, however, it aids in the identification of contourite deposits past and present. In this section, we examine the geochemical signatures from a single sediment core and foraminiferal tests with the aim of 1) identifying the key signatures of specific watermasses in the past and present from sediment core and foraminiferal data, and 2) considering the driving factors for the variations in geochemical signatures observed through time.

This work makes use of a 6-metre sediment core (UPC164) collected from the contourite terrace located at the modern interface between two critical intermediate watermasses, known as Antarctic Intermediate Water (AAIW) and Upper Circumpolar Deepwater (UCDW). The piston core was collected during expedition J14092 conducted by BG Group on the Uruguay continental margin in 2014. The core was selected for palaeoceanographic study due to the sample location, good recovery, and because an adjacent repeat core was taken from the same site on the same expedition.

The core represents an extended record of sandy contourite deposition on the contourite terrace (Fig. 5.1 B & 5.2) The analysis presented herein is the first attempt that has been made to reconstruct the palaeoceanography of the watermasses at this depth (700 – 1000 mbsl) from a record on the terrace. As the terrace is one of the most conspicuous sedimentary features on the Uruguay slope, it is important to understand the processes and watermasses that led to its formation, as this will also provide new data on the migrations of Antarctic watermasses in the South Atlantic and the implications this has for Atlantic Ocean circulation in the past and present.

#### 5.1.2 Oceanographic Regime

The location of this study on the Uruguayan margin is vital for understanding South Atlantic oceanographic processes, as it provides evidence of a variety of critical watermasses sourced from northern and southern origins that flow close to the sea floor. The focus of this study will be on Antarctic-sourced waters, primarily Antarctic Intermediate Water (AAIW), which is formed in the Southwest Atlantic and Southeast Pacific (Piola & Gordon, 1989) (Figure 5.1). This intermediate watermass flows through the Drake Passage and transforms into Atlantic AAIW. It originates by subduction of cold/fresh Antarctic Surface Water across the Antarctic Polar Front, with additional contributions of Sub-Antarctic Mode Water during deep winter convection north of the Sub-Antarctic Front (Naveira Garabato *et al.*, 2009). Antarctic Intermediate Water is advected through the Drake Passage and flows northwards into and along the western edge of the Argentine Basin and gets incorporated into the South Atlantic subtropical gyre (Figure 5.1). The injection of cold/fresh AAIW into the subtropical gyre likely has important implications for the budget of heat and salinity in the Atlantic. Altering



this budget would have a knock-on effect for the rate of North Atlantic Deep Water (NADW) formation through increasing or decreasing density gradients (Rintoul, 1991; Graham *et al.*, 2011). Once AAIW enters the interior of the Atlantic (via the cold water route) it begins to be modified. Its components are incorporated into warm and salty varieties, such as the Agulhas current (warm water route) by interactions with the atmosphere and interior mixing. These currents become the upper limb of Atlantic Meridional Overturning Circulation (AMOC) which is a major mechanism of inter-hemispheric heat exchange (Lumpkin & Speer, 2007) (Figure 5.1). AMOC requires a volume transport balance of exports and imports from water masses, southward-flowing watermasses exported into the South Atlantic require an equal return flow. It has been suggested that southern-sourced watermass contributions balance the return flow and their thermohaline properties control the Atlantic Ocean's meridional heat and freshwater fluxes (Poole & Tomczak, 1999).

Previous studies have observed abrupt changes in AAIW flow to the north linked to AMOC reduction in North Atlantic deglacial cold periods, Heinrich Stadial 1 and Younger Dryas (Marchitto *et al.*, 1998; Laj *et al.*, 2002; Rickaby & Elderfield, 2005; Came *et al.*, 2008; Pahnke *et al.*, 2008; Thornalley *et al.*, 2011; Xie *et al.*, 2012; Huang *et al.*, 2014; Voigt *et al.*, 2016). However, there is no consensus as to whether AAIW strengthens or weakens during cold deglacial events.

Abrupt changes in AMOC during the Holocene and the forcing mechanisms behind them are still poorly understood. This is despite its capacity for dramatic and rapid changes, altering the distribution of oceanic heat, salt and carbon, with important repercussions for global climate. An important example of this behaviour is the bipolar “see-saw” process-linked changes in North Atlantic

freshwater budgets. The thermal bipolar see-saw hypothesis is the current explanation for the coupling of Dansgaard-Oeschger (DO) and Antarctic Isotope Maxima (AIM) events (these were rapid climate fluctuations in the northern and southern hemisphere that occurred in the last glacial period). Stocker & Johnsen, (2003) suggest that the temperature anomalies in Greenland and Antarctica during these events could be explained by changes in the rate of cross-equatorial ocean heat transport in the Atlantic, that are modulated at southern high latitudes by a large heat reservoir (the Southern Ocean). Evidence gleaned from climate archives suggests that abrupt transitions in the past were foreshadowed by systematic behaviour of the climate that could potentially provide early warning indicators. If AMOC were to undergo any significant changes it would have major repercussions on Earth's climate. For example, a slowdown of AMOC is associated with a warming of the Southern Ocean and Antarctica in a 'see-saw' response (Masson-Delmotte et al., 2013; Rahmstorf, 2002). The long-term cooling of the subpolar Atlantic contrasts with the simultaneous global warming since the industrial era began, raising concerns that we are currently in the early stages of such a "see-saw" process (Caesar *et al.* 2018). It is important to fully understand the dynamics, control and impact of changes in AMOC polarity, which is inhibited by the very advanced level of constraint on past circulation changes in the northern hemisphere compared to the southern. It is critically important to address the knowledge deficit about interior circulation changes in the south Atlantic so that conceptual models concerning see-saw events are not excessively linked to northern hemisphere changes.

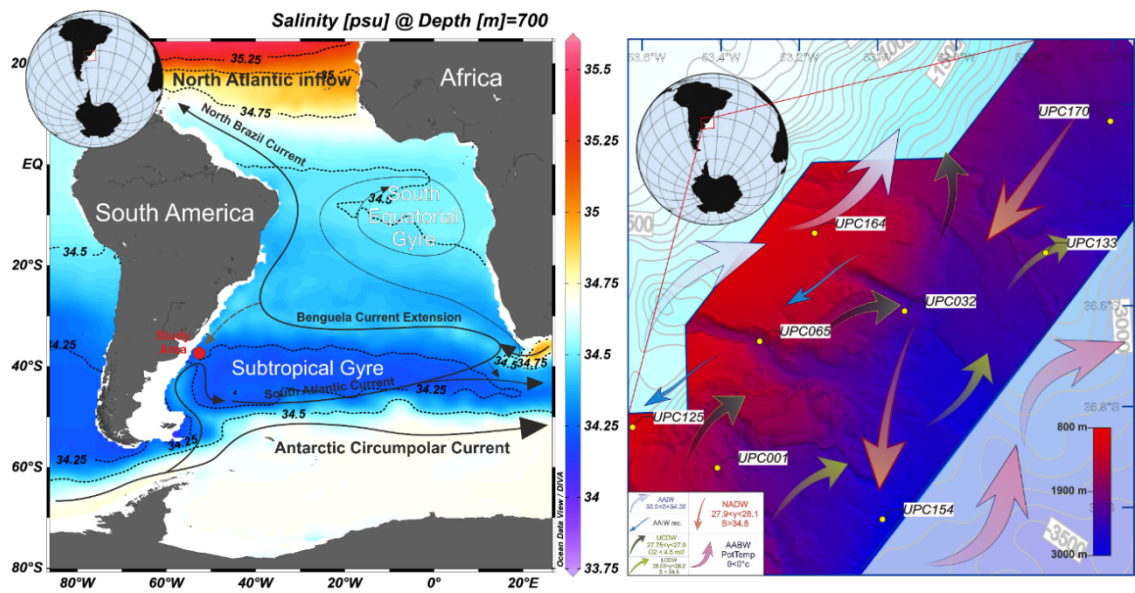


Figure 47 A: Modern annual salinity mean at 700 m water depth and flow of southern-sourced waters (black arrows) showing primary cold and warm water contributions to the South Atlantic. Southwestern Atlantic study area indicated in red. B: Enlargement of study area seabed generated in Petrel. Yellow dot indicates the location of core UPC164 on the Ewing terrace, on the interface between AAIW and UCDW. Flow paths of the main watermasses are indicated by arrows and table with upper and lower property limits. AAIW = Antarctic Intermediate Water; UCDW = Upper Circumpolar Deep Water; NADW = North Atlantic Deep Water; LCDW = Lower Circumpolar Deep Water; AABW = Antarctic Bottom Water. Prepared using Petrel, ArcGIS and Ocean Data View (<http://odv.awi.de>).

This dataset provides an opportunity to address the knowledge deficit about interior circulation changes in the South Atlantic since the last glacial period, but first the watermass components that make up this interior, all of which are observed offshore Uruguay must be characterised (Figure 5.1; 5.2 & 5.3). The upper parts of the ocean circulation offshore Uruguay contain the southward-flowing Brazil Current (BC), made up of Tropical Water (TW) and South Atlantic Central Water (SACW), and the northward-flowing Malvinas Current (MC), composed of Antarctic Intermediate Water (AAIW) and Upper Circumpolar Deep Water (UCDW) components. The northward-flowing Malvinas Current is the focus of this study, as it is topographically steered along the 1400 m isobath and

is thought to be linked to the formation of an extensive contourite terrace on the Argentine and Uruguay margins (Preu et al., 2013). The Brazil and Malvinas currents converge at a point located around 38°S directly offshore Uruguay, this creates the Brazil-Malvinas Confluence (BMC: Gordon & Greengrove, 1986; Piola & Matano, 2008; Stramma & England, 1999). The confluence is characterised by sharp gradients in temperature and salinity within the surface and subsurface watermasses. However, in contrast with the near surface layer Preu et al. (2013) found that there is no clear subsurface transition from watermasses of southern and northern origin. For example, their analysis shows that South Atlantic Central water (SACW) ( $\theta > 8\text{ }^{\circ}\text{C}$ ,  $S > 34.8$ ) detaches from the Western margin of the Atlantic around 36°S, while southern-sourced and northward flowing AAIW ( $S < 32.25$ ) flows along the margin to 30°S. It also suggests that southward flowing recirculated AAIW deviates from the margin around 29°S, while the North Atlantic Deep Water (NADW) extends to 38°S. Therefore the BMC should be thought of on a regional scale rather than a narrow strip. Importantly, migrations of the BMC over glacial-interglacial transitions are thought to influence the stratification of the watermasses below (Gordon and Greengrove, 1986; Gordon, 1989). Fluctuations on this scale are known to influence the South Atlantic subtropical gyre and therefore global ocean circulation and global climate, by linking back into the hypothesis of a bipolar see-saw operating within the Atlantic heat budget.

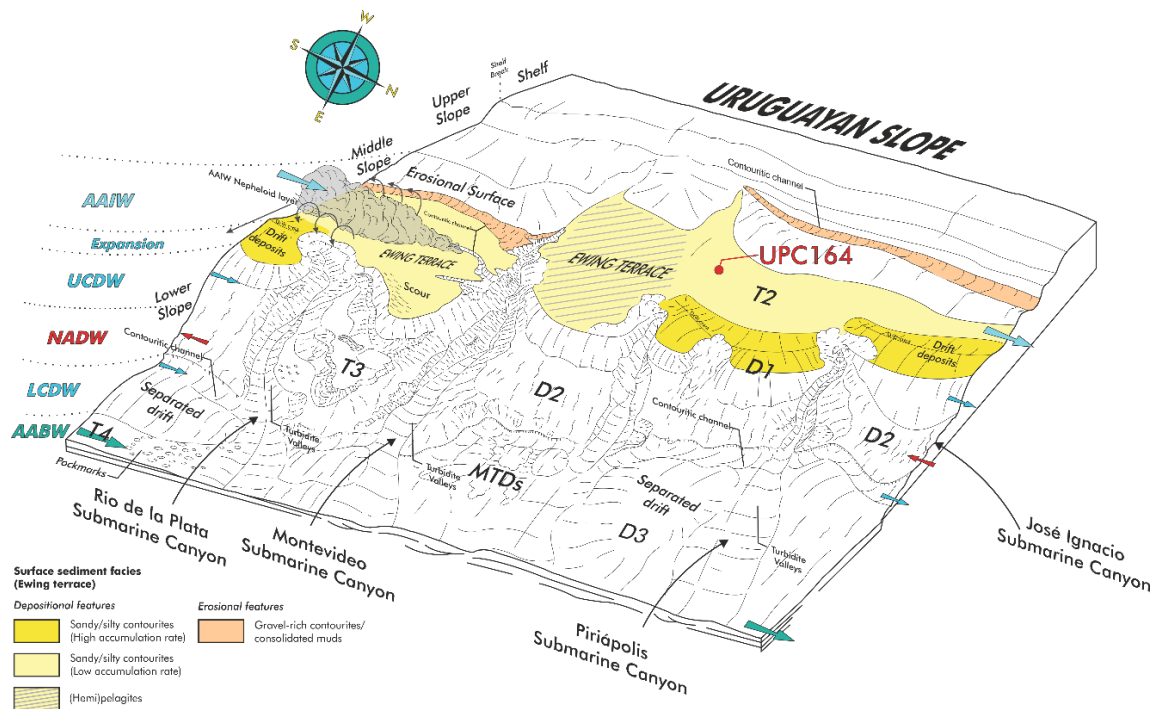


Figure 48 Modern morpho-sedimentary map of Uruguay continental margin (after Hernández-Molina et al., 2016; Preu et al., 2013; Voigt et al., 2013). Shows Ewing terrace contourite system incised by multiple submarine canyon systems. Yellow-coloured areas define Ewing terrace, located at interface of AAIW and UCDW. Voigt et al. (2013) showed lowermost portion of AAIW contains distinct nepheloid layer. Surface sediment facies defined following Bozzano, Violante, & Cerredo, 2011 and Hernández-Molina et al., 2016. Red circle shows location of core UPC164 investigated in this study. AAIW = Antarctic Intermediate Water; UCDW = Upper Circumpolar Deep Water; NADW = North Atlantic Deep Water; LCDW = Lower Circumpolar Deep Water; AABW = Antarctic Bottom Water; T2 = Terrace 2; D1 = Drift 1; D2 = Drift 2; T3 = Terrace 3; D3 = Drift 3; T4 = Terrace 4; MTDs = Mass Transport Deposits. Expansion zones relate to Holocene change and retreat of deeper water masses to increased NADW and AAIW.

To understand the distribution of water masses at depth, we must assign values to their physical and chemical properties (Table 5.1) and oceanographic transects (Fig. 5.3).

*Table 5.1 Summary of key watermasses located offshore Uruguay, their properties and characteristic flow directions. Criteria overlap with one another so only key parameters used to identify each watermass are listed below. ( $\theta$ =temperature; S=salinity; O<sub>2</sub>=oxygenation)*

| Watermass                           | Criteria   | Flow direction and deviation from seafloor (°S) |
|-------------------------------------|--|---|
| South Atlantic Central Water (SACW) | $\theta > 8\text{ }^{\circ}\text{C}$ , $S > 34.80$ | Northwards to 36°S                              |
| Antarctic Intermediate Water (AAIW) | $S < 32.25$  | Northwards to 30°S                              |
| Upper Circumpolar Deep Water (UCDW) | $\text{O}_2 < 4.50\text{ ml/l}$                    | Northwards to 35°S                              |
| North Atlantic Deep Water (NADW)    | $S > 34.80$  | Southwards to 38°S                              |
| Lower Circumpolar Deep Water (LCDW) | $S < 34.80$  | Northwards to ~36°S                             |
| Antarctic Bottom Water (AABW)       | $\theta < 0\text{ }^{\circ}\text{C}$               | Northwards depths below 3.5 km                  |

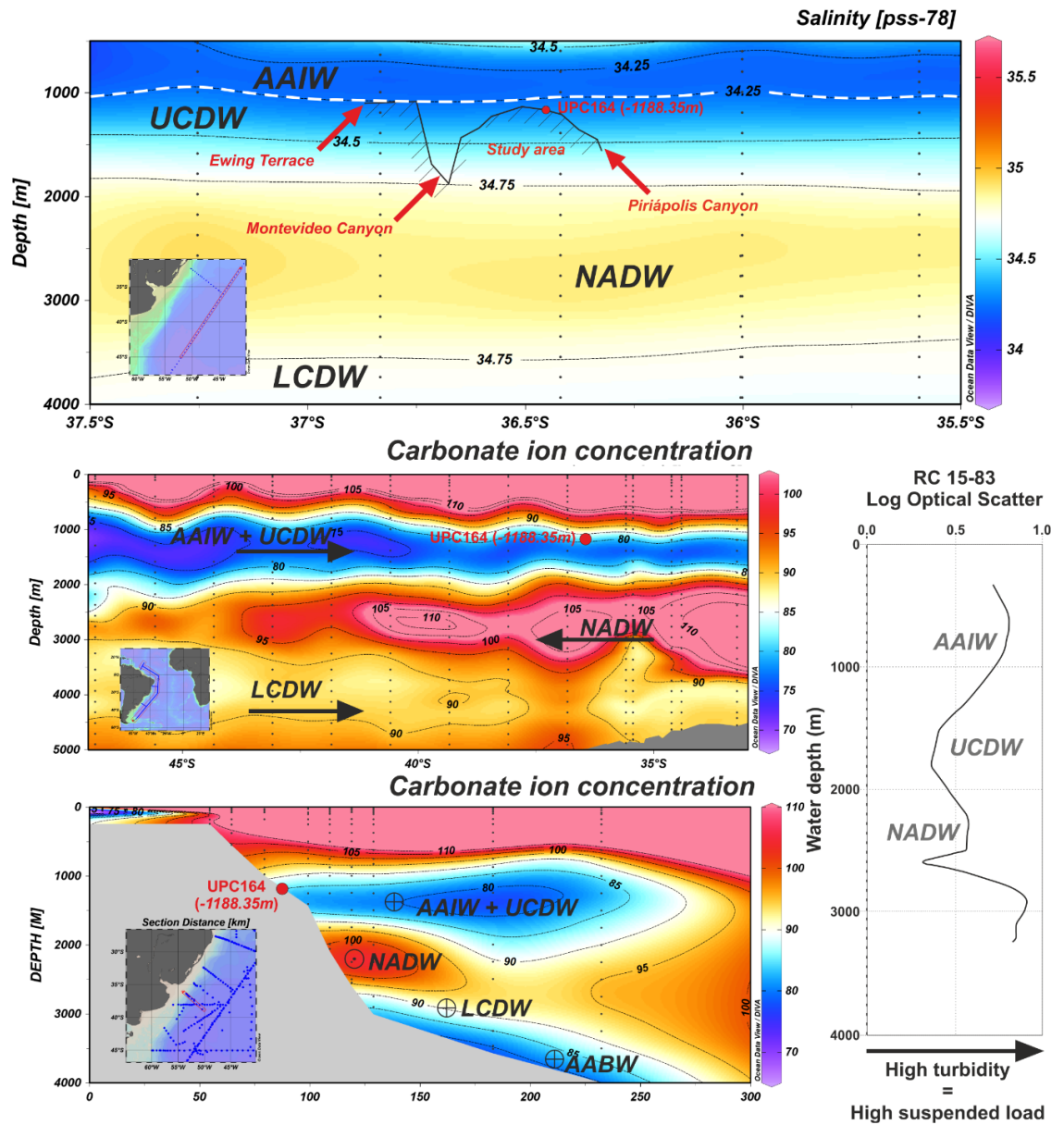


Figure 49 A: Section of salinity across the study area offshore Uruguay. A trace of the bathymetry along the Ewing terrace shows the intersecting Montevideo Canyon and Piriápolis Canyon. The red dot indicates the location of core UPC164 used in this study. The dashed white line indicates the interface between Antarctic Intermediate Water (AAIW) and Upper Circumpolar Deepwater (UCDW). B: Modern day carbonate ion concentration ( $\text{CO}_3^{2-}$ ) in the SW Atlantic, show in along and cross slope sections. The red dot shows the location of core UPC164 currently situated in the upper portion of the AAIW/UCDW. C: Turbidity depth profile taken to the south of the study area (Lamont-Doherty Earth Observatory) there is an increase in turbidity from ~700 – 1000 m where a nepheloid layer associated with the strong current activity within the range of AAIW. Prepared using Ocean Data View (<http://odv.awi.de>).

## 5.2 Materials & Methods

Piston core UPC 164 was recovered from the AAIW/UCDW interface on the contourite feature known as the Ewing terrace, offshore Uruguay. The cores were collected by BG Group in 2014 during expedition J14092.

*Table 5.2 Location of sediment core in this study*

| Cruise | Core   | Latitude  | Longitude    | Water depth (m) | Recovery (m) |
|--------|--------|-----------|--------------|-----------------|--------------|
| J14092 | UPC164 | -36.45574 | -53.16191263 | -1188.35        | 5.38         |

Weight percentage grain-size fractions were used to infer past variation of southern-sourced water flow speeds, and apply the planktonic foraminifera fragmentation index and ITRAX bulk geochemical ratios to detect calcite dissolution, oxygenation, productivity and current velocity within seafloor sediments. The core site is located at the interface between the southern (Glacial-CDW/AAIW/UCDW) and northern (Glacial-NCW/NADW) sourced water masses (Fig. 5.3). Northern-sourced waters enable good preservation of calcareous sediment due to calcite being supersaturated. In contrast, the overlying southern-sourced water has a lower carbonate ion concentration, which causes the dissolution of carbonate in the sediment. Using the foram fragmentation index (indicates corrosivity of seawater) and elemental ratios (quick guide for carbonate and heavy mineral content in sediment) allows us to determine vertical shifts of the interfaces between southern and northern sourced water, and the relationship between these shifts and the strength of the overlying watermass. We combine this with stable isotopes of oxygen and carbon obtained from benthic foraminifera to detect glacial-interglacial changes in surface and bottom water densities.



Lastly, we use planktonic foraminiferal assemblages (*N. pachyderma* (sinistral) percentage (NPS%), benthic/planktic ratios, warm vs. cold water dwellers) to detect shifts in sea surface temperature during the deglaciation. To reduce the impact of dissolution we only obtained dates from foraminiferal tests that showed no discolouration, fragmentation or recrystallisation.

## 5.3 Results

### 5.3.1 Chronostratigraphy

The results from the accelerator mass spectrometry radiocarbon dates and interpolated dates from the age/depth model calculated using the R Bchron package are present in Table 5.3.

Table 5.3 Accelerator mass spectrometry (AMS) radiocarbon dates and calibrated ages. IRMS isotope values from *G. inflata* included

| Species           | Probability | Conventional age | Calibrated age<br>95.4% probability<br>(cal ka B.P.) | Calibrated age,                             |          |                           |
|-------------------|-------------|------------------|--|---|----------|---------------------------|
|                   |             |                  |  | Interpolated<br>from model<br>(cal ka B.P.) | IRM<br>S | IRMS<br>d <sup>18</sup> O |
| <i>G. inflata</i> | 95.40%      | 1900 +/- 30 BP   | 1529 - 1358 cal BP                                   | 1470  | 1.70     | 2.59                      |
| <i>G. inflata</i> | 95.40%      | 4550 +/- 30 BP   | 4835 - 4646 cal BP                                   | 4762  | 1.60     | 2.68                      |
| <i>G. inflata</i> | 95.40%      | 8540 +/- 30 BP   | 9285 - 9051 cal BP                                   | 7932.5                                      | 1.40     | 2.73                      |
| <i>G. inflata</i> | 95.40%      | 8330 +/- 30 BP   | 8996 - 8771 cal BP                                   | 8915  | 1.50     | 2.79                      |
| <i>G. inflata</i> | 95.40%      | 10250 +/- 30 BP  | 11327 - 11147 cal BP                                 | 11218                                       | 1.30     | 3.09                      |
| <i>G. inflata</i> | 95.40%      | 10470 +/- 40 BP  | 11861 - 11346 cal BP                                 | 11488                                       | -0.60    | 1.60                      |
| <i>G. inflata</i> | 95.40%      | 10770 +/- 30 BP  | 12432 - 12046 cal BP                                 | 11698                                       | 1.20     | 3.00                      |
| <i>G. inflata</i> | 95.40%      | 10580 +/- 30 BP  | 12035 - 11693 cal BP                                 | 11877                                       | 1.40     | 3.05                      |
| <i>G. inflata</i> | 95.40%      | 10670 +/- 40 BP  | 12260 - 11825 cal BP                                 | 12022                                       | 1.40     | 3.13                      |
| <i>G. inflata</i> | 95.40%      | 10680 +/- 40 BP  | 12294 - 11843 cal BP                                 | 12181.5                                     | 1.00     | 2.77                      |
| <i>G. inflata</i> | 95.40%      | 10140 +/- 40 BP  | 11236 - 11040 cal BP                                 | 12726.5                                     | 1.20     | 3.20                      |
| <i>G. inflata</i> | 95.40%      | 12600 +/- 40 BP  | 14218 - 13940 cal BP                                 | 13886.5                                     | 0.20     | 2.41                      |

The radiocarbon results in this study in 12 species-specific samples of planktonic foraminifera *Globorotalia inflata* in the size fraction  $>150\ \mu\text{m}$  (BETA Analytic, Table 5.3). The radiocarbon dates were calibrated by BETA Analytic with the high-probability density (HPD) range method using the MARINE13 calibration curve and no  $\Delta R$  (Reimer et al., 2013). All ages are given in calibrated thousands of years before present (ka B.P.). The age-depth model, sedimentation/accumulation rates and activity (taking the calibrated ages and summing the probability distributions with the aim of estimating activity at the site through age as a proxy) were all calculated using the Bchron R package (Figure 5.4).

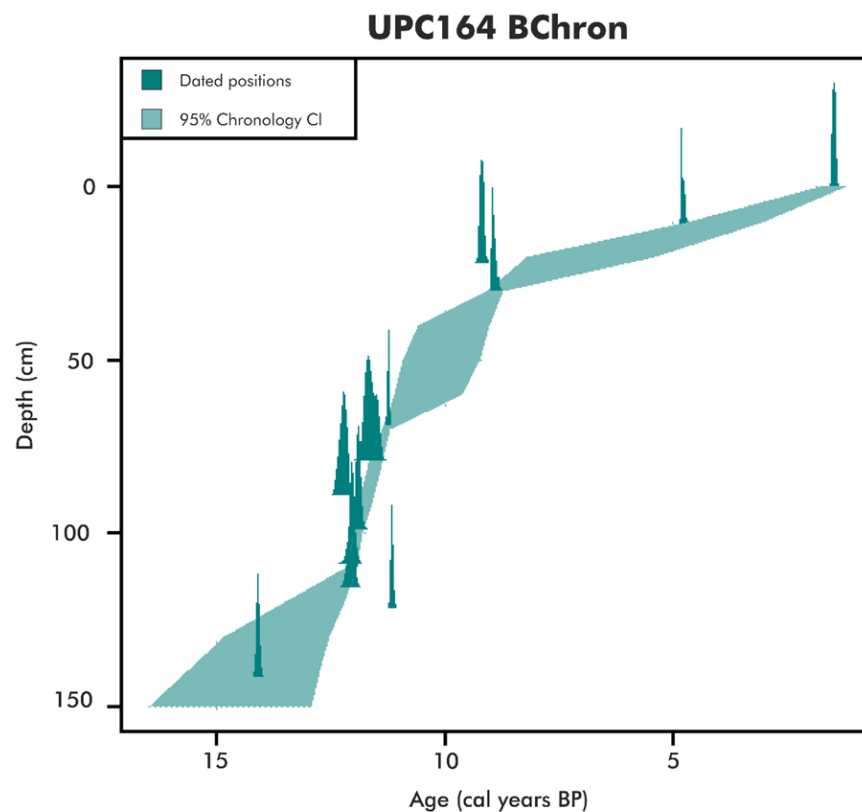


Figure 50 Age-depth model calculated from BChron R package for the 12 radiocarbon dates in Table 5.3

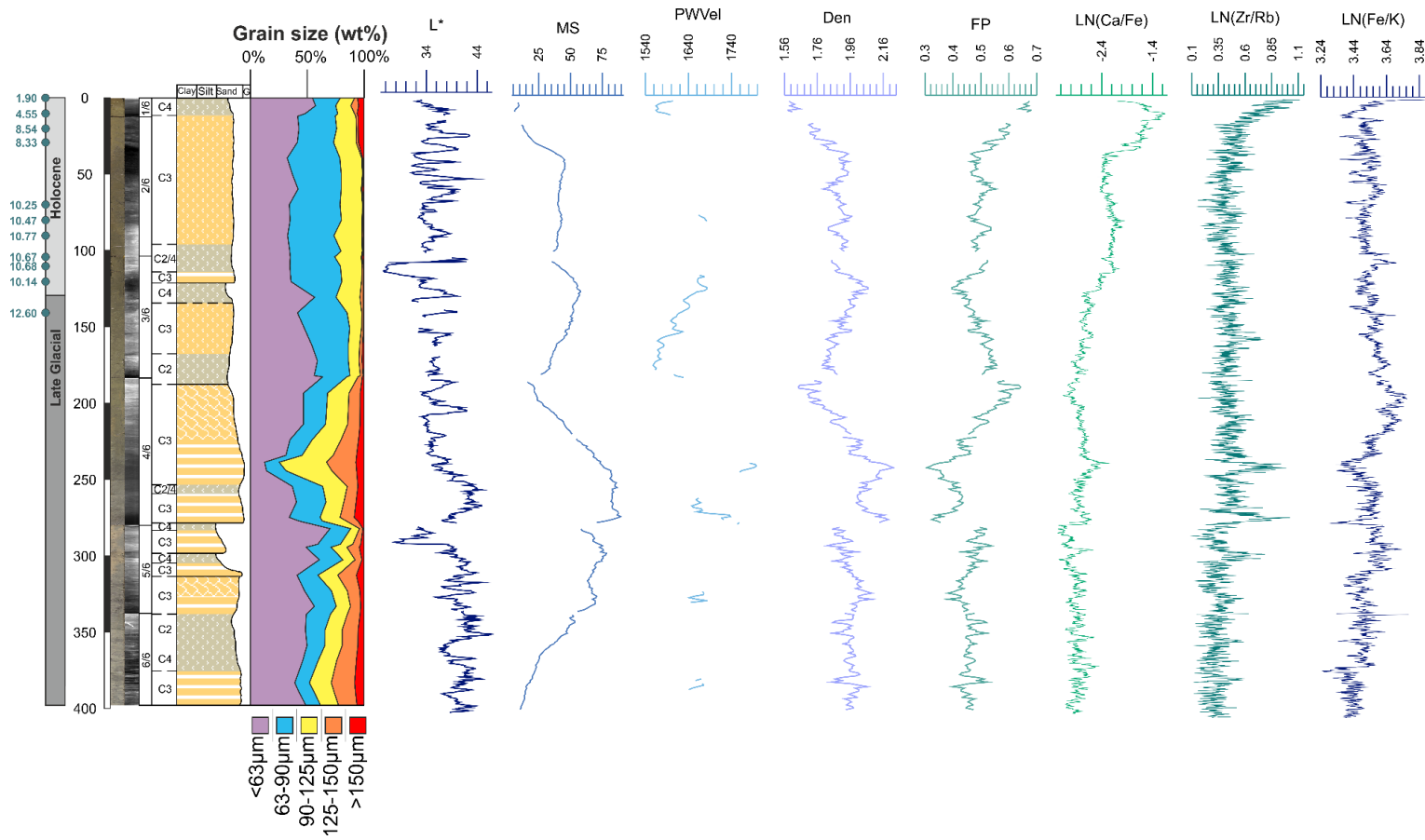


Figure 51 Summary of the sedimentary data collected for core UPC164 before conversion to age scale. Line scan images, radiographs, interpreted sedimentary facies, grain-size weight percentages downcore, L\* for lightness, MSCL-S physical properties and key ITRAX elemental ratios plotted as 5 point moving averages

### 5.3.2 Down-Core Trends

#### 5.3.2.1 Visual Logging & Facies Analysis

Visual logs were combined with radiographs, MSCL and ITRAX data to give a detailed log of the chosen sediment core UPC164 (Fig. 5.5). This core was selected for detailed palaeoceanographic study based on its recovery, availability of data already collected, sand content, depositional environment and position on the slope. Samples were taken at high-resolution (10 g of sediment taken at least every 10 cm down core) to aid core description, provide gravimetric grain size analyses and a low resolution radiocarbon, oxygen isotopes and foraminiferal assemblage indices. UPC164 was initially targeted to characterise the sandier localities in the study area for facies analysis (assessed in Chapter 4). The 6 metre core was logged at high resolution and changing facies, discontinuities and sedimentary units have been identified (Ch. 4 section 4.3.2.7). The core reveals a dynamic sedimentary system with an overall decrease in sedimentation rate that is interrupted by periods of non-deposition or erosion. The age model in Figure 5.4 suggests highly variable sedimentation rates in the core across the last deglaciation, from ~10 cm/kyr in the Holocene to ~50 cm/kyr during deglaciation. This trend is also seen in upstream sites of similar depths in proximity to Drake's Passage (Lamy *et al.*, 2015). The core is dominated by coarse-silt facies without many primary sedimentary structures probably due to a high intensity of bioturbation that is pervasive in these settings or other post depositional removal (Wetzel *et al.*, 2008). A coarser grain size during the Last Glacial Maximum, followed by a decrease in grain size from 70% to 20% particles being >63 µm between 18-15 ka, and an increase in grain size of 20% to 50%

particles being  $>63 \mu\text{m}$  from 15-10 ka. We see a general fining of grain size 50% to 30% particles being  $>63 \mu\text{m}$  throughout the Holocene section of the core.

The glacial sections of the core show layers of fine sand of a yellow to grey colour (Fig. 5.5) associated with the high manganese content in the sediment (this could indicate hiatuses/erosive surfaces that cannot be confirmed due to a restricted dateable zone to the Holocene portion of the core). The Holocene portions are characterised by a transition to homogeneous, strongly bioturbated coarse-silt facies. The early Holocene in the core is characterised by high sedimentation rates that decrease through to the late Holocene as indicated by calibrated AMS- $^{14}\text{C}$  ages shown in Table 5.3. Physical parameters and gravimetric grain size analysis, down-core high-resolution physical sediment properties of magnetic susceptibility, p-wave velocity, density, fractional porosity and lightness ( $L^*$ ) confirm the same glacial-interglacial transition observed in the visual logging results (Figure 5.5).  $L^*$  or lightness has successfully been used to reflect changes in local particle flux. It has been used as a reliable indicator of important sedimentological components such as carbonate (Rogerson *et al.*, 2006). It forms an important component for the initial chronostratigraphic model development for long marine sediment cores collected by the International Ocean Discovery Program as it can be used as a reliable indicator for the state of the climate (Ortiz *et al.*, 1999). Here, while it does appear to show a glacial-interglacial change, lightness does not increase into the interglacial. In the glacial, it is characterised by roughly correlating to changing grain size with broad intervals of change up to ~220 cm where it transitions to a more constant trend with short intervals of higher  $L^*$  values.

Magnetic susceptibility is used primarily as a relative proxy indicator for mineralogical changes in composition that can be linked to climatic processes. It is also extremely useful in core-to-core correlation. It is plotted alongside other key measurements of physical properties, P-wave velocity (stratigraphic correlation to seismic and determination of grain-size variations), Density (Proxy for the density (grains + fluid)) in the sediment and fractional porosity (mass-based calculation from gamma bulk density). The results from UPC164 (Figure 5.5) show a glacial-interglacial transition with a higher magnetic susceptibility response in the glacial sections of the core. The interglacial has a lower response and appears to have cyclicity. The higher values correspond with coarser grain sizes, indicating a mineralogical change within the sandier units. These sandier units are also observed to have higher densities, velocities and lower fractional porosity than the Holocene finer facies.

## 5.3.2.3 ITRAX Results

In total, eighteen elemental ratios were calculated for this project shown in Table 3.2, a summary of the ratios used in this chapter are shown in Table 5.4. These are difficult to accurately translate into element concentration (Section 3.3.1.3). Therefore, the ratios are used to only show down-core changes and as an aid to correlation between cores (Weltje & Tjallingii, 2008).

Table 5.4 Summary of elemental ratios used in this chapter, their importance and key studies

| <b>Elemental Ratio</b> | <b>Importance</b>  | <b>Case study</b>   |
|------------------------|--|---|
| Ca/Fe                  | Carbonate stratigraphy; core correlation; terrigenous turbidite mud discrimination.                                    | (Rothwell and Rack, 2006)   |
| Si/Al                  | Changes in aluminosilicates; biogenic production   | (Tisserand <i>et al.</i> , 2009)<br>(Dickson <i>et al.</i> , 2010)  |
| Ti/Al                  | Increase in particle size, environmental energy changes  | (Spofforth, Pälike and Green, 2008)   |
| K/Al                   | Provenance changes   | (Spofforth, Pälike and Green, 2008)   |
| Zr/Al                  | Bottom current intensity   | (van der Schee <i>et al.</i> , 2016)  |
| Zr/Rb                  | Increased heavy resistate minerals   | (Rothwell and Rack, 2006)   |
| Br/Cl                  | Presence of organic-rich layers, increased porosity  | (Rothwell and Rack, 2006)   |
| Mn/Fe                  | Identification of redox transitions, sub-oxic diagenesis   | (Marsh <i>et al.</i> , 2007)  |
| Fe/K                   | Basaltic material in IRD, changes in terrigenous mineralogy, used as north/south source indicator and core correlation | (Kuijpers <i>et al.</i> , 2003)<br>(Blanchet, Thouveny and Vidal, 2009)<br>(Warratz <i>et al.</i> , 2017) |

In Figure 5.5 where the Ca/Fe ratio is plotted against depth, we can see a gradual decrease in values down-core. The highest values are reported from the



Holocene in the upper portions of the core. Zr/Rb indicates an increase in heavy, resistate minerals such as zirconium, compared to rubidium which is enhanced in clays. It shows prominent peaks within the sandier facies and so Zr/Rb can be used as an indicator of increased winnowing. Fe/K indicates a change in terrigenous mineralogy and can be used to identify basaltic ice rafted debris (IRD) or source of the sediment. It is also useful as a core correlation tool. In Figure 5.5 Fe/K shows a shift in values of  $\sim 0.20$  at  $\sim 220$  cm, at the same depth there is an interglacial change in sediment grain size.

Once the elemental ratios are plotted onto an age scale in Figure 5.6 intensity of elemental responses can be linked to particular intervals of time.. By plotting such proxies for current velocities (Figures 5.5 & 5.6) alongside sediment grain size we can see that an increase in sand fraction corresponds with periods of increased winnowing shown by Zr/Al, Si/Al, Ti/Al, K/Al and Zr/Rb ratios. A decreased Ca/Fe ratio (Figure 5.6 D), meanwhile, coincides with periods of decreased current velocities (by proxy of grain size and elemental ratios) as seen from 300 – 275 cm and 200 – 150 cm.

Plotting  $\ln(\text{Ca/Fe})$  against age there is a clear decrease in values towards the LGM, but with three intervals of higher values. These values visually mirror our  $\delta^{18}\text{O}$  signal, foraminiferal total counts, and fragmentation index (Figure 5.7 & 5.8). Important periods of Ca/Fe lows include AIM-1, 11.5 – 10 ka BP and Late Holocene. Ratios of Br/Cl (Figure 5.6 C) which are a proxy for productivity, show an inverse correlation with Ca/Fe up to the Holocene where they show a common increasing trend. The ratios associated with an increase in current velocity (Zr/Al, Si/Al, Ti/Al, K/Al and Zr/Rb) show eight significant peaks; the most pronounced being at 15–14.5 ka BP, 11.5–10 ka BP,  $\sim 8$  ka BP, and 3–2 ka BP, while there

are significant troughs during 18–15 ka BP and at 13–11.5 ka BP. Down-core natural log ratios of Ca/Fe, Mn/Fe and Zr/Al show different chemical properties through the glacial-interglacial transition. Ca/Fe reflects a dramatic reduction of carbonate content into the glacial associated with more corrosive bottom waters, a signal seen across the entire study area (Figure 5.8). Mn/Fe shows pronounced high value peaks when colder conditions prevail (LGM and ACR) and lower values when climate was warming (Early-Mid Holocene and AIM-1). Zr/Rb linked above in Figure 5.5 to changes in winnowing intensity does not appear to correlate with the other winnowing indicators plotted in Figure 5.6. Two intervals where it diverges from the trend are the exit of the LGM at ~18 ka and in the Mid to Late Holocene it shows a much more pronounced increase in values than the other winnowing indicator ratios. This divergence may indicate a change in provenance rather than a change in relative current velocity.

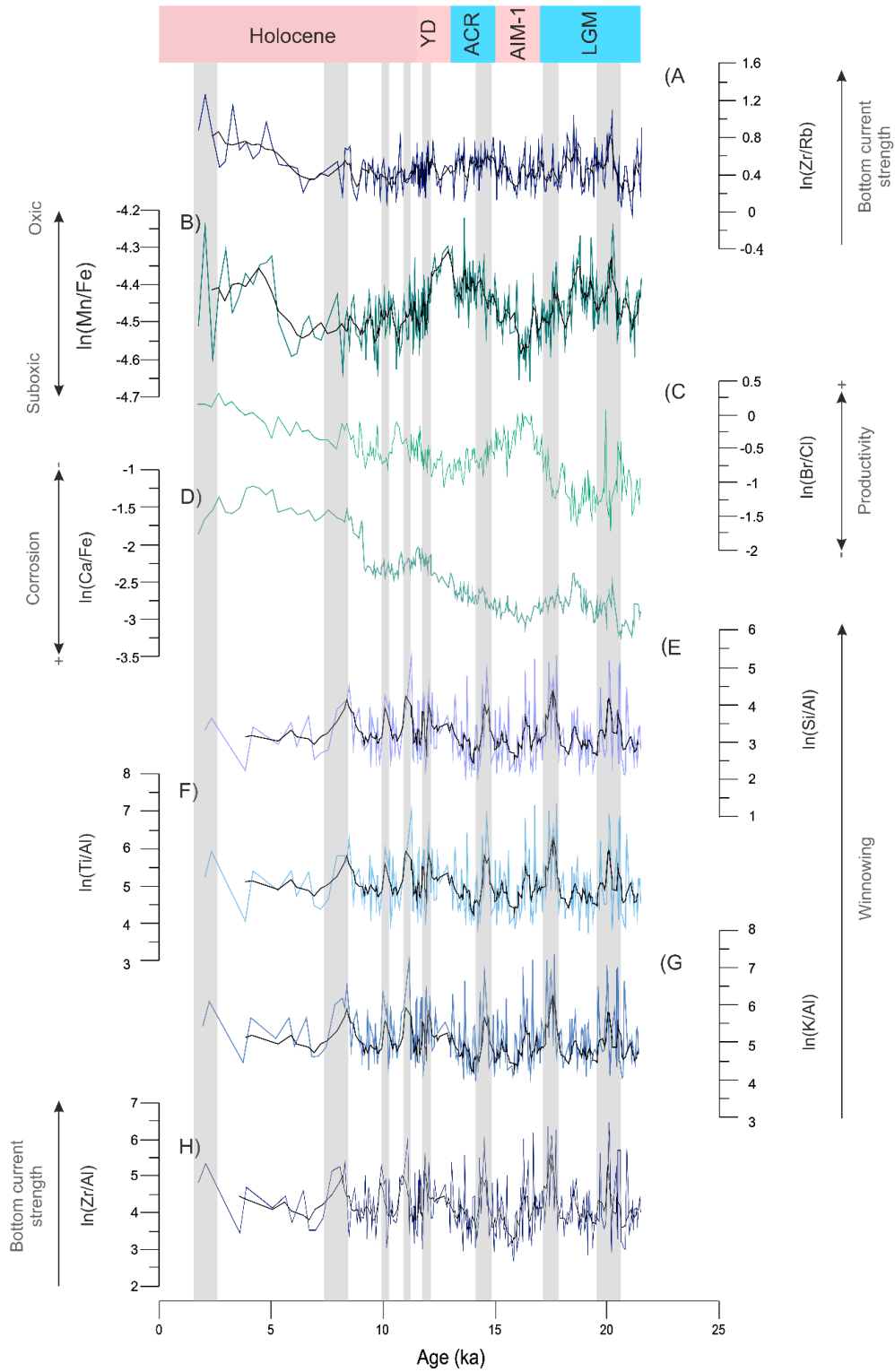


Figure 52 Age-adjusted key ITRAX elemental ratios for core UPC164. Time periods indicated across the top in pink for warming and blue for cooling in the Southern Hemisphere. Grey-shading indicates periods of more intense winnowing activity. Elemental ratio (A-H) use and key case studies listed in Table 5.4. (YD = Younger Dryas; ACR = Antarctic Cold Reversal; AIM-1 = Antarctic Isotope Maximum 1; LGM = Last Glacial Maximum)

#### 5.3.2.4 Oxygen Isotope Results

The data in Figure 5.7 reveal important deglacial changes in surface and deep ocean conditions. The benthic  $\delta^{18}\text{O}$  isotope record from our study site shows similar trends to the isotope record of the EPICA Dronning Maud Land (EDML) ice core when plotted alongside each other (Figure 5.7 B and C). Significant intervals where the benthic  $\delta^{18}\text{O}$  isotope values lighten are across AIM-1 and Younger Dryas. They appear heavier during the Last Glacial Maximum and Antarctic Cold Reversal. Overall a general decrease in values is observed into the interglacial. This record is very similar to the EDML ice core record over the same interval of time. Comparison of the benthic  $\delta^{18}\text{O}$  isotope record from UPC164 to the EDML  $\delta^{18}\text{O}$  isotope provides the most accurate chronology for interpretation of climate records. The EDML ice core records high resolution  $\delta^{18}\text{O}$  isotope measurements that can be used as a proxy for ice cap extent. The intermediate to deep ocean waters over our site therefore track changes in the O isotope record from the Southern Hemisphere.

#### 5.3.2.5 Micropalaeontology Results

The micropalaeontology data (Figure 5.7) can be indirectly compared to the O isotope records to examine how foraminifera responded to changes in climate in the South Atlantic as O isotopes reflect the amount of ice present at the poles and can therefore be an indicator of warmer or colder climatic conditions. This is done by assemblage counts of warm and cold-water species and percentage of sinistral (left coiling) *N. pachyderma*. The relative abundance of dextral versus sinistral *Neogloboquadrina pachyderma* has been used as a palaeo-indicator of Sea Surface Temperature (Bé & Tolderlund, 1971; Reynolds & Thunell, 1986; Pflaumann *et al.*, 2003; Žarić *et al.*, 2005). These counts are combined with

indices for benthic foraminifera diversity, the fragmentation index and percentage sand contained in each sample. The fragmentation index (Figure 5.7 G) shows highest values during AIM-1, YD and late Holocene. Fragmentation decreases during the ACR (100% to 10%) and early to mid-Holocene (50% to 10%). Across the ACR there is an increase in warm species 0% to 10%, with a decrease in NPS% from 80% to 40% (Figure 5.7 F and H). Benthic diversity also expands over this period from values of 0 Shannon Diversity Index (SDI) at 15 ka to values over 2 SDI for much of the Holocene. The ACR is seen as a relative cooling from  $\delta^{18}\text{O}$  and NPS% values. We see evidence for this cooling in our benthic  $\delta^{18}\text{O}$  isotope record and the increasing percentage of cold-water dwelling taxa. During the mid-ACR, a dramatic increase in carbonate preservation and benthic species diversity is recorded, coinciding with the beginning of the 15–10 ka BP increase in sand fraction.

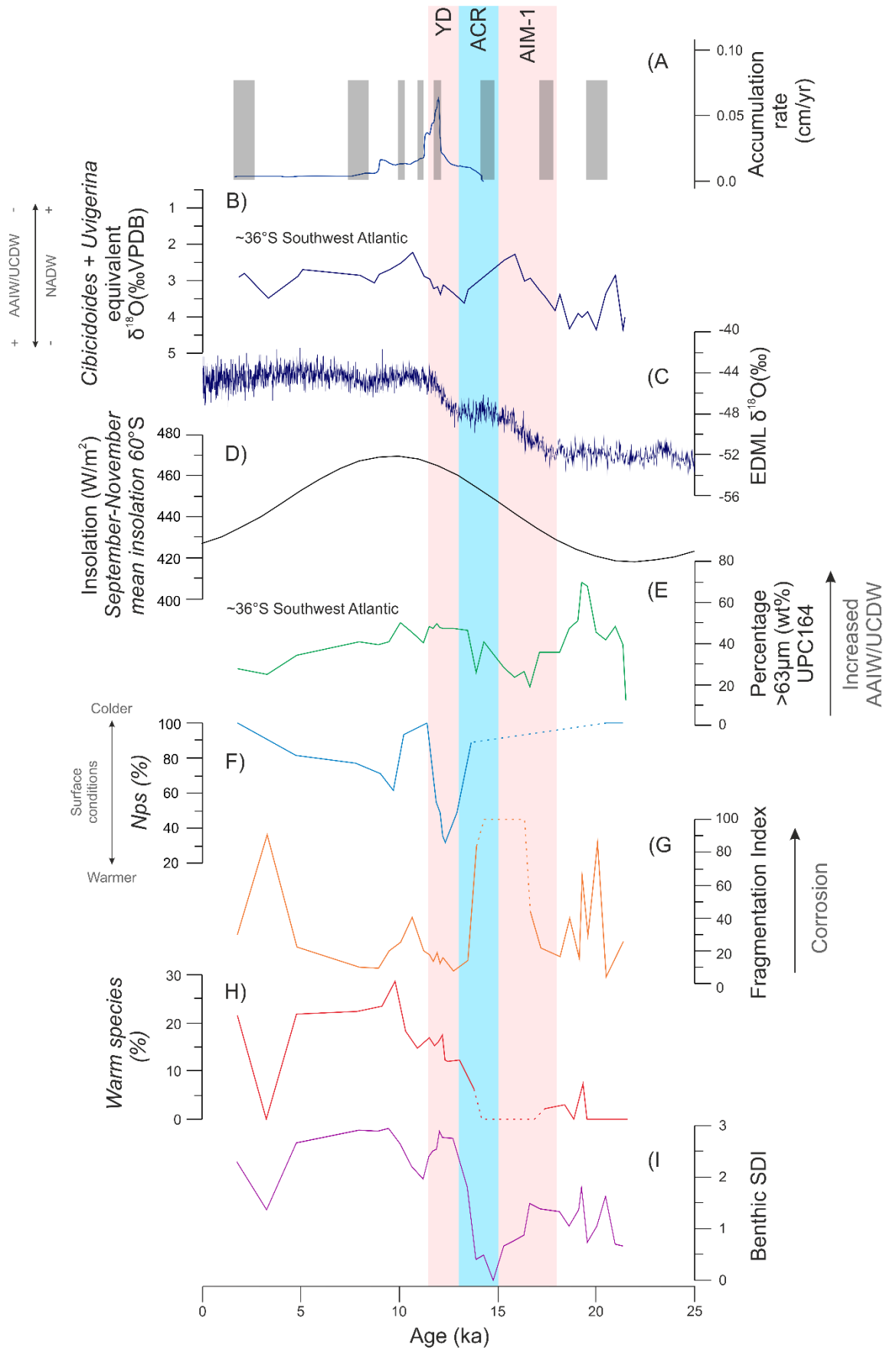


*Figure 53 Summary of micropalaeontological data collected from core UPC164. A: Grey shading shows periods of increased bottom current activity overlain on sediment accumulation rate. B: Cibicidoides + Uvigerina equivalent  $\delta^{18}\text{O}$  showing shifting position of AAIW through the last ~20 ka. C: Stable oxygen isotopes  $\delta^{18}\text{O}$  of ice core EDML. D: Austral spring (September–November) mean insolation at 60°S (Berger & Loutre, 1991; Renssen et al., 2005) E: Percentage sand fraction of core UPC164 F: %NPS is the percentage of left-coiling *Neogloboquadrina pachyderma* out of total *N. pachyderma*, with higher values reflecting colder surface conditions. G: Fragmentation Index of core UPC164. H: %warm is the combined contribution of warm planktonic foraminiferal species to the entire assemblage. I: Benthic Shannon Diversity Index showing higher diversity into the Holocene. Data recorded down core from the >150  $\mu\text{m}$  fraction.*

At the end of the ACR, a period of renewed warming begins (the Younger Dryas) with an increase in warm, surface-water foram species (Figure 5.7 H), alongside an increase in fragmented benthic tests and in sedimentation rate (Figure 5.7 G and 5.7 A). Fragmentation increases between 11.5 and 10 ka BP with a decrease in sedimentation rate. Entering the Holocene Thermal Maximum (HTM) we see a return of warm-water species and decrease of fragmentation on the seafloor.

### 5.3.3 Regional Downcore Trends

Further evidence for correlating trends in climate, current strength and foram community turnover across the core set regionally was gathered from plotting the ITRAX data from other cores against the stable oxygen isotopes  $\delta^{18}\text{O}$  of ice core EDML. This yields not only important information about sediment composition, but also about potential local or regional climatic signals that may be recorded in the sedimentary record. In addition to this, if an event can be identified across multiple cores, it allows a further constraint on core correlation. Ca/Fe ratio results have proven to be significant use in this study in correlation to other cores in the study area (Figure 5.5 and 5.6). Plotting Ca/Fe ratios against depth down core show common trends within each sedimentary environment. Both UPC001 and UPC065 show high levels of variability, with a general increasing trend down

core. UPC125 shows relatively consistent values of Ca/Fe with depth, with a slight increase in values within the finer grained section of the core. Within UPC164 high values are observed in the uppermost section of the core, with a gradual decrease in values with depth. Cores UPC154 and UPC170 show similar trends where high ratios are observed in the upper portions of the cores before decreasing dramatically down core



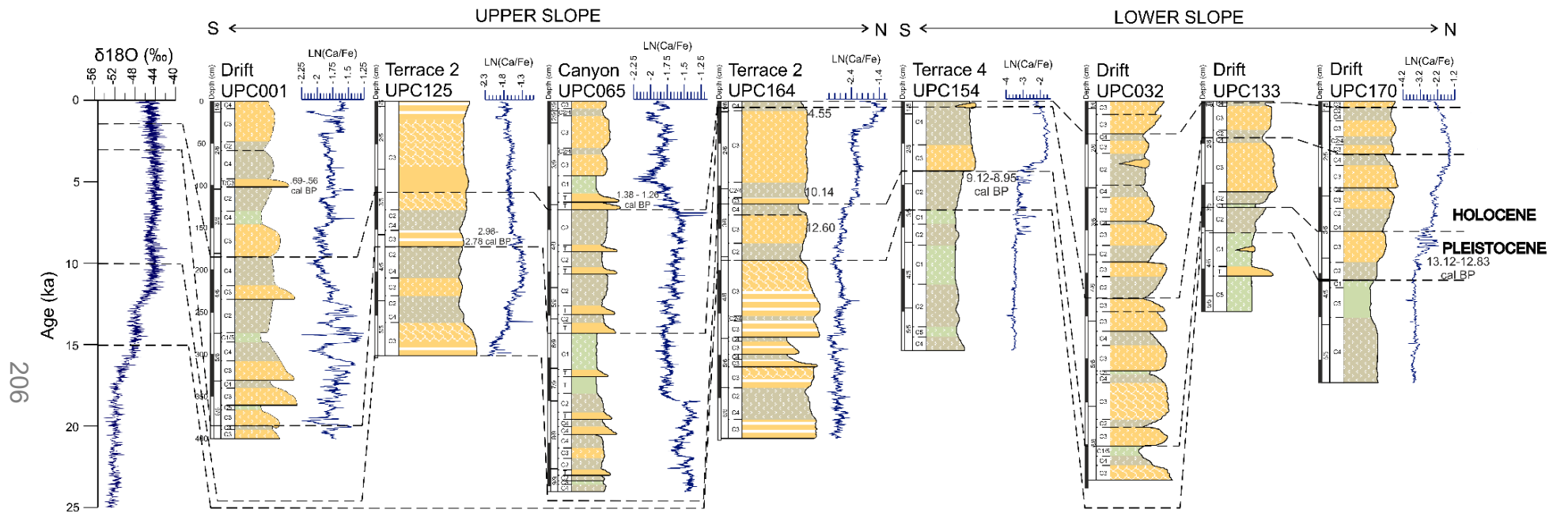


Figure 54 Stratigraphic table showing sedimentary logs of each core with ITRAX Ca/Fe elemental ratios for the upper and lower slopes from South to North. Dashed lines are interpreted tie points associated with radiocarbon dates and specific fluctuations observed in the Ca/Fe record. Lines are tied to the EDML oxygen isotope record (Barbante et al., 2006)

## 5.4 Discussion

### 5.4.1 Sediment Supply to the Ewing Terrace

The sedimentary analysis of core UPC164 provided here and in Chapter 4 shows the dominance of bottom-current activity on the Ewing terrace. The core shows evidence of the deposition of sand-silty contourites and hemipelagic deposits. All but the lowermost portions of the core are extensively bioturbated, destroying most of the primary sedimentary structures. Pervasive bioturbation has been previously recorded in contourites (Wetzel, Werner and Stow, 2008) and is seen as one of the key criteria in distinguishing deposits influenced by continuous bottom current activity on the seafloor, from those that are not (Stow *et al.*, 2002). A significant portion of our deposits contain 50 to 70% sand, in an area of the deep ocean that is not expected to be in the range of strong downslope transport. Accumulation rates also vary with periods of high deposition (weaker currents) and low accumulation to hiatus/erosional (from 10 mm per year to 0 mm). This indicates that Southern Component Water current velocity changed through time.

Data from the ITRAX support a changing current velocity as well as a change in the chemistry of the overlying water mass. The elemental ratios measured are proxies for changes in winnowing intensity (Bahr *et al.*, 2014b), strong peaks in values indicate that the terrace was exposed to periods of increased current velocities. These peaks occur at significant periods of climatic change and are likely due to a restructuring of watermasses and the passage of zones of higher velocity over the core site as a watermass interface deepens or shoals (Figure 5.9). Variations in K/Al in particular could indicate a changing sediment source: as a proxy for the clay mineral illite it indicates low intensities of chemical weathering on land associated with the Antarctic regions and are likely of this

origin here (Lantzsch *et al.*, 2014). Higher values of K/Al are used here as a proxy for the influence of Southern Component Water vs Northern Component Water on the terrace and show Northern Component Water dominates the terrace during the Holocene (Figure 5.6).

The decrease in grain size and winnowing intensity seen exiting the Last Glacial Maximum into AIM-1 is associated with the glacial expansion of deep Southern Component Water (Freeman *et al.*, 2016; Warratz *et al.*, 2017). Expansion of deeper waters would cause an upward shift of the high energy glacial-Circumpolar Deepwater/Northern Component Water interface, with an associated decline in current velocities and ventilation at the study site. The introduction and subsequent deepening of the of the Antarctic Intermediate Water/Northern Component Water interface across the Antarctic Cold Reversal to the depth range (700 – 1000 mbsl) of the study site could have resulted in increased current velocity (Preu *et al.*, 2013). The interface was positioned at this depth (700 – 1000 mbsl) until the Younger Dryas when we interpret an expansion of the Circumpolar Deepwater and movement of the interface upslope, replacing Northern Component Water. After the Younger Dryas, a reinvigorated Northern Component Water split the Circumpolar Deepwater into Upper and Lower Circumpolar Deepwater, confining them to the upper and lower slope respectively. The new Antarctic Intermediate Water/Upper Circumpolar Deepwater interface then moved upslope, away from our study area depth. This resulted in a decrease of current velocity and increase in sedimentation rate at the sampled site. Entering the Holocene, the Antarctic Intermediate Water/Upper Circumpolar Deepwater interface deepened initially over our core site in the Holocene Thermal Maximum and then began to deepen even further in the late

Holocene. The downward migration is tracked by a decrease in grain size and winnowing activity as indicated by Ti, Si, K and Zr proxies. The Holocene core interval shows a re-initiation and enhanced influence of modern North Atlantic Deepwater, compared to a relatively weak deep Southern Component Water flow (Böhm et al., 2015).

Our proposed vertical migrations of water masses support the construction of contourite terraces offshore Uruguay as observed by Hernández-Molina et al., (2016). The interaction between the local bottom current regime and the margin physiography results in terrace formation via a locally confined velocity maximum watermass core, interfacing with a much lower velocity watermass core of different depths and properties, carving a contourite channel at the base of the slope (Fig. 5.2). Sediment removed from the locality or resuspended from downslope channels is transported along the terrace and deposited on the seaward limit to form drifts, or into submarine canyons that intersect the terrace, where current velocity decreases. It is likely that the stronger currents and shallower position of the Antarctic Intermediate Water/Upper Circumpolar Deepwater interface during glacial periods changed the mode of terrace formation from phases of deposition/erosion of drifts over our core site (Preu et al., 2013).

#### 5.4.2 Carbonate Preservation as a Proxy for Variations in Southwest Atlantic Water Mass Structure

A lack of carbonate in the lowermost core samples (formed during the Last Glacial Maximum) and in parts of the deglacial interval could be explained by strong corrosion, low carbonate production, or both. The Ca/Fe ratio (a proxy for carbonate content) shows carbonate increasing after the Antarctic Cold Reversal

and in the Holocene Thermal Maximum (Figure 5.6, D). The low carbonate content in samples from the late Last Glacial Maximum is consistent with a shallow glacial-Upper Circumpolar Deepwater equivalent. A shoaling of deeper Southern Component Water to these depths would have severely inhibited vigorous Atlantic Meridional Overturning Circulation in the North Atlantic. As a result, well-ventilated and  $\text{CO}_3^{2-}$ -saturated North Atlantic Deepwater was not present in any great quantities to allow for well-preserved carbonate records. Instead, Upper Circumpolar Deepwater that is undersaturated in  $\text{CO}_3^{2-}$  has caused strong carbonate corrosion on the slope (Henrich *et al.*, 2003). We can therefore interpret carbonate-free sections in the deglacial as an effect of weakened NCW. With the introduction of well-ventilated AAIW at 15 ka BP, carbonate-free sections are then linked to AAIW. The Late Holocene carbonate decrease may be a result of Antarctic Intermediate Water taking on the character of Upper Circumpolar Deepwater, as it acts as a sink for atmospheric  $\text{CO}_2$  (Elmore *et al.*, 2015; Ronge *et al.*, 2015).

Additional factors in the dilution of carbonate during deglaciation include the rate of primary production. Dependent on ventilation, high primary production of organic carbon in the surface layer leads to increased organic input to, and thus suboxic conditions on the seafloor (Berger *et al.*, 1989). The shelf waters over our deep core site are periodically fertilized by La Plata River derived waters when they are not diverted to the north (Voigt *et al.*, 2013). Our Br/Cl record does show variability from cold to warm periods (Figure 5.6, C). While this variability in surface productivity-driven changes in carbonate content may not be negligible, we consider it to have only minor effects when compared to the highly corrosive potential of waters derived from the deep Southern Ocean.

A poorly ventilated, more sluggish Northern Component Water, particularly during the early deglacial and Younger Dryas, could have resulted in more corrosive waters due to an increase in the remineralisation of organic matter. However, our observations of increased winnowing activity and by proxy higher current velocities over the site agree with previous studies that suggest a greater portion of more vigorous deep Southern Component Water in the South Atlantic during the Last Glacial Maximum compared to the modern regime (Howe *et al.*, 2016). This was at the expense of non-corrosive Northern Component Water that was positioned as a shallow water mass beneath the Antarctic Intermediate Water. The first increase in carbonate content we see (enhanced Northern Component Water/Antarctic Intermediate Water) started during the Antarctic Cold Reversal (15 – 13 ka). This testifies to enhanced water mass ventilation that reduced the corrosivity of the waters at 1188 m depth. We see a return to more corrosive waters during the Younger Dryas and for a brief period afterwards due to a decrease in water mass ventilation. The extended period of corrosivity after the Younger Dryas up to 10 ka BP may be explained by the confinement of corrosive Upper Circumpolar Deepwater to the Ewing terrace. Around 10 ka BP is known for reduced Antarctic Intermediate Water production (Voigt *et al.*, 2016) and a reinvigoration of North Atlantic Deepwater after the Younger Dryas (Negre *et al.*, 2010; Skinner *et al.*, 2013; Jonkers *et al.*, 2015). Production of deep Southern Component Water is still increased (Warratz *et al.*, 2017) and this would act to confine the upper portion of the Circumpolar Deepwater to the depth of the terrace, under a shoaled Antarctic Intermediate Water. Entering the Holocene enhanced ventilation and production of Antarctic Intermediate Water keeps carbonate content relatively high.

### 5.4.3 Are these signals traceable on the rest of the margin?

Across cores UPC125, UPC154, UPC164 and UPC170 we observe upper sediment units that have relatively high Ca/Fe values overlying a dramatic reduction in values to the lower units. This transition is interpreted as the Holocene-Pleistocene boundary on the Uruguayan continental margin. Radiocarbon dating supports this interpretation and further microfossil analysis shows that the increase in Ca/Fe is linked to a dramatic increase in shelly material (specifically foraminifera) into the Holocene. This transition can be tracked into core UPC133 based on microfossil content alone. The transition is not recorded in cores UPC001, UPC032 or UPC065 as the cores only record mid to late Holocene at most due to high sedimentation rates at these localities. In fact, cores UPC001 and UPC065 record a slight decrease in Ca/Fe values in the upper portions of the cores. This reduction is present in other cores (UPC125, UPC154, UPC164 and UPC170), just not as dramatic as the Holocene-Pleistocene transition. This reduction appears to have occurred at ~3000 ka and again in both UPC001 and UPC065 at ~1400 ka. Other studies in the region (Voigt *et al.*, 2016) have related this late Holocene reduction in carbonate content to the expansion and renewal of more corrosive AAIW/UCDW at the expense of NADW at these depths. These north/south watermass fluctuations therefore appear to operate on relatively short millennial timescales.

The curves of ratios attributed to increase bottom current velocity (Si/Al, Ti/Al, K/Al and Zr/Al) have been of some use in correlation, however they have proven more useful in recognising periods of climatically driven increases in current velocity within particular watermasses on the slope. By highlighting all of the coincident peaks on the curves across all of the cores it is possible to discern

significant periods when watermass bottom current velocity was significantly reduced. Periods of increased velocity can be related to a number of factors including movement of the high velocity core of a particular watermass over the study site, movement of the turbulent interface between two watermasses over the study site, an increase in density gradient between watermasses, reduced water column accommodation space for a watermass to pass through and/or increased production at the watermass source. Often it is a combination of the above factors which makes it difficult to discern a particular forcing mechanism behind fluctuating bottom current velocities (Roberts, 2017). However, we observe general trends that can be linked to periods of significant changes in watermass properties in the Southwest Atlantic. At the depth of AAIW/UCDW (UPC125 and UPC164) there is a general increase in values through the Holocene after a period of low values. We attribute this to increased bottom current velocity due to increased northward advection of AAIW observed at this depth in other studies (Voigt, Chiessi, Piola and Rüdiger Henrich, 2016). At the depth range of NADW (UPC001, UPC065 and UPC170) we see a general increase in values up to the mid to late Holocene before there is an abrupt decrease in values from the mid Holocene to the present. This reduction in bottom current velocity could be linked to a reduction in the strength of NADW in the study area. At the depths of LCDW/AABW (UPC154) there is an increase in the values of the bottom current proxy ratios in the Late Deglacial/Early Holocene before a slight decrease in values from the mid Holocene to the present. The variations in bottom current velocity are linked to depth migrations of each of the watermasses with a changing climate since the Last Glacial Maximum. These



migrations coincide with those of UPC164 in relation to production of deepwater in the Northern and Southern Hemispheres.

In all cores apart from UPC154 we see general increases in Fe/K through the Holocene. The increase across all other cores is likely due to either increased northern watermass influence transporting more Fe-rich sediment from equatorial regions or an increase in continental precipitation transported to the site from the Rio de la Plata. The reduction of values at core site UPC154 could be linked to increased southern-sourced watermass influence at these depths in the early to mid Holocene (Warratz *et al.*, 2017). However, there is an increase in the late Holocene to recent that is most likely the same signal we see in other cores for increased Fe or decreased K into the late Holocene. This record is identical to the Ti/K record in every core, it is therefore likely to be a signal of terrigenous input to the different sites rather than an indicator of watermass influence. An increase or decrease in Fe and Ti can be linked to increased or decreased continental runoff and sediment supply to the shelf.

Proxies for productivity and organic carbon Ba/Al and Br/Cl increase in all cores upon entering the Holocene. Here we link this increase in surface water productivity to more vigorous oceanic overturning circulation and therefore upwelling more nutrient-rich deep waters since the deglaciation. There are intervals in cores UPC001 and UPC065 that show peaks in Br/Cl. These may be due to enhanced organic carbon preservation in turbidite mud caps. Palaeoxygenation proxies (Mn/Fe & Mn/Ti) show an inverse relationship to proxies of productivity (Br/Cl), as increased productivity would result in reduced oxygen conditions in seafloor sediments. Proxies for clay content and composition (Fe/Rb, K/Rb, Zr/Rb and Ti/Rb) have been useful alongside the

discrete grain size measurements in identifying sediments that may be linked to turbidite deposition, particularly in cores UPC001 and UPC065 where we see peaks in Fe/Rb associated with turbidite mud caps and potentially in the C1, 4 and 5 divisions of contouritic sediments. Zr/Rb does not correlate with the other Rb ratios in all cores. Higher values of Zr/Rb appear to correspond more with the defined intervals of increased current velocity. Unlike the other Rb proxies, it does not identify more clay-rich units and instead appears to pick out units that are more sand-rich that have had their fines winnowed away by the action of vigorous bottom currents. It may also be useful in identifying discontinuity horizons within the sediment column as there are several peaks that correspond with intervals interpreted as periods of non-deposition/erosional surfaces. These can be seen in cores UPC154 at intervals 80 cm and 165 cm, UPC164 at 120 cm, 150 cm, 240 cm, 260 cm and 300 cm, and UPC170 at 190 cm.

#### 5.4.4 Glacial-Interglacial Variation of Atlantic Intermediate Waters

The flux of southern-sourced water entering the Atlantic has an effect on the thermohaline properties of the northward return flow. During the Last Glacial Maximum to early deglacial, Atlantic Meridional Overturning Circulation was suppressed by denser glacial expanded southern-sourced waters such as the Circumpolar Deepwater and Antarctic Bottom Water (Voigt *et al.*, 2016). Northern Component Water expanded into an intermediate depth/poorly ventilated watermass; we see evidence for this in the suboxic conditions identified from the Mn/Fe record of AIM-1 (Figure 5.6 B). At 15 ka BP, a southward shift of the South Atlantic Front (Roberts, 2017) delivered a greater volume of cold Subantarctic Mode Water into the Atlantic Basin and would have resulted in the formation of a freshened Antarctic Intermediate Water. An injection of fresh southern-sourced

water into the Atlantic would have increased the density gradient in the North Atlantic, allowing a reinvigoration of Atlantic Meridional Overturning Circulation. The Antarctic Cold Reversal is characterised by intense Atlantic Meridional Overturning Circulation that siphoned heat from the Southern hemisphere, which we observe as a cooling of surface water NPS% and a significant increase in the benthic O isotope record (Figure 5.7 B, F). From 14.5 ka BP this increased ventilation and contributions from Antarctic Intermediate Water and Northern Component Water to the bottom water column improved the preservation of planktonic foraminifera and there was a return to more oxygen-rich conditions.

The Younger Dryas was a period of renewed warming, due to the shutdown of Atlantic Meridional Overturning Circulation. During the Younger Dryas, warm-water species expanded into the surface waters and test fragmentation occurred on the seafloor (Figure 5.7 G). Fragmentation increases from 11.5 – 10 ka BP associated with a reinvigorated Atlantic Meridional Overturning Circulation and weak Antarctic Intermediate Waters. Austral spring mean insolation in the region of Antarctic Intermediate Water formation has been shown to have a strong link to its relative strength (Figure 5.7, D). An insolation maximum in this interval would have limited Antarctic Intermediate Water expansion. The return of a strong Northern Component Water splits Circumpolar Deepwater, confining its fresher but poorly ventilated component to the terrace beneath a fresh/shoaled Antarctic Intermediate Water. Confining low-oxygen Upper Circumpolar Deepwater over the location of our core site explains the increase of fragmentation and drop in Mn/Fe ratio over this interval. Atlantic Meridional Overturning Circulation continues to strengthen entering the Holocene Thermal Maximum and we see a return of warm water species and decrease of fragmentation on the seafloor. This

period of increased ventilation lasts through the early to mid-Holocene until we see an expansion of southern-sourced, oxygen-rich Antarctic Intermediate Water in the late Holocene (See Figure 5.9 for summary).

#### 5.4.5 Glacial-Interglacial Bottom Water Production Around Antarctica

The ocean's thermohaline circulation is sustained by continuous generation of cold and saline bottom waters in production areas at high-latitudes, these include the Norwegian-Greenland Sea, Labrador Sea, Bering Sea, Weddell Sea and other areas in the Southern Ocean (Rahmstorf, 2006). Differences in the timing of bottom water production between Northern and Southern Hemispheres have been observed, and this has been called the see-saw effect (Steig *et al.*, 1998). Intermediate waters are produced in marginal basins and surrounding seas. Production of these intermediate waters is thought to be the prevailing conditions for bottom water generation during interglacials (Gross & Gross, 1996).

In the Southern Hemisphere, the link between climate, sea level and bottom water production efficiency is poorly understood (Roberts, 2017). What is known is that it is far more complex than the processes linked to Northern Hemisphere bottom water generation. An expanded influence of Antarctic Bottom Water into the Atlantic has been observed during glacial periods, alongside a lower sea level. However, there is less evidence for increased velocity of bottom current at this time (McCave *et al.*, 1995; Orsi *et al.*, 1999; Schmittner, 2003; Barbante *et al.*, 2006; Negre *et al.*, 2010). The expanded influence of Southern Component Waters could largely be due to increased space in the water column left by a reduced generation of Northern Component Waters at this time. However, there is a good deal of evidence for a more vigorous Antarctic Circumpolar Current at depth during glacials, but it is difficult to link this to increased bottom current

generation alone as this surface current is largely driven by surface wind shear (Naveira Garabato *et al.*, 2009).

In the Antarctic, during periods of extensive sea-ice development, water circulation migrates basinward, and therefore the location of bottom water production migrates also. There is clear evidence for this from observations of watermasses around Antarctica where the Antarctic Circumpolar Current moves to the north during intervals of sea-ice expansion (Rebesco *et al.*, 1997). This could have the effect of forcing the bottom currents away from the slope where the current stops interacting with the seafloor morphology which would decrease bottom current velocities. However, there is evidence that parts of the deep shelf areas around Antarctica maintained ice shelves in periods of lower sea level during glacials and would have therefore maintained the same effective method of bottom water generation as highstands. The combination of colder water and a greater level of freezing for sea ice formation, there is a possibility that there could have been increased bottom water generation during glacial periods. This would support observations of higher bottom current velocities being linked to colder climates for the Southwest Pacific Gateway and along the Argentine and Uruguay margin (Goosse *et al.*, 2001; Carter *et al.*, 2004; Hernández-Molina *et al.*, 2009; Hernández-Molina *et al.*, 2010; This Study).

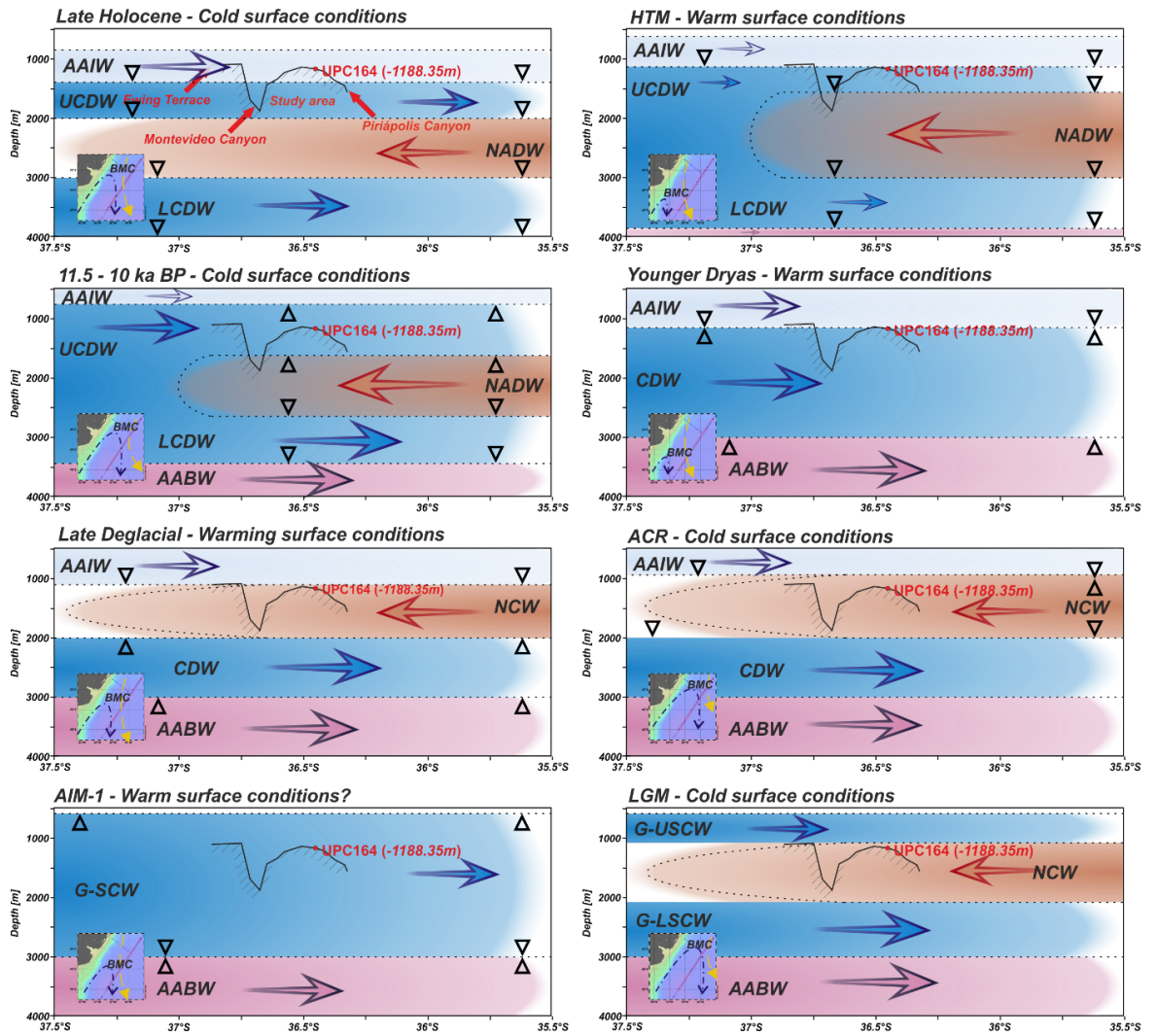


Figure 55 Diagram representing the migration of main water masses present offshore Uruguay since the Last Glacial Maximum. Arrows indicate relative intensity and direction of flow. Hollow black arrows indicate the migration of interfaces in each period. Inset is interpreted position of the BMC. Location and bathymetry of UPC164 is overlain.

## 5.5 Conclusions

This chapter presents the first AMS radiocarbon-based age model extending back to the Last Glacial Maximum for a sediment core in the range of intermediate Southern Component Water (Antarctic Intermediate Water/Upper Circumpolar Deepwater) on the Uruguayan continental margin. We use the surface assemblages and fragmentation index of planktonic foraminifera to determine changes in water column ventilation. Poorly ventilated/weak Atlantic Meridional Overturning/strong southern-sourced waters dominated during AIM-1, Younger Dryas, and Holocene Thermal Maximum. In these periods we see an associated warming of surface waters as poorly ventilated Southern Component Water dominate. In the ventilated/strong Atlantic Meridional Overturning Circulation/Northern Component Water and Antarctic Intermediate Water-influenced Antarctic Cold Reversal, late deglacial and late Holocene ventilation increases. Surface waters cool in periods of ventilation, as there is more siphoning of heat to the Northern Hemisphere. These periods are either represented in the sediment cores as an abundance of warm water species of forams and a reduction in carbonate content (poor ventilation), or an abundance of cold water forams and increased carbonate preservation (more vigorous ventilation).

Based on the corrosivity of Southern Component Water, we propose that the absence of carbonate across the entire study area during the glacial to early deglacial interval, and in the period 11.5 – 10 ka BP, coupled with the increase in carbonate during the late deglacial and early to mid-Holocene, reflect a shift of the Circumpolar Deepwater downslope. Between 20 and 15 ka BP, we suggest that an intermediate Northern Component Water interacted with a glacial

Southern Component Water in the Southwestern Atlantic, the evidence for this is the reduced carbonate preservation seen in the foram and Ca/Fe ratios across this period. An increase in Antarctic Intermediate Water at 15 ka BP led to an upper Southern Component Water intermediate water expansion. This intermediate Southern Component Water was composed of a lower corrosive water mass (Upper Circumpolar Deepwater) and an upper non-corrosive watermass (Antarctic Intermediate Water). The high velocity interface of these watermasses lay at the depth of the terrace as indicated by an increased grain size and high elemental ratios used as a proxy for increased winnowing by bottom currents (~1000m depth in the Atlantic) until the mid-Holocene where it began to migrate downwards in the water column enhancing carbonate preservation. In the late Holocene, there was an increase in corrosivity which may relate to the upper non-corrosive Southern Component Water taking on the characteristics of its deeper corrosive Southern Component Water counterparts. As the Antarctic ice shelf continues to retreat with global warming, the production of intermediate Southern Component Water increases. An associated effect of this is that it can take up more carbon from the atmosphere and store it at intermediate depths. This will have the effect of increasing the corrosivity of the intermediate Southern Component Water, becoming more like its deeper Southern Component Water counterparts. The apparent merging of intermediate Southern Component Waters may act to further weaken Atlantic Meridional Overturning Circulation in the future.



# CHAPTER 6

## MICROPALAEONTOLOGY

### *A New Method to Differentiate Along- and Down-Slope Processes*

#### 6.1 Introduction

This chapter uses benthic foraminifera assemblages, gravimetric grain size analyses, core logging and ITRAX elemental ratios to distinguish sediment transportation mechanisms within a mixed sedimentary system, on the passive Uruguayan continental margin where horizontal environmental gradients are high (See Fig. 6.1). This has implications for distinguishing strong versus weak bottom current deposits, and their distinction from turbidite and open slope deposits.

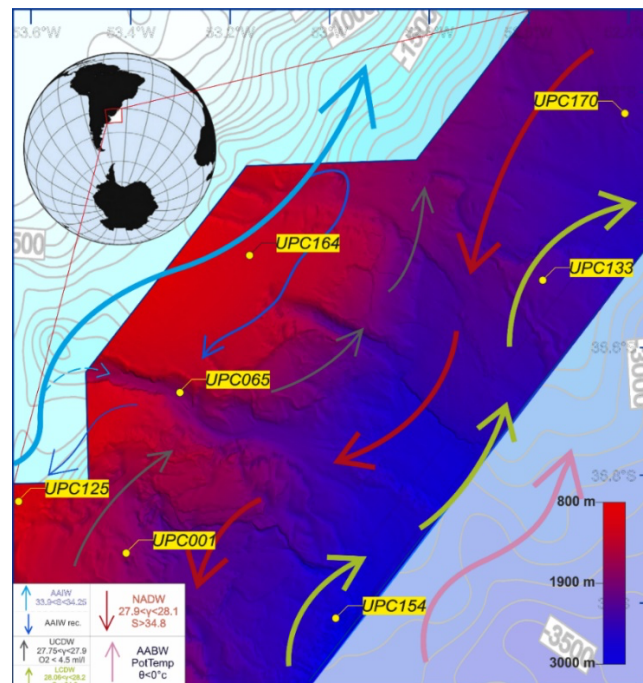


Figure 56.1 Location of the J14092 cruise core localities in this study and present day pathways of the Southern and Northern sourced watermasses based on (Hernández-Molina et al., 2016)

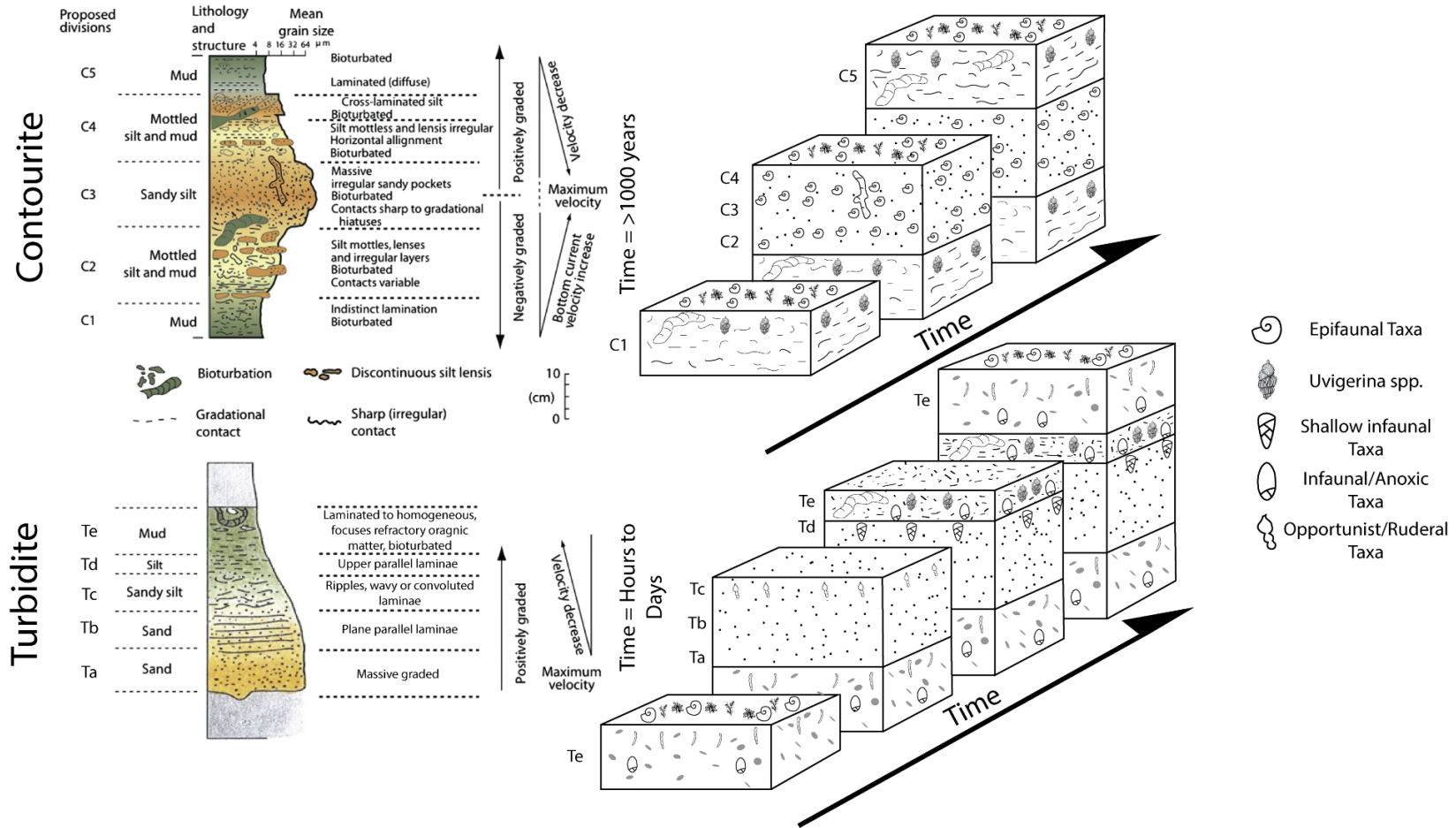


Figure 57 Summarised schematic adapted from (Hess et al., 2005) which documents the various foraminiferal responses to the deposition of a turbidite. In addition is a hypothesised schematic of how foraminifera may respond to contourrite deposition using various observations of the studies discussed in this chapter.

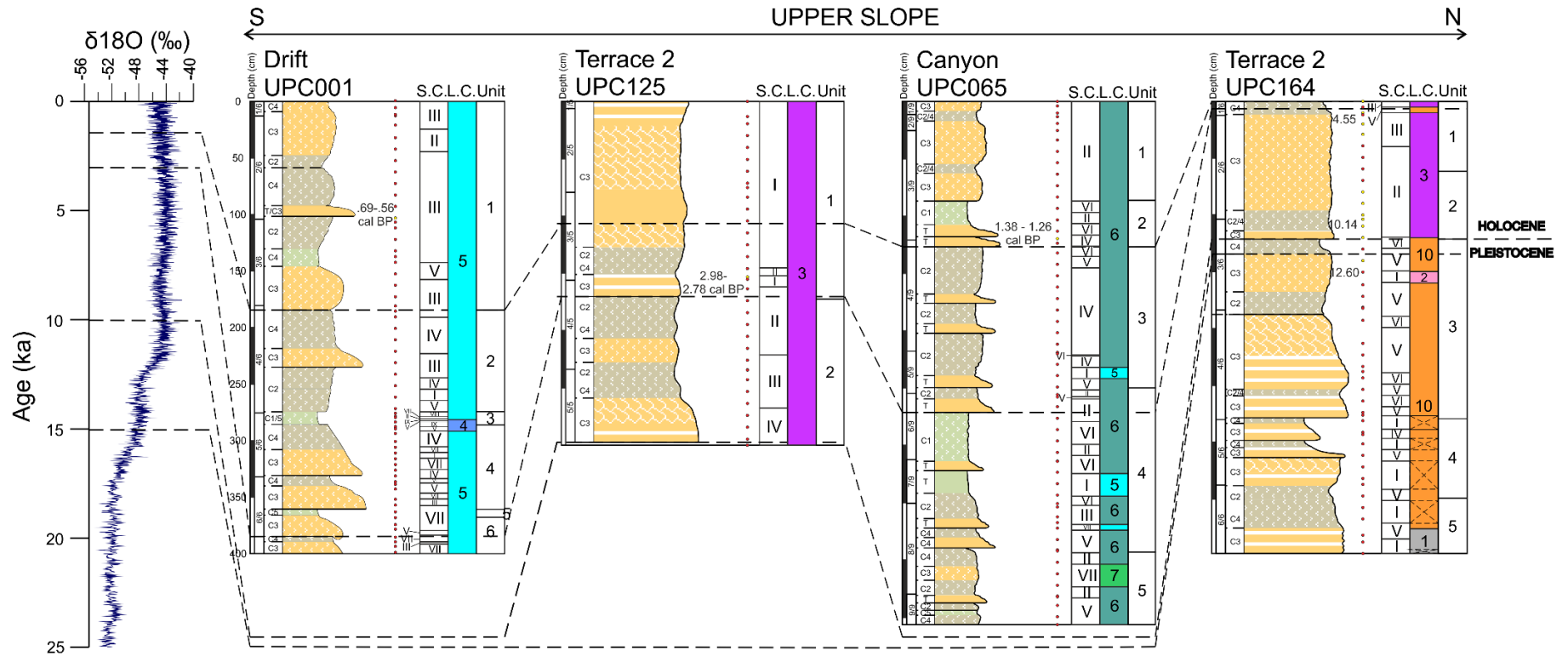


Figure 58 Sedimentary logs from South to North on the Upper Slope correlated to EDML Stable  $\delta^{18}\text{O}$  Isotope Ice Core Record (‰). Sampled intervals in red and yellow (dated) dots. Cores UPC001, UPC125, UPC065 and UPC164 with corresponding clusters within each individual core (letters) and overall clusters (colour coded, 1 - 11) across study area.

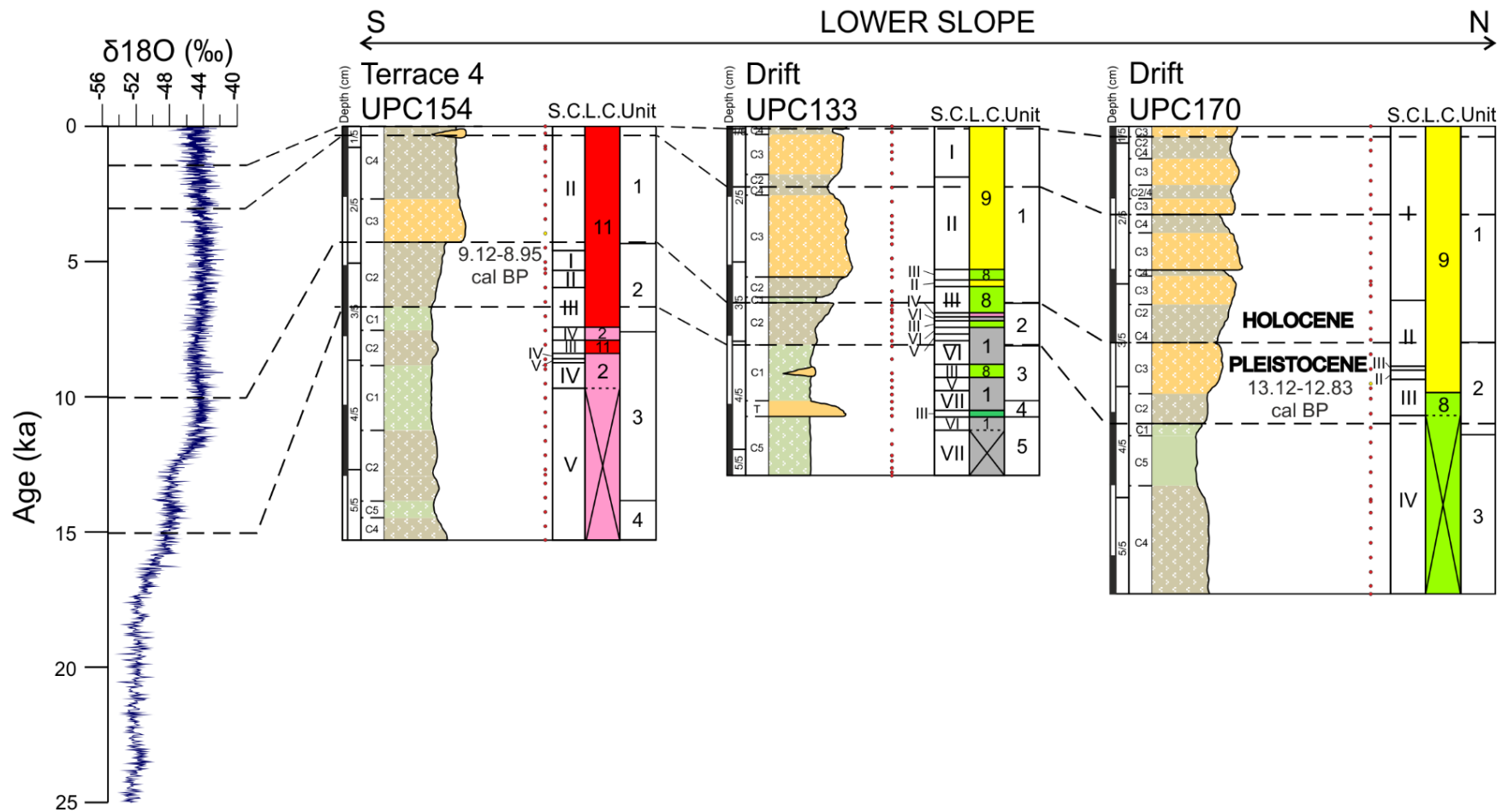


Figure 59 Sedimentary logs from South to North on the Lower Slope correlated to EDML Stable  $\delta^{18}\text{O}$  Isotope Ice Core Record (%). Sampled intervals in red and yellow (dated) dots. Cores UPC154, UPC133 and UPC170 with corresponding clusters within each individual core (letters) and overall clusters (colour coded, 1 -11) across study area

## 6.2 Results

### 6.2.1 Foraminiferal Analysis

Bulk sediment samples of approximately 10 cm<sup>3</sup> were collected from the cores as described in Section 3.3.1.5 for micropaleontological and gravimetric grain size analysis. In this chapter we present the micropaleontological data collected

*Table 6.1 Summary of sedimentary environments and prevailing energy conditions sampled*

| Environment (Core No.)         | Water Depth (m) | Prevailing energy conditions | Unit Designation | Number of samples analysed |
|--------------------------------|-----------------|------------------------------|------------------|----------------------------|
|                                |                 | High                         | 1, 2, 4, 5, 6    | 54                         |
| Drift 1 (001)                  | -2053.05        | Low                          | 3                | 5                          |
| Drift (032)                    | -2513.29        | Medium                       | 1, 2, 3, 4       | 0                          |
| Submarine Canyon System (065)  | -1896.61        | High                         | 1, 2, 3          | 31                         |
|                                |                 | Low                          | 4, 5             | 25                         |
| Scoured Terrace 2 (125)        | -1121.22        | High                         | 1, 2             | 33                         |
|                                |                 | Medium                       | 1                | 18                         |
| Separated Drift 3 (133)        | -2451           | Low                          | 2, 3, 4, 5       | 23                         |
| Pockmarked Terrace 4 (154)     | -3158.49        | Low                          | 1, 2, 3, 4       | 35                         |
|                                |                 | High                         | 1, 2             | 16                         |
|                                |                 | Medium                       | 3, 5             | 22                         |
| Drift Terrace 2 (164)          | -1188.35        | Low                          | 4                | 10                         |
|                                |                 | High                         | 1, 2             | 24                         |
| Drift 2/Turbidite Valley (170) | -2535           | Low                          | 3                | 13                         |

A total of 95,021 benthic foraminiferal shells (average: 299.75 tests/sample) from 173 taxa have been picked and identified from the sample material. Calculated total numbers of benthic foraminifera are presented in Appendix 3.1. Abundance patterns of the most common species up to a contribution of 3% in each cluster by the SIMPER analysis (Table 6.2) are plotted in Figures 6.6 – 6.12. The foraminiferal assemblages reveal several major environmental preferences that are well expressed in the distribution of clusters (Fig. 6.3 & 6.4). A total of 91,204 planktic foraminiferal shells (average: 287.71 tests/sample) were counted for Benthic/Planktic Ratios and Fragmentation Index (170,631 fragments; average: 538.27 fragments/sample).

Out of the 317 samples, 45 were found to be barren of specimens and 160 contained <300. (Appendix 3.1). Preservation of the foraminiferal tests was often poor in the lower sections of the cores with lower sedimentation rates (e.g. UPC125, UPC133, UPC154, UPC164 and UPC170). This complicated species identification, led to the large amounts of barren samples or samples not reaching >300 individuals. For taxonomic references, see the appendix at the end of this thesis.

Abundances of epifaunal and infaunal taxa have been contrasted down each core to infer changes in export productivity/bottom water oxygenation throughout the studied interval in each of the interpreted environments (Jorissen *et al.*, 2007). A list of taxa with clear microhabitat preferences based on previous studies was collected for this study and considered in this analysis (Appendix 3.2).

### 6.2.2 Foraminifera Observed in Sedimentary Units

In Chapter 4 sedimentary units were defined based on similar characteristics of prevailing current energy conditions. Here we simplify the characteristics of each sedimentary unit into high, medium and low energy sedimentary environments. Within each of the discrete samples taken from the sedimentary units there are distinct sets of foraminiferal facies we can define within each unit. The percentage ranges of each species below are the percentage ranges of this species within each sedimentary unit's foram assemblage. The species listed are the most abundant in each unit or are seen as key indicator species of a particular microhabitat. The foram assemblages from the samples taken in the depth ranges of each sedimentary unit are defined below.

#### *UPC001*

UPC001 was collected from Contourite Drift 1 in Chapter 4 is composed of six sedimentary units (Fig 6.1 and 6.3).

The high energy environment in Unit 1 is composed of an assemblage of *Stainforthia complanta* (17–23%), *Cassidulina subglobosa* (12%), *Globobulimina turgida* (7–10%), *Bulimina marginata* (5-10%) and *Cibicides lobatulus* (5-10%). This unit has reduced *Chilostomella oolina* (~8%), *Cibicidoides pachyderma* (<5%), *Nonionella spp.* (<4%) and *Trifarina angulosa* (<6%) and no *Discorbis sp.* when compared to deeper sedimentary units in the core.

High energy conditions in Unit 2 are composed of *Stainforthia complanata* (20-25%), *Chilostomella oolina* (3-15%), *Trifarina angulosa* (>5%), *Cibicidoides pachyderma* (>5%), *Globobulimina turgida* (5-10%). This unit has less *Cassidulina subglobosa* (often <5%) and *Bulimina marginata* (often <5%) than

other units in this core. It has small numbers of *Nonionella atlantica* (<5%) and *Discorbis sp.* (~3%) but rare *Nonionella turgida*. At the base of this unit we see an increase in *Rutherfordoides corunata* (>5%).

Low energy setting of Unit 3 is easily identified by the presence of abundant *Nonionella spp.* (>10%) and *Globobulimina turgida* (>10%). This unit contains some *Eggerella bradiana* (>4%) and *Chilostomella oolina* can dominate the assemblage with values >20%. Unit 3 has relatively reduced *Stainforthia complanata* (often <10%) when compared to other units.

The high energy environment in Unit 4 assemblage is characterised by peaks of *Chilostomella oolina* (~20%), *Globobulimina turgida* (>10%), *Rutherfordoides corunata* (~15%) and *Cassidulina subglobosa* (~30%), however these species are in lower abundance outside of these peak values. Unit 4 has reduced *Nonionella spp.* than units 3, 5 and 6 (<5%). *Cibicidoides wuellerstorfi* increases in Unit 4 from Unit 5. Unit 4 has higher abundances of *Discorbis sp.* (~10%), but relatively lower *Trifarina angulosa* (<5%), *Cibicides lobatulus* (<5%) and *Stainforthia complanata* (often <15%) than other units.

#### UPC065

UPC065 has been collected from the Montevideo submarine canyon system. The core contains five sedimentary units defined in Chapter 4. The foraminiferal facies in each unit are listed below.

High energy conditions prevail in Unit 1 that is dominated by *Bulimina marginata* (>33%), *Chilostomella oolina* (>12%) and *Rutherfordoides corunata* (>8%). Significant foraminifera found in this unit include *Trifarina angulosa* (>5%), *Glaphyrammina americana* (>5%) and important contributions by *Cibicidoides*



*wuellerstorfi* (>3%). This unit has reduced *Stainforthia complanata* (<5%), *Cassidulina subglobosa* (<5%), *Globbulimina turgida* (<5%) and *Uvigerina peregrina* (<5%) when compared to deeper units. *Nonionella* spp. are rare or absent, with little or no *Gyroidina soldanii*, *Melonis* spp. and *Pyrgo* spp.

The high energy setting of Unit 2 is also dominated by *Bulimina marginata* (>20%) and *Chilostomella oolina* (>10%). *Cassidulina subglobosa* (>5%), *Trifarina angulosa* (>5%), *Uvigerina peregrina* (>5%) and *Globbulimina turgida* (~10%) are found in significant quantities. *Stainforthia complanata* decreases through this unit from unit three to values ~10%. *Rutherfordoides corunata* is relatively low compared to units 1 and 3 at <10% and so is *Cibicidoides wuellerstorfi* (<3%). There is little to no *Nonionella* spp., *Gyroidina soldanii*, *Melonis* spp. or *Pyrgo* spp. in this unit.

High energy Unit 3 is one of the only units not dominated by *Bulimina marginata* in this core, however it is still present in values around 15%. It is replaced by higher values of *Chilostomella oolina* (>15%), *Stainforthia complanata* (~15%), *Rutherfordoides corunata* (~8%). Significant quantities of the agglutinated taxa *Glaphryammia americana* are found in this unit (>5%) alongside more minor *Melonis affinis* (~3%) and *Gyroidina soldanii* (~3%). *Uvigerina* is reduced in this unit (<3%).

Low energy Unit 4 has peaks of *Bulimina marginata* reaching >40% in its upper section and this is replaced by a *Stainforthia complanata* peak (>30%) in its lower section. Overall, this unit has lower *Chilostomella oolina* (<10%), but high values of *Nonionella* spp. (>5%), *Cassidulina subglobosa* (>5%) and *Trifarina angulosa*

(>5%). Unit 4 has higher values of *Uvigerina peregrina* (~5%) and *Cibicidoides wuellerstorfi* (~5%) than Unit 5, but lower *Pyrgo spp.* (<5%).

Low energy conditions in Unit 5 are characterised by an abundance of *Pyrgo spp.* (>20%) and *Rutherfordoides corunata* (>15%). *Bulimina marginata* (>10%), *Chilostomella oolina* (>5%), and *Trifarina angulosa* (5%) are all present in significant quantities. There are minor contributions from *Globobulimina turgida* (~3%) and *Cibicidoides wuellerstorfi* (3%) and *Stainforthia complanta* (~5%) and *Cassidulina subglobosa* (<5%) are less common.

#### UPC125

UPC125 has been collected from the depositional portion of the sandy contourite Terrace 2. The core contains two sedimentary units that are defined in Chapter 4. The foraminiferal facies for each of the units are outlined below.

The high energy environment in Unit 1 is characterised by *Trifarina angulosa* (~15%), *Cassidulina laevigata* (~15%), *Bulimina marginata* (~8%), *Planulina ariminensis* (~8%), *Oridorsalis umbonatus* (>5%), *Pullenia bulloides* (>5%), *Melonis affinis* (~5%), *Stainforthia complanata* (~5%) and minor *Cibicidoides wuellerstorfi* (~3%). Unit 1 has higher *Chilostomella oolina* than Unit 2 at ~5%, but lower *Uvigerina peregrina* and *Sphaeroidina dehiscens* (<5%).

High energy conditions in Unit 2 are dominated by *Trifarina angulosa* (20-40%) and *Cassidulina laevigata* (>15%), present in higher abundances than Unit 1. *Uvigerina peregrina* (up to 10%) and *Sphaeroidina dehiscens* (>5%) are present in higher quantities than Unit 1. *Bulimina marginata* (<5%), *Planulina ariminensis* (<5%), *Pullenia bulloides* (<5%), *Melonis affinis* (<5%), *Stainforthia complanata* (<5%), *Chilostomella oolina* (<3%) and *Cibicidoides wuellerstorfi* (<3%) are all

present in lower abundances than Unit 1. *Hoeglundina elegans* contributes an important ~3% to this facies.

### *UPC133*

UPC133 has been collected from separated contourite Drift 3. The core contains five sedimentary units. The foraminiferal facies associated with these units are listed below.

Medium energy Unit 1 is characterised by *Bulimina aculeata* (5-30%), *Uvigerina mediterranea* (>10%), *Cibicoides pachyderma* (>10%), *Uvigerina peregrina* (~10%), *Cibicoides subhaidingerii* (>5%), and *Uvigerina auberiana* (~5%). There are less *Globobulimina* spp. (~5%), *Pullenia bulloides* (<5%), *Lagena laevis* (<5%), *Melonis affinis* (<5%) and *Stainforthia complanata* (<10%). There are minor amounts of *Fissurina* spp. (<5%), *Bulimina marginata* (<5%), *Pyrgo* spp. (~10%) and *Eggerella bradyana* (<5%). There are also minor but important contributions of *Cibicides refulgens* (~3%).

Low energy Unit 2 is characterised by *Globobulimina* spp. (>15%), *Pullenia bulloides* (>10%), *Stainforthia complanata* (10-50%), *Lagena laevis* (peak of 10%), *Melonis affinis* (10-50%), *Rhabdammina linearis* (0-50%) and *Hyperammina elongata* (0-50%).

Low energy Unit 3 is dominated by few taxa. Overall, *Nonionella* spp. (5-30%) and *Stainforthia complanata* (0-75%) and *Fissurina* spp. (~5%) make up calcareous forms, while agglutinates *Hyperammina elongata* (0-100%) and *Rhabdammina linearis* (0-100%) are presented in significant amounts.

Low energy Unit 4 is similar to Unit 1. It consists of *Uvigerina peregrina* (~5%), *Cibicoides subhaidingerii* (~5%), *Cibicides refulgens* (~5%), *Gyroidina soldanii*

(~5%), *Bulimina marginata* (~5%), *Pyrgo spp.* (5-10%) and *Eggerella bradiana* (5-10%). The facies contain small amounts of *Pullenia bulloides* (<3%), *Lagena laevis* (<3%) and *Melonis affinis* (<5%). Agglutinated species *Psammospaera fusca* (~50%) and *Rhabdammina linearis* (~50%) are in abundance.

Unit 5 is mostly barren of foraminifera.

#### UPC154

UPC154 was collected from the lower slope contourite Terrace 4. The core is divided into four sedimentary units. The foraminifera associated with each of these units are outlined below.

Low energy Unit 1 is dominated by *Uvigerina peregrina* (>40%), *Uvigerina mediterranea* (>10%), *Uvigerina bradyana* (>5%), *Cibicidoides subhaidingerii* (~5%), *Uvigerina aubriana* (>3%) and *Cibicidoides pachyderma* (~3%). This unit contains no *Melonis spp.*

Low energy Unit 2 contains *Uvigerina mediterranea* (>10%) and peak *Uvigerina peregrina* (~40%). *Melonis spp.* (<10%), *Globobulimina turgida* (<10%) and *Uvigerina bradyana* (<10%) all begin to decrease within this unit from high values in Unit 3 to low values in Unit 1. We see the first appearance of *Cibicidoides subhaidingerii* (<5%) in this unit. *Uvigerina auberiana* (>15%) is in peak abundance and we see the only appearance of *Nonion spp.* (>10%) within this unit. There are also minor contributions from *Globobulimina affinis* (~10%) and *Fissurina spp.* (~10%).

Low energy Unit 3 is dominated by a peak in *Uvigerina mediterranea* abundance (~40%), with *Melonis spp.* (0-40%) and *Globobulimina turgida* (0-50%) in

abundance. There are minor contributions from *Globobulimina affinis* (~15%) and *Fissurina bisulcata* (~20%).

Low energy Unit 4 is mostly barren of foraminifera.

#### *UPC164*

UPC164 was collected from the erosional/non-depositional portion of the sand-rich contourite Terrace 2. The core has been divided into five sedimentary units and the foraminiferal assemblages found within each are outlined below.

High energy Unit 1 is characterised by an abundance of *Cassidulina laevigata* (>10%), *Planulina ariminensis* (>10%), *Hoeglundina elegans* (>5%), *Chilostomella oolina* (>5%), *Pullenia bulloides* (~5%), *Cibicides lobatulus* (~5%), *Uvigerina bifurcata* (peak >10%) and *Bulimina marginata* (~10%). Unit 1 has reduced numbers of *Rutherfordoides coronata* (<5%), *Melonis affinis* (<10%), *Oridorsalis umbonatus* (<10%) and *Trifarina angulosa* (<5%) compared to Unit 2.

High energy Unit 2 has increased *Rutherfordoides coronata* (>15%), *Melonis affinis* (>10%), *Oridorsalis umbonatus* (>10%), *Trifarina angulosa* (>5%), *Chilostomella oolina* (>5%) and *Bulimina marginata* (>10%). However, Unit 2 has lower abundances of *Cassidulina laevigata* (<5%), *Planulina ariminensis* (<5%), *Hoeglundina elegans* (<5%), *Pullenia bulloides* (<5%) and *Cibicides lobatulus* (<5%) compared to Unit 1 and reduced *Uvigerina peregrina* (~10%) compared to Unit 3. Unit 2 has minor contributions from *Epistomella exigua* (~3%) and *Sigmoilopsis schlumbergeri* (~3%).

Medium energy Unit 3 has major contributions from *Uvigerina bifurcata* (>15%), *Uvigerina peregrina* (>50%) and *Globobulimina turgida* (>30%). The unit contains

some *Rutherfordoides corunata* (~3%), *Melonis spp.* (<5%) and *Trifarina angulosa* (<10%), but no other taxa from Units 1 or 2.

Low energy Unit 4 has reduced benthic counts and contains few *Uvigerina spp.* (often 100% of the assemblage) and a peak in *Bulimina marginata* abundance at 100% of the assemblage, but is otherwise barren of foraminifera.

Medium energy Unit 5 contains few *Uvigerina peregrina* (100%) but is otherwise barren.

### *UPC170*

UPC170 was collected from the plastered contourite drift 2. The core contains three sedimentary units that were described in Chapter 4. Below, the foraminiferal assemblages associated with each unit are outlined.

High energy Unit 1 is characterised by high abundances of *Uvigerina peregrina* (>10%), *Bulimina marginata* (>10%), *Cibicidoides pachyderma* (>5%), *Cibicidoides subhaidingerii* (>5%), *Uvigerina mediterranea* (>5%), *Cibicidoides mundulus* (~5%) and *Hyperammia elongata* (~5%). *Globobulimina turgida* (<5%) and *Gyroidina soldanii* (<5%) are not as abundant in this unit compared to Unit 2.

High energy Unit 2 contains high abundance of *Globobulimina turgida* (~10%), *Gyroidina soldanii* (~5%), *Melonis affinis* (>5%), *Chilostomella oolina* (~5%), *Pullenia bulloides* (~5%), *Glandulina ovula* (>5%), *Fissurina seimarginata* (>5%), *Cibicides refulgens* (~5%) and *Oolina globosa* (~5%). There are also minor but important contributions from *Oridorsalis umbonatus* (~4%), *Cassidulina subglobosa* (~4%) and *Stainforthia complanta* (~3%).

Low energy Unit 3 is barren of foraminifera.

### 6.2.3 Statistical Analysis

Multivariate statistical analyses were performed by using the PAST software package (version 3.0). Q-mode cluster analysis (Unweighted Pair group method with arithmetic mean (UPGMA) algorithm, Bray-curtis similarity index for abundance data) has been applied in order to group the samples according to their similarity in foraminiferal content (Figure 6.5) (Øyvind *et al.*, 2001). Fifty-nine species, occurring with abundances >5% in at least one sample and representing on average 96.5% of the total fauna, have been included in this analysis (Appendix 3.3). A one-way ANOSIM was performed to obtain the P value (significance levels) and a R value (strength of the factors on the samples). R value varies between 0 and 1, with a value close to 1 indicating high separation between levels of factors, R close to 0 indicates no separation. P value determines the significance of the factor with values P >0.1 of weak or no significance to P <0.05 of strong significance. A Similarity Percentage analysis (SIMPER, Bray-Curtis similarity index, all samples pooled, Table 6.2) has been performed on the same data-set (Clarke, 1993).

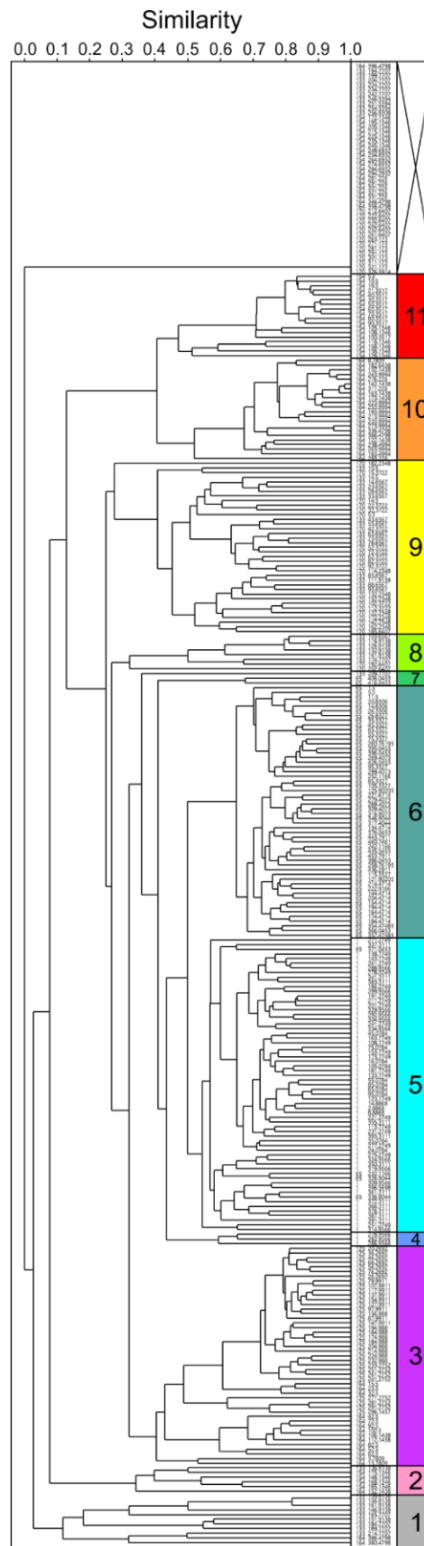


Figure 60 Q-mode cluster analysis (UPGMA, Bray Curtis; correlation: 0.90) for autochthonous benthic foraminifera >150  $\mu\text{m}$  from all cores. Numerals indicate groups of samples with a similar composition of foraminifera, representing foraminiferal assemblages. Sample numbers indicated and coloured in accordance with overall regional assemblages. Autochthonous taxa occurring >5% abundance in at least one sample have been considered for this analysis.



We present the results from the overall data-set (Table 6.2) but have included a high resolution breakdown of separate analyses conducted on each core to identify any small scale changes in (Appendix 6.1). The separate core analysis followed the same statistical methods as the one conducted on the larger data-set. This was done to prove the ability of foraminiferal assemblages in identifying environmental changes that would otherwise be invisible through sedimentary analysis alone.

*Table 6.2 Summary of one-way ANOSIM results for statistical significance of factor for Clusters 1 - 11*

|                          |          |
|--------------------------|----------|
| <b>ANOSIM</b>            |          |
| <b>Permutation N</b>     | 9999     |
| <b>Mean Rank within</b>  | 4318     |
| <b>Mean rank between</b> | 2.10E+04 |
| <b><i>R</i></b>          | 0.9034   |
| <b><i>p</i>(same)</b>    | 0.0001   |

Table 6.3 Pairwise ANOSIM *p*-values, uncorrected significance for each Cluster 1 - 11

| <i>p</i> -values | Cluster 1 | Cluster 2 | Cluster 3 | Cluster 4 | Cluster 5 | Cluster 6 | Cluster 7 | Cluster 8 | Cluster 9 | Cluster 10 | Cluster 11 |
|------------------|-----------|-----------|-----------|-----------|-----------|-----------|-----------|-----------|-----------|------------|------------|
| Cluster 1        |           | 0.0002    | 0.0001    | 0.0035    | 0.0001    | 0.0001    | 0.0175    | 0.0002    | 0.0001    | 0.0001     | 0.0001     |
| Cluster 2        | 0.0002    |           | 0.0001    | 0.0135    | 0.0001    | 0.0001    | 0.0127    | 0.0002    | 0.0001    | 0.0001     | 0.0001     |
| Cluster 3        | 0.0001    | 0.0001    |           | 0.0001    | 0.0001    | 0.0001    | 0.0002    | 0.0001    | 0.0001    | 0.0001     | 0.0001     |
| Cluster 4        | 0.0035    | 0.0135    | 0.0001    |           | 0.0002    | 0.0002    | 0.0968    | 0.0071    | 0.0001    | 0.0003     | 0.0009     |
| Cluster 5        | 0.0001    | 0.0001    | 0.0001    | 0.0002    |           | 0.0001    | 0.0001    | 0.0001    | 0.0001    | 0.0001     | 0.0001     |
| Cluster 6        | 0.0001    | 0.0001    | 0.0001    | 0.0002    | 0.0001    |           | 0.0001    | 0.0001    | 0.0001    | 0.0001     | 0.0001     |
| Cluster 7        | 0.0175    | 0.0127    | 0.0002    | 0.0968    | 0.0001    | 0.0001    |           | 0.0066    | 0.0003    | 0.0008     | 0.001      |
| Cluster 8        | 0.0002    | 0.0002    | 0.0001    | 0.0071    | 0.0001    | 0.0001    | 0.0066    |           | 0.0001    | 0.0001     | 0.0001     |
| Cluster 9        | 0.0001    | 0.0001    | 0.0001    | 0.0001    | 0.0001    | 0.0001    | 0.0003    | 0.0001    |           | 0.0001     | 0.0001     |
| Cluster 10       | 0.0001    | 0.0001    | 0.0001    | 0.0003    | 0.0001    | 0.0001    | 0.0008    | 0.0001    | 0.0001    |            | 0.0001     |
| Cluster 11       | 0.0001    | 0.0001    | 0.0001    | 0.0009    | 0.0001    | 0.0001    | 0.001     | 0.0001    | 0.0001    | 0.0001     |            |

Table 6.4 Pairwise ANOSIM R values for each Cluster 1 - 11

| <b>R-values</b>   | <b>Cluster 1</b> | <b>Cluster 2</b> | <b>Cluster 3</b> | <b>Cluster 4</b> | <b>Cluster 5</b> | <b>Cluster 6</b> | <b>Cluster 7</b> | <b>Cluster 8</b> | <b>Cluster 9</b> | <b>Cluster 10</b> | <b>Cluster 11</b> |
|-------------------|------------------|------------------|------------------|------------------|------------------|------------------|------------------|------------------|------------------|-------------------|-------------------|
| <b>Cluster 1</b>  |                  | 0.6868           | 0.9758           | 0.5684           | 0.9865           | 0.9818           | 0.4399           | 0.5988           | 0.9539           | 0.9336            | 0.8748            |
| <b>Cluster 2</b>  | 0.6868           |                  | 0.9994           | 0.9259           | 0.9996           | 0.9998           | 0.9753           | 0.8847           | 0.9829           | 1                 | 0.9606            |
| <b>Cluster 3</b>  | 0.9758           | 0.9994           |                  | 0.9751           | 0.9474           | 0.8805           | 0.85             | 0.9754           | 0.9568           | 0.9864            | 0.9949            |
| <b>Cluster 4</b>  | 0.5684           | 0.9259           | 0.9751           |                  | 0.8396           | 0.997            | 0.6667           | 0.8656           | 0.9271           | 1                 | 1                 |
| <b>Cluster 5</b>  | 0.9865           | 0.9996           | 0.9474           | 0.8396           |                  | 0.7681           | 0.9742           | 0.9277           | 0.9141           | 1                 | 1                 |
| <b>Cluster 6</b>  | 0.9818           | 0.9998           | 0.8805           | 0.997            | 0.7681           |                  | 0.8896           | 0.9977           | 0.9705           | 1                 | 1                 |
| <b>Cluster 7</b>  | 0.4399           | 0.9753           | 0.85             | 0.6667           | 0.9742           | 0.8896           |                  | 0.8333           | 0.9085           | 1                 | 1                 |
| <b>Cluster 8</b>  | 0.5988           | 0.8847           | 0.9754           | 0.8656           | 0.9277           | 0.9977           | 0.8333           |                  | 0.775            | 1                 | 0.9939            |
| <b>Cluster 9</b>  | 0.9539           | 0.9829           | 0.9568           | 0.9271           | 0.9141           | 0.9705           | 0.9085           | 0.775            |                  | 0.9969            | 0.6375            |
| <b>Cluster 10</b> | 0.9336           | 1                | 0.9864           | 1                | 1                | 1                | 1                | 1                | 0.9969           |                   | 0.8555            |
| <b>Cluster 11</b> | 0.8748           | 0.9606           | 0.9949           | 1                | 1                | 1                | 1                | 0.9939           | 0.6375           | 0.8555            |                   |

Table 6.5 Similarity percentage (SIMPER) analysis for benthic foraminiferal assemblages >150 µm (combined fractions) in all cores. Overall average dissimilarity: 76.59. Taxa occurring at least once at >5% abundance were included in the data matrix.

| Taxon (ALLCORES)                | Average dissimilarity of species | Contribution (%) | Cumulative (%) | Mean Cluster 1 | Mean Cluster 2 | Mean Cluster 3 | Mean Cluster 4 | Mean Cluster 5 | Mean Cluster 6 | Mean Cluster 7 | Mean Cluster 8 | Mean Cluster 9 | Mean Cluster 10 | Mean Cluster 11 |
|---------------------------------|----------------------------------|------------------|----------------|----------------|----------------|----------------|----------------|----------------|----------------|----------------|----------------|----------------|-----------------|-----------------|
| <i>Uvigerina peregrina</i>      | 9.6                              | 12.5             | 12.5           | 0.0            | 0.0            | 4.6            | 0.0            | 1.5            | 3.3            | 2.0            | 0.5            | 9.3            | 67.9            | 38.0            |
| <i>Stainforthia complanata</i>  | 6.9                              | 9.0              | 21.5           | 4.5            | 0.0            | 2.3            | 9.2            | 22.9           | 9.4            | 9.1            | 45.2           | 6.7            | 0.0             | 0.3             |
| <i>Bulimina marginata</i>       | 6.0                              | 7.8              | 29.3           | 0.2            | 0.0            | 8.4            | 0.3            | 6.3            | 25.0           | 11.0           | 0.5            | 0.6            | 3.8             | 0.4             |
| <i>Chilostomella oolina</i>     | 3.9                              | 5.1              | 34.4           | 0.0            | 0.0            | 3.0            | 22.0           | 11.2           | 12.6           | 3.0            | 1.1            | 2.1            | 0.0             | 0.8             |
| <i>Globobulimina turgida</i>    | 3.6                              | 4.7              | 39.1           | 0.0            | 45.1           | 1.4            | 10.7           | 7.2            | 5.2            | 2.8            | 13.4           | 5.7            | 0.5             | 4.2             |
| <i>Trifarina angulosa</i>       | 3.6                              | 4.6              | 43.8           | 0.0            | 0.0            | 16.1           | 3.1            | 4.5            | 5.9            | 3.5            | 0.7            | 1.5            | 1.7             | 1.1             |
| <i>Rutherfordoides corunata</i> | 2.8                              | 3.7              | 47.4           | 0.0            | 0.0            | 3.8            | 0.6            | 4.6            | 8.5            | 15.6           | 0.0            | 0.2            | 0.9             | 0.0             |
| <i>Cassidulina subglobulosa</i> | 2.3                              | 3.0              | 50.5           | 0.0            | 0.0            | 0.2            | 3.9            | 9.1            | 3.1            | 1.9            | 1.3            | 1.3            | 0.0             | 0.3             |
| <i>Rhabdammina linearis</i>     | 2.1                              | 2.7              | 53.2           | 41.4           | 0.0            | 0.0            | 0.0            | 0.0            | 0.0            | 4.8            | 0.1            | 0.6            | 0.0             | 0.0             |
| <i>Cassidulina laevigata</i>    | 2.0                              | 2.7              | 55.8           | 0.0            | 0.0            | 10.6           | 1.5            | 0.8            | 0.4            | 0.2            | 0.1            | 0.8            | 0.0             | 0.1             |
| <i>Uvigerina mediterranea</i>   | 2.0                              | 2.6              | 58.4           | 0.0            | 8.3            | 0.0            | 0.0            | 0.1            | 0.2            | 0.0            | 1.3            | 6.7            | 0.0             | 12.0            |
| <i>Melonis affinis</i>          | 1.8                              | 2.4              | 60.8           | 4.6            | 2.1            | 6.2            | 0.0            | 0.3            | 0.4            | 3.0            | 6.7            | 1.9            | 0.8             | 0.0             |
| <i>Uvigerina bifurcata</i>      | 1.7                              | 2.2              | 63.0           | 0.0            | 0.0            | 1.1            | 0.0            | 0.1            | 1.5            | 0.9            | 0.0            | 0.0            | 14.9            | 0.0             |
| <i>Bulimina aculeata</i>        | 1.6                              | 2.1              | 65.2           | 0.0            | 0.0            | 0.3            | 0.0            | 0.2            | 0.1            | 0.3            | 0.0            | 10.5           | 0.3             | 0.3             |
| <i>Cibicidoides pachyderma</i>  | 1.5                              | 2.0              | 67.2           | 0.0            | 0.0            | 0.1            | 1.0            | 2.3            | 0.1            | 0.0            | 2.3            | 7.2            | 0.0             | 2.4             |
| <i>Hyperammina elongata</i>     | 1.4                              | 1.9              | 69.0           | 20.2           | 1.0            | 0.0            | 0.0            | 0.0            | 0.0            | 0.5            | 2.6            | 2.5            | 0.0             | 0.3             |
| <i>Oridorsalis umbonatus</i>    | 1.3                              | 1.7              | 70.8           | 0.0            | 0.0            | 6.2            | 1.2            | 1.0            | 1.1            | 1.6            | 1.0            | 1.1            | 0.3             | 0.4             |

|                                  |     |     |      |      |      |     |      |     |     |      |     |     |     |     |
|----------------------------------|-----|-----|------|------|------|-----|------|-----|-----|------|-----|-----|-----|-----|
| <i>Cibicides lobatulus</i>       | 1.3 | 1.7 | 72.4 | 0.0  | 0.0  | 1.8 | 3.0  | 5.2 | 1.4 | 1.7  | 0.3 | 1.3 | 0.1 | 0.3 |
| <i>Cibicoides subhaidingerii</i> | 1.3 | 1.6 | 74.1 | 0.2  | 2.1  | 0.0 | 0.0  | 0.0 | 0.0 | 0.5  | 0.7 | 6.8 | 0.0 | 3.5 |
| <i>Planulina ariminensis</i>     | 1.2 | 1.6 | 75.7 | 0.0  | 0.0  | 5.5 | 0.3  | 1.4 | 0.4 | 0.3  | 0.0 | 0.4 | 0.0 | 0.1 |
| <i>Cibicoides wuellerstorfi</i>  | 1.1 | 1.4 | 77.1 | 0.0  | 0.0  | 1.7 | 3.6  | 3.4 | 2.0 | 2.1  | 1.4 | 1.9 | 0.0 | 0.7 |
| <i>Nonionella atlantica</i>      | 1.1 | 1.4 | 78.5 | 3.0  | 0.0  | 0.2 | 11.4 | 1.9 | 2.4 | 0.0  | 0.0 | 0.1 | 0.1 | 0.0 |
| <i>Pullenia bulloides</i>        | 1.0 | 1.3 | 79.9 | 0.0  | 2.1  | 4.0 | 0.0  | 1.6 | 1.8 | 0.8  | 1.2 | 1.3 | 0.6 | 0.4 |
| <i>Psammosphaera fusca</i>       | 0.9 | 1.2 | 81.1 | 14.8 | 1.9  | 0.0 | 0.0  | 0.1 | 0.0 | 0.0  | 0.4 | 0.5 | 0.0 | 0.3 |
| <i>Gyroidina soldani</i>         | 0.9 | 1.2 | 82.3 | 0.0  | 1.0  | 1.4 | 0.6  | 1.6 | 0.7 | 3.0  | 1.4 | 3.0 | 0.0 | 1.4 |
| <i>Melonis barleeanus</i>        | 0.9 | 1.1 | 83.4 | 0.0  | 22.3 | 0.1 | 0.0  | 0.0 | 0.2 | 0.0  | 0.0 | 0.1 | 0.0 | 3.2 |
| <i>Nonionella auris</i>          | 0.9 | 1.1 | 84.5 | 1.4  | 0.0  | 0.8 | 10.3 | 1.3 | 2.3 | 0.6  | 0.1 | 0.0 | 0.0 | 0.0 |
| <i>Glaphyrammina americana</i>   | 0.8 | 1.0 | 85.5 | 0.0  | 0.0  | 0.5 | 0.0  | 0.1 | 3.3 | 0.2  | 0.0 | 0.4 | 0.0 | 0.4 |
| <i>Uvigerina bradyana</i>        | 0.7 | 1.0 | 86.5 | 0.0  | 1.0  | 0.0 | 0.0  | 0.0 | 0.0 | 0.0  | 0.0 | 0.8 | 0.0 | 8.2 |
| <i>Cibicides refulgens</i>       | 0.7 | 1.0 | 87.5 | 0.2  | 0.0  | 1.6 | 0.6  | 0.8 | 0.3 | 1.1  | 2.1 | 2.4 | 0.1 | 0.9 |
| <i>Globobulimina affinis</i>     | 0.7 | 0.9 | 88.4 | 0.0  | 6.0  | 0.1 | 0.8  | 1.0 | 1.0 | 0.0  | 1.6 | 1.2 | 0.0 | 2.1 |
| <i>Hoeglundia elegans</i>        | 0.7 | 0.9 | 89.3 | 0.0  | 0.0  | 2.9 | 0.0  | 0.2 | 0.1 | 0.0  | 1.1 | 0.9 | 0.2 | 1.5 |
| <i>Uvigerina aubriana</i>        | 0.7 | 0.9 | 90.2 | 0.0  | 1.0  | 0.0 | 0.0  | 0.0 | 0.0 | 0.0  | 0.1 | 2.2 | 0.0 | 4.8 |
| <i>Prygo nasuta</i>              | 0.6 | 0.7 | 90.9 | 0.0  | 0.0  | 0.1 | 0.0  | 0.4 | 1.0 | 14.6 | 0.0 | 1.1 | 0.0 | 0.5 |
| <i>Sphaeroidina dehiscens</i>    | 0.6 | 0.7 | 91.7 | 0.2  | 0.0  | 2.8 | 0.0  | 0.0 | 0.0 | 0.0  | 1.4 | 0.1 | 0.0 | 0.0 |
| <i>Nonionella stella</i>         | 0.5 | 0.7 | 92.4 | 0.0  | 0.0  | 0.3 | 2.5  | 1.2 | 1.4 | 0.0  | 0.0 | 0.1 | 0.0 | 0.0 |
| <i>Fissurina semimarginata</i>   | 0.5 | 0.6 | 93.0 | 0.0  | 0.0  | 0.4 | 0.0  | 1.1 | 0.3 | 0.0  | 3.2 | 0.5 | 0.0 | 0.7 |
| <i>Discorbis spp.</i>            | 0.5 | 0.6 | 93.6 | 0.0  | 0.0  | 0.6 | 0.9  | 1.2 | 0.2 | 1.0  | 0.0 | 0.8 | 0.0 | 0.0 |
| <i>Prygo murrhina</i>            | 0.4 | 0.6 | 94.1 | 0.0  | 0.0  | 0.3 | 0.0  | 0.3 | 0.8 | 4.9  | 0.0 | 1.3 | 0.0 | 0.4 |
| <i>Uvigerina striata</i>         | 0.4 | 0.6 | 94.7 | 0.0  | 0.0  | 1.8 | 0.0  | 0.2 | 0.3 | 2.4  | 0.0 | 0.0 | 0.1 | 0.0 |

|                                      |     |     |       |     |     |     |     |     |     |     |     |     |     |     |
|--------------------------------------|-----|-----|-------|-----|-----|-----|-----|-----|-----|-----|-----|-----|-----|-----|
| <i>Fissurina bisulcata</i>           | 0.4 | 0.5 | 95.2  | 0.2 | 3.8 | 0.7 | 0.0 | 0.2 | 0.1 | 1.0 | 0.2 | 0.8 | 0.0 | 0.8 |
| <i>Cibicides mundulus</i>            | 0.4 | 0.5 | 95.8  | 0.0 | 0.0 | 0.0 | 0.0 | 0.0 | 0.0 | 0.0 | 0.1 | 2.0 | 0.0 | 1.6 |
| <i>Ehrenbergina pupa</i>             | 0.4 | 0.5 | 96.2  | 0.0 | 0.0 | 1.8 | 0.3 | 0.0 | 0.3 | 0.0 | 0.1 | 0.1 | 0.0 | 0.0 |
| <i>Cibicoides bradyi</i>             | 0.4 | 0.5 | 96.7  | 0.0 | 0.0 | 0.0 | 0.0 | 0.0 | 0.0 | 0.0 | 0.0 | 1.4 | 0.0 | 2.2 |
| <i>Eggerella bradiana</i>            | 0.4 | 0.5 | 97.2  | 0.0 | 0.0 | 0.0 | 1.0 | 1.0 | 0.0 | 2.4 | 0.3 | 0.8 | 0.0 | 0.2 |
| <i>Lagena laevis</i>                 | 0.3 | 0.4 | 97.6  | 0.0 | 2.1 | 0.1 | 0.0 | 0.4 | 0.2 | 0.6 | 0.6 | 0.6 | 0.1 | 0.4 |
| <i>Nonionella turgida</i>            | 0.3 | 0.4 | 97.9  | 0.1 | 0.0 | 0.3 | 8.6 | 0.4 | 0.2 | 0.0 | 0.2 | 0.1 | 0.0 | 0.1 |
| <i>Bulimina mexicana</i>             | 0.3 | 0.4 | 98.3  | 0.0 | 0.0 | 0.0 | 0.0 | 0.0 | 0.5 | 0.0 | 0.6 | 1.0 | 0.0 | 0.4 |
| <i>Uvigerina holicki</i>             | 0.3 | 0.3 | 98.7  | 0.0 | 0.0 | 0.0 | 0.0 | 0.0 | 0.0 | 0.0 | 0.0 | 0.0 | 2.8 | 0.0 |
| <i>Oolina globulosa</i>              | 0.2 | 0.3 | 98.9  | 0.0 | 0.0 | 0.1 | 0.6 | 0.1 | 0.0 | 0.6 | 2.2 | 0.4 | 0.1 | 0.5 |
| <i>Epistomella exigua</i>            | 0.2 | 0.3 | 99.2  | 0.0 | 0.0 | 0.3 | 0.0 | 0.1 | 0.0 | 0.0 | 0.1 | 0.4 | 1.1 | 0.1 |
| <i>Glandulina ovula</i>              | 0.2 | 0.3 | 99.5  | 0.0 | 0.0 | 0.1 | 0.0 | 0.0 | 0.0 | 0.0 | 1.6 | 0.6 | 0.2 | 0.4 |
| <i>Uvigerina canariensis</i>         | 0.1 | 0.1 | 99.6  | 0.0 | 0.0 | 0.0 | 0.0 | 0.0 | 0.0 | 0.0 | 0.0 | 0.0 | 0.9 | 0.0 |
| <i>Rhabdammina abyssorum</i>         | 0.1 | 0.1 | 99.7  | 0.6 | 0.0 | 0.0 | 0.0 | 0.0 | 0.0 | 0.0 | 0.0 | 0.3 | 0.0 | 0.0 |
| <i>Reophax subfusiformis</i>         | 0.1 | 0.1 | 99.8  | 1.0 | 0.0 | 0.0 | 0.0 | 0.0 | 0.0 | 0.0 | 0.0 | 0.0 | 0.0 | 0.0 |
| <i>Nonion barleeianum</i>            | 0.1 | 0.1 | 99.8  | 0.0 | 0.0 | 0.0 | 0.0 | 0.0 | 0.0 | 0.0 | 0.0 | 0.0 | 0.0 | 0.8 |
| <i>Sigmoilopsis schlumbergeri</i>    | 0.1 | 0.1 | 99.9  | 0.5 | 0.0 | 0.0 | 0.0 | 0.0 | 0.0 | 0.0 | 0.0 | 0.0 | 0.1 | 0.0 |
| <i>Globocassidulina subglobulosa</i> | 0.0 | 0.0 | 100.0 | 0.0 | 0.0 | 0.0 | 0.0 | 0.0 | 0.0 | 0.0 | 0.0 | 0.0 | 0.3 | 0.0 |
| <i>Buzasima ringens</i>              | 0.0 | 0.0 | 100.0 | 0.0 | 0.0 | 0.0 | 0.0 | 0.0 | 0.0 | 0.0 | 0.0 | 0.2 | 0.0 | 0.0 |

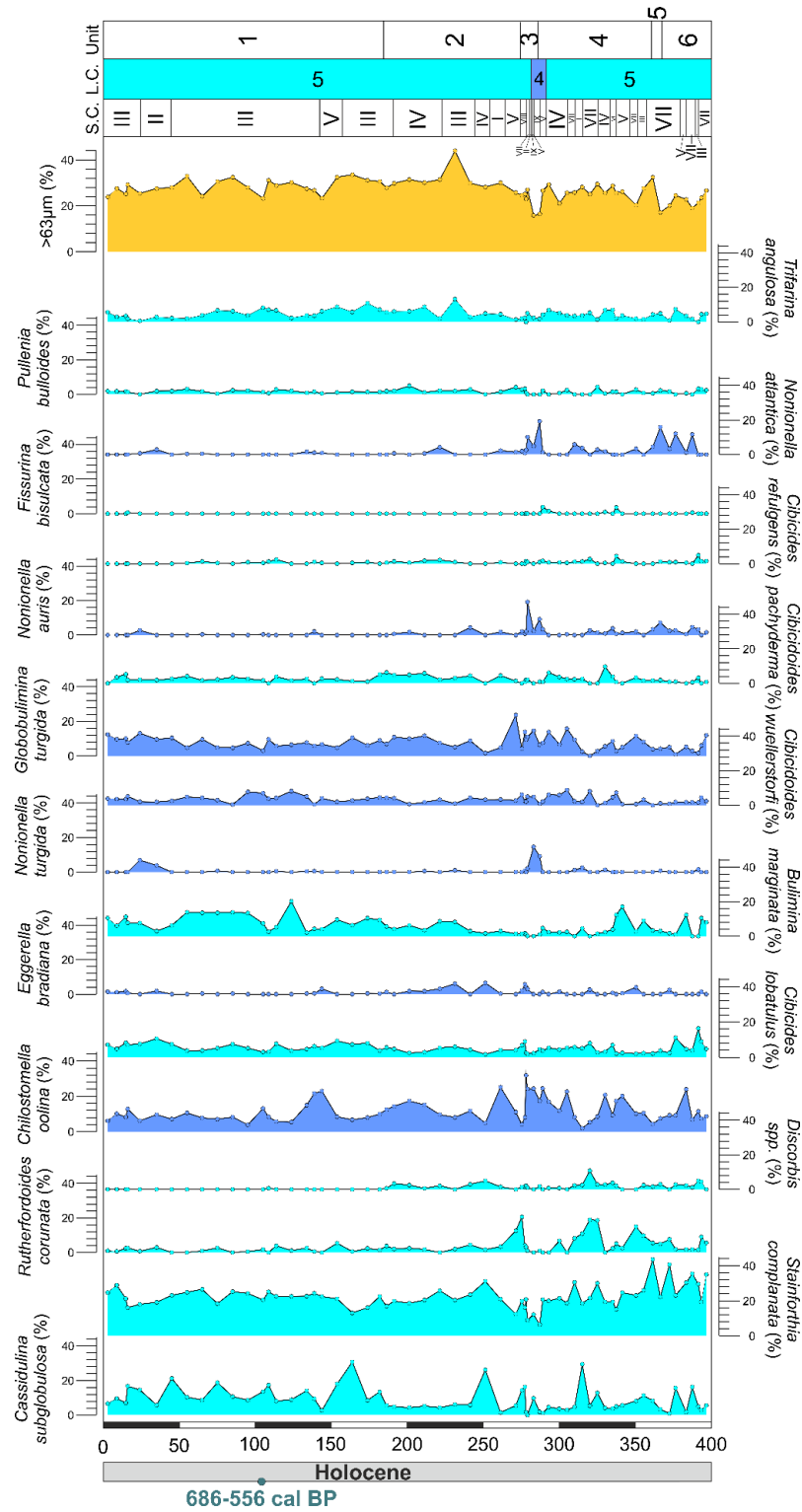


Figure 61 Variations in relative abundances of major benthic foraminiferal taxa in core UPC001 from disturbed drift. Colours and numbers correspond to foraminiferal assemblages characterising the sample clustering across the different environments/sediment core set. Uncoloured numerals correspond to foraminiferal assemblages within the sediment core. Grey bars indicate periods of increased bottom current activity as represented by high values of  $\ln(Zr/Al)$  ratios. Percentage gravimetric grain size  $>63 \mu\text{m}$  in yellow.

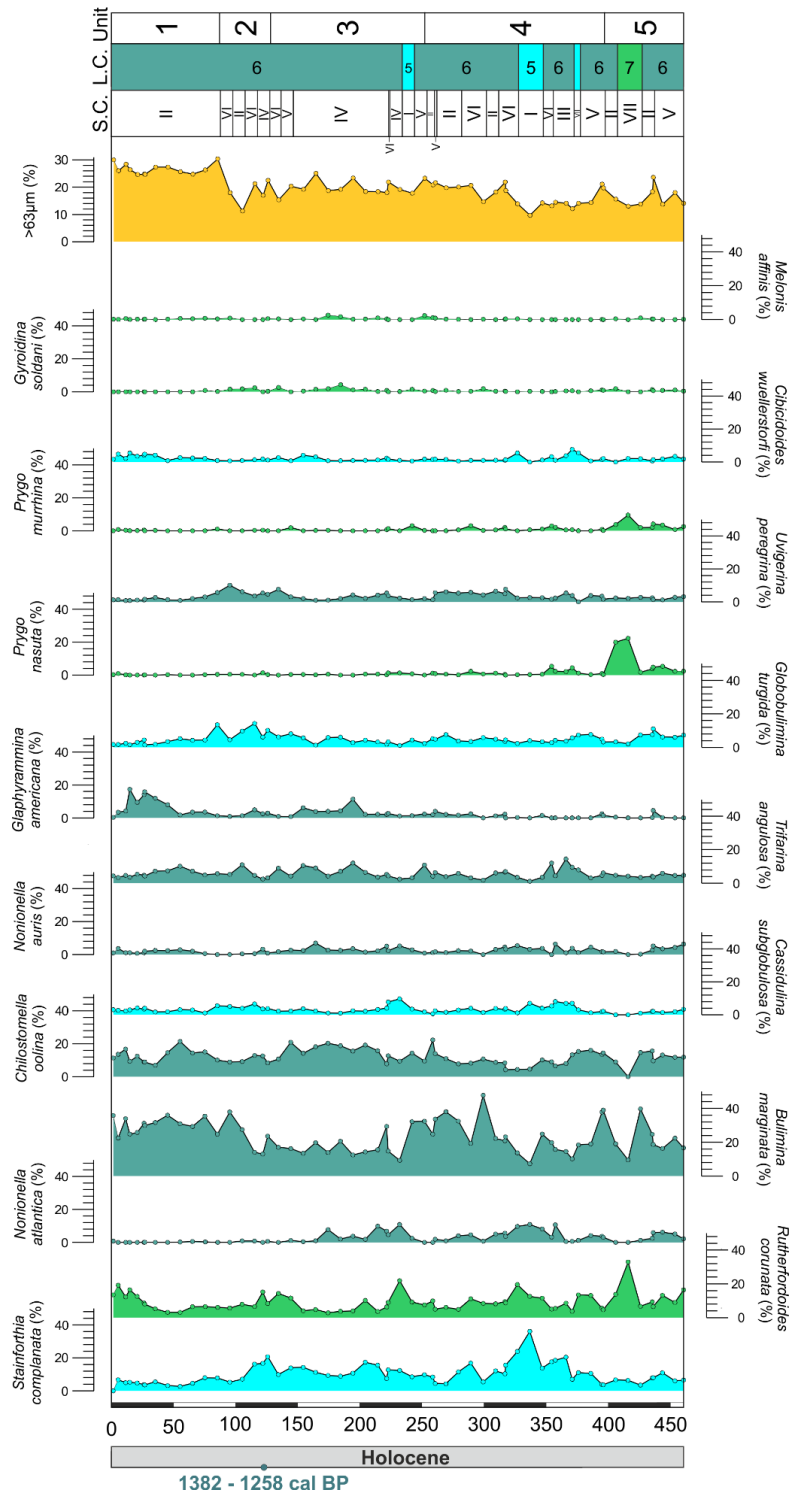


Figure 62 Variations in relative abundances of major benthic foraminiferal taxa from core UPC065 within a submarine canyon system. Colours and numbers correspond to foraminiferal assemblages characterising the sample clustering across the different environments/sediment core set. Uncoloured numerals correspond to foraminiferal assemblages within the sediment core. Grey bars indicate periods of increased bottom current activity as represented by high values of  $\ln(Zr/Al)$  ratios. Percentage gravimetric grain size  $>63 \mu\text{m}$  in yellow.



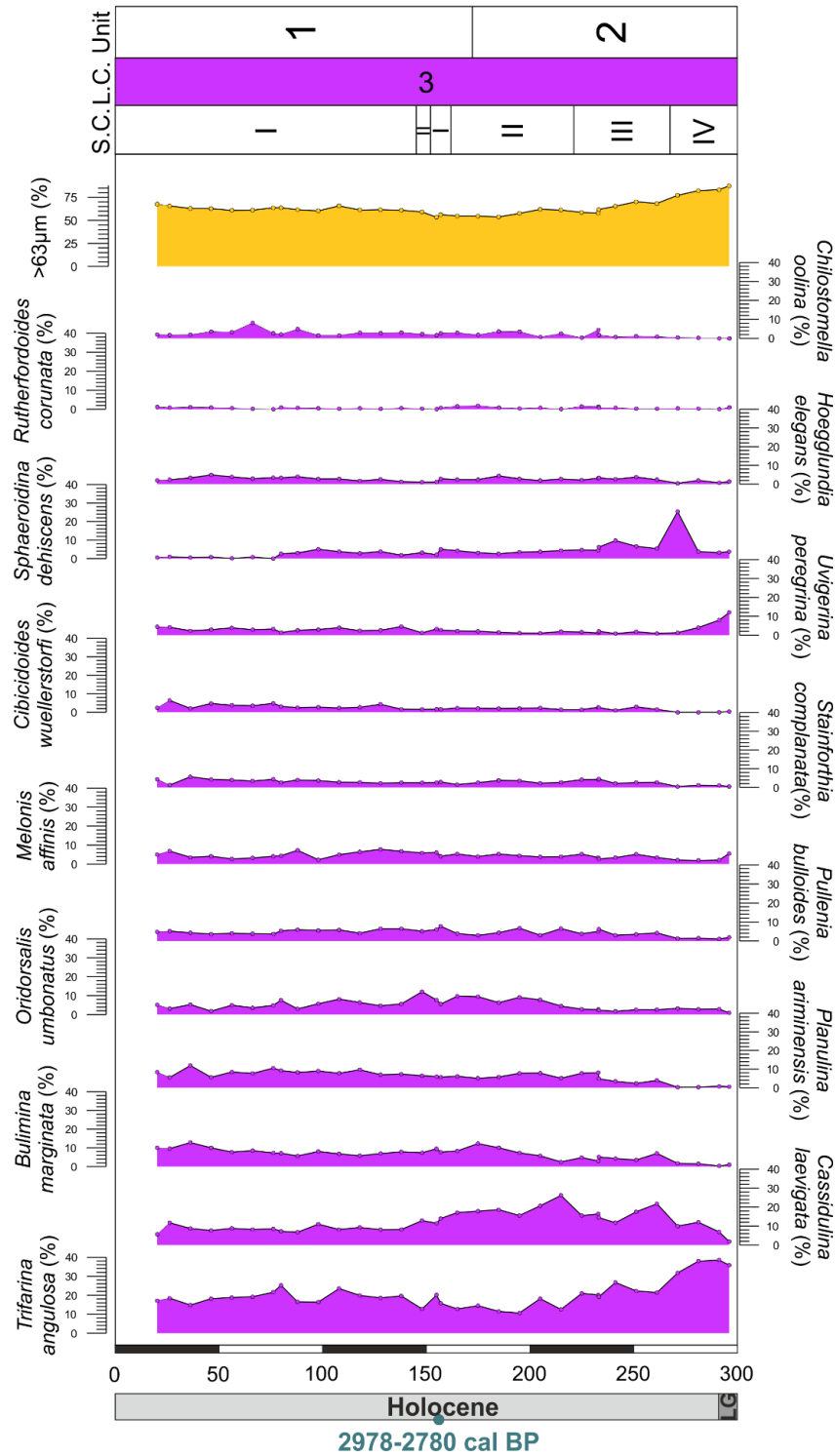
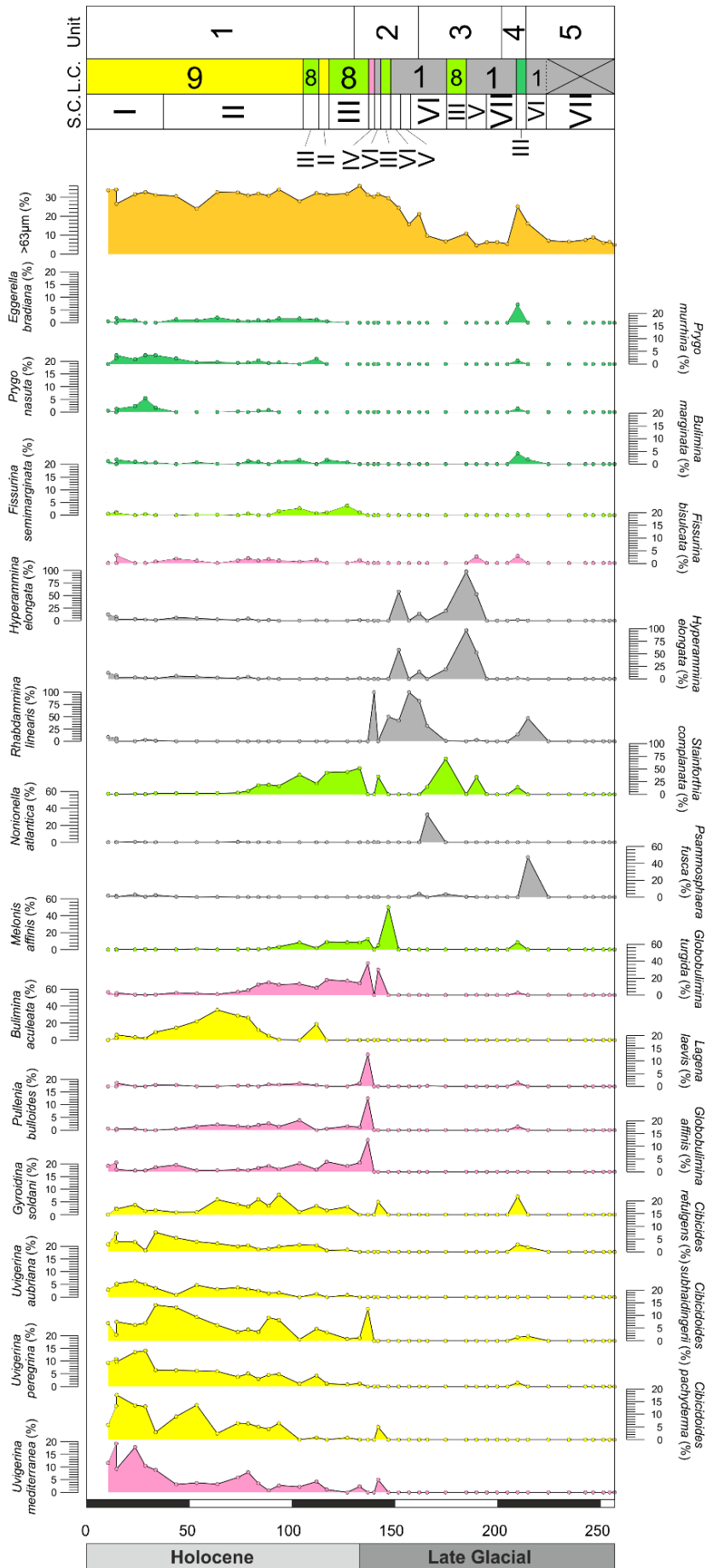


Figure 63 Variations in relative abundances of major benthic foraminiferal taxa within core UPC125 from the upper slope contourite terrace. Colours and numbers correspond to foraminiferal assemblages characterising the sample clustering across the different environments/sediment core set. Uncoloured numerals correspond to foraminiferal assemblages within the sediment core. Grey bars indicate periods of increased bottom current activity as represented by high values of  $\ln(\text{Zr}/\text{Al})$  ratios. Percentage gravimetric grain size >63 µm in yellow.



*Figure 64 Variations in relative abundances of major benthic foraminiferal taxa within core UPC133 on the separated drift. Colours and numbers correspond to foraminiferal assemblages characterising the sample clustering across the different environments/sediment core set. Uncoloured numerals correspond to foraminiferal assemblages within the sediment core. Percentage gravimetric grain size >63 µm in yellow.*

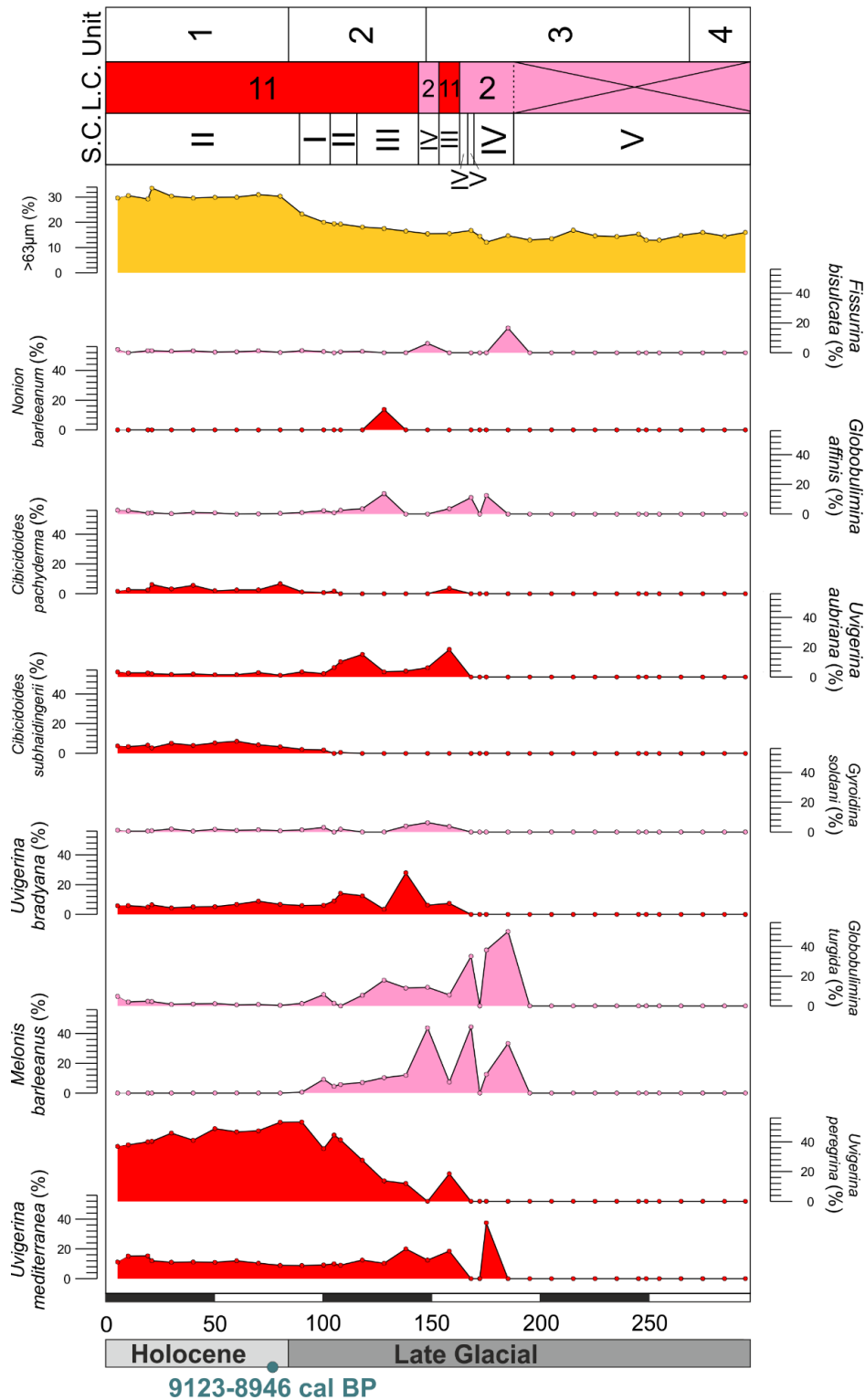


Figure 65 Variations in relative abundances of major benthic foraminiferal taxa within core UPC154 from the lower slope terrace. Colours and numbers correspond to foraminiferal assemblages characterising the sample clustering across the different environments/sediment core set. Uncoloured numerals correspond to foraminiferal assemblages within the sediment core. Grey bars indicate periods of increased bottom current activity as represented by high values of  $\ln(\text{Zr}/\text{Al})$  ratios. Percentage gravimetric grain size  $>63 \mu\text{m}$  in yellow.

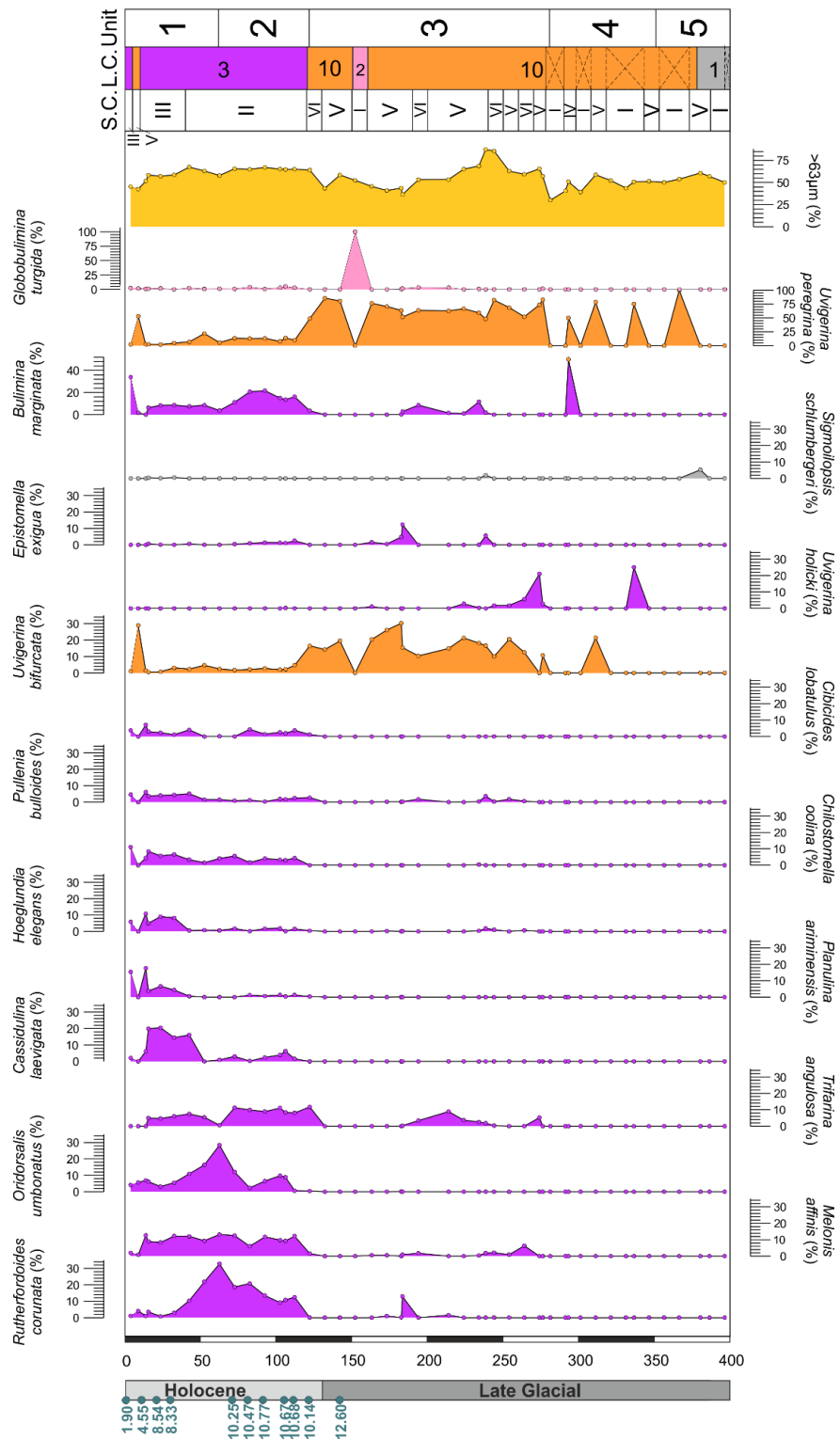


Figure 66 Variations in relative abundances of major benthic foraminiferal taxa within core UPC164 from the upper slope terrace. Colours and numbers correspond to foraminiferal assemblages characterising the sample clustering across the different environments/sediment core set. Uncoloured numerals correspond to foraminiferal assemblages within the sediment core. Grey bars indicate periods of increased bottom current activity as represented by high values of  $\ln(\text{Zr}/\text{Al})$  ratios. Percentage gravimetric grain size  $>63 \mu\text{m}$  in yellow.

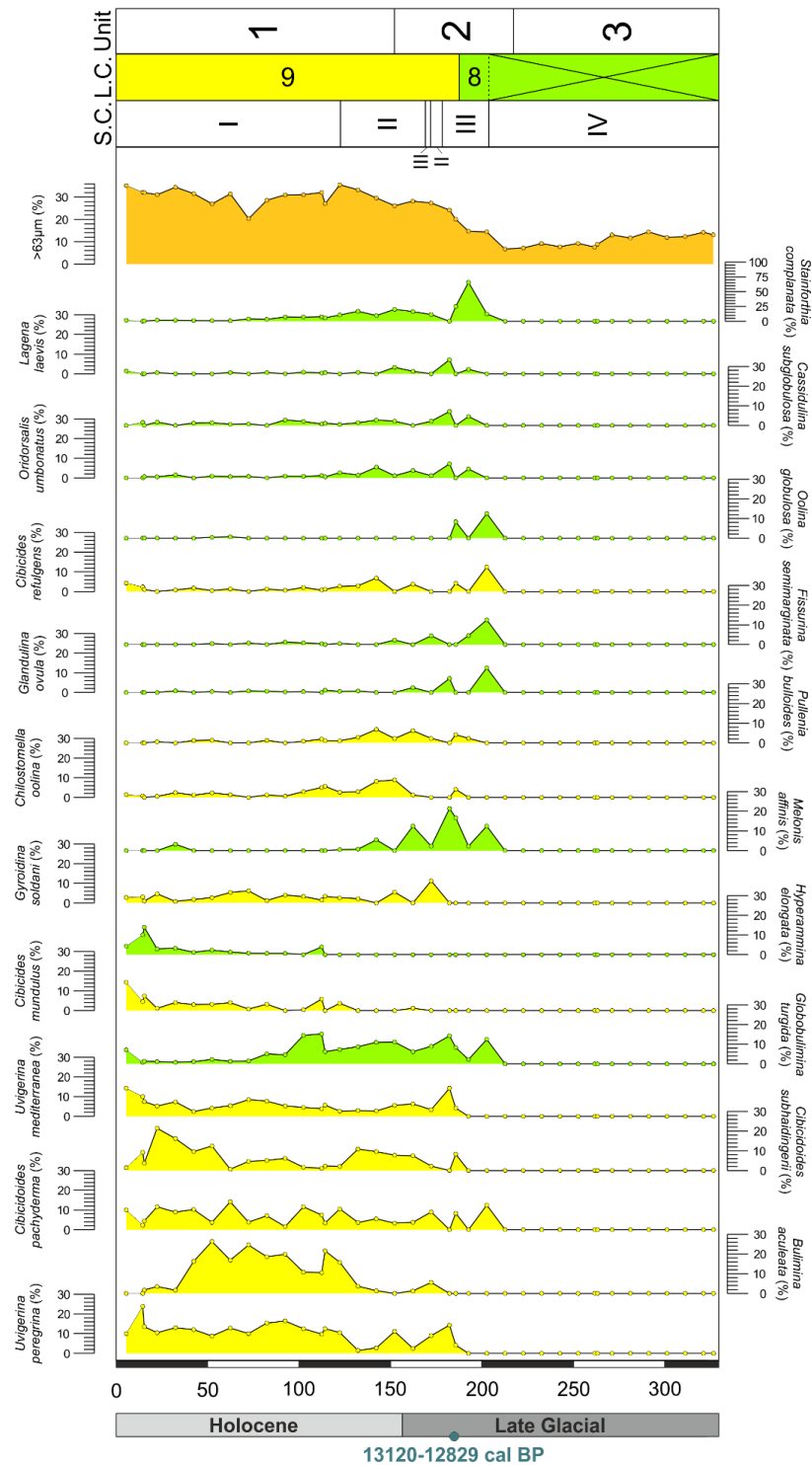


Figure 67 Variations in relative abundances of major benthic foraminiferal taxa from core UPC170 on the plastered drift. Colours and numbers correspond to foraminiferal assemblages characterising the sample clustering across the different environments/sediment core set. Uncoloured numerals correspond to foraminiferal assemblages within the sediment core. Grey bars indicate periods of increased bottom current activity as represented by high values of  $\ln(\text{Zr}/\text{Al})$  ratios. Percentage gravimetric grain size  $>63 \mu\text{m}$  in dark yellow.

#### 6.2.4 Multivariate Statistics & Foraminiferal Indices

Eleven groups of samples (minus those samples barren from dissolution) can be distinguished as a result of the Q-mode cluster analysis (correlation coefficient: 0.90) (Figure 6.5). Each cluster represents groups of samples according to similarities in foraminiferal composition.

A significant statistical difference was found (Table 6.2) between the Clusters with R values  $> 0.90$  and p values  $< 0.05$  in many samples. Clusters that appear to be more similar to one another or the differences do not appear to be as significant between Cluster 7 and Clusters 1 and 4, as well as Cluster 8 and Cluster 1. This is likely due to a smaller sample size and relatively similar environments.

SIMPER analysis on the foraminiferal dataset shows the principal foraminiferal species contributing to differences between clusters (Table 6.5). Only 8 taxa are responsible for 50.5% of the differences between the clusters (Table 6.5).

A number of diversity and foraminiferal indices have been applied to the dataset. Here we apply the indices to each individual cluster to help better understand ecological and environmental factors. Dominance (D) ranges from 0 (all taxa are equally present) to 1 (one taxon dominates the community completely). Shannon Index (H) (entropy) accounts for the number of individuals as well as number of taxa. Varies from 0 for communities with only a single taxon to high values for communities with many taxa, each with few individuals. Equitability (J) measures the evenness with which individuals are divided among the taxa present. Fisher's alpha ( $\alpha$ ) is a diversity index that is used in many foraminiferal studies. It describes the relationship between number of species and the number of

individuals in those species. The small number of abundant species and the large proportion of rare species (class with a single individual is the largest) predicted by the logarithmic series model suggest that, it will be most useful in situations where one or a few factors dominate the ecology of a community. These indices are explained in detail in (Øyvind *et al.*, 2001). For the Foraminiferal Fragmentation Index, the foraminiferal test is considered as fragmented when a test portion is less than two thirds of its original size. The index for each sample was calculated using the equation defined in Section 3.3.1.5. In the equation the number of fragments is divided by 8 because on foraminifer generally breaks into this number of fragments. It is the proportion of fragmented foraminifera and not the number of fragments themselves that has a close to linear relationship with dissolution (Shackleton *et al.*, 1992). Benthic foraminifera cannot be included in this index as they are more resistant to dissolution than planktic foraminifera as benthics generally have less porous chamber walls. Using the indices outlined above it was possible to define 11 foraminiferal assemblages with the relevant index results given for each.

#### 6.2.4.1 Cluster 1 *Rhabdammina* spp-*Hyperammina elongata* assemblage

Found in sedimentary units 2-5 in UPC133 and unit 5 in UPC164. Major contributors to cluster 1 are *Rhabdammina linearis* (41.4%), *Hyperammina elongata* (20.2%), *Psammosphaera fusca* (14.8%), *Melonis affinis* (4.55%), *Stainforthia complanata* (4.49%), and *Nonionella atlantica* (2.98%). This cluster is characterised by very high Dominance (D) up to 0.8 and high Evenness (J) 0.5 to 0.9. Diversity indices of Shannon (H) and Fisher's Alpha ( $\alpha$ ) are low around 1 and 2. Fragmentation of planktic foraminifera is high, up to 1 on the index (not a



single whole individual surviving). Benthics per gram is very low to barren and dominated by infaunal species at >75%. Grain sizes are low at <10% >63  $\mu\text{m}$ .

#### 6.2.4.2 Cluster 2 *Globobulimina* spp.-*Melonis barleeanus* assemblage

Observed in sedimentary units 3 and 4 in UPC154 and sedimentary unit 3 of UPC164. Cluster 2 is dominated by *Globobulimina turgida* (45.1%), *Melonis barleeanus* (22.3%), *Uvigerina mediterranea* (8.33%), *Globobulimina affinis* (6.02%) and *Fissurina bisulcata* (3.82%). The cluster shows a high Dominance values of 0.2 to 0.3 and high values of Evenness up to 0.7. Diversity indices are low/medium at  $H = 2.0$  and  $a = 6$ . The fragmentation indices range from 0.3 to 1.0 and there are commonly <10 benthics per gram of sediment in these samples that are dominated by infaunal species (>75%). Grain sizes are low with only 10 – 30 % >63  $\mu\text{m}$ .

#### 6.2.4.3 Cluster 3 *Trifarina angulosa*-*Cassidulina laevigata* assemblage

The primary foraminiferal assemblage in sedimentary units 1 and 2 of UPC125 and units 1 and 2 in UPC164. Cluster 3 is characterised by *Trifarina angulosa* (16.1%), *Cassidulina laevigata* (10.6%), *Bulimina marginata* (8.37%), *Oridorsalis umbonatus* (6.17%), *Melonis affinis* (6.15%), *Planulina ariminensis* (5.48%), *Uvigerina peregrina* (4.58%), *Pullenia bulloides* (3.96%), *Rutherfordoides coronata* (3.84%) and minor, but significant contributions of *Chilostomella oolina* (3.03%), *Hoeglundina elegans* (2.85%), *Sphaeroidina bulloides* (2.81%). Cluster 3 has a low dominance from any one species at 0.05 to 0.16 and medium values of evenness at 0.3 to 0.5. Diversity indices are very high with  $H = 2.5$  to 3.0 and  $a = 8$  to 11. Fragmentation stays low to medium at values of 0.2 to 0.4 with high benthic counts per gram of 50 to 200 with an assemblage dominated by epifaunal species (>75%). Grain sizes are the highest observed with 50 – 75% >63  $\mu\text{m}$ .

#### 6.2.4.4 Cluster 4 *Chilostomella oolina*-*Nonionella atlantica* assemblage

Only observed in sedimentary unit 3 of UPC001. Cluster 4 is mainly composed of *Chilostomella oolina* (22%), *Nonionella atlantica* (11.4%), *Globobulimina turgida* (10.7%), *Nonionella auris* (10.3%), *Stainforthia complanata* (9.24%), *Nonionella turgida* (8.61%), *Cassidulina subglobulosa* (3.86%), *Cibicidoides wuellerstorfi* (3.62%), *Trifarina angulosa* (3.11%) and *Cibicides lobatulus* (3.02%). Cluster 4 has low to medium dominance values ~0.1 with high evenness values ~0.7. Diversity indices are medium to high with Shannon values of 2.5 to 2.7 and Fisher's alpha of 8 to 11. Fragmentation index values are low at 0.1 to 0.2, with low benthic counts of <20 per gram and are mainly composed of infaunal species (>75%). Grain sizes are low at <20% >63 µm in samples.

#### 6.2.4.5 Cluster 5 *Stainforthia complanata*-*Chilostomella oolina* assemblage

Dominant in UPC001 sedimentary units 1, 2, 4, 5 and 6 and observed in UPC065 unit 3 and 4. Contributors to cluster 5 are *Stainforthia complanata* (22.9%), *Chilostomella oolina* (11.2%), *Cassidulina subglobulosa* (9.12%), *Globobulimina turgida* (7.21%), *Bulimina marginata* (6.29%), *Cibicides lobatulus* (5.17%), *Rutherfordoides coronata* (4.61%), *Trifarina angulosa* (4.47%) and *Cibicidoides wuellerstorfi* (3.37%). Dominance values are low to medium at 0.1 to 0.2 with medium evenness values of 0.4 to 0.7. Diversity is medium to high with values of  $H = 2.4$  to  $2.8$  and Fisher's alpha = 7 to 12. Fragmentation index values are low at 0.1, with medium counts of benthics per gram at 50 to 100. The assemblages are dominated by epifaunal species (>75%). Grain sizes are medium at 30 to 40% >63 µm in samples.

#### 6.2.4.6 Cluster 6 *Bulimina marginata*-*Chilostomella oolina* assemblage

The primary foraminiferal assemblage of UPC065 sedimentary units. Cluster 6 is mainly composed of *Bulimina marginata* (25%), *Chilostomella oolina* (12.6%), *Stainforthia complanata* (9.41%), *Rutherfordoides coronata* (8.51%), *Trifarina angulosa* (5.92%), *Globobulimina turgida* (5.15%), *Glaphyrammina americana* (3.3%), *Uvigerina peregrina* (3.25%) and *Cassidulina subglobulosa* (3.12%). This cluster is characterised by low to medium dominance values of 0.1 to 0.2 and evenness values of 0.3 to 0.5. Diversity values are medium to high at Shannon Index values of 2.25 to 2.75 and Fisher's alpha of 7 to 10. Fragmentation is low at 0.1 with medium to high benthic counts at 100 to 200 tests per gram. Assemblages are dominated by infaunal species (>75%) and grain sizes are low to medium at 20 to 30% >63 µm in samples.

#### 6.2.4.7 Cluster 7 *Rutherfordoides coronata*-*Prygo* spp. assemblage

Observed in unit 5 of UPC065 and unit 4 of UPC133. Cluster 7 is dominated by *Rutherfordoides coronata* (15.6%), *Prygo nasuta* (14.6%), *Bulimina marginata* (11%), *Stainforthia complanata* (9.11%), *Prygo murrhina* (4.94%), *Rhabdammina linearis* (4.76%), *Trifarina angulosa* (3.48%) and minor contributions of *Chilostomella oolina* (3.02%), *Gyroidina soldani* (3.02%), *Melonis affinis* (3.02%), *Globobulimina turgida* (2.77%), *Eggerella bradiana* (2.38%). Cluster 7 has medium dominance values at 0.16 and medium to high evenness values ~0.6. Diversity values are low with Shannon Index values ~2 and Fisher's alpha values ~3.5. Fragmentation values are low at 0.1 with low benthic counts per gram of <50 tests. Epifaunal and Infaunal species are evenly matched and grain sizes are low at <20% >63 µm in samples.

#### 6.2.4.8 Cluster 8 *Stainforthia complanta*-*Globobulimina turgida* assemblage

Observed in UPC133 sedimentary units 1, 2 and 3 and in UPC170 units 2 and 3. Cluster 8 has only 4 major contributors in *Stainforthia complanata* (45.2%), *Globobulimina turgida* (13.4%), *Melonis affinis* (6.72%) and *Fissurina semimarginata* (3.24%). Dominance values are medium ~0.2 and low evenness values ~0.25. Diversity indices are low to medium at Shannon values of 1 to 2 and Fisher's alpha of 5 to 10. Fragmentation values are medium to high at 0.2 to 0.3 with low benthic counts of <50 tests per gram. Assemblages are dominated by infaunal species (>75%) and low grain sizes of <30% >63 µm in samples.

#### 6.2.4.9 Cluster 9 *Bulimina aculeata*-*Uvigerina* spp. assemblage

Found to be dominant in unit 1 of UPC133 and units 1 and 2 of UPC170. Major contributors to cluster 9 are *Bulimina aculeata* (10.5%), *Uvigerina peregrina* (9.32%), *Cibicidoides pachyderma* (7.17%), *Cibicidoides subhaidingerii* (6.79%), *Stainforthia complanata* (6.72%), *Uvigerina mediterranea* (6.66%), *Globobulimina turgida* (5.69%) and *Gyroidina soldani* (3.01%). Dominance values are very low ~0.06, with low to medium evenness values of 0.4 to 0.7. Diversity indices are high with Shannon index values of 2.5 to 3.0 and Fisher's alpha values of 10 to 20. Fragmentation values are low at 0.04 to 0.24, with low to medium benthic counts of 20 to 60 per gram. Epifaunal and infaunal species are in equilibrium to each other with medium grain sizes of 30% >63 µm in samples.

#### 6.2.4.10 Cluster 10 *Uvigerina* spp.-*Bulimina marginata* assemblage

Only found in units 3,4 and 5 of UPC164. Cluster 10 has three major contributors *Uvigerina peregrina* (67.9%), *Uvigerina bifurcata* (14.9%) and *Bulimina marginata* (3.75%). Dominance values in cluster 10 are high at 0.55 to 0.90 and evenness

values are medium to high at 0.16 to 0.76. Diversity indices are very low with Shannon values of less than 1 and Fisher's alpha values of less than 2.5. Fragmentation index values are very high from 0.25 to entirely fragmented with no whole tests surviving. Benthic counts per gram are low at <50 tests and assemblages are dominated by > 75% infaunal species. >50% of the grain size values are >63 µm (sand fraction) indicating a sediment with reduced fine fraction and a coarser grain size.

#### 6.2.4.11 Cluster 11 *Uvigerina* spp-*Globobulimina turgida* assemblage

Finally, Cluster 11 is observed in units 1, 2 and the top of unit 3 in UPC154. This assemblage is dominated by *Uvigerina peregrina* (38%), *Uvigerina mediterranea* (12%), *Uvigerina bradyana* (8.18%), *Uvigerina aubriana* (4.76%), *Globobulimina turgida* (4.23%), *Cibicidoides subhaidingerii* (3.47%) and *Melonis barleeanus* (3.17%). This cluster has medium dominance values of 0.18 to 0.28 and medium to high evenness values of 0.16 to 0.76. Diversity indices are medium to high with Shannon indices between 2 and 2.5 and Fisher's alpha values of 7 to 12. Fragmentation is medium to high at 0.2 to 0.3 with high benthic counts per gram at 100 to 200 and is dominated by infaunal species (>75%). Grain sizes are medium ~30% >63 µm.

#### 6.2.5 Stratigraphy of Foraminiferal Assemblages

Figures 6.3 and 6.4 show the distribution of sample clusters from each core, each showing different foraminiferal compositions. Intervals of core have been coloured accordingly. Foraminiferal assemblages have been assigned according to the cluster in which they are most dominant (above 3% contribution in each cluster according to the SIMPER analysis), these most dominant taxa are represented in the same colours as the corresponding cluster (Fig. 6.6 – 6.19).

There are several marked changes in assemblage distribution from core to core and within each core that allow the cores to be subdivided by the 11 clusters defined above.

#### *6.2.5.1 Upper Slope Distributions*

UPC001 located on Drift 1 is composed of fine sand and silt units and finer clay and silt intervals. Samples from assemblage 5 are most common in the coarser sediment units 1, 2 4 and 5 within this core. Within the clay-rich unit 3, assemblage 4 becomes more dominant. UPC125 on Terrace 2 is dominated by assemblage 3 with a composition of coarse (Unit 2) to medium sand (Unit 1) throughout the entire core. UPC065 in the submarine channel system consists of alternating units of clay, silt to sandy silt units. The clay to silt fractions (units 3, 4 and 5) are dominated by assemblages 5 and 7, while the sandier units are mainly composed of assemblage 6 e.g. Unit 1. UPC164 on Terrace 2 is the only core on the upper slope to show evidence for dissolution in the lowermost sections of the core. The sediments in the core are composed of transitions from silty clay, sandy silt to silty sand. The lowermost sandy units 3, 4 and 5 are dominated by assemblages 1, 2 and 10 within the Last Glacial. These assemblages are likely to have been influenced by dissolution as seen by the increase in the foraminiferal fragmentation. A major shift in foraminiferal composition occurs in the uppermost units 1 and 2, across the Holocene-Pleistocene boundary, where silty sands dominate with assemblage 3, this is similar to core UPC125.

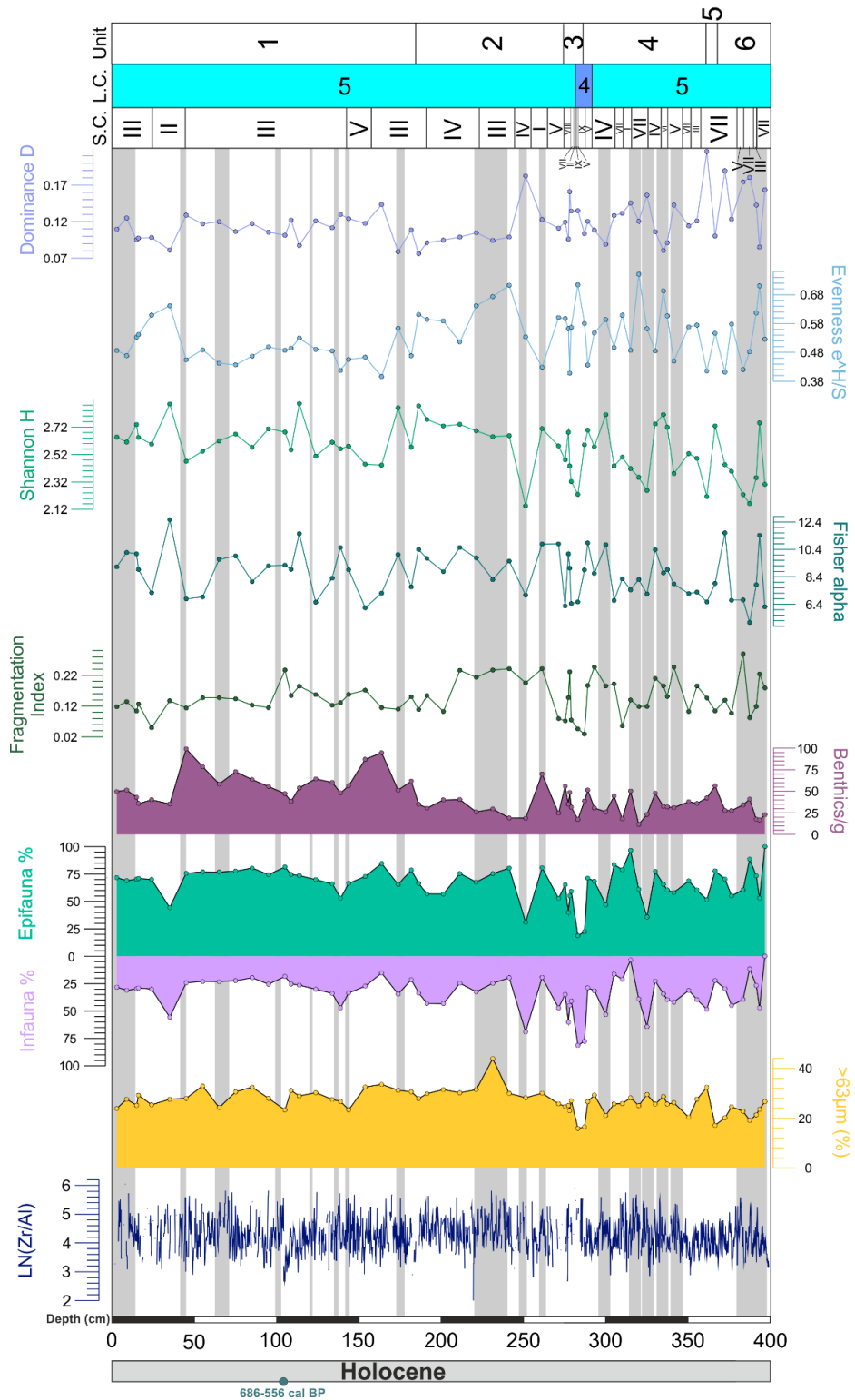


Figure 68 Variations in assemblage indices for core UPC001. Dominance (D), Evenness (J), Shannon Diversity (H) and Fisher's Alpha Index. Fragmentation Index based in proportion of fragmented planktonic foraminifera down core. Benthic tests per gram. Relative abundances of epifaunal/shallow infaunal (green, %) vs. infauna intermediate/deep infauna (purple, %) from Appendix 3.2. Percentage gravimetric grain size >63µm in yellow. Ln(Zr/Al) ratio (blue, 3-point running average).

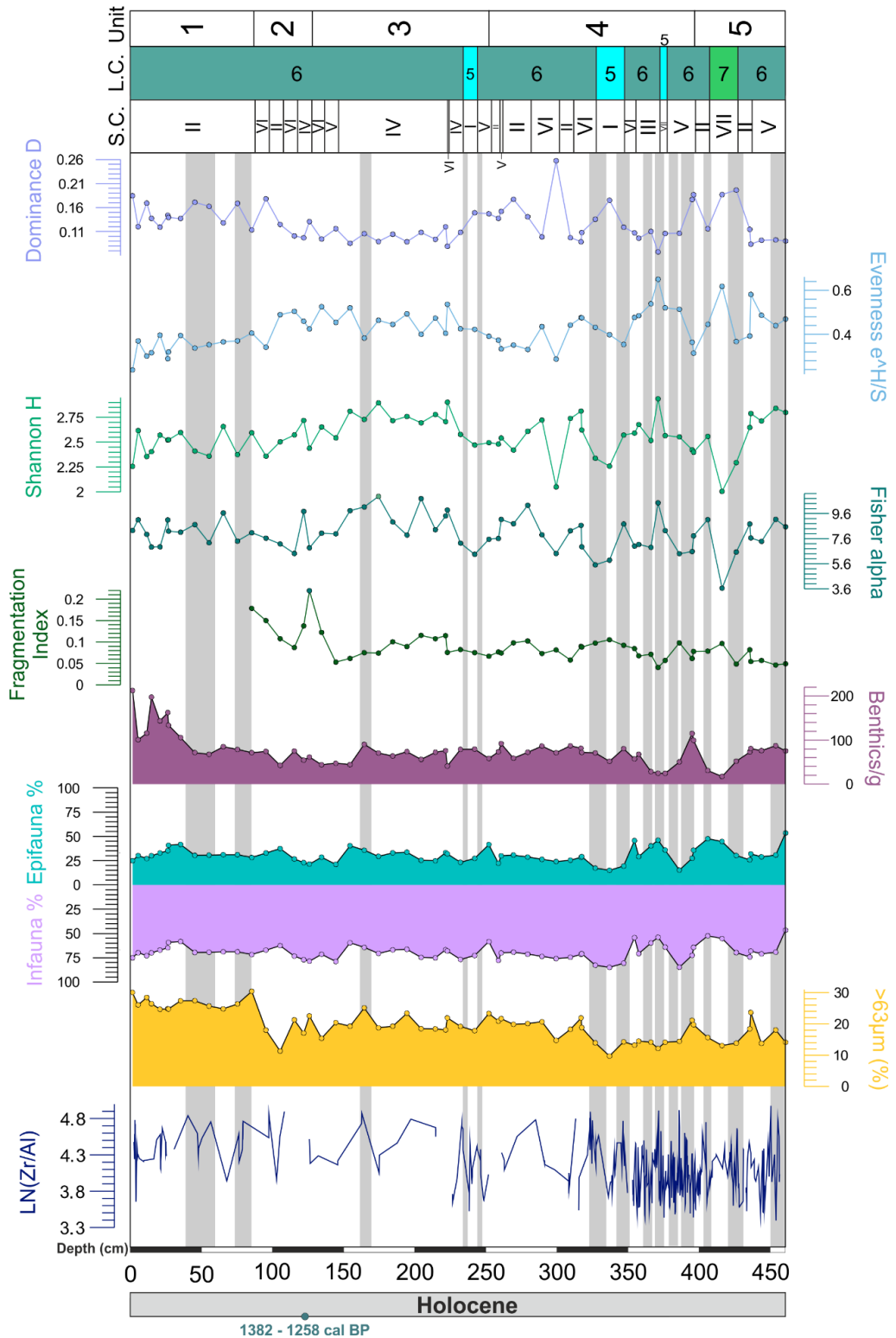


Figure 69 Variations in assemblage indices for UPC065. Dominance (D), Evenness (J), Shannon Diversity (H) and Fisher's Alpha Index. Fragmentation Index based in proportion of fragmented planktonic foraminifera down core. Benthic tests per gram. Relative abundances of epifaunal/shallow infaunal (green, %) vs. infauna intermediate/deep infauna (purple, %) from Appendix 3.2. Percentage gravimetric grain size  $>63\mu m$  in yellow. Ln(Zr/Al) ratio (blue, 3-point running average).



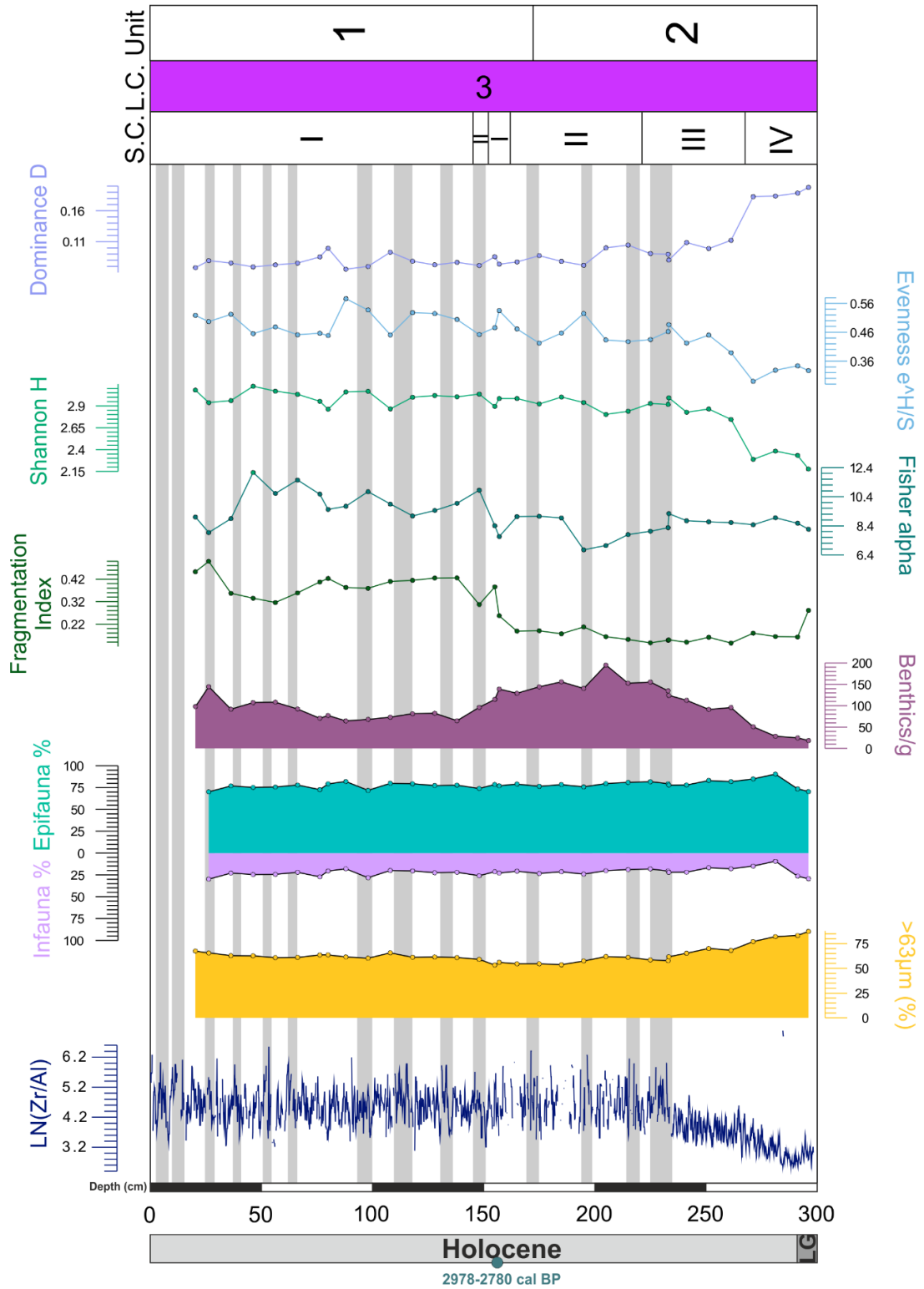


Figure 70 Variations in assemblage indices for UPC125. Dominance (D), Evenness (J), Shannon Diversity (H) and Fisher's Alpha Index. Fragmentation Index based in proportion of fragmented planktonic foraminifera down core. Benthic tests per gram. Relative abundances of epifaunal/shallow infaunal (green, %) vs. infauna intermediate/deep infauna (purple, %) from Appendix 3.2. Percentage gravimetric grain size  $>63\mu\text{m}$  in yellow.  $\text{Ln}(\text{Zr}/\text{Al})$  ratio (blue, 3-point running average).

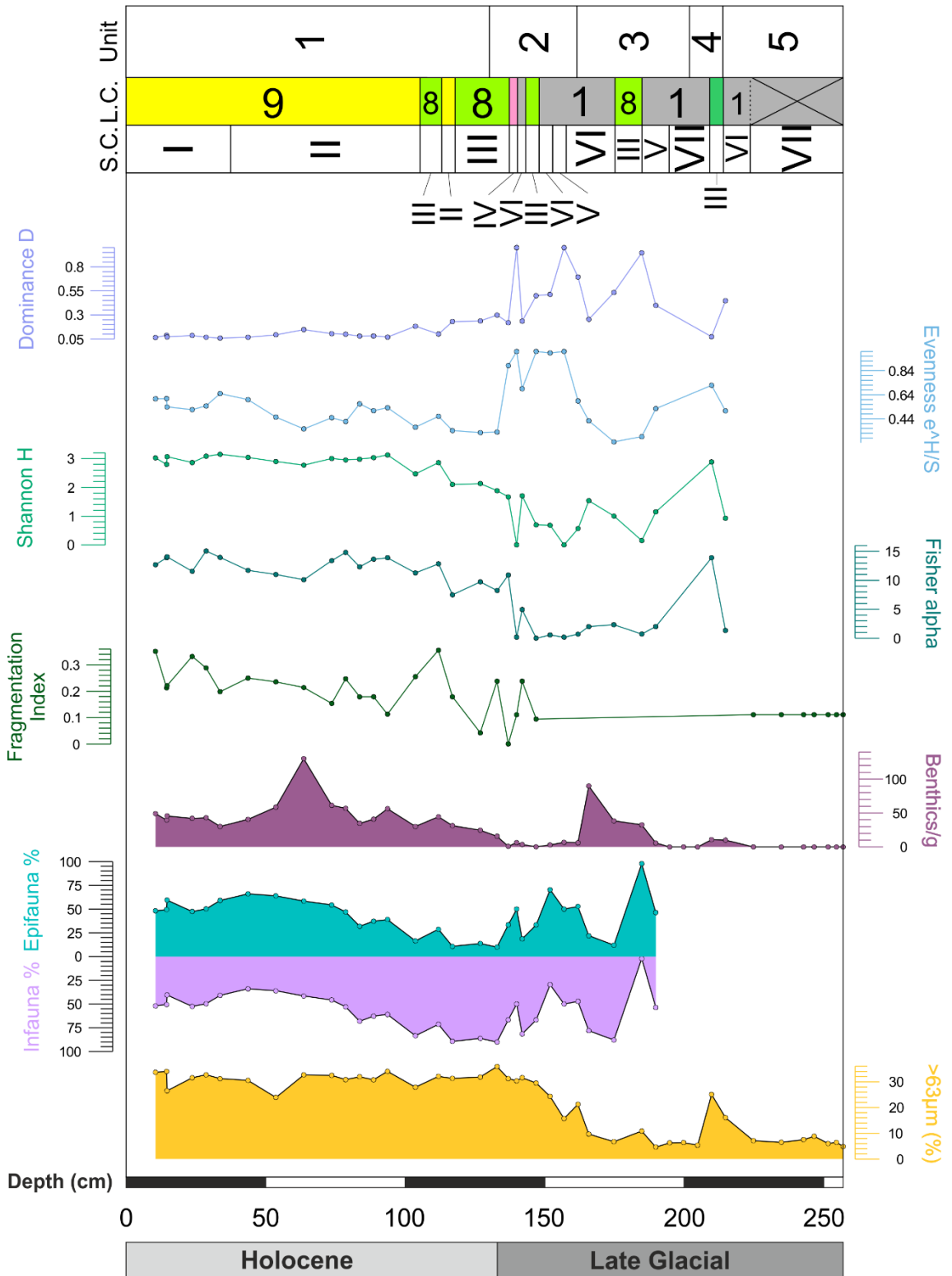


Figure 71 Variations in assemblage indices for UPC133. Dominance (D), Evenness (J), Shannon Diversity (H) and Fisher's Alpha Index. Fragmentation Index based in proportion of fragmented planktonic foraminifera down core. Benthic tests per gram. Relative abundances of epifaunal/shallow infaunal (green, %) vs. infauna intermediate/deep infauna (purple, %) from Appendix 3.2. Percentage gravimetric grain size >63µm in yellow. Ln(Zr/Al) ratio (blue, 3-point running average).

#### 6.2.5.2 Lower Slope Distributions

The sediment in core UPC154 is mainly composed of clays (Hemipelagic/Pelagic) and silts. The lowermost section is barren of foraminifera, mainly clay-rich units 3 and 4, are dominated by assemblage 2. This section of core is likely influenced by dissolution. There is a major shift in foraminiferal assemblage composition in the upper core units 1 and 2 across the Holocene-Pleistocene boundary to a silty sediment with assemblage 11 becoming dominant. UPC133 has the most heterogeneous foraminiferal compositions. The core contains sediment units ranging from clays to silts to fine sand. The clays and silts (units 2, 3 and 5) are dominated by assemblages 1, 2 and 8. These units are found in the lowermost sections of the core and are likely influenced by dissolution. There is a sandier unit 4 that is mainly composed of assemblage 7 and in the uppermost core there is a transition across the Holocene-Pleistocene boundary to sandy silt unit 1 where assemblage 9 becomes the dominant assemblage. In core UPC170 there is a transition from clay and silt units 2 and 3 in the lowermost core to sandy silty unit 1 in the upper core. Assemblage 8 is dominant in the clays and silts (units 2 and 3), while assemblage 9 is dominant in the sandy silt (unit 1). This is a similar transition seen in UPC133.

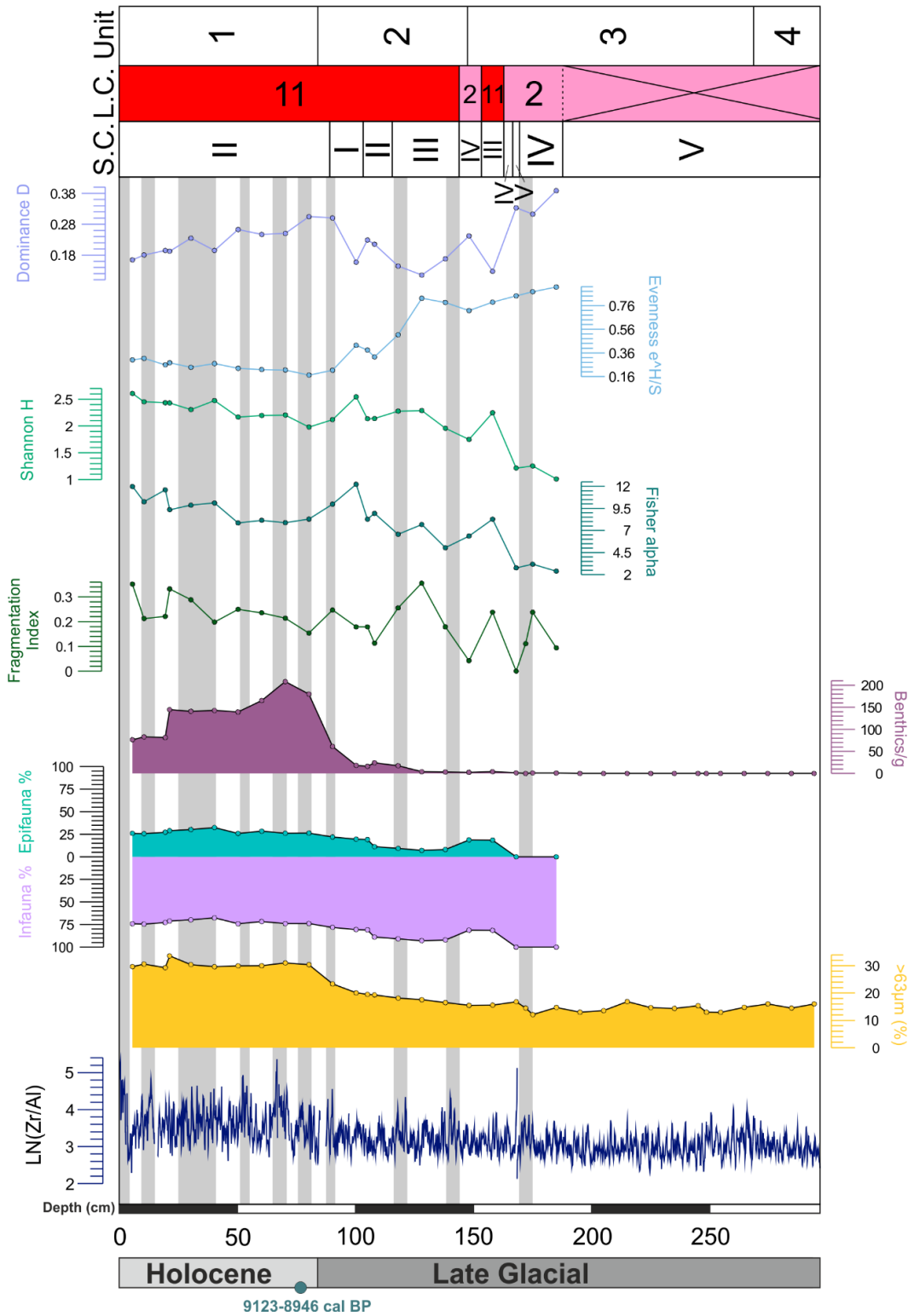


Figure 72 Variations in assemblage indices for UPC154. Dominance (D), Evenness (J), Shannon Diversity (H) and Fisher's Alpha Index. Fragmentation Index based in proportion of fragmented planktonic foraminifera down core. Benthic tests per gram. Relative abundances of epifaunal/shallow infaunal (green, %) vs. infauna intermediate/deep infauna (purple, %) from Appendix 3.2. Percentage gravimetric grain size >63µm in yellow. Ln(Zr/Al) ratio (blue, 3-point running average).



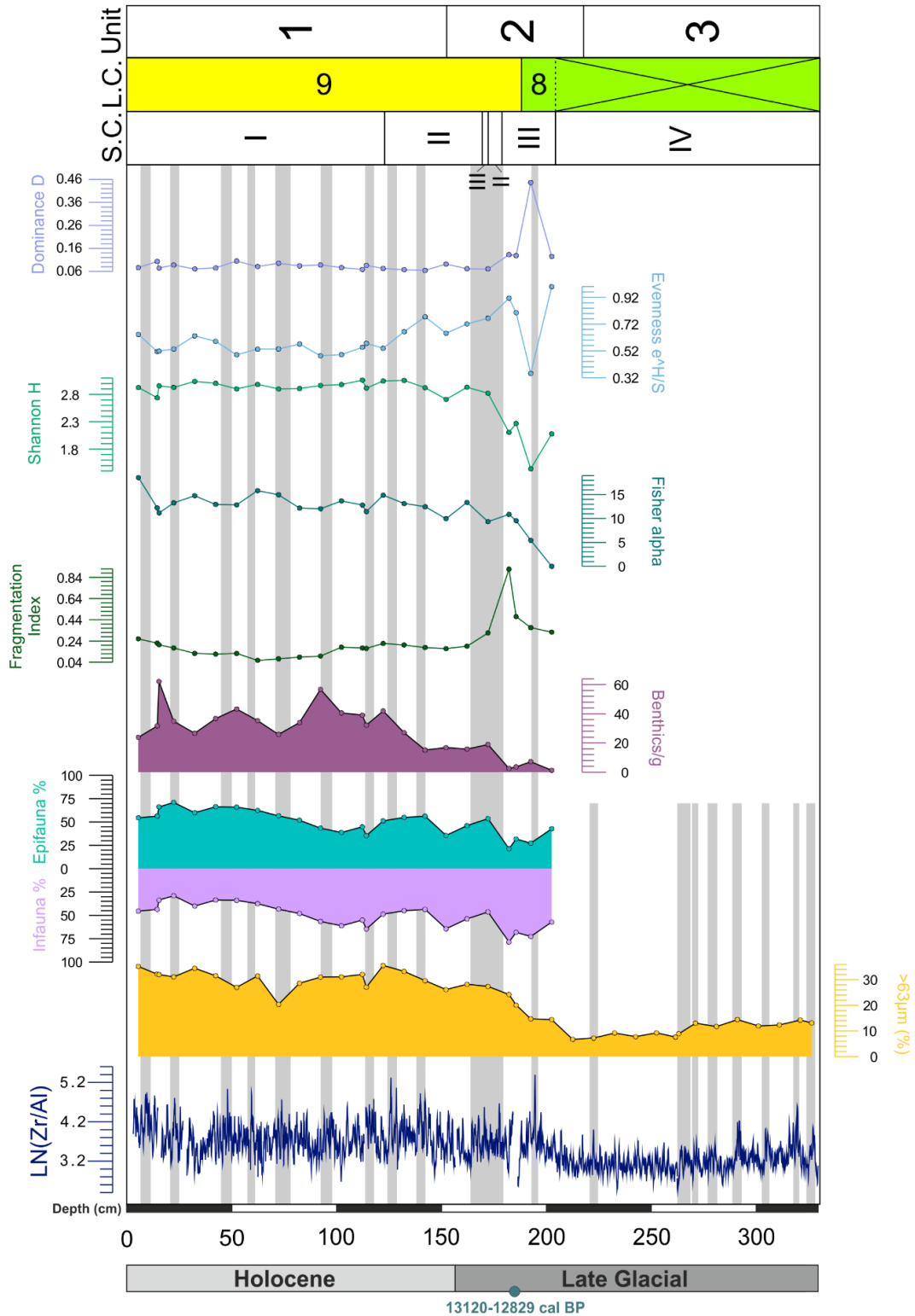


Figure 74 Variations in assemblage indices for UPC170. Dominance (D), Evenness (J), Shannon Diversity (H) and Fisher's Alpha Index. Fragmentation Index based in proportion of fragmented planktonic foraminifera down core. Benthic tests per gram. Relative abundances of epifaunal/shallow infaunal (green, %) vs. infauna intermediate/deep infauna (purple, %) from Appendix 3.2. Percentage gravimetric grain size >63µm in yellow. Ln(Zr/Al) ratio (blue, 3-point running average).

### 6.3 Discussion

Foraminiferal abundances and statistical analyses resulted in eleven distinct faunal assemblages being identified in the core set studied from Uruguay, indicating six prevailing (palaeo)environments. With the aid of the sedimentary analysis in identifying key facies, these can be generalised into a higher energy upper slope associated with a strong modern AAIW bottom current velocity and a lower energy lower slope associated with weak modern LCDW and AABW. Assemblages found in sections of core older than the Holocene-Pleistocene boundary cannot be attributed to prevailing environmental conditions as hydrography in the region has changed significantly since the LGM. Assemblages 1, 2, 8 and 10 are mostly found within these sections. As discussed in previous chapters, increased Antarctic water production led to increased dissolution of benthic tests on the entire slope. However, within these Pleistocene sections the presence of key indicator species may still provide clues to past conditions. The remaining seven assemblages can be associated with changes in grain size, oxygenation, food supply and disturbance under much less corrosive Holocene water mass properties.

#### 6.3.1 Foraminiferal Assemblages & Morphosedimentary Environments

##### *6.3.1.1 Pleistocene Dissolution Intervals*

The foraminiferal assemblages 1, 2, 8 and 10 characterise the dissolution intervals from the lower sections of core in UPC133, UPC154, UPC164 and UPC170. All of these core localities show lower sedimentation rates than the other localities in the region. Therefore, the sedimentary record extends back into the Pleistocene. All these sampled intervals are dated as late Pleistocene in age and can therefore give some insight into glacial conditions on the continental

slope. The Pleistocene dissolution interval on the terrace (UPC164) is characterised by assemblage 10 with intervals of 1 and 2 associated with stronger periods of dissolution/benthic exclusion. There is evidence for substantial bottom current activity in the Pleistocene on the terrace, sediment grain size ranges from silt to medium sand, that show both fining and coarsening upwards sequences. Within cluster 10 there are continuous abundances of *U. peregrina* and *U. bifurcata*, with peak abundances of *B. marginata* within the silts. This suggests mesotrophic conditions prevailing on the terrace during this period. *Uvigerinids* are generally described as shallow infaunal species able to feed on relatively fresh organic detritus (De Rijk *et al.*, 2000; Schmiedl *et al.*, 2000; Fontanier *et al.*, 2002, 2003, 2006, 2008; Eberwein & Mackensen, 2006; Koho *et al.*, 2008, 2007; Duros *et al.*, 2011, 2013; Contreras-Rosales *et al.*, 2012). *Uvigerina peregrina* can behave as an opportunistic taxon feeding on freshly exported phytodetritus in slope environments, while *Uvigerina bifurcata* generally requires a more elevated oxygen content than *U. peregrina* (Kaiho & Hasegawa, 1994; Bubenshchikova *et al.*, 2008). Peaks in abundance of *B. marginata* being found within the finer sediments is significant as this may indicate periods of weakened bottom current activity allowing more organic matter to settle on the seafloor or periods where the La Plata plume extends over the core site. *B. marginata* is an opportunistic fauna that inhabits food-rich zones, that shows a positive correlation with nutrient content (Donnici, *et al.* 2002) and is therefore tolerant of low-oxygen conditions (Murray, 1991; Jorissen *et al.*, 1992). The appearance of assemblages 1 and 2 also within the finer sediments on the terrace may suggest brief periods more eutrophic conditions caused by enhanced phytodetritus delivery to the seafloor.



Foraminiferal assemblage 1 is found in the lowermost section of the terrace core (UPC164) and generally characterises the Pleistocene section of the deeper separated contourite drift (UPC133). Sections of core where assemblage 1 are dominated by muddy sediments. Assemblage 1 is composed mostly of agglutinated foraminifera that can survive corrosive water masses and/or below the CCD. Despite the muddy nature of the sediment the foraminiferal microhabitat appears well-oxygenated. Foraminifera found here include *Rhabdammina linearis* and *Hyperammina elongata* that are known passive suspension feeders in low to high bottom current conditions in distal marine settings (Schönfeld, 2002c; Murray, 2006). This may suggest low food supply to seafloor, resulting in a more elevated position within the water column being more advantageous. The only infaunal taxa found in significant abundances is *Stainforthia complanata* that is seen to survive in a variety of settings but is generally seen as an opportunist with “bloom-feeding” characteristics (Kuhnt *et al.*, 2005). There is a single peak in abundance of *Psammosphaera fusca* within the separated drift core (UPC133) associated with assemblage 1. The peak in abundance of *P. fusca* coincides with a fine-grained turbidite deposit. Indeed, *P. fusca* is a stress tolerant, opportunistic taxa found in sediment poor in organic matter, documented as potential recolonisers of freshly disturbed areas (Kaminski, 1985; Hess & Kuhnt, 1996; Hess *et al.*, 2005; Hess & Jorissen, 2009; Fontanier *et al.*, 2012; Duros *et al.*, 2013). This turbidite interval also contains taxa such as *Melonis affinis* and *Nonionella spp.* that will be discussed below.

Foraminiferal assemblage 2 is found to dominate the Pleistocene sections of the lower contourite terrace core (UPC154) and is found in short intervals within UPC164 and UPC133. It is characterised by a predominance of infaunal species

adapted to eutrophic conditions such as *Globobulimina turgida*, *Melonis barleeanus*, *Uvigerina mediteranea*, *Globobulimina affinis* (Sen Gupta, 1999a). This assemblage is again generally found in the muddier samples giving an indication that bottom currents had low velocities in these intervals. *Globobulimina turgida* occupy niches deep in the sediment often below the maximum oxygen penetration depth (can vary from a few mm to 10s of cm depth) (Sen Gupta, 1999; Gooday *et al.*, 2000). In very eutrophic conditions the species is often found solely at the sediment water interface (Koho *et al.*, 2008), however this is probably not the case in this setting. The association of this species within assemblage 2 with *U. mediterranea* and *M. barleeanus* shows that mesotrophic conditions prevail. *M. barleeanus* thrives in deep microhabitats below the sediment-water interface feeding on degraded organic matter (Schmiedl *et al.*, 2000; Fontanier *et al.*, 2003, 2005, 2008; Licari *et al.*, 2003; Koho *et al.*, 2007; Duros *et al.*, 2011, 2013). *U. mediterranea* being a opportunistic species able to grow and reproduce when food is available on the surface sediment (Fontanier *et al.*, 2003; Duros *et al.*, 2011, 2013). The presence of *G. turgida*, *M. barleeanus* and *U. mediterranea* with contributions from *G. affinis* suggests a sediment rich in organic content. These highly specialised taxa are capable of relying on low-quality organic detritus that collects in depressions of canyons or in the weaker/distal portions of bottom currents (Fontanier *et al.*, 2005, 2008). *G. affinis* alternate in abundance maxima with *Fissurina spp.* and *Uvigerina spp.* in the Pleistocene sections of core UPC154. This may suggest episodic delivery of fine, low quality organic material to the lower terrace in the Last Glacial. *Fissurina spp.* are generally found within more oligotrophic settings, adapted to a carnivorous life strategy as an epifaunal foraminifera (Kitazato, 1988). It has been observed

to be highly mobile within the sediment (Kitazato, 1988). This switch from eutrophic to oligotrophic conditions may suggest a punctuated delivery of degraded organic material from the canyon mouths upslope from this location. One alternative interpretation of this switching could be from episodic gas hydrate emission within the pockmark field on the lower terrace where UPC154 is located. These pockmark environments are rich in degraded organic matter with episodic blooms of bacterial mats related to methane gas seepage providing food for opportunistic taxa such as *Fissurina* spp. (Fontanier *et al.*, 2015).

Assemblage 8 dominates the Pleistocene sections of the plastered drift core (UPC170) and alternates with assemblage 1 in the separated drift core (UPC133). The assemblage appears similar to assemblage 2 but has some key differences. Firstly, the sections of core characterised by assemblage 8 are generally siltier than other assemblage intervals indicating stronger near bottom currents. It is composed of *S. complanata*, *G. turgida*, *M. affinis* and *Fissurina* spp. with minor contributions from *C. refulgens* and *C. pachyderma*. *Stainforthia complanata* is capable of surviving in a variety of different microhabitats, however it is generally seen as an opportunist in food-rich environments (Alve, 1995). It shows remarkably high abundances (up to 75%) at the late Glacial transition before tapering off into the Holocene seen in cores UPC133 and UPC170. This species is known to have rapid fluctuations in population size and is an extremely successful recoloniser of formerly anoxic environments (Alve, 1995) as well as new recently established habitats (Alve, 1999). It exploits food resources in organic-rich, oxygen-depleted muddy sediments and is inferred to grow and reproduce quickly throughout the year and to have a high turnover rate (Murray, 1991). Live specimens are associated with organically enriched microhabitats,

always occurring in aggregates of fresh phytodetritus (Gooday & Alve, 2001) and not the degraded supply seen as a requirement for assemblage 2. *Melonis affinis* shows a similar high abundance at the late Glacial transition before tailing off into the Holocene. This species is generally found in more mesotrophic to well-oxygenated environments than the similar looking *M. barleeanus* (Caralp, 1989a, 1989b; Schmiedl *et al.*, 2000; Kurbjeweit *et al.*, 2000; Fontanier *et al.*, 2003, 2005, 2008; Licari *et al.*, 2003; Koho *et al.*, 2007; Duros *et al.*, 2011, 2013), as is the case for *Fissurina* spp. discussed previously. Critically, we find this assemblage associated with *Cibicides refulgens* a passive suspension feeder attached to objects above the sediment/water interface to catch food particles (Linke and Lutze, 1993) and *Cibicidoides pachyderma* colonises exposed oxygenated habitats with an epibenthic lifestyle. These two species indicate enhanced bottom current conditions exiting the last Glacial. Alongside the bottom current activity, productivity in the water column increases supplying a new habitat to be colonised through the Holocene. Assemblage 8 can therefore be seen as a transition fauna on the lower slope contourite drifts from less favourable conditions in the late Pleistocene to favourable Holocene conditions. This is likely due to increased seasonality, leading to increases in phytodetritus input on the seafloor.

#### 6.3.1.2 Open Slope/Hemipelagic Environments

All of the open slope samples have been dated to no older than Holocene age. After exiting the last Glacial, these sites show a recovery to very stable environmental conditions without any faunal turnover or disturbance. These settings are dominated by infaunal taxa in muddy to silty sediment. The main assemblages found in these settings are assemblages 10 (upper slope) and 11

(lower slope). Assemblage 10 has already been linked to dissolution intervals and is therefore not assumed to be representative of the whole original living benthic assemblage. However, it shows many similarities to assemblage 11 as both are found in contourite terrace environments and dominated by *U. peregrina*. Other species contributions include *U. mediterranea*, *U. bradyana*, *U. aubriana*, *G. turgida*, *C. subhaidingerii/pachyderma* and *M. barleeanus*. *U. peregrina* and *U. mediterranea* are generally described as shallow infaunal species able to feed on relatively fresh organic detritus in mesotrophic environments (De Rijk *et al.*, 2000; Schmiedl *et al.*, 2000; Fontanier *et al.*, 2002, 2003, 2006, 2008; Eberwein and Mackensen, 2006; Koho *et al.*, 2008, 2007; Duros *et al.*, 2011, 2013; Contreras-Rosales *et al.*, 2012). *Uvigerina peregrina* can behave as an opportunistic taxon feeding on freshly exported phytodetritus in canyon and slope environments, whereas *U. mediterranea* is an opportunistic species able to grow and reproduce when food is available in the surface sediment (Fontanier *et al.*, 2003; Duros *et al.*, 2011, 2013). The faunal association between *M. barleeanus* and uvigerinids shows that mesotrophic conditions prevail naturally in these settings. The two species of *Cibicidoides* spp. are regarded as epibenthic (Jorissen *et al.*, 1995). They have an affinity to colonise exposed habitats from field studies (Alexander & Delaca, 1987; Lutze & Thiel, 1989; Linke & Lutze, 1993; Schönfeld, 2002c) and they are also seen as a facultative endobenthic organisms by (Licari, 2006). Food availability appears to be a living mode determining parameter in oligotrophic settings, *C. pachyderma* is an epibenthic or shallow infaunal (Schmiedl *et al.*, 2000). At eutrophic sites the species lives a predominantly endobenthic lifestyle (Jorissen *et al.*, 1995; Licari, 2006). Therefore, bottom current activity appears to

have little influence, other than keeping the site relatively mesotrophic when compared to earlier eutrophic glacial intervals.

#### 6.3.1.3 Stable *Contourite* Drift Environments (Low Energy)

Low energy contourite drift deposits are characterised by sandy silt and a high degree of bioturbation seen in the Holocene sections of cores UPC133 and UPC170. The foraminiferal assemblage has high diversity and relatively equal proportions of epifaunal and infaunal taxa. The Holocene intervals in both cores are entirely made up of assemblage 9 and represent an equilibrium fauna reached after the transition from assemblage 8. *Bulimina aculeata*, *Uvigerina peregrina*, *Cibicidoides pachyderma*, *Cibicidoides subhaidingerii*, *Stainforthia complanata*, *Uvigerina mediterranea*, *Globobulimina turgida*, *Gyroidina soldani* and associated with *Cibicides refulgens* throughout. *B. aculeata* shows maximum abundances following the Glacial transition (due to its specialised lifestyle) but decreases in abundances dramatically in the upper portions of the cores to be replaced by *Cibicidoides* spp. and *Uvigerina* spp. *B. aculeata* occupies deep microhabitats, typical of high organic matter input and or oxygen depleted environments (Mojtahid *et al.*, 2009). It has been shown to be associated with a mix of marine and continental organic matter in the Gulf of Lions (Goineau *et al.*, 2011) where riverine inputs dominate the flux of particulate matter to the seafloor. It is able to respond quickly to fresh organic matter inputs (Kitazato *et al.*, 2000; Eberwein & Mackensen, 2006; Nomaki *et al.*, 2008) and therefore it is assumed that upon entering the Holocene there was increased seasonality, in particular stronger El Niño events. This increased seasonality is backed up by the Si/Al records from sediment cores in Chapter 4 that show positive incursions into the Holocene, indicating increased supply of siliceous microfossils onto the seafloor.

Large positive precipitation anomalies over SE South America associated with El Niño events significantly increased the discharge of the La Plata River that in turn enhanced the primary production (Voigt *et al.*, 2013). Due to atmospheric circulation and precipitation anomalies the La Plata plume spread offshore, leading to event-like accumulation of biogenic-rich layers over the Uruguayan slope (Voigt *et al.*, 2013). The faunal transition from more eutrophic fauna such as *B. aculeata*, *S. complanata* and *G. turgida* to a more eutrophic/oligotrophic faunal assemblage with *Uvigerina spp.* and *Cibicidoides spp.* in the late Holocene implies less of a La Plata plume influence as it is now diverted northwards to the Rio Grande cone. The presence of *Gyroidina soldanii* and *Cibicides refulgens* would imply that the drift are now swept by well-oxygenated bottom currents, even if they are relatively weak. *Cibicides refulgens* is regarded as an elevated epifaunal species (Schönfeld, 2002b) and *Gyroidina soldanii* cannot survive in low oxygen conditions (Abu-Zied *et al.*, 2008) and is typical of oligotrophic basins (Fontanier *et al.*, 2008, 2012). The case for these species being allothonous tests transported from the shelf is unlikely due to the absence of any other shallow water species, and no obvious source of delivery to these drift deposits.

#### 6.3.1.4 Stable Contourite Drift Environments (High Energy)

The high energy contourite drift deposits are primarily found upon the large contourite terraces incised into the slope. The Holocene terraces are characterised by sand-rich deposits that are characterised by foraminiferal assemblage 3. This high diversity assemblage is dominated by epifaunal foraminiferal species. The absence of shelf dwelling foraminifera in this sandy assemblage suggests that the effects of downslope transport are minimal on at these sites. The assemblage is composed of *Trifarina angulosa*, *Cassidulina*

*laevigata*, *Bulimina marginata*, *Oridorsalis umbonatus*, *Melonis affinis*, *Planulina ariminensis*, *Uvigerina peregrina*, *Pullenia bulloides*, *Rutherfordoides coronata* and minor, but significant contributions of *Chilostomella oolina*, *Hoeglundina elegans*, *Sphaeroidina bulloides* and *Cibicide lobatulus*. *T. angulosa* is continuously found in high abundances (>20%) in samples from the contourite terrace. This is a cosmopolitan, shallow infaunal species (De Stigter *et al.*, 1999; Schönfeld, 2001), and occurs in low to moderate abundances from subtidal to middle bathyal depths e.g. (Seiler, 1975; Lutze & Coulbourn, 1984; Jorissen, 1988). High percentages are recorded from current-swept passages (Hayward & Hollis, 1994), coarse, biogenic sands on the inner shelf (McGann & Sloan, 1996), and deep, high-energy environments on the outer shelf and upper slope (Mackensen *et al.*, 1985; Violanti, 1996). It is often associated as in this case with *C. lobatulus*, *C. refulgens*, and *Planulina ariminensis*. Apparently, *T. angulosa* is adapted to strong water turbulences of varying intensity (Mackensen, 1987). As observations of living specimens attached to large particles have not been reported to date, the species seemingly occupies interstitial microhabitats in the coarse-grained sediments where it may withstand water turbulence. *Trifarina angulosa*, seemingly can withstand permanent winnowing and redeposition in environment such as this. Other species in the assemblage such as *Planulina ariminensis* and *Cibicide lobatulus* preferred attached and elevated positions above the sediment surface catching suspended food particles from enhanced bottom currents (Altenbach, 1987; Lutze & Thiel, 1989; Linke & Lutze, 1993). Other species in the assemblage give some indications of a changing food supply/oxygenation through the Holocene. *C. laevigata* is much more abundant in the early Holocene, being replaced by species such as



*Oridorsalis umbonatus* in the late Holocene. *C. laevigata* do not occur below 1 °C (Østby & Nagy, 1982; Klitgaard-Kristensen *et al.*, 2002) showing it is relatively sensitive to bottom water temperature. Laboratory experiments by (Alve, 2010) showed this taxa died off after a period of two years without a supply of fresh phytodetritus, requiring relatively suboxic conditions (Kaiho & Hasegawa, 1994). On the otherhand, *Oridorsalis umbonatus* is a detritivore and has a shallow infaunal microhabitat (Murray, 1991). It is tolerant of changing environmental conditions and occurs with high abundance in areas with low flux rates of particulate organic matter (Friedrich - Wilhelm & Pflaumann, 1989; Schonfeld & Spiegler, 1995). This suggests a decrease in food supply through the Holocene to the terrace either caused by strengthening of bottom currents (resulting in fine particulate matter bypassing the seafloor) or a decrease in productivity in the water column (with an associated decrease in fresh phytodetritus). The relatively constant low abundances of *B. marginata*, *P. bulloides*, *S. bulloides* and *H. elegans* suggest cold well-oxygenated waters with low quantities of organic matter. All these species require seasonal inputs of fresh phytodetritus to the seafloor and have adapted to be incredibly fast moving within the sediment to reach fresh sources of food (Lutze & Coulbourn, 1984; Linke & Lutze, 1993; Schönfeld, 1997, 2001; Gross, 2000; Licari & Mackensen, 2005; Murray, 2006; Koho *et al.*, 2008) this suggests a highly productive water column. However, there are significant contributions of species classed as specialists in dysoxic to anoxic environments that primarily feed on labile organic matter. Species such as *Chilostomella oolina*, *Rutherfordoides coronata* and *Melonis affinis* are all specialists in utilising poor-quality organic matter transferred deep into the sediment. *Chilostomella oolina* inhabits a depth in the sediment at or below the penetration of nitrate. The species

has been observed to benefit from labile organic matter directly by consumption or indirectly through associated bacteria populations. The latter option has been observed in experiments by Nomaki *et al.*, 2008, so it is the more likely feeding strategy. *C. oolina* does not migrate in the sediment column to make use of fresh food inputs, so is seen as a specialist in anoxic environments (Koho *et al.*, 2008). This is anoxic lifestyle is also thought to be the case for *Rutherfordoides coronata*. This species has been observed to occupy surface sediments in the oxygen minimum zones of the California inner borderland basins (2–15 mmol/L) and from, the bathyal anoxic environments of Sagami Bay, Japan, even seen to thrive here (Douglas & Heitman, 1979; Bernhard, Sen Gupta & Borne, 1997; Diekmann *et al.*, 2000; Nomaki *et al.*, 2008; Bernhard *et al.*, 2012). TEM observations show that the species is likely to be a detritus feeder and symbiont free bacteriovore and capable of denitrification (Bernhard *et al.*, 2012). Chloroplasts that become sequestered into the cytoplasm of both *C. oolina* and *R. coronata* may provide a nitrate reductase that is needed for nitrate respiration (Bernhard & Sen Gupta, 1999; Grzymski *et al.*, 2002; Bernhard *et al.*, 2012). This specialist lifestyle indicates that both of these species are likely to be facultative anaerobes. To find such anoxic specialists in what is an otherwise oxygen-rich environment requires an extremely high input of degraded organic matter onto the surface sediment of the terrace. This is interpreted as periods of nepheloid plume deposition, where the fine fraction is deposited over the site as the strong core of bottom currents have migrated up or down slope or have decreased in strength. These dysoxic zones are also found at the limit of drift sedimentation in the Gulf of Cadiz on the lower limit of Mediterranean Outflow activity where degraded organic matter is focused by bottom current activity (Rogerson *et al.*, 2011). This is where

refractory organic matter accumulates in a similar fashion to the outer parts of submarine canyons (Fontanier *et al.*, 2005; Rogerson *et al.*, 2006). It has been termed a dysoxic “halo” zone by (Rogerson *et al.*, 2011) where it is also found at the edge of plume activity. However, in this study it is imagined at more of a dysoxic “strip” that can migrate up and down the slope.

#### 6.3.1.5 Unstable Contourite Drift Environments

Mounded contourite drifts occur on the outer edge of contourite terraces and on the up-current side of submarine canyons. During periods of intensified bottom current activity, sediment accumulation increases. This increase in sediment load and possible undercutting by strong currents downslope causes instability that increases the frequency of slope failures with their associated gravity currents. These settings are characterised by high accumulation rates, with a range of grain sizes from mud units to sandy-silts and silty-sands. Core UPC001 is characteristic of this environment, while there is some evidence of drift type sediment found within the submarine canyon core UPC065. The sediments contain a moderately diverse assemblage of foraminifera that is dominated by epifaunal taxa of assemblage 5, except within the mud units where infaunal species dominate in assemblage 4. The coarser-grained assemblage 5 is found to contain *Stainforthia complanata*, *Chilostomella oolina*, *Cassidulina subglobosa*, *Globobulimina turgida*, *Bulimina marginata*, *Cibicides lobatulus*, *Rutherfordoides corunata*, *Trifarina angulosa*, *Cibicoides wuellerstorfi*, and minor contributions of *Discorbis spp.* UPC001 show evidence for increased bottom current activity and associated instability in the deeper half of the core. Here, we see pulses of coarser grained sediment interbedded with muddy units. These sections show peaks of high abundances of *S. complanta*, *B. marginata*

and *C. subglobosa* alongside minor *P. bulloides* and *Fissurina spp.* peaks. All typical of mesotrophic to suboxic environments with pulses inputs of fresh organic matter. The muddier units are composed of Assemblage 4, largely composed of the same assemblage as 5, but with the addition of *Nonionella spp.* *Nonionella spp.* behaves like an intermediate-infaunal species. It has been documented in anoxic sediments from shelf environments (Ikeya, 1971; Leutenegger, 1984; Kitazato *et al.*, 2000) and in dysoxic to anoxic sediments from several OMZs in the Pacific Ocean (0–15 mmol/L; Phleger & Soutar, 1973; Bernhard, Sen Gupta and Borne, 1997; Bernhard *et al.*, 2012; Mallon *et al.*, 2012). As with *R. coronata* and *C. oolina*, it is interpreted as a facultative anerobe. Therefore, these mud units are thought to of similar origin to the anoxic “strips” seen elsewhere on the terrace, where there is a high accumulation of degraded organic matter from the lower limits of the bottom current plume. In the upper portions of core UPC001 *C. subglobosa* increases in abundance and we observed less frequent abundance peaks of opportunistic species. However, *C. subglobosa* shows cyclic abundance increases possibly linked to pulsed food inputs (Gooday, 1994; Gupta & Thomas, 2003). This species is associated with phytodetritus input (Gooday, 1988, 1993; Gooday, Bowser & Bernhard, 1996) as they selectively feed on phytodetritus (Suhr *et al.*, 2003; Suhr & Pond, 2006) Despite this increased food input they are generally found in oxic environments possibly linked to UCDW (Violante *et al.*, 2014). Furthermore, they have been linked to enhanced bottom current velocities (Schmiedl *et al.*, 1997). Clearly, even though assemblages 4 and 5 show an environment prone to periods of decreased oxygen availability, species such as *C. subglobosa*, *C. lobatulus*, *T. angulosa*, *C. wuellerstorfi* and *Discorbis spp.* show the environment is still swept by oxygen-rich bottom currents to allow these

species to be present in such high abundances feeding directly from the bottom current.

#### 6.3.1.6 Turbidite Environments

Turbidite deposits are mainly found within the submarine canyons and plastered drifts on the lower continental slope. Turbidite activity on the slope has been directly linked to drift instability and failure on the slope. However, the foraminiferal assemblage found within these deposits is uniquely made up of a low to moderately diverse fauna of infaunal opportunists. The sediment composition ranges from mud through to sandy silt to silty sand. Apart from a few sections of the submarine canyon core UPC065 that are composed of assemblage 5 (drift sedimentation directly into the canyon), the units interpreted as turbidite in origin are entirely composed of assemblage 6 in the canyon and 7 on the lower slope drifts in core UPC133. The canyon turbidite assemblage 6 is composed of *Bulimina marginata*, *Chilostomella oolina*, *Stainforthia complanata*, *Rutherfordoides corunata*, *Trifarina angulosa*, *Globobulimina turgida*, *Glaphryamma americana*, *Uvigerina peregrina* and *Cassidulina subglobosa*. Of these species, the opportunist *B. marginata* and the recoloniser *S. complanata* dominate the assemblage, with percentages frequently over 30% with peaks of over 40% within some units, suggesting that these are coloniser species. Alongside these coloniser species, there are significant contributions to the assemblage from facultative anaerobes *C. oolina*, *R. corunata*, *Globobulimina spp.* and *Nonionella spp.* indicative of an environment where degraded organic matter can pool and result in anoxic conditions within the sediments. However, the associated uvigerinids and *Melonis affinis* throughout the core shows a more typically mesotrophic canyon environment. The canyon environment is the only

set of samples where we see agglutinated taxa make up a significant percentage of the assemblage (~10%) *Glaphryammina americana* is a shallow infaunal agglutinated taxon (Licari, 2006). It is often associated with the development of a “flysch fauna” which occurs when disturbance is frequent enough to exclude calcareous benthic foraminifera. Disturbance will preferentially exclude calcareous benthic taxa, however, agglutinated taxa are delicate and are often either found in the smaller sediment size fraction or destroyed during sieving and cleaning (Kaminski *et al.*, 1996). However, an agglutinated/calcareous ratio may be useful for finer grain size fractions. Assemblage 5 associated with drift sedimentation is found within the finer sediments within the canyon. This is likely due to the canyon environment being undisturbed for enough time for a drift fauna to establish themselves. Therefore, background sedimentation within the canyon is similar to that of the unstable drift. This is in agreement with observations from (Voigt *et al.*, 2013) where the canyons are fed by drift progradation during periods of increased bottom current activity.

Assemblage 7 is found in cores UPC065 from the canyon and UPC133 from the plastered drift. This is associated with silty-sandy sediment in fining upwards sequences. The assemblage is dominated by *Rutherfordoides corunata*, *Pyrgo nasuta*, *Bulimina marginata*, *Stainforthia complanata*, *Pyrgo murrhina*, *Rhabdammina linearis*, *Trifarina angulosa*, *Chilostomella oolina*, *Gyroidina soldani* and *Eggerella bradyi*. This is largely similar to the other disturbed assemblages with the opportunists *B. marginata*, *S. complanata* and *R. linearis* and the facultative anerobes *R. corunata*, *C. oolina* and *Globobulimina spp.* However, the presence of *Pyrgo spp.*, *E. bradyi*, *G. soldani* and *T. angulosa* suggests oxygen-rich/high velocity bottom currents. These are the only areas on

the slope where we find *Pyrgo spp.*, *E. bradyi* and *G. soldani* in high abundance. All are found in oligotrophic conditions with low carbon fluxes (Burke *et al.*, 1993; Altenbach *et al.*, 1999; Gupta & Thomas, 2003). *Pyrgo spp.* are fast moving species and can react rapidly to influxes of organic matter, choosing to be epifaunal or infaunal. Generally, for their tests to be preserved there needs to be good conditions for carbonate preservation, not common on the Uruguayan continental margin (Gupta & Thomas, 2003). Here, we suggest that these have been transported down from drift slope failures under the influence of non-corrosive and oxygenated North Atlantic Deep Water. This water mass is shown as an anomaly on the >150 micron surface grain size map, where large planktic and *Pyrgo spp.* tests artificially increase the sediment grain size due to more favourable carbonate preservation conditions. Unfortunately, cores from this area of slope are not included in our dataset.

### 6.3.2 Benthic Foraminifera as Indicators of Strong vs. Weak Bottom Currents, Stable vs. Unstable & Open Slope Environments.

It is clear from the analyses in this chapter that the strict interpretation of a morphosedimentary environment as along- or downslope process dominated is oversimplifying the complex interactions of both deep-sea processes. All sedimentary systems, even the classic contourite systems in the Gulf of Cadiz, should be viewed as mixed systems from a seismic to microscopic scale. Turbiditic and contouritic processes operate on different timescales but are both relatively constant on a geological scale. Both will wax and wane dependent on climatic and tectonic processes, but rarely will an environment of strong hydrographic gradients be exposed to just one of the processes. Sediment will be transported to and from a continental margin by both processes, even in

settings such as the Uruguayan Continental Margin, where both processes are low energy/low frequency compared to the more well-studied environments. However, by using foraminiferal assemblages we can still distinguish at least 6 different sedimentary environments based on disturbance frequency, bottom current strength and food supply to the benthic fauna. While much of the sediment microhabitats match interpretations of the morphosedimentary environments from (Hernández-Molina *et al.*, 2016), the microhabitats reveal more complex interactions with bottom currents, sediment supply, disturbance and organic matter flux. The environments and their associated assemblages are summarised in Figure 6.20. There are many expected outcomes of the foraminiferal assemblages, such as increased percentages of epifauna and their related indicator taxa in areas prone to increased bottom current velocities such as the contourite terrace and contourite drifts. The increased epifaunal signal is seen in both coarser and finer grained sediment, so is most likely driven by low disturbance and an increased import of food within the near bottom current. A strong bottom current will keep the sediment oxygenated, even a relatively weak current will keep the environment relatively mesotrophic. However, with increased amounts of food either through increased productivity in the water column or increase input of refractory organic matter the most abundant taxa will obscure the indicator species (De Rijk *et al.*, 2000). Seasonal species that rely on these influxes of food will be overrepresented in the fossil record, as they will bloom and die, contributing a large amount of tests to the sediment (Jorissen, 1999). Therefore, as food supply/seasonality increase, bottom current signal becomes less clear, particularly in weaker bottom currents where vertical flux



from fresh phytodetritus can be deposited on the sediment surface without being reworked by the current.

There are some morphosedimentary environments interpreted as bottom current dominated where the microhabitat would suggest otherwise. This is particularly evident on the lower slope contourite terrace (core UPC154) where infaunal taxa dominate for the entire Holocene. The assemblage is similar to those found in the more quiescent areas around submarine canyons and canyon mouths or those found around gas hydrate deposits. This setting is downslope of several submarine canyons and is located in the middle of a dense pockmark field that could be associated with gas hydrate escape from the seafloor. These processes are therefore thought to be the most recent dominant processes and the large-scale feature of the contourite terrace was formed in a period when the deep Antarctic-sourced watermasses had higher current velocities. The current needs to be capable of erosion and reworking large amounts of sediment in order to form a feature of this size and therefore the lower terrace is not thought to be presently active.

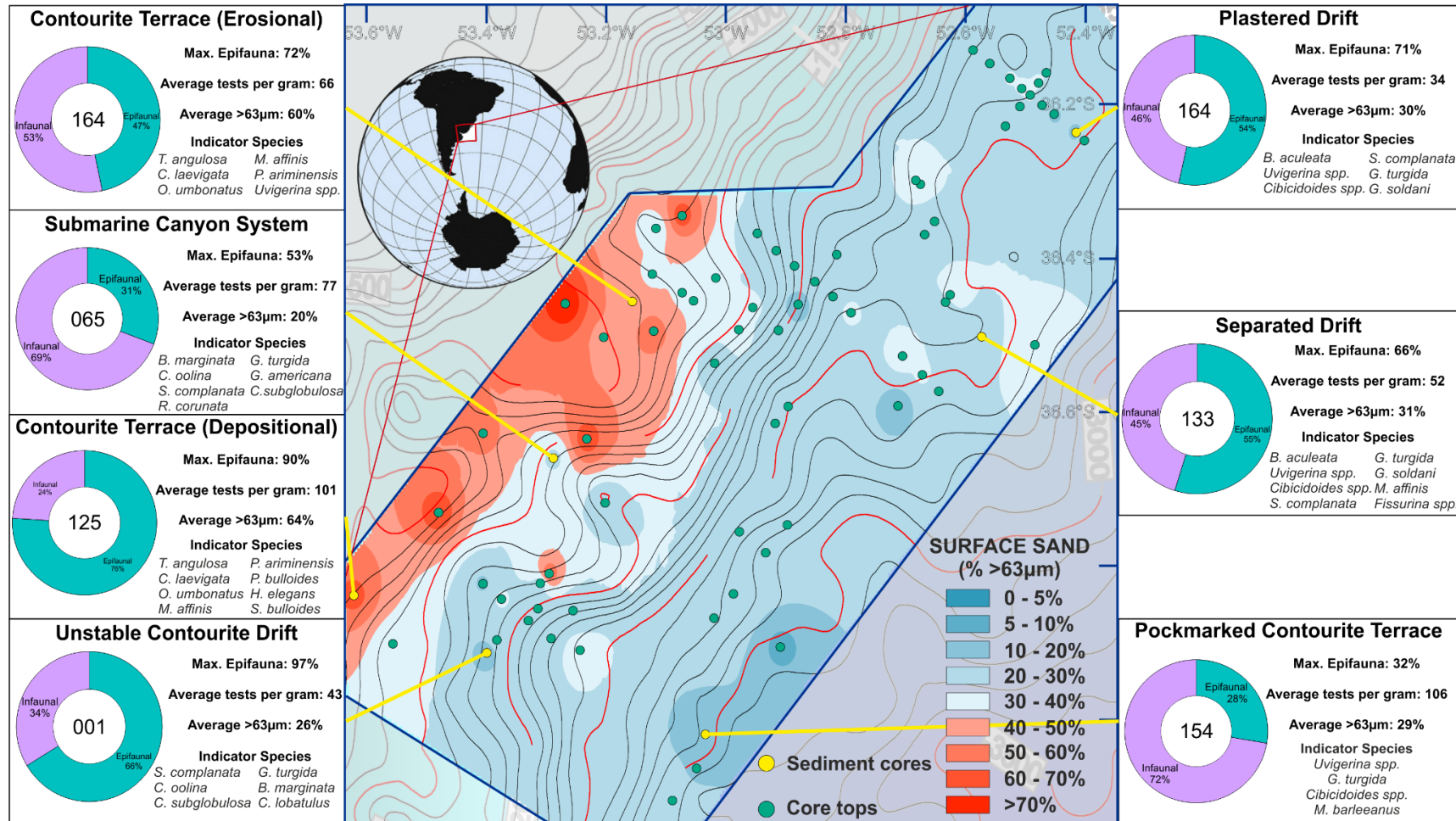


Figure 75 Summary of foraminiferal proxies in relation to sediment grain size on the slope (bottom current velocity). Major indicator species are listed for each interpreted morphosedimentary environment

Another morphosedimentary environment not showing expected assemblage compositions is within the submarine canyons (UPC065) incised into the upper slope terrace. While the sediments do show typical signs of sediments from turbidite deposition, containing a high percentage of infaunal taxa dominated by opportunists, we do not observe barren samples, any shelf transported tests or ruderal/recoloniser taxa. In many cases, the assemblages resemble more of a contourite drift assemblage than one that is dominated by large energetic downslope transport events. Therefore, the canyons offshore Uruguay do not show the typical processes or microhabitats as those found in the NE Atlantic or in the Mediterranean. Instead, our results agree with the interpretations of (Voigt *et al.*, 2013) and others that the canyons are fed by sediment sourced from the terrace and are most active during periods of drift progradation and failure into the canyon. However, there are relatively high and constant accumulation rates within the canyon due to sediment deposition directly from the nepheloid layer into the canyon due to a weakening of flow strength as the current passes over the canyon. The canyon sediment assemblages are therefore composed of reworked terrace and drift fauna within an environment prone to instability. Despite these contouritic processes feeding the canyon, a disturbance dominated fauna is still apparent being dominated by opportunist/early colonisers *Bulimina marginata* and *Stainforthia complanata*. While allochthonous taxa within the canyon give the polluting drift faunal signal such as *Trifarina angulosa* and *Pyrgo spp.* In more energetic settings from the NE Atlantic (Hess *et al.*, 2005; Duros *et al.*, 2017) observed early colonisers and ruderal taxa within the canyon assemblage along with a high percentage of allochthonous taxa from the shallow shelf. We do not observe any of these in the Uruguayan canyon assemblage.

However, Duros *et al.*, (2017) found evidence for bottom current activity having an influence on the recolonization of a barren substrate within and around the canyon environment following a turbidity current. A turbidite assemblage should therefore be defined as an assemblage showing signals of increased disturbance compared to background levels on the Uruguayan slope. Turbidite activity appears to be too infrequent to have major implications for the fauna found in morphosedimentary environments prone to turbidity currents to result microhabitats observed in other more energetic environments such as barren sediment units or assemblages dominated by ruderal/early colonisers. Other foraminiferal taxa that are useful indicators of a turbidite dominated environment such as one dominated by facultative anaerobes are useful, however offshore Uruguay they are found in both canyon and terrace settings, so should only be used as indicators in the absence of any oxygen-dependent taxa. Figure 6.21 summarises where the eleven foraminiferal assemblages fall on a disturbance/bottom current/food supply phase diagram, while Figure 6.22 show the interpreted disturbance/succession model for the foraminiferal assemblages found offshore Uruguay.

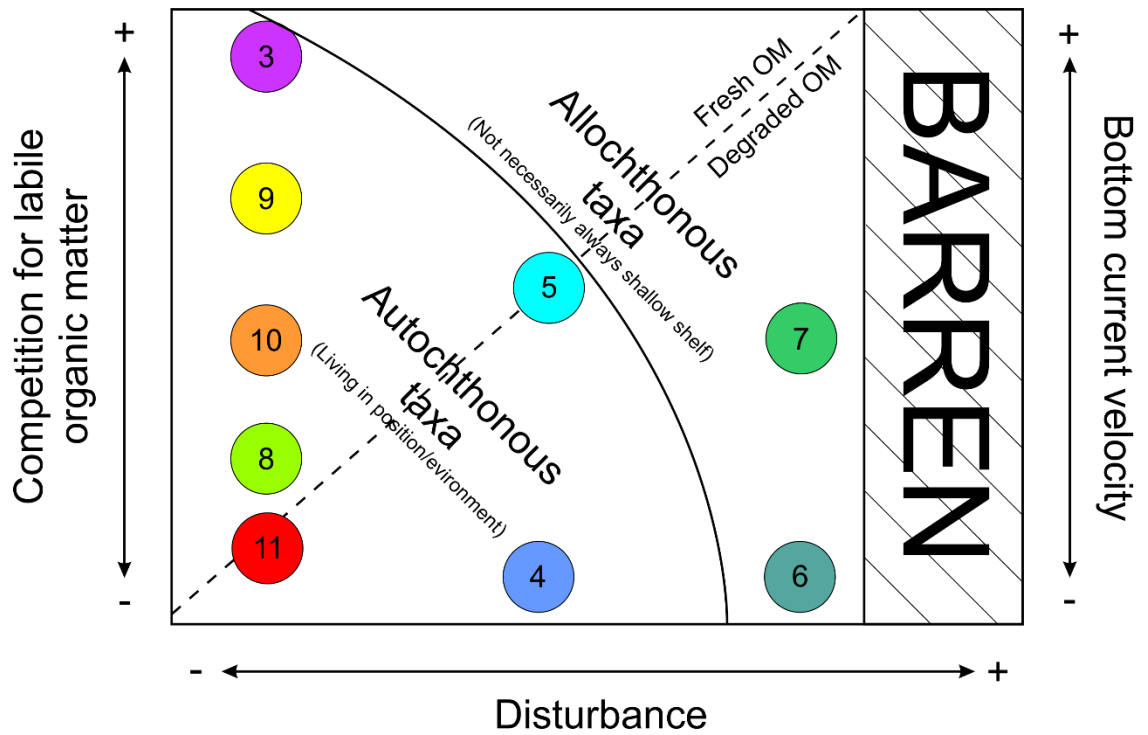


Figure 76.21 Phase diagram summarising the positions of each assemblage against levels of disturbance, competition for food and bottom current strength. Stippled line divided the fresh organic matter supplied via phytodetritus vs. degraded refractory material from turbidites. Solid black line marks the likely boundary where downslope transport can supply enough material from the shelf to be deposited or bottom currents are strong enough to prevent shelf material making it downslope.

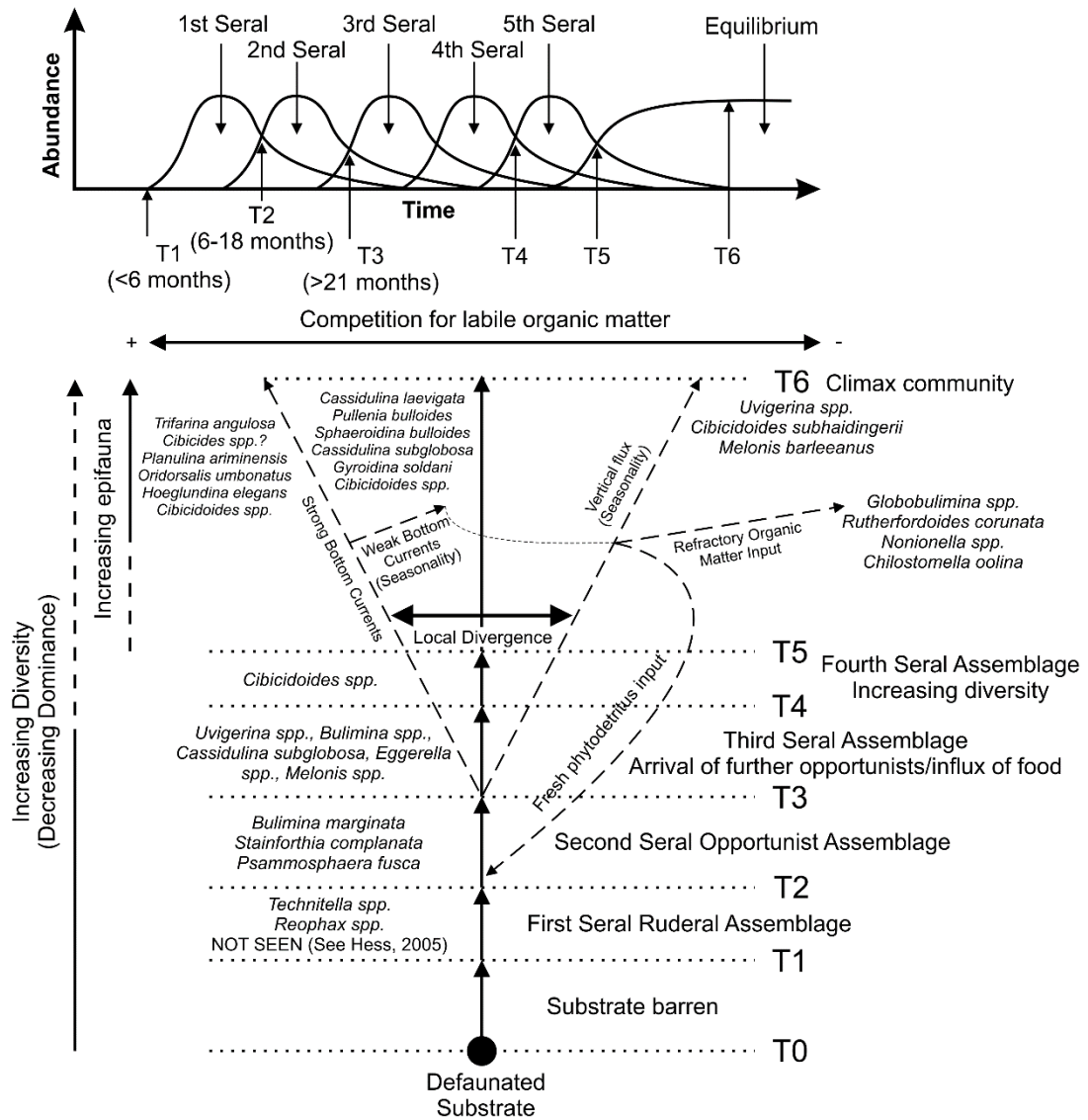


Figure 77 Conceptual model for the succession of benthic foraminifera adapted from (S. Hess et al., 2005; Rogerson, Kouwenhoven, et al., 2006). Assemblages are outlined on the righthand side of the diagram. Key indicator taxa are named within the dashed horizontal lines for T. The T values are those adapted from (Hess et al., 2005). Branching structure shows the arrival of specialist taxa into the prevailing environment. Assemblages of taxa shown here are site specific.

Previous to this study, the morphosedimentary settings interpreted as contourite in origin have been based on seismic, sedimentological and geochemical data. Of these, the seismic data has remained the only possible way to confidently determine the origin of a sedimentary body. During the course of this project identification of a contourite through sedimentology (beds, grain-size) or

geochemistry (Zr/Al,  $\delta^{18}\text{O}$ ) proved immensely difficult. While the onset of a high energy event can be identified by an increase in grain size or a change in chemical composition, these changes offshore Uruguay are often too diffuse or the core too poorly consolidated to identify the origin of the event. Therefore, the origin of sand bodies, whether sourced from along- or downslope sedimentation remains an unknown. As discussed previously, the new microfossil data provide additional means to address this issue and have proven to be very suitable water mass indicators throughout the Holocene. Table 6.6 is a summary of biological and sedimentological indicators for both along and down slope sedimentation in the mud and sand grain size fractions.

Table 6.6 A comparison of the expected patterns of bioturbation in hemipelagic, turbiditic and contouritic sedimentary environments. Adapted from (Wetzel, et al., 2008) to include foraminiferal patterns. Assemblages are grouped into there associated interpreted lithological facies.

|                              | Hemipelagic  | Turbidite   |  | Contourite  |  |
|------------------------------|--|---|--|---|--|
|                              |  | Mud   | Sand   | Mud   | Sand   |
| <b>Sediment Accumulation</b> | Continuous and slow  | Instant & rapid   | Instant & rapid  | Semi-continuous deposition with reworking   | Intermittent deposition & reworking  |
| <b>Organic Matter Influx</b> | Vertical flux  | Vertical flux & suspension transportation   | Vertical flux & suspension transportation  | Vertical flux and lateral input   | Vertical flux & lateral input  |
| <b>Fauna Stability</b>       | Continuous   | Death & decolonisation in turbidite events  | Death & decolonisation in turbidite events                                       | Continuous  | Deep infauna may survive   |
| <b>Fauna Abundance</b>       | Average/Low  | Dependent on frequency of turbidite events  | Low  | Very high   | Fine Sand = High<br>Coarse Sand = Low  |
| <b>Bioturbation Rate</b>     | Average - regulated by vertical flux   | Generally low   | Low  | Very high   | Fine Sand = High<br>Coarse Sand = Low  |
| <b>Foram indicator</b>       | Assemblage = 8, 9 & 11<br><i>Uvigerina</i> spp.<br><i>Cibicidoides</i> spp.<br><i>Melonis</i> spp.<br><i>Globobulimina</i> spp.<br>+ <i>Opportunists</i> | Assemblage = 4, 5, 6, & 7<br><i>C. oolina</i><br><i>R. coronata</i><br><i>Globobulimina</i> spp.<br><i>Nonionella</i> spp.<br><i>C. subglobosa</i><br>+ <i>Opportunists</i> | Assemblage = 7 or barren<br><i>Transported tests</i><br>+<br><i>Opportunists</i> | Assemblage = 5, 9 & 10<br><i>Uvigerina</i> spp.<br><i>Bulimina</i> spp.<br><i>Cibicidoides</i> spp.<br><i>Globobulimina</i> spp.<br>+ <i>Oligotrophic species</i> | Assemblage = 3<br><i>T. angulosa</i><br><i>C. laevigata</i><br><i>B. marginata</i><br><i>O. umbonatus</i><br><i>P. ariminensis</i><br><i>P. bulloides</i><br><i>H. elegans</i><br>+ <i>anaerobes</i> |

The term “elevated epifauna” pertains to the group of benthic foraminiferal species that inhabit elevated substrates above the sediment surface to optimise food acquisition under the influence of strong bottom currents (Schönfeld, 1997, 2002c, 2002b). The percentage abundance of these taxa within the assemblage have been directly related to the presence of increased bottom currents (Schönfeld, 2002c; Rogerson *et al.*, 2011; Singh *et al.*, 2015). However, this approach has not yet been used as evidence for strong bottom currents in more open ocean/mud dominated settings until this study. In our samples, the elevated epifauna is represented by *Planulina ariminensis*, *Cibicides lobatulus*, *Cibicides refulgens* and *Globocassidulina subglobosa*. Due to the much lower bottom



current velocities offshore Uruguay we also include other species known to prefer epifaunal/shallow infaunal oligotrophic conditions, many of which are commonly found in areas known to be exposed to increased current velocities. Species such as *Cibicidoides* spp., *C. laevigata*, *O. umbonatus*, *P. bulloides* and *H. elegans* are cosmopolitan species, however in distinguishing oxic environments swept by bottom currents they prove useful here. Mackensen *et al.*, 1995 found a faunal association dominated by *Trifarina angulosa*, correlated with very coarse-grained sediments and strong bottom current activity, we find this same correlation within assemblage 3 in cores UPC125 and UPC164. This species appears to be adapted to being reworked by bottom currents within the sediment. Since these species only become dominant in geomorphic settings interpreted as being constructed under the influence of pervasive bottom current activity and within coarser grain sizes, this assemblage is thought to represent our contourite assemblage.

However, the development of such a bottom current indicator requires more ecological studies using living and subfossil faunas, in order to better understand the influence of taphonomy on the final assemblage record of current regimes (Schönfeld, 1997, 2002b). To calibrate a bottom current velocity proxy is severely hampered by the paucity of detailed bottom current velocity measurements in regions where there is information on benthic assemblages available. For example, in the Bay of Biscay foraminiferal microhabitats have been well studied (Fontanier *et al.*, 2002, 2003, 2005, 2006; Hess *et al.*, 2005; Duros *et al.*, 2017) but there are no precise current measurements available. As we have attempted in this study, non-faunal proxies for bottom current activity can be used with some success, such as grain size analysis, X-ray photographs, elemental ratios,

sedimentary structures in the core and other methods not used here such as  $^{210}\text{Pb}$  and/or  $^{234}\text{Th}$  profiles of the upper sediment layers can also be used (Fontanier *et al.*, 2005). One of the main potential flaws of using elevated taxa as indicators of stronger bottom currents is the fact that there are no observations of benthic foraminifera living on elevated substrates being suspension feeders. Some of the species used in this study as indicators of higher current velocities, have also been found in shallow infaunal microhabitats e.g. *Cibicidoides spp.* in (Corliss, 1985; Rathburn & Corliss, 1994; Fontanier *et al.*, 2002; *Planulina ariminensis* in De Stigter *et al.*, 1999). Species such as *Cibicides lobatulus*, *Planulina ariminensis*, *Oridorsalis umbonatus*, *Trifarina angulosa* and *Hoeglundina elegans* are common in areas where there are no indications of bottom current activity. Most of these species appear to occupy oligotrophic environments, where a position close to the sediment-water interface may be advantageous for suspension feeding.

What is clear, is that within environments interpreted here to be more unstable and prone to frequent disturbance and defaunation, there is a significantly different, more infaunal life-strategy adopted. Despite the assemblages not representing a classic turbidite benthic foraminiferal assemblage, with early colonisers and abundant transported tests from the shelf, there is a distinct reduction in epibenthic taxa. We link the absence of shelf taxa in the turbidite assemblage to the difference of canyon sediment source (from the Ewing terrace), when compared to more well-studied classic canyon systems (Bay of Biscay). The shallower terrace sediment has a distinct assemblage and elements of it can be seen to have been potentially reworked into the canyon e.g. *Trifarina angulosa*, *Cibicidoides spp.* and *Gyroidina soldanii* peaks coincide with periods

of interpreted Zr/Al maxima in UPC065. Therefore, the turbidite signal is likely being polluted to some degree by the reworked of epibenthic taxa from the contourite terrace. Early colonising species are likely to be found within these samples, either in the finer fractions or have been destroyed during processing. These species are usually small and have agglutinated tests, making them more fragile than their calcareous counterparts. However, they have been found from turbidite deposits in other systems e.g. Hess *et al.*, (2005). The reduction in epifaunal taxa must be linked to reduced bottom current activity and higher disturbance in turbidite settings. These different processes will fundamentally change the the preferred life-strategy in order to compete for a food source. The available food within the canyon is likely degraded refractory organic matter, resulting in an infaunal deposit feeding strategy, while the frequent disturbance leads to a dominance of early coloniser and opportunist specialist taxa. This difference in feeding strategy can easily be seen between the contourite (assemblage 3) and the turbidite (assemblage 6) deposits.

## 6.4 Conclusions

Sedimentary features indicate that disturbance and bottom current velocity (i.e. turbidite deposits, contourite deposits, hemipelagites) vary across each of the morphosedimentary environments. In the 7 studied sites, different foraminiferal responses to various sedimentary processes are observed revealing the complexity of a mixed sedimentary system (Fig. 6.20, 6.21 and 6.22).

1. Foraminiferal assemblages with low diversity and high dominance, which are dominated by pioneer species and opportunists such as *Stainforthia complanata* and ruderal (simple) taxa (not seen here) are typical of frequently disturbed canyon environments that sustain fauna in the early stage of recolonization. No barren assemblages were observed within the canyon which contradicts previous studies that suggest a canyon (highly disturbed environment should be kept barren of a benthic foraminifera microhabitat (Rogerson, *et al.*, 2006).
2. A low diversity assemblage with a high dominance of *Bulimina marginata* and *Stainforthia complanata*. These opportunistic taxa occupy a superficial microhabitat. Such specialist fauna indicate strongly food-enriched sediment, but unstable conditions. These taxa are found in every sedimentary environment on the slope and is consistent with a high amount of fine-grained sediment accumulating. However, peaks occur within areas prone to turbidites and in other areas where peaks are likely due to deposition of seasonal fresh phytodetritus.
3. A more diverse assemblage composed of *Uvigerina spp.*, *Bulimina spp.*, *Cassidulina subglobosa*, *Eggerella spp.* and *Melonis spp.* is believed to belong to a second generation of colonisers and represents an advanced stage of recolonization after disturbance. This is interpreted as relatively

mesotrophic conditions found in most environments at least some stage during the Holocene. With increasing bottom current energy/increased oxygenation of the seafloor *Cibicidoides spp.* is found within this late stage assemblage too.

4. A climax community without external influence other than seasonal vertical flux of food is observed as a diverse, low dominance and deep microhabitat assemblage composed of *Uvigerina spp.*, *Cibicidoides subhaidingerii* and *Melonis barleeanus*. These species are K strategists, highly specialised, large in size and not capable of withstanding a catastrophic change in conditions such as the deposition of a turbidite. These quiescent conditions allow a diverse foraminiferal community to develop.
5. The climax community has a continuous gradient into three relatively diverse assemblages dependent on food supply and bottom current velocity over the site. In sites on the edge of nepheloid layer and within canyon environments there is an increased supply of refracted organic matter. This leads to an assemblage of deep infaunal/facultative anaerobes *Rutherfordoides coronata*, *Globobulimina spp.*, *Nonionella spp.* and *Chilostomella oolina* that have adapted to cope with an anaerobic/nitrogen fixing feeding strategy. Under weak bottom currents, an oligotrophic assemblage with a seasonal input of fresh food to the seafloor is observed. Under very strong oligotrophic bottom currents, occupying an elevated position above the sediment becomes advantageous to the suspension filtering feeding strategy of epifaunal species. An ability to survive reworking and a poor-quality food supply may also prove advantageous.

The absence of numerous neritic allochthonous species in all studied sites points towards the unique sedimentary set up dominated by strong intermediate watermass bottom currents that prevent a supply of sediment from the adjacent shelf.

The identification of more detailed periods of change in the sedimentary environment not revealed by the geochemical or grain size proxies shows that benthic foraminifera are incredibly useful in the reconstruction of palaeoceanographic regimes. They should therefore be used in any study where other sedimentological approaches have proven inconclusive.

In the following chapter (Chapter 7), the results of this entire study are synthesised in terms of key findings, wider implications, limitations of this research and any future work that may possibly address these limitations.

# CHAPTER 7

---

## SYNTHESIS AND CONCLUSION

### *Key Findings, Limitations and Future Work*

#### 7.1 Introduction

The research presented in this thesis sought to further our knowledge of deep marine sedimentary systems past and present, their mechanisms of particulate transport, identification of the characteristics of their deposits, the ability of these deposits to record palaeoceanographic change, and what the microfossils contained within the deposits can tell us about all of the above. This study has gathered, analysed and interpreted a brand new sediment core data-set from the Uruguay continental margin. This core data-set is the first and only high resolution coring campaign conducted on the Uruguay continental margin. The cores have been integrated with previously collected bathymetric and 3D seismic data collected in the same area to ground-truth and give new understanding of mixed/hybrid contourite depositional systems. A range of representative core tops were sampled from across the study area to understand current surface sediment conditions on the slope. From these core tops, a subset of full sediment cores were selected, split, logged and sampled from each interpreted sedimentary environment. From this, the sediments were characterised in terms of facies and grain parameters in **Chapter 4**, with the aim of aiding the identification of contourite and turbidite facies from similar mixed/hybrid contourite systems in the future. The controls of contourite and turbidite

sedimentation were assessed using the data from this study and found to have unappreciated complexity when compared to existing studies from the Gulf of Cadiz and Argentine continental slope. Sedimentation on the slope was seen to have some influence from bottom current activity and their associated watermasses in every setting sampled which adds to the complexity when interpreting a deposit as mostly turbidite or mostly contourite. In combination with geochemical and foraminiferal proxies in **Chapter 5**, intermediate to deep watermasses in the South Atlantic Ocean are found to be much more mobile and variable than previously thought (Preu *et al.*, 2013). Despite this complexity, in **Chapter 6** a combination of previous morphosedimentary interpretation from seismic and bathymetry (Hernández-Molina *et al.*, 2016), benthic foraminiferal assemblages have been used to accurately identify contourite facies, and their distinction from other deep-water sediments, in particular those sourced from disturbance-related events such as turbidity currents.

In this chapter, the key research outputs from this study are synthesised, and reference is given to the wider implications of this work and the contribution it will make to the advancement of marine geology. A summary of the limitations is also given, of which are addressed in the proposal for future work. This chapter will conclude with a brief summary of how the overarching aim of this research and the seven research objectives of this thesis (outlined in **Chapter 1**) have been met.



## 7.2 Key Research Outputs

This research has spanned three key research themes, which include 1) determining whether sediments collected from different geomorphic settings that originate from along-slope (contourite) or gravitational (turbidite) processes. 2) Whether micropalaeontological analysis can resolve long-standing problems with differentiating along- and down-slope processes in the geological record and 3) do the drift sediments contain a record of palaeoceanographic change? Key research outputs under each of these themes are given in this section. This is followed by a more holistic synthesis of the wider implications of this research in terms of its scientific importance.

### 7.2.1 Verification of Morphosedimentary Environments

**Chapter 4** outlined the sediment distribution on the Uruguay continental slope. Even by using a mixture of bathymetric, facies and sedimentary data it is clear that contouritic features are difficult to identify within a mixed system. Many of the features identified e.g. channels, mounds etc. can also be attributed to those seen in other deposits such as turbidites. Despite these complications, the core data validate the interpretations and morphosedimentary map produced by Hernández-Molina *et al.*, (2016) that divided the Uruguay slope into distinct areas of contouritic and turbiditic/mass wasting influence. Each sedimentary environment has a higher level of complexity on glacial-interglacial timescales (as seen in the ITRAX and grain size records), but the broad geological interpretations of each environment as under the dominant influence of turbidites or contourites over glacial-interglacial timescales are correct from the sedimentary ground-truthing presented. Positive identification of a particular sedimentary facies as contourite is extremely challenging. Mud-rich contourites

are easily misidentified as pelagic and hemipelagic sediments, whereas silty to sandy contourites can be confused with turbidites and vice-versa. However, we can identify particular sedimentary facies within our cores using a set of physical, chemical and biological criteria.

### 7.2.2 A Palaeoceanographic Record

In **Chapter 5** we presented the first Accelerated Mass Spectrometer (AMS) radiocarbon-based age model extending back to the Last Glacial Maximum for a sediment core in the spatial influence of the intermediate Southern Component Water (Antarctic Intermediate Water/Upper Circumpolar Deepwater) on the Uruguayan continental margin. We used the assemblages and fragmentation index of planktonic foraminifera to determine changes in water column ventilation. Poorly ventilated/weak Atlantic Meridional Overturning/strong southern-sourced waters dominated during the AIM-1, the Younger Dryas, and the Holocene Thermal Maximum. In these periods we see an associated warming of surface waters as poorly ventilated Southern Component Water dominates. In the ventilated/strong Atlantic Meridional Overturning Circulation/Northern Component Water and Antarctic Intermediate Water-influenced Antarctic Cold Reversal, late deglacial and late Holocene ventilation increases. Surface waters cool in periods of ventilation, as there is more siphoning of heat to the Northern Hemisphere. This interpreted sequence of climatic events supports observations made from studies from the Drake Passage, Argentine and Brazil Margin (Elmore *et al.*, 2015; Voigt *et al.*, 2016; Warratz *et al.*, 2017)

Based on the corrosivity of Southern Component Water (e.g.  $[\text{CO}_3^{2-}]/I < 100 \mu\text{mol}$  (Henrich *et al.*, 2003)) , we proposed that the absence of carbonate during the glacial to early deglacial interval, and in the period 11.5–10 ka BP, coupled with

the increase in carbonate during the late deglacial and early to mid-Holocene, reflect a shift of the Circumpolar Deepwater downslope. Between 20 and 15 ka BP, we suggest that an intermediate Northern Component Water interacted with a glacial Southern Component Water in the Southwestern Atlantic, reducing carbonate preservation. An increase in Antarctic Intermediate Water at 15 ka BP led to an upper Southern Component Water intermediate water expansion. This intermediate Southern Component Water was composed of a lower corrosive water mass (Upper Circumpolar Deepwater) and an upper non-corrosive watermass (Antarctic Intermediate Water). The interface of these watermasses lay at the depth of the terrace (~1000m depth in the Atlantic) until the mid-Holocene where it began to migrate downwards in the water column enhancing carbonate preservation. In the late Holocene, we observe an increase in corrosivity which may relate to the upper non-corrosive Southern Component Water taking on the characteristics of its deeper corrosive Southern Component Water counterparts.

### 7.2.3 A Micropalaeontological Tool to Differentiate Along- & Down-Slope Transport Processes in the Geological Record

In **Chapter 6** we developed a micropalaeontological tool to distinguish along- and down-slope sedimentation using benthic foraminiferal assemblages that can be applied to the Geological Record where we cannot observe these processes in situ. To demonstrate this tool, we gathered a set of representative sediment core samples from each interpreted morphosedimentary environment on the Uruguay continental slope, incorporating the greatest range of sediment grain sizes as possible from the sedimentary analysis in **Chapter 4**. We identified the foraminifera species present in each of the 8 sedimentary facies. The facies were

grouped into 2 to 6 units per sediment core, with each unit being a set of common facies that were interpreted as representing a particular environmental condition. Using a combination of traditional benthic assemblage counts (Murray, 2006), foraminiferal indices (such as fragmentation), benthic microhabitat preferences (from morphological and microcosim experiments) and statistics (Pair-wise Anosim and SIMPER analyses), we identified eleven foraminiferal facies that define six environmental settings on the continental margin. The six environmental settings ranged from hemipelagic (no disturbance and/or no bottom current activity) to sandy (disturbed and/or high velocity bottom current activity). Each of these assemblages can be interpreted as representing a transition between end members high-low food supply, high-low bottom current velocity and high-low disturbance frequency that are all observed to have an effect on benthic communities elsewhere (Alve, 1999; Schönfeld, 2002b; Duros *et al.*, 2017).

The foraminiferal facies found within the sedimentary environment most likely to be sand dominated and deposited from vigorous along-slope processes contained the highest percentages of taxa that feed from the water column by attaching themselves to elevated substrates or “elevated-epifauna”. Under strong bottom currents occupying an elevated position above the sediment becomes advantageous to epifauna with a suspension/filter feeding strategy. An ability to survive reworking and a poor-quality food supply may also prove advantageous as we also observe high percentages of species known to withstand transport within coarse grained sediment (Schönfeld, 1997, 2002b; Chapter 6, Fig. 6.20).

Whereas, the foraminiferal facies found within the sedimentary environment most likely to contain sand deposited from catastrophic down-slope processes contain

higher percentages of infaunal opportunistic species and taxa that can be defined by “flysch fauna”. Therefore, a deposit can be interpreted as contourite or turbidite from foraminiferal assemblages alone. Assemblage counting can quickly be done alongside the initial sediment sieving for grain size without the need for complex sedimentary analyses such as sortable silt (SS) (McCave, 2008).

### 7.3 Key Findings & Wider Implications of this Research

From the key outputs given in Section 7.2, three primary implications of this research can be depicted. These relate to 1) the contribution to verifying the processes recorded by sedimentary facies to seismic scale morphosedimentary environments, 2) the application of these tools to increase our understanding of contourites as records of palaeoclimate and 3) our simple micropalaeontological tool can be used to reduce the risk of exploration targets where depositional geometry is unknown, as well as aiding well planning, basin modelling, production strategy and improving our understanding of the geological record of these geometrically complex depositional systems. Each of these themes are discussed further in this section.

#### 7.3.1 The Requirement for Multiscale Contourite Identification Criteria

Hydrocarbon exploration begins at the basin scale, beginning with seismic surveys and interpreting the seismic data to find potential reservoirs. Therefore identifying potential contourite sand reservoirs from seismic data is of great interest in the hydrocarbon industry, as well as for the understanding of continental slope stability and past and present continental margin current movements. Identifying contourite reservoirs in seismic data has previously been incredibly challenging for sands as contourite drifts are easy to identify from muds because they show significant external morphology and internal architecture, however coarser sediment bodies are often difficult to identify as their features are so similar to those seen in turbidite depositional systems.

Therefore, it is important once these deposits are drilled and cored that a set of diagnostic criteria can be used to positively identify deposits as contourite in origin. Until now a clear set of diagnostic and unambiguous criteria for the

identification of contourite deposits has proven to be an impossible task (Stow et al., 2020). Instead a number of separate observations must be made to derive the environmental context so that the likely regions of contourite sedimentation can be identified. This sediment and core data should always be used together with seismic data in order to build the case for the depositional process. We demonstrated in **Chapter 4** that by using a set of key features such as reverse and normal grading, erosional surfaces with slight grading above and below, high bioturbation rates in fine sediments and intervals with laminations and/or cross lamination identified through classical core logging, gravimetric grain size, advanced core scanning and x-radiographs, allowed the identification of potential contourite facies. However, as we also had a full set of seismic data to provide us with context, contourite characterisation still requires the integration of acoustic, core and sediment data without a new tool for contourite identification. Palaeoceanographic and margin reconstruction remains essential for building the case for contourite deposition in all settings even with a simple tool for identification, such as the foram method developed here.

### 7.3.2 Contourite Depositional Systems & the Currents that Create Them

In **Chapter 5** we demonstrated that Antarctic-sourced watermasses flowing into the Atlantic basin are much more mobile and variable than previously thought (Preu *et al.*, 2013). There is evidence that the migration of these watermasses and their associated bottom currents have influenced different sectors of the slope on glacial-interglacial cycles by controlling sedimentary and biological processes.

As the Antarctic ice shelf continues to retreat with global warming, the production of Antarctic-sourced water increases its contribution into the watermasses of the

Atlantic basin (Roberts, 2017). An associated effect of this is that the intermediate watermasses can take up more carbon from the atmosphere and store it at intermediate depths. This will have the effect of increasing the corrosivity of the Antarctic water. Homogenising Antarctic Waters such as this may act to further weaken Atlantic Meridional Overturning Circulation in the future which would have potentially catastrophic implications for Northern Hemisphere climates (Caesar *et al.*, 2018).

### 7.3.3 A Simple Unambiguous Method to Identify a Contourite Sand

New criteria for distinguishing contourite (along-slope) and turbidite (down-slope) sediments remain key to unlocking the unique potential of contourite depositional systems as high-resolution archives of palaeoceanography and palaeoclimate. In **Chapter 6** we demonstrated the ability of traditional micropalaeontological techniques to differentiate contourite from turbidite deposits. In principal this means that contourite and turbidite materials should be distinguishable, even at hand-specimen scale in a relatively fast and cost-effective method.



## 7.4 Limitations

### 7.4.1 Facies Identification

Identifying contourite facies from hand sample to core scale (even in outcrop) is extremely challenging. With our present understanding and identifying criteria (listed in section 7.3.1), a sedimentologist without specialist knowledge of deep marine sedimentology would struggle without some level of context to the sedimentary record they are attempting to interpret. In **Chapter 4** we overcame this challenge preconditioned with interpretations from seismic data and advanced core scanning techniques that allowed identification of sedimentary characteristics that are impossible to see with the naked eye. Even when presenting type localities of contourite deposits on field trips, where there is ample evidence for bottom current activity in a deep-marine setting, people remain unconvinced that such a process is possible. Therefore, a simple set of identifying criteria are needed at a hand sample to outcrop scale. This thesis goes some ways to address this problem but would argue for an even simpler visual method for contourite identification in the field or in the sediment core lab that unequivocally identifies a deposit as contourite in origin.

### 7.4.2 Carbonate Preservation – Modern versus Palaeo-Hydrography

One of the major problems with the sediments collected in this study is their exposure to typical deep sea processes such as dissolution, bioturbation, reworking and winnowing (Archer, 1996; Wetzel *et al.*, 2008). These factors cause potential bias within our foraminiferal  $^{14}\text{C}$  ages and would influence the reliability and accuracy of ages and paleoecological data reported (Barker *et al.*, 2007; Mekik, 2014). Dissolution could play a major part in causing foraminiferal  $^{14}\text{C}$  estimate bias (Broecker *et al.*, 1991; Keir & Michel, 1993; Barker *et al.*, 2007).

Our record shows that the Uruguay cores have been exposed to dissolution in the past, with poor carbonate preservation in several core intervals, with complete dissolution in the lowermost intervals of some cores. This shows that despite the modern calcite lysocline and compensation depths in the South Atlantic being located at ~4000 m and 5300m respectively (Bramlette, 1961; Archer, 1996; Dittert & Henrich, 1999), the intermediate depths experienced variations in carbonate ion concentrations ( $[\text{CO}_3^{2-}]$ ) since the last glacial period. We attribute this to the influence of southern sourced waters from Antarctica, which are known to have low  $\text{CO}_3^{2-}$  (Henrich *et al.* 2003). This limited our ability to track palaeoecological downcore trends in many of the sections with larger grain sizes or within glacial intervals. The sandier sections where of greatest interest to us and unfortunately (or fortunately) the strongest currents were linked to the most corrosive watermasses (**Chapter 5**). This also limits our ability to track subsurface palaeohydrographical/palaeoecological conditions and related them to present hydrography/ecological conditions. This is even more of a problem when considering ancient examples of contourites e.g. Petra Tou Romiou, Cyprus or the Rifian Corridor in Morocco (Capella *et al.*, 2018b; Miguez-Salas *et al.*, 2019).

#### 7.4.3 Benthic Foraminifera as Indicators of Current Velocity

The use of the benthic foraminiferal assemblages themselves as a proxy for past bottom current conditions is complicated by the fact that the active currents forming these deposits may form one of the major taphonomical factors that lead to the winnowing of or addition of taxa to the assemblage. Schönfeld (1997) suggested the use of the >250  $\mu\text{m}$  size fraction benthic foraminifera as a proxy for bottom current regimes as tests in this large size fraction are least affected by transport as discussed in **Chapter 2**. The proxy that distinguishes the contourite

deposits from turbidite deposits in this thesis relies on this assumption. The calibration of such a proxy is hampered by the lack of precise measurements of bottom current conditions in regions where benthic foraminiferal assemblages are available. Another challenge is the fact there are no direct observations that the taxa interpreted in this thesis as living on elevated substrates are suspension feeders at all. This feeding strategy is entirely inferred from living position of taxa on the seafloor and their test morphologies. Species listed in Appendix 3.2 as “elevated” epifauna also occur in shallow infaunal microhabitats (e.g. *Cibicidoides* spp. and *Planulina ariminensis*). Species such as *Cibicides lobatulus* and *Planulina ariminensis* are common in areas where there are no indications of any bottom current activity. It appears that these species are common in oligotrophic conditions (Schönfeld, 2002b), where the shallow infaunal microhabitat already makes the suspension feeding life strategy advantageous.

## 7.5 Future Work & Addressing Limitations

Insights from this research and limitations encountered has given insight into deep marine sedimentary, oceanographic and benthic biological systems. This section briefly describes some key areas of future work and applications of the new micropalaeontological tool.

### 7.5.1 Grain Size Characteristics & Foraminifera from Core Tops

This study used an extensive data-set collected from the Uruguay Continental Margin by ANCAP and provides the largest sedimentological analyses of the margin sediments to date (See Figure 4.2). This increases the geographical range of contourite depositional examples and will allow comparisons to other, classical examples e.g. the Gulf of Cadiz. Analysis of the sediment core tops from the study area appear to represent current seafloor conditions accurately (See **Chapters 4 and 5**). The core tops may present a wider opportunity to use more advanced grain size parameters (e.g. sortable silt) than used here to distinguish between different depositional processes and then compare these results to the benthic foraminiferal assemblages within the core tops. Sedimentary analysis that quantifies parameters such as sorting and skewness can show grouping of properties relating to depositional process e.g. turbidite vs. contourite. This has the added advantage of removing problems of uncertainty reconstructing palaeohydrographic and palaeoecological conditions as measurements from the seafloor can be made in real time and compared to the results of the more detailed core top analysis.

### 7.5.2 Precise Current Measurements from the Seafloor

There is a lack of precise and highly detailed measurements of bottom current velocities in regions where there are vigorous bottom currents and where

information on benthic foraminiferal assemblages are available. If measurement of bottom current velocities proves an impossible task in some settings, there are other proxies for current velocity that could be used, some of which have been used in this study with some success e.g. Zr/Al, Zr/Rb, bioturbation, x-radiographs and others such as  $^{210}\text{Pb}$  and/or  $^{234}\text{Th}$  profiles of the upper sediment layers. The development of a benthic foraminiferal proxy for bottom currents will require more ecological studies on living and sub fossil assemblages that are not covered here and would require the collection of cores that preserve the sediment surface (e.g. Mebo coring techniques). This type of ecological study of fauna associated with recently deposited contouritic sediments is required to understand the taphonomical modifications and the record of faunal response to current regimes and how they are recorded in the sediment characteristics.

### 7.5.3 Linking to Ancient Outcrop Examples

One of the original objectives of this project was to ascertain whether micropalaeotological tool used in this study could also be applied to an ancient example from a similar sedimentary system i.e. mixed hybrid contourite depositional system. The intended examples were the Lefkara and Pakhna formations in the Eocene-Miocene of Cyprus. This palaeoenvironment is more carbonate-rich than our Uruguay setting as the succession is dominated by calcilutite and calcarenite beds that were deposited under vertical flux from pelagic and hemipelagic sedimentation. These conditions are punctuated by increased bottom current activity and distal turbidity current events (Kahler, 1994; Kähler & Stow, 1998; Miguez-Salas & Rodríguez-Tovar, 2019). The 100% exposure and ease of access to sections at Petra Tou Romiou and Agios Konstantinos have resulted in these sections being recommended as type

examples of ancient contourite sections (Stow et al., 2002). Recent studies of these sections have focused on differentiating between bottom-current and gravity-flow induced deposits through the use of facies, microfacies and trace fossil analyses (Miguez-Salas & Rodríguez-Tovar, 2019). A small pilot study found the both the calcilutite and calcarenite beds of the Petra Tou Romiou section contained an abundance of larger ( $> 250 \mu\text{m}$ ) benthic foraminifera *Nummulites*. There is an abundance of *A-type* tests (tests of a specific size, shape, density and volume) only observed within the '*Nummulites Banks*' of the Middle Eocene Pederiva Bank, Northern Italy (Jorry et al., 2006; Yordanova & Hohenegger, 2007; Hohenegger & Briguglio, 2012), based on our new model (Section 6.4.2) this would suggest that the Pakhna sections of the succession are downslope of such a bank and tests are being reworked downslope and winnowed by the action of bottom currents. Therefore, there is obvious potential for foraminiferal methods developed in this study to be incorporated into future studies on the contourite depositional models from Cyprus and other ancient examples.

## 7.6 Conclusion

The main purpose of the research was to test if a simple micropalaeontological tool can help with the problem of distinguishing contourites from turbidites and gain insights into how the influence of bottom currents and their associated watermasses can be applied to understanding the dynamics of novel contourite sedimentary systems in the deep sea.

Through the work completed in this thesis, insight into deep sea contourite sedimentary systems and their mechanisms of particulate transport has been gained by developing and applying the simple micropalaeontological tool described in **Chapter 6**. The work has also contributed to the understanding of complex contourite sedimentary systems through the use of simple sedimentological tools and advanced palaeoceanographic techniques employed in **Chapters 4** and **5**.

This was achieved through the use of data collected from gravimetric grain size, visual sediment core logging, foraminiferal indices, stable and radiometric isotopes of foraminiferal tests, physical and ITRAX core logging techniques. The data were from 86 sampled core tops and 8 piston cores sampled at at least 10 cm depth intervals, totalling 25 metres of sediment representing 20,000 years of never-before studied palaeoclimatic records from the South Atlantic. This record was explored for changes in sediment properties and foraminifera under different sedimentary environments determined to be influenced by both contourite and turbidite depositional processes from previous seismic and bathymetric studies of the seafloor offshore of Uruguay. From this data a simple micropalaeontological model and index was developed and tested to distinguish the two sedimentary processes that influence the slope.

The exploration of the sediment record from the Last Glacial Maximum and transition to the current interglacial suggests an unprecedented amount of cold, fast-flowing and corrosive water entering the South Atlantic and travelling at intermediate depths to reach the Uruguayan shelf at the end of the LGM. This injection would have had profound effects on AMOC and could have contributed to the disruption and reinvigorating of ocean circulation across the Younger Dryas. The exploration of the micropalaeontological record and the development of a foraminiferal model to distinguish contourites from turbidites can be used by industry and scientific expeditions to cut time and make targeting deep sea contourite and/or turbidite deposits easier and safer in the future as they will immediately (from core cap sampling) be able to recognise and predict the drilled deposit's geometry, internal properties and potential as a prospect for hydrocarbon exploration, carbon capture and/or palaeoclimatic records. A quick method of identifying geometric sediment bodies and the sediment processes that influence them on the Uruguayan slope may also assist in mitigating risk to communities and vital deep seafloor infrastructure such as pipelines and cables from slope stability geohazards.

The aim of the study has been achieved by meeting the seven principal research objectives, which were given in **Chapter 1**. Each of the Research Objectives (1-7) are addressed in Table 7.1-7.7.



Table 7.1 Research Objective 1 and how it has been addressed in this thesis

|  |  |
|--|--|
| <p><b>Research Objective</b></p>                       | <p><b>Objective 1:</b> Collect, curate and select core sample set, by first selecting, splitting, scanning logging and then sampling cores from a range of morphosedimentary environments from both along- and down-slope deposits</p>   |
| <p><b>Chapter Reference</b></p>                        | <p>Chapter 3 and Chapter 4</p>   |
| <p><b>How has the Research Objective been met?</b></p> | <p>Over 200 piston cores were curated in the British Ocean Sediment Core Facility (BOSCORF), so that they are now stored and secured in numerical order. This process required consultation of previously collected bathymetric/seismic data and core location maps. This allowed for the selection of the 86 core tops and 8 complete cores that were most likely to contain a range of grain sizes from both along- and down-slope deposits.</p> |

Table 67.2 Research Objective 2 and how it has been addressed in this thesis

|   |  |
|---|--|
| <b>Research Objective</b>                       | <b>Objective 2:</b> Use a combination of multi-sensor core logging, radiocarbon and oxygen isotopes to identify where changes in the subsurface sediment properties were through time.   |
| <b>Chapter Reference</b>                        | Chapter 4 and Chapter 5  |
| <b>How has the Research Objective been met?</b> | Using a combination of multisensor coreloggers (MSCL), ITRAX and mass spectrometers we obtained a high resolution record of changes in subsurface sediments properties and their associated changes during glacial and interglacials from the late Pleistocene through the Holocene. |

Table 7.3 Research Objective 3 and how it has been addressed in this thesis

|   |  |
|---|--|
| <b>Research Objective</b>                       | <b>Objective 3:</b> Collect samples from key sections of core from the Uruguay shelf to conduct sediment gravimetric grain size analysis and benthic foraminifera censuses. Develop use core scanning techniques to determine sedimentological and palaeoceanographic controls influenced the core material with the aid of gravimetric grain size and traditional core logging techniques.  |
| <b>Chapter Reference</b>                        | Chapters 4, 5 and 6  |
| <b>How has the Research Objective been met?</b> | 77 core tops that were considered most representative of those available were selected for grain size analysis. Subsequently 8 complete cores were selected for description of the subsurface characteristics, gravimetric grain size and facies analysis of the 8 cores selected to be representative of the depositional types found in the core tops. These data were then compared and contrasted to the data collected from core scanning techniques. The results demonstrated that core scanning techniques are a fast and effective way of gathering information on the sedimentological and palaeoceanographical controls in core material by proxy. |

Table 7.4 Research Objective 4 and how it has been addressed in this thesis

|   |   |
|---|---|
| <b>Research Objective</b>                       | <b>Objective 4:</b> Reconstruct the depositional history of the chosen sites by using a combination of multi-sensor core logging, radiocarbon and oxygen isotopes.  |
| <b>Chapter Reference</b>                        | Chapter 4 and Chapter 5   |
| <b>How has the Research Objective been met?</b> | The development of an Accelerator Mass Spectrometer (AMS) radiocarbon-based age model extending back to the Last Glacial Maximum for a sediment core in the depth coverage of intermediate Southern Component Water (Antarctic Intermediate Water/Upper Circumpolar Deepwater) on the Uruguayan continental margin. We used the surface assemblages and fragmentation index of planktonic foraminifera to determine changes in water column ventilation. These indices were used in conjunction with the stable oxygen isotope record from benthic foraminifera to reconstruct ice sheet extent and watermass density since the LGM. It is suggested that watermasses in the South Atlantic have changed their characteristics and depth ranges on several occasions over the last deglaciation, having a knock on effect on the Atlantic Meridional Overturning Circulation and thus Global Climate. |

Table 7.5 Research Objective 5 and how it has been addressed in this thesis

|   |  |
|---|--|
| <b>Research Objective</b>                       | <b>Objective 5:</b> Develop and test the ability of foraminiferal assemblages to discriminate between contouritic and turbiditic depositional systems in order to constrain reservoir geometry.  |
| <b>Chapter Reference</b>                        | Chapter 6  |
| <b>How has the Research Objective been met?</b> | Using standard micropalaeotological approaches (by counting assemblages and calculating indices of foraminifera in the sand-sized fraction) we were able to clearly discriminate between sediment samples from interpreted turbidite and contourite prone environments. This was confirmed by standard palaeontological statistical analyses from foraminiferal census data and interpreted groupings of sedimentary units based on intervals sharing similar sedimentary facies. Under very strong oligotrophic bottom currents, occupying an elevated position above the sediment becomes advantageous to the suspension filtering feeding strategy of epifaunal species. An ability to survive reworking and a poor-quality food supply may also prove advantageous. Meanwhile, in an environment prone to a high frequency of disturbance events (such as turbidites), foraminiferal assemblages with low diversity and high dominance, which are dominated by pioneer species and opportunists and ruderal taxa are observed. This environment sustains fauna in the early stage of recolonization. |

Table 7.6 Research Objective 6 and how it has been addressed in this thesis

|   |   |
|---|---|
| <b>Research Objective</b>                       | <b>Objective 6:</b> Infer the processes responsible for each identified assemblage e.g. flow strength/sedimentological/oceanographic conditions using framework from earlier chapters   |
| <b>Chapter Reference</b>                        | Chapters 4, 5 and 6   |
| <b>How has the Research Objective been met?</b> | <p>This objective was met in the process of completing objectives 1 – 5. The resolution and quantity of data collected from previous chapters allowed the identification of a range of foraminiferal assemblages between the contourite and turbidite end members. Correlating the foraminiferal data to the physical properties, ITRAX and geochemical data collected, alongside palaeoceanographic interpretations made in previous chapters.</p> <p>These foraminiferal assemblages highlighted the complexity of foraminiferal life strategies and that food supply (not only disturbance) is a major factor on foraminiferal assemblages observed.</p> |

Table 7.7 Research Objective 7 and how it has been addressed in this thesis

|   |  |
|---|--|
| <b>Research Objective</b>                       | <b>Objective 7:</b> Determine whether bottom currents can influence the sedimentation, stability and biology on the Uruguay continental slope  |
| <b>Chapters</b>                                 | Chapters 4 and 6   |
| <b>How has the Research Objective been met?</b> | <p>Particulate transport processes and fluxes control the geometry, distribution and internal architecture of deep-sea sediment accumulations. Therefore it is a first-order issue to constrain when creating a detailed reconstruction of a depositional sequence. Depositional sequences form the critical long-term archives (&gt;100 years) for investigations into the response of the planet's interconnected systems to climate change, and the risks posed by natural hazards. An understanding how sediment and associated pollutants are transported from source (on land) to sink (the deep-ocean) and subsequently dispersed are critical to improve societal resilience to planetary change and the hazards we face as a species. Understanding mixed/hybrid depositional systems such as the Uruguayan continental margin are critical in achieving this goal. In the identification of sedimentary environments here we have recognised the importance of bottom current driven instability on the slope, climatic shifts on a millennial timescale and their how a bottom current and its associated watermass determines the ability for life to thrive or die on the seafloor, which in our example has a direct link to the ability of our oceans as a carbon sink.</p> |

# REFERENCES

---

Abu-Zied, R. H. *et al.* (2008) 'Benthic foraminiferal response to changes in bottom-water oxygenation and organic carbon flux in the eastern Mediterranean during LGM to Recent times', *Marine Micropaleontology*. doi: 10.1016/j.marmicro.2007.08.006.

Akhmetzhanov, A. M. *et al.* (2007) 'North Atlantic contourite sand channels', in *Geological Society, London, Special Publications*. doi: 10.1144/GSL.SP.2007.276.01.02.

Alexander, S. P. and Delaca, T. E. (1987) 'Feeding adaptations of the foraminiferan *Cibicides refulgens* living epizoically and parasitically on the Antarctic scallop *Adamussium colbecki*', *Biological Bulletin*. doi: 10.2307/1541868.

Allen, P. A. (2009) *Earth Surface Processes, Earth Surface Processes*. doi: 10.1002/9781444313574.

Altenbach, A. V. (1987) 'The measurement of organic carbon in foraminifera.', *Journal of Foraminiferal Research*. doi: 10.2113/gsjfr.17.2.106.

Altenbach, A. V. *et al.* (1999) 'Scaling percentages and distributional patterns of benthic foraminifera with flux rates of organic carbon', *Journal of Foraminiferal Research*.

Alve, E. (1995) 'Benthic foraminiferal distribution and recolonization of formerly anoxic environments in Drammensfjord, southern Norway', *Marine*



*Micropaleontology*. doi: 10.1016/0377-8398(95)00007-N.

Alve, E. (1999) 'Colonization of new habitats by benthic foraminifera: A review', *Earth Science Reviews*. doi: 10.1016/S0012-8252(99)00016-1.

Alve, E. (2010) 'Benthic foraminiferal responses to absence of fresh phytodetritus: A two-year experiment', *Marine Micropaleontology*. doi: 10.1016/j.marmicro.2010.05.003.

Ambar, I. and Howe, M. R. (1979) 'Observations of the Mediterranean outflow-l mixing in the Mediterranean outflow', *Deep Sea Research Part A, Oceanographic Research Papers*. doi: 10.1016/0198-0149(79)90095-5.

Angela Kelham (2011) *Investigation into the post-mortem transport of benthic foraminifera*. University of Hull.

Anschutz, P., Jorissen, F.J., Chaillou, G., Abu-Zeid, R. and Fontanier, C. (2002) 'Recent turbidite deposition in the eastern Atlantic: Early diagenesis and biotic recovery.', *Journal of Marine Research*, 60, pp. 835–854.

Archer, D. (1996) 'A data-driven model of the global calcite lysocline', *Global Biogeochemical Cycles*. doi: 10.1029/96GB01521.

*Atlas of Deep-Water Outcrops* (2008) *Atlas of Deep-Water Outcrops*. doi: 10.1306/st561240.

B.C. Heezen, G. L. J. (1969) 'Mediterranean undercurrent and microphysiography west of Gibraltar', *Bull. Inst. Océanogr. Monaco*, 67, pp. 1–95.

Bahr, A. *et al.* (2014a) 'Deciphering bottom current velocity and paleoclimate

signals from contourite deposits in the Gulf of Cádiz during the last 140 kyr: An inorganic geochemical approach', *Geochemistry, Geophysics, Geosystems*. doi: 10.1002/2014GC005356.

Bahr, A. *et al.* (2014b) 'Deciphering bottom current velocity and paleoclimate signals from contourite deposits in the Gulf of Cádiz during the last 140 kyr: An inorganic geochemical approach', *Geochemistry, Geophysics, Geosystems*. doi: 10.1002/2014GC005356.

Baldwin, C. T. and McCave, I. N. (2007) 'Bioturbation in an Active Deep-Sea Area: Implications for Models of Trace Fossil Tiering', *PALAIOS*. doi: 10.2307/3515463.

Bandy, O. L. (1964) 'Foraminiferal trends associated with deep water sands, San Pedro and Santa Monica basins, California.', *Journal of Paleontology*, 38, pp. 138–148.

Barbante, C. *et al.* (2006) 'One-to-one coupling of glacial climate variability in Greenland and Antarctica', *Nature*. doi: 10.1038/nature05301.

Barbieri, R. (2001) 'Taphonomic implications of foraminiferal composition and abundance in intertidal mudflats, Colorado River Delta (Mexico).', *Micropaleontology*, 47, pp. 73–86.

Baringer, M. O. N. and Price, J. F. (1999) 'A review of the physical oceanography of the Mediterranean outflow', *Marine Geology*. doi: 10.1016/S0025-3227(98)00141-8.

Barker, S. *et al.* (2007) 'Radiocarbon age offsets of foraminifera resulting from differential dissolution and fragmentation within the sedimentary bioturbated

zone', *Paleoceanography*. doi: 10.1029/2006PA001354.

Basu, S. and Mackey, K. R. M. (2018) 'Phytoplankton as key mediators of the biological carbon pump: Their responses to a changing climate', *Sustainability (Switzerland)*. doi: 10.3390/su10030869.

Bé, A. W. H. and Tolderlund, D. S. (1971) 'Distribution and Ecology of Living Planktonic Foraminifera in Surface Waters of the Atlantic and Indian Oceans', *Micropalaeontology of marine bottom sediments*.

Berger, A. and Loutre, M. F. (1991) 'Insolation values for the climate of the last 10 million years', *Quaternary Science Reviews*. doi: 10.1016/0277-3791(91)90033-Q.

Berger, W. H., Smetacek, V. S. and Wefer, G. (1989) 'Ocean productivity and paleoproductivity - an overview', *Productivity of the Ocean: Present and Past*. doi: 10013/epic.10860.

Bernhard, J. M. (2009) 'Foraminiferal biotopes in Explorers Cove, McMurdo Sound, Antarctica', *The Journal of Foraminiferal Research*. doi: 10.2113/gsjfr.17.4.286.

Bernhard, J. M. *et al.* (2012) 'Potential importance of physiologically diverse benthic foraminifera in sedimentary nitrate storage and respiration', *Journal of Geophysical Research: Biogeosciences*. doi: 10.1029/2012JG001949.

Bernhard, J. M. and Sen Gupta, B. K. (1999) 'Foraminifera of oxygen-depleted environments', in *Modern Foraminifera*. doi: 10.1007/0-306-48104-9\_12.

Bernhard, J. M., Sen Gupta, B. K. and Borne, P. F. (1997) 'Benthic foraminiferal proxy to estimate dysoxic bottom-water oxygen concentrations: Santa Barbara Basin, U.S. Pacific continental margin', *Journal of Foraminiferal Research*. doi:

10.2113/gsjfr.27.4.301.

Blanchet, C. L., Thouveny, N. and Vidal, L. (2009) 'Formation and preservation of greigite (Fe<sub>3</sub>S<sub>4</sub>) in sediments from the Santa Barbara Basin: Implications for paleoenvironmental changes during the past 35 ka', *Paleoceanography*. doi: 10.1029/2008PA001719.

Bohm, E. *et al.* (2015) 'Strong and deep Atlantic meridional overturning circulation during the last glacial cycle', *Nature*. doi: 10.1038/nature14059.

Bolliet, T. *et al.* (2014) 'Benthic foraminifera from Capbreton Canyon revisited; faunal evolution after repetitive sediment disturbance', *Deep-Sea Research Part II: Topical Studies in Oceanography*. doi: 10.1016/j.dsr2.2013.09.009.

Bouma, A. H. (1962) 'Sedimentology of some Flysch deposits; a graphic approach to facies interpretation', *Elsevier*. doi: -.

Bouma, A. H. (1964) 'Turbidites', *Developments in Sedimentology*. doi: 10.1016/S0070-4571(08)70967-1.

Bouma, A. H. and Hollister, C. D. (1973) 'Deep ocean basin sedimentation', in *Turbidites and Deep-Water Sedimentation*. doi: -.

Bozzano, G., Violante, R. A. and Cerredo, M. E. (2011) 'Middle slope contourite deposits and associated sedimentary facies off NE Argentina', *Geo-Marine Letters*. doi: 10.1007/s00367-011-0239-x.

Bramlette, M. N. (1961) 'Pelagic Sediments', in Sears, M. (ed.) *Oceanography*. American Association for the Advancement of Sciences, pp. 345–366.

Brendryen, J., Hafliðason, H. and Sejrup, H. P. (2010) 'Norwegian Sea tephrostratigraphy of marine isotope stages 4 and 5: Prospects and problems for tephrochronology in the North Atlantic region', *Quaternary Science Reviews*. doi: 10.1016/j.quascirev.2009.12.004.

Briguglio, A. and Hohenegger, J. (2009) 'Nummulitids hydrodynamics: An example using nummulites globulus leymerie, 1846', *Bollettino della Societa Paleontologica Italiana*. doi: 10.1002/asia.201100576.

Brocheray, S. *et al.* (2014) '2000 years of frequent turbidite activity in the Capbreton Canyon (Bay of Biscay)', *Marine Geology*. doi: 10.1016/j.margeo.2013.11.009.

Broecker, W. S. *et al.* (1991) 'Radiocarbon decay and oxygen utilization in the Deep Atlantic Ocean', *Global Biogeochemical Cycles*. doi: 10.1029/90GB02279.

Bubenshchikova, N. *et al.* (2008) 'Living benthic foraminifera of the Okhotsk Sea: Faunal composition, standing stocks and microhabitats', *Marine Micropaleontology*. doi: 10.1016/j.marmicro.2008.09.002.

Burke, S. K. *et al.* (1993) 'Benthic foraminifera in box core ERDC 112, Ontong Java Plateau', *Journal of Foraminiferal Research*. doi: 10.2113/gsjfr.23.1.19.

Buzas-Stephens, P. (2005) 'POPULATION DYNAMICS AND DISSOLUTION OF FORAMINIFERA IN NUECES BAY, TEXAS', *The Journal of Foraminiferal Research*. doi: 10.2113/35.3.248.

Caesar, L. *et al.* (2018) 'Observed fingerprint of a weakening Atlantic Ocean overturning circulation', *Nature*. doi: 10.1038/s41586-018-0006-5.

Came, R. E. *et al.* (2008) 'Deglacial variability in the surface return flow of the

Atlantic meridional overturning circulation', *Paleoceanography*. doi: 10.1029/2007PA001450.

Candela, J. (2001) 'Mediterranean water and global circulation', in *Ocean Circulation and Climate*. doi: 10.1016/S0074-6142(01)80132-7.

Capella, W. *et al.* (2017) 'Sandy contourite drift in the late Miocene Rifian Corridor (Morocco): Reconstruction of depositional environments in a foreland-basin seaway', *Sedimentary Geology*. doi: 10.1016/j.sedgeo.2017.04.004.

Capella, W. *et al.* (2018a) 'Data on lithofacies, sedimentology and palaeontology of South Rifian Corridor sections (Morocco)', *Data in Brief*. doi: 10.1016/j.dib.2018.05.047.

Capella, W. *et al.* (2018b) 'Palaeogeographic evolution of the late Miocene Rifian Corridor (Morocco): Reconstructions from surface and subsurface data', *Earth-Science Reviews*. doi: 10.1016/j.earscirev.2018.02.017.

Caralp, M. H. (1989a) 'Abundance of *Bulimina exilis* and *Melonis barleeanum*: Relationship to the quality of marine organic matter', *Geo-Marine Letters*. doi: 10.1007/BF02262816.

Caralp, M. H. (1989b) 'Size and morphology of the benthic foraminifer *Melonis barleeanum*: relationships with marine organic matter', *Journal of Foraminiferal Research*. doi: 10.2113/gsjfr.19.3.235.

Carter, L., Carter, R. M. and McCave, I. N. (2004) 'Evolution of the sedimentary system beneath the deep Pacific inflow off eastern New Zealand', *Marine Geology*. doi: 10.1016/S0025-3227(04)00016-7.

Caspers, H. (1980) 'Atlas of Benthic Shelf Foraminifera of the Southwest Atlantic. Edited by E. Boltovskoy, G. Giussani, S. Watanabe, R. Wright. - 36 plates, 17 figs., 147 pp. The Hague-Boston-London: Dr. W. Junk by Publishers 1980. ISBN 90-6193-604-7. Hfl 110,-, US \$ 57.90', *Internationale Revue der gesamten Hydrobiologie und Hydrographie*. doi: 10.1002/iroh.19800650609.

Caswell, B. A., Paine, M. and Frid, C. L. J. (2018) 'Seafloor ecological functioning over two decades of organic enrichment', *Marine Pollution Bulletin*. doi: 10.1016/j.marpolbul.2018.08.041.

Chiessi, C. M. *et al.* (2009) 'Possible impact of the Atlantic Multidecadal Oscillation on the South American summer monsoon', *Geophysical Research Letters*. doi: 10.1029/2009GL039914.

CLARKE, K. R. (1993) 'Non-parametric multivariate analyses of changes in community structure', *Australian Journal of Ecology*. doi: 10.1111/j.1442-9993.1993.tb00438.x.

Contreras-Rosales, L. A. *et al.* (2012) 'Living deep-sea benthic foraminifera from the Cap de Creus Canyon (western Mediterranean): Faunal-geochemical interactions', *Deep-Sea Research Part I: Oceanographic Research Papers*. doi: 10.1016/j.dsr.2012.01.010.

Corliss, B. H. (1985) 'Microhabitats of benthic foraminifera within deep-sea sediments', *Nature*. doi: 10.1038/314435a0.

Courtene-Jones, W. *et al.* (2019) 'Consistent microplastic ingestion by deep-sea invertebrates over the last four decades (1976–2015), a study from the North East Atlantic', *Environmental Pollution*. doi: 10.1016/j.envpol.2018.10.090.

Croudace, I. W., Rindby, A. and Rothwell, R. G. (2006) 'ITRAX: description and evaluation of a new multi-function X-ray core scanner', *Geological Society, London, Special Publications*. doi: 10.1144/GSL.SP.2006.267.01.04.

Croudace, I. W. and Rothwell, R. G. (2015) *Micro-XRF Studies of Sediment Cores: Applications of a non-destructive tool for the environmental sciences, Developments in Paleoenvironmental Research*. doi: 10.1007/978-94-017-9849-5.

Dickson, A. J. *et al.* (2010) 'Oceanic, atmospheric and ice-sheet forcing of South East Atlantic Ocean productivity and South African monsoon intensity during MIS-12 to 10', *Quaternary Science Reviews*. doi: 10.1016/j.quascirev.2010.09.014.

Diekmann, B. *et al.* (2000) 'Terrigenous sediment supply in the Scotia Sea (Southern Ocean): Response to Late Quaternary ice dynamics in Patagonia and on the Antarctic Peninsula', *Palaeogeography, Palaeoclimatology, Palaeoecology*. doi: 10.1016/S0031-0182(00)00138-3.

Dittert, N. and Henrich, R. (1999) 'Carbonate dissolution in the South Atlantic Ocean: Evidence from ultrastructure breakdown in *Globigerina bulloides*', *Deep-Sea Research Part I: Oceanographic Research Papers*. doi: 10.1016/S0967-0637(99)00069-2.

Donald R. Lowe (1982) 'Sediment Gravity Flows: II Depositional Models with Special Reference to the Deposits of High-Density Turbidity Currents', *SEPM Journal of Sedimentary Research*. doi: 10.1306/212F7F31-2B24-11D7-8648000102C1865D.

Donnici, S. and Serandrei Barbero, R. (2002) 'The benthic foraminiferal communities of the northern Adriatic continental shelf', *Marine Micropaleontology*.



doi: 10.1016/S0377-8398(01)00043-3.

Douglas, R. G. and Heitman, H. L. (1979) 'Slope and basin benthic foraminifera of the California borderland.', *Geology of continental slopes*.

Ducassou, E. *et al.* (2008) 'Nile floods recorded in deep Mediterranean sediments', *Quaternary Research*. doi: 10.1016/j.yqres.2008.02.011.

Duros, P. *et al.* (2011) 'Live (stained) benthic foraminifera in the Whittard Canyon, Celtic margin (NE Atlantic)', *Deep-Sea Research Part I: Oceanographic Research Papers*. doi: 10.1016/j.dsr.2010.11.008.

Duros, P. *et al.* (2013) 'Live (stained) benthic foraminifera from the Cap-Ferret Canyon (Bay of Biscay, NE Atlantic): A comparison between the canyon axis and the surrounding areas', *Deep-Sea Research Part I: Oceanographic Research Papers*. doi: 10.1016/j.dsr.2013.01.004.

Duros, P. *et al.* (2014) 'Benthic foraminiferal thanatocoenoses from the Cap-Ferret Canyon area (NE Atlantic): A complex interplay between hydro-sedimentary and biological processes', *Deep-Sea Research Part II: Topical Studies in Oceanography*. doi: 10.1016/j.dsr2.2013.09.024.

Duros, P. *et al.* (2017) 'Benthic foraminiferal response to sedimentary disturbance in the Capbreton canyon (Bay of Biscay, NE Atlantic)', *Deep-Sea Research Part I: Oceanographic Research Papers*. doi: 10.1016/j.dsr.2016.11.012.

Eberwein, A. and Mackensen, A. (2006) 'Regional primary productivity differences off Morocco (NW-Africa) recorded by modern benthic foraminifera and their stable carbon isotopic composition', *Deep-Sea Research Part I: Oceanographic*

*Research Papers*. doi: 10.1016/j.dsr.2006.04.001.

Elmore, A. C. *et al.* (2015) 'Antarctic Intermediate Water properties since 400 ka recorded in infaunal (*Uvigerina peregrina*) and epifaunal (*Planulina wuellerstorfi*) benthic foraminifera', *Earth and Planetary Science Letters*. doi: 10.1016/j.epsl.2015.07.013.

Erlenkeuser, H. (1980) '14C age and vertical mixing of deep-sea sediments', *Earth and Planetary Science Letters*. doi: 10.1016/0012-821X(80)90018-7.

Ewing, M. and Lonardi, A. G. (1971) 'Sediment transport and distribution in the Argentine Basin. 5. Sedimentary structure of the Argentine margin, basin, and related provinces', *Physics and Chemistry of the Earth*. doi: 10.1016/0079-1946(71)90017-6.

Faugères, J.-C. *et al.* (2008) 'The Columbia Channel-levee system: a fan drift in the southern Brazil Basin', *Geological Society, London, Memoirs*. doi: 10.1144/gsl.mem.2002.022.01.16.

Faugères, J. C. *et al.* (1999) 'Seismic features diagnostic of contourite drifts', *Marine Geology*. doi: 10.1016/S0025-3227(99)00068-7.

Faugeres, J. C., Gonthier, E. and Stow, D. A. V. (1984) 'Contourite drift molded by deep Mediterranean outflow.', *Geology*. doi: 10.1130/0091-7613(1984)12<296:CDMBDM>2.0.CO;2.

Faugères, J. C. and Stow, D. A. V. (1993) 'Bottom-current-controlled sedimentation: a synthesis of the contourite problem', *Sedimentary Geology*. doi: 10.1016/0037-0738(93)90127-Q.

Fontanier, C. *et al.* (2002) 'Live benthic foraminiferal faunas from the Bay of Biscay: Faunal density, composition, and microhabitats', *Deep-Sea Research Part I: Oceanographic Research Papers*. doi: 10.1016/S0967-0637(01)00078-4.

Fontanier, C. *et al.* (2003) 'Seasonal and interannual variability of benthic foraminiferal faunas at 550 m depth in the Bay of Biscay', *Deep-Sea Research Part I: Oceanographic Research Papers*. doi: 10.1016/S0967-0637(02)00167-X.

Fontanier, C. *et al.* (2005) 'Live foraminiferal faunas from a 2800 m deep lower canyon station from the Bay of Biscay: Faunal response to focusing of refractory organic matter', *Deep-Sea Research Part I: Oceanographic Research Papers*. doi: 10.1016/j.dsr.2005.01.006.

Fontanier, C. *et al.* (2006) 'Stable oxygen and carbon isotopes of live benthic foraminifera from the Bay of Biscay: Microhabitat impact and seasonal variability', *Marine Micropaleontology*. doi: 10.1016/j.marmicro.2005.09.004.

Fontanier, C. *et al.* (2008) 'Live foraminifera from the open slope between Grand Rhône and Petit Rhône Canyons (Gulf of Lions, NW Mediterranean)', *Deep-Sea Research Part I: Oceanographic Research Papers*. doi: 10.1016/j.dsr.2008.07.003.

Fontanier, C. *et al.* (2012) 'Deep-sea foraminifera from the Cassidaigne Canyon (NW Mediterranean): Assessing the environmental impact of bauxite red mud disposal', *Marine Pollution Bulletin*. doi: 10.1016/j.marpolbul.2012.06.016.

Fontanier, C. *et al.* (2015) 'Deep-sea benthic foraminifera in an area around the Cassidaigne Canyon (NW Mediterranean) affected by bauxite discharges', *Marine Biodiversity*. doi: 10.1007/s12526-014-0281-9.

Franke, D. *et al.* (2006) 'Crustal structure across the Colorado Basin, offshore Argentina', *Geophysical Journal International*. doi: 10.1111/j.1365-246X.2006.02907.x.

Freeman, E. *et al.* (2016) 'Radiocarbon evidence for enhanced respired carbon storage in the Atlantic at the Last Glacial Maximum', *Nature Communications*. doi: 10.1038/ncomms11998.

Friedrich-Wilhelm *et al.* (1989) 'Late Pleistocene foraminiferal stratigraphy on the Vøring Plateau, Norwegian Sea', *Boreas*, 18(4).

Galy, V. *et al.* (2007) 'Efficient organic carbon burial in the Bengal fan sustained by the Himalayan erosional system', *Nature*. doi: 10.1038/nature06273.

García-Gallardo, Á. *et al.* (2017) 'Benthic foraminifera-based reconstruction of the first Mediterranean-Atlantic exchange in the early Pliocene Gulf of Cadiz', *Palaeogeography, Palaeoclimatology, Palaeoecology*. doi: 10.1016/j.palaeo.2017.02.009.

Gaudin, M. *et al.* (2006) 'Massive sand beds attributed to deposition by dense water cascades in the Bourcart canyon head, Gulf of Lions (northwestern Mediterranean Sea)', *Marine Geology*. doi: 10.1016/j.margeo.2006.09.020.

Georgi, D. T. (1981) 'Circulation of bottom waters in the southwestern South Atlantic', *Deep Sea Research Part A, Oceanographic Research Papers*. doi: 10.1016/0198-0149(81)90012-1.

Giberto, D. A. *et al.* (2004) 'Large-scale spatial patterns of benthic assemblages in the SW Atlantic: The Río de la Plata estuary and adjacent shelf waters', *Estuarine*,

*Coastal and Shelf Science*. doi: 10.1016/j.ecss.2004.03.015.

Giosan, L. *et al.* (2002) 'Paleoceanographic significance of sediment color on western North Atlantic Drifts: II. Late Pliocene-Pleistocene sedimentation', *Marine Geology*. doi: 10.1016/S0025-3227(02)00322-5.

Giosan, L., Flood, R. D. and Aller, R. C. (2002) 'Paleoceanographic significance of sediment color on western North Atlantic drifts: I. Origin of color', *Marine Geology*. doi: 10.1016/S0025-3227(02)00321-3.

Goineau, A. *et al.* (2011) 'Live (stained) benthic foraminifera from the Rhône prodelta (Gulf of Lion, NW Mediterranean): Environmental controls on a river-dominated shelf', *Journal of Sea Research*. doi: 10.1016/j.seares.2010.07.007.

Gonthier, E. G., Faugères, J.-C. and Stow, D. A. V. (1984) 'Contourite facies of the Faro Drift, Gulf of Cadiz', *Geological Society, London, Special Publications*. doi: 10.1144/GSL.SP.1984.015.01.18.

Gooday, A. J. (1988) 'A response by benthic Foraminifera to the deposition of phytodetritus in the deep sea', *Nature*. doi: 10.1038/332070a0.

Gooday, A. J. (1993) 'Deep-sea benthic foraminiferal species which exploit phytodetritus: Characteristic features and controls on distribution', *Marine Micropaleontology*. doi: 10.1016/0377-8398(93)90043-W.

Gooday, A. J. (1994) 'The Biology of Deep-Sea Foraminifera: A Review of Some Advances and Their Applications in Paleoceanography', *PALAIOS*. doi: 10.2307/3515075.

Gooday, A. J. *et al.* (2000) 'Foraminifera in the Arabian Sea oxygen minimum zone

and other oxygen-deficient settings: taxonomic â€¦', *Deep-Sea Research Part II - Topical Studies in Oceanography*.

Gooday, A. J. (2003) 'Benthic foraminifera (protista) as tools in deep-water palaeoceanography: Environmental influences on faunal characteristics', *Advances in Marine Biology*. doi: 10.1016/S0065-2881(03)46002-1.

Gooday, A. J. and Alve, E. (2001) 'Morphological and ecological parallels between sublittoral and abyssal foraminiferal species in the NE atlantic: A comparison of *Stainforthia fusiformis* and *Stainforthia* sp.', *Progress in Oceanography*. doi: 10.1016/S0079-6611(01)00057-X.

Gooday, A. J., Bowser, S. S. and Bernhard, J. M. (1996) 'Benthic foraminiferal assemblages in Explorers Cove, Antarctica: A shallow-water site with deep-sea characteristics', *Progress in Oceanography*. doi: 10.1016/S0079-6611(96)00007-9.

Goosse, H., Campin, J. M. and Tartinville, B. (2001) 'The sources of Antarctic bottom water in a global ice-ocean model', *Ocean Modelling*. doi: 10.1016/S1463-5003(00)00017-2.

Gordon, A. L. (1989) 'Brazil-Malvinas Confluence-1984', *Deep Sea Research Part A, Oceanographic Research Papers*. doi: 10.1016/0198-0149(89)90042-3.

Gordon, A. L. *et al.* (1992) 'Thermocline and intermediate water communication between the south Atlantic and Indian oceans', *Journal of Geophysical Research*. doi: 10.1029/92JC00485.

Gordon, A. L. and Greengrove, C. L. (1986) 'Geostrophic circulation of the Brazil-

Falkland confluence', *Deep Sea Research Part A, Oceanographic Research Papers*. doi: 10.1016/0198-0149(86)90054-3.

Graham, J. A. *et al.* (2011) 'North Atlantic climate responses to perturbations in Antarctic Intermediate Water', *Climate Dynamics*. doi: 10.1007/s00382-010-0981-1.

Gross, M. G. and Gross, E. (1996) *Oceanography: A View of the Earth*. 7th Editio.

Gross, O. (2000) 'Influence of temperature, oxygen and food availability on the migrational activity of bathyal benthic foraminifera: Evidence by microcosm experiments', in *Hydrobiologia*. doi: 10.1023/A:1003930831220.

Grzymiski, J. *et al.* (2002) 'The function of plastids in the deep-sea benthic foraminifer, *Nonionella stella*', *Limnology and Oceanography*. doi: 10.4319/lo.2002.47.6.1569.

Gupta, A. K. and Thomas, E. (2003) 'Initiation of Northern Hemisphere glaciation and strengthening of the northeast Indian monsoon: Ocean drilling program site 758, eastern equatorial Indian Ocean', *Geology*. doi: 10.1130/0091-7613(2003)031<0047:IONHGA>2.0.CO;2.

Sen Gupta, B. K. (1999a) 'Foraminifera in marginal marine environments', in *Modern Foraminifera*. doi: 10.1007/0-306-48104-9\_9.

Sen Gupta, B. K. (1999b) 'Systematics of moder Foraminifera', in *Modern Foraminifera*. doi: 10.1007/0-306-48104-9\_2.

Sen Gupta, B. K. and Machain-Castillo, M. L. (1993) 'Benthic foraminifera in oxygen-poor habitats', *Marine Micropaleontology*. doi: 10.1016/0377-

8398(93)90032-S.

Gwilliam, C. S. (1996) '- Modelling the global ocean circulation on the T3D', in *Parallel Computational Fluid Dynamics 1995 Implementations and Results Using Parallel Computers*, pp. 33–40.

Habgood, E. L. *et al.* (2003) 'Deep-water sediment wave fields, bottom current sand channels and gravity flow channel-lobe systems: Gulf of Cadiz, NE Atlantic', *Sedimentology*. doi: 10.1046/j.1365-3091.2003.00561.x.

Hage, S. *et al.* (2018) 'How to recognize crescentic bedforms formed by supercritical turbidity currents in the geologic record: Insights from active submarine channels', *Geology*. doi: 10.1130/G40095.1.

Hans Nelson, C., Baraza, J. and Maldonado, A. (1993) 'Mediterranean undercurrent sandy contourites, Gulf of Cadiz, Spain', *Sedimentary Geology*. doi: 10.1016/0037-0738(93)90116-M.

Hayek, L.-A. C. and Buzas, M. A. (2016) *Surveying Natural Populations, Surveying Natural Populations*. doi: 10.7312/haye14620.

Haynes, J. R. (1981) *Foraminifera*. Mac Millan, London.

Hayward, B. W. and Hollis, C. J. (1994) 'Brackish foraminifera in New Zealand: A taxonomic and ecologic review', *MICROPALAEONTOLOGY*.

Heezen, B. C., Hollister, C. D. and Ruddiman, W. F. (1966) 'Shaping of the continental rise by deep geostrophic contour currents', *Science*. doi: 10.1126/science.152.3721.502.



Henrich R.; Baumann K-H.; Gerhardt S.; Gröger M.; Volbers A. (2003) 'Carbonate Preservation in Deep and Intermediate Water Masses in the South Atlantic: Evaluation and Geological Record (a Review)', in Wefer, G., Mulitza, S., and Ratmeyer, V. (eds) *The South Atlantic in the Late Quaternary*. Berlin: Springer, Berlin, Heidelberg, pp. 645–670. doi: 10.1007/978-3-642-18917-3\_28.

Hepp, D. A. *et al.* (2009) 'A late Miocene-early Pliocene Antarctic deepwater record of repeated iron reduction events', *Marine Geology*. doi: 10.1016/j.margeo.2009.08.006.

Hernández-Molina, F. J. *et al.* (2009) 'Contourite depositional system on the Argentine slope: An exceptional record of the influence of Antarctic water masses', *Geology*. doi: 10.1130/G25578A.1.

Hernández-Molina, F. J. *et al.* (2006) 'The contourite depositional system of the Gulf of Cádiz: A sedimentary model related to the bottom current activity of the Mediterranean outflow water and its interaction with the continental margin', *Deep-Sea Research Part II: Topical Studies in Oceanography*. doi: 10.1016/j.dsr2.2006.04.016.

Hernández-Molina, F. J. *et al.* (2010) 'Giant mounded drifts in the Argentine Continental Margin: Origins, and global implications for the history of thermohaline circulation', *Marine and Petroleum Geology*. doi: 10.1016/j.marpetgeo.2010.04.003.

Hernández-Molina, F. J. *et al.* (2013) 'IODP Expedition 339 in the Gulf of Cadiz and off West Iberia: Decoding the environmental significance of the Mediterranean outflow water and its global influence', *Scientific Drilling*. doi: 10.5194/sd-16-1-

2013.

Hernández-Molina, F. J. *et al.* (2014) 'Contourite processes associated with the Mediterranean Outflow Water after its exit from the Strait of Gibraltar: Global and conceptual implications', *Geology*. doi: 10.1130/G35083.1.

Hernández-Molina, F. J. *et al.* (2016) 'A contourite depositional system along the Uruguayan continental margin: Sedimentary, oceanographic and paleoceanographic implications', *Marine Geology*. doi: 10.1016/j.margeo.2015.10.008.

Hernández-Molina, F. J. *et al.* (2018) 'Large bedforms on contourite terraces: Sedimentary and conceptual implications', *Geology*. doi: 10.1130/G39655.1.

Hernández-Molina, F. J., Llave, E. and Stow, D. A. V. (2008) 'Chapter 19 Continental Slope Contourites', *Developments in Sedimentology*. doi: 10.1016/S0070-4571(08)10019-X.

Hernández-Molina, F. J., Llave, E. and Stow, D. A. V. (2008) 'Continental slope contourites', in *Developments in Sedimentology*. doi: 10.1016/S0070-4571(08)10019-X.

Hess, S. *et al.* (2005) 'Benthic foraminiferal recovery after recent turbidite deposition in Cap Breton Canyon, Bay of Biscay', *Journal of Foraminiferal Research*. doi: 10.2113/35.2.114.

Hess, S. *et al.* (2005) 'Benthic foraminiferal recovery after recent turbidite deposition in Cap Breton Canyon, Bay of Biscay', *The Journal of Foraminiferal Research*. doi: 10.2113/35.2.114.

Hess, S. and Jorissen, F. J. (2009) 'Distribution patterns of living benthic foraminifera from Cap Breton canyon, Bay of Biscay: Faunal response to sediment instability', *Deep-Sea Research Part I: Oceanographic Research Papers*. doi: 10.1016/j.dsr.2009.04.003.

Hess, S. and Kuhnt, W. (1996) 'Deep-sea benthic foraminiferal recolonization of the 1991 Mt. Pinatubo ash layer in the South China Sea', *Marine Micropaleontology*. doi: 10.1016/0377-8398(95)00080-1.

Hesse, R. (1975) 'Turbiditic and non-turbiditic mudstone of Cretaceous flysch sections of the East Alps and other basins', *Sedimentology*. doi: 10.1111/j.1365-3091.1975.tb01638.x.

Hodell, D. A. *et al.* (2008) 'Onset of "Hudson Strait" Heinrich events in the eastern North Atlantic at the end of the middle Pleistocene transition (~640 ka)?', *Paleoceanography*. doi: 10.1029/2008PA001591.

Hodgson, D. M. *et al.* (2018) 'Grand challenges (And great opportunities) in sedimentology, stratigraphy, and diagenesis research', *Frontiers in Earth Science*. doi: 10.3389/feart.2018.00173.

Hohenegger, J. and Briguglio, A. (2012) 'Axially oriented sections of nummulitids: A tool to interpret larger benthic foraminiferal deposits', *Journal of Foraminiferal Research*. doi: 10.2113/gsjfr.42.2.134.

Hohenegger, J. and Yordanova, E. K. (2001) 'Displacement of Larger Foraminifera at the Western Slope of Motobu Peninsula (Okinawa, Japan)', *Palaios*. doi: 10.2307/3515552.

Holbourn, A., Henderson, A. S. and MacLeod, N. (2013) *Atlas of Benthic Foraminifera, Atlas of Benthic Foraminifera*. doi: 10.1002/9781118452493.

Hollister, C. D. (1967) *Sediment Distribution and Deep Circulation in the Western North Atlantic (Ph.D. dissertation)*. Columbia University, New York.

Hollister, C. D. (1994) 'The concept of deep-sea contourites-reply', *Sedimentary Geology*. doi: 10.1016/0037-0738(94)90069-8.

Hoogakker, B. *et al.* (2010) 'Benthic foraminiferal oxygen isotope offsets over the last glacial-interglacial cycle', *Paleoceanography*. doi: 10.1029/2009PA001870.

Horton, B. P., Edwards, R. J. and Lloyd, J. M. (1999) 'A FORAMINIFERAL-BASED TRANSFER FUNCTION: IMPLICATIONS FOR SEA-LEVEL STUDIES', *The Journal of Foraminiferal Research*. doi: 10.2113/gsjfr.29.2.117.

Howe, J. N. W. *et al.* (2016) 'North Atlantic Deep Water Production during the Last Glacial Maximum', *Nature Communications*. doi: 10.1038/ncomms11765.

Hsü, K.J. (1964) 'Cross-laminated sequence in graded bed sequence', *Journal of Sedimentary Petrology*, 34, pp. 379–388.

Hsu, S. K. *et al.* (2008) 'Turbidity currents, submarine landslides and the 2006 Pingtung earthquake off SW Taiwan', *Terrestrial, Atmospheric and Oceanic Sciences*. doi: 10.3319/TAO.2008.19.6.767(PT).

Huang, K. F., Oppo, D. W. and Curry, W. B. (2014) 'Decreased influence of Antarctic intermediate water in the tropical Atlantic during North Atlantic cold events', *Earth and Planetary Science Letters*. doi: 10.1016/j.epsl.2013.12.037.

Hubert, J. F. (1964) 'Textural evidence for deposition of many western North Atlantic deep-sea sands by oceanbottom currents rather than turbidity currents', *Journal of Geology*, 72, pp. 757–785.

Hunt, J. E. *et al.* (2011) 'Sedimentological and geochemical evidence for multistage failure of volcanic island landslides: A case study from Icod landslide on north Tenerife, Canary Islands', *Geochemistry, Geophysics, Geosystems*. doi: 10.1029/2011GC003740.

Huvenne, V. A. I., Masson, D. G. and Wheeler, A. J. (2009) 'Sediment dynamics of a sandy contourite: The sedimentary context of the Darwin cold-water coral mounds, Northern Rockall Trough', *International Journal of Earth Sciences*. doi: 10.1007/s00531-008-0312-5.

Ikeya, N. (1971) 'Species diversity of recent benthonic foraminifera off the Pacific coast of north Japan', *Reports of Faculty of Science, Shizuoka University*, 6.

Jorga, M. C. and Lozier, M. S. (1999) 'Signatures of the Mediterranean outflow from a North Atlantic climatology: 1. Salinity and density fields', *Journal of Geophysical Research: Oceans*. doi: 10.1029/1999jc900115.

IPCC (2013) '(Intergovernmental Panel on Climate Change). Working Group I Contribution to the IPCC Fifth Assessment Report - Summary for Policymakers', *Climate Change 2013: The Physical Science Basis*. doi: 10.1017/CBO9781107415324.004.

J.R. Reid (1996) 'On the Circulation of the South Atlantic Ocean', in G. Wefer *et al.* (ed.) *The South Atlantic*. First. New York: Springer-Verlag, pp. 13–44. doi: 10.1007/978-3-642-80353-6\_2.

Jansen, J. H. F. *et al.* (1998) 'CORTEX, a shipboard XRF-scanner for element analyses in split sediment cores', *Marine Geology*. doi: 10.1016/S0025-3227(98)00074-7.

Jones, R. W. (1994) *The Challenger Foraminifera*. Oxford University Press.

Jones, R. W. (2011) *Applications of palaeontology: Techniques and case studies, Applications of Palaeontology: Techniques and Case Studies*. doi: 10.1017/CBO9780511793752.

Jonkers, L. *et al.* (2015) 'Deep circulation changes in the central South Atlantic during the past 145 kyrs reflected in a combined  $^{231}\text{Pa}/^{230}\text{Th}$ , Neodymium isotope and benthic  $\delta^{13}\text{C}$  record', *Earth and Planetary Science Letters*. doi: 10.1016/j.epsl.2015.03.004.

Jorissen, F. J. (1988) 'Benthic foraminifera from the Adriatic Sea: principles of phenotypic variation', *Utrecht Micropaleontol Bull*.

Jorissen, F. J. *et al.* (1992) 'Vertical distribution of benthic foraminifera in the northern Adriatic Sea: The relation with the organic flux', *Marine Micropaleontology*. doi: 10.1016/0377-8398(92)90025-F.

Jorissen, F. J. (1999) 'Benthic foraminiferal microhabitats below the sediment-water interface', in *Modern Foraminifera*. doi: 10.1007/0-306-48104-9\_10.

Jorissen, F. J., Fontanier, C. and Thomas, E. (2007) 'Chapter Seven Paleooceanographical Proxies Based on Deep-Sea Benthic Foraminiferal Assemblage Characteristics', *Developments in Marine Geology*. doi: 10.1016/S1572-5480(07)01012-3.

Jorissen, F. J., de Stigter, H. C. and Widmark, J. G. V. (1995) 'A conceptual model explaining benthic foraminiferal microhabitats', *Marine Micropaleontology*. doi: 10.1016/0377-8398(95)00047-X.

Jorry, S. J., Hasler, C. A. and Davaud, E. (2006) 'Hydrodynamic behaviour of Nummulites: Implications for depositional models', *Facies*. doi: 10.1007/s10347-005-0035-z.

Kahler, G. (1994) *Stratigraphy and sedimentology of the Paleogene Lefkara Formation, Cyprus*. University of Southampton.

Kähler, G. and Stow, D. A. V. (1998) 'Turbidites and contourites of the Palaeogene Lefkara Formation, southern Cyprus', *Sedimentary Geology*. doi: 10.1016/S0037-0738(97)00094-8.

Kaiho, K. and Hasegawa, T. (1994) 'End-Cenomanian benthic foraminiferal extinctions and oceanic dysoxic events in the northwestern Pacific Ocean', *Palaeogeography, Palaeoclimatology, Palaeoecology*. doi: 10.1016/0031-0182(94)90346-8.

Kaminski, M. A. (1985) 'Evidence for control of abyssal agglutinated foraminiferal community structure by substrate disturbance: Results from the HEBBLE Area', *Marine Geology*. doi: 10.1016/0025-3227(85)90025-8.

Kaminski, M. A., Kuhnt, W. and Radley, J. D. (1996) 'Palaeocene-Eocene deep water agglutinated foraminifera from the Numidian Flysch (Rif, Northern Morocco): their significance for the palaeoceanography of the Gibraltar gateway', *Journal of Micropalaeontology*. doi: 10.1144/jm.15.1.1.

Kane, I. A. and Clare, M. A. (2019) 'Dispersion, accumulation, and the ultimate fate of microplastics in deep-marine environments: A review and future directions', *Frontiers in Earth Science*. doi: 10.3389/feart.2019.00080.

Keigwin, L. D. and Guilderson, T. P. (2009) 'Bioturbation artifacts in zero-age sediments', *Paleoceanography*. doi: 10.1029/2008PA001727.

Keir, R. S. and Michel, R. L. (1993) 'Interface dissolution control of the  $^{14}\text{C}$  profile in marine sediment', *Geochimica et Cosmochimica Acta*. doi: 10.1016/0016-7037(93)90139-N.

Kitazato, H. (1988) 'Locomotion of some benthic Foraminifera in and on sediments', *Journal of Foraminiferal Research*. doi: 10.2113/gsjfr.18.4.344.

Kitazato, H. *et al.* (2000) 'Seasonal phytodetritus deposition and responses of bathyal benthic foraminiferal populations in Sagami Bay, Japan: Preliminary results from "Project Sagami 1996-1999"', in *Marine Micropaleontology*. doi: 10.1016/S0377-8398(00)00036-0.

Klaus, A. and Ledbetter, M. T. (1988) 'Deep-sea sedimentary processes in the Argentine Basin revealed by high-resolution seismic records (3.5 kHz echograms)', *Deep Sea Research Part A, Oceanographic Research Papers*. doi: 10.1016/0198-0149(88)90067-2.

Klein, G. de V. (1975) 'Resedimented pelagic carbonate and volcanoclastic sediments and sedimentary structures in leg 30 dsdp cores from the western equatorial Pacific', *Geology*. doi: 10.1130/0091-7613(1975)3<39:RPCAVS>2.0.CO;2.



Klinck, J. M. (1996) 'Circulation near submarine canyons: A modeling study', *Journal of Geophysical Research C: Oceans*. doi: 10.1029/95JC02901.

Klitgaard-Kristensen, D., Sejrup, H. P. and Hafliðason, H. (2002) 'Distribution of recent calcareous benthic foraminifera in the northern North Sea and relation to the environment', *Polar Research*.

Knutz, P. C. (2008) 'Chapter 24 Palaeoceanographic Significance of Contourite Drifts', *Developments in Sedimentology*. doi: 10.1016/S0070-4571(08)10024-3.

Koho, K. A. *et al.* (2007) 'Benthic foraminifera in the Nazaré Canyon, Portuguese continental margin: Sedimentary environments and disturbance', *Marine Micropaleontology*. doi: 10.1016/j.marmicro.2007.07.005.

Koho, K. A. *et al.* (2008) 'Sedimentary labile organic carbon and pore water redox control on species distribution of benthic foraminifera: A case study from Lisbon-Setúbal Canyon (southern Portugal)', *Progress in Oceanography*. doi: 10.1016/j.pocean.2008.07.004.

Kotler, E., Martin, R. E. and Liddell, D. W. (1992) 'Experimental Analysis of Abrasion and Dissolution Resistance of Modern Reef-Dwelling Foraminifera: Preservation of the Implications for Biogenic Carbonate', *SEPM Society for Sedimentary Geology*. doi: 10.2307/3514972.

Krastel, S. *et al.* (2011) 'Sediment dynamics and geohazards off Uruguay and the de la Plata River region (northern Argentina and Uruguay)', *Geo-Marine Letters*. doi: 10.1007/s00367-011-0232-4.

Kuenen, P. H.; Migliorini, C., I. (1950) 'Turbidity Currents as a Cause for Graded

Bedding', *The Journal of Geology*. doi: 10.1086/625710.

Kuenen, P. H. (1951) 'Properties of turbidity currents of high density', in *Turbidity Currents and the Transportation of Coarse Sediments to Deep Water*. doi: 10.2110/pec.51.02.0014.

Kuhnt, W. *et al.* (2005) 'The impact of the 1991 Mt. Pinatubo eruption on deep-sea foraminiferal communities: A model for the Cretaceous-Tertiary (K/T) boundary?', in *Palaeogeography, Palaeoclimatology, Palaeoecology*. doi: 10.1016/j.palaeo.2005.03.042.

Kuijpers, A. *et al.* (2003) 'Late Quaternary sedimentary processes and ocean circulation changes at the Southeast Greenland margin', *Marine Geology*. doi: 10.1016/S0025-3227(02)00684-9.

Kurbjewit, F. *et al.* (2000) 'Distribution, biomass and diversity of benthic foraminifera in relation to sediment geochemistry in the Arabian Sea', *Deep-Sea Research Part II: Topical Studies in Oceanography*. doi: 10.1016/S0967-0645(00)00053-9.

Laberg, J. S. and Camerlenghi, A. (2008) 'Chapter 25 The Significance of Contourites for Submarine Slope Stability', *Developments in Sedimentology*. doi: 10.1016/S0070-4571(08)10025-5.

Laj, C. *et al.* (2002) 'Suborbital intermediate water variability inferred from paired benthic foraminiferal Cd/Ca and  $\delta^{13}\text{C}$  in the tropical West Atlantic and linking with North Atlantic climates', *Earth and Planetary Science Letters*. doi: 10.1016/S0012-821X(02)00613-1.

Lamy, F. *et al.* (2015) 'Glacial reduction and millennial-scale variations in Drake Passage throughflow', *Proceedings of the National Academy of Sciences*. doi: 10.1073/pnas.1509203112.

Lantsch, H. *et al.* (2014) 'The high-supply, current-dominated continental margin of southeastern South America during the late quaternary', *Quaternary Research (United States)*. doi: 10.1016/j.yqres.2014.01.003.

Leutenegger, S. (1984) 'Symbiosis in benthic foraminifera: specificity and host adaptations.', *Journal of Foraminiferal Research*. doi: 10.2113/gsjfr.14.1.16.

Licari, L. (2006) 'Ecological Preferences of Benthic Foraminifera in the Eastern South Atlantic: Distribution Patterns, Stable Carbon Isotopic Composition, and Paleoceanographic Implications', *Atlantic*. doi: 10.1003/epic.10537.d001.

Licari, L. and Mackensen, A. (2005) 'Benthic foraminifera off West Africa (1°N to 32°S): Do live assemblages from the topmost sediment reliably record environmental variability?', *Marine Micropaleontology*. doi: 10.1016/j.marmicro.2005.03.001.

Licari, L. N. *et al.* (2003) 'Communities and microhabitats of living benthic foraminifera from the tropical East Atlantic: Impact of different productivity regimes', *Journal of Foraminiferal Research*. doi: 10.2113/0330010.

Linke, P. and Lutze, G. F. (1993) 'Microhabitat preferences of benthic foraminifera- a static concept or a dynamic adaptation to optimize food acquisition?', *Marine Micropaleontology*. doi: 10.1016/0377-8398(93)90034-U.

Lirer, F. (2000) 'A new technique for retrieving calcareous microfossils from lithified

lime deposits', *Micropaleontology*.

Liu, J. T. *et al.* (2016) 'From the highest to the deepest: The Gaoping River-Gaoping Submarine Canyon dispersal system', *Earth-Science Reviews*. doi: 10.1016/j.earscirev.2015.10.012.

Loeblich, A.R. Jn., & Tappan, H. (1988) *Foraminifera genera and their classification*. New York: Van Nostrand Reinhold.

Loeblich, A. R. and Tappan, H. (1988) 'Foraminiferal genera and their classification. Two volumes', *Foraminiferal genera and their classification. Two volumes*.

Lonardi, A. G. and Ewing, M. (1971) 'Sediment transport and distribution in the Argentine Basin. 4. Bathymetry of the continental margin, Argentine Basin and other related provinces. Canyons and sources of sediments', *Physics and Chemistry of the Earth*. doi: 10.1016/0079-1946(71)90016-4.

Lonsdale, P., Normark, W. R. and Newman, W. A. (1972) 'Sedimentation and Erosion on Horizon Guyot', *Bulletin of the Geological Society of America*. doi: 10.1130/0016-7606(1972)83[289:SAEOHG]2.0.CO;2.

Lovell, J. P. B. and Stow, D. A. V. (1981) 'Identification of ancient sandy contourites.', *Geology*. doi: 10.1130/0091-7613(1981)9<347:IOASC>2.0.CO;2.

Löwemark, L. *et al.* (2004) 'Trace fossils as a paleoceanographic tool: Evidence from Late Quaternary sediments of the southwestern Iberian margin', *Marine Geology*. doi: 10.1016/S0025-3227(03)00351-7.

Lumpkin, R. and Speer, K. (2007) 'Global Ocean Meridional Overturning', *Journal*

of *Physical Oceanography*. doi: 10.1175/JPO3130.1.

Lutze, G. F. and Coulbourn, W. T. (1984) 'Recent benthic foraminifera from the continental margin of northwest Africa: Community structure and distribution', *Marine Micropaleontology*. doi: 10.1016/0377-8398(84)90002-1.

Lutze, G. F. and Thiel, H. (1989) 'Epibenthic Foraminifera from elevated microhabitats: *Cibicidoides wuellerstorfi* and *Planulina ariminensis*', *Journal of Foraminiferal Research*. doi: 10.2113/gsjfr.19.2.153.

Mackensen, A. (1987) 'Benthische Foraminiferen auf dem Island-Schottland Rücken: Umwelt-Anzeiger an der Grenze zweier ozeanischer Räume', *Paläontologische Zeitschrift*. doi: 10.1007/BF02985902.

Mackensen, A. *et al.* (1995) 'Deep-sea foraminifera in the South Atlantic Ocean: Ecology and assemblage generation', *Micropaleontology*.

Mackensen, A., Sejrup, H. P. and Jansen, E. (1985) 'The distribution of living benthic foraminifera on the continental slope and rise off southwest Norway', *Marine Micropaleontology*. doi: 10.1016/0377-8398(85)90001-5.

Mallon, J., Glock, N., and Schönfeld, J. (2012) 'The response of benthic foraminifera to low-oxygen conditions of the Peruvian oxygen minimum zone', in *Anoxia: Evidence for Eukaryote Survival and Palaeontological Strategies*. Springer, pp. 305–321.

Marchès, E. *et al.* (2007) 'Contourite drift construction influenced by capture of Mediterranean Outflow Water deep-sea current by the Portimão submarine canyon (Gulf of Cadiz, South Portugal)', *Marine Geology*. doi:

10.1016/j.margeo.2007.03.013.

Marchitto, J., Curry, W. B. and Oppo, D. W. (1998) 'Millennial-scale changes in North Atlantic circulation since the last glaciation', *Nature*. doi: 10.1038/31197.

Marsh, R. *et al.* (2007) 'Controls on sediment geochemistry in the Crozet region', *Deep-Sea Research Part II: Topical Studies in Oceanography*. doi: 10.1016/j.dsr2.2007.06.004.

Martín-Chivelet, J., Fregenal-Martínez, M. A. and Chacón, B. (2003) 'Mid-depth calcareous contourites in the latest Cretaceous of Caravaca (Subbetic Zone, SE Spain). Origin and palaeohydrological significance', *Sedimentary Geology*. doi: 10.1016/S0037-0738(03)00176-3.

Martín-Chivelet, J., Fregenal-Martínez, M. A. and Chacón, B. (2008) 'Chapter 10 Traction Structures in Contourites', *Developments in Sedimentology*. doi: 10.1016/S0070-4571(08)10010-3.

Martin, R.E. & Liddell, W. D. (1991) 'The taphonomy of foraminifera in modern carbonate environments: implications for the formation of foraminiferal assemblages.', in *The Processes of Fossilisation*. London: Belhaven Press, pp. 170–193.

Masson-Delmotte, V. *et al.* (2013) '5th assessment IPCC report, cap.5: Information from Paleoclimate Archives', *Climate Change 2013: The Physical Science Basis. Contribution of Working Group I to the Fifth Assessment Report of the Intergovernmental Panel on Climate Change*. doi: 10.1017/CBO9781107415324.

Masson, D. G. *et al.* (2010) 'Sedimentology and depositional history of Holocene sandy contourites on the lower slope of the Faroe-Shetland Channel, northwest of the UK', *Marine Geology*. doi: 10.1016/j.margeo.2009.10.014.

McCall, J. *et al.* (2005) 'Encyclopedia of Geology', *Elsevier*. doi: 10.1016/B0-12-369396-9/00102-7.

McCave, I. N. (2008) 'Chapter 8 Size Sorting During Transport and Deposition of Fine Sediments. Sortable Silt and Flow Speed', *Developments in Sedimentology*. doi: 10.1016/S0070-4571(08)10008-5.

McCave, I. N., Manighetti, B. and Beveridge, N. A. S. (1995) 'Circulation in the glacial North Atlantic inferred from grain-size measurements', *Nature*. doi: 10.1038/374149a0.

McGann, M. and Sloan, D. (1996) 'Recent introduction of the foraminifer *Trochammina hadai* Uchio into San Francisco Bay, California, USA', *Marine Micropaleontology*. doi: 10.1016/0377-8398(95)00077-1.

Meinke, J., Siedler, G., Zenk, W. (1975) 'Some current observations near the continental slope off Portugal.', *Meteor Forsch.-Ergebn.*, A(16), pp. 15–22.

Mekik, F. (2014) 'Radiocarbon dating of planktonic foraminifer shells: A cautionary tale', *Paleoceanography*. doi: 10.1002/2013PA002532.

Middleton, G. V and Hampton, M. (1976) 'Subaqueous sediment transport and deposition by sediment gravity waves', in *Marine Sediment Transport and Environmental Management*. doi: 10.1080/02626660109492803.

Miguez-Salas, O. and Rodríguez-Tovar, F. J. (2019) 'Stable deep-sea

macrobenthic trace maker associations in disturbed environments from the Eocene Lefkara Formation, Cyprus', *Geobios*. doi: 10.1016/j.geobios.2018.11.002.

Mikhalevich, V. I. (2013) 'New insight into the systematics and evolution of the foraminifera', *Micropaleontology*.

Miller, M. C. and Komar, P. D. (1977) 'The development of sediment threshold curves for unusual environments (Mars) and for inadequately studied materials (foram sands)', *Sedimentology*. doi: 10.1111/j.1365-3091.1977.tb00266.x.

Miller, M. C., McCave, I. N. and Komar, P. D. (1977) 'Threshold of sediment motion under unidirectional currents', *Sedimentology*. doi: 10.1111/j.1365-3091.1977.tb00136.x.

Miramontes, E. *et al.* (2018) 'Morphological control of slope instability in contourites: a geotechnical approach', *Landslides*. doi: 10.1007/s10346-018-0956-6.

Moernaut, J. *et al.* (2014) 'Lacustrine turbidites as a tool for quantitative earthquake reconstruction: New evidence for a variable rupture mode in south central Chile', *Journal of Geophysical Research: Solid Earth*. doi: 10.1002/2013JB010738.

Mojtahid, M. *et al.* (2009) 'Spatial distribution of live benthic foraminifera in the Rhône prodelta: Faunal response to a continental-marine organic matter gradient', *Marine Micropaleontology*. doi: 10.1016/j.marmicro.2008.12.006.

Moraes, M. A. S. *et al.* (2007a) 'Bottom-current reworked Palaeocene-Eocene deep-water reservoirs of the Campos Basin, Brazil', *Geological Society, London, Special Publications*. doi: 10.1144/GSL.SP.2007.276.01.04.



Moraes, M. A. S. *et al.* (2007b) 'Bottom-current reworked Palaeocene-Eocene deep-water reservoirs of the Campos Basin, Brazil', *Geological Society, London, Special Publications*. doi: 10.1144/gsl.sp.2007.276.01.04.

Mulder, T. *et al.* (2003) 'Marine hyperpycnal flows: Initiation, behavior and related deposits. A review', *Marine and Petroleum Geology*. doi: 10.1016/j.marpetgeo.2003.01.003.

Mulder, T. *et al.* (2004) 'Understanding continent-ocean sediment transfer', *Eos*. doi: 10.1029/2004EO270001.

Mulder, T. *et al.* (2006) 'The western part of the Gulf of Cadiz: Contour currents and turbidity currents interactions', *Geo-Marine Letters*. doi: 10.1007/s00367-005-0013-z.

Mulder, T. *et al.* (2009) 'Sediment failures and flows in the Gulf of Cadiz (eastern Atlantic)', *Marine and Petroleum Geology*. doi: 10.1016/j.marpetgeo.2008.02.009.

Mulder, T. and Alexander, J. (2001) 'The physical character of subaqueous sedimentary density flow and their deposits', *Sedimentology*. doi: 10.1046/j.1365-3091.2001.00360.x.

Mulder, T., Faugères, J. C. and Gonthier, E. (2008) 'Chapter 21 Mixed Turbidite-Contourite Systems', *Developments in Sedimentology*. doi: 10.1016/S0070-4571(08)10021-8.

Murray, John William, 1937 (1991) *Ecology and palaeoecology of benthic foraminifera* / John W. Murray. - Version details - Trove, Harlow, Essex, England : Longman Scientific and Technical ; New York : Wiley.

Murray, J. W. (1991) 'Ecology and distribution of planktonic foraminifera', in *Biology of the foraminifera*.

Murray, J. W. (1998) *When does environmental variability become environmental change? The proxy record of benthic foraminifera, Soton eprints*.

Murray, J. W. (2006) *Ecology and applications of benthic foraminifera, Ecology and Applications of Benthic Foraminifera*. doi: 10.1017/CBO9780511535529.

Mutti, E. (1992) 'Turbidite Sandstones', *Special publication, Agip, Milan*, p. 275.

Mutti, E. and Carminatti, M. (2012) 'Deep-water sands of the Brazilian offshore basins', in *AAPG International Conference and Exhibition*. doi: 10.1017/S0305000900012381.

N. Antia, A., Von Bodungen, B. and Peinert, R. (1999) 'Particle flux across the mid-European continental margin', *Deep-Sea Research Part I: Oceanographic Research Papers*. doi: 10.1016/S0967-0637(99)00041-2.

Näkki, P., Setälä, O. and Lehtiniemi, M. (2017) 'Bioturbation transports secondary microplastics to deeper layers in soft marine sediments of the northern Baltic Sea', *Marine Pollution Bulletin*. doi: 10.1016/j.marpolbul.2017.03.065.

Naveira Garabato, A. C. *et al.* (2009) 'Variability of Subantarctic Mode Water and Antarctic Intermediate Water in the Drake Passage during the late-twentieth and early-twenty-first centuries', *Journal of Climate*. doi: 10.1175/2009JCLI2621.1.

Negre, C. *et al.* (2010) 'Reversed flow of Atlantic deep water during the Last Glacial Maximum', *Nature*. doi: 10.1038/nature09508.

Nelson, C. H. *et al.* (1999) 'Influence of the Atlantic inflow and Mediterranean outflow currents on late Quaternary sedimentary facies of the Gulf of Cadiz continental margin', *Marine Geology*. doi: 10.1016/S0025-3227(98)00143-1.

Nielsen, T., Knutz, P. C. and Kuijpers, A. (2008) 'Chapter 16 Seismic Expression of Contourite Depositional Systems', *Developments in Sedimentology*. doi: 10.1016/S0070-4571(08)10016-4.

Nomaki, H. *et al.* (2008) 'Benthic foraminifera as trophic links between phytodetritus and benthic metazoans: Carbon and nitrogen isotopic evidence', *Marine Ecology Progress Series*. doi: 10.3354/meps07309.

O'Brien, N. R., Nakazawa, K. and Tokuhashi, S. (2009) 'Use of clay fabric to distinguish turbiditic and hemipelagic siltstones and silts', in *Deep-Water Turbidite Systems*. doi: 10.1002/9781444304473.ch19.

Orsi, A. H., Johnson, G. C. and Bullister, J. L. (1999) 'Circulation, mixing, and production of Antarctic Bottom Water', *Progress in Oceanography*. doi: 10.1016/S0079-6611(99)00004-X.

Ortiz, J. *et al.* (1999) 'Diffuse spectral reflectance as a proxy for percent carbonate content in North Atlantic sediments', *Paleoceanography*. doi: 10.1029/1998PA900021.

Østby, K. L. and Nagy, J. (1982) 'Foraminiferal distribution in the western Barents Sea, Recent and Quaternary', *Polar Research*. doi: 10.1111/j.1751-8369.1982.tb00472.x.

Øyvind Hammer, David A.T. Harper, and P. D. R. (2001) 'PAST: Paleontological

statistics software package for education and data analysis', *Palaeontologia Electronica*, 4(1), p. 9pp.

Pahnke, K., Goldstein, S. L. and Hemming, S. R. (2008) 'Abrupt changes in antarctic intermediate water circulation over the past 25,000 years', *Nature Geoscience*. doi: 10.1038/ngeo360.

Parsons, J. D., Bush, J. W. M. and Syvitski, J. P. M. (2001) 'Hyperpycnal plume formation from riverine outflows with small sediment concentrations', *Sedimentology*. doi: 10.1046/j.1365-3091.2001.00384.x.

Paull, C. K. *et al.* (2018) 'Powerful turbidity currents driven by dense basal layers', *Nature Communications*. doi: 10.1038/s41467-018-06254-6.

Pawlowski, J. *et al.* (2003) 'The evolution of early Foraminifera', *Proceedings of the National Academy of Sciences*. doi: 10.1073/pnas.2035132100.

Pequegnat, W. E. (1972) 'A deep bottom-current on the Mississippi Cone', in Capurro, L.R.A., Reid, J.L. (Eds.), *Contribution on the Physical Oceanography of the Gulf of Mexico, Texas A&M University Oceanographic Studies 2*. Houston, TX: Gulf Publishing, pp. 65–87.

Pflaumann, U. *et al.* (2003) 'Glacial North Atlantic: Sea-surface conditions reconstructed by GLAMAP 2000', *Paleoceanography*. doi: 10.1029/2002pa000774.

Phleger, F. B. and Soutar, A. (1973) 'Production of Benthic Foraminifera in Three East Pacific Oxygen Minima', *Micropaleontology*. doi: 10.2307/1484973.

Piola, A. R. and Gordon, A. L. (1989) 'Intermediate waters in the southwest South

Atlantic', *Deep Sea Research Part A, Oceanographic Research Papers*. doi: 10.1016/0198-0149(89)90015-0.

Piola, A. R. and Matano, R. P. (2008) 'The South Atlantic Western Boundary Currents Brazil/Falkland (Malvinas) Currents', *Encyclopedia of Ocean Sciences: Second Edition*, (May 2014), pp. 422–430. doi: 10.1016/B978-012374473-9.00358-1.

Poole, R. and Tomczak, M. (1999) 'Optimum multiparameter analysis of the water mass structure in the Atlantic Ocean thermocline', *Deep-Sea Research Part I: Oceanographic Research Papers*. doi: 10.1016/S0967-0637(99)00025-4.

Preu, B. *et al.* (2013) 'Morphosedimentary and hydrographic features of the northern Argentine margin: The interplay between erosive, depositional and gravitational processes and its conceptual implications', *Deep-Sea Research Part I: Oceanographic Research Papers*. doi: 10.1016/j.dsr.2012.12.013.

Prins, M. A. *et al.* (2001) 'The Late Quaternary Sedimentary Record of Reykjanes Ridge, North Atlantic', *Radiocarbon*. doi: 10.1017/S0033822200041606.

R. H. Dott, Jr. (1964) 'Wacke, Graywacke and Matrix--What Approach to Immature Sandstone Classification?', *SEPM Journal of Sedimentary Research*. doi: 10.1306/74D71109-2B21-11D7-8648000102C1865D.

Rahmstorf, S. (2002) 'Ocean circulation and climate during the past 120,000 years', *Nature*. doi: 10.1038/nature01090.

Rahmstorf, S. (2006) 'Thermohaline ocean circulation', *Encyclopedia of Quaternary Science*. doi: 10.1016/B0-44-452747-8/00014-4.

Rathburn, A. E. and Corliss, B. H. (1994) 'The ecology of living (stained) deep-sea benthic foraminifera from the Sulu Sea', *Paleoceanography*. doi: 10.1029/93PA02327.

Rebesco, M. *et al.* (1997) 'The history of sedimentation on the continental rise west of the Antarctic Peninsula', *Geology and Seismic Stratigraphy of the Antarctic Margin*, v.2. doi: 10.1007/BF02202600.

Rebesco, M. *et al.* (2014) 'Contourites and associated sediments controlled by deep-water circulation processes: State-of-the-art and future considerations', *Marine Geology*. doi: 10.1016/j.margeo.2014.03.011.

Reimer, P. J. *et al.* (2013) 'IntCal 13 and Marine 13 radiocarbon age calibration curves 0–50,000 years cal BP', *Radiocarbon*. doi: 10.2458/azu.

Renssen, H. *et al.* (2005) 'Holocene climate evolution in the high-latitude Southern Hemisphere simulated by a coupled atmosphere-sea ice-ocean-vegetation model', *Holocene*. doi: 10.1191/0959683605hl869ra.

Reynolds, L. A. and Thunell, R. C. (1986) 'Seasonal Production and Morphologic Variation of *Neogloboquadrina pachyderma* (Ehrenberg) in the Northeast Pacific', *Micropaleontology*. doi: 10.2307/1485696.

Richter, T. O. *et al.* (2006) 'The Avaatech XRF Core Scanner: technical description and applications to NE Atlantic sediments', *Geological Society, London, Special Publications*. doi: 10.1144/GSL.SP.2006.267.01.03.

Rickaby, R. E. M. and Elderfield, H. (2005) 'Evidence from the high-latitude North Atlantic for variations in Antarctic Intermediate water flow during the last

deglaciation', *Geochemistry, Geophysics, Geosystems*. doi: 10.1029/2004GC000858.

De Rijk, S. *et al.* (2000) 'Organic flux control on bathymetric zonation of Mediterranean benthic foraminifera', in *Marine Micropaleontology*. doi: 10.1016/S0377-8398(00)00037-2.

Rintoul, S. R. (1991) 'South Atlantic Interbasin Exchange', *JOURNAL OF GEOPHYSICAL RESEARCH*. doi: 10.1029/90JC02422.

Roberts, J. (2017) 'Deglacial changes in flow and frontal structure through the Drake Passage Deglacial changes in flow and frontal structure through the Drake Passage', *Earth and Planetary Science Letters*. Elsevier B.V., (July). doi: 10.1016/j.epsl.2017.07.004.

Rogerson, M., Kouwenhoven, T. J., *et al.* (2006) 'Benthic foraminifera of a Miocene canyon and fan', *Marine Micropaleontology*. doi: 10.1016/j.marmicro.2006.06.002.

Rogerson, M., Weaver, P. P. E., Rohling, E. J., Lourens, L. J., Murray, J. W. and Hayes, A. (2006) 'Colour logging as a tool in high-resolution palaeoceanography', in *New Techniques in Sediment Core Analysis*. doi: 10.1144/GSL.SP.2006.267.01.07.

Rogerson, M., Weaver, P. P. E., Rohling, E. J., Lourens, L. J., Murray, J. W. and Hayes, a. (2006) 'Colour logging as a tool in high-resolution palaeoceanography', *Geological Society, London, Special Publications*. doi: 10.1144/GSL.SP.2006.267.01.07.

Rogerson, M., Schönfeld, J. and Leng, M. J. (2011) 'Qualitative and quantitative

approaches in palaeohydrography: A case study from core-top parameters in the Gulf of Cadiz', *Marine Geology*. doi: 10.1016/j.margeo.2010.12.008.

Ronge, T. A. *et al.* (2015) 'Pushing the boundaries: Glacial/interglacial variability of intermediate and deep waters in the southwest Pacific over the last 350,000 years', *Paleoceanography*. doi: 10.1002/2014PA002727.

Van Rooij, D. *et al.* (2010) 'The Le Danois Contourite Depositional System: Interactions between the Mediterranean Outflow Water and the upper Cantabrian slope (North Iberian margin)', *Marine Geology*. doi: 10.1016/j.margeo.2010.03.001.

Roth, P.H. & Berger, W. H. (1975) 'Distribution and dissolution of coccoliths in the South and Central Pacific.', *Cushman Foundation for Foraminiferal Research, Special Publication*, 13, pp. 87–113.

Rothwell, R. G. and Rack, F. R. (2006) 'New techniques in sediment core analysis: an introduction', *Geological Society, London, Special Publications*. doi: 10.1144/GSL.SP.2006.267.01.01.

Rowe, G. T., Polloni, P. T. and Haedrich, R. L. (1982) 'The deep-sea macrobenthos on the continental margin of the northwest Atlantic Ocean', *Deep Sea Research Part A, Oceanographic Research Papers*. doi: 10.1016/0198-0149(82)90113-3.

Sanders, J.E., Freidman, G. . (1997) 'History of petroleum exploration in turbidites and related deepwater deposits.', *Northeastern Geology and Environmental Sciences*, 19, pp. 67–102.

Sanders, J. E. (1963) 'Concepts of fluid mechanics provided by primary



sedimentary structures', *JOURNAL OF SEDIMENTARY RESEARCH*. doi: 10.1306/74D70DF3-2B21-11D7-8648000102C1865D.

Savoie, B., Piper, D. J. W. and Droz, L. (1993) 'Plio-Pleistocene evolution of the Var deep-sea fan off the French Riviera', *Marine and Petroleum Geology*. doi: 10.1016/0264-8172(93)90059-2.

van der Schee, M. *et al.* (2016) 'Evidence of early bottom water current flow after the Messinian Salinity Crisis in the Gulf of Cadiz', *Marine Geology*. doi: 10.1016/j.margeo.2016.04.005.

Schiebel, R. (2002) 'Planktic foraminiferal sedimentation and the marine calcite budget', *Global Biogeochemical Cycles*. doi: 10.1029/2001gb001459.

Schiebel, R. *et al.* (2007) 'Planktic foraminiferal dissolution in the twilight zone', *Deep-Sea Research Part II: Topical Studies in Oceanography*. doi: 10.1016/j.dsr2.2007.01.009.

Schmiedl, G. *et al.* (1998) 'Impact of climatic changes on the benthic foraminiferal fauna in the Ionian Sea during the last 330,000 years', *Paleoceanography*. doi: 10.1029/98PA01864.

Schmiedl, G. *et al.* (2000) 'Trophic control of benthic foraminiferal abundance and microhabitat in the bathyal Gulf of Lions, western Mediterranean Sea', in *Marine Micropaleontology*. doi: 10.1016/S0377-8398(00)00038-4.

Schmiedl, G., Mackensen, A. and Müller, P. J. (1997) 'Recent benthic foraminifera from the eastern South Atlantic Ocean: Dependence on food supply and water masses', *Marine Micropaleontology*. doi: 10.1016/S0377-8398(97)00023-6.

Schmittner, A. (2003) 'Southern Ocean sea ice and radiocarbon ages of glacial bottom waters', *Earth and Planetary Science Letters*. doi: 10.1016/S0012-821X(03)00291-7.

Schönfeld, J. (1997) 'The impact of the Mediterranean Outflow Water (MOW) on benthic foraminiferal assemblages and surface sediments at the southern Portuguese continental margin', *Marine Micropaleontology*. doi: 10.1016/S0377-8398(96)00050-3.

Schönfeld, J. (2001) 'Benthic foraminifera and pore-water oxygen profiles: A re-assessment of species boundary conditions at the western Iberian Margin', *Journal of Foraminiferal Research*. doi: 10.2113/0310086.

Schönfeld, J. (2002a) 'A new benthic foraminiferal proxy for near-bottom current velocities in the Gulf of Cadiz, northeastern Atlantic Ocean', *Deep-Sea Research Part I: Oceanographic Research Papers*. doi: 10.1016/S0967-0637(02)00088-2.

Schönfeld, J. (2002b) 'A new benthic foraminiferal proxy for near-bottom current velocities in the Gulf of Cadiz, northeastern Atlantic Ocean', *Deep-Sea Research Part I: Oceanographic Research Papers*. doi: 10.1016/S0967-0637(02)00088-2.

Schönfeld, J. (2002c) 'Recent benthic foraminiferal assemblages in deep high-energy environments from the Gulf of Cadiz (Spain)', *Marine Micropaleontology*. doi: 10.1016/S0377-8398(01)00039-1.

Schönfeld, J. *et al.* (2012) 'The FOBIMO (FOraminiferal Blo-MOnitoring) initiative-Towards a standardised protocol for soft-bottom benthic foraminiferal monitoring studies', *Marine Micropaleontology*. doi: 10.1016/j.marmicro.2012.06.001.

Schonfeld, J. and Spiegler, D. (1995) 'Benthic Foraminiferal Biostratigraphy of Site 861, Chile Triple Junction, Southeastern Pacific', in *Proceedings of the Ocean Drilling Program, 141 Scientific Results*. doi: 10.2973/odp.proc.sr.141.010.1995.

Schönfeld, J. and Zahn, R. (2000) 'Late Glacial to Holocene history of the Mediterranean outflow. Evidence from benthic foraminiferal assemblages and stable isotopes at the Portuguese margin', *Palaeogeography, Palaeoclimatology, Palaeoecology*. doi: 10.1016/S0031-0182(00)00035-3.

Schröder-Adams, C. J. *et al.* (2008) 'Influence of sediment transport dynamics and ocean floor morphology on benthic foraminifera, offshore Fraser Island, Australia', *Marine Geology*. doi: 10.1016/j.margeo.2008.05.002.

Seiler, W. (1975) 'Tiefenverteilung benthischer Foraminiferen am portugiesischen Kontinentalhang.', *Meteor Forschungsergebnisse, Deutsche Forschungsgemeinschaft, Reihe C Geologie und Geophysik, Gebrüder Bornträger*, C23,(47–94).

Shackleton, N. J. *et al.* (1992) 'Carbon isotope records from pacific surface waters and atmospheric carbon dioxide', *Quaternary Science Reviews*. doi: 10.1016/0277-3791(92)90021-Y.

Shanmugam, G. (1996) 'High-density turbidity currents; are they sandy debris flows?', *Journal of Sedimentary Research*. doi: 10.1306/D426828E-2B26-11D7-8648000102C1865D.

Shanmugam, G. (2003) 'Deep-marine tidal bottom currents and their reworked sands in modern and ancient submarine canyons', *Marine and Petroleum Geology*. doi: 10.1016/S0264-8172(03)00063-1.

Shanmugam, G. (2006) *Deep-water processes and facies models: implications for sandstone petroleum reservoirs - Handbook of petroleum exploration and production 5*, Elsevier. doi: 10.1017/CBO9781107415324.004.

Shanmugam, G. (2008) 'Chapter 5 Deep-water Bottom Currents and their Deposits', *Developments in Sedimentology*. doi: 10.1016/S0070-4571(08)10005-X.

Shanmugam, G. (2012) *New Perspectives on Deep-water Sandstones - Origin, Recognition, Initiation and Reservoir Quality, Handbook of Petroleum Exploration and Production*. doi: 10.1016/B978-0-444-56335-4.00005-9.

Shanmugam, G. (2013) 'New perspectives on deep-water sandstones: Implications', *Petroleum Exploration and Development*. doi: 10.1016/S1876-3804(13)60038-5.

Shanmugam, G. (2016) 'Submarine fans: A critical retrospective (1950–2015)', *Journal of Palaeogeography*. doi: 10.1016/j.jop.2015.08.011.

Shanmugam, G. (2017) 'The Contourite Problem', in *Sediment Provenance*. doi: 10.1016/B978-0-12-803386-9.00009-5.

Shanmugam, G. (2018) 'Slides, Slumps, Debris Flows, Turbidity Currents, Hyperpycnal Flows, and Bottom Currents ☆', in *Reference Module in Earth Systems and Environmental Sciences*. doi: 10.1016/B978-0-12-409548-9.10884-X.

Shanmugam, G., Spalding, T. D. and Rofheart, D. H. (1993) 'Process sedimentology and reservoir quality of deep-marine bottom-current reworked

sands (sandy contourites): an example from the Gulf of Mexico', *American Association of Petroleum Geologists Bulletin*. doi: -.

Shanmugam, G., Spalding, T. D. and Rofheart, D. H. (2014) 'Deep-marine bottom-current reworked sand (pliocene and pleistocene), ewing bank 826 field, Gulf of Mexico', in *Turbidites and Associated Deep-Water Facies*. doi: 10.2110/cor.95.20.0025.

Siani, G. *et al.* (2010) 'Late Glacial to Holocene terrigenous sediment record in the Northern Patagonian margin: Paleoclimate implications', *Palaeogeography, Palaeoclimatology, Palaeoecology*. doi: 10.1016/j.palaeo.2010.07.011.

Singh, A. D. *et al.* (2015) 'Fluctuations of Mediterranean Outflow Water circulation in the Gulf of Cadiz during MIS 5 to 7: Evidence from benthic foraminiferal assemblage and stable isotope records', *Global and Planetary Change*. doi: 10.1016/j.gloplacha.2015.08.005.

Skinner, L. C. *et al.* (2013) 'North atlantic versus southern ocean contributions to a deglacial surge in deep ocean ventilation', *Geology*. doi: 10.1130/G34133.1.

Soetaert, K. and Heip, C. (1995) 'Nematode assemblages of deep-sea and shelf break sites in the North Atlantic and Mediterranean Sea', *Marine Ecology Progress Series*. doi: 10.3354/meps125171.

Soto, M. *et al.* (2011) 'The continental margin of uruguay: Crustal architecture and segmentation', *Marine and Petroleum Geology*. doi: 10.1016/j.marpetgeo.2011.07.001.

Spofforth, D. J. A., Pälike, H. and Green, D. (2008) 'Paleogene record of elemental

concentrations in sediments from the Arctic Ocean obtained by XRF analyses', *Paleoceanography*. doi: 10.1029/2007PA001489.

Stanley, D. J. (1993) 'Model for turbidite-to-contourite continuum and multiple process transport in deep marine settings: examples in the rock record', *Sedimentary Geology*. doi: 10.1016/0037-0738(93)90124-N.

Steig, E. J. *et al.* (1998) 'Synchronous climate changes in Antarctica and the North Atlantic', *Science*. doi: 10.1126/science.282.5386.92.

De Stigter, H. C., Van Der Zwaan, G. J. and Langone, L. (1999) 'Differential rates of benthic foraminiferal test production in surface and subsurface sediment habitats in the southern Adriatic Sea', *Palaeogeography, Palaeoclimatology, Palaeoecology*. doi: 10.1016/S0031-0182(98)00193-X.

Stocker, T. F. and Johnsen, S. J. (2003) 'A minimum thermodynamic model for the bipolar seesaw', *Paleoceanography*. doi: 10.1029/2003PA000920.

Stow, D.A.V., H.G. Reading, and J. D. C. (1996) 'Deep Seas', in *Sedimentary Environments: Processes, Facies and Stratigraphy*. 3rd edn. Oxford: Blackwell Science Ltd.

Stow, D. A. V. (1985) 'Fine-grained sediments in deep water: An overview of processes and facies models', *Geo-Marine Letters: An International Journal of Marine Geology*. doi: 10.1007/BF02629792.

Stow, D. A. V. *et al.* (2002) 'Bottom currents, contourites and deep-sea sediment drifts: current state-of-the-art', *Geological Society, London, Memoirs*. doi: 10.1144/GSL.MEM.2002.022.01.02.

Stow, D. A. V. *et al.* (2009) 'Bedform-velocity matrix: The estimation of bottom current velocity from bedform observations', *Geology*. doi: 10.1130/G25259A.1.

Stow, D. A. V. and Faugères, J. C. (2008) 'Chapter 13 Contourite Facies and the Facies Model', *Developments in Sedimentology*. doi: 10.1016/S0070-4571(08)10013-9.

Stow, D. A. V., Faugères, J. C. and Gonthier, E. (1986) 'Facies distribution and textural variation in Faro Drift contourites: Velocity fluctuation and drift growth', *Marine Geology*. doi: 10.1016/0025-3227(86)90100-3.

Stow, D. A. V., Kahler, G. and Reeder, M. (2002) 'Fossil contourites: type example from an Oligocene palaeoslope system, Cyprus', *Geological Society, London, Memoirs*. doi: 10.1144/GSL.MEM.2002.022.01.31.

Stow, D. A. V. and Lovell, J. P. B. (1979) 'Contourites: Their recognition in modern and ancient sediments', *Earth Science Reviews*. doi: 10.1016/0012-8252(79)90002-3.

Stow, D. A. V. and Shanmugam, G. (1980) 'Sequence of structures in fine-grained turbidites: Comparison of recent deep-sea and ancient flysch sediments', *Sedimentary Geology*. doi: 10.1016/0037-0738(80)90052-4.

Stow, D. A. V. and Tabrez, A. R. (1998) 'Hemipelagites: processes, facies and model', *Geological Society, London, Special Publications*. doi: 10.1144/GSL.SP.1998.129.01.19.

Stow, D. A. V., Viana, A. R. and Faugeres, J. C. (1998) 'Bottom-current-controlled sand deposits - a review of modern shallow- to deep-water environments',

*Sedimentary Geology.*

Stow, D. and Smillie, Z. (2020) 'Distinguishing between deep-water sediment facies: Turbidites, contourites and hemipelagites', *Geosciences (Switzerland)*. doi: 10.3390/geosciences10020068.

Stramma, L. and England, M. (1999) 'On the water masses and mean circulation of the South Atlantic Ocean', *Journal of Geophysical Research: Oceans*. doi: 10.1029/1999JC900139.

Suhr, S. B. *et al.* (2003) 'Selective feeding by benthic foraminifera on phytodetritus on the western Antarctic Peninsula shelf: Evidence from fatty acid biomarker analysis', *Marine Ecology Progress Series*. doi: 10.3354/meps262153.

Suhr, S. B. and Pond, D. W. (2006) 'Antarctic benthic foraminifera facilitate rapid cycling of phytoplankton-derived organic carbon', *Deep-Sea Research Part II: Topical Studies in Oceanography*. doi: 10.1016/j.dsr2.2006.02.002.

Sumner, E. J. *et al.* (2013) 'Can turbidites be used to reconstruct a paleoearthquake record for the central Sumatran margin?', *Geology*. doi: 10.1130/G34298.1.

Susana M. Lebreiro (1 \*), I. Nichol (2003) 'Late Quaternary Turbidite Emplacement on the Horseshoe Abyssal Plain (Iberian Margin)', *SEPM Journal of Sedimentary Research*. doi: 10.1306/d4268658-2b26-11d7-8648000102c1865d.

Talley, L. D. (1999) 'Some aspects of ocean heat transport by the shallow, intermediate and deep overturning circulations', in *Geophysical Monograph Series*. doi: 10.1029/GM112p0001.



- Thomson, J., Croudace, I. W. and Rothwell, R. G. (2006) 'A geochemical application of the ITRAX scanner to a sediment core containing eastern Mediterranean sapropel units', *Geological Society, London, Special Publications*. doi: 10.1144/GSL.SP.2006.267.01.05.
- Thornalley, D. J. R. *et al.* (2011) 'The deglacial evolution of north atlantic deep convection', *Science*. doi: 10.1126/science.1196812.
- Thorpe, S. A. (1976) 'Variability of the mediterranean undercurrent in the Gulf of Cadiz', *Deep Sea Research and Oceanographic Abstracts*. doi: 10.1016/s0011-7471(76)80016-2.
- Tisserand, A. *et al.* (2009) 'African monsoon enhancement during the penultimate glacial period (MIS 6.5 ~ 170 ka) and its atmospheric impact', *Paleoceanography*. doi: 10.1029/2008PA001630.
- Toucanne, S. *et al.* (2007) 'Contourites of the Gulf of Cadiz: A high-resolution record of the paleocirculation of the Mediterranean outflow water during the last 50,000 years', *Palaeogeography, Palaeoclimatology, Palaeoecology*. doi: 10.1016/j.palaeo.2006.10.007.
- Vetter, E. W. and Dayton, P. K. (1998) 'Macrofaunal communities within and adjacent to a detritus-rich submarine canyon system', *Deep-Sea Research Part II: Topical Studies in Oceanography*. doi: 10.1016/S0967-0645(97)00048-9.
- Viana, A. R. (2008) 'Chapter 23 Economic Relevance of Contourites', *Developments in Sedimentology*. doi: 10.1016/S0070-4571(08)10023-1.
- Viana, A. R., Faugères, J. C. and Stow, D. A. V. (1998) 'Bottom-current-controlled

sand deposits - A review of modern shallow- to deep-water environments', *Sedimentary Geology*. doi: 10.1016/S0037-0738(97)00087-0.

Viana, A. R. and Fauglères, J.-C. (1998) 'Upper slope sand deposits: the example of Campos Basin, a latest Pleistocene-Holocene record of the interaction between alongslope and downslope currents', in *Geological Processes on Continental Margins: Sedimentation, Mass-Wasting and Stability*. doi: 10.1144/gsl.sp.1998.129.01.18.

Violante, R. A. *et al.* (2014) 'The Argentine continental shelf: Morphology, sediments, processes and evolution since the last glacial maximum', *Geological Society Memoir*. doi: 10.1144/M41.6.

Violanti, D. (1996) 'Taxonomy and distribution of recent benthic foraminifers from Terra Nova Bay (Ross Sea, Antarctica), oceanographic campaign 1987/1988', *Palaeontographica Italica*, 83, pp. 25–71.

Voigt, I. *et al.* (2013) 'A submarine canyon as a climate archive - Interaction of the antarctic intermediate water with the mar del plata canyon (southwest atlantic)', *Marine Geology*. doi: 10.1016/j.margeo.2013.05.002.

Voigt, I., Chiessi, C. M., Piola, A. R. and Henrich, Rüdiger (2016) 'Holocene changes in Antarctic Intermediate Water flow strength in the Southwest Atlantic', *Palaeogeography, Palaeoclimatology, Palaeoecology*. doi: 10.1016/j.palaeo.2016.09.018.

Voigt, I., Chiessi, C. M., Piola, A. R. and Henrich, Rüdiger (2016) 'Holocene changes in Antarctic Intermediate Water flow strength in the Southwest Atlantic', *Palaeogeography, Palaeoclimatology, Palaeoecology*. doi:

10.1016/j.palaeo.2016.09.018.

Walker, M. (2006) *Quaternary Dating Methods*. Mike J.C. Walker, Wiley, Chichester, West Sussex, England (2005) (286p.)., *Quaternary Geochronology*. doi: 10.1016/j.quageo.2006.08.004.

Warratz, G. *et al.* (2017) 'Deglacial changes in the strength of deep southern component water and sediment supply at the Argentine continental margin', *Paleoceanography*. doi: 10.1002/2016PA003079.

Weltje, G. J. and Tjallingii, R. (2008) 'Calibration of XRF core scanners for quantitative geochemical logging of sediment cores: Theory and application', *Earth and Planetary Science Letters*. doi: 10.1016/j.epsl.2008.07.054.

Wetzel, A., Werner, F. and Stow, D. A. V. (2008) 'Chapter 11 Bioturbation and Biogenic Sedimentary Structures in Contourites', *Developments in Sedimentology*. doi: 10.1016/S0070-4571(08)10011-5.

Xie, R. C., Marcantonio, F. and Schmidt, M. W. (2012) 'Deglacial variability of Antarctic Intermediate Water penetration into the North Atlantic from authigenic neodymium isotope ratios', *Paleoceanography*. doi: 10.1029/2012PA002337.

Xu, J. P. *et al.* (2010) 'Event-driven sediment flux in Hueneme and Mugu submarine canyons, southern California', *Marine Geology*. doi: 10.1016/j.margeo.2009.12.007.

Xu, J. P., Sequeiros, O. E. and Noble, M. A. (2014) 'Sediment concentrations, flow conditions, and downstream evolution of two turbidity currents, Monterey Canyon, USA', *Deep-Sea Research Part I: Oceanographic Research Papers*. doi:

10.1016/j.dsr.2014.04.001.

Yordanova, E. K. and Hohenegger, J. (2007) 'Studies on settling, traction and entrainment of larger benthic foraminiferal tests: Implications for accumulation in shallow marine sediments', *Sedimentology*. doi: 10.1111/j.1365-3091.2007.00881.x.

Žarić, S. *et al.* (2005) 'Sensitivity of planktic foraminifera to sea surface temperature and export production as derived from sediment trap data', *Marine Micropaleontology*. doi: 10.1016/j.marmicro.2005.01.002.

Zenck (1980) 'The sub-Mediterranean undercurrent', *Deep Sea Res.*, A(27), pp. 97–98.

Zhang, L., Liddell, W.D. & Martin, R. E. (1993) 'Hydraulic properties of foraminifera from shallow-water siliciclastic environments: A possible transport indicator in the stratigraphic record.', *Geological Society of America Annual Meeting Abstracts with Programs*, 25(A428).

Van Der Zwaan, G. J. *et al.* (1999) 'Benthic foraminifers: Proxies or problems? A review of paleocological concepts', *Earth Science Reviews*. doi: 10.1016/S0012-8252(99)00011-2.

# APPENDICES

---

# TABLE OF APPENDICES

---

|   |            |
|---|------------|
| <b>APPENDIX 3.1.....</b>                                  | <b>380</b> |
| SIGNIFICANT FORAM COUNTS AND SEDIMENT CHARACTERISTICS.... | 380        |
| <b>APPENDIX 3.2.....</b>                                  | <b>404</b> |
| MICROHABITAT PREFERENCES .....                            | 404        |
| <b>APPENDIX 4.1.....</b>                                  | <b>411</b> |
| SEDIMENTARY LOGS.....                                     | 411        |
| <b>APPENDIX 4.2.....</b>                                  | <b>417</b> |
| GRAIN SIZE TABLES.....                                    | 417        |
| <b>APPENDIX 4.3.....</b>                                  | <b>419</b> |
| FULL ITRAX DATA.....                                      | 419        |
| <b>APPENDIX 6.1.....</b>                                  | <b>424</b> |
| Q-MODE CLUSTERS PER CORE .....                            | 424        |
| <b>APPENDIX 6.2.....</b>                                  | <b>431</b> |
| TAXONOMIC REFERENCES .....                                | 431        |

# APPENDIX 3.1

## SIGNIFICANT FORAM COUNTS AND SEDIMENT CHARACTERISTICS

Cited in Chapter 3 & 6

Table 3.1 Counts of foraminifera contributing >5% of overall assemblage - *B. aculeata* to *F. semimarginata* and sediment characteristics

| Core | Point Depth (cm) | Water Depth (mbsl) | Environment (Contourite/Turbidite) | >63µm (%) | Sediment    | <i>Bullimina aculeata</i> | <i>Bullimina marginata</i> | <i>Bullimina mexicana</i> | <i>Buzasina ringens</i> | <i>Cassidulina laevigata</i> | <i>Cassidulina subglobulosa</i> | <i>Chilostomella oolina</i> | <i>Cibicides lobatulus</i> | <i>Cibicides mundulus</i> | <i>Cibicides refulgens</i> | <i>Cibicides bradyi</i> | <i>Cibicides paucyferma</i> | <i>Cibicides subhadingeri</i> | <i>Cibicides wuellerstorfi</i> | <i>Discorbis spp.</i> | <i>Eggerella bradiana</i> | <i>Ehrenbergina pupa</i> | <i>Epistominella exigua</i> | <i>Fissurina bisulcata</i> | <i>Fissurina semimarginata</i> |
|------|------------------|--------------------|------------------------------------|-----------|-------------|---------------------------|----------------------------|---------------------------|-------------------------|------------------------------|---------------------------------|-----------------------------|----------------------------|---------------------------|----------------------------|-------------------------|-----------------------------|-------------------------------|--------------------------------|-----------------------|---------------------------|--------------------------|-----------------------------|----------------------------|--------------------------------|
| 1    | 2.89             | -2053.1            | C                                  | 23.9      | Sand y Silt | 0                         | 22                         | 0                         | 0                       | 3                            | 14                              | 13                          | 15                         | 0                         | 0                          | 0                       | 0                           | 0                             | 8                              | 0                     | 3                         | 1                        | 1                           | 0                          | 3                              |
| 1    | 8.89             | -2053.1            | C                                  | 27.6      | Sand y Silt | 0                         | 10                         | 0                         | 0                       | 2                            | 16                              | 17                          | 8                          | 0                         | 0                          | 0                       | 6                           | 0                             | 6                              | 0                     | 2                         | 0                        | 1                           | 0                          | 0                              |
| 1    | 14.9             | -2053.1            | C                                  | 25.2      | Sand y Silt | 0                         | 19                         | 0                         | 0                       | 3                            | 12                              | 14                          | 14                         | 0                         | 0                          | 0                       | 9                           | 0                             | 6                              | 0                     | 3                         | 0                        | 1                           | 0                          | 2                              |
| 1    | 16.1             | -2053.1            | C                                  | 29.2      | Sand y Silt | 0                         | 12                         | 0                         | 0                       | 0                            | 26                              | 20                          | 11                         | 0                         | 0                          | 0                       | 3                           | 0                             | 8                              | 0                     | 1                         | 0                        | 0                           | 1                          | 1                              |
| 1    | 24.1             | -2053.1            | C                                  | 25.4      | Sand y Silt | 0                         | 11                         | 0                         | 0                       | 7                            | 21                              | 9                           | 11                         | 0                         | 0                          | 0                       | 3                           | 0                             | 3                              | 0                     | 0                         | 0                        | 0                           | 0                          | 0                              |
| 1    | 35.1             | -2053.1            | C                                  | 27.6      | Sand y Silt | 0                         | 3                          | 0                         | 1                       | 2                            | 6                               | 10                          | 11                         | 0                         | 0                          | 0                       | 2                           | 0                             | 2                              | 0                     | 2                         | 0                        | 0                           | 0                          | 0                              |
| 1    | 45.1             | -2053.1            | C                                  | 28        | Sand y Silt | 0                         | 19                         | 0                         | 0                       | 2                            | 65                              | 22                          | 23                         | 0                         | 0                          | 0                       | 8                           | 0                             | 8                              | 0                     | 0                         | 0                        | 0                           | 0                          | 0                              |
| 1    | 55.1             | -2053.1            | C                                  | 32.9      | Sand y Silt | 0                         | 40                         | 0                         | 0                       | 0                            | 30                              | 31                          | 11                         | 0                         | 1                          | 0                       | 12                          | 0                             | 14                             | 0                     | 0                         | 0                        | 0                           | 0                          | 0                              |
| 1    | 65.1             | -2053.1            | C                                  | 24.2      | Sand y Silt | 1                         | 31                         | 0                         | 1                       | 3                            | 20                              | 18                          | 9                          | 0                         | 3                          | 0                       | 4                           | 0                             | 10                             | 0                     | 1                         | 0                        | 1                           | 0                          | 0                              |
| 1    | 75.1             | -2053.1            | C                                  | 30.6      | Sand y Silt | 2                         | 36                         | 0                         | 0                       | 4                            | 50                              | 19                          | 14                         | 0                         | 1                          | 0                       | 6                           | 0                             | 8                              | 0                     | 0                         | 0                        | 0                           | 0                          | 0                              |
| 1    | 85.1             | -2053.1            | C                                  | 32.4      | Sand y Silt | 0                         | 35                         | 0                         | 0                       | 2                            | 27                              | 21                          | 19                         | 0                         | 0                          | 0                       | 9                           | 0                             | 1                              | 0                     | 1                         | 0                        | 1                           | 0                          | 0                              |
| 1    | 95.1             | -2053.1            | C                                  | 28        | Sand y Silt | 1                         | 31                         | 0                         | 0                       | 4                            | 20                              | 9                           | 12                         | 0                         | 2                          | 0                       | 6                           | 0                             | 18                             | 0                     | 0                         | 0                        | 0                           | 0                          | 0                              |
| 1    | 105.1            | -2053.1            | C                                  | 23.3      | Sand y Silt | 0                         | 17                         | 0                         | 0                       | 4                            | 31                              | 30                          | 7                          | 0                         | 1                          | 0                       | 4                           | 0                             | 16                             | 0                     | 0                         | 0                        | 0                           | 0                          | 0                              |
| 1    | 109.1            | -2053.1            | C                                  | 31.1      | Sand y Silt | 0                         | 4                          | 0                         | 0                       | 1                            | 27                              | 13                          | 5                          | 0                         | 2                          | 0                       | 0                           | 0                             | 6                              | 1                     | 0                         | 1                        | 1                           | 0                          | 0                              |
| 1    | 114.1            | -2053.1            | C                                  | 28.9      | Sand y Silt | 0                         | 11                         | 0                         | 0                       | 1                            | 17                              | 12                          | 16                         | 0                         | 5                          | 0                       | 8                           | 0                             | 9                              | 0                     | 0                         | 0                        | 0                           | 0                          | 9                              |
| 1    | 124.1            | -2053.1            | C                                  | 30.3      | Sand y Silt | 0                         | 59                         | 0                         | 0                       | 5                            | 26                              | 16                          | 11                         | 0                         | 0                          | 0                       | 5                           | 0                             | 24                             | 0                     | 0                         | 0                        | 0                           | 0                          | 0                              |
| 1    | 134.1            | -2053.1            | C                                  | 27.5      | Sand y Silt | 0                         | 5                          | 0                         | 0                       | 2                            | 33                              | 35                          | 11                         | 0                         | 0                          | 0                       | 6                           | 0                             | 12                             | 0                     | 1                         | 1                        | 0                           | 0                          | 0                              |
| 1    | 139.1            | -2053.1            | C                                  | 26.7      | Sand y Silt | 0                         | 8                          | 0                         | 0                       | 1                            | 18                              | 41                          | 12                         | 0                         | 2                          | 0                       | 0                           | 0                             | 1                              | 0                     | 1                         | 0                        | 0                           | 0                          | 2                              |
| 1    | 144.1            | -2053.1            | C                                  | 23.3      | Sand y Silt | 0                         | 9                          | 0                         | 0                       | 1                            | 6                               | 51                          | 12                         | 0                         | 1                          | 0                       | 6                           | 0                             | 9                              | 0                     | 7                         | 0                        | 2                           | 0                          | 8                              |
| 1    | 154.1            | -2053.1            | C                                  | 32.5      | Sand y Silt | 0                         | 34                         | 0                         | 0                       | 2                            | 64                              | 30                          | 33                         | 0                         | 0                          | 0                       | 8                           | 0                             | 7                              | 0                     | 0                         | 0                        | 0                           | 0                          | 2                              |
| 1    | 164.1            | -2053.1            | C                                  | 33.5      | Sand y Silt | 0                         | 25                         | 0                         | 0                       | 5                            | 122                             | 27                          | 29                         | 0                         | 2                          | 0                       | 5                           | 0                             | 11                             | 0                     | 0                         | 0                        | 0                           | 0                          | 3                              |
| 1    | 174.1            | -2053.1            | C                                  | 31.2      | Sand y Silt | 2                         | 22                         | 0                         | 0                       | 4                            | 18                              | 17                          | 17                         | 0                         | 2                          | 0                       | 2                           | 0                             | 8                              | 0                     | 1                         | 0                        | 0                           | 0                          | 0                              |
| 1    | 182.1            | -2053.1            | C                                  | 30.6      | Sand y Silt | 0                         | 27                         | 0                         | 0                       | 2                            | 39                              | 29                          | 11                         | 0                         | 0                          | 0                       | 15                          | 0                             | 13                             | 0                     | 1                         | 0                        | 0                           | 0                          | 1                              |

|    |      |         |   |      |             |   |    |   |    |   |    |    |    |    |   |   |    |   |    |   |   |   |   |   |   |   |
|----|------|---------|---|------|-------------|---|----|---|----|---|----|----|----|----|---|---|----|---|----|---|---|---|---|---|---|---|
| 1  | 186  | -2053.1 | C | 27.9 | Sand y Silt | 0 | 9  | 0 | 0  | 1 | 9  | 20 | 9  | 0  | 1 | 0 | 10 | 0 | 7  | 1 | 2 | 0 | 0 | 0 | 0 | 1 |
| 1  | 191  | -2053.1 | C | 29.8 | Sand y Silt | 0 | 6  | 0 | 0  | 2 | 7  | 21 | 7  | 0  | 2 | 0 | 7  | 0 | 6  | 5 | 0 | 0 | 0 | 0 | 0 | 2 |
| 1  | 201  | -2053.1 | C | 31.5 | Sand y Silt | 0 | 10 | 0 | 0  | 2 | 7  | 28 | 4  | 0  | 1 | 0 | 8  | 0 | 1  | 4 | 3 | 0 | 0 | 0 | 4 |   |
| 1  | 211  | -2053.1 | C | 30.2 | Sand y Silt | 0 | 6  | 0 | 0  | 3 | 9  | 26 | 5  | 0  | 3 | 0 | 10 | 0 | 3  | 1 | 3 | 0 | 0 | 0 | 1 |   |
| 1  | 221  | -2053.1 | C | 31.5 | Sand y Silt | 0 | 8  | 0 | 0  | 1 | 4  | 9  | 5  | 0  | 2 | 0 | 2  | 0 | 3  | 2 | 3 | 0 | 0 | 0 | 2 |   |
| 1  | 231  | -2053.1 | C | 43.9 | Sand y Silt | 1 | 8  | 0 | 0  | 0 | 6  | 8  | 6  | 0  | 1 | 0 | 3  | 0 | 1  | 0 | 6 | 0 | 0 | 0 | 6 |   |
| 1  | 241  | -2053.1 | C | 29.9 | Sand y Silt | 0 | 2  | 0 | 0  | 0 | 4  | 8  | 3  | 0  | 0 | 0 | 3  | 0 | 3  | 2 | 0 | 0 | 0 | 0 | 4 |   |
| 1  | 251  | -2053.1 | T | 28.2 | Silt        | 0 | 1  | 0 | 0  | 0 | 16 | 3  | 1  | 0  | 0 | 0 | 0  | 0 | 2  | 3 | 4 | 0 | 0 | 0 | 2 |   |
| 1  | 261  | -2053.1 | T | 30.1 | Sand y Silt | 0 | 8  | 0 | 0  | 2 | 4  | 67 | 11 | 0  | 2 | 0 | 12 | 0 | 9  | 4 | 1 | 0 | 0 | 0 | 8 |   |
| 1  | 271  | -2053.1 | T | 25.8 | Silt        | 0 | 1  | 0 | 0  | 1 | 4  | 8  | 3  | 0  | 0 | 0 | 1  | 0 | 2  | 0 | 0 | 0 | 0 | 0 | 0 |   |
| 1  | 275  | -2053.1 | T | 24.7 | Silt        | 3 | 2  | 0 | 0  | 3 | 21 | 6  | 10 | 0  | 0 | 0 | 0  | 0 | 9  | 2 | 3 | 0 | 0 | 0 | 2 |   |
| 1  | 277  | -2053.1 | T | 25.1 | Silt        | 0 | 2  | 0 | 0  | 0 | 20 | 10 | 11 | 0  | 0 | 0 | 1  | 0 | 3  | 2 | 7 | 0 | 0 | 0 | 0 |   |
| 1  | 278  | -2053.1 | T | 23   | Sand y Silt | 1 | 2  | 0 | 0  | 0 | 3  | 61 | 5  | 0  | 3 | 0 | 4  | 0 | 4  | 4 | 8 | 0 | 0 | 0 | 3 |   |
| 1  | 279  | -2053.1 | T | 27   | Silt        | 0 | 0  | 0 | 0  | 1 | 0  | 24 | 2  | 0  | 1 | 0 | 2  | 0 | 5  | 1 | 3 | 1 | 0 | 0 | 0 |   |
| 1  | 283  | -2053.1 | T | 15.9 | Clay        | 0 | 0  | 0 | 0  | 1 | 4  | 10 | 1  | 0  | 0 | 0 | 0  | 0 | 2  | 0 | 0 | 0 | 0 | 0 | 0 |   |
| 1  | 287  | -2053.1 | T | 16.5 | Clay        | 0 | 1  | 0 | 0  | 1 | 2  | 19 | 5  | 0  | 1 | 0 | 1  | 0 | 1  | 2 | 0 | 0 | 0 | 0 | 0 |   |
| 1  | 289  | -2053.1 | T | 26.6 | Sand y Silt | 1 | 11 | 0 | 0  | 2 | 3  | 58 | 9  | 0  | 4 | 0 | 2  | 0 | 5  | 0 | 3 | 0 | 0 | 9 | 1 |   |
| 1  | 293  | -2053.1 | T | 29.3 | Sand y Silt | 1 | 3  | 0 | 0  | 0 | 6  | 22 | 7  | 0  | 1 | 0 | 8  | 0 | 8  | 1 | 0 | 0 | 0 | 2 | 0 |   |
| 1  | 300  | -2053.1 | T | 21.1 | Silt        | 0 | 3  | 0 | 0  | 3 | 5  | 16 | 6  | 0  | 1 | 0 | 5  | 0 | 8  | 1 | 2 | 0 | 0 | 0 | 0 |   |
| 1  | 305  | -2053.1 | T | 25.7 | Sand y Silt | 2 | 5  | 0 | 0  | 2 | 6  | 46 | 11 | 0  | 1 | 0 | 5  | 0 | 18 | 0 | 0 | 0 | 0 | 0 | 4 |   |
| 1  | 310  | -2053.1 | T | 25.8 | Silt        | 0 | 0  | 0 | 0  | 1 | 4  | 7  | 5  | 0  | 1 | 0 | 2  | 0 | 2  | 2 | 0 | 0 | 0 | 0 | 2 |   |
| 1  | 315  | -2053.1 | T | 28.2 | Sand y Silt | 0 | 7  | 0 | 0  | 1 | 46 | 3  | 8  | 0  | 2 | 0 | 4  | 0 | 3  | 4 | 0 | 0 | 1 | 0 | 2 |   |
| 1  | 320  | -2053.1 | T | 25.1 | Silt        | 0 | 0  | 0 | 0  | 0 | 2  | 2  | 3  | 0  | 1 | 0 | 0  | 0 | 3  | 4 | 1 | 0 | 0 | 0 | 1 |   |
| 1  | 325  | -2053.1 | T | 29.5 | Silt        | 0 | 1  | 0 | 0  | 1 | 9  | 6  | 2  | 0  | 0 | 0 | 0  | 0 | 0  | 2 | 0 | 0 | 0 | 0 | 0 |   |
| 1  | 330  | -2053.1 | T | 25.7 | Sand y Silt | 3 | 5  | 0 | 0  | 1 | 9  | 45 | 7  | 0  | 1 | 0 | 21 | 0 | 3  | 6 | 0 | 0 | 0 | 2 | 3 |   |
| 1  | 335  | -2053.1 | T | 28.7 | Sand y Silt | 0 | 5  | 0 | 0  | 0 | 5  | 12 | 9  | 0  | 0 | 0 | 5  | 0 | 6  | 5 | 1 | 0 | 0 | 0 | 3 |   |
| 1  | 337  | -2053.1 | T | 25.7 | Silt        | 0 | 17 | 0 | 0  | 1 | 7  | 24 | 3  | 0  | 6 | 0 | 1  | 0 | 10 | 3 | 0 | 0 | 0 | 5 | 3 |   |
| 1  | 341  | -2053.1 | T | 28.2 | Sand y Silt | 3 | 27 | 0 | 0  | 0 | 9  | 32 | 4  | 0  | 2 | 0 | 0  | 0 | 1  | 0 | 1 | 0 | 1 | 0 | 2 |   |
| 1  | 350  | -2053.1 | T | 20.4 | Silt        | 0 | 4  | 0 | 0  | 1 | 12 | 15 | 3  | 0  | 0 | 0 | 5  | 0 | 1  | 0 | 6 | 0 | 0 | 0 | 0 |   |
| 1  | 355  | -2053.1 | T | 27.6 | Silt        | 0 | 11 | 0 | 0  | 0 | 14 | 13 | 3  | 0  | 0 | 0 | 2  | 0 | 4  | 3 | 0 | 0 | 0 | 0 | 2 |   |
| 1  | 361  | -2053.1 | T | 32.4 | Sand y Silt | 1 | 6  | 0 | 0  | 1 | 15 | 8  | 4  | 0  | 0 | 0 | 3  | 0 | 0  | 3 | 0 | 0 | 0 | 0 | 0 |   |
| 1  | 366  | -2053.1 | T | 17.2 | Clay        | 1 | 8  | 0 | 0  | 4 | 9  | 20 | 10 | 0  | 3 | 0 | 5  | 0 | 3  | 8 | 0 | 0 | 0 | 0 | 4 |   |
| 1  | 372  | -2053.1 | T | 20.1 | Silt        | 0 | 2  | 0 | 0  | 1 | 1  | 11 | 3  | 0  | 1 | 0 | 1  | 0 | 1  | 0 | 3 | 0 | 0 | 0 | 0 |   |
| 1  | 376  | -2053.1 | T | 24.6 | Silt        | 0 | 1  | 0 | 0  | 0 | 17 | 10 | 12 | 0  | 1 | 0 | 1  | 0 | 2  | 3 | 0 | 0 | 0 | 0 | 1 |   |
| 1  | 383  | -2053.1 | T | 22.8 | Silt        | 0 | 21 | 0 | 0  | 0 | 3  | 41 | 8  | 0  | 1 | 0 | 0  | 0 | 3  | 4 | 0 | 0 | 0 | 0 | 4 |   |
| 1  | 387  | -2053.1 | T | 19.1 | Clay        | 0 | 0  | 0 | 0  | 0 | 28 | 12 | 7  | 0  | 0 | 0 | 1  | 0 | 3  | 2 | 0 | 0 | 0 | 1 | 0 |   |
| 1  | 391  | -2053.1 | T | 21.3 | Silt        | 0 | 0  | 0 | 0  | 1 | 3  | 7  | 10 | 0  | 3 | 0 | 2  | 0 | 1  | 3 | 0 | 0 | 0 | 0 | 0 |   |
| 1  | 393  | -2053.1 | T | 23.6 | Silt        | 1 | 7  | 0 | 0  | 0 | 2  | 5  | 6  | 0  | 1 | 0 | 0  | 0 | 3  | 3 | 1 | 0 | 0 | 0 | 2 |   |
| 1  | 397  | -2053.1 | T | 26.7 | Sand y Silt | 1 | 10 | 0 | 0  | 0 | 7  | 11 | 6  | 0  | 2 | 0 | 1  | 0 | 3  | 0 | 0 | 0 | 0 | 0 | 3 |   |
| 65 | 1.5  | -1896.6 | C | 30   | Sand y Silt | 0 | 37 | 7 | 0  | 1 | 32 | 11 | 9  | 25 | 0 | 0 | 0  | 0 | 17 | 0 | 0 | 5 | 1 | 2 | 0 |   |
| 65 | 5.5  | -1896.6 | C | 26   | Sand y Silt | 1 | 11 | 7 | 0  | 1 | 14 | 71 | 14 | 0  | 0 | 0 | 0  | 0 | 25 | 0 | 0 | 3 | 1 | 0 | 0 |   |
| 65 | 11.5 | -1896.6 | C | 28.4 | Sand y Silt | 1 | 21 | 8 | 11 | 0 | 15 | 10 | 8  | 25 | 0 | 0 | 0  | 0 | 14 | 0 | 0 | 4 | 1 | 1 | 0 |   |
| 65 | 14.8 | -1896.6 | C | 26.4 | Sand y Silt | 2 | 26 | 6 | 21 | 0 | 32 | 10 | 1  | 18 | 0 | 0 | 0  | 0 | 58 | 0 | 0 | 4 | 0 | 0 | 0 |   |
| 65 | 20.8 | -1896.6 | C | 24.7 | Sand y Silt | 0 | 20 | 5 | 22 | 0 | 33 | 99 | 27 | 0  | 0 | 1 | 0  | 0 | 28 | 0 | 0 | 3 | 0 | 1 | 5 |   |



|    |      |         |   |       |             |   |      |    |   |   |    |      |    |   |   |   |   |   |    |   |   |   |   |   |   |
|----|------|---------|---|-------|-------------|---|------|----|---|---|----|------|----|---|---|---|---|---|----|---|---|---|---|---|---|
| 65 | 26.3 | -1896.6 | C | 24.8  | Sand y Silt | 1 | 31.8 | 27 | 0 | 3 | 35 | 92   | 11 | 0 | 0 | 1 | 0 | 0 | 42 | 0 | 0 | 2 | 1 | 0 | 1 |
| 65 | 26.8 | -1896.6 | C | 24.7  | Sand y Silt | 2 | 28.3 | 17 | 0 | 1 | 38 | 85   | 30 | 0 | 0 | 0 | 0 | 0 | 45 | 0 | 0 | 3 | 1 | 0 | 5 |
| 65 | 35.3 | -1896.6 | C | 27.4  | Sand y Silt | 1 | 16.7 | 13 | 0 | 4 | 9  | 37   | 13 | 0 | 0 | 0 | 0 | 0 | 22 | 0 | 1 | 7 | 0 | 0 | 4 |
| 65 | 45.3 | -1896.6 | C | 27.4  | Sand y Silt | 1 | 13.5 | 18 | 0 | 0 | 7  | 55   | 6  | 0 | 0 | 0 | 0 | 0 | 3  | 0 | 0 | 2 | 1 | 1 | 1 |
| 65 | 55.3 | -1896.6 | C | 25.7  | Sand y Silt | 0 | 13.7 | 19 | 0 | 2 | 14 | 95   | 7  | 0 | 0 | 0 | 0 | 0 | 12 | 0 | 0 | 2 | 0 | 0 | 0 |
| 65 | 65.3 | -1896.6 | C | 24.8  | Sand y Silt | 1 | 15.8 | 27 | 0 | 3 | 16 | 78   | 5  | 0 | 0 | 0 | 0 | 0 | 13 | 0 | 0 | 2 | 0 | 1 | 1 |
| 65 | 75.3 | -1896.6 | C | 26.3  | Sand y Silt | 0 | 12.9 | 0  | 0 | 1 | 4  | 55   | 12 | 0 | 1 | 0 | 0 | 0 | 8  | 0 | 0 | 0 | 0 | 0 | 1 |
| 65 | 85.3 | -1896.6 | C | 30.4  | Sand y Silt | 1 | 11.7 | 0  | 0 | 0 | 26 | 48   | 9  | 0 | 2 | 0 | 0 | 0 | 4  | 0 | 1 | 0 | 0 | 0 | 2 |
| 65 | 95.3 | -1896.6 | T | 18    | Silt        | 0 | 16.5 | 0  | 0 | 0 | 22 | 39   | 3  | 0 | 1 | 0 | 1 | 0 | 3  | 3 | 0 | 0 | 0 | 1 | 0 |
| 65 | 10.5 | -1896.6 | T | 11.3  | Silt        | 0 | 62   | 0  | 0 | 1 | 9  | 21   | 2  | 0 | 2 | 0 | 0 | 0 | 2  | 3 | 0 | 0 | 0 | 0 | 0 |
| 65 | 11.5 | -1896.6 | T | 21.3  | Sand y Silt | 0 | 51   | 0  | 0 | 0 | 24 | 47   | 2  | 0 | 1 | 0 | 0 | 0 | 5  | 0 | 0 | 0 | 0 | 0 | 0 |
| 65 | 12.2 | -1896.6 | T | 17    | Silt        | 1 | 36   | 0  | 0 | 1 | 10 | 35   | 2  | 0 | 2 | 0 | 1 | 0 | 5  | 0 | 0 | 5 | 0 | 0 | 0 |
| 65 | 12.6 | -1896.6 | T | 22.5  | Sand y Silt | 0 | 81   | 0  | 0 | 2 | 13 | 29   | 0  | 0 | 1 | 0 | 0 | 0 | 4  | 0 | 0 | 1 | 0 | 0 | 2 |
| 65 | 13.4 | -1896.6 | T | 15.4  | Clay        | 0 | 38   | 0  | 0 | 0 | 5  | 24   | 2  | 0 | 0 | 0 | 0 | 0 | 6  | 0 | 0 | 0 | 0 | 0 | 1 |
| 65 | 14.4 | -1896.6 | T | 20.4  | Sand y Silt | 0 | 42   | 0  | 0 | 0 | 6  | 54   | 5  | 0 | 2 | 0 | 2 | 0 | 2  | 1 | 0 | 1 | 0 | 2 | 0 |
| 65 | 15.4 | -1896.6 | T | 19.2  | Silt        | 0 | 33   | 0  | 0 | 1 | 9  | 35   | 3  | 0 | 0 | 0 | 1 | 0 | 10 | 4 | 0 | 3 | 0 | 3 | 1 |
| 65 | 16.4 | -1896.6 | T | 25.1  | Sand y Silt | 0 | 10.2 | 0  | 0 | 2 | 12 | 94   | 5  | 0 | 0 | 0 | 0 | 0 | 16 | 4 | 0 | 5 | 0 | 0 | 3 |
| 65 | 17.4 | -1896.6 | T | 18.7  | Silt        | 0 | 52   | 0  | 0 | 0 | 4  | 76   | 3  | 0 | 4 | 0 | 1 | 0 | 3  | 1 | 0 | 0 | 0 | 3 | 3 |
| 65 | 18.4 | -1896.6 | T | 19.2  | Silt        | 1 | 81   | 0  | 0 | 0 | 4  | 74   | 7  | 0 | 1 | 0 | 0 | 0 | 3  | 0 | 2 | 3 | 0 | 1 | 0 |
| 65 | 19.4 | -1896.6 | T | 23.4  | Sand y Silt | 0 | 56   | 0  | 0 | 5 | 11 | 70   | 3  | 0 | 0 | 0 | 0 | 0 | 4  | 0 | 0 | 4 | 0 | 0 | 0 |
| 65 | 20.4 | -1896.6 | T | 18.4  | Silt        | 0 | 46   | 0  | 0 | 3 | 7  | 62   | 2  | 0 | 0 | 0 | 0 | 0 | 3  | 0 | 1 | 1 | 0 | 0 | 5 |
| 65 | 21.4 | -1896.6 | T | 18.4  | Silt        | 0 | 76   | 0  | 0 | 1 | 16 | 77   | 8  | 0 | 0 | 0 | 0 | 0 | 6  | 0 | 1 | 1 | 0 | 0 | 0 |
| 65 | 22.2 | -1896.6 | T | 18    | Silt        | 1 | 13.8 | 0  | 0 | 2 | 19 | 37   | 2  | 0 | 0 | 0 | 0 | 0 | 11 | 0 | 0 | 2 | 0 | 0 | 2 |
| 65 | 22.3 | -1896.6 | T | 21.9  | Sand y Silt | 0 | 44   | 0  | 0 | 2 | 23 | 38   | 4  | 0 | 0 | 0 | 0 | 0 | 5  | 0 | 0 | 4 | 0 | 0 | 1 |
| 65 | 23.2 | -1896.6 | T | 19.2  | Silt        | 0 | 48   | 0  | 0 | 1 | 50 | 49   | 2  | 0 | 0 | 0 | 0 | 0 | 5  | 0 | 0 | 4 | 0 | 0 | 0 |
| 65 | 24.2 | -1896.6 | T | 17.8  | Silt        | 0 | 16.6 | 0  | 0 | 3 | 18 | 74   | 4  | 0 | 0 | 0 | 0 | 0 | 3  | 0 | 0 | 0 | 0 | 0 | 2 |
| 65 | 25.2 | -1896.6 | T | 23.3  | Sand y Silt | 3 | 14.6 | 0  | 0 | 1 | 8  | 43   | 13 | 0 | 2 | 0 | 0 | 0 | 8  | 4 | 0 | 5 | 0 | 0 | 1 |
| 65 | 25.9 | -1896.6 | T | 20.9  | Sand y Silt | 0 | 12.4 | 0  | 0 | 5 | 3  | 11.2 | 10 | 0 | 1 | 0 | 1 | 0 | 8  | 2 | 0 | 0 | 0 | 0 | 3 |
| 65 | 26.1 | -1896.6 | T | 21.7  | Sand y Silt | 2 | 19.4 | 0  | 0 | 3 | 14 | 81   | 5  | 0 | 1 | 0 | 1 | 0 | 10 | 1 | 0 | 2 | 0 | 0 | 0 |
| 65 | 26.9 | -1896.6 | T | 19.8  | Silt        | 1 | 12.4 | 0  | 0 | 0 | 5  | 36   | 4  | 0 | 2 | 0 | 1 | 0 | 5  | 0 | 0 | 0 | 0 | 0 | 3 |
| 65 | 27.9 | -1896.6 | T | 20.1  | Sand y Silt | 1 | 17.8 | 0  | 0 | 0 | 16 | 43   | 4  | 0 | 3 | 0 | 1 | 0 | 3  | 3 | 0 | 0 | 0 | 0 | 2 |
| 65 | 28.9 | -1896.6 | T | 20.7  | Sand y Silt | 0 | 12.6 | 0  | 0 | 8 | 26 | 54   | 3  | 0 | 3 | 0 | 1 | 0 | 6  | 0 | 0 | 1 | 0 | 0 | 3 |
| 65 | 29.9 | -1896.6 | T | 14.7  | Clay        | 0 | 20.3 | 0  | 0 | 4 | 6  | 46   | 1  | 0 | 2 | 0 | 1 | 0 | 4  | 1 | 0 | 0 | 1 | 0 | 0 |
| 65 | 30.9 | -1896.6 | T | 18.2  | Silt        | 0 | 12.7 | 0  | 0 | 4 | 22 | 50   | 2  | 0 | 3 | 0 | 0 | 0 | 6  | 1 | 0 | 0 | 1 | 0 | 2 |
| 65 | 31.7 | -1896.6 | T | 21.9  | Sand y Silt | 1 | 10.1 | 0  | 0 | 6 | 16 | 41   | 8  | 0 | 1 | 0 | 0 | 0 | 5  | 1 | 0 | 0 | 0 | 0 | 3 |
| 65 | 31.7 | -1896.6 | T | 18.8  | Silt        | 0 | 10.3 | 0  | 0 | 0 | 17 | 19   | 3  | 0 | 1 | 0 | 0 | 0 | 6  | 1 | 0 | 0 | 0 | 0 | 4 |
| 65 | 32.7 | -1896.6 | T | 13.9  | Clay        | 0 | 58   | 0  | 0 | 2 | 5  | 19   | 0  | 0 | 2 | 0 | 0 | 0 | 23 | 1 | 0 | 0 | 0 | 0 | 1 |
| 65 | 33.7 | -1896.6 | T | 9.6.8 | Clay        | 1 | 25   | 0  | 0 | 2 | 24 | 16   | 5  | 0 | 0 | 0 | 0 | 0 | 0  | 1 | 0 | 0 | 0 | 0 | 0 |
| 65 | 34.7 | -1896.6 | T | 14.2  | Silt        | 0 | 14.6 | 0  | 0 | 4 | 24 | 60   | 1  | 0 | 0 | 0 | 1 | 0 | 7  | 0 | 0 | 0 | 0 | 0 | 0 |
| 65 | 35.4 | -1896.6 | T | 13.2  | Clay        | 0 | 74   | 0  | 0 | 0 | 20 | 34   | 2  | 0 | 1 | 0 | 0 | 0 | 12 | 2 | 0 | 2 | 0 | 0 | 0 |
| 65 | 35.7 | -1896.6 | T | 14.5  | Clay        | 2 | 74   | 0  | 0 | 4 | 38 | 31   | 5  | 0 | 0 | 0 | 0 | 0 | 5  | 0 | 0 | 0 | 0 | 0 | 2 |
| 65 | 36.6 | -1896.6 | T | 14.1  | Clay        | 0 | 27   | 0  | 0 | 0 | 13 | 15   | 3  | 0 | 0 | 0 | 0 | 0 | 7  | 0 | 0 | 0 | 0 | 0 | 0 |
| 65 | 37.1 | -1896.6 | T | 12.1  | Clay        | 0 | 16   | 0  | 0 | 0 | 11 | 21   | 5  | 0 | 1 | 0 | 1 | 0 | 12 | 2 | 0 | 0 | 0 | 0 | 0 |
| 65 | 37.6 | -1896.6 | T | 14.1  | Clay        | 1 | 30   | 0  | 0 | 2 | 5  | 25   | 4  | 0 | 3 | 0 | 0 | 0 | 9  | 2 | 0 | 0 | 0 | 0 | 1 |

|    |     |      |   |     |        |   |    |   |   |    |    |    |    |   |    |   |    |   |    |    |   |    |   |     |   |
|----|-----|------|---|-----|--------|---|----|---|---|----|----|----|----|---|----|---|----|---|----|----|---|----|---|-----|---|
| 65 | 38  | -    | T | 14. | Clay   | 0 | 59 | 0 | 0 | 2  | 4  | 50 | 1  | 0 | 1  | 0 | 0  | 0 | 2  | 0  | 0 | 0  | 0 | 0   | 1 |
|    | 6   | 1896 |   | 4   |        |   |    |   |   |    |    |    |    |   |    |   |    |   |    |    |   |    |   |     |   |
|    |     | .6   |   |     |        |   |    |   |   |    |    |    |    |   |    |   |    |   |    |    |   |    |   |     |   |
| 65 | 39  | -    | T | 21. | Sand   | 0 | 27 | 0 | 0 | 3  | 14 | 98 | 10 | 0 | 0  | 0 | 0  | 0 | 11 | 0  | 0 | 3  | 0 | 1   | 2 |
|    | 5   | 1896 |   | 1   | y Silt |   | 5  |   |   |    |    |    |    |   |    |   |    |   |    |    |   |    |   |     |   |
|    |     | .6   |   |     |        |   |    |   |   |    |    |    |    |   |    |   |    |   |    |    |   |    |   |     |   |
| 65 | 39  | -    | T | 19. | Silt   | 0 | 26 | 0 | 0 | 0  | 15 | 98 | 12 | 0 | 13 | 0 | 0  | 0 | 14 | 1  | 0 | 0  | 0 | 4   |   |
|    | 6   | 1896 |   | 7   |        |   | 4  |   |   |    |    |    |    |   |    |   |    |   |    |    |   |    |   |     |   |
|    |     | .6   |   |     |        |   |    |   |   |    |    |    |    |   |    |   |    |   |    |    |   |    |   |     |   |
| 65 | 40  | -    | T | 15. | Clay   | 2 | 40 | 0 | 0 | 1  | 0  | 19 | 3  | 0 | 1  | 0 | 0  | 0 | 0  | 0  | 0 | 0  | 0 | 0   |   |
|    | 6   | 1896 |   | 6   |        |   |    |   |   |    |    |    |    |   |    |   |    |   |    |    |   |    |   |     |   |
|    |     | .6   |   |     |        |   |    |   |   |    |    |    |    |   |    |   |    |   |    |    |   |    |   |     |   |
| 65 | 41  | -    | T | 13  | Clay   | 0 | 9  | 0 | 0 | 0  | 0  | 0  | 2  | 0 | 0  | 0 | 0  | 0 | 2  | 0  | 0 | 0  | 0 | 0   |   |
|    | 6   | 1896 |   |     |        |   |    |   |   |    |    |    |    |   |    |   |    |   |    |    |   |    |   |     |   |
|    |     | .6   |   |     |        |   |    |   |   |    |    |    |    |   |    |   |    |   |    |    |   |    |   |     |   |
| 65 | 42  | -    | T | 13. | Clay   | 2 | 15 | 0 | 0 | 2  | 4  | 59 | 7  | 0 | 0  | 0 | 0  | 0 | 8  | 4  | 0 | 0  | 1 | 3   |   |
|    | 6   | 1896 |   | 8   |        |   | 9  |   |   |    |    |    |    |   |    |   |    |   |    |    |   |    |   |     |   |
|    |     | .6   |   |     |        |   |    |   |   |    |    |    |    |   |    |   |    |   |    |    |   |    |   |     |   |
| 65 | 43  | -    | T | 18. | Silt   | 0 | 12 | 0 | 0 | 0  | 11 | 82 | 3  | 0 | 4  | 0 | 0  | 0 | 3  | 1  | 0 | 0  | 0 | 1   |   |
|    | 6   | 1896 |   | 4   |        |   | 9  |   |   |    |    |    |    |   |    |   |    |   |    |    |   |    |   |     |   |
|    |     | .6   |   |     |        |   |    |   |   |    |    |    |    |   |    |   |    |   |    |    |   |    |   |     |   |
| 65 | 43  | -    | T | 23. | Sand   | 1 | 54 | 0 | 0 | 0  | 6  | 28 | 3  | 0 | 1  | 0 | 1  | 0 | 4  | 0  | 0 | 0  | 0 | 1   |   |
|    | 6   | 1896 |   | 6   | y Silt |   |    |   |   |    |    |    |    |   |    |   |    |   |    |    |   |    |   |     |   |
|    |     | .6   |   |     |        |   |    |   |   |    |    |    |    |   |    |   |    |   |    |    |   |    |   |     |   |
| 65 | 44  | -    | T | 13. | Clay   | 2 | 79 | 0 | 0 | 1  | 7  | 64 | 3  | 0 | 3  | 0 | 0  | 0 | 9  | 2  | 0 | 0  | 0 | 0   |   |
|    | 4   | 1896 |   | 7   |        |   |    |   |   |    |    |    |    |   |    |   |    |   |    |    |   |    |   |     |   |
|    |     | .6   |   |     |        |   |    |   |   |    |    |    |    |   |    |   |    |   |    |    |   |    |   |     |   |
| 65 | 45  | -    | T | 18  | Silt   | 1 | 14 | 0 | 0 | 5  | 12 | 76 | 7  | 0 | 11 | 0 | 0  | 0 | 22 | 3  | 0 | 0  | 0 | 1   |   |
|    | 4   | 1896 |   |     |        |   | 4  |   |   |    |    |    |    |   |    |   |    |   |    |    |   |    |   |     |   |
|    |     | .6   |   |     |        |   |    |   |   |    |    |    |    |   |    |   |    |   |    |    |   |    |   |     |   |
| 65 | 46  | -    | T | 14. | Clay   | 3 | 84 | 0 | 0 | 5  | 17 | 60 | 8  | 0 | 6  | 0 | 2  | 0 | 9  | 2  | 0 | 0  | 1 | 0   |   |
|    | 1   | 1896 |   | 1   |        |   |    |   |   |    |    |    |    |   |    |   |    |   |    |    |   |    |   |     |   |
|    |     | .6   |   |     |        |   |    |   |   |    |    |    |    |   |    |   |    |   |    |    |   |    |   |     |   |
| 12 | 7.5 | -    | C | 96. | Silty  | 0 | 0  | 0 | 0 | 0  | 0  | 0  | 0  | 0 | 0  | 0 | 0  | 0 | 0  | 0  | 0 | 0  | 0 | 0   |   |
|    | 5   | 1121 |   | 6   | Sand   |   |    |   |   |    |    |    |    |   |    |   |    |   |    |    |   |    |   |     |   |
|    |     | .2   |   |     |        |   |    |   |   |    |    |    |    |   |    |   |    |   |    |    |   |    |   |     |   |
| 12 | 20. | -    | C | 96. | Silty  | 0 | 95 | 0 | 0 | 54 | 8  | 19 | 26 | 0 | 19 | 0 | 2  | 0 | 23 | 0  | 0 | 1  | 0 | 4   |   |
|    | 5   | 1121 |   | 5   | Sand   |   |    |   |   |    |    |    |    |   |    |   |    |   |    |    |   |    |   |     |   |
|    |     | .2   |   |     |        |   |    |   |   |    |    |    |    |   |    |   |    |   |    |    |   |    |   |     |   |
| 12 | 26  | -    | C | 96. | Silty  | 0 | 91 | 0 | 0 | 11 | 2  | 17 | 9  | 0 | 12 | 0 | 0  | 0 | 61 | 2  | 0 | 15 | 2 | 14  |   |
|    | 5   | 1121 |   | 7   | Sand   |   |    |   |   | 1  |    |    |    |   |    |   |    |   |    |    |   |    |   |     |   |
|    |     | .2   |   |     |        |   |    |   |   |    |    |    |    |   |    |   |    |   |    |    |   |    |   |     |   |
| 12 | 36. | -    | C | 96. | Silty  | 0 | 72 | 0 | 0 | 49 | 1  | 11 | 10 | 0 | 5  | 0 | 0  | 0 | 12 | 5  | 0 | 6  | 0 | 2   |   |
|    | 5   | 1121 |   | 4   | Sand   |   |    |   |   |    |    |    |    |   |    |   |    |   |    |    |   |    |   |     |   |
|    |     | .2   |   |     |        |   |    |   |   |    |    |    |    |   |    |   |    |   |    |    |   |    |   |     |   |
| 12 | 46. | -    | C | 95. | Silty  | 0 | 75 | 0 | 0 | 58 | 5  | 27 | 27 | 0 | 12 | 0 | 1  | 0 | 36 | 3  | 1 | 15 | 0 | 5   |   |
|    | 5   | 1121 |   | 6   | Sand   |   |    |   |   |    |    |    |    |   |    |   |    |   |    |    |   |    |   |     |   |
|    |     | .2   |   |     |        |   |    |   |   |    |    |    |    |   |    |   |    |   |    |    |   |    |   |     |   |
| 12 | 56. | -    | C | 96  | Silty  | 0 | 56 | 0 | 0 | 64 | 6  | 24 | 10 | 0 | 15 | 0 | 0  | 0 | 28 | 11 | 0 | 33 | 0 | 4   |   |
|    | 5   | 1121 |   |     | Sand   |   |    |   |   |    |    |    |    |   |    |   |    |   |    |    |   |    |   |     |   |
|    |     | .2   |   |     |        |   |    |   |   |    |    |    |    |   |    |   |    |   |    |    |   |    |   |     |   |
| 12 | 66. | -    | C | 95. | Silty  | 0 | 52 | 0 | 0 | 50 | 2  | 50 | 13 | 0 | 0  | 0 | 0  | 0 | 22 | 5  | 1 | 10 | 0 | 2   |   |
|    | 5   | 1121 |   | 4   | Sand   |   |    |   |   |    |    |    |    |   |    |   |    |   |    |    |   |    |   |     |   |
|    |     | .2   |   |     |        |   |    |   |   |    |    |    |    |   |    |   |    |   |    |    |   |    |   |     |   |
| 12 | 76. | -    | C | 96. | Silty  | 0 | 40 | 0 | 0 | 47 | 9  | 15 | 7  | 0 | 4  | 0 | 2  | 0 | 27 | 7  | 0 | 4  | 2 | 5   |   |
|    | 5   | 1121 |   | 6   | Sand   |   |    |   |   |    |    |    |    |   |    |   |    |   |    |    |   |    |   |     |   |
|    |     | .2   |   |     |        |   |    |   |   |    |    |    |    |   |    |   |    |   |    |    |   |    |   |     |   |
| 12 | 80  | -    | C | 96. | Silty  | 0 | 40 | 0 | 0 | 41 | 0  | 12 | 3  | 0 | 1  | 0 | 0  | 0 | 18 | 3  | 0 | 6  | 1 | 3   |   |
|    | 5   | 1121 |   | 1   | Sand   |   |    |   |   |    |    |    |    |   |    |   |    |   |    |    |   |    |   |     |   |
|    |     | .2   |   |     |        |   |    |   |   |    |    |    |    |   |    |   |    |   |    |    |   |    |   |     |   |
| 12 | 88  | -    | C | 96. | Silty  | 0 | 24 | 0 | 0 | 29 | 0  | 21 | 7  | 0 | 8  | 0 | 2  | 0 | 11 | 2  | 1 | 8  | 0 | 1   |   |
|    | 5   | 1121 |   | 3   | Sand   |   |    |   |   |    |    |    |    |   |    |   |    |   |    |    |   |    |   |     |   |
|    |     | .2   |   |     |        |   |    |   |   |    |    |    |    |   |    |   |    |   |    |    |   |    |   |     |   |
| 12 | 98  | -    | C | 96. | Silty  | 0 | 35 | 0 | 0 | 48 | 0  | 7  | 3  | 0 | 3  | 0 | 3  | 0 | 12 | 5  | 0 | 9  | 0 | 5   |   |
|    | 5   | 1121 |   | 3   | Sand   |   |    |   |   |    |    |    |    |   |    |   |    |   |    |    |   |    |   |     |   |
|    |     | .2   |   |     |        |   |    |   |   |    |    |    |    |   |    |   |    |   |    |    |   |    |   |     |   |
| 12 | 10  | -    | C | 96. | Silty  | 0 | 34 | 0 | 0 | 41 | 0  | 8  | 5  | 0 | 2  | 0 | 0  | 0 | 12 | 3  | 0 | 11 | 0 | 3   |   |
|    | 5   | 1121 |   | 9   | Sand   |   |    |   |   |    |    |    |    |   |    |   |    |   |    |    |   |    |   |     |   |
|    |     | .2   |   |     |        |   |    |   |   |    |    |    |    |   |    |   |    |   |    |    |   |    |   |     |   |
| 12 | 11  | -    | C | 97. | Silty  | 0 | 34 | 0 | 0 | 55 | 0  | 18 | 13 | 0 | 6  | 0 | 3  | 0 | 16 | 5  | 0 | 12 | 0 | 0   |   |
|    | 5   | 1121 |   | 2   | Sand   |   |    |   |   |    |    |    |    |   |    |   |    |   |    |    |   |    |   |     |   |
|    |     | .2   |   |     |        |   |    |   |   |    |    |    |    |   |    |   |    |   |    |    |   |    |   |     |   |
| 12 | 12  | -    | C | 97. | Silty  | 0 | 40 | 0 | 0 | 47 | 3  | 16 | 11 | 0 | 6  | 0 | 0  | 0 | 25 | 0  | 0 | 13 | 1 | 8   |   |
|    | 5   | 1121 |   | 3   | Sand   |   |    |   |   |    |    |    |    |   |    |   |    |   |    |    |   |    |   |     |   |
|    |     | .2   |   |     |        |   |    |   |   |    |    |    |    |   |    |   |    |   |    |    |   |    |   |     |   |
| 12 | 13  | -    | C | 97. | Silty  | 0 | 43 | 0 | 0 | 45 | 0  | 17 | 7  | 0 | 8  | 0 | 6  | 0 | 9  | 3  | 0 | 12 | 1 | 4   |   |
|    | 5   | 1121 |   | 7   | Sand   |   |    |   |   |    |    |    |    |   |    |   |    |   |    |    |   |    |   |     |   |
|    |     | .2   |   |     |        |   |    |   |   |    |    |    |    |   |    |   |    |   |    |    |   |    |   |     |   |
| 12 | 14  | -    | C | 96. | Silty  | 0 | 55 | 0 | 0 | 96 | 4  | 17 | 10 | 0 | 11 | 0 | 4  | 0 | 12 | 0  | 1 | 0  | 0 | 6   |   |
|    | 5   | 1121 |   | 5   | Sand   |   |    |   |   |    |    |    |    |   |    |   |    |   |    |    |   |    |   |     |   |
|    |     | .2   |   |     |        |   |    |   |   |    |    |    |    |   |    |   |    |   |    |    |   |    |   |     |   |
| 12 | 15  | -    | C | 97  | Silty  | 2 | 73 | 0 | 0 | 88 | 0  | 13 | 9  | 0 | 10 | 0 | 0  | 0 | 13 | 6  | 0 | 0  | 0 | 6   |   |
|    | 5   | 1121 |   |     | Sand   |   |    |   |   |    |    |    |    |   |    |   |    |   |    |    |   |    |   |     |   |
|    |     | .2   |   |     |        |   |    |   |   |    |    |    |    |   |    |   |    |   |    |    |   |    |   |     |   |
| 12 | 15  | -    | C | 96. | Silty  | 0 | 74 | 0 | 0 | 13 | 0  | 26 | 16 | 0 | 18 | 0 | 0  | 0 | 16 | 6  | 0 | 12 | 0 | 0   |   |
|    | 5   | 1121 |   | 8   | Sand   |   |    |   |   | 3  |    |    |    |   |    |   |    |   |    |    |   |    |   |     |   |
|    |     | .2   |   |     |        |   |    |   |   |    |    |    |    |   |    |   |    |   |    |    |   |    |   |     |   |
| 12 | 16  | -    | C | 96. | Silty  | 0 | 78 | 0 | 0 | 16 | 0  | 28 | 13 | 0 | 18 | 0 | 6  | 0 | 22 | 6  | 1 | 2  | 0 | 6   |   |
|    | 5   | 1121 |   | 4   | Sand   |   |    |   |   | 0  |    |    |    |   |    |   |    |   |    |    |   |    |   |     |   |
|    |     | .2   |   |     |        |   |    |   |   |    |    |    |    |   |    |   |    |   |    |    |   |    |   |     |   |
| 12 | 17  | -    | C | 96. | Silty  | 0 | 14 | 0 | 0 | 20 | 0  | 22 | 15 | 0 | 18 | 0 | 4  | 0 | 25 | 8  | 2 | 11 | 0 | 4   |   |
|    | 5   | 1121 |   | 2   | Sand   |   |    |   |   | 7  |    |    |    |   |    |   |    |   |    |    |   |    |   |     |   |
|    |     | .2   |   |     |        |   |    |   |   |    |    |    |    |   |    |   |    |   |    |    |   |    |   |     |   |
| 12 | 18  | -    | C | 97  | Silty  | 0 | 12 | 0 | 0 | 22 | 0  | 45 | 16 | 0 | 18 | 0 | 18 | 0 | 26 | 0  | 0 | 10 | 2 | 4</ |   |

|     |     |         |   |      |             |     |   |   |    |    |    |    |    |    |    |    |    |    |    |    |    |   |   |    |   |
|-----|-----|---------|---|------|-------------|-----|---|---|----|----|----|----|----|----|----|----|----|----|----|----|----|---|---|----|---|
| 125 | 296 | -1121.2 | C | 99.3 | Sand        | 0   | 2 | 0 | 0  | 4  | 0  | 0  | 1  | 0  | 0  | 0  | 0  | 0  | 1  | 1  | 0  | 1 | 3 | 4  | 4 |
| 133 | 105 | -2451   | C | 33.7 | Sand y Silt | 0   | 2 | 0 | 11 | 0  | 0  | 6  | 2  | 0  | 5  | 0  | 10 | 12 | 0  | 0  | 1  | 0 | 0 | 0  | 1 |
| 133 | 145 | -2451   | C | 34   | Sand y Silt | 2   | 0 | 1 | 1  | 0  | 0  | 1  | 1  | 0  | 6  | 1  | 11 | 2  | 0  | 1  | 0  | 0 | 1 | 0  | 1 |
| 133 | 147 | -2451   | C | 26.5 | Sand y Silt | 14  | 4 | 0 | 0  | 1  | 0  | 3  | 0  | 0  | 9  | 0  | 40 | 17 | 0  | 3  | 4  | 0 | 1 | 7  | 2 |
| 133 | 237 | -2451   | C | 31.6 | Sand y Silt | 7   | 2 | 1 | 0  | 0  | 1  | 1  | 2  | 0  | 8  | 0  | 28 | 13 | 0  | 3  | 2  | 0 | 0 | 0  | 0 |
| 133 | 287 | -2451   | C | 32.7 | Sand y Silt | 4   | 1 | 1 | 0  | 0  | 7  | 3  | 2  | 8  | 1  | 0  | 26 | 14 | 0  | 3  | 0  | 0 | 0 | 0  | 1 |
| 133 | 337 | -2451   | C | 31.2 | Sand y Silt | 16  | 1 | 0 | 0  | 1  | 2  | 5  | 4  | 1  | 13 | 0  | 5  | 24 | 3  | 6  | 0  | 0 | 3 | 1  | 0 |
| 133 | 437 | -2451   | C | 30.6 | Sand y Silt | 32  | 0 | 3 | 0  | 2  | 0  | 1  | 3  | 8  | 12 | 0  | 20 | 29 | 9  | 3  | 3  | 0 | 1 | 4  | 0 |
| 133 | 537 | -2451   | C | 23.9 | Sand y Silt | 90  | 3 | 6 | 0  | 1  | 2  | 3  | 6  | 3  | 16 | 0  | 55 | 38 | 10 | 2  | 4  | 0 | 1 | 4  | 1 |
| 133 | 637 | -2451   | C | 32.7 | Sand y Silt | 305 | 1 | 2 | 0  | 12 | 7  | 6  | 21 | 16 | 28 | 0  | 21 | 53 | 17 | 14 | 18 | 0 | 0 | 0  | 2 |
| 133 | 737 | -2451   | C | 32.5 | Sand y Silt | 107 | 0 | 5 | 0  | 8  | 11 | 4  | 5  | 2  | 8  | 0  | 24 | 13 | 12 | 6  | 3  | 1 | 0 | 4  | 0 |
| 133 | 787 | -2451   | C | 30.8 | Sand y Silt | 83  | 4 | 1 | 0  | 1  | 4  | 1  | 5  | 4  | 8  | 0  | 20 | 14 | 2  | 5  | 2  | 0 | 1 | 6  | 2 |
| 133 | 837 | -2451   | C | 32   | Sand y Silt | 24  | 2 | 1 | 0  | 1  | 4  | 5  | 0  | 0  | 2  | 0  | 10 | 7  | 0  | 0  | 2  | 0 | 0 | 2  | 0 |
| 133 | 887 | -2451   | C | 30.8 | Sand y Silt | 13  | 0 | 2 | 0  | 2  | 2  | 4  | 5  | 7  | 3  | 0  | 11 | 24 | 14 | 0  | 2  | 0 | 2 | 4  | 0 |
| 133 | 937 | -2451   | C | 34.1 | Sand y Silt | 1   | 3 | 0 | 0  | 5  | 0  | 7  | 4  | 4  | 6  | 0  | 19 | 24 | 9  | 0  | 5  | 0 | 2 | 3  | 5 |
| 133 | 104 | -2451   | C | 27.9 | Sand y Silt | 0   | 3 | 1 | 0  | 2  | 3  | 3  | 2  | 0  | 5  | 0  | 0  | 1  | 3  | 0  | 3  | 0 | 1 | 1  | 5 |
| 133 | 112 | -2451   | C | 32.1 | Sand y Silt | 44  | 0 | 2 | 0  | 2  | 8  | 7  | 4  | 2  | 6  | 0  | 2  | 11 | 3  | 0  | 3  | 0 | 1 | 3  | 2 |
| 133 | 117 | -2451   | C | 31.4 | Sand y Silt | 0   | 3 | 1 | 0  | 0  | 4  | 3  | 0  | 0  | 1  | 0  | 0  | 6  | 3  | 0  | 1  | 0 | 0 | 0  | 2 |
| 133 | 127 | -2451   | C | 31.8 | Sand y Silt | 0   | 1 | 2 | 0  | 0  | 2  | 4  | 0  | 1  | 1  | 0  | 1  | 1  | 2  | 0  | 0  | 1 | 0 | 0  | 5 |
| 133 | 133 | -2451   | C | 35.9 | Sand y Silt | 0   | 0 | 0 | 0  | 0  | 0  | 2  | 1  | 0  | 0  | 0  | 0  | 1  | 1  | 0  | 0  | 0 | 0 | 1  | 1 |
| 133 | 137 | -2451   | C | 31.3 | Sand y Silt | 0   | 0 | 0 | 0  | 0  | 0  | 0  | 0  | 0  | 0  | 0  | 0  | 1  | 0  | 0  | 0  | 0 | 0 | 0  | 0 |
| 133 | 140 | -2451   | C | 30.4 | Sand y Silt | 0   | 0 | 0 | 0  | 0  | 0  | 0  | 0  | 0  | 0  | 0  | 0  | 0  | 0  | 0  | 0  | 0 | 0 | 0  | 0 |
| 133 | 142 | -2451   | C | 31.6 | Sand y Silt | 0   | 0 | 0 | 0  | 0  | 0  | 0  | 0  | 0  | 0  | 0  | 1  | 0  | 1  | 0  | 0  | 0 | 0 | 0  | 0 |
| 133 | 147 | -2451   | C | 29.5 | Sand y Silt | 0   | 0 | 0 | 0  | 0  | 0  | 0  | 0  | 0  | 0  | 0  | 0  | 0  | 0  | 0  | 0  | 0 | 0 | 0  | 0 |
| 133 | 152 | -2451   | C | 24.3 | Sand y Silt | 0   | 0 | 0 | 0  | 0  | 0  | 0  | 0  | 0  | 0  | 0  | 0  | 0  | 0  | 0  | 0  | 0 | 0 | 0  | 0 |
| 133 | 157 | -2451   | C | 15.7 | Silt        | 0   | 0 | 0 | 0  | 0  | 0  | 0  | 0  | 0  | 0  | 0  | 0  | 0  | 0  | 0  | 0  | 0 | 0 | 0  | 0 |
| 133 | 162 | -2451   | C | 21.2 | Silt        | 0   | 0 | 0 | 0  | 0  | 0  | 0  | 0  | 0  | 0  | 0  | 0  | 0  | 0  | 0  | 0  | 0 | 0 | 0  | 0 |
| 133 | 166 | -2451   | C | 9.7  | Clay        | 0   | 0 | 0 | 0  | 0  | 1  | 1  | 0  | 0  | 0  | 0  | 0  | 0  | 0  | 0  | 0  | 0 | 0 | 0  | 0 |
| 133 | 175 | -2451   | C | 6.7  | Clay        | 0   | 0 | 0 | 0  | 0  | 0  | 0  | 1  | 0  | 0  | 0  | 0  | 0  | 0  | 0  | 0  | 0 | 0 | 0  | 0 |
| 133 | 185 | -2451   | C | 10.9 | Clay        | 0   | 0 | 0 | 0  | 0  | 0  | 0  | 0  | 0  | 0  | 0  | 0  | 0  | 0  | 0  | 0  | 0 | 0 | 0  | 0 |
| 133 | 190 | -2451   | C | 4.6  | Clay        | 0   | 0 | 0 | 0  | 0  | 0  | 0  | 0  | 0  | 0  | 0  | 0  | 0  | 0  | 0  | 0  | 0 | 0 | 1  | 0 |
| 133 | 195 | -2451   | C | 6.3  | Clay        | 0   | 0 | 0 | 0  | 0  | 0  | 0  | 0  | 0  | 0  | 0  | 0  | 0  | 0  | 0  | 0  | 0 | 0 | 0  | 0 |
| 133 | 200 | -2451   | C | 6.3  | Clay        | 0   | 0 | 0 | 0  | 0  | 0  | 0  | 0  | 0  | 0  | 0  | 0  | 0  | 0  | 0  | 0  | 0 | 0 | 0  | 0 |
| 133 | 205 | -2451   | C | 5.4  | Clay        | 0   | 0 | 0 | 0  | 0  | 0  | 0  | 0  | 0  | 0  | 0  | 0  | 0  | 0  | 0  | 0  | 0 | 0 | 0  | 0 |
| 133 | 210 | -2451   | C | 25.1 | Fine Silt   | 0   | 3 | 0 | 0  | 0  | 4  | 0  | 1  | 0  | 2  | 0  | 0  | 1  | 3  | 2  | 5  | 0 | 0 | 2  | 0 |
| 133 | 215 | -2451   | C | 16.1 | Silt        | 0   | 1 | 0 | 0  | 0  | 0  | 0  | 0  | 0  | 1  | 0  | 0  | 1  | 0  | 0  | 0  | 0 | 0 | 0  | 0 |
| 133 | 225 | -2451   | C | 7.1  | Clay        | 0   | 0 | 0 | 0  | 0  | 0  | 0  | 0  | 0  | 0  | 0  | 0  | 0  | 0  | 0  | 0  | 0 | 0 | 0  | 0 |
| 133 | 235 | -2451   | C | 6.5  | Clay        | 0   | 0 | 0 | 0  | 0  | 0  | 0  | 0  | 0  | 0  | 0  | 0  | 0  | 0  | 0  | 0  | 0 | 0 | 0  | 0 |
| 133 | 243 | -2451   | C | 7.5  | Clay        | 0   | 0 | 0 | 0  | 0  | 0  | 0  | 0  | 0  | 0  | 0  | 0  | 0  | 0  | 0  | 0  | 0 | 0 | 0  | 0 |
| 133 | 247 | -2451   | C | 8.8  | Clay        | 0   | 0 | 0 | 0  | 0  | 0  | 0  | 0  | 0  | 0  | 0  | 0  | 0  | 0  | 0  | 0  | 0 | 0 | 0  | 0 |
| 133 | 252 | -2451   | C | 6.0  | Clay        | 0   | 0 | 0 | 0  | 0  | 0  | 0  | 0  | 0  | 0  | 0  | 0  | 0  | 0  | 0  | 0  | 0 | 0 | 0  | 0 |
| 133 | 255 | -2451   | C | 6.4  | Clay        | 0   | 0 | 0 | 0  | 0  | 0  | 0  | 0  | 0  | 0  | 0  | 0  | 0  | 0  | 0  | 0  | 0 | 0 | 0  | 0 |
| 133 | 257 | -2451   | C | 4.8  | Clay        | 0   | 0 | 0 | 0  | 0  | 0  | 0  | 0  | 0  | 0  | 0  | 0  | 0  | 0  | 0  | 0  | 0 | 0 | 0  | 0 |
| 154 | 56  | 3158.5  | C | 29.7 | Sand y Silt | 0   | 0 | 3 | 0  | 2  | 1  | 11 | 0  | 14 | 2  | 12 | 8  | 25 | 4  | 0  | 0  | 1 | 2 | 11 | 7 |



|         |          |                 |   |          |                |    |    |   |   |    |   |    |    |    |    |    |    |    |    |   |   |    |    |   |   |
|---------|----------|-----------------|---|----------|----------------|----|----|---|---|----|---|----|----|----|----|----|----|----|----|---|---|----|----|---|---|
| 16<br>4 | 82<br>5  | -<br>1188<br>.4 | C | 99.<br>1 | Silty<br>Sand  | 0  | 86 | 0 | 0 | 1  | 0 | 7  | 18 | 0  | 15 | 0  | 0  | 0  | 0  | 0 | 0 | 4  | 4  | 1 | 0 |
| 16<br>4 | 92<br>5  | -<br>1188<br>.4 | C | 99.<br>3 | Silty<br>Sand  | 0  | 63 | 0 | 0 | 7  | 0 | 12 | 4  | 1  | 2  | 0  | 0  | 0  | 0  | 0 | 0 | 4  | 4  | 0 | 0 |
| 16<br>4 | 10<br>3  | -<br>1188<br>.4 | C | 99.<br>2 | Silty<br>Sand  | 3  | 46 | 1 | 0 | 12 | 0 | 10 | 8  | 0  | 7  | 0  | 0  | 0  | 0  | 0 | 0 | 13 | 4  | 0 | 0 |
| 16<br>4 | 10<br>6  | -<br>1188<br>.4 | C | 98.<br>7 | Silty<br>Sand  | 2  | 63 | 0 | 0 | 29 | 0 | 14 | 9  | 0  | 4  | 0  | 0  | 0  | 0  | 0 | 0 | 11 | 5  | 0 | 0 |
| 16<br>4 | 11<br>2  | -<br>1188<br>.4 | C | 99.<br>1 | Silty<br>Sand  | 1  | 52 | 0 | 0 | 5  | 0 | 14 | 12 | 0  | 1  | 0  | 0  | 0  | 0  | 0 | 0 | 17 | 8  | 0 | 0 |
| 16<br>4 | 12<br>2  | -<br>1188<br>.4 | C | 99.<br>4 | Silty<br>Sand  | 0  | 9  | 0 | 0 | 0  | 0 | 0  | 3  | 0  | 5  | 0  | 0  | 0  | 0  | 0 | 0 | 1  | 0  | 0 | 0 |
| 16<br>4 | 13<br>2  | -<br>1188<br>.4 | C | 99.<br>2 | Sand<br>y Silt | 0  | 0  | 0 | 0 | 0  | 0 | 0  | 0  | 0  | 0  | 0  | 0  | 0  | 0  | 0 | 0 | 0  | 0  | 0 | 0 |
| 16<br>4 | 14<br>2  | -<br>1188<br>.4 | C | 99.<br>4 | Silty<br>Sand  | 0  | 0  | 0 | 0 | 0  | 0 | 0  | 0  | 0  | 0  | 0  | 0  | 0  | 0  | 0 | 0 | 0  | 0  | 0 | 0 |
| 16<br>4 | 15<br>2  | -<br>1188<br>.4 | C | 99.<br>4 | Silty<br>Sand  | 0  | 0  | 0 | 0 | 0  | 0 | 0  | 0  | 0  | 0  | 0  | 0  | 0  | 0  | 0 | 0 | 0  | 0  | 0 | 0 |
| 16<br>4 | 16<br>3  | -<br>1188<br>.4 | C | 98.<br>6 | Sand<br>y Silt | 0  | 0  | 0 | 0 | 0  | 0 | 0  | 0  | 0  | 0  | 0  | 0  | 0  | 0  | 0 | 0 | 0  | 3  | 0 | 0 |
| 16<br>4 | 17<br>3  | -<br>1188<br>.4 | C | 98.<br>2 | Sand<br>y Silt | 0  | 0  | 0 | 0 | 0  | 0 | 0  | 0  | 0  | 0  | 0  | 0  | 0  | 0  | 0 | 0 | 0  | 2  | 0 | 0 |
| 16<br>4 | 18<br>3  | -<br>1188<br>.4 | C | 99.<br>1 | Sand<br>y Silt | 0  | 1  | 0 | 0 | 0  | 0 | 0  | 0  | 0  | 0  | 0  | 0  | 0  | 0  | 0 | 0 | 0  | 42 | 0 | 0 |
| 16<br>4 | 18<br>3  | -<br>1188<br>.4 | C | 98.<br>4 | Sand<br>y Silt | 0  | 18 | 0 | 0 | 0  | 0 | 0  | 0  | 0  | 0  | 0  | 0  | 0  | 0  | 0 | 0 | 0  | 79 | 0 | 0 |
| 16<br>4 | 19<br>4  | -<br>1188<br>.4 | C | 96.<br>5 | Silty<br>Sand  | 0  | 5  | 0 | 0 | 0  | 0 | 0  | 0  | 0  | 0  | 0  | 0  | 0  | 0  | 0 | 0 | 0  | 0  | 0 | 0 |
| 16<br>4 | 21<br>4  | -<br>1188<br>.4 | C | 96.<br>4 | Silty<br>Sand  | 1  | 1  | 0 | 0 | 0  | 0 | 0  | 0  | 0  | 0  | 0  | 0  | 0  | 0  | 0 | 0 | 0  | 0  | 0 | 0 |
| 16<br>4 | 22<br>4  | -<br>1188<br>.4 | C | 95.<br>1 | Silty<br>Sand  | 2  | 1  | 0 | 0 | 0  | 0 | 0  | 0  | 0  | 0  | 0  | 0  | 0  | 0  | 0 | 0 | 0  | 0  | 0 | 0 |
| 16<br>4 | 23<br>4  | -<br>1188<br>.4 | C | 93.<br>5 | Silty<br>Sand  | 4  | 32 | 0 | 0 | 0  | 0 | 1  | 0  | 0  | 0  | 0  | 0  | 0  | 0  | 0 | 0 | 0  | 0  | 0 | 0 |
| 16<br>4 | 23<br>8  | -<br>1188<br>.4 | C | 92.<br>8 | Sand           | 1  | 1  | 0 | 0 | 0  | 0 | 0  | 0  | 0  | 0  | 0  | 0  | 0  | 0  | 0 | 0 | 0  | 3  | 0 | 0 |
| 16<br>4 | 24<br>4  | -<br>1188<br>.4 | C | 93.<br>4 | Sand           | 0  | 0  | 0 | 0 | 0  | 0 | 0  | 0  | 0  | 0  | 0  | 0  | 0  | 0  | 0 | 0 | 0  | 0  | 0 | 0 |
| 16<br>4 | 25<br>4  | -<br>1188<br>.4 | C | 94.<br>5 | Silty<br>Sand  | 0  | 0  | 0 | 0 | 0  | 0 | 0  | 0  | 0  | 0  | 0  | 0  | 0  | 0  | 0 | 0 | 0  | 0  | 0 | 0 |
| 16<br>4 | 26<br>4  | -<br>1188<br>.4 | C | 92.<br>9 | Silty<br>Sand  | 0  | 0  | 0 | 0 | 0  | 0 | 0  | 0  | 0  | 0  | 0  | 0  | 0  | 0  | 0 | 0 | 0  | 0  | 0 | 0 |
| 16<br>4 | 27<br>4  | -<br>1188<br>.4 | C | 91.<br>5 | Silty<br>Sand  | 0  | 0  | 0 | 0 | 0  | 0 | 0  | 0  | 0  | 0  | 0  | 0  | 0  | 0  | 0 | 0 | 0  | 0  | 0 | 0 |
| 16<br>4 | 27<br>6  | -<br>1188<br>.4 | C | 94.<br>5 | Silty<br>Sand  | 0  | 0  | 0 | 0 | 0  | 0 | 0  | 0  | 0  | 0  | 0  | 0  | 0  | 0  | 0 | 0 | 0  | 0  | 0 | 0 |
| 16<br>4 | 28<br>1  | -<br>1188<br>.4 | C | 99       | Sand<br>y Silt | 0  | 0  | 0 | 0 | 0  | 0 | 0  | 0  | 0  | 0  | 0  | 0  | 0  | 0  | 0 | 0 | 0  | 0  | 0 | 0 |
| 16<br>4 | 29<br>1  | -<br>1188<br>.4 | C | 97.<br>2 | Sand<br>y Silt | 0  | 0  | 0 | 0 | 0  | 0 | 0  | 0  | 0  | 0  | 0  | 0  | 0  | 0  | 0 | 0 | 0  | 0  | 0 | 0 |
| 16<br>4 | 29<br>3  | -<br>1188<br>.4 | C | 95.<br>7 | Silty<br>Sand  | 0  | 1  | 0 | 0 | 0  | 0 | 0  | 0  | 0  | 0  | 0  | 0  | 0  | 0  | 0 | 0 | 0  | 0  | 0 | 0 |
| 16<br>4 | 30<br>1  | -<br>1188<br>.4 | C | 98       | Sand<br>y Silt | 0  | 0  | 0 | 0 | 0  | 0 | 0  | 0  | 0  | 0  | 0  | 0  | 0  | 0  | 0 | 0 | 0  | 0  | 0 | 0 |
| 16<br>4 | 31<br>1  | -<br>1188<br>.4 | C | 93.<br>2 | Silty<br>Sand  | 0  | 0  | 0 | 0 | 0  | 0 | 0  | 0  | 0  | 0  | 0  | 0  | 0  | 0  | 0 | 0 | 0  | 0  | 0 | 0 |
| 16<br>4 | 32<br>1  | -<br>1188<br>.4 | C | 96.<br>2 | Silty<br>Sand  | 0  | 0  | 0 | 0 | 0  | 0 | 0  | 0  | 0  | 0  | 0  | 0  | 0  | 0  | 0 | 0 | 0  | 0  | 0 | 0 |
| 16<br>4 | 33<br>1  | -<br>1188<br>.4 | C | 97.<br>1 | Sand<br>y Silt | 0  | 0  | 0 | 0 | 0  | 0 | 0  | 0  | 0  | 0  | 0  | 0  | 0  | 0  | 0 | 0 | 0  | 0  | 0 | 0 |
| 16<br>4 | 33<br>6  | -<br>1188<br>.4 | C | 96.<br>4 | Silty<br>Sand  | 0  | 0  | 0 | 0 | 0  | 0 | 0  | 0  | 0  | 0  | 0  | 0  | 0  | 0  | 0 | 0 | 0  | 0  | 0 | 0 |
| 16<br>4 | 34<br>6  | -<br>1188<br>.4 | C | 94.<br>8 | Silty<br>Sand  | 0  | 0  | 0 | 0 | 0  | 0 | 0  | 0  | 0  | 0  | 0  | 0  | 0  | 0  | 0 | 0 | 0  | 0  | 0 | 0 |
| 16<br>4 | 35<br>6  | -<br>1188<br>.4 | C | 94.<br>5 | Silty<br>Sand  | 0  | 0  | 0 | 0 | 0  | 0 | 0  | 0  | 0  | 0  | 0  | 0  | 0  | 0  | 0 | 0 | 0  | 0  | 0 | 0 |
| 16<br>4 | 36<br>6  | -<br>1188<br>.4 | C | 93       | Silty<br>Sand  | 0  | 0  | 0 | 0 | 0  | 0 | 0  | 0  | 0  | 0  | 0  | 0  | 0  | 0  | 0 | 0 | 0  | 0  | 0 | 0 |
| 16<br>4 | 38<br>0  | -<br>1188<br>.4 | C | 91.<br>8 | Silty<br>Sand  | 0  | 0  | 0 | 0 | 0  | 0 | 0  | 0  | 0  | 0  | 0  | 0  | 0  | 0  | 0 | 0 | 0  | 0  | 0 | 0 |
| 16<br>4 | 38<br>6  | -<br>1188<br>.4 | C | 92.<br>4 | Silty<br>Sand  | 0  | 0  | 0 | 0 | 0  | 0 | 0  | 0  | 0  | 0  | 0  | 0  | 0  | 0  | 0 | 0 | 0  | 0  | 0 | 0 |
| 16<br>4 | 39<br>6  | -<br>1188<br>.4 | C | 93.<br>9 | Silty<br>Sand  | 0  | 0  | 0 | 0 | 0  | 0 | 0  | 0  | 0  | 0  | 0  | 0  | 0  | 0  | 0 | 0 | 0  | 0  | 0 | 0 |
| 17<br>0 | 5.5      | -<br>2535       | C | 35.<br>2 | Sand<br>y Silt | 0  | 1  | 0 | 0 | 0  | 0 | 1  | 0  | 10 | 3  | 0  | 7  | 1  | 1  | 1 | 0 | 0  | 1  | 1 | 0 |
| 17<br>0 | 14.<br>5 | -<br>2535       | C | 32.<br>2 | Sand<br>y Silt | 0  | 1  | 1 | 0 | 0  | 2 | 1  | 1  | 6  | 3  | 13 | 3  | 12 | 3  | 1 | 0 | 1  | 0  | 0 | 0 |
| 17<br>0 | 15.<br>4 | -<br>2535       | C | 32       | Sand<br>y Silt | 5  | 0  | 2 | 0 | 1  | 0 | 0  | 2  | 22 | 3  | 6  | 13 | 11 | 2  | 0 | 1 | 0  | 2  | 2 | 0 |
| 17<br>0 | 22.<br>4 | -<br>2535       | C | 31.<br>1 | Sand<br>y Silt | 6  | 1  | 5 | 0 | 0  | 3 | 1  | 2  | 2  | 0  | 11 | 20 | 37 | 7  | 0 | 2 | 0  | 0  | 1 | 0 |
| 17<br>0 | 32.<br>4 | -<br>2535       | C | 34.<br>5 | Sand<br>y Silt | 2  | 4  | 2 | 0 | 1  | 0 | 3  | 2  | 5  | 1  | 5  | 11 | 20 | 4  | 1 | 0 | 0  | 0  | 0 | 0 |
| 17<br>0 | 42.<br>4 | -<br>2535       | C | 31.<br>6 | Sand<br>y Silt | 27 | 5  | 6 | 0 | 2  | 2 | 2  | 2  | 5  | 3  | 1  | 17 | 16 | 13 | 3 | 2 | 0  | 0  | 0 | 0 |
| 17<br>0 | 52.<br>4 | -<br>2535       | C | 27       | Sand<br>y Silt | 57 | 0  | 3 | 0 | 9  | 3 | 5  | 2  | 7  | 1  | 2  | 8  | 27 | 2  | 5 | 3 | 0  | 0  | 3 | 1 |

|     |      |       |   |      |             |    |   |   |   |   |   |    |   |    |   |   |    |    |   |   |   |   |   |   |   |
|-----|------|-------|---|------|-------------|----|---|---|---|---|---|----|---|----|---|---|----|----|---|---|---|---|---|---|---|
| 170 | 62.4 | -2535 | C | 31.5 | Sand y Silt | 25 | 0 | 3 | 0 | 5 | 1 | 2  | 1 | 6  | 2 | 7 | 21 | 1  | 2 | 3 | 3 | 0 | 1 | 0 | 0 |
| 170 | 72.4 | -2535 | C | 20.4 | Silt        | 32 | 0 | 1 | 0 | 3 | 1 | 0  | 0 | 1  | 0 | 2 | 5  | 6  | 5 | 3 | 3 | 0 | 1 | 0 | 1 |
| 170 | 82.4 | -2535 | C | 28.6 | Sand y Silt | 29 | 0 | 0 | 0 | 4 | 0 | 2  | 2 | 5  | 2 | 8 | 11 | 8  | 5 | 1 | 2 | 0 | 0 | 2 | 0 |
| 170 | 92.4 | -2535 | C | 31   | Sand y Silt | 64 | 5 | 6 | 0 | 8 | 9 | 2  | 3 | 0  | 2 | 6 | 5  | 20 | 5 | 0 | 2 | 0 | 0 | 1 | 4 |
| 170 | 102  | -2535 | C | 31.1 | Sand y Silt | 26 | 1 | 1 | 0 | 1 | 5 | 7  | 1 | 1  | 5 | 0 | 28 | 4  | 1 | 1 | 0 | 0 | 0 | 2 | 2 |
| 170 | 112  | -2535 | C | 32.1 | Sand y Silt | 27 | 0 | 0 | 0 | 0 | 2 | 13 | 1 | 15 | 2 | 6 | 19 | 3  | 4 | 1 | 1 | 0 | 1 | 4 | 1 |
| 170 | 114  | -2535 | C | 27.1 | Sand y Silt | 38 | 2 | 5 | 0 | 1 | 2 | 10 | 3 | 0  | 2 | 4 | 6  | 4  | 4 | 0 | 1 | 0 | 2 | 0 | 0 |
| 170 | 122  | -2535 | C | 35.5 | Sand y Silt | 30 | 0 | 0 | 0 | 0 | 1 | 5  | 2 | 7  | 5 | 1 | 20 | 4  | 3 | 2 | 0 | 1 | 1 | 2 | 1 |
| 170 | 132  | -2535 | C | 33.2 | Sand y Silt | 5  | 0 | 1 | 0 | 0 | 2 | 4  | 1 | 0  | 4 | 8 | 5  | 15 | 0 | 0 | 4 | 0 | 0 | 0 | 0 |
| 170 | 142  | -2535 | C | 29.6 | Sand y Silt | 1  | 0 | 1 | 0 | 1 | 2 | 6  | 2 | 0  | 5 | 2 | 4  | 7  | 1 | 0 | 0 | 0 | 0 | 4 | 0 |
| 170 | 152  | -2535 | C | 26.1 | Sand y Silt | 0  | 0 | 3 | 0 | 0 | 2 | 8  | 2 | 0  | 0 | 0 | 3  | 7  | 0 | 0 | 0 | 0 | 0 | 0 | 2 |
| 170 | 162  | -2535 | C | 28.2 | Sand y Silt | 1  | 0 | 2 | 0 | 0 | 0 | 1  | 2 | 1  | 3 | 0 | 3  | 6  | 0 | 1 | 0 | 1 | 1 | 0 | 0 |
| 170 | 172  | -2535 | C | 27.4 | Sand y Silt | 5  | 0 | 2 | 0 | 0 | 2 | 0  | 5 | 0  | 0 | 0 | 8  | 2  | 7 | 0 | 0 | 0 | 0 | 0 | 4 |
| 170 | 182  | -2535 | C | 24.2 | Sand y Silt | 0  | 0 | 0 | 0 | 0 | 1 | 0  | 0 | 0  | 0 | 0 | 0  | 0  | 0 | 0 | 0 | 0 | 0 | 0 | 0 |
| 170 | 186  | -2535 | C | 20.1 | Silt        | 0  | 0 | 0 | 0 | 0 | 0 | 1  | 0 | 0  | 1 | 0 | 2  | 2  | 0 | 0 | 0 | 0 | 0 | 0 | 0 |
| 170 | 193  | -2535 | C | 14.7 | Silt        | 0  | 0 | 1 | 0 | 0 | 2 | 0  | 0 | 0  | 0 | 0 | 0  | 0  | 0 | 0 | 0 | 0 | 0 | 0 | 2 |
| 170 | 203  | -2535 | C | 14.4 | Silt        | 0  | 0 | 0 | 0 | 0 | 0 | 0  | 0 | 0  | 1 | 0 | 1  | 0  | 0 | 0 | 0 | 0 | 0 | 0 | 1 |
| 170 | 213  | -2535 | C | 6.71 | Clay        | 0  | 0 | 0 | 0 | 0 | 0 | 0  | 0 | 0  | 0 | 0 | 0  | 0  | 0 | 0 | 0 | 0 | 0 | 0 | 0 |
| 170 | 223  | -2535 | C | 7.2  | Clay        | 0  | 0 | 0 | 0 | 0 | 0 | 0  | 0 | 0  | 0 | 0 | 0  | 0  | 0 | 0 | 0 | 0 | 0 | 0 | 0 |
| 170 | 233  | -2535 | C | 9.19 | Clay        | 0  | 0 | 0 | 0 | 0 | 0 | 0  | 0 | 0  | 0 | 0 | 0  | 0  | 0 | 0 | 0 | 0 | 0 | 0 | 0 |
| 170 | 243  | -2535 | C | 7.75 | Clay        | 0  | 0 | 0 | 0 | 0 | 0 | 0  | 0 | 0  | 0 | 0 | 0  | 0  | 0 | 0 | 0 | 0 | 0 | 0 | 0 |
| 170 | 253  | -2535 | C | 9.26 | Clay        | 0  | 0 | 0 | 0 | 0 | 0 | 0  | 0 | 0  | 0 | 0 | 0  | 0  | 0 | 0 | 0 | 0 | 0 | 0 | 0 |
| 170 | 262  | -2535 | C | 7.6  | Clay        | 0  | 0 | 0 | 0 | 0 | 0 | 0  | 0 | 0  | 0 | 0 | 0  | 0  | 0 | 0 | 0 | 0 | 0 | 0 | 0 |
| 170 | 263  | -2535 | C | 8.88 | Clay        | 0  | 0 | 0 | 0 | 0 | 0 | 0  | 0 | 0  | 0 | 0 | 0  | 0  | 0 | 0 | 0 | 0 | 0 | 0 | 0 |
| 170 | 271  | -2535 | C | 13   | Silt        | 0  | 0 | 0 | 0 | 0 | 0 | 0  | 0 | 0  | 0 | 0 | 0  | 0  | 0 | 0 | 0 | 0 | 0 | 0 | 0 |
| 170 | 281  | -2535 | C | 11.7 | Silt        | 0  | 0 | 0 | 0 | 0 | 0 | 0  | 0 | 0  | 0 | 0 | 0  | 0  | 0 | 0 | 0 | 0 | 0 | 0 | 0 |
| 170 | 291  | -2535 | C | 14.4 | Silt        | 0  | 0 | 0 | 0 | 0 | 0 | 0  | 0 | 0  | 0 | 0 | 0  | 0  | 0 | 0 | 0 | 0 | 0 | 0 | 0 |
| 170 | 301  | -2535 | C | 11.9 | Silt        | 0  | 0 | 0 | 0 | 0 | 0 | 0  | 0 | 0  | 0 | 0 | 0  | 0  | 0 | 0 | 0 | 0 | 0 | 0 | 0 |
| 170 | 311  | -2535 | C | 12.3 | Silt        | 0  | 0 | 0 | 0 | 0 | 0 | 0  | 0 | 0  | 0 | 0 | 0  | 0  | 0 | 0 | 0 | 0 | 0 | 0 | 0 |
| 170 | 321  | -2535 | C | 14.3 | Silt        | 0  | 0 | 0 | 0 | 0 | 0 | 0  | 0 | 0  | 0 | 0 | 0  | 0  | 0 | 0 | 0 | 0 | 0 | 0 | 0 |
| 170 | 327  | -2535 | C | 13.1 | Silt        | 0  | 0 | 0 | 0 | 0 | 0 | 0  | 0 | 0  | 0 | 0 | 0  | 0  | 0 | 0 | 0 | 0 | 0 | 0 | 0 |

Table 3.2 Counts of foraminifera contributing >5% of overall assemblage - *G. americana* to *P. nasuta* and sediment characteristics

| Core | Point Depth (cm) | Water Depth (mbs) | Environment (Contourite/Turbidite) | >63µm (%) | Sediment   | <i>Glaphyrammina americana</i> | <i>Glandulina ovula</i> | <i>Globobulimina affinis</i> | <i>Globobulimina turgida</i> | <i>Globocassidulina subglobulosa</i> | <i>Gyroidina solidani</i> | <i>Hoeglundia elegans</i> | <i>Hyperammina elongata</i> | <i>Lagena laevis</i> | <i>Melonis affinis</i> | <i>Melonis barleeanus</i> | <i>Nonion barleeanum</i> | <i>Nonionella atlantica</i> | <i>Nonionella auris</i> | <i>Nonionella stella</i> | <i>Nonionella turgida</i> | <i>Oolina globulosa</i> | <i>Oridorsalis umbonatus</i> | <i>Planulina ariminhensis</i> | <i>Pygo murrhina</i> | <i>Pygo nasuta</i> |
|------|------------------|-------------------|------------------------------------|-----------|------------|--------------------------------|-------------------------|------------------------------|------------------------------|--------------------------------------|---------------------------|---------------------------|-----------------------------|----------------------|------------------------|---------------------------|--------------------------|-----------------------------|-------------------------|--------------------------|---------------------------|-------------------------|------------------------------|-------------------------------|----------------------|--------------------|
| 1    | 2.89             | -205.3.1          | C                                  | 23.9      | Sandy Silt | 0                              | 0                       | 2                            | 26                           | 0                                    | 9                         | 0                         | 0                           | 1                    | 0                      | 0                         | 0                        | 0                           | 0                       | 0                        | 0                         | 0                       | 3                            | 2                             | 0                    | 1                  |
| 1    | 8.89             | -205.3.1          | C                                  | 27.6      | Sandy Silt | 0                              | 0                       | 1                            | 16                           | 0                                    | 2                         | 0                         | 0                           | 1                    | 1                      | 0                         | 0                        | 0                           | 0                       | 5                        | 0                         | 0                       | 0                            | 3                             | 0                    | 2                  |
| 1    | 14.9             | -205.3.1          | C                                  | 25.2      | Sandy Silt | 0                              | 0                       | 1                            | 17                           | 0                                    | 2                         | 1                         | 0                           | 0                    | 0                      | 0                         | 0                        | 0                           | 0                       | 3                        | 0                         | 0                       | 1                            | 0                             | 0                    | 1                  |
| 1    | 16.1             | -205.3.1          | C                                  | 29.2      | Sandy Silt | 2                              | 0                       | 1                            | 12                           | 0                                    | 10                        | 0                         | 0                           | 1                    | 0                      | 0                         | 0                        | 0                           | 0                       | 0                        | 0                         | 0                       | 2                            | 0                             | 1                    | 0                  |
| 1    | 24.1             | -205.3.1          | C                                  | 25.4      | Sandy Silt | 0                              | 0                       | 0                            | 19                           | 0                                    | 5                         | 1                         | 0                           | 0                    | 1                      | 0                         | 0                        | 1                           | 4                       | 3                        | 10                        | 0                       | 3                            | 2                             | 0                    | 1                  |
| 1    | 35.1             | -205.3.1          | C                                  | 27.6      | Sandy Silt | 0                              | 0                       | 1                            | 10                           | 0                                    | 2                         | 1                         | 0                           | 0                    | 1                      | 0                         | 0                        | 3                           | 0                       | 2                        | 4                         | 0                       | 1                            | 0                             | 0                    | 0                  |
| 1    | 45.1             | -205.3.1          | C                                  | 28        | Sandy Silt | 0                              | 0                       | 3                            | 32                           | 0                                    | 9                         | 6                         | 0                           | 1                    | 0                      | 0                         | 0                        | 0                           | 0                       | 1                        | 0                         | 0                       | 2                            | 3                             | 0                    | 2                  |
| 1    | 55.1             | -205.3.1          | C                                  | 32.9      | Sandy Silt | 0                              | 0                       | 0                            | 14                           | 0                                    | 2                         | 2                         | 0                           | 2                    | 0                      | 0                         | 0                        | 1                           | 0                       | 0                        | 0                         | 1                       | 4                            | 0                             | 5                    | 0                  |
| 1    | 65.1             | -205.3.1          | C                                  | 24.2      | Sandy Silt | 0                              | 0                       | 2                            | 22                           | 0                                    | 4                         | 0                         | 0                           | 1                    | 0                      | 0                         | 0                        | 1                           | 1                       | 0                        | 0                         | 0                       | 5                            | 2                             | 2                    | 3                  |
| 1    | 75.1             | -205.3.1          | C                                  | 30.6      | Sandy Silt | 0                              | 0                       | 2                            | 13                           | 0                                    | 1                         | 1                         | 0                           | 1                    | 0                      | 0                         | 0                        | 0                           | 0                       | 1                        | 2                         | 0                       | 6                            | 2                             | 1                    | 1                  |
| 1    | 85.1             | -205.3.1          | C                                  | 32.4      | Sandy Silt | 0                              | 0                       | 3                            | 12                           | 0                                    | 3                         | 0                         | 0                           | 2                    | 2                      | 0                         | 0                        | 0                           | 0                       | 0                        | 0                         | 0                       | 5                            | 2                             | 1                    | 5                  |
| 1    | 95.1             | -205.3.1          | C                                  | 28        | Sandy Silt | 0                              | 0                       | 3                            | 17                           | 0                                    | 4                         | 0                         | 0                           | 0                    | 1                      | 0                         | 0                        | 0                           | 0                       | 0                        | 0                         | 0                       | 5                            | 4                             | 0                    | 1                  |
| 1    | 10.5             | -205.3.1          | C                                  | 23.3      | Sandy Silt | 0                              | 0                       | 2                            | 7                            | 0                                    | 6                         | 1                         | 0                           | 0                    | 0                      | 0                         | 0                        | 0                           | 1                       | 0                        | 0                         | 0                       | 0                            | 4                             | 5                    | 0                  |
| 1    | 10.9             | -205.3.1          | C                                  | 31.1      | Sandy Silt | 0                              | 0                       | 2                            | 15                           | 0                                    | 1                         | 2                         | 0                           | 0                    | 0                      | 0                         | 0                        | 0                           | 0                       | 0                        | 0                         | 0                       | 0                            | 2                             | 0                    | 0                  |
| 1    | 11.4             | -205.3.1          | C                                  | 28.9      | Sandy Silt | 0                              | 0                       | 2                            | 12                           | 0                                    | 2                         | 1                         | 0                           | 0                    | 0                      | 0                         | 0                        | 0                           | 0                       | 1                        | 1                         | 1                       | 3                            | 4                             | 0                    | 1                  |
| 1    | 12.4             | -205.3.1          | C                                  | 30.3      | Sandy Silt | 0                              | 0                       | 2                            | 19                           | 0                                    | 5                         | 0                         | 0                           | 1                    | 0                      | 0                         | 0                        | 0                           | 0                       | 0                        | 0                         | 0                       | 6                            | 14                            | 1                    | 3                  |
| 1    | 13.4             | -205.3.1          | C                                  | 27.5      | Sandy Silt | 0                              | 0                       | 1                            | 18                           | 0                                    | 1                         | 0                         | 0                           | 1                    | 0                      | 0                         | 0                        | 4                           | 0                       | 12                       | 1                         | 0                       | 3                            | 3                             | 4                    | 0                  |
| 1    | 13.9             | -205.3.1          | C                                  | 26.7      | Sandy Silt | 0                              | 0                       | 2                            | 11                           | 0                                    | 2                         | 0                         | 0                           | 2                    | 2                      | 0                         | 0                        | 2                           | 4                       | 8                        | 1                         | 2                       | 1                            | 3                             | 0                    | 0                  |
| 1    | 14.4             | -205.3.1          | C                                  | 23.3      | Sandy Silt | 0                              | 0                       | 2                            | 15                           | 0                                    | 1                         | 0                         | 0                           | 0                    | 4                      | 0                         | 0                        | 2                           | 0                       | 4                        | 0                         | 0                       | 4                            | 6                             | 1                    | 0                  |
| 1    | 15.4             | -205.3.1          | C                                  | 32.5      | Sandy Silt | 0                              | 1                       | 1                            | 17                           | 0                                    | 7                         | 0                         | 0                           | 0                    | 0                      | 0                         | 0                        | 0                           | 0                       | 1                        | 0                         | 0                       | 4                            | 2                             | 0                    | 1                  |
| 1    | 16.4             | -205.3.1          | C                                  | 33.5      | Sandy Silt | 0                              | 0                       | 6                            | 42                           | 0                                    | 5                         | 0                         | 0                           | 0                    | 1                      | 0                         | 0                        | 0                           | 0                       | 1                        | 0                         | 0                       | 5                            | 7                             | 5                    | 0                  |
| 1    | 17.4             | -205.3.1          | C                                  | 31.2      | Sandy Silt | 0                              | 0                       | 2                            | 13                           | 0                                    | 7                         | 0                         | 0                           | 2                    | 1                      | 0                         | 0                        | 0                           | 0                       | 5                        | 0                         | 0                       | 2                            | 6                             | 1                    | 0                  |
| 1    | 18.2             | -205.3.1          | C                                  | 30.6      | Sandy Silt | 0                              | 0                       | 4                            | 26                           | 0                                    | 6                         | 0                         | 0                           | 2                    | 0                      | 0                         | 0                        | 0                           | 0                       | 2                        | 0                         | 0                       | 4                            | 0                             | 0                    | 1                  |
| 1    | 18.6             | -205.3.1          | C                                  | 27.9      | Sandy Silt | 0                              | 0                       | 4                            | 11                           | 0                                    | 6                         | 1                         | 0                           | 1                    | 1                      | 0                         | 0                        | 0                           | 0                       | 0                        | 0                         | 0                       | 2                            | 5                             | 1                    | 0                  |
| 1    | 19.1             | -205.3.1          | C                                  | 29.8      | Sandy Silt | 2                              | 0                       | 3                            | 16                           | 0                                    | 2                         | 1                         | 0                           | 0                    | 0                      | 0                         | 0                        | 1                           | 1                       | 0                        | 0                         | 0                       | 5                            | 0                             | 0                    | 0                  |
| 1    | 20.1             | -205.3.1          | C                                  | 31.5      | Sandy Silt | 0                              | 0                       | 3                            | 16                           | 0                                    | 3                         | 0                         | 0                           | 0                    | 1                      | 0                         | 0                        | 0                           | 3                       | 0                        | 0                         | 0                       | 2                            | 1                             | 0                    | 1                  |
| 1    | 21.1             | -205.3.1          | C                                  | 30.2      | Sandy Silt | 0                              | 0                       | 3                            | 20                           | 0                                    | 3                         | 0                         | 0                           | 0                    | 0                      | 0                         | 0                        | 1                           | 0                       | 0                        | 1                         | 1                       | 1                            | 0                             | 2                    | 2                  |
| 1    | 22.1             | -205.3.1          | C                                  | 31.5      | Sandy Silt | 0                              | 0                       | 0                            | 7                            | 0                                    | 0                         | 0                         | 0                           | 0                    | 0                      | 0                         | 0                        | 4                           | 0                       | 1                        | 0                         | 0                       | 2                            | 2                             | 0                    | 0                  |
| 1    | 23.1             | -205.3.1          | C                                  | 43.9      | Sandy Silt | 0                              | 0                       | 2                            | 5                            | 0                                    | 3                         | 0                         | 0                           | 0                    | 0                      | 0                         | 0                        | 0                           | 0                       | 1                        | 0                         | 0                       | 1                            | 0                             | 0                    | 0                  |
| 1    | 24.1             | -205.3.1          | C                                  | 29.9      | Sandy Silt | 0                              | 0                       | 0                            | 6                            | 0                                    | 1                         | 0                         | 0                           | 2                    | 0                      | 0                         | 0                        | 0                           | 3                       | 0                        | 0                         | 0                       | 0                            | 0                             | 0                    | 0                  |
| 1    | 25.1             | -205.3.1          | T                                  | 28.2      | Silt       | 0                              | 0                       | 0                            | 1                            | 0                                    | 1                         | 0                         | 0                           | 0                    | 0                      | 0                         | 0                        | 0                           | 0                       | 2                        | 0                         | 0                       | 0                            | 0                             | 0                    | 0                  |

|    |    |     |   |    |      |    |   |    |    |   |   |   |   |   |   |   |    |    |    |    |   |   |    |   |   |   |
|----|----|-----|---|----|------|----|---|----|----|---|---|---|---|---|---|---|----|----|----|----|---|---|----|---|---|---|
| 1  | 26 | -   | T | 30 | Sand | 0  | 0 | 2  | 13 | 0 | 2 | 2 | 0 | 0 | 1 | 0 | 0  | 6  | 5  | 0  | 0 | 1 | 1  | 4 | 0 | 0 |
| 1  | 27 | 205 | T | 25 | Silt | 0  | 0 | 2  | 17 | 0 | 0 | 0 | 0 | 0 | 0 | 0 | 1  | 0  | 0  | 0  | 0 | 2 | 2  | 1 | 1 |   |
| 1  | 27 | -   | T | 24 | Silt | 0  | 0 | 0  | 6  | 0 | 0 | 0 | 0 | 0 | 0 | 0 | 3  | 3  | 0  | 0  | 0 | 1 | 5  | 0 | 0 |   |
| 1  | 27 | 205 | T | 25 | Silt | 0  | 0 | 3  | 17 | 0 | 3 | 0 | 0 | 0 | 0 | 0 | 1  | 1  | 0  | 1  | 0 | 1 | 0  | 0 | 1 |   |
| 1  | 27 | -   | T | 23 | Sand | 0  | 0 | 1  | 18 | 0 | 2 | 0 | 0 | 3 | 0 | 0 | 0  | 5  | 4  | 0  | 0 | 0 | 4  | 2 | 0 | 0 |
| 1  | 27 | 205 | T | 27 | Silt | 0  | 0 | 0  | 11 | 0 | 1 | 0 | 0 | 0 | 0 | 0 | 10 | 19 | 0  | 2  | 0 | 0 | 0  | 0 | 0 |   |
| 1  | 28 | -   | T | 15 | Clay | 0  | 0 | 1  | 6  | 0 | 0 | 0 | 0 | 0 | 0 | 0 | 2  | 1  | 0  | 6  | 0 | 0 | 0  | 0 | 0 |   |
| 1  | 28 | 205 | T | 16 | Clay | 0  | 0 | 0  | 7  | 0 | 1 | 0 | 0 | 0 | 0 | 0 | 21 | 10 | 8  | 10 | 2 | 4 | 1  | 0 | 0 |   |
| 1  | 28 | -   | T | 26 | Sand | 0  | 0 | 3  | 18 | 0 | 4 | 2 | 0 | 0 | 0 | 0 | 3  | 8  | 1  | 0  | 0 | 6 | 6  | 1 | 0 |   |
| 1  | 29 | 205 | T | 29 | Sand | 0  | 0 | 2  | 18 | 0 | 0 | 1 | 0 | 1 | 1 | 0 | 0  | 0  | 2  | 0  | 0 | 2 | 4  | 1 | 0 |   |
| 1  | 30 | -   | T | 21 | Silt | 0  | 0 | 2  | 9  | 0 | 4 | 0 | 0 | 1 | 2 | 0 | 0  | 0  | 1  | 0  | 1 | 0 | 10 | 0 | 0 |   |
| 1  | 30 | 205 | T | 25 | Sand | 0  | 0 | 4  | 32 | 0 | 0 | 0 | 0 | 2 | 0 | 0 | 0  | 0  | 1  | 1  | 0 | 0 | 1  | 6 | 0 | 0 |
| 1  | 31 | -   | T | 25 | Silt | 0  | 0 | 0  | 8  | 0 | 2 | 0 | 0 | 3 | 0 | 0 | 0  | 5  | 0  | 0  | 1 | 1 | 0  | 2 | 0 | 0 |
| 1  | 31 | 205 | T | 28 | Sand | 0  | 0 | 0  | 4  | 0 | 1 | 0 | 0 | 4 | 0 | 0 | 0  | 6  | 0  | 0  | 4 | 0 | 1  | 0 | 0 | 0 |
| 1  | 32 | -   | T | 25 | Silt | 0  | 0 | 0  | 0  | 0 | 0 | 0 | 0 | 0 | 0 | 0 | 0  | 1  | 0  | 0  | 0 | 0 | 1  | 0 | 0 | 0 |
| 1  | 32 | 205 | T | 29 | Silt | 0  | 0 | 0  | 2  | 0 | 1 | 0 | 0 | 0 | 0 | 0 | 2  | 1  | 0  | 0  | 0 | 2 | 0  | 0 | 0 | 0 |
| 1  | 33 | -   | T | 25 | Sand | 0  | 0 | 1  | 12 | 0 | 4 | 0 | 0 | 2 | 0 | 0 | 0  | 4  | 2  | 0  | 3 | 0 | 3  | 5 | 2 | 3 |
| 1  | 33 | 205 | T | 28 | Sand | 0  | 0 | 0  | 11 | 0 | 1 | 0 | 0 | 1 | 0 | 0 | 0  | 5  | 6  | 0  | 0 | 3 | 7  | 0 | 0 | 0 |
| 1  | 33 | -   | T | 25 | Silt | 0  | 0 | 10 | 4  | 0 | 2 | 0 | 0 | 0 | 0 | 0 | 0  | 1  | 0  | 0  | 0 | 2 | 0  | 0 | 2 | 0 |
| 1  | 34 | 205 | T | 26 | Sand | 0  | 0 | 1  | 8  | 0 | 6 | 0 | 0 | 1 | 0 | 0 | 0  | 2  | 1  | 0  | 0 | 2 | 0  | 0 | 0 | 0 |
| 1  | 35 | -   | T | 20 | Silt | 0  | 0 | 3  | 17 | 0 | 3 | 0 | 0 | 0 | 1 | 0 | 0  | 5  | 3  | 0  | 0 | 0 | 0  | 2 | 0 | 0 |
| 1  | 35 | 205 | T | 27 | Silt | 0  | 0 | 2  | 10 | 0 | 3 | 1 | 0 | 1 | 0 | 0 | 0  | 0  | 2  | 0  | 0 | 0 | 2  | 1 | 0 | 0 |
| 1  | 36 | -   | T | 32 | Sand | 0  | 0 | 0  | 7  | 0 | 0 | 0 | 0 | 0 | 0 | 0 | 8  | 6  | 12 | 0  | 0 | 0 | 1  | 1 | 0 | 0 |
| 1  | 36 | 205 | T | 17 | Clay | 0  | 0 | 0  | 11 | 0 | 1 | 0 | 0 | 2 | 0 | 0 | 0  | 42 | 19 | 7  | 2 | 0 | 0  | 7 | 0 | 0 |
| 1  | 37 | -   | T | 20 | Silt | 0  | 0 | 1  | 6  | 0 | 3 | 1 | 0 | 0 | 2 | 0 | 0  | 4  | 3  | 3  | 0 | 0 | 0  | 0 | 0 | 2 |
| 1  | 37 | 205 | T | 24 | Silt | 0  | 0 | 0  | 1  | 0 | 2 | 0 | 0 | 0 | 0 | 0 | 13 | 3  | 0  | 0  | 0 | 0 | 3  | 0 | 1 | 0 |
| 1  | 38 | -   | T | 22 | Silt | 0  | 0 | 2  | 9  | 0 | 0 | 0 | 0 | 0 | 3 | 0 | 0  | 2  | 1  | 1  | 0 | 0 | 0  | 0 | 1 | 0 |
| 1  | 38 | 205 | T | 19 | Clay | 0  | 0 | 0  | 5  | 0 | 7 | 0 | 0 | 0 | 0 | 0 | 20 | 8  | 8  | 0  | 0 | 0 | 0  | 0 | 0 | 1 |
| 1  | 39 | -   | T | 21 | Silt | 0  | 0 | 0  | 1  | 0 | 2 | 0 | 0 | 1 | 0 | 0 | 0  | 2  | 3  | 1  | 0 | 0 | 0  | 0 | 0 | 0 |
| 1  | 39 | 205 | T | 23 | Silt | 0  | 0 | 1  | 4  | 0 | 1 | 0 | 0 | 0 | 0 | 0 | 0  | 0  | 1  | 0  | 0 | 2 | 0  | 0 | 0 | 0 |
| 1  | 39 | -   | T | 26 | Sand | 0  | 0 | 0  | 15 | 0 | 1 | 0 | 0 | 0 | 1 | 0 | 0  | 2  | 0  | 0  | 0 | 0 | 0  | 0 | 0 | 0 |
| 65 | 1. | 189 | C | 30 | Sand | 3  | 0 | 5  | 18 | 1 | 0 | 1 | 0 | 1 | 3 | 0 | 0  | 8  | 10 | 14 | 6 | 0 | 2  | 1 | 0 | 3 |
| 65 | 5. | 189 | C | 26 | Sand | 18 | 0 | 2  | 9  | 0 | 0 | 1 | 0 | 5 | 1 | 0 | 0  | 0  | 19 | 2  | 3 | 0 | 4  | 5 | 4 | 5 |
| 65 | 11 | -   | C | 28 | Sand | 27 | 0 | 5  | 16 | 0 | 0 | 0 | 0 | 2 | 4 | 0 | 0  | 0  | 7  | 8  | 2 | 0 | 2  | 0 | 2 | 1 |
| 65 | 14 | 189 | C | 26 | Sand | 18 | 0 | 7  | 17 | 0 | 0 | 0 | 0 | 1 | 1 | 0 | 0  | 0  | 12 | 0  | 2 | 0 | 9  | 7 | 1 | 0 |
| 65 | 20 | -   | C | 24 | Sand | 75 | 0 | 9  | 24 | 0 | 0 | 1 | 0 | 0 | 2 | 0 | 0  | 0  | 6  | 23 | 1 | 0 | 6  | 0 | 1 | 0 |
| 65 | 26 | 189 | C | 24 | Sand | 14 | 0 | 13 | 45 | 0 | 0 | 1 | 0 | 3 | 2 | 0 | 0  | 0  | 11 | 4  | 4 | 0 | 4  | 6 | 5 | 0 |
| 65 | 26 | -   | C | 24 | Sand | 15 | 0 | 10 | 14 | 0 | 0 | 0 | 0 | 1 | 3 | 0 | 0  | 1  | 19 | 7  | 2 | 0 | 11 | 3 | 0 | 1 |
| 65 | 35 | 189 | C | 27 | Sand | 63 | 1 | 9  | 10 | 0 | 0 | 0 | 0 | 2 | 0 | 0 | 0  | 0  | 13 | 2  | 4 | 0 | 4  | 2 | 1 | 0 |
| 65 | 45 | -   | C | 27 | Sand | 30 | 1 | 4  | 13 | 0 | 0 | 0 | 0 | 0 | 1 | 0 | 0  | 0  | 9  | 4  | 3 | 0 | 2  | 0 | 0 | 1 |
| 65 | 55 | 189 | C | 25 | Sand | 8  | 0 | 9  | 23 | 0 | 0 | 0 | 0 | 1 | 3 | 0 | 0  | 1  | 13 | 5  | 4 | 0 | 0  | 0 | 0 | 0 |
| 65 | 65 | -   | C | 24 | Sand | 19 | 2 | 6  | 23 | 0 | 0 | 0 | 0 | 0 | 3 | 0 | 0  | 3  | 11 | 2  | 4 | 1 | 6  | 2 | 0 | 0 |
| 65 | 75 | 189 | C | 26 | Sand | 13 | 0 | 4  | 16 | 0 | 3 | 0 | 0 | 0 | 3 | 0 | 0  | 1  | 2  | 0  | 0 | 0 | 5  | 4 | 0 | 1 |
| 65 | 85 | -   | C | 30 | Sand | 6  | 0 | 10 | 64 | 0 | 1 | 0 | 0 | 1 | 2 | 1 | 0  | 0  | 0  | 1  | 0 | 0 | 2  | 2 | 5 | 2 |



|    |      |          |   |      |            |    |   |    |    |   |    |   |   |   |    |   |   |    |    |    |   |   |    |   |    |    |
|----|------|----------|---|------|------------|----|---|----|----|---|----|---|---|---|----|---|---|----|----|----|---|---|----|---|----|----|
| 65 | 95.3 | -189.6.6 | T | 18   | Silt       | 4  | 0 | 8  | 20 | 0 | 7  | 3 | 0 | 0 | 4  | 1 | 0 | 0  | 0  | 1  | 0 | 0 | 8  | 0 | 0  | 2  |
| 65 | 105  | -189.6.6 | T | 11.3 | Silt       | 3  | 0 | 2  | 22 | 0 | 4  | 0 | 0 | 0 | 0  | 2 | 0 | 2  | 1  | 0  | 0 | 0 | 3  | 0 | 0  | 1  |
| 65 | 115  | -189.6.6 | T | 21.3 | Sandy Silt | 18 | 0 | 9  | 52 | 0 | 9  | 1 | 0 | 1 | 0  | 0 | 0 | 3  | 2  | 0  | 1 | 0 | 8  | 1 | 1  | 0  |
| 65 | 122  | -189.6.6 | T | 17   | Silt       | 7  | 0 | 1  | 17 | 0 | 0  | 1 | 0 | 1 | 0  | 0 | 0 | 0  | 9  | 5  | 0 | 0 | 5  | 1 | 1  | 4  |
| 65 | 126  | -189.6.6 | T | 22.5 | Sandy Silt | 10 | 0 | 2  | 35 | 0 | 1  | 0 | 0 | 0 | 2  | 0 | 0 | 2  | 3  | 0  | 0 | 0 | 8  | 1 | 0  | 1  |
| 65 | 134  | -189.6.6 | T | 15.4 | Clay       | 2  | 0 | 1  | 14 | 0 | 6  | 0 | 0 | 1 | 1  | 0 | 0 | 0  | 4  | 0  | 0 | 0 | 2  | 2 | 0  | 0  |
| 65 | 144  | -189.6.6 | T | 20.4 | Sandy Silt | 2  | 0 | 3  | 21 | 0 | 0  | 0 | 0 | 0 | 0  | 2 | 0 | 3  | 7  | 0  | 0 | 0 | 1  | 0 | 5  | 1  |
| 65 | 154  | -189.6.6 | T | 19.2 | Silt       | 15 | 0 | 1  | 14 | 0 | 1  | 0 | 0 | 1 | 1  | 3 | 0 | 1  | 6  | 0  | 0 | 0 | 4  | 3 | 0  | 1  |
| 65 | 164  | -189.6.6 | T | 25.1 | Sandy Silt | 20 | 0 | 5  | 7  | 0 | 8  | 0 | 0 | 3 | 0  | 4 | 0 | 5  | 36 | 3  | 1 | 1 | 7  | 2 | 1  | 1  |
| 65 | 174  | -189.6.6 | T | 18.7 | Silt       | 15 | 0 | 4  | 22 | 0 | 7  | 1 | 1 | 3 | 10 | 6 | 0 | 29 | 10 | 6  | 2 | 0 | 5  | 8 | 1  | 2  |
| 65 | 184  | -189.6.6 | T | 19.2 | Silt       | 17 | 0 | 4  | 24 | 0 | 17 | 1 | 0 | 1 | 7  | 4 | 0 | 8  | 10 | 0  | 0 | 0 | 9  | 3 | 0  | 0  |
| 65 | 194  | -189.6.6 | T | 23.4 | Sandy Silt | 51 | 0 | 2  | 13 | 0 | 5  | 0 | 0 | 1 | 1  | 5 | 0 | 17 | 16 | 8  | 0 | 1 | 9  | 2 | 0  | 0  |
| 65 | 204  | -189.6.6 | T | 18.4 | Silt       | 7  | 0 | 3  | 14 | 0 | 5  | 1 | 0 | 1 | 1  | 1 | 0 | 6  | 5  | 4  | 0 | 0 | 3  | 0 | 0  | 2  |
| 65 | 214  | -189.6.6 | T | 18.4 | Silt       | 11 | 0 | 4  | 16 | 0 | 1  | 0 | 0 | 4 | 5  | 3 | 0 | 48 | 11 | 6  | 0 | 0 | 11 | 1 | 0  | 3  |
| 65 | 222  | -189.6.6 | T | 18   | Silt       | 10 | 0 | 2  | 9  | 0 | 4  | 0 | 0 | 6 | 2  | 0 | 0 | 32 | 24 | 4  | 1 | 0 | 4  | 3 | 3  | 1  |
| 65 | 223  | -189.6.6 | T | 21.9 | Sandy Silt | 8  | 0 | 3  | 10 | 0 | 0  | 0 | 0 | 1 | 0  | 2 | 0 | 14 | 7  | 6  | 1 | 0 | 5  | 0 | 4  | 4  |
| 65 | 232  | -189.6.6 | T | 19.2 | Silt       | 6  | 0 | 1  | 6  | 0 | 1  | 1 | 0 | 1 | 0  | 5 | 0 | 56 | 27 | 11 | 1 | 0 | 7  | 0 | 0  | 7  |
| 65 | 242  | -189.6.6 | T | 17.8 | Silt       | 7  | 0 | 6  | 23 | 0 | 8  | 1 | 0 | 0 | 0  | 4 | 0 | 13 | 15 | 6  | 0 | 0 | 7  | 0 | 16 | 4  |
| 65 | 252  | -189.6.6 | T | 23.3 | Sandy Silt | 11 | 0 | 3  | 11 | 0 | 2  | 0 | 0 | 0 | 11 | 0 | 0 | 0  | 4  | 5  | 0 | 1 | 7  | 0 | 1  | 0  |
| 65 | 259  | -189.6.6 | T | 20.9 | Sandy Silt | 10 | 0 | 7  | 26 | 0 | 4  | 0 | 0 | 3 | 6  | 0 | 0 | 0  | 6  | 24 | 2 | 0 | 4  | 1 | 0  | 6  |
| 65 | 261  | -189.6.6 | T | 21.7 | Sandy Silt | 23 | 0 | 7  | 28 | 0 | 1  | 0 | 0 | 0 | 5  | 0 | 0 | 11 | 10 | 6  | 4 | 1 | 5  | 0 | 0  | 5  |
| 65 | 269  | -189.6.6 | T | 19.8 | Silt       | 7  | 0 | 2  | 25 | 0 | 3  | 0 | 0 | 1 | 1  | 2 | 0 | 3  | 4  | 0  | 1 | 2 | 3  | 0 | 0  | 2  |
| 65 | 279  | -189.6.6 | T | 20.1 | Sandy Silt | 9  | 0 | 8  | 21 | 0 | 1  | 0 | 0 | 3 | 1  | 0 | 0 | 22 | 13 | 7  | 0 | 1 | 9  | 2 | 3  | 1  |
| 65 | 289  | -189.6.6 | T | 20.7 | Sandy Silt | 16 | 0 | 6  | 23 | 0 | 2  | 0 | 0 | 1 | 0  | 0 | 0 | 30 | 14 | 12 | 0 | 1 | 9  | 0 | 20 | 15 |
| 65 | 299  | -189.6.6 | T | 14.7 | Clay       | 0  | 0 | 7  | 25 | 0 | 8  | 0 | 0 | 2 | 1  | 0 | 0 | 3  | 0  | 2  | 0 | 0 | 3  | 1 | 1  | 3  |
| 65 | 309  | -189.6.6 | T | 18.2 | Silt       | 7  | 0 | 7  | 28 | 0 | 2  | 0 | 0 | 0 | 0  | 0 | 0 | 29 | 18 | 7  | 1 | 1 | 3  | 1 | 3  | 7  |
| 65 | 317  | -189.6.6 | T | 21.9 | Sandy Silt | 11 | 0 | 7  | 17 | 0 | 2  | 1 | 0 | 1 | 1  | 0 | 0 | 27 | 22 | 15 | 0 | 0 | 0  | 2 | 10 | 2  |
| 65 | 317  | -189.6.6 | T | 18.8 | Silt       | 0  | 0 | 2  | 20 | 0 | 1  | 0 | 0 | 1 | 2  | 0 | 0 | 16 | 15 | 7  | 1 | 0 | 8  | 3 | 5  | 0  |
| 65 | 327  | -189.6.6 | T | 13.9 | Clay       | 1  | 0 | 0  | 10 | 0 | 0  | 0 | 0 | 0 | 2  | 1 | 0 | 41 | 23 | 10 | 1 | 0 | 1  | 0 | 0  | 1  |
| 65 | 337  | -189.6.6 | T | 9.68 | Clay       | 0  | 0 | 2  | 14 | 0 | 1  | 0 | 0 | 3 | 0  | 0 | 0 | 37 | 11 | 9  | 0 | 0 | 0  | 0 | 2  | 1  |
| 65 | 347  | -189.6.6 | T | 14.2 | Silt       | 9  | 1 | 2  | 20 | 0 | 1  | 0 | 0 | 0 | 0  | 0 | 0 | 48 | 22 | 13 | 0 | 1 | 2  | 1 | 6  | 3  |
| 65 | 354  | -189.6.6 | T | 13.2 | Clay       | 0  | 0 | 1  | 11 | 0 | 0  | 0 | 0 | 2 | 0  | 0 | 0 | 12 | 0  | 11 | 0 | 0 | 4  | 0 | 11 | 20 |
| 65 | 357  | -189.6.6 | T | 14.5 | Clay       | 0  | 0 | 4  | 20 | 0 | 1  | 0 | 0 | 0 | 0  | 0 | 0 | 50 | 30 | 15 | 0 | 0 | 4  | 2 | 10 | 11 |
| 65 | 366  | -189.6.6 | T | 14.1 | Clay       | 0  | 0 | 0  | 7  | 0 | 1  | 0 | 0 | 0 | 0  | 0 | 0 | 1  | 2  | 1  | 1 | 0 | 2  | 2 | 1  | 4  |
| 65 | 371  | -189.6.6 | T | 12.1 | Clay       | 0  | 0 | 3  | 9  | 0 | 1  | 0 | 0 | 0 | 0  | 0 | 0 | 1  | 6  | 6  | 0 | 0 | 1  | 3 | 1  | 7  |
| 65 | 376  | -189.6.6 | T | 14.1 | Clay       | 0  | 0 | 1  | 12 | 0 | 0  | 0 | 0 | 0 | 0  | 0 | 0 | 2  | 2  | 2  | 0 | 0 | 1  | 1 | 0  | 2  |
| 65 | 386  | -189.6.6 | T | 14.4 | Clay       | 0  | 0 | 11 | 24 | 0 | 2  | 0 | 0 | 0 | 0  | 1 | 0 | 13 | 14 | 8  | 0 | 0 | 5  | 0 | 0  | 1  |
| 65 | 395  | -189.6.6 | T | 21.1 | Sandy Silt | 18 | 0 | 0  | 36 | 0 | 8  | 0 | 0 | 0 | 1  | 0 | 0 | 27 | 13 | 16 | 0 | 0 | 9  | 2 | 6  | 7  |
| 65 | 396  | -189.6.6 | T | 19.7 | Silt       | 10 | 1 | 2  | 22 | 0 | 6  | 0 | 0 | 1 | 0  | 0 | 0 | 21 | 11 | 6  | 3 | 0 | 10 | 2 | 1  | 2  |
| 65 | 406  | -189.6.6 | T | 15.6 | Clay       | 1  | 0 | 0  | 7  | 0 | 4  | 0 | 0 | 1 | 1  | 0 | 0 | 0  | 4  | 0  | 0 | 1 | 1  | 2 | 8  | 42 |
| 65 | 416  | -189.6.6 | T | 13   | Clay       | 0  | 0 | 0  | 2  | 0 | 0  | 0 | 0 | 0 | 0  | 0 | 0 | 0  | 0  | 0  | 0 | 0 | 0  | 0 | 9  | 21 |
| 65 | 426  | -189.6.6 | T | 13.8 | Clay       | 0  | 0 | 9  | 30 | 0 | 0  | 0 | 0 | 0 | 4  | 0 | 0 | 5  | 1  | 0  | 0 | 0 | 4  | 0 | 8  | 7  |
| 65 | 436  | -189.6.6 | T | 18.4 | Silt       | 1  | 0 | 7  | 40 | 0 | 7  | 0 | 0 | 0 | 2  | 2 | 0 | 13 | 14 | 14 | 0 | 1 | 5  | 1 | 11 | 20 |
| 65 | 436  | -189.6.6 | T | 23.6 | Sandy Silt | 13 | 0 | 5  | 32 | 0 | 2  | 0 | 0 | 0 | 1  | 0 | 0 | 17 | 15 | 3  | 0 | 0 | 6  | 0 | 12 | 14 |



|    |    |   |   |    |       |    |   |    |    |   |    |    |    |   |    |   |   |    |    |   |   |    |    |    |   |
|----|----|---|---|----|-------|----|---|----|----|---|----|----|----|---|----|---|---|----|----|---|---|----|----|----|---|
| 13 | 53 | - | C | 23 | Sandy | 0  | 0 | 2  | 8  | 0 | 4  | 5  | 18 | 0 | 3  | 0 | 0 | 0  | 0  | 0 | 2 | 0  | 3  | 3  | 0 |
| 13 | 63 | - | C | 32 | Sandy | 0  | 3 | 5  | 9  | 0 | 51 | 7  | 22 | 0 | 0  | 0 | 0 | 0  | 0  | 0 | 3 | 4  | 13 | 7  | 0 |
| 13 | 73 | - | C | 32 | Sandy | 0  | 3 | 3  | 14 | 0 | 15 | 0  | 5  | 1 | 1  | 0 | 0 | 1  | 0  | 1 | 0 | 9  | 3  | 2  | 1 |
| 13 | 78 | - | C | 30 | Sandy | 0  | 0 | 2  | 18 | 0 | 10 | 3  | 13 | 1 | 2  | 0 | 0 | 0  | 0  | 1 | 1 | 0  | 2  | 0  |   |
| 13 | 83 | - | C | 32 | Sandy | 0  | 0 | 3  | 25 | 0 | 12 | 3  | 0  | 0 | 1  | 1 | 0 | 0  | 0  | 0 | 0 | 4  | 0  | 3  | 1 |
| 13 | 88 | - | C | 30 | Sandy | 0  | 2 | 6  | 39 | 0 | 9  | 2  | 3  | 2 | 3  | 3 | 0 | 0  | 0  | 0 | 2 | 1  | 3  | 1  | 2 |
| 13 | 93 | - | C | 34 | Sandy | 0  | 2 | 3  | 36 | 0 | 23 | 3  | 0  | 2 | 10 | 0 | 0 | 0  | 0  | 0 | 2 | 7  | 3  | 2  | 0 |
| 13 | 10 | - | C | 27 | Sandy | 0  | 1 | 6  | 24 | 0 | 2  | 1  | 0  | 2 | 15 | 0 | 0 | 0  | 0  | 0 | 3 | 2  | 0  | 0  | 0 |
| 13 | 11 | - | C | 32 | Sandy | 0  | 2 | 2  | 20 | 0 | 8  | 4  | 1  | 1 | 4  | 0 | 0 | 0  | 0  | 0 | 1 | 0  | 1  | 5  | 0 |
| 13 | 11 | - | C | 31 | Sandy | 0  | 0 | 7  | 32 | 0 | 3  | 4  | 0  | 0 | 16 | 0 | 0 | 0  | 0  | 0 | 3 | 0  | 0  | 0  | 0 |
| 13 | 12 | - | C | 31 | Sandy | 0  | 0 | 3  | 22 | 0 | 4  | 2  | 0  | 0 | 11 | 0 | 0 | 0  | 0  | 0 | 1 | 0  | 0  | 0  | 0 |
| 13 | 13 | - | C | 35 | Sandy | 0  | 0 | 3  | 12 | 0 | 0  | 0  | 1  | 1 | 7  | 0 | 0 | 0  | 0  | 0 | 0 | 2  | 0  | 0  | 0 |
| 13 | 13 | - | C | 31 | Sandy | 0  | 0 | 1  | 3  | 0 | 0  | 0  | 0  | 1 | 1  | 0 | 0 | 0  | 0  | 0 | 0 | 0  | 0  | 0  | 0 |
| 13 | 14 | - | C | 30 | Sandy | 0  | 0 | 0  | 0  | 0 | 0  | 0  | 0  | 0 | 0  | 0 | 0 | 0  | 0  | 0 | 0 | 0  | 0  | 0  | 0 |
| 13 | 14 | - | C | 31 | Sandy | 0  | 0 | 0  | 6  | 0 | 1  | 0  | 0  | 0 | 1  | 0 | 0 | 0  | 0  | 0 | 0 | 0  | 0  | 0  | 0 |
| 13 | 14 | - | C | 29 | Sandy | 0  | 0 | 0  | 0  | 0 | 0  | 0  | 0  | 0 | 1  | 0 | 0 | 0  | 0  | 0 | 0 | 0  | 0  | 0  | 0 |
| 13 | 15 | - | C | 24 | Sandy | 0  | 0 | 0  | 0  | 0 | 0  | 0  | 11 | 0 | 0  | 0 | 0 | 0  | 0  | 0 | 0 | 0  | 0  | 0  | 0 |
| 13 | 15 | - | C | 15 | Silt  | 0  | 0 | 0  | 0  | 0 | 0  | 0  | 0  | 0 | 0  | 0 | 0 | 0  | 0  | 0 | 0 | 0  | 0  | 0  | 0 |
| 13 | 16 | - | C | 21 | Silt  | 0  | 0 | 0  | 0  | 0 | 0  | 0  | 7  | 0 | 0  | 0 | 0 | 0  | 0  | 0 | 0 | 0  | 0  | 0  | 0 |
| 13 | 16 | - | C | 9  | Cla   | 0  | 0 | 0  | 0  | 0 | 0  | 0  | 0  | 1 | 0  | 0 | 0 | 16 | 74 | 0 | 8 | 0  | 0  | 0  | 0 |
| 13 | 17 | - | C | 6  | Cla   | 0  | 0 | 0  | 0  | 0 | 0  | 0  | 50 | 0 | 0  | 0 | 0 | 0  | 3  | 0 | 5 | 2  | 0  | 0  | 0 |
| 13 | 18 | - | C | 10 | Cla   | 1  | 0 | 0  | 0  | 0 | 0  | 0  | 17 | 0 | 0  | 0 | 0 | 0  | 0  | 0 | 0 | 0  | 0  | 0  | 0 |
| 13 | 19 | - | C | 4  | Cla   | 0  | 0 | 0  | 0  | 0 | 0  | 0  | 20 | 0 | 0  | 0 | 0 | 0  | 0  | 0 | 0 | 0  | 0  | 0  | 0 |
| 13 | 19 | - | C | 6  | Cla   | 0  | 0 | 0  | 0  | 0 | 0  | 0  | 0  | 0 | 0  | 0 | 0 | 0  | 0  | 0 | 0 | 0  | 0  | 0  | 0 |
| 13 | 20 | - | C | 6  | Cla   | 0  | 0 | 0  | 0  | 0 | 0  | 0  | 0  | 0 | 0  | 0 | 0 | 0  | 0  | 0 | 0 | 0  | 0  | 0  | 0 |
| 13 | 20 | - | C | 5  | Cla   | 0  | 0 | 0  | 0  | 0 | 0  | 0  | 0  | 0 | 0  | 0 | 0 | 0  | 0  | 0 | 0 | 0  | 0  | 0  | 0 |
| 13 | 21 | - | C | 25 | Fine  | 0  | 0 | 0  | 2  | 0 | 5  | 0  | 1  | 1 | 6  | 0 | 0 | 0  | 0  | 0 | 1 | 3  | 0  | 1  | 1 |
| 13 | 21 | - | C | 16 | Silt  | 0  | 0 | 0  | 0  | 0 | 0  | 0  | 0  | 0 | 0  | 0 | 0 | 0  | 0  | 0 | 0 | 0  | 0  | 0  | 0 |
| 13 | 22 | - | C | 7  | Cla   | 0  | 0 | 0  | 0  | 0 | 0  | 0  | 0  | 0 | 0  | 0 | 0 | 0  | 0  | 0 | 0 | 0  | 0  | 0  | 0 |
| 13 | 23 | - | C | 6  | Cla   | 0  | 0 | 0  | 0  | 0 | 0  | 0  | 0  | 0 | 0  | 0 | 0 | 0  | 0  | 0 | 0 | 0  | 0  | 0  | 0 |
| 13 | 24 | - | C | 7  | Cla   | 0  | 0 | 0  | 0  | 0 | 0  | 0  | 0  | 0 | 0  | 0 | 0 | 0  | 0  | 0 | 0 | 0  | 0  | 0  | 0 |
| 13 | 24 | - | C | 8  | Cla   | 0  | 0 | 0  | 0  | 0 | 0  | 0  | 0  | 0 | 0  | 0 | 0 | 0  | 0  | 0 | 0 | 0  | 0  | 0  | 0 |
| 13 | 25 | - | C | 6  | Cla   | 0  | 0 | 0  | 0  | 0 | 0  | 0  | 0  | 0 | 0  | 0 | 0 | 0  | 0  | 0 | 0 | 0  | 0  | 0  | 0 |
| 13 | 25 | - | C | 6  | Cla   | 0  | 0 | 0  | 0  | 0 | 0  | 0  | 0  | 0 | 0  | 0 | 0 | 0  | 0  | 0 | 0 | 0  | 0  | 0  | 0 |
| 13 | 25 | - | C | 4  | Cla   | 0  | 0 | 0  | 0  | 0 | 0  | 0  | 0  | 0 | 0  | 0 | 0 | 0  | 0  | 0 | 0 | 0  | 0  | 0  | 0 |
| 15 | 5  | - | C | 29 | Sandy | 0  | 0 | 13 | 32 | 0 | 6  | 4  | 6  | 4 | 0  | 0 | 0 | 0  | 0  | 0 | 2 | 0  | 3  | 0  | 3 |
| 15 | 10 | - | C | 30 | Sandy | 17 | 1 | 9  | 10 | 0 | 2  | 9  | 7  | 2 | 0  | 0 | 0 | 0  | 0  | 0 | 1 | 4  | 0  | 0  | 1 |
| 15 | 19 | - | C | 29 | Sandy | 1  | 2 | 3  | 16 | 0 | 3  | 15 | 3  | 1 | 0  | 0 | 0 | 0  | 0  | 0 | 1 | 1  | 2  | 1  | 3 |
| 15 | 21 | - | C | 33 | Sandy | 1  | 2 | 6  | 22 | 0 | 6  | 9  | 4  | 0 | 0  | 0 | 0 | 0  | 0  | 0 | 2 | 2  | 2  | 1  | 0 |
| 15 | 30 | - | C | 30 | Sandy | 1  | 2 | 2  | 7  | 0 | 14 | 15 | 2  | 0 | 0  | 0 | 0 | 0  | 0  | 0 | 3 | 0  | 2  | 4  |   |
| 15 | 40 | - | C | 29 | Sandy | 0  | 2 | 8  | 10 | 0 | 4  | 25 | 1  | 4 | 0  | 0 | 0 | 0  | 0  | 2 | 0 | 4  | 3  | 0  | 2 |
| 15 | 50 | - | C | 29 | Sandy | 0  | 0 | 8  | 15 | 0 | 18 | 22 | 2  | 0 | 0  | 0 | 0 | 0  | 0  | 2 | 4 | 9  | 0  | 5  |   |
| 15 | 60 | - | C | 30 | Sandy | 0  | 3 | 0  | 9  | 0 | 13 | 29 | 0  | 0 | 0  | 0 | 0 | 0  | 0  | 2 | 0 | 10 | 1  | 15 |   |
| 15 | 70 | - | C | 31 | Sandy | 0  | 2 | 2  | 16 | 0 | 24 | 20 | 4  | 0 | 0  | 0 | 0 | 0  | 0  | 0 | 6 | 4  | 2  | 22 |   |





|     |     |        |   |      |            |   |   |   |    |   |    |   |   |   |    |   |   |   |   |   |   |   |   |   |   |   |
|-----|-----|--------|---|------|------------|---|---|---|----|---|----|---|---|---|----|---|---|---|---|---|---|---|---|---|---|---|
| 170 | 132 | -253.5 | C | 33.2 | Sandy Silt | 0 | 1 | 6 | 12 | 0 | 3  | 4 | 0 | 1 | 1  | 0 | 0 | 0 | 0 | 0 | 0 | 0 | 2 | 1 | 3 | 3 |
| 170 | 142 | -253.5 | C | 29.6 | Sandy Silt | 0 | 0 | 0 | 8  | 0 | 0  | 1 | 0 | 0 | 4  | 0 | 0 | 0 | 0 | 0 | 0 | 0 | 4 | 0 | 0 | 0 |
| 170 | 152 | -253.5 | C | 26.1 | Sandy Silt | 0 | 0 | 0 | 10 | 0 | 5  | 0 | 0 | 3 | 0  | 0 | 0 | 0 | 0 | 0 | 0 | 0 | 1 | 0 | 0 | 0 |
| 170 | 162 | -253.5 | C | 28.2 | Sandy Silt | 0 | 2 | 2 | 5  | 0 | 0  | 3 | 0 | 1 | 10 | 0 | 0 | 0 | 0 | 0 | 0 | 0 | 3 | 2 | 0 | 0 |
| 170 | 172 | -253.5 | C | 27.4 | Sandy Silt | 0 | 0 | 4 | 8  | 0 | 10 | 0 | 0 | 0 | 2  | 0 | 0 | 0 | 0 | 0 | 0 | 0 | 1 | 1 | 0 | 0 |
| 170 | 182 | -253.5 | C | 24.2 | Sandy Silt | 0 | 1 | 0 | 2  | 0 | 0  | 0 | 0 | 1 | 3  | 0 | 0 | 0 | 0 | 0 | 0 | 0 | 1 | 0 | 0 | 0 |
| 170 | 186 | -253.5 | C | 20.1 | Silt       | 0 | 0 | 0 | 2  | 0 | 0  | 0 | 0 | 0 | 4  | 0 | 0 | 0 | 0 | 0 | 0 | 0 | 2 | 0 | 0 | 0 |
| 170 | 193 | -253.5 | C | 14.7 | Silt       | 0 | 0 | 0 | 1  | 0 | 0  | 2 | 0 | 1 | 1  | 0 | 0 | 0 | 0 | 0 | 0 | 0 | 2 | 0 | 0 | 0 |
| 170 | 203 | -253.5 | C | 14.4 | Silt       | 0 | 1 | 0 | 1  | 0 | 0  | 0 | 0 | 0 | 1  | 0 | 0 | 0 | 0 | 0 | 0 | 0 | 1 | 0 | 0 | 0 |
| 170 | 213 | -253.5 | C | 6.71 | Clay       | 0 | 0 | 0 | 0  | 0 | 0  | 0 | 0 | 0 | 0  | 0 | 0 | 0 | 0 | 0 | 0 | 0 | 0 | 0 | 0 | 0 |
| 170 | 223 | -253.5 | C | 7.2  | Clay       | 0 | 0 | 0 | 0  | 0 | 0  | 0 | 0 | 0 | 0  | 0 | 0 | 0 | 0 | 0 | 0 | 0 | 0 | 0 | 0 | 0 |
| 170 | 233 | -253.5 | C | 9.19 | Clay       | 0 | 0 | 0 | 0  | 0 | 0  | 0 | 0 | 0 | 0  | 0 | 0 | 0 | 0 | 0 | 0 | 0 | 0 | 0 | 0 | 0 |
| 170 | 243 | -253.5 | C | 7.75 | Clay       | 0 | 0 | 0 | 0  | 0 | 0  | 0 | 0 | 0 | 0  | 0 | 0 | 0 | 0 | 0 | 0 | 0 | 0 | 0 | 0 | 0 |
| 170 | 253 | -253.5 | C | 9.26 | Clay       | 0 | 0 | 0 | 0  | 0 | 0  | 0 | 0 | 0 | 0  | 0 | 0 | 0 | 0 | 0 | 0 | 0 | 0 | 0 | 0 | 0 |
| 170 | 262 | -253.5 | C | 7.6  | Clay       | 0 | 0 | 0 | 0  | 0 | 0  | 0 | 0 | 0 | 0  | 0 | 0 | 0 | 0 | 0 | 0 | 0 | 0 | 0 | 0 | 0 |
| 170 | 263 | -253.5 | C | 8.88 | Clay       | 0 | 0 | 0 | 0  | 0 | 0  | 0 | 0 | 0 | 0  | 0 | 0 | 0 | 0 | 0 | 0 | 0 | 0 | 0 | 0 | 0 |
| 170 | 271 | -253.5 | C | 13   | Silt       | 0 | 0 | 0 | 0  | 0 | 0  | 0 | 0 | 0 | 0  | 0 | 0 | 0 | 0 | 0 | 0 | 0 | 0 | 0 | 0 | 0 |
| 170 | 281 | -253.5 | C | 11.7 | Silt       | 0 | 0 | 0 | 0  | 0 | 0  | 0 | 0 | 0 | 0  | 0 | 0 | 0 | 0 | 0 | 0 | 0 | 0 | 0 | 0 | 0 |
| 170 | 291 | -253.5 | C | 14.4 | Silt       | 0 | 0 | 0 | 0  | 0 | 0  | 0 | 0 | 0 | 0  | 0 | 0 | 0 | 0 | 0 | 0 | 0 | 0 | 0 | 0 | 0 |
| 170 | 301 | -253.5 | C | 11.9 | Silt       | 0 | 0 | 0 | 0  | 0 | 0  | 0 | 0 | 0 | 0  | 0 | 0 | 0 | 0 | 0 | 0 | 0 | 0 | 0 | 0 | 0 |
| 170 | 311 | -253.5 | C | 12.3 | Silt       | 0 | 0 | 0 | 0  | 0 | 0  | 0 | 0 | 0 | 0  | 0 | 0 | 0 | 0 | 0 | 0 | 0 | 0 | 0 | 0 | 0 |
| 170 | 321 | -253.5 | C | 14.3 | Silt       | 0 | 0 | 0 | 0  | 0 | 0  | 0 | 0 | 0 | 0  | 0 | 0 | 0 | 0 | 0 | 0 | 0 | 0 | 0 | 0 | 0 |
| 170 | 327 | -253.5 | C | 13.1 | Silt       | 0 | 0 | 0 | 0  | 0 | 0  | 0 | 0 | 0 | 0  | 0 | 0 | 0 | 0 | 0 | 0 | 0 | 0 | 0 | 0 | 0 |

Table 3.3 Counts of foraminifera contributing >5% of overall assemblage - *P. fusca* to *U. striata* and sediment characteristics

| Core | Point Depth (cm) | Water Depth (mbs) | Environment (Contourite/Turbidite) | >63µm (%) | Sediment   | <i>Psammosphaera fusca</i> | <i>Pullenia bulloides</i> | <i>Reophax subuliformis</i> | <i>Rhabdammina abyssorum</i> | <i>Rhabdammina linearis</i> | <i>Rutherfordoides coronata</i> | <i>Sigmaliopsis schlumbergeri</i> | <i>Sphaeroidina deliscens</i> | <i>Stainforthia complanata</i> | <i>Trifarina angulosa</i> | <i>Uvigerina aubriana</i> | <i>Uvigerina bifurcata</i> | <i>Uvigerina bradyana</i> | <i>Uvigerina canariensis</i> | <i>Uvigerina holicki</i> | <i>Uvigerina mediterranea</i> | <i>Uvigerina peregrina</i> | <i>Uvigerina striata</i> |
|------|------------------|-------------------|------------------------------------|-----------|------------|----------------------------|---------------------------|-----------------------------|------------------------------|-----------------------------|---------------------------------|-----------------------------------|-------------------------------|--------------------------------|---------------------------|---------------------------|----------------------------|---------------------------|------------------------------|--------------------------|-------------------------------|----------------------------|--------------------------|
| 1    | 2.89             | -2053.1           | C                                  | 23.9      | Sandy Silt | 1                          | 4                         | 0                           | 0                            | 0                           | 2                               | 0                                 | 0                             | 52                             | 12                        | 0                         | 0                          | 0                         | 0                            | 0                        | 1                             | 4                          | 0                        |
| 1    | 8.89             | -2053.1           | C                                  | 27.6      | Sandy Silt | 1                          | 3                         | 0                           | 0                            | 0                           | 1                               | 0                                 | 0                             | 48                             | 5                         | 0                         | 1                          | 0                         | 0                            | 0                        | 3                             | 1                          | 0                        |
| 1    | 14.9             | -2053.1           | C                                  | 25.2      | Sandy Silt | 0                          | 3                         | 0                           | 0                            | 0                           | 4                               | 0                                 | 0                             | 36                             | 6                         | 0                         | 0                          | 0                         | 0                            | 0                        | 3                             | 0                          | 0                        |
| 1    | 16.1             | -2053.1           | C                                  | 29.2      | Sandy Silt | 2                          | 2                         | 0                           | 0                            | 0                           | 4                               | 0                                 | 0                             | 25                             | 3                         | 0                         | 0                          | 0                         | 0                            | 0                        | 3                             | 1                          | 0                        |
| 1    | 24.1             | -2053.1           | C                                  | 25.4      | Sandy Silt | 0                          | 0                         | 0                           | 0                            | 0                           | 1                               | 0                                 | 0                             | 26                             | 1                         | 0                         | 0                          | 0                         | 0                            | 0                        | 0                             | 0                          | 0                        |
| 1    | 35.1             | -2053.1           | C                                  | 27.6      | Sandy Silt | 0                          | 2                         | 0                           | 0                            | 0                           | 3                               | 0                                 | 0                             | 20                             | 3                         | 0                         | 0                          | 0                         | 0                            | 0                        | 1                             | 4                          | 1                        |
| 1    | 45.1             | -2053.1           | C                                  | 28        | Sandy Silt | 0                          | 6                         | 0                           | 0                            | 0                           | 0                               | 0                                 | 0                             | 71                             | 7                         | 0                         | 0                          | 0                         | 0                            | 0                        | 3                             | 2                          | 1                        |
| 1    | 55.1             | -2053.1           | C                                  | 32.9      | Sandy Silt | 0                          | 9                         | 0                           | 0                            | 0                           | 0                               | 0                                 | 0                             | 72                             | 6                         | 0                         | 2                          | 0                         | 0                            | 0                        | 0                             | 12                         | 2                        |
| 1    | 65.1             | -2053.1           | C                                  | 24.2      | Sandy Silt | 0                          | 4                         | 0                           | 0                            | 0                           | 2                               | 0                                 | 0                             | 61                             | 9                         | 0                         | 0                          | 0                         | 0                            | 0                        | 0                             | 3                          | 1                        |
| 1    | 75.1             | -2053.1           | C                                  | 30.6      | Sandy Silt | 0                          | 1                         | 0                           | 0                            | 0                           | 7                               | 0                                 | 0                             | 49                             | 18                        | 0                         | 1                          | 0                         | 0                            | 0                        | 0                             | 4                          | 1                        |
| 1    | 85.1             | -2053.1           | C                                  | 32.4      | Sandy Silt | 0                          | 6                         | 0                           | 0                            | 0                           | 0                               | 0                                 | 0                             | 64                             | 16                        | 0                         | 0                          | 0                         | 0                            | 0                        | 0                             | 5                          | 1                        |
| 1    | 95.1             | -2053.1           | C                                  | 28        | Sandy Silt | 0                          | 5                         | 0                           | 0                            | 0                           | 1                               | 0                                 | 0                             | 56                             | 9                         | 0                         | 0                          | 0                         | 0                            | 0                        | 0                             | 4                          | 2                        |
| 1    | 105              | -2053.1           | C                                  | 23.3      | Sandy Silt | 0                          | 3                         | 0                           | 0                            | 0                           | 4                               | 0                                 | 0                             | 47                             | 19                        | 1                         | 0                          | 0                         | 0                            | 0                        | 1                             | 2                          | 0                        |
| 1    | 109              | -2053.1           | C                                  | 31.1      | Sandy Silt | 0                          | 1                         | 0                           | 0                            | 0                           | 0                               | 0                                 | 0                             | 39                             | 11                        | 0                         | 0                          | 0                         | 0                            | 0                        | 0                             | 4                          | 1                        |
| 1    | 114              | -2053.1           | C                                  | 28.9      | Sandy Silt | 0                          | 6                         | 0                           | 0                            | 0                           | 8                               | 0                                 | 0                             | 47                             | 14                        | 0                         | 0                          | 1                         | 0                            | 0                        | 0                             | 3                          | 0                        |
| 1    | 124              | -2053.1           | C                                  | 30.3      | Sandy Silt | 0                          | 6                         | 0                           | 0                            | 0                           | 3                               | 0                                 | 0                             | 66                             | 7                         | 0                         | 0                          | 0                         | 0                            | 0                        | 0                             | 8                          | 1                        |
| 1    | 134              | -2053.1           | C                                  | 27.5      | Sandy Silt | 0                          | 2                         | 0                           | 0                            | 0                           | 6                               | 1                                 | 0                             | 53                             | 9                         | 0                         | 0                          | 0                         | 0                            | 0                        | 0                             | 3                          | 0                        |
| 1    | 139              | -2053.1           | C                                  | 26.7      | Sandy Silt | 1                          | 3                         | 0                           | 0                            | 0                           | 1                               | 0                                 | 0                             | 46                             | 7                         | 0                         | 0                          | 0                         | 0                            | 0                        | 0                             | 0                          | 0                        |
| 1    | 144              | -2053.1           | C                                  | 23.3      | Sandy Silt | 1                          | 1                         | 0                           | 0                            | 0                           | 0                               | 0                                 | 0                             | 50                             | 14                        | 0                         | 0                          | 0                         | 0                            | 0                        | 0                             | 1                          | 0                        |
| 1    | 154              | -2053.1           | C                                  | 32.5      | Sandy Silt | 0                          | 4                         | 0                           | 0                            | 0                           | 19                              | 0                                 | 0                             | 75                             | 31                        | 0                         | 0                          | 1                         | 0                            | 0                        | 0                             | 7                          | 1                        |
| 1    | 164              | -2053.1           | C                                  | 33.5      | Sandy Silt | 0                          | 6                         | 0                           | 0                            | 0                           | 2                               | 0                                 | 0                             | 52                             | 23                        | 0                         | 2                          | 0                         | 0                            | 0                        | 0                             | 3                          | 0                        |
| 1    | 174              | -2053.1           | C                                  | 31.2      | Sandy Silt | 0                          | 3                         | 0                           | 0                            | 0                           | 5                               | 0                                 | 0                             | 34                             | 23                        | 2                         | 2                          | 0                         | 0                            | 0                        | 0                             | 4                          | 0                        |
| 1    | 182              | -2053.1           | C                                  | 30.6      | Sandy Silt | 0                          | 4                         | 0                           | 0                            | 0                           | 4                               | 0                                 | 0                             | 65                             | 21                        | 0                         | 0                          | 0                         | 0                            | 0                        | 0                             | 2                          | 0                        |
| 1    | 186              | -2053.1           | C                                  | 27.9      | Sandy Silt | 0                          | 3                         | 0                           | 0                            | 0                           | 6                               | 0                                 | 0                             | 27                             | 9                         | 1                         | 1                          | 0                         | 0                            | 0                        | 0                             | 8                          | 0                        |
| 1    | 191              | -2053.1           | C                                  | 29.8      | Sandy Silt | 0                          | 3                         | 0                           | 0                            | 0                           | 3                               | 0                                 | 0                             | 29                             | 9                         | 0                         | 0                          | 0                         | 0                            | 0                        | 0                             | 2                          | 0                        |
| 1    | 201              | -2053.1           | C                                  | 31.5      | Sandy Silt | 0                          | 8                         | 0                           | 0                            | 0                           | 4                               | 0                                 | 0                             | 30                             | 10                        | 0                         | 0                          | 0                         | 0                            | 0                        | 0                             | 5                          | 0                        |
| 1    | 211              | -2053.1           | C                                  | 30.2      | Sandy Silt | 0                          | 2                         | 0                           | 0                            | 2                           | 3                               | 0                                 | 0                             | 35                             | 15                        | 0                         | 0                          | 0                         | 0                            | 0                        | 0                             | 6                          | 1                        |
| 1    | 221              | -2053.1           | C                                  | 31.5      | Sandy Silt | 0                          | 2                         | 0                           | 0                            | 0                           | 0                               | 0                                 | 0                             | 24                             | 2                         | 0                         | 0                          | 0                         | 0                            | 0                        | 0                             | 5                          | 0                        |
| 1    | 231              | -2053.1           | C                                  | 43.9      | Sandy Silt | 0                          | 2                         | 0                           | 0                            | 0                           | 2                               | 0                                 | 0                             | 20                             | 13                        | 0                         | 0                          | 0                         | 0                            | 0                        | 0                             | 2                          | 0                        |
| 1    | 241              | -2053.1           | C                                  | 29.9      | Sandy Silt | 1                          | 2                         | 0                           | 0                            | 0                           | 3                               | 0                                 | 0                             | 16                             | 2                         | 0                         | 0                          | 0                         | 0                            | 0                        | 0                             | 0                          | 1                        |
| 1    | 251              | -2053.1           | T                                  | 28.2      | Silt       | 0                          | 0                         | 0                           | 0                            | 0                           | 1                               | 0                                 | 0                             | 19                             | 3                         | 0                         | 0                          | 0                         | 0                            | 0                        | 0                             | 0                          | 0                        |
| 1    | 261              | -2053.1           | T                                  | 30.1      | Sandy Silt | 0                          | 4                         | 0                           | 0                            | 0                           | 9                               | 0                                 | 0                             | 56                             | 12                        | 1                         | 0                          | 0                         | 0                            | 0                        | 0                             | 5                          | 1                        |

|    |      |             |   |      |            |   |    |   |   |   |    |   |   |    |    |   |    |   |   |   |   |    |    |    |
|----|------|-------------|---|------|------------|---|----|---|---|---|----|---|---|----|----|---|----|---|---|---|---|----|----|----|
| 1  | 271  | -<br>2053.1 | T | 25.8 | Silt       | 0 | 3  | 0 | 0 | 0 | 9  | 0 | 0 | 9  | 1  | 0 | 0  | 0 | 0 | 0 | 0 | 0  | 1  | 0  |
| 1  | 275  | -<br>2053.1 | T | 24.7 | Silt       | 0 | 4  | 0 | 0 | 0 | 30 | 0 | 0 | 29 | 3  | 0 | 0  | 0 | 0 | 0 | 0 | 0  | 0  | 0  |
| 1  | 277  | -<br>2053.1 | T | 25.1 | Silt       | 1 | 4  | 0 | 0 | 0 | 5  | 0 | 0 | 20 | 3  | 0 | 0  | 0 | 0 | 0 | 0 | 0  | 1  | 0  |
| 1  | 278  | -<br>2053.1 | T | 23   | Sandy Silt | 0 | 2  | 0 | 0 | 0 | 6  | 0 | 0 | 40 | 0  | 0 | 0  | 0 | 0 | 0 | 0 | 0  | 1  | 0  |
| 1  | 279  | -<br>2053.1 | T | 27   | Silt       | 0 | 0  | 0 | 0 | 0 | 1  | 0 | 0 | 9  | 5  | 0 | 0  | 0 | 0 | 0 | 0 | 0  | 0  | 0  |
| 1  | 283  | -<br>2053.1 | T | 15.9 | Clay       | 0 | 0  | 0 | 0 | 0 | 0  | 0 | 0 | 5  | 1  | 0 | 0  | 0 | 0 | 0 | 0 | 0  | 0  | 0  |
| 1  | 287  | -<br>2053.1 | T | 16.5 | Clay       | 0 | 0  | 0 | 0 | 0 | 1  | 0 | 0 | 7  | 2  | 0 | 0  | 0 | 0 | 0 | 0 | 0  | 0  | 0  |
| 1  | 289  | -<br>2053.1 | T | 26.6 | Sandy Silt | 1 | 5  | 0 | 0 | 0 | 0  | 0 | 0 | 49 | 10 | 0 | 0  | 0 | 0 | 0 | 0 | 0  | 4  | 0  |
| 1  | 293  | -<br>2053.1 | T | 29.3 | Sandy Silt | 0 | 0  | 0 | 0 | 0 | 0  | 0 | 0 | 26 | 9  | 0 | 0  | 0 | 0 | 0 | 0 | 0  | 2  | 0  |
| 1  | 300  | -<br>2053.1 | T | 21.1 | Silt       | 0 | 1  | 0 | 0 | 0 | 9  | 0 | 0 | 29 | 7  | 0 | 0  | 0 | 0 | 0 | 0 | 0  | 3  | 2  |
| 1  | 305  | -<br>2053.1 | T | 25.7 | Sandy Silt | 0 | 5  | 0 | 0 | 0 | 0  | 0 | 0 | 38 | 8  | 0 | 0  | 0 | 0 | 0 | 0 | 0  | 2  | 0  |
| 1  | 310  | -<br>2053.1 | T | 25.8 | Silt       | 0 | 0  | 0 | 0 | 0 | 7  | 0 | 0 | 26 | 3  | 0 | 0  | 0 | 0 | 0 | 0 | 0  | 0  | 0  |
| 1  | 315  | -<br>2053.1 | T | 28.2 | Sandy Silt | 0 | 0  | 0 | 0 | 0 | 17 | 0 | 0 | 29 | 6  | 0 | 0  | 0 | 0 | 0 | 0 | 0  | 0  | 0  |
| 1  | 320  | -<br>2053.1 | T | 25.1 | Silt       | 0 | 0  | 0 | 0 | 0 | 7  | 0 | 0 | 8  | 2  | 0 | 0  | 0 | 0 | 0 | 0 | 0  | 0  | 0  |
| 1  | 325  | -<br>2053.1 | T | 29.5 | Silt       | 0 | 3  | 0 | 0 | 0 | 13 | 0 | 0 | 21 | 1  | 0 | 0  | 0 | 0 | 0 | 0 | 0  | 2  | 0  |
| 1  | 330  | -<br>2053.1 | T | 25.7 | Sandy Silt | 0 | 1  | 0 | 0 | 0 | 0  | 0 | 0 | 42 | 15 | 0 | 0  | 0 | 0 | 0 | 0 | 0  | 5  | 0  |
| 1  | 335  | -<br>2053.1 | T | 28.7 | Sandy Silt | 0 | 2  | 0 | 0 | 0 | 3  | 0 | 0 | 25 | 9  | 0 | 0  | 0 | 0 | 0 | 0 | 0  | 1  | 1  |
| 1  | 337  | -<br>2053.1 | T | 25.7 | Silt       | 0 | 2  | 0 | 0 | 0 | 7  | 0 | 0 | 21 | 3  | 0 | 0  | 0 | 0 | 0 | 0 | 0  | 0  | 1  |
| 1  | 341  | -<br>2053.1 | T | 26.2 | Sandy Silt | 0 | 0  | 0 | 0 | 0 | 4  | 0 | 0 | 39 | 6  | 0 | 0  | 0 | 0 | 0 | 0 | 0  | 0  | 3  |
| 1  | 350  | -<br>2053.1 | T | 20.4 | Silt       | 0 | 4  | 0 | 0 | 0 | 22 | 0 | 0 | 34 | 3  | 0 | 0  | 0 | 0 | 0 | 0 | 0  | 0  | 0  |
| 1  | 355  | -<br>2053.1 | T | 27.6 | Silt       | 0 | 1  | 0 | 0 | 0 | 12 | 0 | 0 | 32 | 2  | 0 | 0  | 0 | 0 | 0 | 0 | 0  | 2  | 0  |
| 1  | 361  | -<br>2053.1 | T | 32.4 | Sandy Silt | 0 | 1  | 0 | 0 | 0 | 10 | 0 | 0 | 79 | 8  | 0 | 0  | 0 | 0 | 0 | 0 | 0  | 3  | 0  |
| 1  | 366  | -<br>2053.1 | T | 17.2 | Clay       | 0 | 6  | 0 | 0 | 0 | 13 | 0 | 0 | 59 | 13 | 0 | 0  | 0 | 0 | 0 | 0 | 0  | 2  | 0  |
| 1  | 372  | -<br>2053.1 | T | 20.1 | Silt       | 0 | 2  | 0 | 0 | 0 | 9  | 0 | 0 | 48 | 1  | 0 | 0  | 0 | 0 | 0 | 0 | 0  | 2  | 0  |
| 1  | 376  | -<br>2053.1 | T | 24.6 | Silt       | 0 | 0  | 0 | 0 | 0 | 2  | 0 | 0 | 25 | 8  | 0 | 0  | 0 | 0 | 0 | 0 | 0  | 2  | 0  |
| 1  | 383  | -<br>2053.1 | T | 22.8 | Silt       | 0 | 1  | 0 | 0 | 0 | 3  | 0 | 0 | 52 | 6  | 0 | 0  | 0 | 0 | 0 | 0 | 0  | 2  | 0  |
| 1  | 387  | -<br>2053.1 | T | 19.1 | Clay       | 0 | 0  | 0 | 0 | 0 | 3  | 0 | 0 | 61 | 3  | 0 | 0  | 0 | 0 | 0 | 0 | 1  | 0  | 0  |
| 1  | 391  | -<br>2053.1 | T | 21.3 | Silt       | 0 | 2  | 0 | 0 | 0 | 1  | 0 | 0 | 18 | 0  | 0 | 0  | 0 | 0 | 0 | 0 | 0  | 0  | 0  |
| 1  | 393  | -<br>2053.1 | T | 23.6 | Silt       | 0 | 2  | 0 | 0 | 0 | 6  | 0 | 0 | 13 | 3  | 0 | 0  | 0 | 0 | 0 | 0 | 0  | 1  | 0  |
| 1  | 397  | -<br>2053.1 | T | 26.7 | Sandy Silt | 0 | 3  | 0 | 0 | 0 | 7  | 0 | 0 | 44 | 6  | 0 | 0  | 0 | 0 | 0 | 0 | 0  | 0  | 0  |
| 65 | 1.5  | -<br>1896.6 | C | 30   | Sandy Silt | 2 | 10 | 0 | 0 | 0 | 14 | 0 | 0 | 0  | 46 | 0 | 3  | 0 | 0 | 0 | 0 | 7  | 13 | 0  |
| 65 | 5.5  | -<br>1896.6 | C | 26   | Sandy Silt | 0 | 7  | 0 | 0 | 0 | 10 | 0 | 0 | 35 | 18 | 0 | 0  | 0 | 0 | 0 | 0 | 4  | 7  | 0  |
| 65 | 11.5 | -<br>1896.6 | C | 28.4 | Sandy Silt | 0 | 3  | 0 | 0 | 0 | 79 | 0 | 0 | 32 | 30 | 0 | 2  | 0 | 0 | 0 | 0 | 3  | 5  | 0  |
| 65 | 14.8 | -<br>1896.6 | C | 26.4 | Sandy Silt | 0 | 5  | 0 | 0 | 0 | 17 | 0 | 0 | 56 | 39 | 0 | 4  | 0 | 0 | 0 | 0 | 13 | 9  | 0  |
| 65 | 20.8 | -<br>1896.6 | C | 24.7 | Sandy Silt | 0 | 4  | 0 | 0 | 0 | 10 | 0 | 0 | 38 | 43 | 0 | 5  | 0 | 0 | 0 | 0 | 4  | 9  | 0  |
| 65 | 26.3 | -<br>1896.6 | C | 24.8 | Sandy Silt | 0 | 11 | 0 | 0 | 0 | 89 | 0 | 0 | 39 | 49 | 0 | 3  | 0 | 0 | 0 | 0 | 9  | 11 | 0  |
| 65 | 26.8 | -<br>1896.6 | C | 24.7 | Sandy Silt | 0 | 15 | 0 | 0 | 0 | 76 | 0 | 0 | 34 | 41 | 0 | 3  | 0 | 0 | 0 | 0 | 8  | 15 | 0  |
| 65 | 35.3 | -<br>1896.6 | C | 27.4 | Sandy Silt | 0 | 10 | 0 | 0 | 0 | 28 | 0 | 0 | 29 | 38 | 0 | 0  | 0 | 0 | 0 | 0 | 4  | 14 | 0  |
| 65 | 45.3 | -<br>1896.6 | C | 27.4 | Sandy Silt | 0 | 5  | 0 | 0 | 0 | 12 | 0 | 0 | 12 | 28 | 0 | 0  | 0 | 0 | 0 | 0 | 3  | 5  | 0  |
| 65 | 55.3 | -<br>1896.6 | C | 25.7 | Sandy Silt | 0 | 3  | 0 | 0 | 0 | 14 | 0 | 0 | 12 | 45 | 0 | 0  | 0 | 0 | 0 | 0 | 2  | 4  | 0  |
| 65 | 65.3 | -<br>1896.6 | C | 24.8 | Sandy Silt | 0 | 15 | 0 | 0 | 0 | 35 | 0 | 0 | 25 | 39 | 0 | 4  | 0 | 0 | 0 | 0 | 6  | 11 | 0  |
| 65 | 75.3 | -<br>1896.6 | C | 26.3 | Sandy Silt | 0 | 6  | 0 | 0 | 0 | 24 | 0 | 0 | 29 | 18 | 0 | 7  | 0 | 0 | 0 | 0 | 0  | 11 | 0  |
| 65 | 85.3 | -<br>1896.6 | C | 30.4 | Sandy Silt | 0 | 11 | 0 | 0 | 0 | 29 | 1 | 0 | 37 | 27 | 0 | 18 | 0 | 0 | 0 | 0 | 0  | 27 | 10 |
| 65 | 95.3 | -<br>1896.6 | T | 18   | Silt       | 0 | 3  | 0 | 0 | 0 | 25 | 0 | 1 | 23 | 23 | 0 | 13 | 0 | 0 | 0 | 0 | 0  | 44 | 1  |



|    |     |             |   |       |            |   |    |   |   |   |      |   |   |      |    |   |    |   |   |   |   |    |    |
|----|-----|-------------|---|-------|------------|---|----|---|---|---|------|---|---|------|----|---|----|---|---|---|---|----|----|
| 65 | 105 | -<br>1896.6 | T | 11.3  | Silt       | 0 | 6  | 0 | 0 | 0 | 18   | 0 | 0 | 16   | 25 | 0 | 3  | 0 | 0 | 0 | 0 | 14 | 0  |
| 65 | 115 | -<br>1896.6 | T | 21.3  | Sandy Silt | 0 | 7  | 0 | 0 | 0 | 24   | 0 | 0 | 59   | 17 | 0 | 5  | 0 | 0 | 0 | 0 | 13 | 0  |
| 65 | 122 | -<br>1896.6 | T | 17    | Silt       | 0 | 5  | 0 | 0 | 0 | 42   | 0 | 0 | 46   | 7  | 0 | 4  | 0 | 0 | 0 | 0 | 15 | 0  |
| 65 | 126 | -<br>1896.6 | T | 22.5  | Sandy Silt | 0 | 8  | 0 | 0 | 0 | 29   | 0 | 0 | 71   | 11 | 0 | 5  | 0 | 0 | 0 | 0 | 16 | 3  |
| 65 | 134 | -<br>1896.6 | T | 15.4  | Clay       | 0 | 4  | 0 | 0 | 0 | 32   | 0 | 0 | 22   | 20 | 0 | 11 | 0 | 0 | 0 | 0 | 17 | 3  |
| 65 | 144 | -<br>1896.6 | T | 20.4  | Sandy Silt | 0 | 5  | 0 | 0 | 0 | 30   | 0 | 0 | 36   | 11 | 0 | 1  | 0 | 0 | 0 | 0 | 8  | 2  |
| 65 | 154 | -<br>1896.6 | T | 19.2  | Silt       | 0 | 6  | 0 | 0 | 0 | 10   | 0 | 0 | 35   | 26 | 0 | 5  | 0 | 0 | 0 | 0 | 5  | 2  |
| 65 | 164 | -<br>1896.6 | T | 25.1  | Sandy Silt | 0 | 11 | 0 | 0 | 0 | 25   | 0 | 0 | 58   | 47 | 0 | 3  | 0 | 0 | 0 | 0 | 5  | 2  |
| 65 | 174 | -<br>1896.6 | T | 18.7  | Silt       | 0 | 15 | 0 | 0 | 0 | 11   | 0 | 0 | 35   | 16 | 0 | 3  | 0 | 0 | 0 | 0 | 4  | 0  |
| 65 | 184 | -<br>1896.6 | T | 19.2  | Silt       | 0 | 12 | 0 | 0 | 0 | 15   | 0 | 0 | 35   | 28 | 0 | 7  | 0 | 0 | 0 | 0 | 8  | 0  |
| 65 | 194 | -<br>1896.6 | T | 23.4  | Sandy Silt | 0 | 9  | 0 | 0 | 0 | 18   | 0 | 0 | 48   | 54 | 0 | 6  | 0 | 0 | 0 | 0 | 19 | 0  |
| 65 | 204 | -<br>1896.6 | T | 18.4  | Silt       | 0 | 5  | 0 | 0 | 0 | 33   | 0 | 0 | 56   | 21 | 0 | 1  | 0 | 0 | 0 | 0 | 7  | 0  |
| 65 | 214 | -<br>1896.6 | T | 18.4  | Silt       | 0 | 13 | 0 | 0 | 0 | 18   | 0 | 0 | 76   | 18 | 0 | 13 | 0 | 0 | 0 | 0 | 20 | 0  |
| 65 | 222 | -<br>1896.6 | T | 18    | Silt       | 0 | 12 | 0 | 0 | 0 | 30   | 0 | 1 | 35   | 25 | 0 | 11 | 0 | 0 | 0 | 0 | 25 | 0  |
| 65 | 223 | -<br>1896.6 | T | 21.9  | Sandy Silt | 0 | 6  | 0 | 0 | 0 | 27   | 0 | 0 | 38   | 13 | 0 | 3  | 0 | 0 | 0 | 0 | 11 | 3  |
| 65 | 232 | -<br>1896.6 | T | 19.2  | Silt       | 0 | 11 | 0 | 0 | 0 | 11.3 | 0 | 0 | 64   | 13 | 0 | 8  | 0 | 0 | 0 | 0 | 12 | 0  |
| 65 | 242 | -<br>1896.6 | T | 17.8  | Silt       | 0 | 5  | 0 | 0 | 0 | 48   | 0 | 0 | 44   | 17 | 0 | 8  | 0 | 0 | 0 | 0 | 7  | 0  |
| 65 | 252 | -<br>1896.6 | T | 23.3  | Sandy Silt | 0 | 10 | 0 | 0 | 0 | 34   | 0 | 0 | 44   | 49 | 0 | 9  | 0 | 0 | 0 | 0 | 9  | 0  |
| 65 | 259 | -<br>1896.6 | T | 20.9  | Sandy Silt | 0 | 6  | 0 | 0 | 0 | 50   | 0 | 0 | 42   | 21 | 0 | 3  | 0 | 0 | 0 | 0 | 7  | 0  |
| 65 | 261 | -<br>1896.6 | T | 21.7  | Sandy Silt | 0 | 10 | 0 | 0 | 0 | 29   | 0 | 0 | 26   | 37 | 0 | 9  | 0 | 0 | 0 | 0 | 32 | 0  |
| 65 | 269 | -<br>1896.6 | T | 19.8  | Silt       | 0 | 12 | 0 | 0 | 0 | 20   | 0 | 0 | 14   | 13 | 0 | 5  | 0 | 0 | 0 | 0 | 20 | 0  |
| 65 | 279 | -<br>1896.6 | T | 20.1  | Sandy Silt | 0 | 11 | 0 | 0 | 0 | 27   | 0 | 0 | 63   | 32 | 0 | 17 | 0 | 0 | 0 | 0 | 29 | 0  |
| 65 | 289 | -<br>1896.6 | T | 20.7  | Sandy Silt | 0 | 9  | 0 | 0 | 0 | 73   | 0 | 0 | 11.0 | 21 | 0 | 12 | 0 | 0 | 0 | 0 | 38 | 0  |
| 65 | 299 | -<br>1896.6 | T | 14.7  | Clay       | 0 | 7  | 0 | 0 | 0 | 36   | 0 | 0 | 23   | 8  | 0 | 8  | 0 | 0 | 0 | 0 | 18 | 0  |
| 65 | 309 | -<br>1896.6 | T | 18.2  | Silt       | 0 | 13 | 0 | 0 | 0 | 47   | 0 | 0 | 69   | 35 | 1 | 19 | 0 | 0 | 0 | 0 | 37 | 10 |
| 65 | 317 | -<br>1896.6 | T | 21.9  | Sandy Silt | 0 | 9  | 0 | 0 | 0 | 46   | 0 | 0 | 50   | 32 | 0 | 13 | 0 | 0 | 0 | 0 | 24 | 0  |
| 65 | 317 | -<br>1896.6 | T | 18.8  | Silt       | 0 | 15 | 0 | 0 | 0 | 39   | 0 | 0 | 69   | 31 | 0 | 17 | 0 | 0 | 0 | 0 | 34 | 0  |
| 65 | 327 | -<br>1896.6 | T | 13.9  | Clay       | 0 | 11 | 0 | 0 | 0 | 83   | 0 | 0 | 10.1 | 15 | 0 | 0  | 0 | 0 | 0 | 0 | 10 | 0  |
| 65 | 337 | -<br>1896.6 | T | 9.6.8 | Clay       | 0 | 3  | 0 | 0 | 0 | 43   | 0 | 1 | 12.3 | 4  | 0 | 0  | 0 | 0 | 0 | 0 | 9  | 3  |
| 65 | 347 | -<br>1896.6 | T | 14.2  | Silt       | 0 | 5  | 0 | 0 | 0 | 68   | 0 | 0 | 81   | 21 | 0 | 7  | 0 | 0 | 0 | 0 | 15 | 3  |
| 65 | 354 | -<br>1896.6 | T | 13.2  | Clay       | 0 | 9  | 0 | 0 | 0 | 19   | 0 | 0 | 66   | 45 | 0 | 2  | 0 | 0 | 0 | 0 | 6  | 0  |
| 65 | 357 | -<br>1896.6 | T | 14.5  | Clay       | 0 | 8  | 0 | 0 | 0 | 26   | 0 | 0 | 87   | 21 | 0 | 2  | 0 | 0 | 0 | 0 | 11 | 0  |
| 65 | 366 | -<br>1896.6 | T | 14.1  | Clay       | 0 | 2  | 0 | 0 | 0 | 16   | 0 | 0 | 38   | 27 | 0 | 3  | 0 | 0 | 0 | 0 | 10 | 0  |
| 65 | 371 | -<br>1896.6 | T | 12.1  | Clay       | 0 | 0  | 0 | 0 | 0 | 6    | 0 | 0 | 11   | 15 | 0 | 1  | 0 | 0 | 0 | 0 | 6  | 0  |
| 65 | 376 | -<br>1896.6 | T | 14.1  | Clay       | 0 | 2  | 0 | 0 | 0 | 22   | 0 | 0 | 18   | 13 | 0 | 0  | 0 | 0 | 0 | 0 | 0  | 0  |
| 65 | 386 | -<br>1896.6 | T | 14.4  | Clay       | 0 | 7  | 0 | 0 | 0 | 41   | 0 | 0 | 33   | 10 | 0 | 7  | 0 | 0 | 0 | 0 | 12 | 0  |
| 65 | 395 | -<br>1896.6 | T | 21.1  | Sandy Silt | 0 | 7  | 0 | 0 | 0 | 41   | 0 | 0 | 28   | 34 | 0 | 16 | 0 | 0 | 0 | 0 | 25 | 10 |
| 65 | 396 | -<br>1896.6 | T | 19.7  | Silt       | 0 | 17 | 0 | 0 | 0 | 32   | 0 | 0 | 25   | 42 | 0 | 16 | 0 | 0 | 0 | 0 | 11 | 9  |
| 65 | 406 | -<br>1896.6 | T | 15.6  | Clay       | 0 | 2  | 0 | 0 | 0 | 29   | 0 | 0 | 14   | 10 | 0 | 1  | 0 | 0 | 0 | 0 | 5  | 6  |
| 65 | 416 | -<br>1896.6 | T | 13    | Clay       | 0 | 0  | 0 | 0 | 0 | 31   | 0 | 0 | 6    | 4  | 0 | 2  | 0 | 0 | 0 | 0 | 2  | 4  |
| 65 | 426 | -<br>1896.6 | T | 13.8  | Clay       | 0 | 3  | 0 | 0 | 0 | 27   | 0 | 0 | 14   | 14 | 0 | 8  | 0 | 0 | 0 | 0 | 11 | 0  |
| 65 | 436 | -<br>1896.6 | T | 18.4  | Silt       | 0 | 6  | 0 | 0 | 0 | 49   | 0 | 0 | 41   | 22 | 0 | 9  | 0 | 0 | 0 | 0 | 13 | 3  |
| 65 | 436 | -<br>1896.6 | T | 23.6  | Sandy Silt | 0 | 8  | 0 | 0 | 0 | 19   | 0 | 0 | 23   | 11 | 0 | 3  | 0 | 0 | 0 | 0 | 4  | 1  |
| 65 | 444 | -<br>1896.6 | T | 13.7  | Clay       | 0 | 7  | 0 | 0 | 0 | 64   | 0 | 0 | 53   | 29 | 0 | 3  | 0 | 0 | 0 | 0 | 6  | 3  |

|     |      |         |   |      |            |   |    |   |   |    |    |   |      |    |      |    |    |   |   |   |    |    |    |
|-----|------|---------|---|------|------------|---|----|---|---|----|----|---|------|----|------|----|----|---|---|---|----|----|----|
| 65  | 454  | -1896.6 | T | 18   | Silt       | 0 | 13 | 0 | 0 | 0  | 58 | 0 | 0    | 39 | 30   | 0  | 17 | 0 | 0 | 0 | 0  | 18 | 5  |
| 65  | 461  | -1896.6 | T | 14.1 | Clay       | 0 | 3  | 0 | 0 | 0  | 83 | 0 | 0    | 33 | 24   | 0  | 6  | 0 | 0 | 0 | 0  | 16 | 7  |
| 125 | 7.54 | -1121.2 | C | 96.6 | Silty Sand | 0 | 0  | 0 | 0 | 0  | 0  | 0 | 0    | 0  | 0    | 0  | 0  | 0 | 0 | 0 | 0  | 0  | 0  |
| 125 | 20.3 | -1121.2 | C | 96.5 | Silty Sand | 0 | 45 | 0 | 0 | 0  | 11 | 0 | 5    | 41 | 16.2 | 0  | 13 | 0 | 0 | 0 | 0  | 42 | 28 |
| 125 | 26.3 | -1121.2 | C | 96.7 | Silty Sand | 0 | 49 | 0 | 0 | 0  | 8  | 0 | 9    | 12 | 17.4 | 0  | 7  | 0 | 0 | 0 | 0  | 40 | 14 |
| 125 | 36.3 | -1121.2 | C | 96.4 | Silty Sand | 0 | 24 | 0 | 0 | 0  | 6  | 0 | 3    | 32 | 83   | 0  | 5  | 0 | 0 | 0 | 0  | 13 | 6  |
| 125 | 46.3 | -1121.2 | C | 95.6 | Silty Sand | 0 | 27 | 1 | 1 | 0  | 7  | 0 | 6    | 32 | 13.6 | 0  | 4  | 0 | 0 | 0 | 0  | 22 | 4  |
| 125 | 56.3 | -1121.2 | C | 96   | Silty Sand | 0 | 29 | 0 | 0 | 0  | 4  | 0 | 1    | 29 | 13.6 | 0  | 6  | 0 | 0 | 0 | 0  | 28 | 8  |
| 125 | 66.3 | -1121.2 | C | 95.4 | Silty Sand | 0 | 23 | 0 | 0 | 0  | 1  | 0 | 5    | 21 | 11.7 | 0  | 4  | 0 | 0 | 0 | 0  | 18 | 9  |
| 125 | 76.3 | -1121.2 | C | 96.6 | Silty Sand | 0 | 20 | 0 | 0 | 0  | 0  | 0 | 0    | 24 | 11.9 | 0  | 3  | 0 | 0 | 0 | 0  | 18 | 9  |
| 125 | 80   | -1121.2 | C | 96.1 | Silty Sand | 0 | 30 | 0 | 0 | 0  | 5  | 1 | 15   | 15 | 14.2 | 0  | 8  | 0 | 0 | 0 | 0  | 8  | 0  |
| 125 | 88   | -1121.2 | C | 96.3 | Silty Sand | 0 | 25 | 0 | 0 | 0  | 3  | 0 | 13   | 17 | 70   | 0  | 2  | 0 | 0 | 0 | 0  | 11 | 8  |
| 125 | 98   | -1121.2 | C | 96.3 | Silty Sand | 0 | 24 | 0 | 0 | 0  | 2  | 0 | 22   | 16 | 71   | 0  | 0  | 0 | 0 | 0 | 0  | 13 | 5  |
| 125 | 108  | -1121.2 | C | 96.9 | Silty Sand | 0 | 29 | 0 | 0 | 0  | 1  | 0 | 19   | 14 | 11.8 | 0  | 1  | 0 | 0 | 0 | 0  | 20 | 9  |
| 125 | 118  | -1121.2 | C | 97.2 | Silty Sand | 0 | 24 | 0 | 0 | 0  | 3  | 0 | 17   | 16 | 11.7 | 0  | 5  | 0 | 0 | 0 | 0  | 14 | 5  |
| 125 | 128  | -1121.2 | C | 97.3 | Silty Sand | 0 | 37 | 0 | 0 | 0  | 1  | 0 | 22   | 13 | 10.7 | 0  | 0  | 0 | 0 | 0 | 0  | 15 | 6  |
| 125 | 138  | -1121.2 | C | 97.7 | Silty Sand | 0 | 35 | 0 | 0 | 0  | 3  | 0 | 10   | 14 | 10.7 | 0  | 5  | 0 | 0 | 0 | 0  | 25 | 7  |
| 125 | 148  | -1121.2 | C | 96.5 | Silty Sand | 0 | 38 | 0 | 0 | 0  | 2  | 1 | 24   | 19 | 95   | 0  | 11 | 0 | 0 | 0 | 1  | 9  | 4  |
| 125 | 155  | -1121.2 | C | 97   | Silty Sand | 0 | 46 | 0 | 0 | 0  | 0  | 0 | 16   | 20 | 15.4 | 0  | 4  | 0 | 0 | 0 | 0  | 25 | 10 |
| 125 | 157  | -1121.2 | C | 96.8 | Silty Sand | 0 | 74 | 0 | 0 | 0  | 7  | 0 | 48   | 28 | 15.0 | 0  | 8  | 0 | 0 | 0 | 0  | 26 | 10 |
| 125 | 165  | -1121.2 | C | 96.4 | Silty Sand | 0 | 36 | 0 | 0 | 0  | 15 | 0 | 40   | 14 | 11.9 | 0  | 3  | 0 | 0 | 0 | 0  | 21 | 16 |
| 125 | 175  | -1121.2 | C | 96.2 | Silty Sand | 0 | 34 | 0 | 0 | 0  | 21 | 2 | 36   | 30 | 16.8 | 0  | 7  | 0 | 0 | 0 | 0  | 24 | 16 |
| 125 | 185  | -1121.2 | C | 97   | Silty Sand | 0 | 53 | 0 | 0 | 0  | 10 | 0 | 32   | 46 | 14.0 | 0  | 8  | 0 | 0 | 0 | 0  | 18 | 13 |
| 125 | 195  | -1121.2 | C | 96.2 | Silty Sand | 0 | 94 | 0 | 0 | 0  | 5  | 0 | 49   | 50 | 14.8 | 0  | 8  | 0 | 0 | 0 | 0  | 16 | 2  |
| 125 | 205  | -1121.2 | C | 95.3 | Silty Sand | 0 | 46 | 0 | 0 | 0  | 12 | 0 | 58   | 35 | 28.1 | 0  | 9  | 0 | 0 | 0 | 0  | 16 | 22 |
| 125 | 215  | -1121.2 | C | 95.8 | Silty Sand | 0 | 85 | 0 | 0 | 0  | 0  | 0 | 57   | 36 | 16.4 | 0  | 3  | 0 | 0 | 0 | 0  | 25 | 22 |
| 125 | 225  | -1121.2 | C | 96.5 | Silty Sand | 0 | 64 | 0 | 0 | 0  | 25 | 0 | 80   | 71 | 35.6 | 0  | 7  | 0 | 0 | 0 | 0  | 28 | 12 |
| 125 | 233  | -1121.2 | C | 95.1 | Silty Sand | 0 | 52 | 0 | 0 | 0  | 14 | 0 | 46   | 43 | 20.8 | 0  | 5  | 0 | 0 | 0 | 0  | 12 | 4  |
| 125 | 233  | -1121.2 | C | 95.3 | Silty Sand | 0 | 48 | 0 | 0 | 0  | 6  | 0 | 48   | 35 | 14.8 | 0  | 4  | 0 | 0 | 0 | 0  | 16 | 18 |
| 125 | 241  | -1121.2 | C | 96.4 | Silty Sand | 0 | 25 | 0 | 0 | 0  | 6  | 0 | 82   | 18 | 22.4 | 0  | 4  | 0 | 0 | 0 | 0  | 7  | 11 |
| 125 | 251  | -1121.2 | C | 97.2 | Silty Sand | 0 | 27 | 0 | 0 | 0  | 2  | 0 | 51   | 20 | 17.1 | 0  | 1  | 0 | 0 | 0 | 0  | 14 | 6  |
| 125 | 261  | -1121.2 | C | 97.1 | Silty Sand | 0 | 37 | 0 | 0 | 0  | 2  | 0 | 48   | 24 | 18.9 | 0  | 0  | 0 | 0 | 0 | 0  | 8  | 6  |
| 125 | 271  | -1121.2 | C | 98.3 | Silty Sand | 0 | 6  | 0 | 0 | 0  | 2  | 0 | 11.7 | 2  | 14.6 | 0  | 1  | 0 | 0 | 0 | 0  | 6  | 7  |
| 125 | 281  | -1121.2 | C | 99.1 | Sand       | 0 | 5  | 0 | 0 | 0  | 1  | 0 | 13   | 4  | 13.2 | 0  | 3  | 0 | 0 | 0 | 0  | 14 | 46 |
| 125 | 291  | -1121.2 | C | 98.9 | Sand       | 0 | 3  | 0 | 0 | 0  | 0  | 0 | 9    | 3  | 10.6 | 0  | 1  | 0 | 0 | 0 | 0  | 22 | 41 |
| 125 | 296  | -1121.2 | C | 99.3 | Sand       | 0 | 4  | 0 | 0 | 0  | 2  | 0 | 8    | 1  | 77   | 0  | 0  | 0 | 0 | 0 | 0  | 26 | 47 |
| 133 | 10.5 | -2451   | C | 33.7 | Sandy Silt | 3 | 1  | 0 | 6 | 15 | 0  | 0 | 1    | 2  | 1    | 5  | 0  | 0 | 0 | 0 | 20 | 16 | 0  |
| 133 | 14.5 | -2451   | C | 34   | Sandy Silt | 1 | 0  | 0 | 1 | 5  | 0  | 0 | 0    | 0  | 1    | 4  | 0  | 0 | 0 | 0 | 16 | 9  | 0  |
| 133 | 14.7 | -2451   | C | 26.5 | Sandy Silt | 1 | 1  | 0 | 1 | 0  | 0  | 0 | 0    | 1  | 9    | 12 | 0  | 0 | 0 | 0 | 21 | 22 | 0  |
| 133 | 23.7 | -2451   | C | 31.6 | Sandy Silt | 6 | 1  | 0 | 0 | 0  | 0  | 0 | 0    | 2  | 6    | 13 | 0  | 0 | 0 | 0 | 37 | 28 | 0  |
| 133 | 28.7 | -2451   | C | 32.7 | Sandy Silt | 1 | 0  | 0 | 0 | 6  | 1  | 2 | 0    | 1  | 7    | 10 | 0  | 0 | 0 | 0 | 21 | 28 | 0  |
| 133 | 33.7 | -2451   | C | 31.2 | Sandy Silt | 4 | 0  | 0 | 0 | 2  | 0  | 0 | 0    | 4  | 4    | 6  | 0  | 0 | 0 | 0 | 15 | 11 | 0  |
| 133 | 43.7 | -2451   | C | 30.6 | Sandy Silt | 1 | 1  | 0 | 0 | 0  | 0  | 0 | 0    | 5  | 5    | 2  | 0  | 0 | 0 | 0 | 7  | 14 | 0  |
| 133 | 53.7 | -2451   | C | 23.9 | Sandy Silt | 0 | 6  | 0 | 0 | 0  | 0  | 0 | 0    | 8  | 9    | 19 | 0  | 0 | 0 | 0 | 15 | 25 | 0  |

|     |      |         |   |      |            |    |    |   |   |     |   |   |   |     |    |    |   |     |   |   |     |     |   |
|-----|------|---------|---|------|------------|----|----|---|---|-----|---|---|---|-----|----|----|---|-----|---|---|-----|-----|---|
| 133 | 63.7 | -2451   | C | 32.7 | Sandy Silt | 1  | 19 | 0 | 0 | 0   | 0 | 2 | 0 | 20  | 16 | 27 | 0 | 0   | 0 | 0 | 28  | 51  | 0 |
| 133 | 73.7 | -2451   | C | 32.5 | Sandy Silt | 0  | 6  | 0 | 0 | 0   | 0 | 0 | 0 | 12  | 9  | 14 | 0 | 0   | 0 | 0 | 22  | 14  | 0 |
| 133 | 78.7 | -2451   | C | 30.8 | Sandy Silt | 0  | 4  | 0 | 0 | 0   | 0 | 0 | 2 | 22  | 7  | 10 | 0 | 0   | 0 | 0 | 25  | 16  | 0 |
| 133 | 83.7 | -2451   | C | 32   | Sandy Silt | 0  | 4  | 0 | 0 | 0   | 0 | 0 | 2 | 36  | 3  | 5  | 0 | 0   | 0 | 0 | 7   | 6   | 0 |
| 133 | 88.7 | -2451   | C | 30.8 | Sandy Silt | 0  | 7  | 0 | 0 | 0   | 1 | 0 | 0 | 49  | 4  | 4  | 0 | 0   | 0 | 0 | 2   | 12  | 0 |
| 133 | 93.7 | -2451   | C | 34.1 | Sandy Silt | 0  | 4  | 0 | 0 | 0   | 1 | 0 | 1 | 48  | 2  | 5  | 0 | 0   | 0 | 0 | 8   | 14  | 0 |
| 133 | 104  | -2451   | C | 27.9 | Sandy Silt | 0  | 7  | 0 | 0 | 0   | 0 | 0 | 0 | 70  | 4  | 0  | 0 | 0   | 0 | 0 | 4   | 2   | 0 |
| 133 | 112  | -2451   | C | 32.1 | Sandy Silt | 0  | 0  | 0 | 0 | 0   | 0 | 0 | 0 | 50  | 2  | 3  | 0 | 0   | 0 | 0 | 10  | 10  | 0 |
| 133 | 117  | -2451   | C | 31.4 | Sandy Silt | 0  | 1  | 0 | 0 | 0   | 0 | 0 | 0 | 76  | 0  | 0  | 0 | 0   | 0 | 0 | 2   | 2   | 0 |
| 133 | 127  | -2451   | C | 31.8 | Sandy Silt | 0  | 2  | 0 | 0 | 0   | 0 | 0 | 1 | 58  | 0  | 1  | 0 | 0   | 0 | 0 | 0   | 1   | 0 |
| 133 | 133  | -2451   | C | 35.9 | Sandy Silt | 0  | 1  | 0 | 0 | 0   | 0 | 0 | 0 | 44  | 1  | 0  | 0 | 0   | 0 | 0 | 2   | 1   | 0 |
| 133 | 137  | -2451   | C | 31.3 | Sandy Silt | 0  | 1  | 0 | 0 | 0   | 0 | 0 | 0 | 0   | 0  | 0  | 0 | 0   | 0 | 0 | 0   | 0   | 0 |
| 133 | 140  | -2451   | C | 30.4 | Sandy Silt | 0  | 0  | 0 | 0 | 53  | 0 | 0 | 0 | 0   | 0  | 0  | 0 | 0   | 0 | 0 | 0   | 0   | 0 |
| 133 | 142  | -2451   | C | 31.6 | Sandy Silt | 0  | 0  | 0 | 0 | 0   | 0 | 0 | 2 | 7   | 0  | 0  | 0 | 0   | 0 | 0 | 1   | 0   | 0 |
| 133 | 147  | -2451   | C | 29.5 | Sandy Silt | 0  | 0  | 0 | 0 | 1   | 0 | 0 | 0 | 0   | 0  | 0  | 0 | 0   | 0 | 0 | 0   | 0   | 0 |
| 133 | 152  | -2451   | C | 24.3 | Sandy Silt | 0  | 0  | 0 | 0 | 8   | 0 | 0 | 0 | 0   | 0  | 0  | 0 | 0   | 0 | 0 | 0   | 0   | 0 |
| 133 | 157  | -2451   | C | 15.7 | Silt       | 0  | 0  | 0 | 0 | 47  | 0 | 0 | 0 | 0   | 0  | 0  | 0 | 0   | 0 | 0 | 0   | 0   | 0 |
| 133 | 162  | -2451   | C | 21.2 | Silt       | 2  | 0  | 0 | 0 | 41  | 0 | 0 | 0 | 0   | 0  | 0  | 0 | 0   | 0 | 0 | 0   | 0   | 0 |
| 133 | 166  | -2451   | C | 9.72 | Clay       | 0  | 0  | 0 | 0 | 154 | 1 | 0 | 0 | 74  | 0  | 0  | 0 | 0   | 0 | 0 | 0   | 0   | 0 |
| 133 | 175  | -2451   | C | 6.76 | Clay       | 9  | 0  | 0 | 0 | 2   | 1 | 0 | 0 | 182 | 0  | 0  | 0 | 0   | 0 | 0 | 0   | 0   | 0 |
| 133 | 185  | -2451   | C | 10.9 | Clay       | 1  | 0  | 0 | 3 | 0   | 0 | 0 | 0 | 0   | 0  | 0  | 0 | 0   | 0 | 0 | 0   | 0   | 0 |
| 133 | 190  | -2451   | C | 4.67 | Clay       | 0  | 0  | 0 | 2 | 1   | 0 | 0 | 1 | 13  | 0  | 0  | 0 | 0   | 0 | 0 | 0   | 0   | 0 |
| 133 | 195  | -2451   | C | 6.31 | Clay       | 0  | 0  | 0 | 0 | 0   | 0 | 0 | 0 | 0   | 0  | 0  | 0 | 0   | 0 | 0 | 0   | 0   | 0 |
| 133 | 200  | -2451   | C | 6.38 | Clay       | 0  | 0  | 0 | 0 | 0   | 0 | 0 | 0 | 0   | 0  | 0  | 0 | 0   | 0 | 0 | 0   | 0   | 0 |
| 133 | 205  | -2451   | C | 5.4  | Clay       | 0  | 0  | 0 | 0 | 0   | 0 | 0 | 0 | 0   | 0  | 0  | 0 | 0   | 0 | 0 | 0   | 0   | 0 |
| 133 | 210  | -2451   | C | 25.1 | Fine Silt  | 0  | 1  | 0 | 0 | 10  | 0 | 0 | 0 | 10  | 1  | 0  | 0 | 0   | 0 | 0 | 0   | 1   | 0 |
| 133 | 215  | -2451   | C | 16.1 | Silt       | 26 | 0  | 0 | 0 | 26  | 0 | 0 | 0 | 0   | 0  | 0  | 0 | 0   | 0 | 0 | 0   | 0   | 0 |
| 133 | 225  | -2451   | C | 7.17 | Clay       | 0  | 0  | 0 | 0 | 0   | 0 | 0 | 0 | 0   | 0  | 0  | 0 | 0   | 0 | 0 | 0   | 0   | 0 |
| 133 | 235  | -2451   | C | 6.54 | Clay       | 0  | 0  | 0 | 0 | 0   | 0 | 0 | 0 | 0   | 0  | 0  | 0 | 0   | 0 | 0 | 0   | 0   | 0 |
| 133 | 243  | -2451   | C | 7.56 | Clay       | 0  | 0  | 0 | 0 | 0   | 0 | 0 | 0 | 0   | 0  | 0  | 0 | 0   | 0 | 0 | 0   | 0   | 0 |
| 133 | 247  | -2451   | C | 8.85 | Clay       | 0  | 0  | 0 | 0 | 0   | 0 | 0 | 0 | 0   | 0  | 0  | 0 | 0   | 0 | 0 | 0   | 0   | 0 |
| 133 | 252  | -2451   | C | 6.03 | Clay       | 0  | 0  | 0 | 0 | 0   | 0 | 0 | 0 | 0   | 0  | 0  | 0 | 0   | 0 | 0 | 0   | 0   | 0 |
| 133 | 255  | -2451   | C | 6.48 | Clay       | 0  | 0  | 0 | 0 | 0   | 0 | 0 | 0 | 0   | 0  | 0  | 0 | 0   | 0 | 0 | 0   | 0   | 0 |
| 133 | 257  | -2451   | C | 4.86 | Clay       | 0  | 0  | 0 | 0 | 0   | 0 | 0 | 0 | 0   | 0  | 0  | 0 | 0   | 0 | 0 | 0   | 0   | 0 |
| 154 | 5.6  | -3158.5 | C | 29.7 | Sandy Silt | 5  | 1  | 0 | 1 | 0   | 1 | 0 | 0 | 3   | 6  | 17 | 0 | 29  | 0 | 0 | 56  | 185 | 0 |
| 154 | 10.5 | -3158.5 | C | 30.6 | Sandy Silt | 4  | 0  | 0 | 0 | 0   | 0 | 0 | 0 | 0   | 5  | 10 | 0 | 22  | 0 | 0 | 56  | 140 | 0 |
| 154 | 19.5 | -3158.5 | C | 29.3 | Sandy Silt | 1  | 4  | 0 | 0 | 0   | 0 | 0 | 0 | 4   | 9  | 14 | 0 | 25  | 0 | 0 | 77  | 201 | 0 |
| 154 | 21.4 | -3158.5 | C | 33.6 | Sandy Silt | 2  | 0  | 0 | 0 | 0   | 0 | 0 | 0 | 2   | 14 | 16 | 0 | 48  | 0 | 0 | 89  | 299 | 0 |
| 154 | 30.4 | -3158.5 | C | 30.4 | Sandy Silt | 0  | 1  | 0 | 0 | 0   | 0 | 0 | 0 | 6   | 9  | 12 | 0 | 30  | 0 | 0 | 76  | 315 | 0 |
| 154 | 40.4 | -3158.5 | C | 29.7 | Sandy Silt | 2  | 6  | 0 | 0 | 0   | 0 | 0 | 0 | 4   | 18 | 16 | 0 | 40  | 0 | 0 | 87  | 318 | 0 |
| 154 | 50.4 | -3158.5 | C | 29.9 | Sandy Silt | 0  | 3  | 0 | 0 | 0   | 0 | 0 | 0 | 0   | 24 | 15 | 0 | 52  | 0 | 0 | 108 | 481 | 0 |
| 154 | 60.4 | -3158.5 | C | 30   | Sandy Silt | 0  | 2  | 0 | 0 | 0   | 4 | 0 | 0 | 0   | 8  | 19 | 0 | 84  | 0 | 0 | 149 | 578 | 0 |
| 154 | 70.4 | -3158.5 | C | 31   | Sandy Silt | 2  | 2  | 0 | 0 | 0   | 0 | 0 | 0 | 0   | 8  | 48 | 0 | 144 | 0 | 0 | 168 | 766 | 0 |
| 154 | 80.4 | -3158.5 | C | 30.4 | Sandy Silt | 1  | 0  | 0 | 0 | 0   | 0 | 0 | 0 | 4   | 12 | 15 | 0 | 89  | 0 | 0 | 117 | 695 | 0 |

|     |      |         |   |      |            |   |    |   |   |   |    |   |   |    |    |    |    |    |    |   |    |     |     |   |
|-----|------|---------|---|------|------------|---|----|---|---|---|----|---|---|----|----|----|----|----|----|---|----|-----|-----|---|
| 154 | 90.4 | -3158.5 | C | 23.3 | Sandy Silt | 0 | 3  | 0 | 0 | 0 | 0  | 1 | 0 | 0  | 0  | 3  | 17 | 0  | 29 | 0 | 0  | 43  | 259 | 0 |
| 154 | 100  | -3158.5 | C | 20.1 | Silt       | 0 | 0  | 0 | 0 | 0 | 0  | 0 | 0 | 1  | 2  | 3  | 0  | 8  | 0  | 0 | 12 | 46  | 0   |   |
| 154 | 105  | -3158.5 | C | 19.5 | Silt       | 0 | 0  | 0 | 0 | 0 | 0  | 0 | 0 | 0  | 2  | 7  | 0  | 10 | 0  | 0 | 11 | 49  | 0   |   |
| 154 | 108  | -3158.5 | C | 19.3 | Silt       | 1 | 1  | 0 | 0 | 0 | 0  | 0 | 0 | 1  | 1  | 16 | 0  | 22 | 0  | 0 | 14 | 64  | 0   |   |
| 154 | 118  | -3158.5 | C | 18.2 | Silt       | 1 | 0  | 0 | 0 | 0 | 0  | 0 | 0 | 0  | 0  | 17 | 0  | 14 | 0  | 0 | 14 | 31  | 0   |   |
| 154 | 128  | -3158.5 | C | 17.6 | Silt       | 0 | 1  | 0 | 0 | 0 | 0  | 0 | 0 | 0  | 0  | 1  | 0  | 1  | 0  | 0 | 3  | 4   | 0   |   |
| 154 | 138  | -3158.5 | C | 16.5 | Silt       | 0 | 0  | 0 | 0 | 0 | 0  | 0 | 0 | 0  | 0  | 1  | 0  | 7  | 0  | 0 | 5  | 3   | 0   |   |
| 154 | 148  | -3158.5 | C | 15.5 | Silt       | 0 | 0  | 0 | 0 | 0 | 0  | 0 | 0 | 0  | 0  | 1  | 0  | 1  | 0  | 0 | 2  | 0   | 0   |   |
| 154 | 158  | -3158.5 | C | 15.6 | Silt       | 0 | 0  | 0 | 0 | 0 | 0  | 0 | 0 | 0  | 0  | 5  | 0  | 2  | 0  | 0 | 5  | 5   | 0   |   |
| 154 | 168  | -3158.5 | C | 16.8 | Silt       | 1 | 0  | 0 | 0 | 0 | 0  | 0 | 0 | 0  | 0  | 0  | 0  | 0  | 0  | 0 | 0  | 0   | 0   |   |
| 154 | 172  | -3158.5 | C | 14.5 | Clay       | 0 | 0  | 0 | 0 | 0 | 0  | 0 | 0 | 0  | 0  | 0  | 0  | 0  | 0  | 0 | 0  | 0   | 0   |   |
| 154 | 175  | -3158.5 | C | 12.1 | Clay       | 0 | 0  | 0 | 0 | 0 | 0  | 0 | 0 | 0  | 0  | 0  | 0  | 0  | 0  | 0 | 3  | 0   | 0   |   |
| 154 | 185  | -3158.5 | C | 14.7 | Silt       | 0 | 0  | 0 | 0 | 0 | 0  | 0 | 0 | 0  | 0  | 0  | 0  | 0  | 0  | 0 | 0  | 0   | 0   |   |
| 154 | 195  | -3158.5 | C | 13   | Silt       | 0 | 0  | 0 | 0 | 0 | 0  | 0 | 0 | 0  | 0  | 0  | 0  | 0  | 0  | 0 | 0  | 0   | 0   |   |
| 154 | 205  | -3158.5 | C | 13.5 | Silt       | 0 | 0  | 0 | 0 | 0 | 0  | 0 | 0 | 0  | 0  | 0  | 0  | 0  | 0  | 0 | 0  | 0   | 0   |   |
| 154 | 215  | -3158.5 | C | 16.9 | Silt       | 0 | 0  | 0 | 0 | 0 | 0  | 0 | 0 | 0  | 0  | 0  | 0  | 0  | 0  | 0 | 0  | 0   | 0   |   |
| 154 | 225  | -3158.5 | C | 14.6 | Silt       | 0 | 0  | 0 | 0 | 0 | 0  | 0 | 0 | 0  | 0  | 0  | 0  | 0  | 0  | 0 | 0  | 0   | 0   |   |
| 154 | 235  | -3158.5 | C | 14.4 | Silt       | 0 | 0  | 0 | 0 | 0 | 0  | 0 | 0 | 0  | 0  | 0  | 0  | 0  | 0  | 0 | 0  | 0   | 0   |   |
| 154 | 245  | -3158.5 | C | 15.4 | Silt       | 0 | 0  | 0 | 0 | 0 | 0  | 0 | 0 | 0  | 0  | 0  | 0  | 0  | 0  | 0 | 0  | 0   | 0   |   |
| 154 | 249  | -3158.5 | C | 13   | Silt       | 0 | 0  | 0 | 0 | 0 | 0  | 0 | 0 | 0  | 0  | 0  | 0  | 0  | 0  | 0 | 0  | 0   | 0   |   |
| 154 | 255  | -3158.5 | C | 12.9 | Clay       | 0 | 0  | 0 | 0 | 0 | 0  | 0 | 0 | 0  | 0  | 0  | 0  | 0  | 0  | 0 | 0  | 0   | 0   |   |
| 154 | 265  | -3158.5 | C | 14.8 | Silt       | 0 | 0  | 0 | 0 | 0 | 0  | 0 | 0 | 0  | 0  | 0  | 0  | 0  | 0  | 0 | 0  | 0   | 0   |   |
| 154 | 275  | -3158.5 | C | 16   | Silt       | 0 | 0  | 0 | 0 | 0 | 0  | 0 | 0 | 0  | 0  | 0  | 0  | 0  | 0  | 0 | 0  | 0   | 0   |   |
| 154 | 285  | -3158.5 | C | 14.5 | Silt       | 0 | 0  | 0 | 0 | 0 | 0  | 0 | 0 | 0  | 0  | 0  | 0  | 0  | 0  | 0 | 0  | 0   | 0   |   |
| 154 | 294  | -3158.5 | C | 16   | Silt       | 0 | 0  | 0 | 0 | 0 | 0  | 0 | 0 | 0  | 0  | 0  | 0  | 0  | 0  | 0 | 0  | 0   | 0   |   |
| 164 | 3.78 | -1188.4 | C | 94.3 | Sandy Silt | 0 | 50 | 0 | 0 | 0 | 12 | 0 | 0 | 0  | 0  | 0  | 11 | 0  | 0  | 0 | 0  | 24  | 0   |   |
| 164 | 8.78 | -1188.4 | C | 95.3 | Sandy Silt | 0 | 0  | 0 | 0 | 0 | 10 | 0 | 0 | 1  | 0  | 0  | 72 | 0  | 4  | 0 | 0  | 132 | 0   |   |
| 164 | 13.8 | -1188.4 | C | 93.9 | Silty Sand | 0 | 47 | 0 | 0 | 0 | 8  | 0 | 0 | 5  | 0  | 5  | 11 | 0  | 0  | 0 | 0  | 18  | 0   |   |
| 164 | 15.5 | -1188.4 | C | 94.7 | Silty Sand | 0 | 30 | 0 | 0 | 0 | 28 | 3 | 0 | 4  | 40 | 0  | 4  | 0  | 0  | 0 | 0  | 20  | 0   |   |
| 164 | 23.5 | -1188.4 | C | 95   | Silty Sand | 0 | 32 | 0 | 0 | 0 | 6  | 1 | 0 | 11 | 37 | 0  | 5  | 1  | 0  | 0 | 0  | 16  | 0   |   |
| 164 | 32.5 | -1188.4 | C | 95.1 | Silty Sand | 0 | 24 | 0 | 0 | 0 | 16 | 3 | 0 | 4  | 33 | 0  | 17 | 0  | 0  | 0 | 0  | 26  | 0   |   |
| 164 | 42.5 | -1188.4 | C | 98.8 | Silty Sand | 0 | 9  | 0 | 0 | 0 | 18 | 0 | 0 | 0  | 13 | 0  | 4  | 0  | 0  | 0 | 0  | 12  | 0   |   |
| 164 | 52.5 | -1188.4 | C | 99.4 | Silty Sand | 0 | 2  | 0 | 0 | 0 | 28 | 0 | 0 | 1  | 7  | 0  | 6  | 0  | 0  | 0 | 0  | 28  | 0   |   |
| 164 | 62.5 | -1188.4 | C | 98.6 | Silty Sand | 0 | 13 | 0 | 0 | 0 | 27 | 0 | 0 | 12 | 5  | 0  | 20 | 0  | 0  | 0 | 0  | 48  | 0   |   |
| 164 | 72.5 | -1188.4 | C | 99.4 | Silty Sand | 0 | 2  | 0 | 0 | 0 | 43 | 0 | 0 | 1  | 26 | 0  | 4  | 0  | 0  | 0 | 0  | 31  | 0   |   |
| 164 | 82.5 | -1188.4 | C | 99.1 | Silty Sand | 0 | 5  | 0 | 0 | 0 | 86 | 0 | 0 | 1  | 41 | 0  | 9  | 0  | 0  | 0 | 0  | 54  | 0   |   |
| 164 | 92.5 | -1188.4 | C | 99.3 | Silty Sand | 0 | 1  | 0 | 0 | 0 | 39 | 0 | 0 | 1  | 26 | 0  | 8  | 0  | 0  | 0 | 0  | 38  | 0   |   |
| 164 | 103  | -1188.4 | C | 99.2 | Silty Sand | 0 | 6  | 0 | 0 | 0 | 28 | 0 | 0 | 2  | 34 | 0  | 6  | 0  | 0  | 0 | 0  | 24  | 0   |   |
| 164 | 106  | -1188.4 | C | 98.7 | Silty Sand | 0 | 8  | 0 | 0 | 0 | 50 | 0 | 0 | 3  | 39 | 0  | 10 | 0  | 0  | 1 | 0  | 64  | 0   |   |
| 164 | 112  | -1188.4 | C | 99.1 | Silty Sand | 0 | 8  | 0 | 0 | 0 | 40 | 0 | 0 | 6  | 26 | 0  | 15 | 0  | 0  | 0 | 0  | 32  | 0   |   |
| 164 | 122  | -1188.4 | C | 99.4 | Silty Sand | 0 | 7  | 0 | 0 | 0 | 0  | 0 | 0 | 0  | 30 | 0  | 42 | 0  | 0  | 0 | 0  | 125 | 0   |   |
| 164 | 132  | -1188.4 | C | 99.2 | Sandy Silt | 0 | 0  | 0 | 0 | 0 | 0  | 0 | 0 | 0  | 0  | 6  | 0  | 0  | 0  | 0 | 0  | 36  | 0   |   |
| 164 | 142  | -1188.4 | C | 99.4 | Silty Sand | 0 | 0  | 0 | 0 | 0 | 0  | 0 | 0 | 0  | 0  | 8  | 0  | 0  | 0  | 0 | 0  | 33  | 0   |   |
| 164 | 152  | -1188.4 | C | 99.4 | Silty Sand | 0 | 0  | 0 | 0 | 0 | 0  | 0 | 0 | 0  | 0  | 0  | 0  | 0  | 0  | 0 | 0  | 0   | 0   |   |



|     |     |       |   |      |            |   |   |   |   |   |   |   |   |    |   |   |   |   |   |   |    |   |
|-----|-----|-------|---|------|------------|---|---|---|---|---|---|---|---|----|---|---|---|---|---|---|----|---|
| 170 | 142 | -2535 | C | 29.6 | Sandy Silt | 0 | 5 | 0 | 0 | 0 | 0 | 0 | 0 | 7  | 0 | 0 | 0 | 0 | 0 | 2 | 2  | 0 |
| 170 | 152 | -2535 | C | 26.1 | Sandy Silt | 0 | 2 | 0 | 0 | 0 | 0 | 0 | 0 | 18 | 1 | 1 | 0 | 0 | 0 | 5 | 10 | 0 |
| 170 | 162 | -2535 | C | 28.2 | Sandy Silt | 0 | 5 | 0 | 0 | 0 | 0 | 0 | 0 | 13 | 1 | 0 | 0 | 0 | 0 | 5 | 2  | 0 |
| 170 | 172 | -2535 | C | 27.4 | Sandy Silt | 0 | 2 | 0 | 0 | 0 | 0 | 0 | 0 | 10 | 1 | 0 | 0 | 0 | 0 | 3 | 8  | 0 |
| 170 | 182 | -2535 | C | 24.2 | Sandy Silt | 0 | 0 | 0 | 0 | 0 | 0 | 0 | 0 | 0  | 0 | 1 | 0 | 0 | 0 | 2 | 2  | 0 |
| 170 | 186 | -2535 | C | 20.1 | Silt       | 0 | 1 | 0 | 0 | 0 | 0 | 0 | 0 | 6  | 1 | 0 | 0 | 0 | 0 | 1 | 1  | 0 |
| 170 | 193 | -2535 | C | 14.7 | Silt       | 0 | 1 | 0 | 0 | 0 | 0 | 0 | 0 | 29 | 1 | 0 | 0 | 0 | 0 | 0 | 0  | 0 |
| 170 | 203 | -2535 | C | 14.4 | Silt       | 0 | 0 | 0 | 0 | 0 | 0 | 0 | 0 | 1  | 0 | 0 | 0 | 0 | 0 | 0 | 0  | 0 |
| 170 | 213 | -2535 | C | 6.71 | Clay       | 0 | 0 | 0 | 0 | 0 | 0 | 0 | 0 | 0  | 0 | 0 | 0 | 0 | 0 | 0 | 0  | 0 |
| 170 | 223 | -2535 | C | 7.2  | Clay       | 0 | 0 | 0 | 0 | 0 | 0 | 0 | 0 | 0  | 0 | 0 | 0 | 0 | 0 | 0 | 0  | 0 |
| 170 | 233 | -2535 | C | 9.19 | Clay       | 0 | 0 | 0 | 0 | 0 | 0 | 0 | 0 | 0  | 0 | 0 | 0 | 0 | 0 | 0 | 0  | 0 |
| 170 | 243 | -2535 | C | 7.75 | Clay       | 0 | 0 | 0 | 0 | 0 | 0 | 0 | 0 | 0  | 0 | 0 | 0 | 0 | 0 | 0 | 0  | 0 |
| 170 | 253 | -2535 | C | 9.26 | Clay       | 0 | 0 | 0 | 0 | 0 | 0 | 0 | 0 | 0  | 0 | 0 | 0 | 0 | 0 | 0 | 0  | 0 |
| 170 | 262 | -2535 | C | 7.6  | Clay       | 0 | 0 | 0 | 0 | 0 | 0 | 0 | 0 | 0  | 0 | 0 | 0 | 0 | 0 | 0 | 0  | 0 |
| 170 | 263 | -2535 | C | 8.88 | Clay       | 0 | 0 | 0 | 0 | 0 | 0 | 0 | 0 | 0  | 0 | 0 | 0 | 0 | 0 | 0 | 0  | 0 |
| 170 | 271 | -2535 | C | 13   | Silt       | 0 | 0 | 0 | 0 | 0 | 0 | 0 | 0 | 0  | 0 | 0 | 0 | 0 | 0 | 0 | 0  | 0 |
| 170 | 281 | -2535 | C | 11.7 | Silt       | 0 | 0 | 0 | 0 | 0 | 0 | 0 | 0 | 0  | 0 | 0 | 0 | 0 | 0 | 0 | 0  | 0 |
| 170 | 291 | -2535 | C | 14.4 | Silt       | 0 | 0 | 0 | 0 | 0 | 0 | 0 | 0 | 0  | 0 | 0 | 0 | 0 | 0 | 0 | 0  | 0 |
| 170 | 301 | -2535 | C | 11.9 | Silt       | 0 | 0 | 0 | 0 | 0 | 0 | 0 | 0 | 0  | 0 | 0 | 0 | 0 | 0 | 0 | 0  | 0 |
| 170 | 311 | -2535 | C | 12.3 | Silt       | 0 | 0 | 0 | 0 | 0 | 0 | 0 | 0 | 0  | 0 | 0 | 0 | 0 | 0 | 0 | 0  | 0 |
| 170 | 321 | -2535 | C | 14.3 | Silt       | 0 | 0 | 0 | 0 | 0 | 0 | 0 | 0 | 0  | 0 | 0 | 0 | 0 | 0 | 0 | 0  | 0 |
| 170 | 327 | -2535 | C | 13.1 | Silt       | 0 | 0 | 0 | 0 | 0 | 0 | 0 | 0 | 0  | 0 | 0 | 0 | 0 | 0 | 0 | 0  | 0 |

# APPENDIX 3.2

## MICROHABITAT PREFERENCES

*Cited in Chapter 3 & 6*

Table 3.4 All Foraminiferal taxa identified in this study and their preferred microhabitat (living depth) according to various references given in Chapter 2 and 6

| <b>Species</b>                    | <b>Preferred Microhabitat</b> | <b>Also observed</b>  |
|-----------------------------------|-------------------------------|-----------------------|
| <i>Ammodiscus gullmarensis</i>    | Epifaunal                     |                       |
| <i>Ammolagena clavata</i>         | Epifaunal                     |                       |
| <i>Ammonia beccarii</i>           | Shallow Infaunal              |                       |
| <i>Ammoscalaria sp.</i>           | Shallow Infaunal              |                       |
| <i>Ammobacculites agglutinans</i> | Shallow Infaunal              |                       |
| <i>Amphycoryna</i>                | Deep Infaunal                 | Intermediate Infaunal |
| <i>Amphycoryna scalaris</i>       | Deep Infaunal                 | Intermediate Infaunal |
| <i>Angulogerina angulosa</i>      | Shallow Infaunal              |                       |
| <i>Astalocus crepidulus</i>       | Shallow Infaunal              |                       |
| <i>Asterigerinata sp.</i>         | Epifaunal                     |                       |
| <i>Astranonion stelligerum</i>    | Epifaunal                     |                       |
| <i>Bolivina ordinaria</i>         | Epifaunal                     |                       |
| <i>Bolivina sp.</i>               | Epifaunal                     |                       |
| <i>Bolivina subspinescens</i>     | Epifaunal                     |                       |
| <i>Bolivina translucens</i>       | Epifaunal                     |                       |
| <i>Bolivina variabilis</i>        | Epifaunal                     |                       |
| <i>Brizalina alata</i>            | Shallow Infaunal              | Intermediate Infaunal |
| <i>Brizalina difformis</i>        | Shallow Infaunal              | Intermediate Infaunal |
| <i>Brizalina dilatata</i>         | Shallow Infaunal              | Intermediate Infaunal |
| <i>Buccella patagonica</i>        | Shallow Infaunal              |                       |
| <i>Buccella peruviana</i>         | Shallow Infaunal              |                       |
| <i>Bulimina aculeata</i>          | Deep Infaunal                 |                       |
| <i>Bulimina barbata</i>           | Shallow Infaunal              |                       |
| <i>Bulimina costata</i>           | Shallow Infaunal              |                       |
| <i>Bulimina elongata</i>          | Shallow Infaunal              |                       |
| <i>Bulimina gibba</i>             | Shallow Infaunal              |                       |
| <i>Bulimina marginata</i>         | Shallow Infaunal              |                       |
| <i>Bulimina mexicana</i>          | Shallow Infaunal              |                       |
| <i>Bulimina ordinaria</i>         | Shallow Infaunal              |                       |
| <i>Bulimina patagonica</i>        | Shallow Infaunal              |                       |
| <i>Bulimina rostrata</i>          | Shallow Infaunal              |                       |
| <i>Bulimina striata</i>           | Deep Infaunal                 | Intermediate Infaunal |

|                                    |                       |                       |
|------------------------------------|-----------------------|-----------------------|
| <i>Bulimina subulata</i>           | Shallow Infaunal      |                       |
| <i>Bulimina translucens</i>        | Shallow Infaunal      |                       |
| <i>Buzasima ringens</i>            | Intermediate Infaunal |                       |
| <i>Cancris spp.</i>                | Epifaunal             |                       |
| <i>Cassidulina laevigata</i>       | Epifaunal             | Elevated              |
| <i>Cassidulina minuta</i>          | Shallow Infaunal      |                       |
| <i>Cassidulina obtusa</i>          | Shallow Infaunal      |                       |
| <i>Cassidulina subglobulosa</i>    | Shallow Infaunal      | Epifaunal             |
| <i>Cassidulinoides mexicana</i>    | Shallow Infaunal      |                       |
| <i>Cassidulinoides parkerianus</i> | Shallow Infaunal      |                       |
| <i>Chilostomella oolina</i>        | Deep Infaunal         | Intermediate Infaunal |
| <i>Chilostomella ovoidea</i>       | Deep Infaunal         | Intermediate Infaunal |
| <i>Cibicides aknerianus</i>        | Epifaunal             | Elevated              |
| <i>Cibicides cicatricosus</i>      | Epifaunal             | Elevated              |
| <i>Cibicides dispars</i>           | Epifaunal             | Elevated              |
| <i>Cibicides fletcheri</i>         | Epifaunal             | Elevated              |
| <i>Cibicides lobatulus</i>         | Epifaunal             | Elevated              |
| <i>Cibicides mckannai</i>          | Epifaunal             | Elevated              |
| <i>Cibicides mundulus</i>          | Epifaunal             | Elevated              |
| <i>Cibicides refulgens</i>         | Epifaunal             | Elevated              |
| <i>Cibicides variabilis</i>        | Epifaunal             | Elevated              |
| <i>Cibicidoides bradyi</i>         | Intermediate Infaunal |                       |
| <i>Cibicidoides dutemplei</i>      | Epifaunal             | Elevated              |
| <i>Cibicidoides globulosus</i>     | Epifaunal             | Elevated              |
| <i>Cibicidoides kullenbergi</i>    | Epifaunal             | Elevated              |
| <i>Cibicidoides pachyderma</i>     | Shallow Infaunal      | Elevated              |
| <i>Cibicidoides sp.</i>            | Epifaunal             | Elevated              |
| <i>Cibicidoides subhaidingerii</i> | Epifaunal             | Elevated              |
| <i>Cibicidoides ungerianus</i>     | Epifaunal             | Elevated              |
| <i>Cibicidoides wuellerstorfi</i>  | Epifaunal             | Elevated              |
| <i>Cornuspira foliacea</i>         | Epifaunal             | Elevated              |
| <i>Cornuspira involvens</i>        | Epifaunal             | Elevated              |
| <i>Cribostomoides subglobosa</i>   | Intermediate Infaunal |                       |
| <i>Cribragoesella robusta</i>      | Epifaunal             |                       |
| <i>Cyclammina cancelata</i>        | Epifaunal             |                       |
| <i>Cystammina sp.</i>              | Intermediate Infaunal |                       |
| <i>Dentalina advena</i>            | Intermediate Infaunal |                       |
| <i>Dentalina communis</i>          | Intermediate Infaunal |                       |
| <i>Dentalina flintii</i>           | Intermediate Infaunal |                       |
| <i>Dentalina striata</i>           | Intermediate Infaunal |                       |
| <i>Dentalinoides canulina</i>      | Intermediate Infaunal |                       |
| <i>Deuterammina dublinensis</i>    | Epifaunal             |                       |
| <i>Discannomalina carinata</i>     | Epifaunal             |                       |
| <i>Discannomalina sp.</i>          | Epifaunal             |                       |



|                                      |                       |                       |
|--------------------------------------|-----------------------|-----------------------|
| <i>Discorbinella sp.</i>             | Epifaunal             |                       |
| <i>Discorbis spp.</i>                | Epifaunal             | Elevated              |
| <i>Discospirina italica</i>          | Epifaunal             |                       |
| <i>Eggerella bradiana</i>            | Intermediate Infaunal |                       |
| <i>Ehrenbergina pacifica</i>         | Epifaunal             |                       |
| <i>Ehrenbergina pupa</i>             | Epifaunal             | Elevated              |
| <i>Elphidium complanatum</i>         | Epifaunal             |                       |
| <i>Elphidium crispum</i>             | Epifaunal             |                       |
| <i>Elphidium excavatum</i>           | Epifaunal             |                       |
| <i>Elphidium incertum</i>            | Epifaunal             |                       |
| <i>Elphidium macellum</i>            | Epifaunal             |                       |
| <i>Elphidium sp.</i>                 | Epifaunal             |                       |
| <i>Elphidium williamsoni</i>         | Epifaunal             |                       |
| <i>Epistomella exigua</i>            | Epifaunal             | Elevated              |
| <i>Eponides sp.</i>                  | Epifaunal             | Elevated              |
| <i>Fissurina bisulcata</i>           | Epifaunal             | Elevated              |
| <i>Fissurina compressa</i>           | Epifaunal             | Elevated              |
| <i>Fissurina formosa</i>             | Epifaunal             | Elevated              |
| <i>Fissurina laevigata</i>           | Epifaunal             | Elevated              |
| <i>Fissurina laevigata</i>           | Epifaunal             | Elevated              |
| <i>Fissurina marginata</i>           | Epifaunal             | Elevated              |
| <i>Fissurina pulchella</i>           | Epifaunal             | Elevated              |
| <i>Fissurina semimarginata</i>       | Epifaunal             | Elevated              |
| <i>Fissurina spp.</i>                | Epifaunal             | Elevated              |
| <i>Fissurina submarginata</i>        | Epifaunal             | Elevated              |
| <i>Fursenkoina sp.</i>               | Deep Infaunal         | Intermediate Infaunal |
| <i>Gaudryina sp.</i>                 | Epifaunal             |                       |
| <i>Glaphyrammina americana</i>       | Shallow Infaunal      |                       |
| <i>Gavellinopsis</i>                 | Epifaunal             |                       |
| <i>Glandulina calomorpha</i>         | Deep Infaunal         | Intermediate Infaunal |
| <i>Glandulina ovula</i>              | Deep Infaunal         | Intermediate Infaunal |
| <i>Glandulina sp.</i>                | Deep Infaunal         | Intermediate Infaunal |
| <i>Globobulimina</i>                 | Deep Infaunal         | Intermediate Infaunal |
| <i>Globobulimina affinis</i>         | Deep Infaunal         | Intermediate Infaunal |
| <i>Globobulimina ovata</i>           | Deep Infaunal         | Intermediate Infaunal |
| <i>Globobulimina ovoidea</i>         | Deep Infaunal         | Intermediate Infaunal |
| <i>Globobulimina turgida</i>         | Deep Infaunal         | Intermediate Infaunal |
| <i>Globocassidulina</i>              | Epifaunal             | Elevated              |
| <i>Globocassidulina crassa</i>       | Epifaunal             | Elevated              |
| <i>Globocassidulina minuta</i>       | Epifaunal             | Elevated              |
| <i>Globocassidulina subglobulosa</i> | Epifaunal             | Elevated              |
| <i>Globulimina pacifica</i>          | Deep Infaunal         | Intermediate Infaunal |
| <i>Globulina sp.</i>                 | Deep Infaunal         | Intermediate Infaunal |
| <i>Glomospira charoides</i>          | Shallow Infaunal      |                       |

|                                   |                       |           |
|-----------------------------------|-----------------------|-----------|
| <i>Glomospira gordialis</i>       | Shallow Infaunal      |           |
| <i>Guttalina lactea</i>           | Epifaunal             | Elevated  |
| <i>Gyroidina orbicularis</i>      | Epifaunal             | Elevated  |
| <i>Gyroidina soldani</i>          | Epifaunal             | Elevated  |
| <i>Gyroidina spp.</i>             | Epifaunal             | Elevated  |
| <i>Gyroidinoides sp.</i>          | Epifaunal             | Elevated  |
| <i>Hanzawaia boueana</i>          | Shallow Infaunal      |           |
| <i>Haplophragmoides quadratus</i> | Shallow Infaunal      |           |
| <i>Haplophragmoides sp.</i>       | Shallow Infaunal      |           |
| <i>Haynesina sp.</i>              | Shallow Infaunal      |           |
| <i>Hippocrepina indivisa</i>      | Shallow Infaunal      |           |
| <i>Hoeglundia elegans</i>         | Epifaunal             | Elevated  |
| <i>Hyalinea balthica</i>          | Epifaunal             | Elevated  |
| <i>Hyalinonetrion clavatum</i>    | Intermediate Infaunal |           |
| <i>Hyalonetrion gracillimum</i>   | Intermediate Infaunal |           |
| <i>Hyperammina cylindrica</i>     | Epifaunal             | Elevated  |
| <i>Hyperammina elongata</i>       | Epifaunal             | Elevated  |
| <i>Hyperammina laevigata</i>      | Epifaunal             | Elevated  |
| <i>Karrerella bradiana</i>        | Epifaunal             | Elevated  |
| <i>Karrerulina conversa</i>       | Epifaunal             | Elevated  |
| <i>Laeidentalina sp.</i>          | Shallow Infaunal      |           |
| <i>Lagena aspera</i>              | Shallow Infaunal      | Epifaunal |
| <i>Lagena cf. interrupta</i>      | Shallow Infaunal      | Epifaunal |
| <i>Lagena clavata</i>             | Shallow Infaunal      | Epifaunal |
| <i>Lagena distoma</i>             | Shallow Infaunal      | Epifaunal |
| <i>Lagena hispida</i>             | Shallow Infaunal      | Epifaunal |
| <i>Lagena hispidula</i>           | Shallow Infaunal      | Epifaunal |
| <i>Lagena interrupta</i>          | Shallow Infaunal      | Epifaunal |
| <i>Lagena laevigata</i>           | Shallow Infaunal      | Epifaunal |
| <i>Lagena laevis</i>              | Shallow Infaunal      | Epifaunal |
| <i>Lagena globulosa</i>           | Shallow Infaunal      | Epifaunal |
| <i>Lagena perlucida</i>           | Shallow Infaunal      | Epifaunal |
| <i>Lagena semilineata</i>         | Shallow Infaunal      | Epifaunal |
| <i>Lagena spp.</i>                | Shallow Infaunal      | Epifaunal |
| <i>Lagena striata</i>             | Shallow Infaunal      | Epifaunal |
| <i>Lagena semimarginata</i>       | Shallow Infaunal      | Epifaunal |
| <i>Lagena sulcata</i>             | Shallow Infaunal      | Epifaunal |
| <i>Laticoryna pauperata</i>       | Epifaunal             |           |
| <i>Lenticulina rotulatus</i>      | Shallow Infaunal      | Epifaunal |
| <i>Lenticulina spp.</i>           | Shallow Infaunal      | Epifaunal |
| <i>Lenticulina vitrea</i>         | Shallow Infaunal      | Epifaunal |
| <i>Lotostomoides calomorphum</i>  | Shallow Infaunal      | Epifaunal |
| <i>Marginulinopsis costata</i>    | Shallow Infaunal      | Epifaunal |
| <i>Martinotiella communis</i>     | Epifaunal             | Elevated  |

|                                    |                       |                       |
|------------------------------------|-----------------------|-----------------------|
| <i>Melonis affinis</i>             | Shallow Infaunal      | Intermediate Infaunal |
| <i>Melonis barleeanus</i>          | Intermediate Infaunal |                       |
| <i>Miliammia fusca</i>             | Epifaunal             | Elevated              |
| <i>Milliolids</i>                  | Epifaunal             | Elevated              |
| <i>Mucronina compressa</i>         | Intermediate Infaunal |                       |
| <i>Neolenticulina sp.</i>          | Epifaunal             | Elevated              |
| <i>Neoponides sp.</i>              | Shallow Infaunal      |                       |
| <i>Nodosaria spp.</i>              | Shallow Infaunal      |                       |
| <i>Nonion barleeenum</i>           | Intermediate Infaunal |                       |
| <i>Nonion commune</i>              | Intermediate Infaunal |                       |
| <i>Nonion fabum</i>                | Intermediate Infaunal |                       |
| <i>Nonion pacifica</i>             | Intermediate Infaunal |                       |
| <i>Nonion pseudotisburyense?</i>   | Intermediate Infaunal |                       |
| <i>Nonion soldanii</i>             | Intermediate Infaunal |                       |
| <i>Nonionella atlantica</i>        | Intermediate Infaunal |                       |
| <i>Nonionella auris</i>            | Intermediate Infaunal |                       |
| <i>Nonionella chiliensis</i>       | Intermediate Infaunal |                       |
| <i>Nonionella sp.</i>              | Intermediate Infaunal |                       |
| <i>Nonionella stella</i>           | Intermediate Infaunal |                       |
| <i>Nonionella turgida</i>          | Deep Infaunal         | Intermediate Infaunal |
| <i>Oolina acuticosta</i>           | Shallow Infaunal      |                       |
| <i>Oolina globulosa</i>            | Shallow Infaunal      |                       |
| <i>Oolina striata</i>              | Shallow Infaunal      |                       |
| <i>Oolina/Favulina acuticosta</i>  | Shallow Infaunal      |                       |
| <i>Oolina/Favulina foveolata</i>   | Shallow Infaunal      |                       |
| <i>Oolina/Favulina hexagona</i>    | Shallow Infaunal      |                       |
| <i>Oolina/Favulina melo</i>        | Shallow Infaunal      |                       |
| <i>Oolina/Favulina squamosa</i>    | Shallow Infaunal      |                       |
| <i>Oridorsalis umbonatus</i>       | Epifaunal             | Elevated              |
| <i>Oridorsalis westi</i>           | Epifaunal             | Elevated              |
| <i>Orthomorphina calomorpha</i>    | Shallow Infaunal      |                       |
| <i>Osangularia sp.</i>             | Epifaunal             | Elevated              |
| <i>Parafissurina basispinata</i>   | Epifaunal             |                       |
| <i>Paratrochammia challengerii</i> | Epifaunal             |                       |
| <i>Patellina corrugata</i>         | Epifaunal             | Elevated              |
| <i>Planodiscorbis sp.</i>          | Epifaunal             | Elevated              |
| <i>Planorbulina mediterransis</i>  | Epifaunal             | Elevated              |
| <i>Planulina ariminensis</i>       | Epifaunal             | Elevated              |
| <i>Planulina wuellerstorfi</i>     | Epifaunal             | Elevated              |
| <i>Procerolagena distoma</i>       | Shallow Infaunal      |                       |
| <i>Prygo murrhina</i>              | Epifaunal             | Elevated              |
| <i>Prygo nasuta</i>                | Epifaunal             | Elevated              |
| <i>Prygo sp.</i>                   | Epifaunal             | Elevated              |
| <i>Psammosphaera fusca</i>         | Shallow Infaunal      |                       |

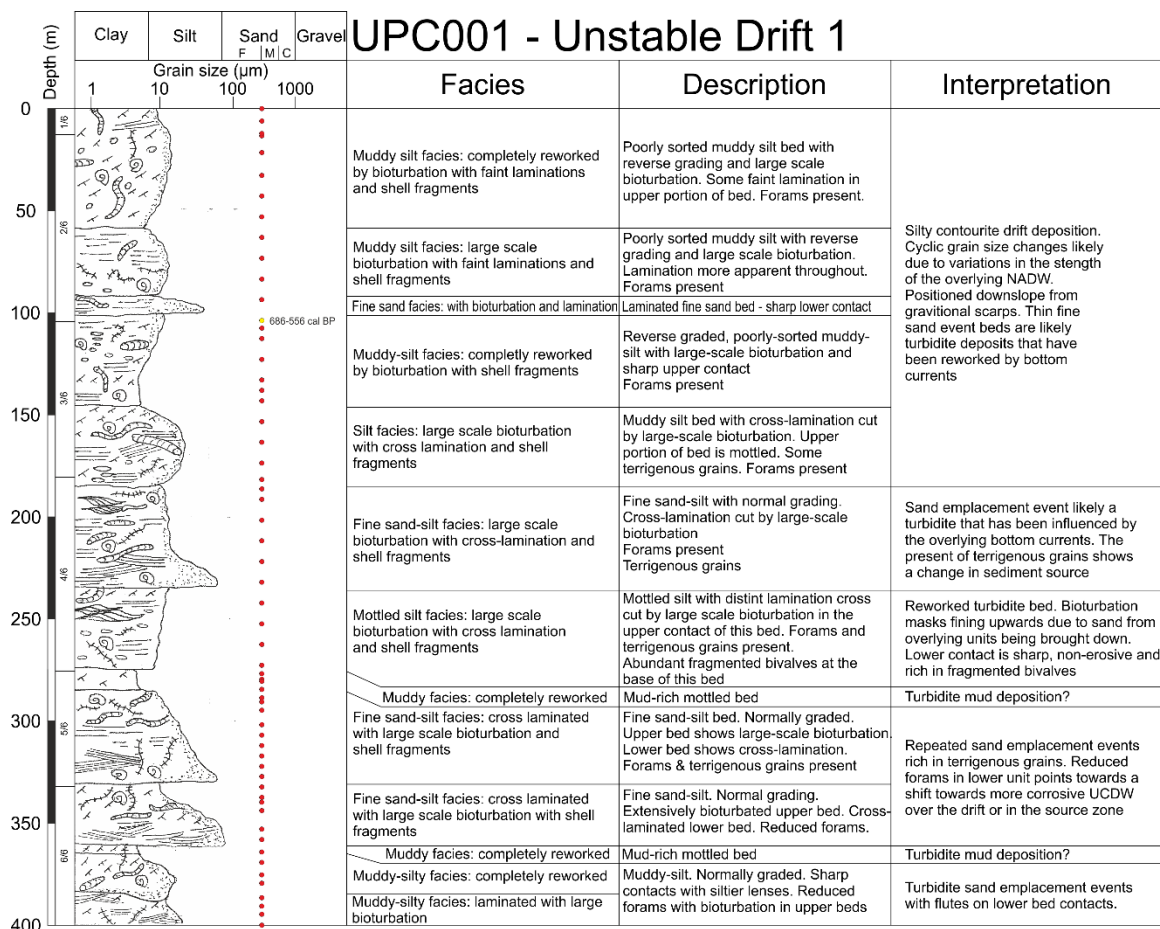
|   |                       |                       |
|---|-----------------------|-----------------------|
| <i>Psammosphaera</i> sp.                | Shallow Infaunal      |                       |
| <i>Pseudonodosaria brevis</i>           | Deep Infaunal         |                       |
| <i>Pseudononion atlanticum</i>          | Deep Infaunal         |                       |
| <i>Pullenia bulloides</i>               | Epifaunal             | Elevated              |
| <i>Pullenia catalinaensis</i>           | Shallow Infaunal      | Intermediate Infaunal |
| <i>Pullenia quadriloba</i>              | Shallow Infaunal      | Intermediate Infaunal |
| <i>Pullenia quinqueloba</i>             | Intermediate Infaunal |                       |
| <i>Pullenia subcarinata</i>             | Epifaunal             | Intermediate Infaunal |
| <i>Pullenia subcarinata quinqueloba</i> | Intermediate Infaunal |                       |
| <i>Pulleniatina</i> sp.?                | Intermediate Infaunal |                       |
| <i>Quinqueloculina patagonica</i>       | Epifaunal             | Elevated              |
| <i>Rectuvigerina bononiensis</i>        | Shallow Infaunal      |                       |
| <i>Rectuvigerina phlegeri</i>           | Shallow Infaunal      |                       |
| <i>Recurvoidella bradyi</i>             | Epifaunal             |                       |
| <i>Reophax subfusiformis</i>            | Shallow Infaunal      |                       |
| <i>Reussella spinulosa</i>              | Shallow Infaunal      |                       |
| <i>Rhabdammina cylindrica</i>           | Epifaunal             | Elevated              |
| <i>Rhabdammina abyssorum</i>            | Epifaunal             | Elevated              |
| <i>Rhabdammina linearis</i>             | Epifaunal             | Elevated              |
| <i>Rhabdamminella cylindrica</i>        | Epifaunal             | Elevated              |
| <i>Robertina</i> sp.                    | Shallow Infaunal      |                       |
| <i>Robulus rotulatus</i>                | Epifaunal             | Elevated              |
| <i>Rosalina globularis</i>              | Epifaunal             | Elevated              |
| <i>Rosalina</i> sp.                     | Epifaunal             | Elevated              |
| <i>Rutherfordoides coronata</i>         | Intermediate Infaunal |                       |
| <i>Saccamina sphaerica</i>              | Shallow Infaunal      |                       |
| <i>Saccorhiza ramosa</i>                | Epifaunal             | Elevated              |
| <i>Sigmoilopsis schlumbergeri</i>       | Epifaunal             | Elevated              |
| <i>Siphonaptera ammophila</i>           | Epifaunal             |                       |
| <i>Siphonina reticulata</i>             | Epifaunal             |                       |
| <i>Siphonoptera ammophila</i>           | Epifaunal             |                       |
| <i>Siphotextularia</i> sp.              | Epifaunal             |                       |
| <i>Siphouvigerina</i> sp.               | Shallow Infaunal      |                       |
| sp. <i>Anox eggii</i>                   | ?                     |                       |
| <i>Sphaeroidina bulloides</i>           | Epifaunal             | Elevated              |
| <i>Sphaeroidina dehiscens</i>           | ?                     | Elevated              |
| <i>Spirillina</i> sp.                   | Epifaunal             |                       |
| <i>Spiroplectamina carinata</i>         | Epifaunal             |                       |
| <i>Spiroplectamina</i> sp.              | Epifaunal             |                       |
| <i>Stainforthia complanata</i>          | Deep Infaunal         | Intermediate Infaunal |
| <i>Textularia agglutinans</i>           | Epifaunal             | Elevated              |
| <i>Textularia candeiana</i>             | Epifaunal             | Elevated              |
| <i>Textularia earlandi</i>              | Epifaunal             | Elevated              |
| <i>Textularia pseudogramen</i>          | Epifaunal             | Elevated              |

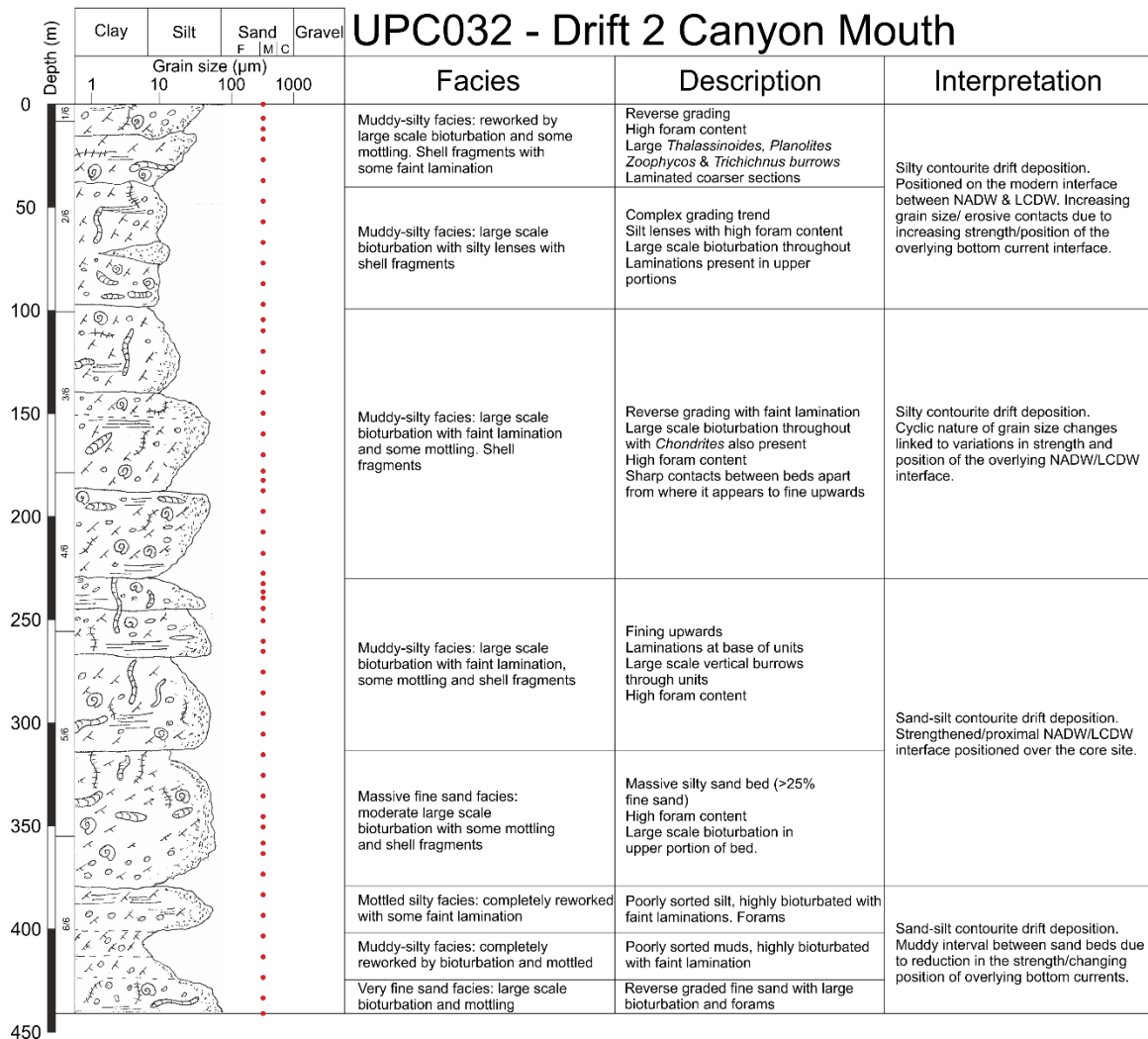
|                                |                       |                       |
|--------------------------------|-----------------------|-----------------------|
| <i>Textularia sagittula</i>    | Epifaunal             | Elevated              |
| <i>Textularia truncata</i>     | Epifaunal             | Elevated              |
| <i>Trifarina angulosa</i>      | Shallow Infaunal      | Epifaunal             |
| <i>Trifarina bradyi</i>        | Shallow Infaunal      | Epifaunal             |
| <i>Triloculina tricarinata</i> | Epifaunal             | Elevated              |
| <i>Trochammina discorbis</i>   | Epifaunal             | Elevated              |
| <i>Trochammina inflata</i>     | Epifaunal             | Elevated              |
| <i>Trochammina squamata</i>    | Epifaunal             | Elevated              |
| <i>Tubinella funalis</i>       | Epifaunal             |                       |
| <i>Usbeckstania chorides</i>   | ?                     |                       |
| <i>Uvigerina aubriana</i>      | Shallow Infaunal      | Intermediate Infaunal |
| <i>Uvigerina aculeata</i>      | Shallow Infaunal      | Intermediate Infaunal |
| <i>Uvigerina bifurcata</i>     | Shallow Infaunal      | Intermediate Infaunal |
| <i>Uvigerina bradyana</i>      | Shallow Infaunal      | Intermediate Infaunal |
| <i>Uvigerina canariensis</i>   | Shallow Infaunal      | Intermediate Infaunal |
| <i>Uvigerina elongata</i>      | DI                    | Intermediate Infaunal |
| <i>Uvigerina holicki</i>       | Shallow Infaunal      | Intermediate Infaunal |
| <i>Uvigerina med/per</i>       | Shallow Infaunal      | Intermediate Infaunal |
| <i>Uvigerina mediterranea</i>  | Shallow Infaunal      | Intermediate Infaunal |
| <i>Uvigerina peregrina</i>     | Shallow Infaunal      | Intermediate Infaunal |
| <i>Uvigerina striata</i>       | Intermediate Infaunal |                       |
| <i>Valvulinera minuta</i>      | Epifaunal             |                       |
| <i>Veleronoides wiesnerix</i>  | Shallow Infaunal      |                       |
| <i>Virgulina riggii</i>        | Deep Infaunal         |                       |

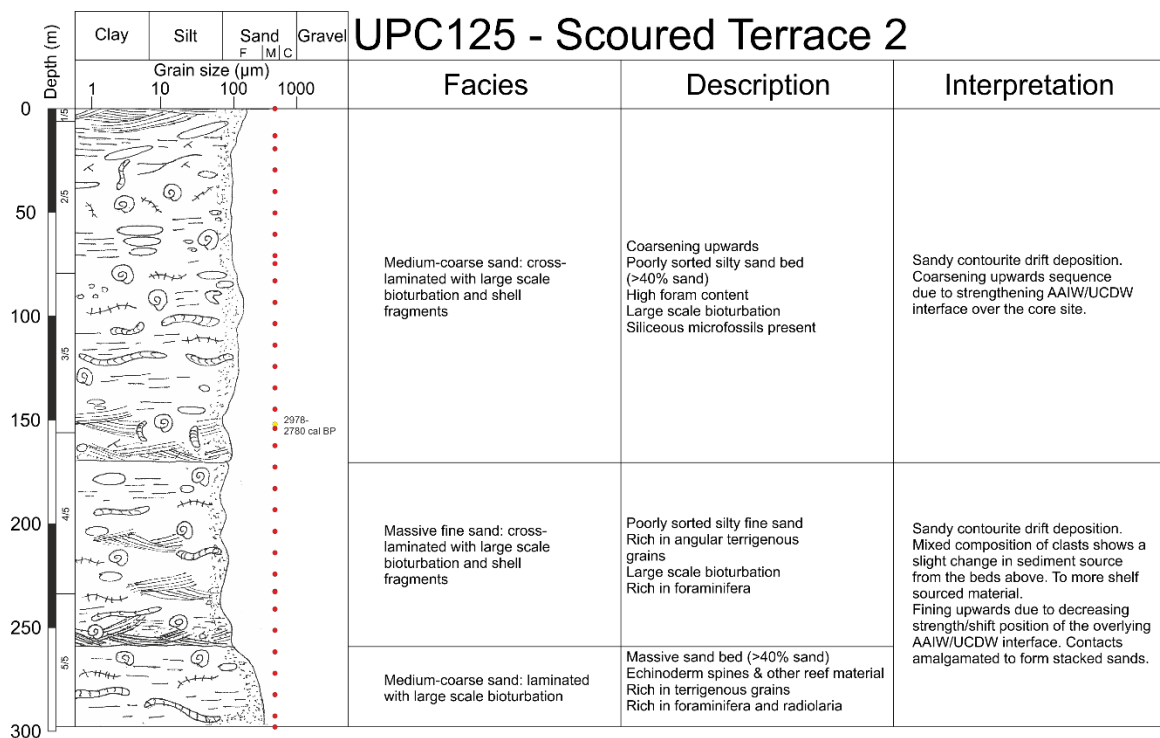
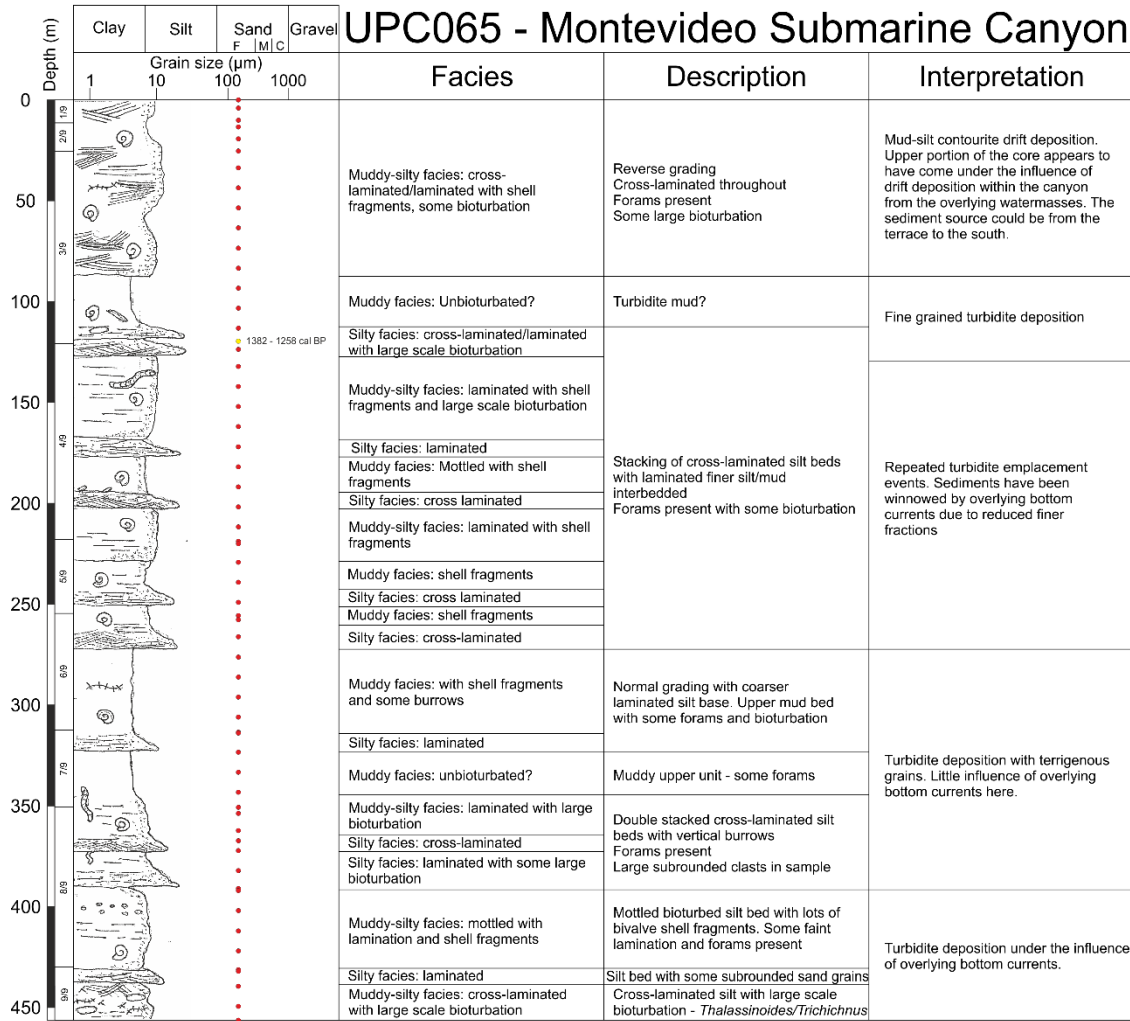
# APPENDIX 4.1

## SEDIMENTARY LOGS

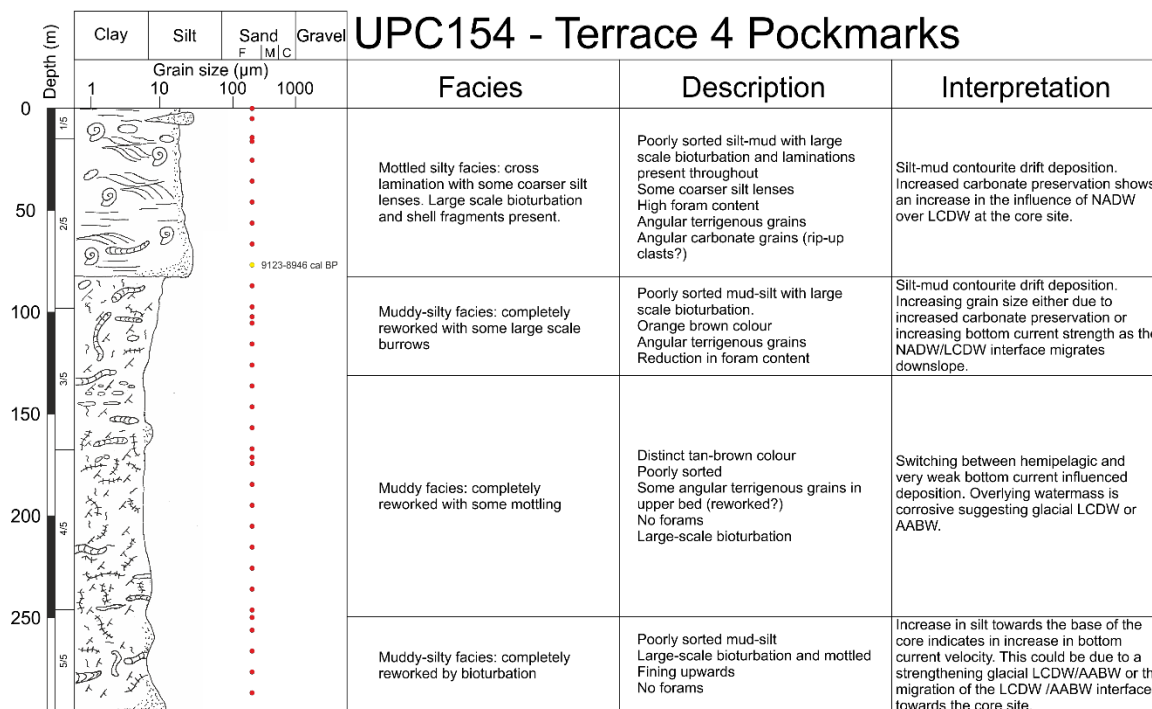
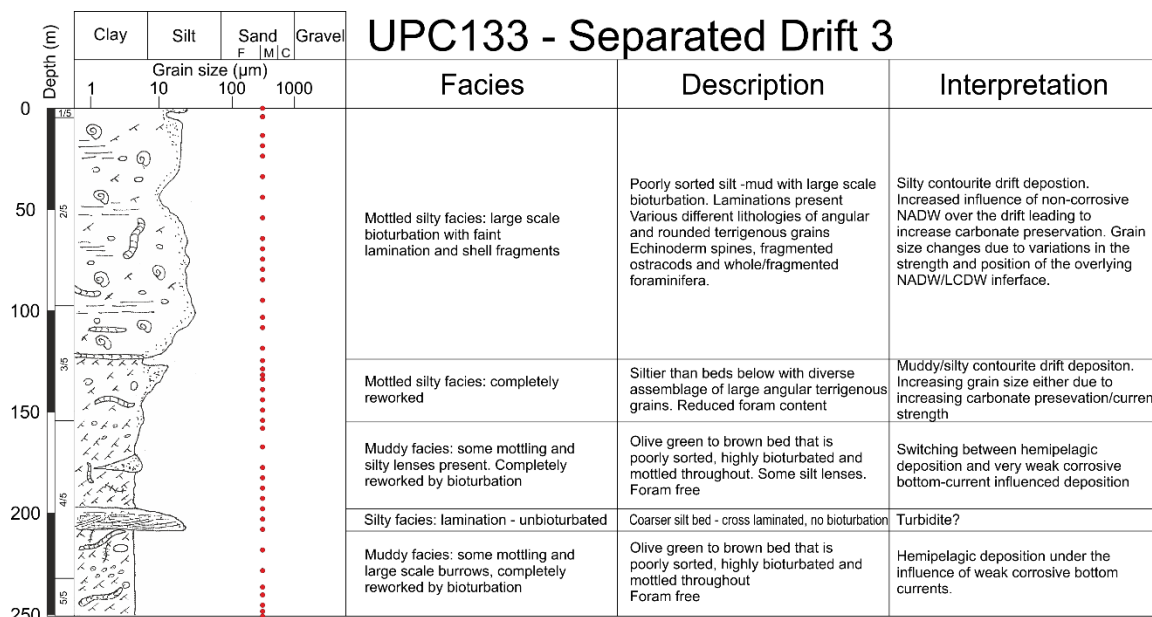
*Cited in Chapter 4*

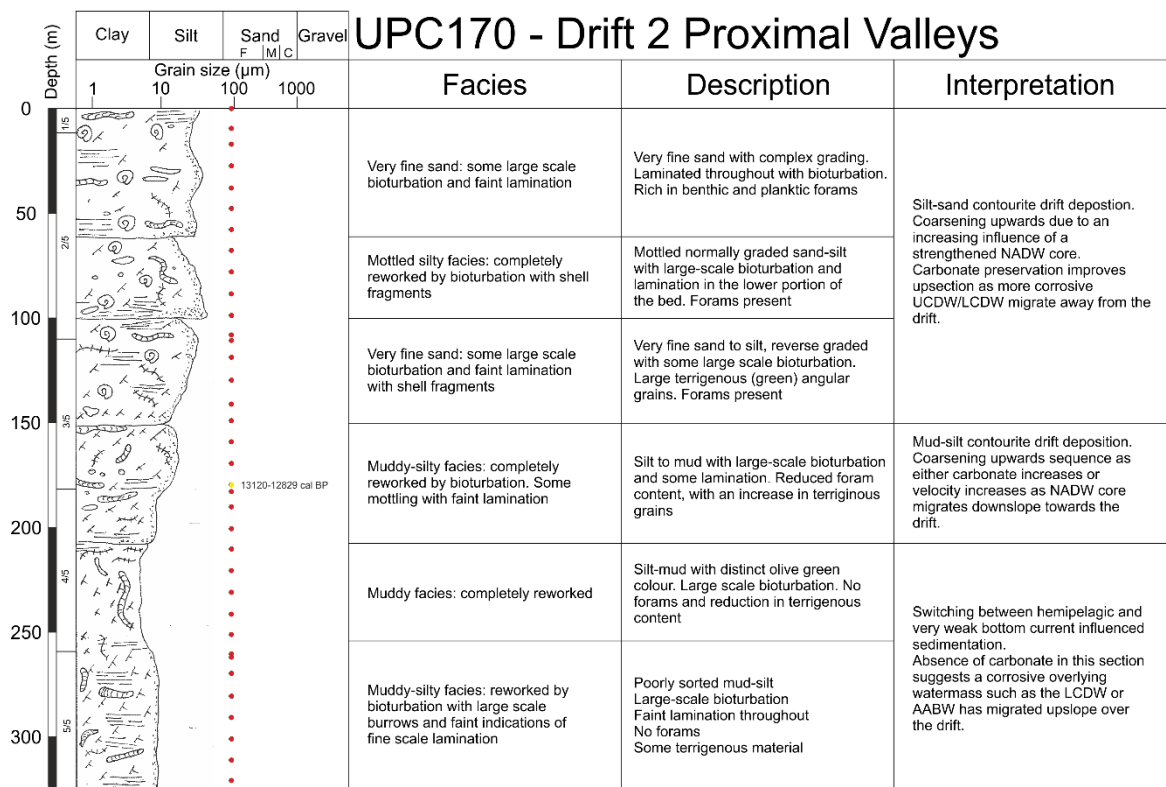
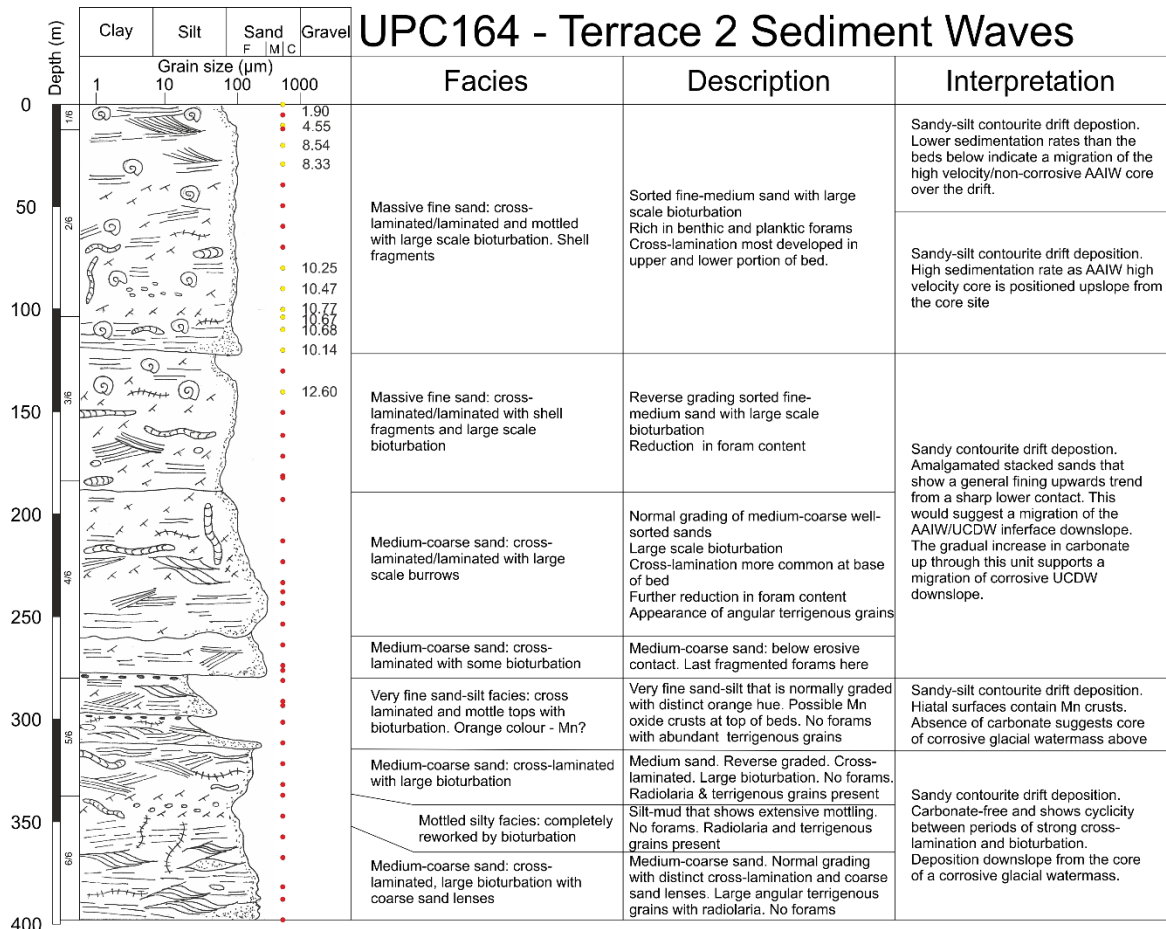












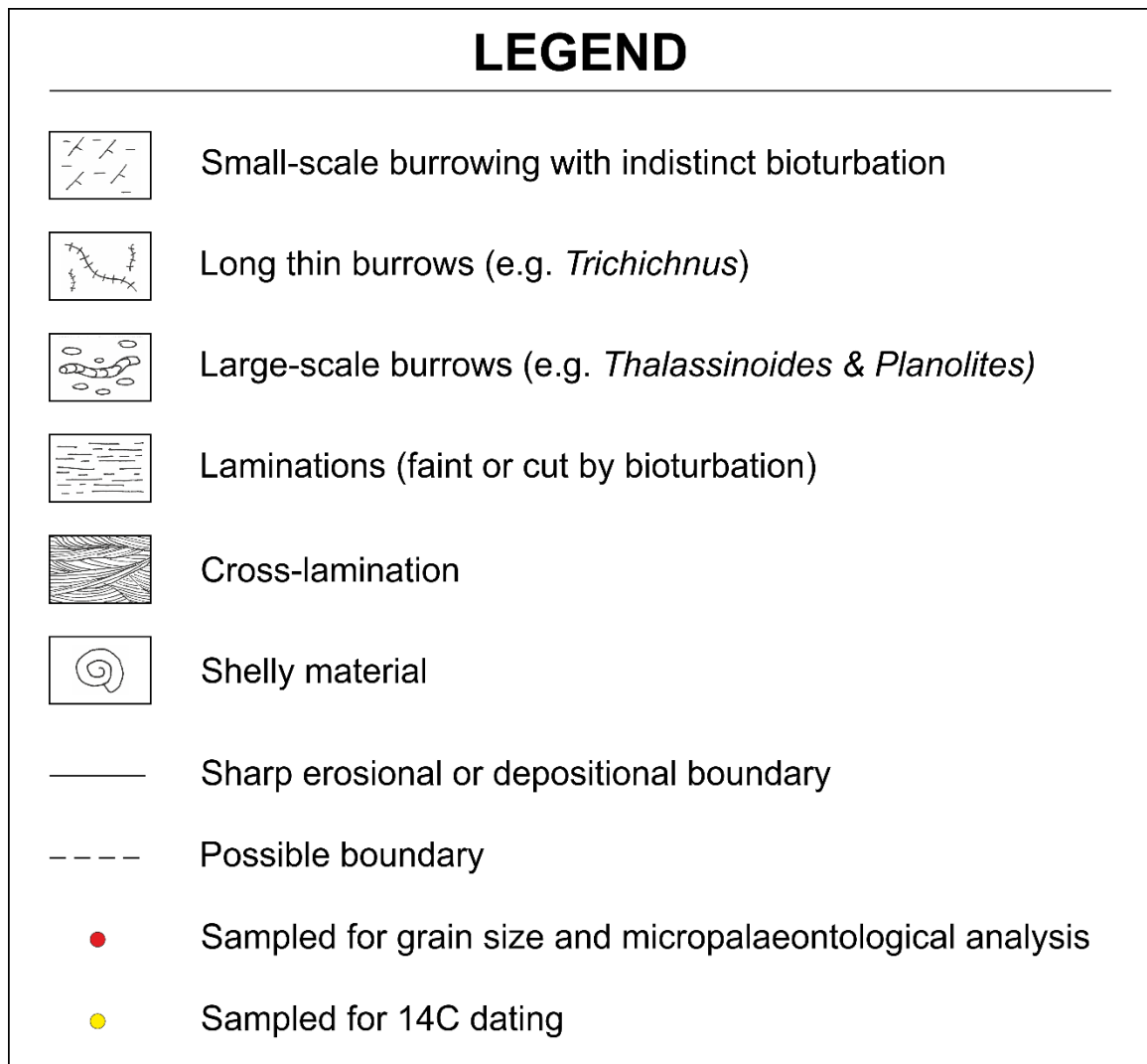


Figure 4.1 Visual logs, sampled intervals, facies identification, sediment description and interpretation for sediment cores UPC001, UPC032, UPC065, UPC125, UPC133, UPC154, UPC164 and UPC170

# APPENDIX 4.2

## GRAIN SIZE TABLES

*Cited in Chapter 4*

Table 4.1 Core water depths, interpreted morphosedimentary environments and grain size weight %

| Core    | Water Depth | Environment         | >250µm (%) | 63-250µm (%) | >63µm (%) | 0% Coarse Sand | V. Fine - M. Sand | Silt - Mud 100% |
|---------|-------------|---------------------|------------|--------------|-----------|----------------|-------------------|-----------------|
| UPC001  | -2053.05    | Drift 1             | 8.1        | 7.1          | 15.2      |                |                   |                 |
| UPC003  | -2205.15    | Drift 1             | 8.0        | 12.1         | 20.1      |                |                   |                 |
| UPC006  | -2376.17    | SCS                 | 4.5        | 23.8         | 28.4      |                |                   |                 |
| UPC007  | -2030.88    | Drift 1             | 2.4        | 29.2         | 31.6      |                |                   |                 |
| UPC015  | -1727.23    | SCS                 | 5.2        | 16.7         | 21.9      |                |                   |                 |
| UPC016  | -1735.54    | SCS                 | 2.9        | 26.0         | 28.9      |                |                   |                 |
| UPC017  | -1921.32    | SCS                 | 6.3        | 20.4         | 26.7      |                |                   |                 |
| UPC018  | -2153.75    | Drift 1             | 7.1        | 13.9         | 21.1      |                |                   |                 |
| UPC019  | -2315.26    | Drift 1             | 6.2        | 23.6         | 29.7      |                |                   |                 |
| UPC020  | -2357.43    | Drift 3             | 7.4        | 24.2         | 31.6      |                |                   |                 |
| UPC021  | -1926.15    | Drift 1             | 9.2        | 10.2         | 19.4      |                |                   |                 |
| UPC022  | -2027.53    | Drift 1             | 7.0        | 7.6          | 14.6      |                |                   |                 |
| UPC023  | -2046.34    | SCS                 | 4.5        | 18.2         | 22.7      |                |                   |                 |
| UPC025  | -2445.71    | SCS                 | 8.6        | 17.1         | 25.8      |                |                   |                 |
| UPC026  | -2403.8     | Turbidite Valley    | 6.6        | 20.1         | 26.7      |                |                   |                 |
| UPC027  | -2379       | Turbidite Valley    | 10.3       | 21.8         | 32.1      |                |                   |                 |
| UPC028  | -2353       | Turbidite Valley    | 9.7        | 20.4         | 30.0      |                |                   |                 |
| UPC029  | -2291       | Turbidite Valley    | 7.5        | 23.1         | 30.5      |                |                   |                 |
| UPC030  | -2345       | Turbidite Valley    | 8.5        | 22.6         | 31.1      |                |                   |                 |
| UPC031  | -2468       | Turbidite Valley    | 5.9        | 11.9         | 17.7      |                |                   |                 |
| UPC032  | -2513.29    | Drift 2             | 2.5        | 27.5         | 30.0      |                |                   |                 |
| UPC033  | -2582.33    | SCS                 | 5.8        | 20.0         | 25.8      |                |                   |                 |
| UPC033R | -2588.53    | SCS                 | 3.0        | 28.6         | 31.6      |                |                   |                 |
| UPC035  | -3026.75    | Turbidite Valley    | 0.6        | 6.1          | 6.7       |                |                   |                 |
| UPC047  | -2221       | SCS                 | 7.7        | 18.9         | 26.6      |                |                   |                 |
| UPC048  | -2568       | Turbidite Valley    | 6.1        | 17.0         | 23.0      |                |                   |                 |
| UPC052  | -1967.23    | Drift 1             | 9.5        | 15.9         | 25.4      |                |                   |                 |
| UPC053  | -2115.24    | SCS                 | 7.5        | 16.3         | 23.9      |                |                   |                 |
| UPC058  | -2255.28    | SCS                 | 9.4        | 12.7         | 22.1      |                |                   |                 |
| UPC059  | -1798.8     | Terrace 3           | 34.9       | 25.7         | 60.6      |                |                   |                 |
| UPC064  | -1263       | Terrace 2           | 3.1        | 53.3         | 56.4      |                |                   |                 |
| UPC065  | -1896.61    | SCS                 | 2.0        | 25.9         | 27.9      |                |                   |                 |
| UPC070  | -2308.6     | SCS                 | 5.2        | 22.7         | 27.9      |                |                   |                 |
| UPC081  | -1895.64    | Terrace 3           | 7.1        | 18.2         | 25.3      |                |                   |                 |
| UPC083  | -2165.47    | Terrace 3           | 6.2        | 12.6         | 18.8      |                |                   |                 |
| UPC087  | -2413.31    | Terrace 3           | 3.1        | 32.7         | 35.8      |                |                   |                 |
| UPC091  | -2644.1     | Turbidite Valley    | 1.6        | 25.4         | 27.1      |                |                   |                 |
| UPC094  | -2945.89    | Pockmarks Terrace 4 | 2.5        | 10.5         | 12.9      |                |                   |                 |
| UPC099  | -3042.41    | Pockmarks Terrace 4 | 0.5        | 18.5         | 19.0      |                |                   |                 |

Table 4.1 continued

| Core    | Water Depth | Environment         | >250µm (%) | 63-250µm (%) | >63µm (%) | 0% Coarse Sand | V. Fine - M. Sand | Silt - Mud 100% |
|---------|-------------|---------------------|------------|--------------|-----------|----------------|-------------------|-----------------|
| UPC102  | -2933.09    | Pockmarks Terrace 4 | 0.6        | 28.3         | 28.8      |                |                   |                 |
| UPC104  | -2726.85    | Turbidite Valley    | 4.4        | 24.6         | 29.0      |                |                   |                 |
| UPC105  | -2732.17    | MTD                 | 3.1        | 23.4         | 26.5      |                |                   |                 |
| UPC106  | -2929.9     | Turbidite Valley    | 8.7        | 20.1         | 28.8      |                |                   |                 |
| UPC108  | -2421.81    | Drift 2             | 3.5        | 31.4         | 34.9      |                |                   |                 |
| UPC109  | -2433.06    | Turbidite Valley    | 3.6        | 22.5         | 26.1      |                |                   |                 |
| UPC110  | -2355.29    | Turbidite Valley    | 4.4        | 21.3         | 25.7      |                |                   |                 |
| UPC114  | -1373       | Terrace 2           | 3.1        | 30.0         | 33.1      |                |                   |                 |
| UPC118  | -1599.87    | Terrace 2           | 5.3        | 27.2         | 32.5      |                |                   |                 |
| UPC119  | -1371.52    | Terrace 2           | 2.7        | 29.9         | 32.6      |                |                   |                 |
| UPC121  | -1476       | SCS                 | 0.7        | 65.1         | 65.8      |                |                   |                 |
| UPC122  | -1154.19    | Terrace 2           | 1.0        | 46.3         | 47.3      |                |                   |                 |
| UPC123  | 1194.3      | Terrace 2           | 1.3        | 45.3         | 46.6      |                |                   |                 |
| UPC124  | -1710.71    | SCS                 | 2.2        | 49.9         | 52.2      |                |                   |                 |
| UPC125  | -1121.22    | Scour Terrace 2     | 0.9        | 61.7         | 62.6      |                |                   |                 |
| UPC126  | -1813.79    | Scour Terrace 2     | 7.3        | 11.0         | 18.3      |                |                   |                 |
| UPC127  | -2359.73    | Drift 2             | 6.3        | 23.1         | 29.4      |                |                   |                 |
| UPC128  | -2546       | Turbidite Valley    | 2.9        | 17.2         | 20.1      |                |                   |                 |
| UPC130  | -2571       | Turbidite Valley    | 11.9       | 27.7         | 39.7      |                |                   |                 |
| UPC132  | -2559.1     | Drift 3             | 6.4        | 21.5         | 27.9      |                |                   |                 |
| UPC133  | -2451       | Drift 3             | 4.7        | 21.3         | 26.0      |                |                   |                 |
| UPC136  | -2499       | Drift 3             | 5.7        | 25.4         | 31.1      |                |                   |                 |
| UPC137  | -2535.53    | MTD                 | 1.2        | 10.0         | 11.3      |                |                   |                 |
| UPC139  | -2499       | Drift 3             | 2.4        | 32.4         | 34.8      |                |                   |                 |
| UPC142  | -2682.11    | Turbidite Valley    | 5.2        | 19.9         | 25.0      |                |                   |                 |
| UPC145  | -1595.39    | Drift 1             | 1.8        | 32.7         | 34.5      |                |                   |                 |
| UPC148B | -2622       | Drift 3             | 2.5        | 36.8         | 39.3      |                |                   |                 |
| UPC149  | -1437.84    | Drift 1             | 2.4        | 32.1         | 34.5      |                |                   |                 |
| UPC158  | -1115.79    | Terrace 2           | 1.3        | 64.7         | 66.0      |                |                   |                 |
| UPC159  | -1460.25    | Terrace 2           | 6.7        | 58.8         | 65.5      |                |                   |                 |
| UPC160  | -1310.81    | Terrace 2           | 1.3        | 38.0         | 39.4      |                |                   |                 |
| UPC161  | -1241.64    | Terrace 2           | 1.9        | 34.7         | 36.6      |                |                   |                 |
| UPC162  | -1285.35    | Terrace 2           | 1.6        | 37.1         | 38.7      |                |                   |                 |
| UPC170  | -2535       | Turbidite Valley    | 6.1        | 12.4         | 18.5      |                |                   |                 |
| UPC171  | -2260.92    | SCS                 | 6.0        | 21.7         | 27.7      |                |                   |                 |
| UPC172  | -2425       | Turbidite Valley    | 10.4       | 12.6         | 23.0      |                |                   |                 |
| UPC177  | -2377       | SCS                 | 13.4       | 17.6         | 31.1      |                |                   |                 |
| UPC182A | -1036       | Terrace 2           | 0.2        | 78.8         | 79.0      |                |                   |                 |

# APPENDIX 4.3

## FULL ITRAX DATA

*Cited in Chapter 4*

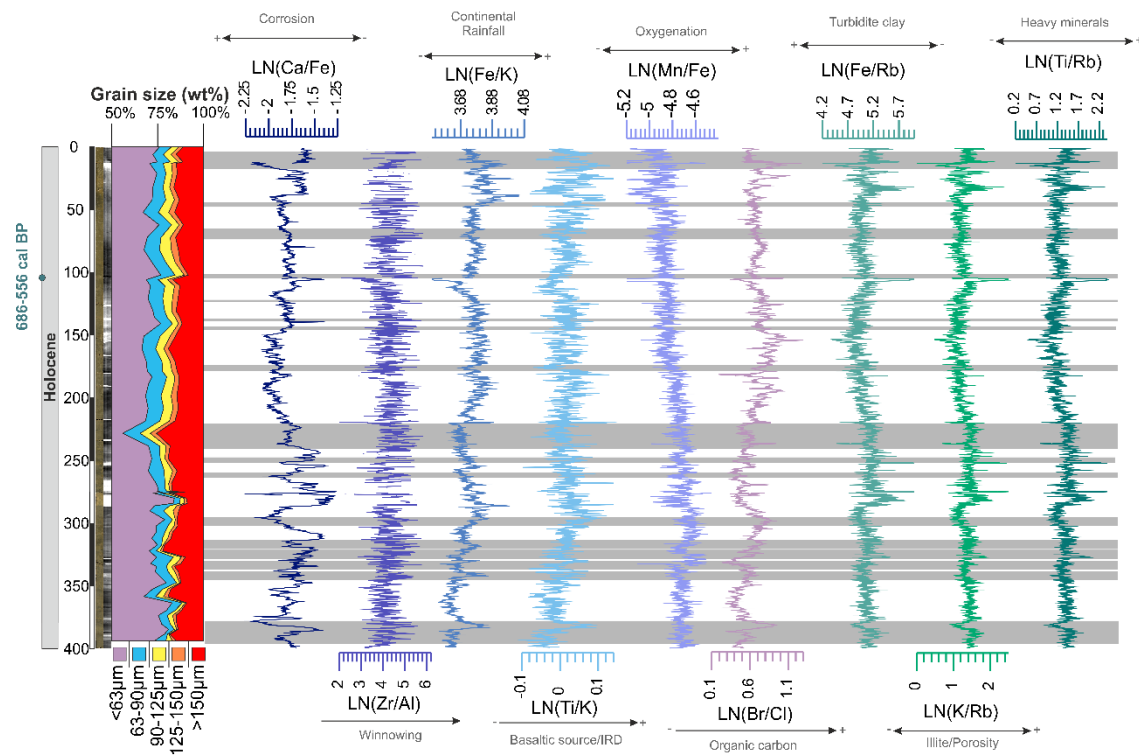


Figure 4.2 Sediment core UPC001 ITRAX elemental ratios plotted against depth and age, alongside grain size weight percentages, core photos and radiographs. Each ratio is labelled with its palaeoclimate proxy. Shaded grey intervals are interpreted periods of increased bottom current intensity according to Zr/Al

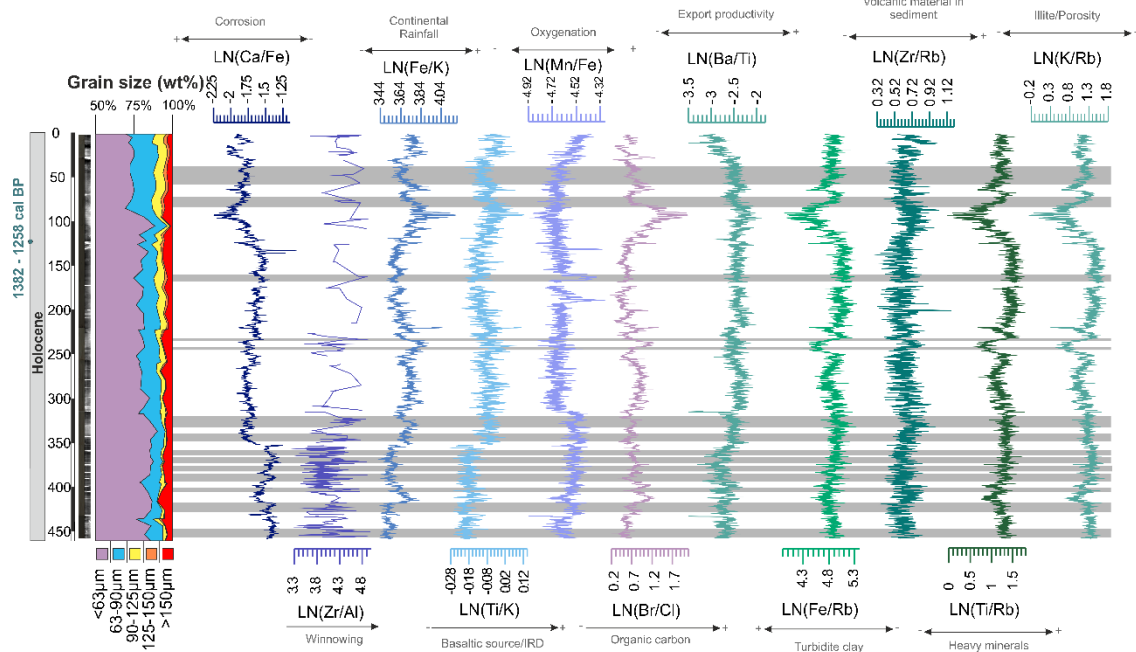


Figure 4.3 Sediment core UPC065 ITRAX elemental ratios plotted against depth and age, alongside grain size weight percentages, core photos and radiographs. Each ratio is labelled with its palaeoclimate proxy. Shaded grey intervals are interpreted periods of increased bottom current intensity according to Zr/Al

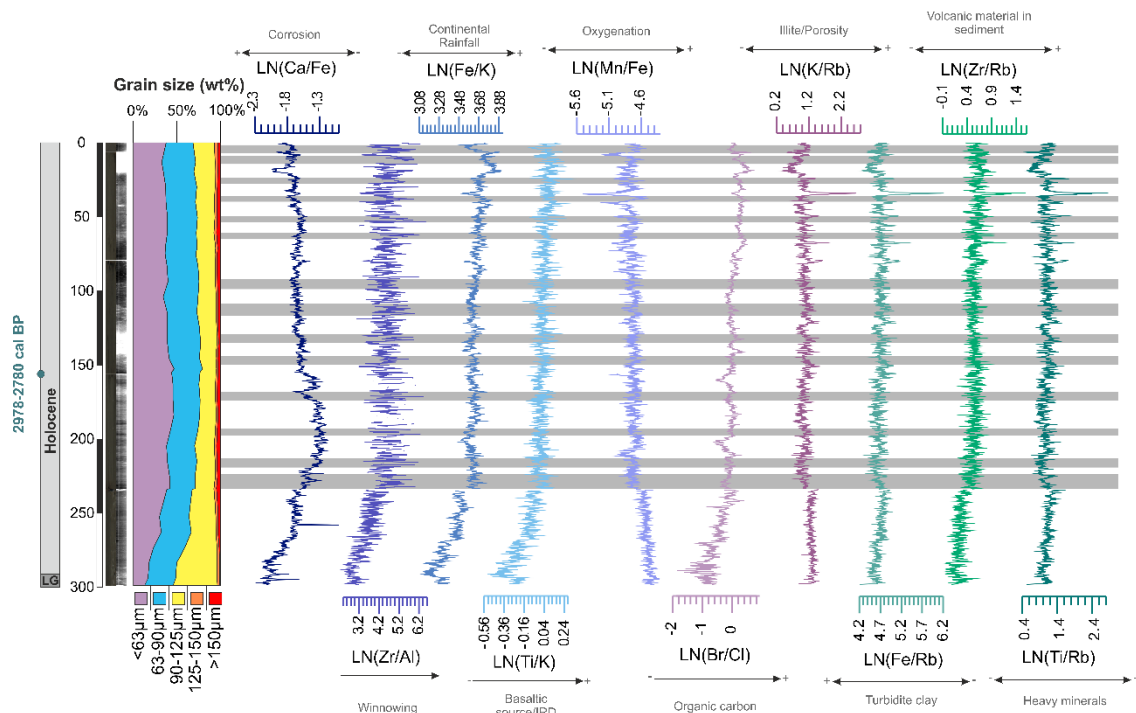


Figure 4.4 Sediment core UPC125 ITRAX elemental ratios plotted against depth and age, alongside grain size weight percentages, core photos and radiographs. Each ratio is labelled with its palaeoclimate proxy. Shaded grey intervals are interpreted periods of increased bottom current intensity according to Zr/Al

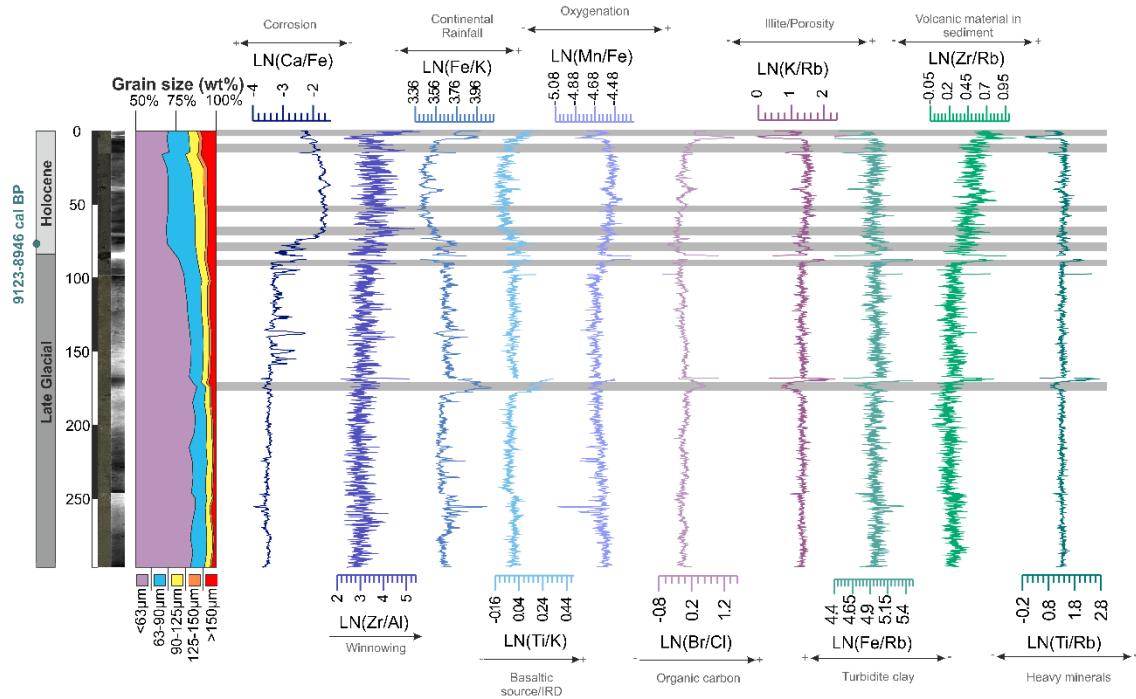


Figure 4.5 Sediment core UPC154 ITRAX elemental ratios plotted against depth and age, alongside grain size weight percentages, core photos and radiographs. Each ratio is labelled with its palaeoclimate proxy. Shaded grey intervals are interpreted periods of increased bottom current intensity according to Zr/Al



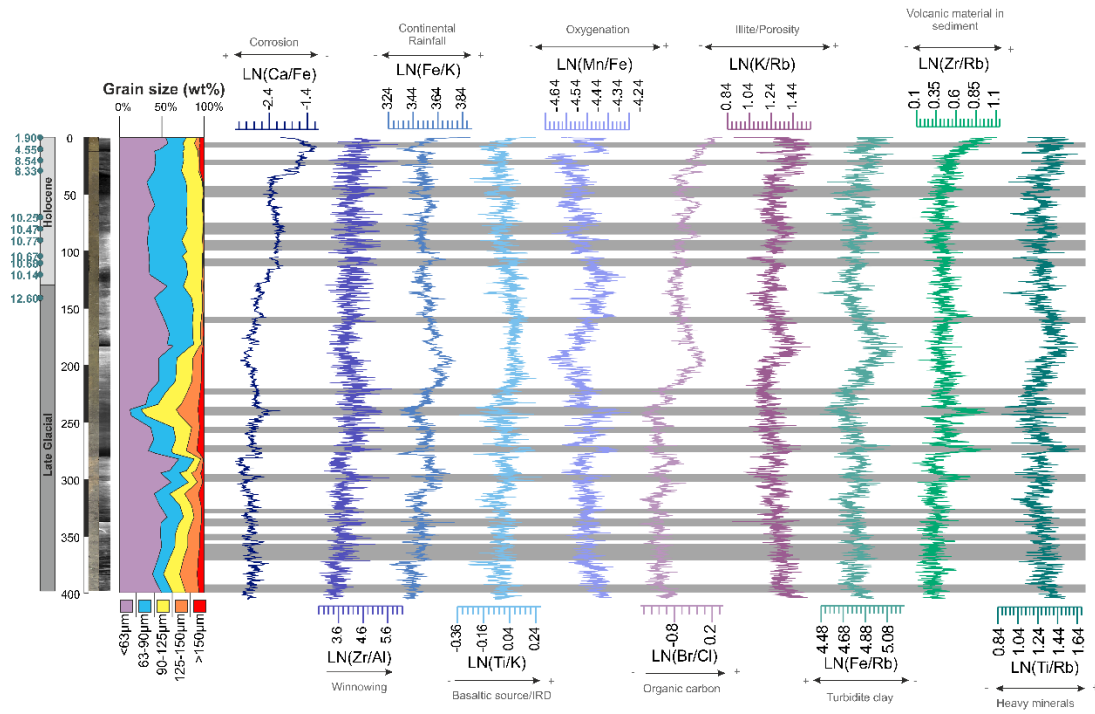


Figure 4.6 Sediment core UPC164 ITRAX elemental ratios plotted against depth and age, alongside grain size weight percentages, core photos and radiographs. Each ratio is labelled with its palaeoclimate proxy. Shaded grey intervals are interpreted periods of increased bottom current intensity according to Zr/Al

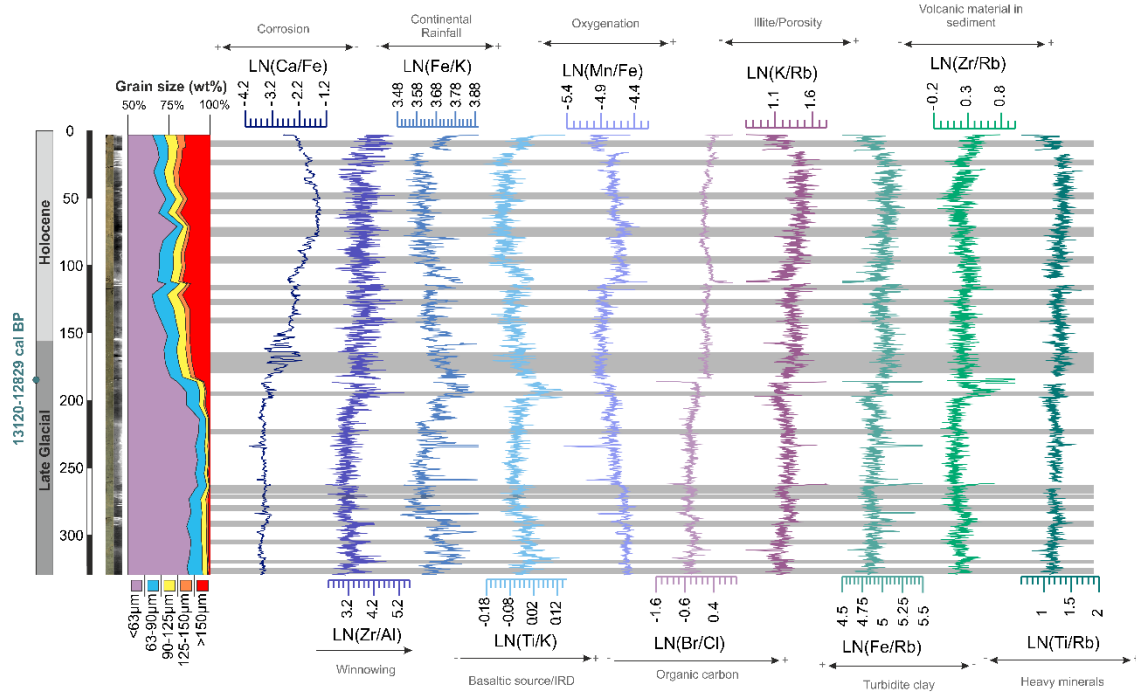


Figure 4.7 Sediment core UPC170 ITRAX elemental ratios plotted against depth and age, alongside grain size weight percentages, core photos and radiographs. Each ratio is labelled with its palaeoclimate proxy. Shaded grey intervals are interpreted periods of increased bottom current intensity according to Zr/Al

# APPENDIX 6.1

## Q-MODE CLUSTERS PER CORE

*Cited in Chapter 6*

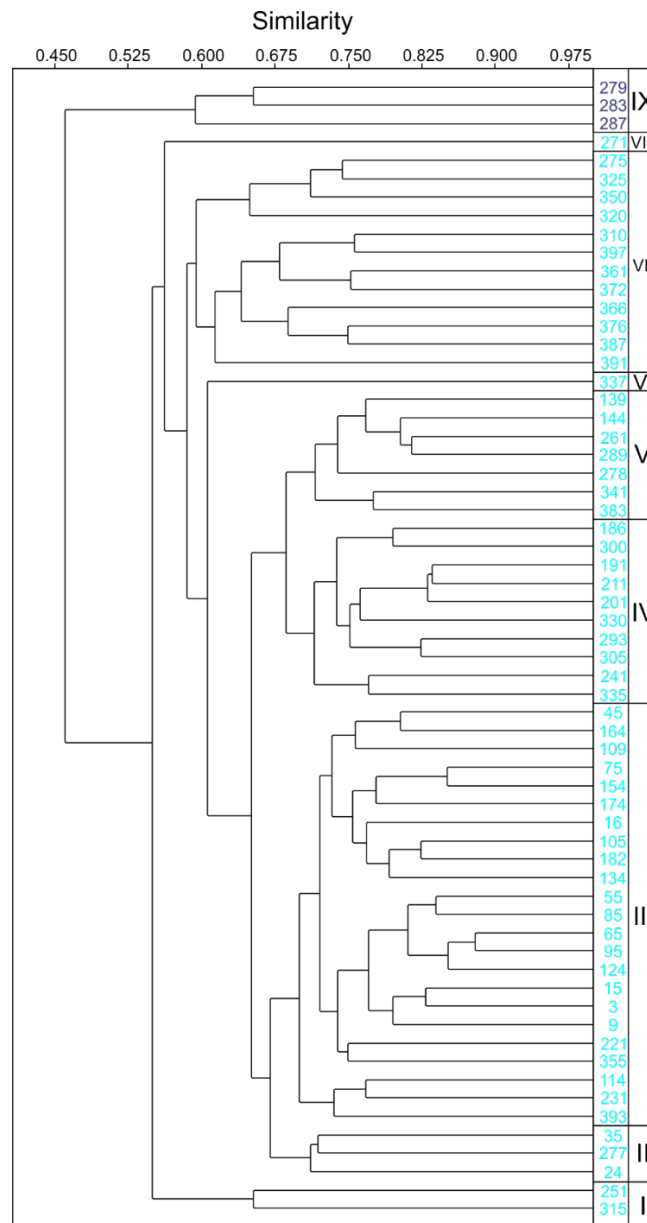


Figure 6.1 UPC001 Q-mode cluster analysis (UPGMA, Bray Curtis) for autochthonous benthic foraminifera >150  $\mu\text{m}$  from all cores. Numerals indicate groups of samples with a similar composition of foraminifera, representing foraminiferal assemblages. Sample numbers indicated and coloured in accordance with overall regional assemblages outlined in Chapter 6. Autochthonous taxa occurring >5% abundance in at least one sample have been considered for this analysis.

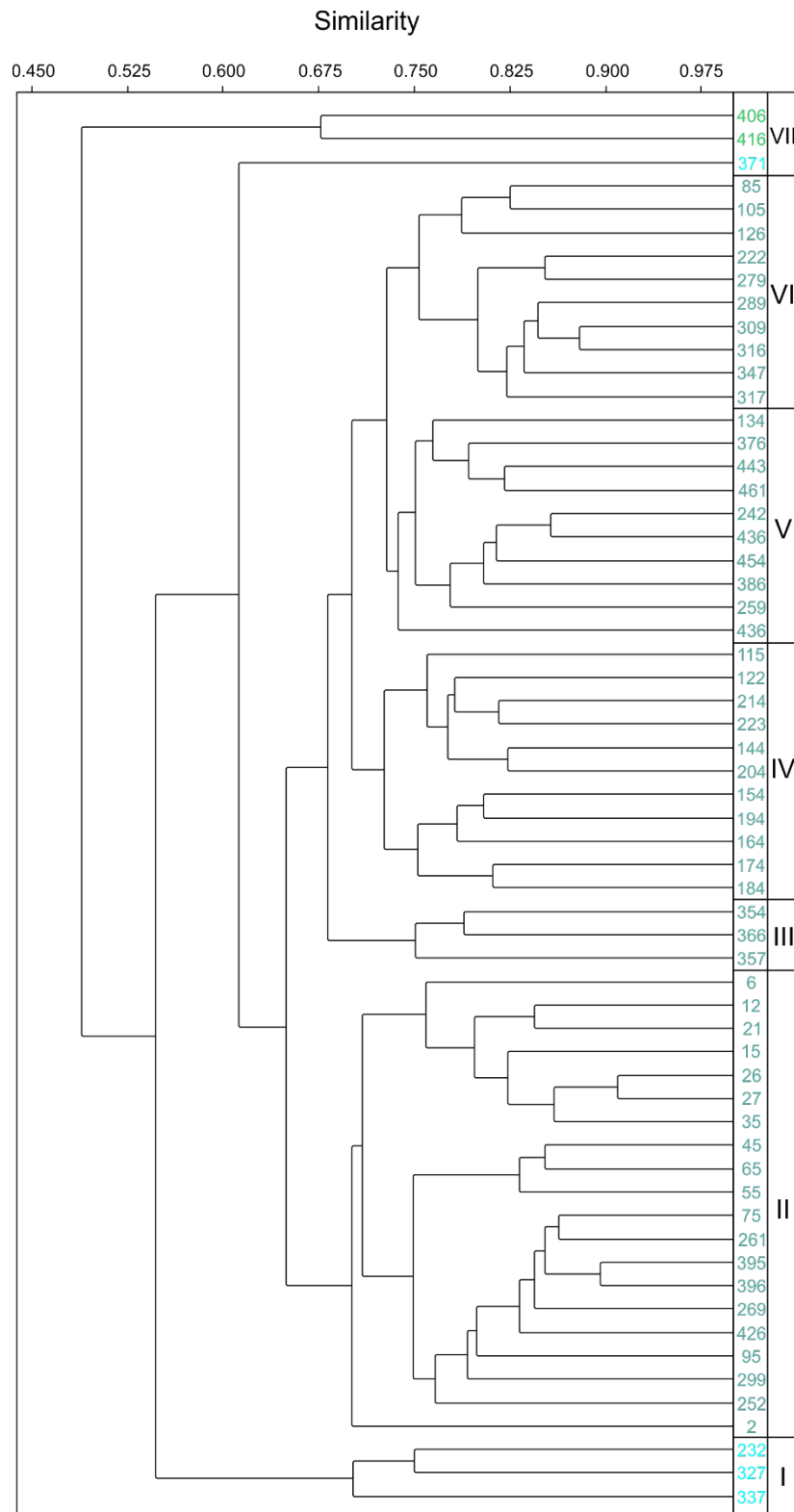


Figure 6.2 UPC065 Q-mode cluster analysis (UPGMA, Bray Curtis) for autochthonous benthic foraminifera >150  $\mu\text{m}$  from all cores. Numerals indicate groups of samples with a similar composition of foraminifera, representing foraminiferal assemblages. Sample numbers indicated and coloured in accordance with overall regional assemblages outlined in Chapter 6. Autochthonous taxa occurring >5% abundance in at least one sample have been considered for this analysis.

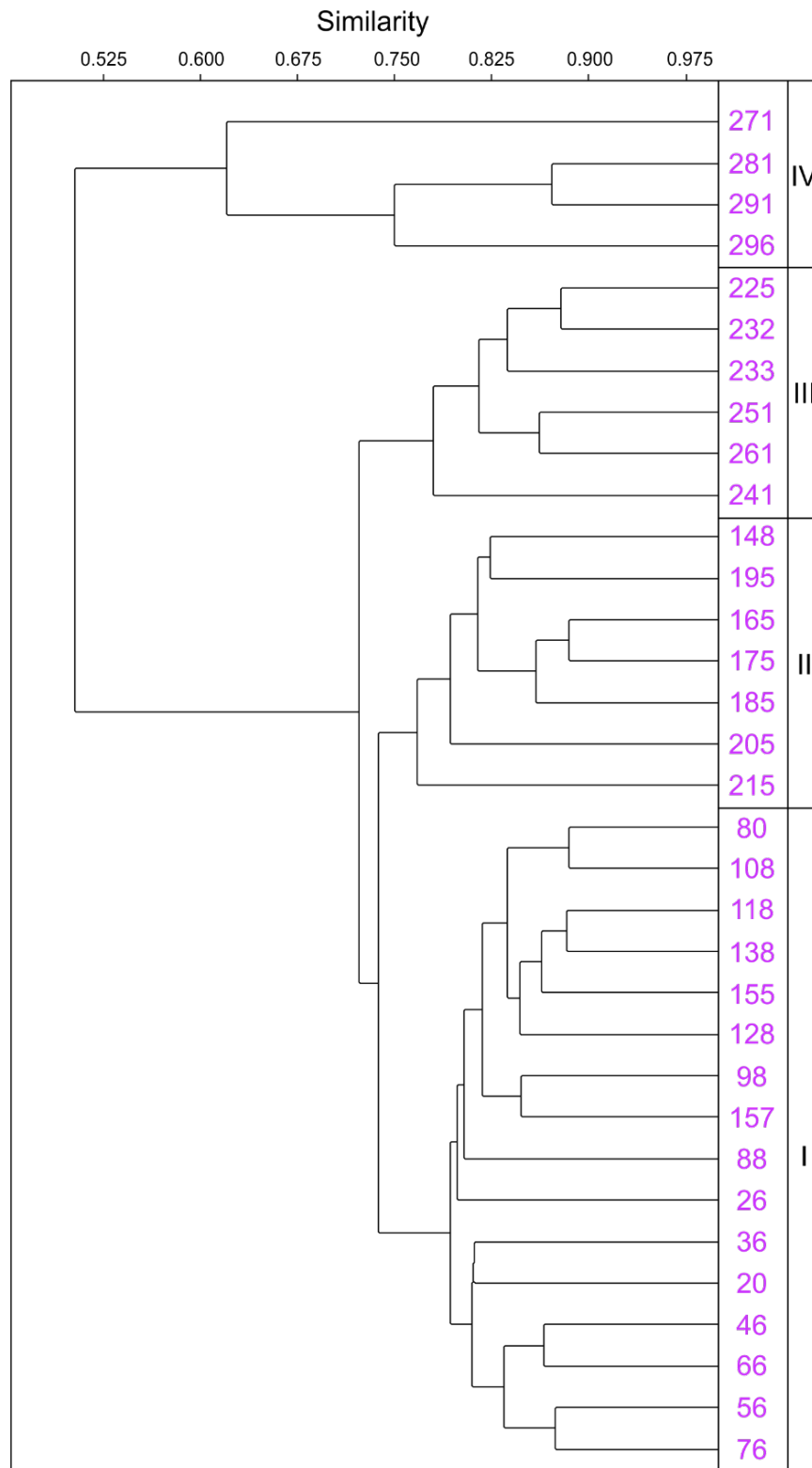


Figure 6.3 UPC125 Q-mode cluster analysis (UPGMA, Bray Curtis) for autochthonous benthic foraminifera >150 μm from all cores. Numerals indicate groups of samples with a similar composition of foraminifera, representing foraminiferal assemblages. Sample numbers indicated and coloured in accordance with overall regional assemblages outlined in Chapter 6. Autochthonous taxa occurring >5% abundance in at least one sample have been considered for this analysis.

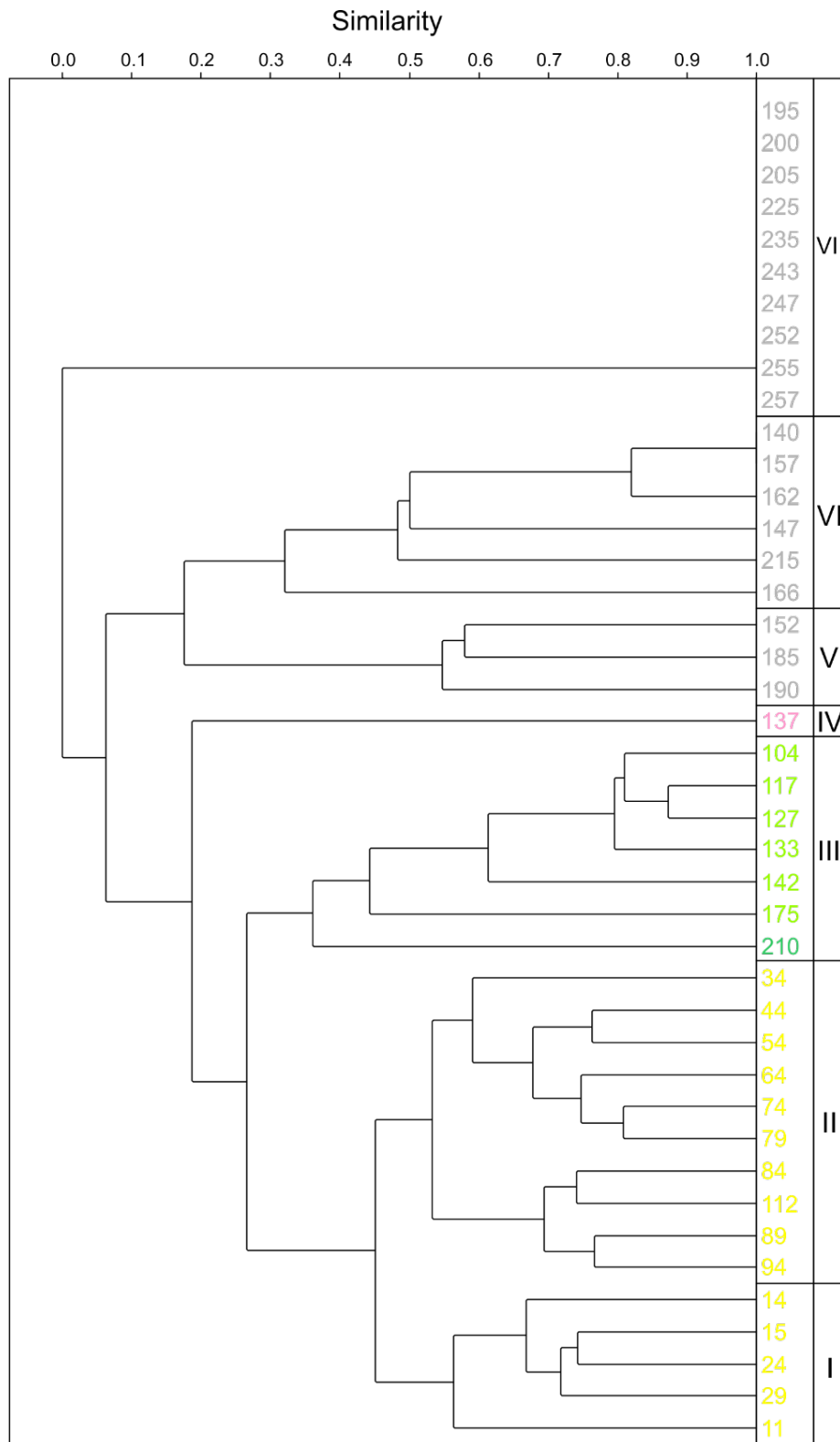


Figure 6.4 UPC133 Q-mode cluster analysis (UPGMA, Bray Curtis) for autochthonous benthic foraminifera >150 μm from all cores. Numerals indicate groups of samples with a similar composition of foraminifera, representing foraminiferal assemblages. Sample numbers indicated and coloured in accordance with overall regional assemblages outlined in Chapter 6. Autochthonous taxa occurring >5% abundance in at least one sample have been considered for this analysis.

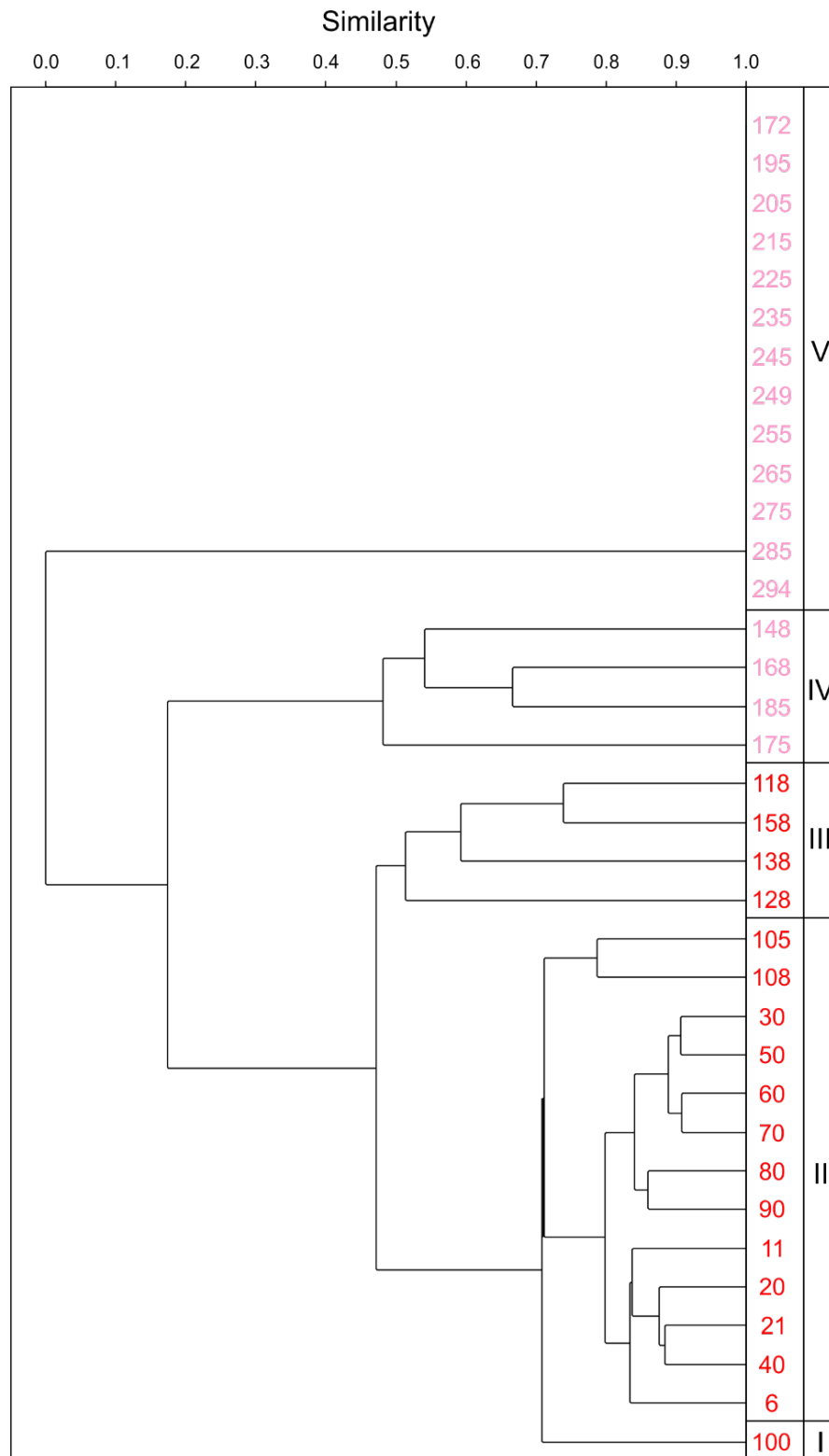


Figure 6.5 UPC154 Q-mode cluster analysis (UPGMA, Bray Curtis) for autochthonous benthic foraminifera >150  $\mu\text{m}$  from all cores. Numerals indicate groups of samples with a similar composition of foraminifera, representing foraminiferal assemblages. Sample numbers indicated and coloured in accordance with overall regional assemblages outlined in Chapter 6. Autochthonous taxa occurring >5% abundance in at least one sample have been considered for this analysis.

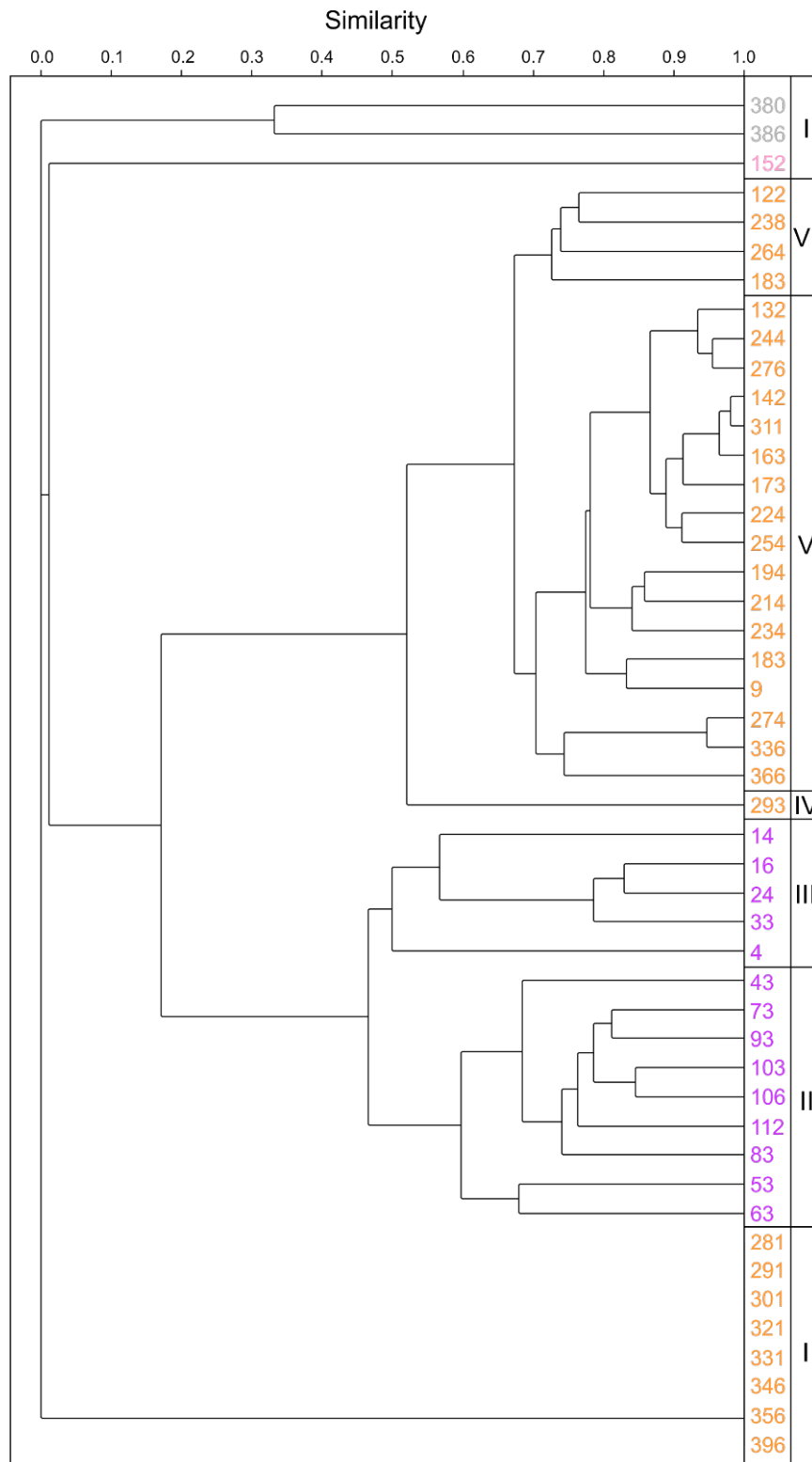


Figure 6.6 UPC164 Q-mode cluster analysis (UPGMA, Bray Curtis) for autochthonous benthic foraminifera >150  $\mu\text{m}$  from all cores. Numerals indicate groups of samples with a similar composition of foraminifera, representing foraminiferal assemblages. Sample numbers indicated and coloured in accordance with overall regional assemblages outlined in Chapter 6. Autochthonous taxa occurring >5% abundance in at least one sample have been considered for this analysis.



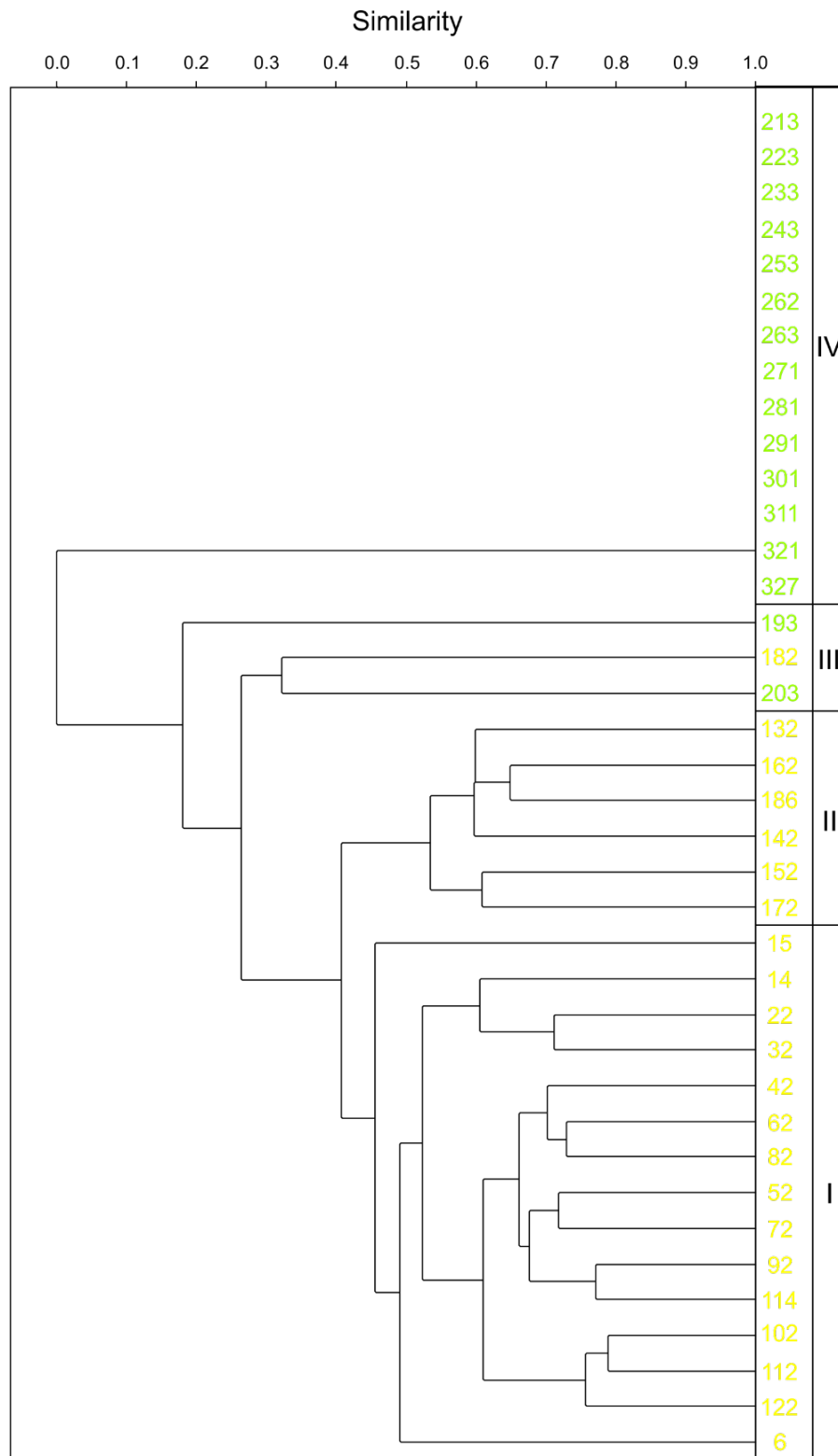


Figure 6.7 UPC170 Q-mode cluster analysis (UPGMA, Bray Curtis) for autochthonous benthic foraminifera >150  $\mu\text{m}$  from all cores. Numerals indicate groups of samples with a similar composition of foraminifera, representing foraminiferal assemblages. Sample numbers indicated and coloured in accordance with overall regional assemblages outlined in Chapter 6. Autochthonous taxa occurring >5% abundance in at least one sample have been considered for this analysis.

# APPENDIX 6.2

---

## TAXONOMIC REFERENCES

*Cited in Chapter 6*

Taxonomic concepts from Holbourn et al. (2013), Jones (1994), Hayward et al. (2019), Boltovskoy et al. (1980), Loeblich & Tappan, (1984) and Cushman (1933)

***Bulimina aculeata*** (d'Orbigny, 1826) sensu Jones (1994), Pl. 51

***Bulimina marginata*** (d'Orbigny, 1826) sensu Jones (1994), Pl. 51

***Bulimina mexicana*** (Cushman, 1922) Holbourn et al. (2013). Pag. 110. Fig. 1,2.

***Buzasima ringens*** (Brady, 1879) Jones (1994), Pl. 40

***Cassidulina laevigata*** (d'Orbigny, 1826) Hayward, B.W.; Le Coze, F.; Vachard, D.; Gross, O. (2019). World Foraminifera Database.

***Cassidulina subglobulosa*** (*unaccepted*) (Brady, 1881) Hayward, B.W.; Le Coze, F.; Vachard, D.; Gross, O. (2019). World Foraminifera Database.

***Chilostomella oolina*** (Schwager, 1878) sensu Jones (1994), Pl. 55

***Cibicides lobatulus*** (Walker and Jakob, 1798) sensu Jones (1994). Plate 93. Fig. 1, 4-5.

***Cibicides mundulus*** (*unaccepted*) Accepted as *Cibicidoides mundulus* (Brady, Parker & Jones, 1888) Hayward, B.W.; Le Coze, F.; Vachard, D.; Gross, O. (2019). World Foraminifera Database.

***Cibicides refulgens*** (de Monfort, 1808) Holbourn et al. (2013). Pag. 154, Fig. 1-3.

- Cibicidoides bradyi*** (Trauth, 1918) Holbourn et al. (2013). Pag. 162, Fig. 1-6.
- Cibicidoides pachyderma*** (Rzehak, 1886) Holbourn et al. (2013). Pag 198. Fig. 1-3.
- Cibicidoides subhaidingerii*** (Parr, 1950) Holbourn et al. (2013) Pag. 204, Fig. 1-3
- Cibicidoides wuellerstorfi*** (Schwager, 1866) sensu Jones (1994), Pl. 93
- Discorbis spp.*** (Lamarck, 1804) Boltovskoy et al. (1980) Pag. 81, Pl. 11
- Eggerella bradyi*** (Cushman, 1911) Holbourn et al. (2013). Pag. 232, Fig. 1-4.
- Ehrenbergina pupa*** (d'Orbigny, 1839) Boltovskoy et al. (1980) Pag. 83, Pl. 12, Fig. 13-14
- Epistomella exigua*** (Brady, 1884) Boltovskoy et al. (1980) Pag. 87, Pl. 14, Fig. 14-17
- Fissurina bisulcata*** (Heron-Allen & Earland, 1932) Boltovskoy et al. (1980) Pag. 89, Pl. 115, Fig. 1-3
- Fissurina semimarginata*** (Reuss, 1870) Boltovskoy et al. (1980) Pag. 91, Pl. 16, Fig. 8-10
- Glaphyrammina americana*** (Cushman, 1910) Loeblich & Tappan, (1984), p. 1161.
- Glandulina ovula*** (d'Obigny, 1846) sensu Jones (1994) Pl. 61
- Globobulimina affinis*** (d'Obigny, 1846) Hayward, B.W.; Le Coze, F.; Vachard, D.; Gross, O. (2019). World Foraminifera Database.
- Globobulimina turgida*** (Bailey, 1851) Hayward, B.W.; Le Coze, F.; Vachard, D.; Gross, O. (2019). World Foraminifera Database.
- Globocassidulina subglobulosa*** (Brady, 1881) Holbourn et al. (2013). Pag. 264, Fig. 1, 2.
- Gyroidina soldani*** (d'Obigny, 1826) Holbourn et al. (2013). Pag.278, Fig. 1-3.

***Hoeglundina elegans*** (d'Orbigny, 1826) Boltovskoy et al. (1980) Pag. 95, Pl. 18, Fig. 14-17

***Hyperammina elongata*** (Brady, 1878) Loeblich & Tappan, 1964, p. 1190.

***Lagena laevis*** (Montagu, 1803) sensu Jones (1994) Pl. 56

***Melonis affinis*** (Reuss, 1851) sensu Jones (1994) Pl. 108

***Melonis barleeanus*** (Williamson, 1858) (*unaccepted subjective junior synonym of *Melonis affinis* in opinion of Hayward et al. (2010)*)

***Nonion barleeanum*** (Williamson, 1858) (*unaccepted subjective junior synonym of *Melonis affinis* in opinion of Hayward et al. (2010)*)

***Nonionella atlantica*** (Cushman, 1947) *unaccepted*

***Nonionella auris*** (d'Orbigny, 1839) Cushman (1933) Part 2 Fig. 1a-1c

***Nonionella stella*** (Cushman & Moyer, 1930) Mendes (2012) Distribution of living benthic foraminifera on the Northern Gulf of Cadiz continental shelf. Journal of Foraminiferal Research, 42(1), 18-38.

***Nonionella turgida*** (Williamson, 1858) *unaccepted* Jones (1994) Pl.108

***Oolina globosa*** (Montagu, 1803) Jones (1994) Pl. 56

***Oridorsalis umbonatus*** (Reuss, 1851) Hayward et al. (1999) p. 258 Pl. 21

***Planulina ariminensis*** (d'Orbigny, 1826) Holbourn et al. (2013). Pag. 402, Fig. 1, 2.

***Prygo murrhina*** (Schwager, 1866) Jones (1994)

***Prygo nasuta*** (Cushman, 1935) Boltovskoy et al. (1980) Pag. 109, Pl. 25, Fig. 18-21

***Psammosphaera fusca*** (Schulze, 1875) Jones (1994)

***Pullenia bulloides*** (d'Orbigny, 1846) Jones (1994) Pl. 83

***Reophax subfusiformis*** (de Monfort, 1808) Brönnimann & Whittaker, (1980)

***Rhabdammina abyssorum*** (Sars, 1869) Jones (1994) Pl.22

***Rhabdammina linearis*** (Brady, 1879) Jones (1994) Pl. 22

***Rutherfordoides corunata*** (Cushman, 1913) Matoba & Yamaguchi (1982), Pl. 3, Fig. 9a, b

***Sigmoilopsis schlumbergeri*** (Finlay, 1947) Jones (1994), Pl. 8

***Sphaeroidina dehiscens*** (d'Orbigny, 1826) Holbourn et al. (2013). Pag. 520, Fig. 1-3.

***Stainforthia complanata*** (Egger, 1893) *unaccepted*, *Fursenkoina complanata* in sensu. Jones (1994), Pl. 52

***Trifarina angulosa*** (Williamson, 1858) sensu Jones (1994) Pl. 74

***Uvigerina aubriana*** (d'Orbigny, 1839) Holbourn et al. (2013). Pag. 584. Fig 1-3.

***Uvigerina bifurcata*** (d'Orbigny, 1839) sensu Jones (1994), Pl 74

***Uvigerina bradyana*** (Fornasini, 1900) sensu Jones (1994), Pl. 74

***Uvigerina canariensis*** (d'Orbigny, 1839) sensu Jones (1994) Pl. 74

***Uvigerina holicki*** (Thalman, 1950) sensu Jones (1994) Pl. 74

***Uvigerina mediterranea*** (Hofker, 1932) sensu Jones (1994) Pl. 74

***Uvigerina peregrina*** (Cushman, 1923) p. 166, Pl. 42, Fig. 2

***Uvigerina striata*** (d'Orbigny, 1839) Boltovskoy et al. (1980) Pag. 127, Pl. 34, Fig. 17-18